WL-TR-97-4055

PROCEEDINGS OF THE 1996 USAF AIRCRAFT STRUCTURAL INTEGRITY PROGRAM CONFERENCE

VOLUME II

ASIP

Gary K. Waggoner
WL/Materials Directorate
Wright-Patterson AFB, Ohio

John W. Lincoln
ASC/Deputy for Engineering
Wright-Patterson AFB, Ohio

James L. Rudd
WL/Flight Dynamics Directorate
Wright-Patterson AFB, Ohio

USAF Aircraft Structural Integrity Program Conference
Hyatt Regency San Antonio
San Antonio, Texas

June 1997

FINAL REPORT FOR PERIOD 3-5 DECEMBER 1996

Approved for public release; distribution unlimited

MATERIALS DIRECTORATE
WRIGHT LABORATORY
AIR FORCE MATERIEL COMMAND
WRIGHT-PATTERSON AFB OH 45433-7734

DTIC QUALITY INSPECTED 3

19970708 074

NOTICE

When government drawings, specifications, or other data are used for any purpose other than in connection with a definitely related government procurement operation, the United States Government thereby incurs no responsibility or any obligation whatsoever; and the fact that the government may have formulated, furnished, or in any way supplied the said drawings, specifications, or other data, is not to be regarded by implication or otherwise as in any manner licensing the holder or any other person or corporation, or conveying any rights or permission to manufacture use, or sell any patented invention that may in any way be related thereto.

This report has been reviewed by the Office of Public Affairs (ASC/PA) and is releasable to the National Technical Information Service (NTIS). At NTIS, it will be available to the general public, including foreign nationals.

This technical report has been reviewed and is approved for publication.

Gary K. Waggoner

GARY K. WAGGONER
Chief
Systems Support Division

Donald R. Kitchen

DONALD R. KITCHEN
Acting Director
Materials Directorate

If your address has changed, if you wish to be removed from our mailing list, or if the addressee is no longer employed by your organization, please notify WL/MLS Bldg 652, 2179 Twelfth St Ste 1, Wright-Patterson AFB, Ohio 45433-7718 to help us maintain a current mailing list.

Copies of this report should not be returned unless return is required by security considerations, contractual obligations, or notice on a specific document.

REPORT DOCUMENTATION PAGE

Form Approved
OMB No. 0704-0188

Public reporting burden for this collection of information is estimated to average 1 hour per response, including the time for reviewing instructions, searching existing data sources, gathering and maintaining the data needed, and completing and reviewing the collection of information. Send comments regarding this burden estimate or any other aspect of this collection of information, including suggestions for reducing this burden, to Washington Headquarters Services, Directorate for Information Operations and Reports, 1215 Jefferson Davis Highway, Suite 1204, Arlington, VA 22202-4302, and to the Office of Management and Budget, Paperwork Reduction Project (0704-0188), Washington, DC 20503.

1. AGENCY USE ONLY *(Leave blank)*	2. REPORT DATE	3. REPORT TYPE AND DATES COVERED
	June 1997	Final, 3-5 December 1996

4. TITLE AND SUBTITLE
PROCEEDINGS OF THE 1996 USAF AIRCRAFT STRUCTURAL INTEGRITY PROGRAM CONFERENCE, VOLUME II

5. FUNDING NUMBERS
PE 62102F
PR 4349
TA LA
WU BR

6. AUTHOR(S)
1-Gary K. Waggoner, Compiler & Editor; 2-John W. Lincoln, ASC/ENF; and 3-James L. Rudd, WL/FIB, Editors

7. PERFORMING ORGANIZATION NAME(S) AND ADDRESS(ES)
1-Materials Directorate and 3-Flight Dynamics Directorate, Wright Laboratory;
2-Aeronautical Systems Center, Deputy for Engineering, all three of the
Air Force Materiel Command
Wright-Patterson AFB OH 45433

8. PERFORMING ORGANIZATION REPORT NUMBER
WL-TR-97-4055

9. SPONSORING/MONITORING AGENCY NAME(S) AND ADDRESS(ES)
Materials Directorate (POC: Gary Waggoner, WL/MLS, 937-255-2282)
Wright Laboratory
Air Force Materiel Command
Wright-Patterson AFB OH 45433-7734

10. SPONSORING/MONITORING AGENCY REPORT NUMBER
WL-TR-97-4055

11. SUPPLEMENTARY NOTES
Volume I - WL-TR-97- 4054

12a. DISTRIBUTION AVAILABILITY STATEMENT
Approved for public release; distribution is unlimited.

12b. DISTRIBUTION CODE

13. ABSTRACT *(Maximum 200 words)*
This report contains the proceedings of the 1996 USAF Structural Integrity Program Conference held at the Hyatt Regency Hotel in San Antonio, Texas, from 3-5 December 1996. The conference, which was sponsored by the Aeronautical Systems Center's Engineering Directorate and the Wright Laboratory's Flight Dynamics and Materials Directorates, was hosted by the San Antonio Air Logistics Center Aircraft Directorate, Aircraft Structural Integrity Branch (SA-ALC/LADD). This conference, as in previous years, was held to permit experts in the field of structural integrity to communicate with each other and to exchange views on how to improve the structural integrity of military weapon systems. Sessions were primarily focused on analysis and testing, engine structural integrity, structural materials and inspections, structural repair, and force management. This year, as in previous years, our friends from outside the U.S. borders provided the audience with outstanding presentations on activities within their countries. It is anticipated this conference will include their contributions in the agenda of future meetings. This year, 18 countries were represented in the audience.

14. SUBJECT TERMS	15. NUMBER OF PAGES
	524
	16. PRICE CODE

17. SECURITY CLASSIFICATION OF REPORT	18. SECURITY CLASSIFICATION OF THIS PAGE	19. SECURITY CLASSIFICATION OF ABSTRACT	20. LIMITATION OF ABSTRACT
UNCLASSIFIED	UNCLASSIFIED	UNCLASSIFIED	SAR

Standard Form 298 (Rev. 2-89) (EG)
Prescribed by ANSI Std. 239.18
Designed using Perform Pro, WHS/DIOR, Oct 94

DTIC QUALITY INSPECTED 2

GENERAL INSTRUCTIONS FOR COMPLETING SF 298

The Report Documentation Page (RDP) is used in announcing and cataloging reports. It is important that this information be consistent with the rest of the report, particularly the cover and title page. Instructions for filling in each block of the form follow. It is important to ***stay within the lines*** to meet ***optical scanning requirements.***

Block 1. Agency Use Only *(Leave blank)*.

Block 2. Report Date. Full publication date including day, month, and year, if available (e.g. 1 Jan 88). Must cite at least the year.

Block 3. Type of Report and Dates Covered. State whether report is interim, final, etc. If applicable, enter inclusive report dates (e.g. 10 Jun 87 - 30 Jun 88).

Block 4. Title and Subtitle. A title is taken from the part of the report that provides the most meaningful and complete information. When a report is prepared in more than one volume, repeat the primary title, add volume number, and include subtitle for the specific volume. On classified documents enter the title classification in parentheses.

Block 5. Funding Numbers. To include contract and grant numbers; may include program element number(s), project number(s), task number(s), and work unit number(s). Use the following labels:

C - Contract	**PR** - Project
G - Grant	**TA** - Task
PE - Program Element	**WU** - Work Unit Accession No.

Block 6. Author(s). Name(s) of person(s) responsible for writing the report, performing the research, or credited with the content of the report. If editor or compiler, this should follow the name(s).

Block 7. Performing Organization Name(s) and Address(es). Self-explanatory.

Block 8. Performing Organization Report Number. Enter the unique alphanumeric report number(s) assigned by the organization performing the report.

Block 9. Sponsoring/Monitoring Agency Name(s) and Address(es). Self-explanatory.

Block 10. Sponsoring/Monitoring Agency Report Number. *(If known)*

Block 11. Supplementary Notes. Enter information not included elsewhere such as: Prepared in cooperation with....; Trans. of....; To be published in.... When a report is revised, include a statement whether the new report supersedes or supplements the older report.

Block 12a. Distribution/Availability Statement. Denotes public availability or limitations. Cite any availability to the public. Enter additional limitations or special markings in all capitals (e.g. NOFORN, REL, ITAR).

- **DOD** - See DoDD 5230.24, "Distribution Statements on Technical Documents."
- **DOE** - See authorities.
- **NASA** - See Handbook NHB 2200.2.
- **NTIS** - Leave blank.

Block 12b. Distribution Code.

- **DOD** - Leave blank.
- **DOE** - Enter DOE distribution categories from the Standard Distribution for Unclassified Scientific and Technical Reports.
- **NASA** - Leave blank.
- **NTIS** - Leave blank.

Block 13. Abstract. Include a brief *(Maximum 200 words)* factual summary of the most significant information contained in the report.

Block 14. Subject Terms. Keywords or phrases identifying major subjects in the report.

Block 15. Number of Pages. Enter the total number of pages.

Block 16. Price Code. Enter appropriate price code *(NTIS only)*.

Blocks 17. - 19. Security Classifications. Self-explanatory. Enter U.S. Security Classification in accordance with U.S. Security Regulations (i.e., UNCLASSIFIED). If form contains classified information, stamp classification on the top and bottom of the page.

Block 20. Limitation of Abstract. This block must be completed to assign a limitation to the abstract. Enter either UL (unlimited) or SAR (same as report). An entry in this block is necessary if the abstract is to be limited. If blank, the abstract is assumed to be unlimited.

Volume II

SESSION V - DYNAMICS/MECSIP

Risk Analysis of Fatigue Cracking in IAF F-16 Aircraft 559
R. Halevi, J. Weihs, H. Cohen and D. Bar-Shalom

Sonic Fatigue - A Problem Requiring Special Handling 597
T. Beier

Application of the MECSIP Process to the B-2 Ground Refueling System 613
E. Wells

SESSION VI - WIDESPREAD FATIGUE DAMAGE

Controlling Multi-Site Damage by Means of Design and Inspection Trade-offs 641
A. Brot

Analysis of Stiffened Panels with Multiple Site Damage 655
M. Heinimann, H. Wang and A. Grandt Jr.

A Proposed Engineering Approach to Assessing the Residual Strength of Aircraft Containing a Lead Crack Interacting with Multiple Site Damage 683
G. Chell, M. Ferrell, R. McClung and S. Hudak Jr.

Enhanced Repair Assessment Procedure and Integrated Design (RAPID) 711
M. Shaio, J. Bakuckas Jr., and C. Bigelow

The Onset of Multiple Site Damage and Widespread Fatigue Damage in Aging Airplanes 729
D. Jeong and P. Tong

SESSION VII - ENGINES

A Probabilistic Approach to Aircraft Turbine Rotor Material Design 753
G. Leverant, D. Littlefield, R. McClung, H. Hillwater and J.Wu

Engine Health Monitoring System for Gas Turbine Engines 793
M. Roemer

The Role of Residual Stress in Low Cycle Fatigue of Gas Turbine Engine Disks 807
E. Bradley, S. Berkley and R. Fairbanks

Quantification of Process Margin for Robust Engine Components 825
P. Domas and H. Popp

Structural Integrity of Composite Containment Structures 837
C. Chamis and P. Gotsis

A Probabilistic Life Method for a Two-Lobed Turbine Disk Attachment 867
C. Date, C. Balis, D. Greving, J. Musgrave, D. Langefels and K. Richardson

PT6A-68 JPATS Engine Structural Integrity Program 879
B. Wilkinson

The Future Direction and Development of Engine Health Monitoring (EHM) Within the United States Air Force 901
Sqn Ldr A.J. Green

SESSION VIII - NDE/I

Computer Monitored Shot Peening, An Update 913
J.R. Harrison

Freeze-Frame Imaging of Operating Turbine Engines Using Synchronous Multiplane Tomography (SMT) 917
T. Kirchner and P. Burstein

Orthogonal-Axis Eddy Current Probes for High Sensitivity/High Productivity Inspection of Aircraft Structure 931
G. Burkhardt, J. Fisher, J. Stolte, S. Kramer and K. Cobble

Eddy Current Inspection of Engine Blade Slots 951
W. Hoppe

SESSION IX - FORCE MANAGEMENT

F-14 Fatigue Tracking 983
R. Dalrymple, T. Fallon and T. Chappell

Achieving an Integrated Usage Based Maintenance Program for the Canadian Forces C-130 1003
T. Padfield, A. McCray and Capt A. van den Hoeven

Aging Aircraft Usage Monitoring in the Royal Australian Air Force 1025
Sqd Ldr M. Wilkin

A Review of a Strain and Flight Parameter Data Based Aircraft Fatigue Usage Monitoring System 1035
L. Molent

ATTENDANCE LIST 1055

SESSION V

DYNAMICS/MECSIP

Chairman: *K. Leikach*, Naval Air Systems Command

RISK ANALYSIS OF FATIGUE CRACKING IN IAF F-16 AIRCRAFT

R. Halevi, J. Weihs, H. Cohen, D. Bar-Shalom
Structures Branch
Israel Air Force
M.O.B. 2158(CT)
I.D.F.
ISRAEL

ABSTRACT

A statistical risk analysis of fatigue failures in a major F-16 fuselage bulkhead and it's implications for the current maintenance policy are presented. A risk analysis based on the Weibull distribution was performed. The distribution was constructed using known in-service failures and estimated failures extrapolated using fatigue analysis. This distribution was in turn used to estimate the failure rate for the remaining aircraft in service. Correlation with planned maintenance action for preventive repairs of the bulkhead yielded an expected number of failures for several different maintenance scenarios. Safety of flight issues were also addressed using the derived failure distribution.

INTRODUCTION

The Lockheed-Martin F-16 fighter was designed for an economical structural fatigue life of 3000 Flight Hours. However, in-service crack findings and results of updated Damage Tolerance Analysis indicate that certain major structural components will need to be repaired at half of the design life. The most critical major component is a fuselage bulkhead at station 341.8 (Fig. 1). The order in which aircraft enter the modification line is determined from the severity of the cracks detected using NDI (Non-Destructive Inspections). Implementation of this modification is in progress on the IAF fleet.

Modification of this bulkhead entails the disassembly of the aircraft, and replacement of the lower half of the bulkhead with a redesigned bulkhead. The upper half of the bulkhead is checked for cracks originating from fastener holes in the upper half of the bulkhead (Fig. 2). The repair of these cracks can be achieved in one of two ways, depending on crack size:

If the crack is small enough, the fastener hole is reamed until the crack is removed. The hole is then cold-worked, an oversize fastener is installed with a radius block. Depending on aircraft model, a special bolt may be fitted.

When the crack length exceeds the allowable reaming diameter, repairing the bulkhead requires cutting the cracked area and splicing a new part to it (Fig. 3). These repairs are costly, and present a fire hazard as the bulkhead is also a fuel tank wall.

The splice-type repair can only be performed at D-Level, while the ream repair is performed at I-Level. The splice type repair costs over $50,000 per aircraft side (up to two per aircraft). The ream repair costs several hundred dollars.

The current maintenance policy calls for a certain number of aircraft to be modified every year, over a span of several years (under a program dubbed "Falcon-Up"). The entire fleet is to be modified.

IAF management commissioned a report to quantify the economic and safety aspects of the current and proposed maintenance policies, which would increase the number of aircraft modified each year. A model would have to be developed to predict when the fatigue cracks in the upper part of the bulkhead would transition from short, easily repairable lengths to splice type repair lengths. The results of such a model, when combined with a maintenance policy, would yield an estimate of the number of splice type repairs incurred by that policy. These results will also be applied towards a safety of flight assessment of the maintenance policies.

TRANSITION PREDICTION MODEL

Attempts to estimate the crack lengths in each aircraft using fatigue tracking measurements failed, due to fatigue tracking model limitations (the models will not account for differing ream sizes). Therefore, conventional methods that would rank the aircraft according to the severity of usage G-spectra or accumulated fatigue damage could not be applied.

A model based upon known failure distributions can be created using a technique called "risk analysis" (see Appendix). This method consists of estimating a failure probability distribution using known failures and maximum likelihood calculations. The integral of this distribution multiplied by a fleet flight hour distribution yields an estimated number of failures. IAF has developed an in-house software package to perform risk analysis, which was used to create all the following data [8]. The term "failure" as used here denotes a splice type repair, also defined as an "economic failure".

A database of NDI results of the critical fastener holes for the fleet was available. A sample of this database is presented in Fig. 4. The data available included date, accumulated flight hours and crack length. Most of the fleet aircraft had discernible cracks. This database was assembled over a period of several years, therefore requiring extrapolation of crack sizes for the current aircraft flight hours.

Since the pending decision was of a binary nature (ream/ splice repair), the data was filtered to include data for splice type repairs only. These repairs were labeled as "failures" - a change of state from ream to splice repair.

The number of "failures" was small compared with the number of reamed holes. A large as possible sample of failures is required for achieving tight confidence bounds. The number of "failures" was extended by estimating the "failure" flight hours for aircraft that had cracks of known sizes. This estimate was accomplished by adding to the flight hours at which the crack size was known, the remaining flight hours to failure (as predicted by fatigue crack growth analysis for this crack size). The remaining flight hours to failure are known at a high confidence level [1]. For every additional 150-200 flight hours the crack grows by one ream over-size. Multiplying this value by the number of remaining over-size ream's (to splice ream size) yield the remaining flight hours to failure. These extrapolations are valid as crack growth predictions for these crack lengths are considered accurate.

estimated failure flight hours = NDI F.H. +
remaining no. of reams * F.H. per ream

Prior to the calculation of the failure probability distribution, an attempt was made to classify the fleet into distinct populations with particular failure distributions. Four populations were recognized, distinguished by differing structural configuration (F-16 model A,B,C,D) and unique usage spectra (IAF / USAF usage). The populations were designated as no. 1 through 4.

For each population, a failure probability distribution was created (see Appendix eq. 4 & Fig. 5). Current fleet accumulated flight hours were used to create a flight hour's probability distribution (Fig. 6) for aircraft that haven't undergone modification.

The results of the risk analysis (predicted number of failures for certain future fleet flight hours) for each of the four sub-populations are presented in Figs. 7 & 8. A graph of these results is presented in Fig. 9.

VERIFICATION OF RESULTS

Once a failure distribution has been calculated, the estimated number of failures may be determined for any fleet flight hours' distribution. To test the failure distribution's accuracy, an estimate of the failures for the current flight hours distribution was made. This estimate was then compared to current crack sizes known from NDI. Summary of this comparison is presented in Fig. 10.
The risk's analysis predication is slightly higher than currently known failures. This may be accounted for in the long time that has passed since, many of the inspections were performed. The cracks may have propagated to failure length by the date this analysis was performed. An attempt to estimate the number of currently failed aircraft according to time since the inspection was made, and good correlation was achieved. The analysis's results therefore may be considered accurate.

INTEGRATION OF MAINTENANCE POLICY

The predicted number of failures does not take into account aircraft modified in the "Falcon-Up" program. Thus, the estimate of the number of aircraft that will be spliced is not readily retrieved from the results of the risk analysis.

A method was developed that integrates risk analysis and maintenance policy data to yield an estimate of the number of overall splices expected.

As risk analysis is a statistical method, no inference may be made from the overall fleet results of the

analysis on the condition of a certain aircraft. Therefore, no assumption can be made on the crack size of an individual aircraft at the date that it will undergo modification.

The following basic assumptions are made:

1. Aircraft entering the modification line are those known to be the most severely cracked.
2. If the number of aircraft that have undergone modification is less than the number of predicated failures (for a certain population), those aircraft are spliced.
3. If there are more aircraft modified than predicted failed, no more splices are required.

Obviously, these assumptions will not hold for the individual dispersion of crack findings on every aircraft entering the modification line. Some aircraft satisfying assumption #2 will not be spliced, and some fulfilling assumption #3 will have to be spliced. However, for estimating the overall number of splices required, this method will provide a reasonable estimate. At worst, this estimate may be used to grade different maintenance policies in respect to the current policy (overall no. of aircraft per year / distribution between sub-populations).

The estimate is made using a graphical technique. The horizontal axis is the time scale (in years), and the vertical axis depicts number of aircraft. Two lines are drawn on the graph (Fig. 11), one representing the number of expected failures. The other line depicts the number of aircraft that have undergone modification. The intersection point of the two lines is the total number of failures expected, given that the lines do not intersect more than once.

RESULTS

The failure rates for sub-populations 1 & 2 are lower than those for sub-populations 3 & 4, but the current overall number of failed aircraft is larger for sub-populations 1 & 2. This is because they have accumulated a significantly higher number of flight hours.

Currently there are about 20 aircraft which will require a splice, and by the end of the year there will be 40 aircraft requiring splices.

The results of the maintenance policy integration are presented in Fig. 12 & 13. Several different options for changing the current maintenance policy of modifying 17 aircraft a year were studied. The resulting number of splices is presented in Fig. 12. A plot of the number of splices vs. no. of aircraft modified each year is introduced in Fig. 13.

Obviously, increasing the number of aircraft modified yearly lowers the number of splices required. However, the fleet has accumulated so much flight hours that many aircraft already must be modified. The number of splices declines with increased modification rates, until it reaches a level from which on the decline tapers off. At infinity (all aircraft modified today), the number of splices equals the number of currently failed aircraft.

An assessment of funds saved for every modification line rate is presented in Fig. 14. The sums presented are a bottom limit, as they are calculated for one splice per aircraft. Some aircraft will probably require two splice repairs.

CONCLUSIONS

The probability distribution for the failure of bulkhead 341.8 (actual failure, not the reaching of splice crack length) and the subsequent failure of the aircraft cannot be determined, since to date non of these failures has occurred. An estimate of the distribution may be made by shifting the splice repair distribution mean. The mean should be shifted by the difference in fatigue life between a crack growing to splice length and a cracking growing to bulkhead failure length. The magnitude of this difference is indeterminate, due to the "lack" of in-service failures to correlate to. Due to this, no estimate may be made of the risk of complete failure of the aircraft. As the "complete bulkhead failure" rate is identical to the "economical" failure rate, an estimate may be made of relative risk amongst the four sub-populations.

At the current aircraft modification rate, most of the fleet will require at least one splice. Once the modification rate is increased for a minimum period (to modify all the "backlogged" aircraft which must be spliced) and afterwards kept at a certain minimum, the IAF will be modifying aircraft before the cracks reach splice lengths.
Increasing the modification rates will enable the modification of aircraft with small cracks and save the splice repairs for these aircraft.

Of the four sub-populations identified, two are the currently critical with many splices. However, the splice rates for these two populations will remain constant during the coming years, and the other two populations (which to date have had few splices) will start require a lot of splice repairs.
At the current maintenance policy, the current high risk level of "complete bulkhead failure" will remain throughout the implementation of the modifications.

Note

For security reasons, all the numbers appearing in this paper have been altered.

REFERENCES

1. "F-16 Durability and Damage Tolerance Analysis", LMTAS Report 16PR12668, Sep. 1995.

2. Christian T. F., Smith H. G., and Saff C. R., "Structural Risk Assessment Using Damage Tolerance Analysis and Flight Usage Data", *Presented at the ASME Winter Annual Meeting* 7-9 Dec. 1986, Anaheim, California.

3. Abernethy R. B., Breneman J. E., Medlin C. H., Reinman G. L., "Weibull Analysis Handbook," USAF Report AFWAL-TR-832079, Nov. 1983.

4. Kennedy J. B., Neville A. M., Basic Statistical Methods for Engineers and Scientists", 3rd ed., *Harper and Row, Publishers, New York*, 1986, pp. 248-253.

5. Nelson W.,"Appllied Life Data Analysis" , *John Wiley and Sons, New York*, 1982.

6. Salzer H.E., Zucker R., "Table of Zeros and Weight Factors of the First Fifteen Laguerre Polynomials", *Bull. Amer. Math. Soc.*, 55, 1949, pp. 1004-1012.

7. Hilderbrand F. B., "Introduction to Numerical Analysis", 2nd ed., *McGraw -Hill, New York*, 1974, pp. 332-334, 392-395.

8. Yosibash Z., "Implementation of Structural Risk Assessment in the IAF for Fleet Managment Using DTA and Aircraft Fleet Usage Data", *AIAA Journal*, 29(4), 1992, pp. 540-544.

APPENDIX - RISK ANALYSIS METHODOLOGY

The following paragraphs contain a detailed description of the methodology employed in structural failure risk analysis. This methodology is not limit to structural failures. A Weibull distribution is used to fit the combined failure data set due to the following reasons: The Weibull distribution is broadly applicable, it provides a simple graphic solution, it can be used even when data is insufficient for other distributions (e.g., sample size is small), and it usually provides the best fit for the type of data encountered in structural fatigue failure [3].
The form for the three-parameter Weibull probability distribution function for hazard is as follows:

$$F_{cr}(t) = 1 - \exp\left[\left[\frac{(t - t_{0cr})}{(n_{cr} - t_{0cr})}\right]^{\beta cr}\right] \quad (1)$$

where t_{ocr} is the minimum expected failure time, η_{cr} is the characteristic failure life and β_{cr} is the Weibull slope parameter for failure life.
Median cumulative distribution function associated with a ranked failure was used in our computations because it is independent of any distribution [4]. An good approximation for the median cumulative function can be shown to be:

$$F(t_i) = \frac{(i - 3)}{(N + 0.4)} \quad (2)$$

where i is the i-th ranked failure, N is the total number of failures in data set and t_i is the i-th ranked failure life. The two parameters for Weibull distribution, β_{cr} and η_{cr}, are determined (assuming $t_{ocr} = 0$) using two methods β_{cr} and η_{cr} are estimated first by Median Rank Regression (MRR), and then by maximum likelihood estimators [5] using MRR estimation of the two parameters [3].
Safety considerations in aerospace operations require corrective action based on a very small sample of failure data. Since this is unusual compared to other Weibull applications, Monte Carlo simulation was used to study the accuracy of Weibull analysis when applied to data from a fleet of several thousand successfully operating components and very few (three to ten) failures [3]. Both rank regression and maximum likelihood tend to overestimate β's with

small failure samples (the slope on the Weibull plot is too steep). This positive bias decreases as the number of failures increases. η is typically underestimated. Rank regression risk forecasts are conservative (overestimate the risk) and less precise when computed with few failures and many suspensions. maximum likelihood risk forecasts are more accurate and precise than rank regression risk forecasts with small failure samples.

The third parameter for Weibull distribution, t_{ocr}, is determined by an iterative method using β_{cr} and η_{cr}. Once β_{cr} and η_{cr} are determined (assuming $t_{ocr} = 0$), we can compute t_{ocr}:

$$t0_{cr} = t2 - \frac{(t3 - t2)\cdot(t2 - t1)}{(t3 - t2) - (t2 - t1)} \qquad (3)$$

where t1 is the first failure time, t3 is the last failure time and t2 is the time corresponding to the linear halfway distance on the Weibull plot vertical axis calculated by :

$$t2 = \exp\{w + \beta_{cr} * \ln(n_{cr})\}$$

where:

$$w = y1 + 0.5*(y3-y1)$$

$$y1 = \ln\{\ln[1/(1-F(t1))]\}$$

$$y3 = \ln\{\ln[1/(1-F(t3))]\}$$

After subtracting t_{ocr} from each failure time of the combined failure data set, the two parameters of the Weibull distribution (β_{cr} and η_{cr}) are re-determined using the "new" combined failure data set. t_{ocr} is re-computed using re-determined β_{cr} and η_{cr}. Those iterations are repeated until convergence of t_{ocr} is achieved. A Weibull distribution is also used to characterise the current aircraft lives. The probability of failure of an aircraft component within the fleet after the next δt flying hours (assuming a uniform fleet flight hour accumulation rate) is determined by the following integral expression [2] :

Probability of failure after the next δt hours =

$$\int_0^{\infty} \exp(-x)\cdot\exp\left[-\left\{\frac{\left[(\eta_{cr} - t0_{cr})\cdot x^{1/\beta_{cr}} + t0_{cr} - t0_{pl} - \delta t\right]}{\eta_{pl} - t0_{pl}}\right\}^{\beta_{pl}}\right] dx \qquad (4)$$

where t_{0pl} is the minimum expected actual aircraft flight hours, η_{pl} is the characteristic flight hours and β_{pl} is the Weibull slope parameter for actual aircraft flight hours. It should be noted that the integral expression in (4) presents the probability of failure after the next δt hours, as long as:

$$t_{ocr} \geq t_{0pl} + \delta t \qquad (5)$$

If the fleet does not accumulate flight hours uniformly, then historical data can be used to estimate the number of flight hours of each aircraft in the next z years. A Weibull distribution will be used to characterise the aircraft expected lives for the next z years. The integral expression in (4) will then be:

Probability of failure after the next z years =

$$\int_0^{\infty} \exp(-x)\cdot\exp\left[-\left\{\frac{\left[(\eta_{cr} - t0_{cr})\cdot x^{1/\beta_{cr}} + t0_{cr} - t0_{pl}(z)\right]}{\eta_{pl}(z) - t0_{pl}(z)}\right\}^{\beta_{pl}(z)}\right] dx \qquad (6)$$

where $\beta_{pl}(z)$, $\eta_{pl}(z)$, $t_{0pl}(z)$ are the three Weibull parameters for expected flight hours for next z years. The integral expressions (4) and (6) are computed numerically using a fifteen point Laguerre-Gauss quadrature [6],[7] :

$$\int_0^{\infty} \exp(-x)\cdot f(x)dx = \sum_{i=1}^{m} Hi\cdot f(x_i) + \text{discretization error} \qquad (7)$$

where x_i is the i-th zero of m-th Laguerre polynomial and H_i is the i-th weight factor while m=1,...,15.

Based on several structural risk analyses, we found that f(x) approaches zero very quickly ($f(x_i) \approx 0.0$ for $x_i \geq 1$), making only the first two terms in the above sum significant. The accuracy of the numerical integration is controlled by computing the error between two consecutive sums, e.g. :

$$\sum_{i=1}^{m} Hi\cdot f(x_i) - \sum_{i=1}^{m-1} Hi\cdot f(x_i)$$

Once the probability of failure is determined as a function of δt (eq. (4)) or as a function of years (eq. (6)), the number of components expected to fail at any time can be determined. For a large, complete (no suspensions) failure data set of size N, the confidence intervals for β_{cr} and η_{cr} can be approximated by the following expressions [3] :

$$\beta_{cr} \cdot \left(\frac{-0.78 \cdot Z\alpha}{\sqrt{N}} \right) \leq \beta_{cr} \leq \beta_{cr} \cdot \left(\frac{0.78 \cdot Z\alpha}{\sqrt{N}} \right) \quad (8)$$

$$\frac{\eta_{cr} \cdot (-1.05 \cdot Z\alpha)}{\beta_{cr} \cdot \sqrt{N}} \leq \eta_{cr} \leq \frac{\eta_{cr} \cdot (1.05 \cdot Z\alpha)}{\beta_{cr} \cdot \sqrt{N}} \quad (9)$$

where Z_α, the upper $\alpha/2$ point of the standard normal distribution, depends on the confidence level chosen. Z_α's for various (typical) confidence levels are presented in many statistical handbooks. The confidence bands are computed by expressions (4) or (6), using the values derived by inequalities (8) and (9). A failure data set may contain more than one mode of failure. In this case, two distinct failure distributions will appear on the Weibull plot. In order to detect this phenomenon, only measured lives for failed components should be incorporated into the failure data set. Risk analysis should be performed for each separate mode of failure.

ACKNOWLEDGMENT

The authors would like to thank Dr. Zohar Yosibash for the development of the computer software used for risk analysis, and for some passages in this appendix[8].

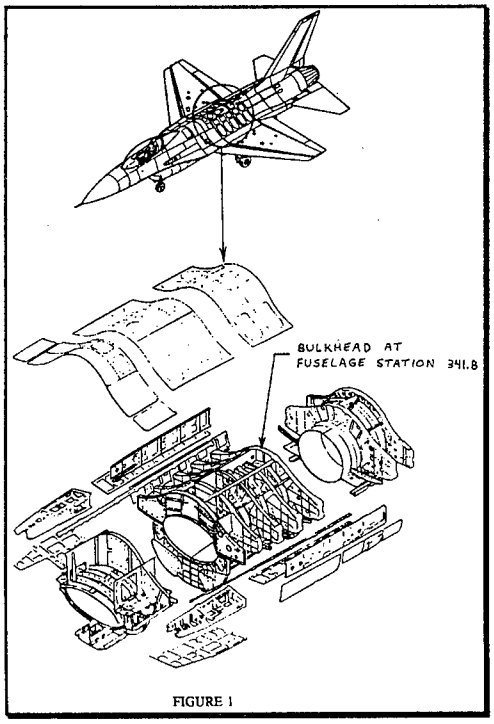

Figure 1. F-16 structral breakdown

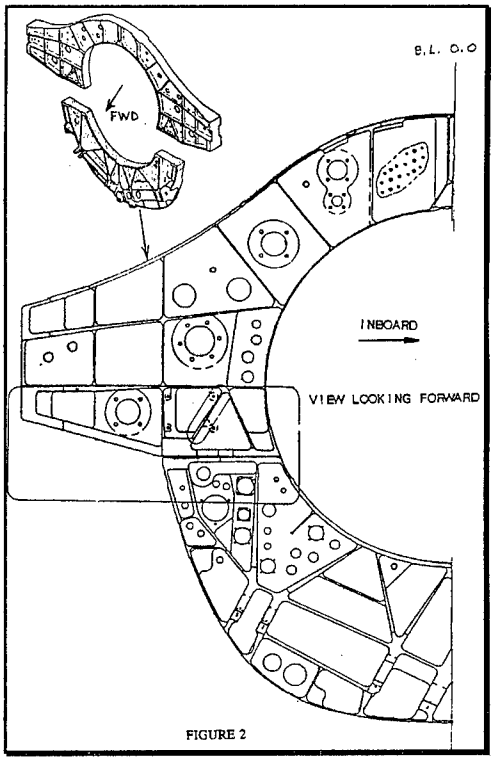

Figure 2. Bulkhead 341.8 detail

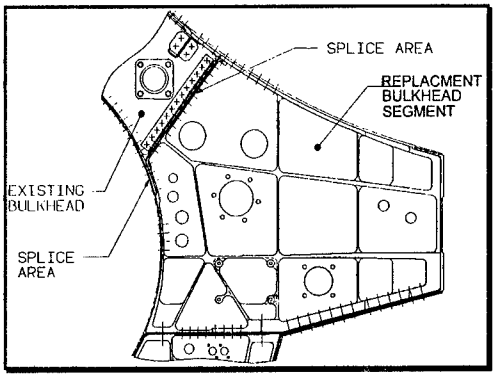

Figure 3. Bulkhead 341.8 splice repair

A/C Type	A/C Number	Date Inspected	Ream Over-Size
F-16A	001	8/95	2
F-16A	002	3/95	4
F-16C	003	1/96	3
.	.	.	.
.	.	.	.

Figure 4. Fatigue crack database

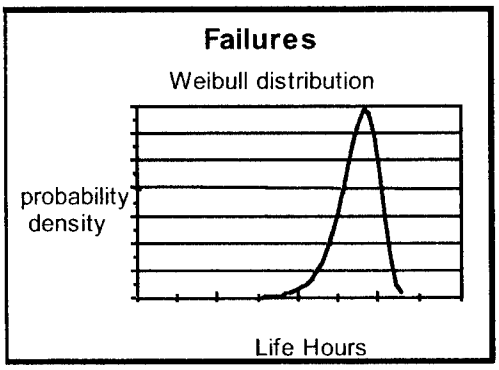

Figure 5. Sub-population failure distribution example

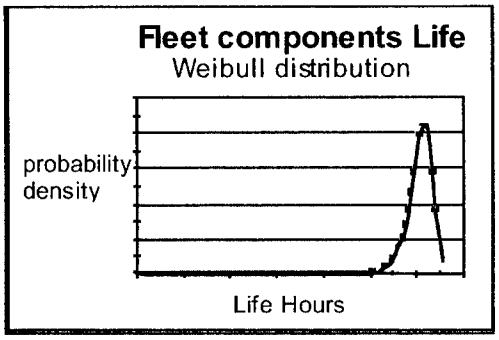

Figure 6. Sub-population life distribution example

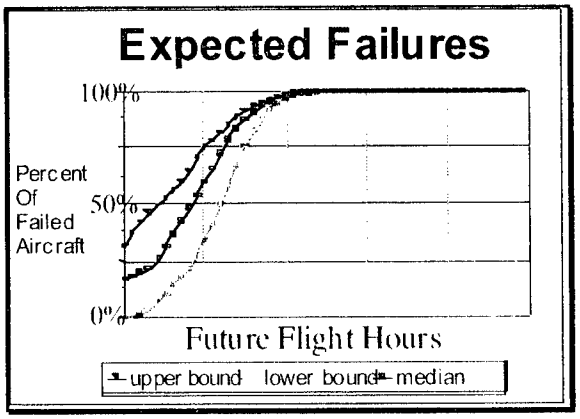

Figure 7. Sub-population expected failures example

Sub-Population					
Year	**1**	**2**	**3**	**4**	**Total**
n	7	9	4	2	22
n+1	12	11	9	6	38
n+2	15	13	14	12	54
n+3	18	16	17	13	64
n+4	21	19	19	13	72
n+5	21	21	19	13	74
n+6	24	24	19	13	80

Figure 8. Comparison of forecasted failures

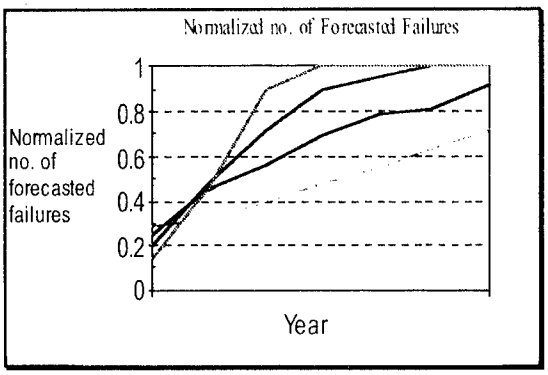

Figure 9. Comparison of sub-population forecasted failures

Sub-Population	Failure Estimate	Known Failures
1	7	4
2	9	7
3	4	3
4	2	3
Total	22	17

Figure 10. Comparison of estimate to known failures

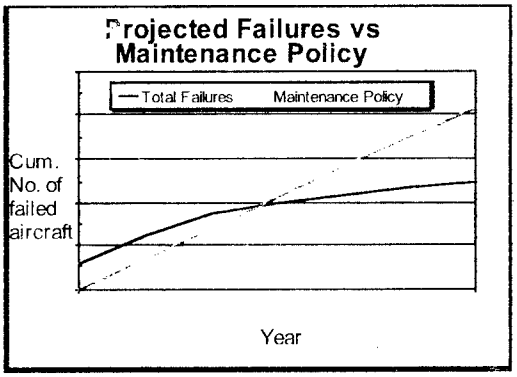

Figure 11. Graphical method for estimation of overall no. of splice repairs

no. of aircraft per year	total no. of splice repairs
17	72
20	68
23	65
27	61
30	58
33	55
37	54
40	52

Figure 12. Total no. of splices required per falcon-up rate

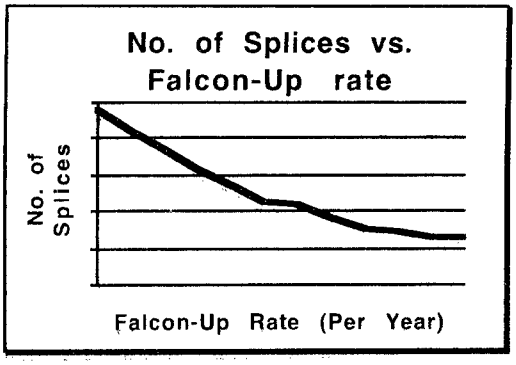

Figure 13. No. of splices vs. falcon-up rate

no. of aircraft per year	funds saved [$US]
17	0 (Ref.)
20	221,000
23	405,000
27	590,000
30	774,000
33	922,000
37	959,000
40	1,113,000

Figure 14. Economic impact of falcon-up rate

RISK ANALYSIS OF FATIGUE CRACKING IN IAF F-16 AIRCRAFT

Major Haim Cohen

Structures Branch
Israel Air Force

Overview

- Introduction
- Analysis Goals
- Method Applied
- Risk Analysis Methodology
- Transition Prediction Model
- Integration Of Maintenance Policy
- Results
- Conclusions

Introduction

- Fatigue Cracking in F-16 Fuselage Bulkhead
  - Bulkhead At F.S. 341.8 Carries Critical Loads From Wings & Fuselage.
  - Cracking occurs at several locations, including fastener holes at upper bulkhead half which link the two bulkhead parts.
  - Cracks too long to ream mandate splicing a new upper bulkhead section. Splice is costly, presents sealing and fire protection challenges.

599

Introduction - Continued

- F-16 Bulkhead 341.8:

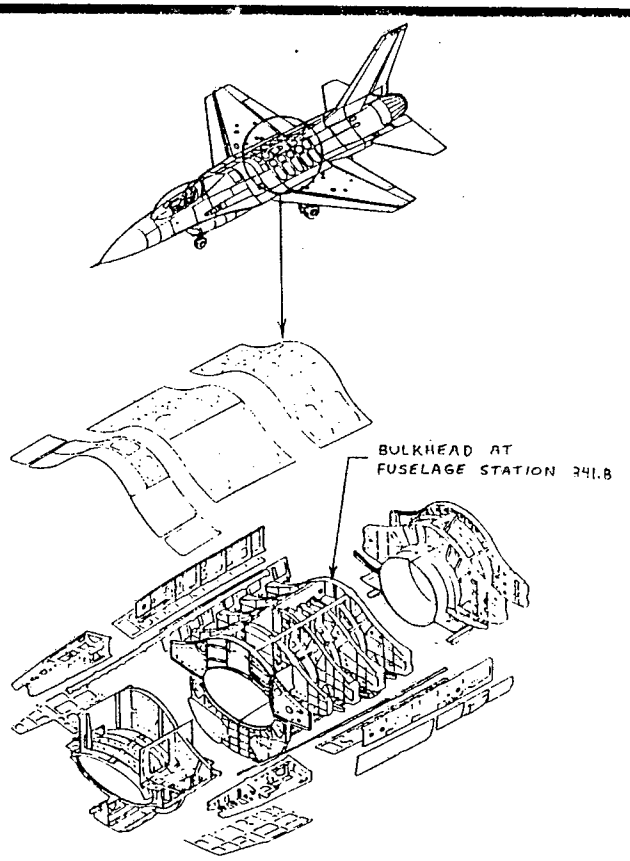

FIGURE 1

Introduction - Continued

- F-16 Bulkhead 341.8:

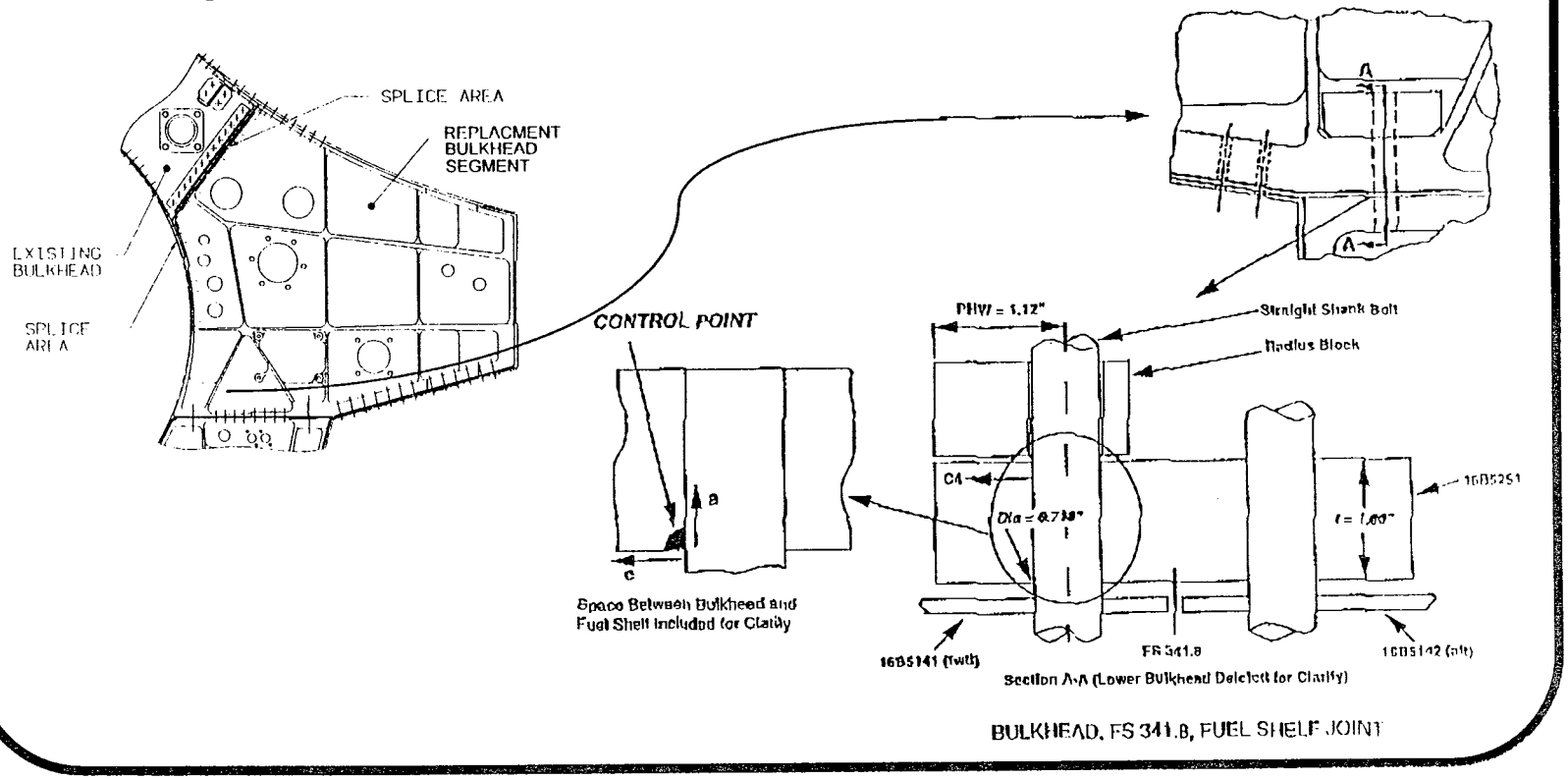

Introduction - Continued

- "Falcon-Up" structural modification line includes replacement of lower bulkhead & rework of upper at station 341.8.
- Line capacity defined by budget constraints and aircraft availability.
- Recently, many aircraft found with non-reamable cracks requiring very costly splices.

Analysis Goals

- Main Goal - Determine optimal Falcon-Up implementation rate, based on safety and economic considerations.
- Secondary Goal - Define line entrance priorities for the different sub-populations.

Method Applied

- Single Control Point selected to define Falcon-Up rate.
- Economic and Safety failure criteria were defined.
- Statistical risk analysis performed to assess future failures without reference to maintenance actions performed.
- Addition of maintenance effects on risk to forecast, and results analysis.

Method Applied - Continued

- Definition of failures:
  - **Economic failure** - crack reaching a size mandating the installation of a splice repair.
  - **Safety failure** - crack growing to critical length through bulkhead, causing it to **fail** and transfer load to neighboring bulkheads.

Method Applied - Continued

- Why Risk Analysis?
  - DTA analysis conservative and do not take into account crack initiation distribution.
  - The presence of a large sample of field measured cracks allows us to directly estimate failure life, instead of using theoretical DTA analysis.
  - Statistical risk analysis accounts for all underlying effects implicitly, such as crack initiation distribution, inspection POD, material property and usage distributions.

Basic Risk Analysis Methodology

- Weibull Statistical Distribution Used:
  - Failure data fit is good.
  - Small failure samples yield acceptable estimates of distribution.
  - Allows for initial failure-free duration.
- Distribution Parameter Estimate:
  - Median Rank Regression.
  - Maximum Likelihood Method.

Methodology - Continued

- Definition of Failure Distribution:
  - Flight hours at splice installation defined as failure.
  - Additional failure hours calculated from crack growth time of near to max. ream size cracks.
- Definition of Fleet Usage Distribution:
  - IAF Fleet cum-to-date flight hours for every aircraft collected.
  - Data fitted to Weibull Distribution.

Methodology - Continued

- Failure Forecast:
  - Integration of failure distribution and current fleet flight hour's distribution yields the estimate of currently failed components:

$$N_{failures} = N_{fleet} \cdot \int_0^{\infty} F_{failures}(\xi) \cdot f_{fleet}(\xi) d\xi$$

  - Shifting the fleet flight hours distribution by ΔT produces an estimate of failed components at time today + ΔT (Assuming uniform fleet operation).

Methodology - Continued

- Sample of risk analysis results:

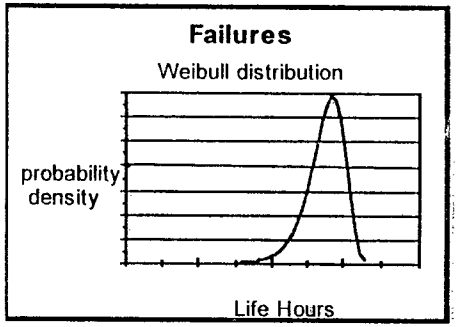

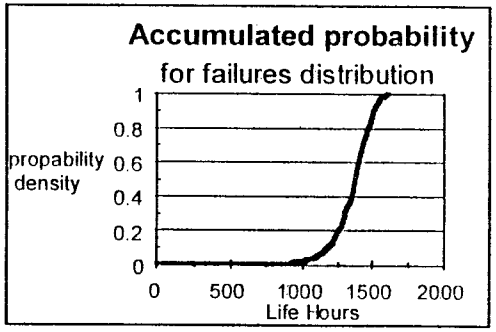

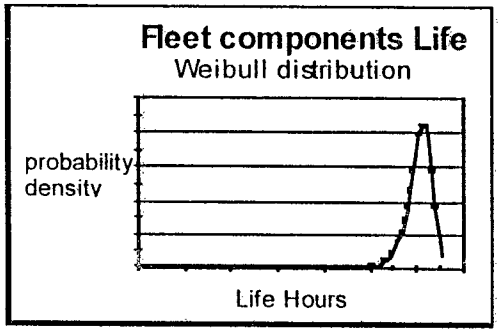

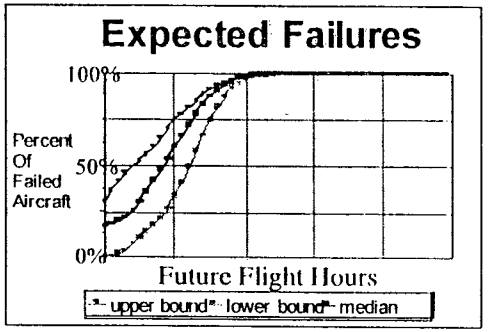

Transition Prediction Model

- A model of fleet splice implementation rates was developed using risk analysis. Transition is defined as a crack exceeding reamable size.
- The IAF fleet was divided into four distinct sub-populations. These were characterized by differing usage and structural configuration.

Transition Prediction Model - Cont.

- For each sub-population, a list of splice repair implementation (failure) flight hours was assembled. Usage (F.H.) was also assembled.
- Risk analysis was run on a PC and results tabulated.
- Results of risk analysis for all sub-populations were summed to provide an estimate for the entire IAF fleet.

Transition Prediction Model - Cont.

- Verification of results:
  - Results of risk analysis for each sub-population were compared to the current data.

Sub-Population	Failure Estimate	Known Failures
1	7	4
2	9	7
3	4	3
4	2	3
Total	22	17

  - Comparison showed risk analysis results are slightly higher than actual findings to-date. This may be due to time passed since reams performed.

Integration Of Maintenance Policy

- The forecast by risk analysis of estimated failures does not take into account maintenance action performed during the Falcon-Up modification line.
- A method of estimating the impact of the Falcon-Up rate on the estimated number of splices is presented.
- Results of risk analysis applicable to entire fleet - not to individual aircraft.

Integration Of Maint. Policy - Cont.

- Basic assumptions for implementation:
  - Aircraft entering the modification line are those known to be the most severely cracked.
  - If the number of aircraft that have undergone modification is less than the number of predicated failures (for a certain population), those aircraft are spliced.
  - If there are more aircraft modified than predicted failed, no more splices are required.

Integration Of Maint. Policy - Cont.

- Based upon previous assumptions, a graphical technique is developed:
  - Draw both risk analysis estimate and planned number of modified aircraft on same graph.

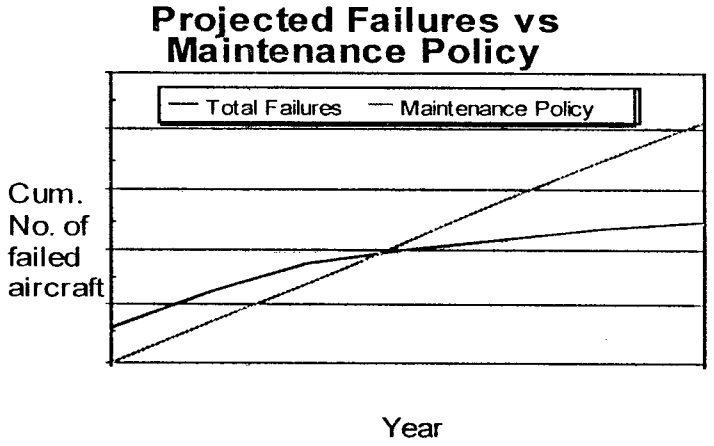

Integration Of Maint. Policy - Cont.

- The estimated number of splices performed after modification line is completed is read off the intersection of the lines.
- This method may be implemented both for a certain sub-population and for the entire fleet.
- Calculations for the fleet are done by the same method for the sum of all sub-populations.

Results

- Different failure rates for sub-populations.

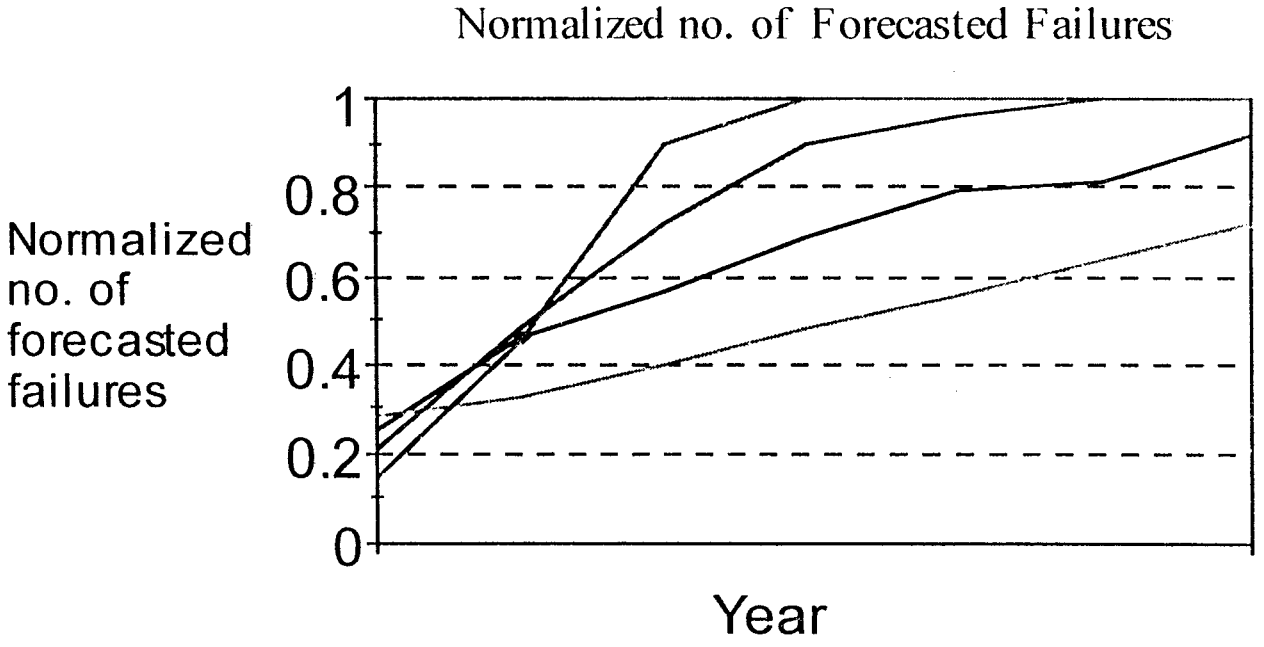

Results - Cont.

- Increasing modification line rate lowers number of splices.

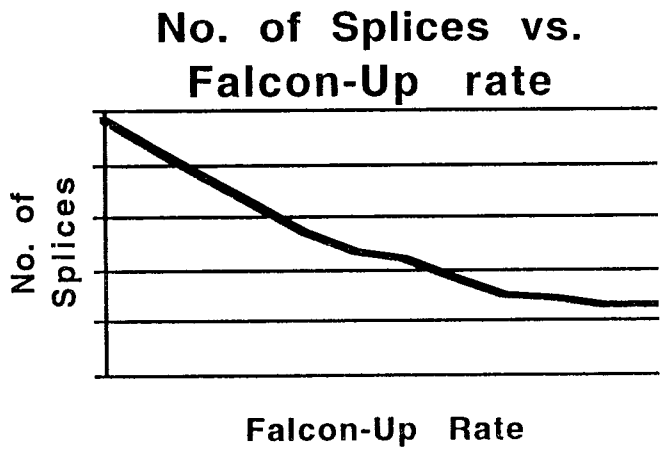

- Number of splices converges to current date estimate at infinity (All a/c modified today).

589

Results - Cont.

- A splice repair adds approximately $55,000 to the price of implementing Falcon-Up on a/c.
- Results of an estimate of the funds saved by increasing the modification rate:

no. of aircraft per year	funds saved [$US]
17	0 (Ref.)
20	221,000
23	405,000
27	590,000
30	774,000
33	922,000
37	959,000
40	1,113,000

Conclusions - Fleet

- At the current fleet rate, most aircraft will require at least one splice repair.
- Modification rates must be increased in order to prevent splices for two reasons:
  - A "backlog" of splice requiring aircraft must be first repaired at increased rate.
  - The overall failure rate is higher than the current modification line rate, so an increase is mandatory to "keep ahead" of the splices.

Conclusions - Safety Issues

- This analysis dealt with splice repairs. The same distribution may be used to estimate actual aircraft failure distribution, given the magnitude of a *shift* in the distribution mean.
  - As this magnitude is currently indeterminate, one can only assess the relative risk between the different sub-populations.
- Increasing mod rate for several years will lower the risk of bulkhead failure and keep it low.

Conclusions - Safety Issues

- Figure depicting relationship between economic and safety failures:

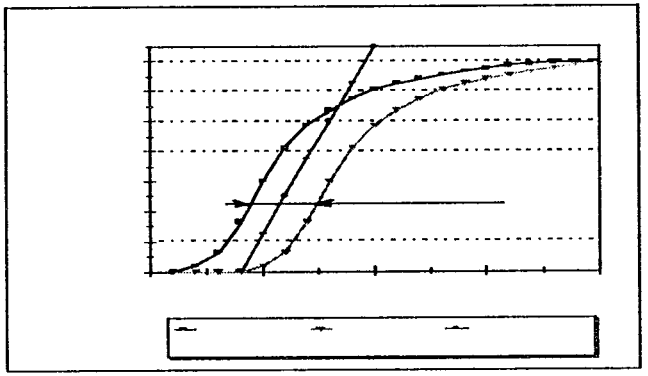

- Should the Falcon-Up rate remain constant, the current high risk of bulkhead failure will remain throughout the following years.

Conclusions - Sub-Populations

- At the time at which the analysis was performed, two sub-populations were deemed critical due to many splice repairs.
- However, the analysis indicated that the other two sub-populations will suffer from many splice repairs shortly.
- This trend was validated lately by many splices required by those sub-populations.

Summary

- A quick and easy to use statistical based method for rough estimates was developed.
- The results of this method should be used for comparison between sub-populations and as a guiding value for planning.
- This tool allows us to deal with a complex problem of determining an optimal Falcon-Up modification line rate, based on economic and safety considerations.

Sonic Fatigue
A Problem Requiring Special Handling

Dr. T. H. Beier
McDonnell Douglas Aerospace
St. Louis, Missouri
4 December 1996

GP64D22001 cvs

As the Performance Level of Aircraft Increase, Sonic (High Cycle) Fatigue Will Increase

- Increased Aircraft Agility
  - Separated Boundary Layers
  - Vortex Impingement
- More Powerful Engines
  - Increased High Q-AOA Flight
  - Increased Acoustic Levels in Inlet
  - Increased Exhaust Velocity and Temperature
- Lighter, Unitized Structure
- Use of Internal Weapons Bays

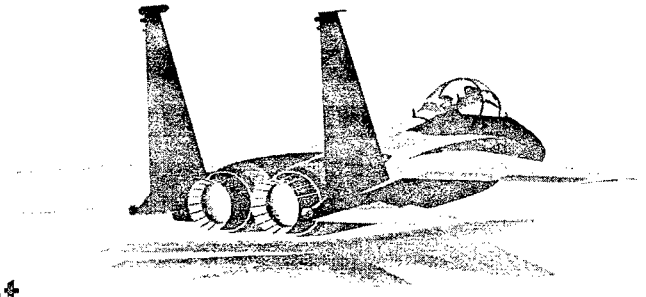

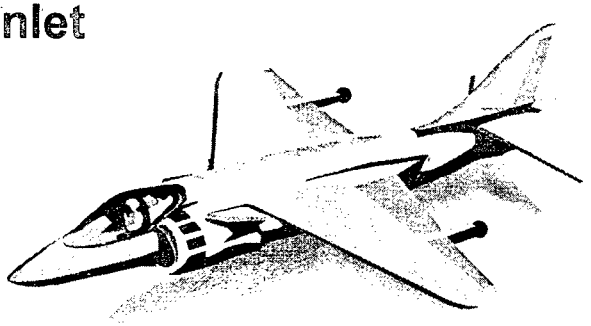

GP64D22002.cvs

Dynamic Fatigue Critical Areas

Dynamic Loads From Separated Flow, Buffeting, Shock Waves, Exhaust Impingement Are Major Cause of Fatigue

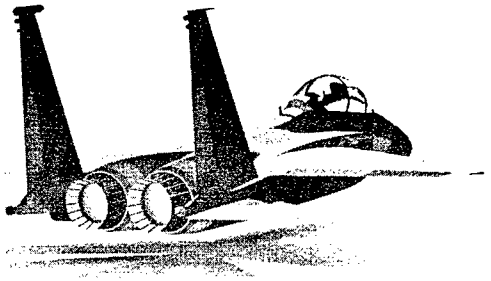

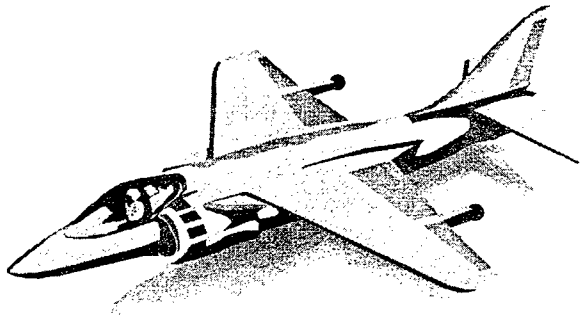

Vertical Tails
Stabilators
Fuselage Skins
Wing Structure
Leading Edges

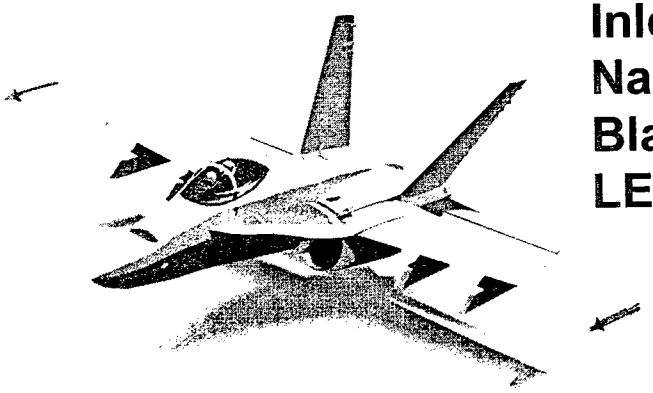

Inlets
Nacelles
Blast Shields
LEX

GP64D22003 cvs

PHANTOM WORKS
MCDONNELL DOUGLAS

Panel Damage From Turbulent Wake

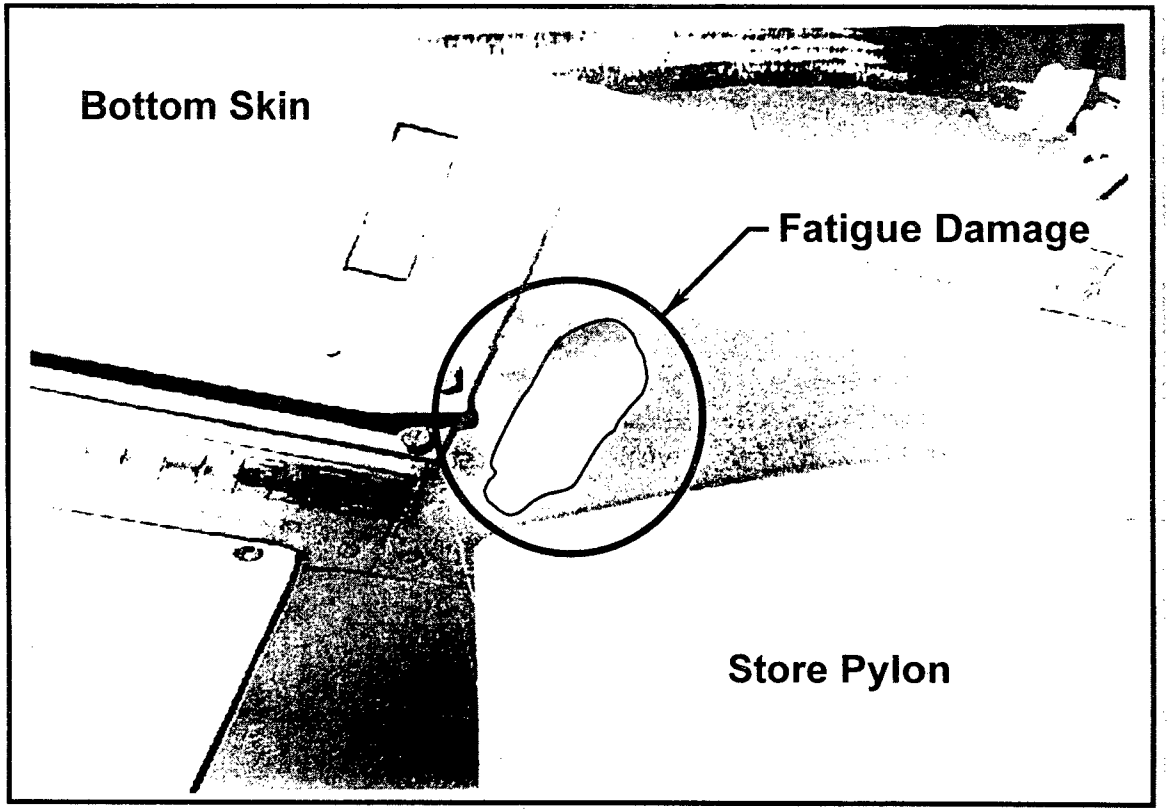

GP64D22004 cvs

Inlet Skin With Pressure Load

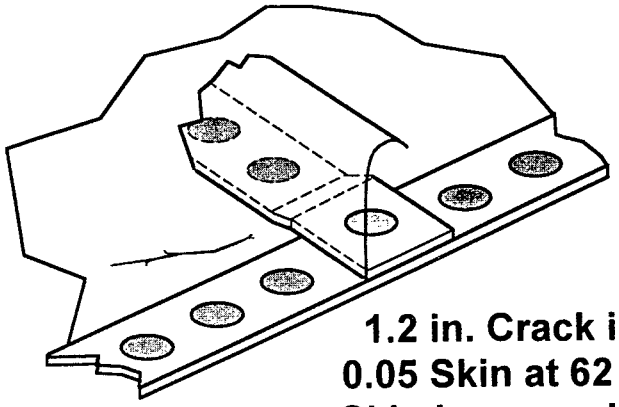

1.2 in. Crack in
0.05 Skin at 62 hr
Skin Increased to
0.071 in.

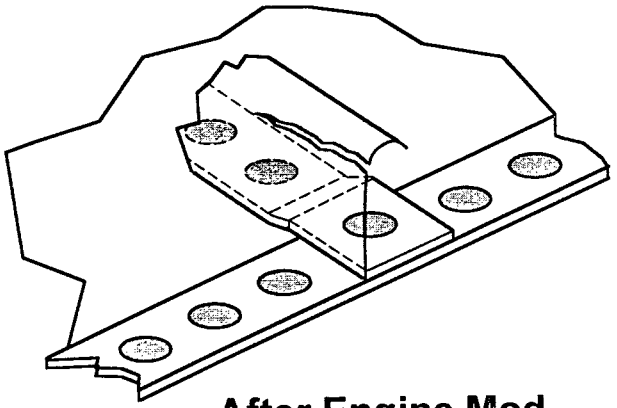

After Engine Mod,
Stringer Flanges
Cracking After 250 hr

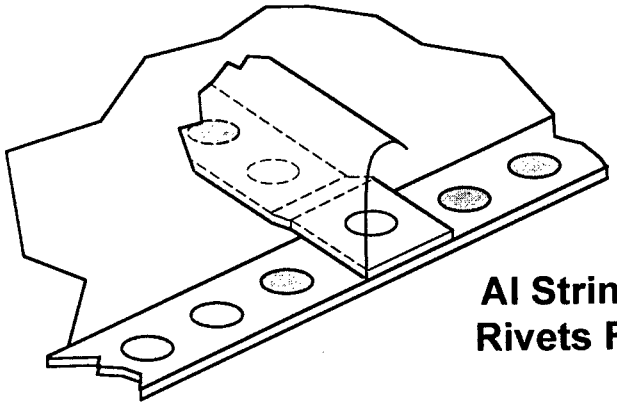

Al Stringers Replaced With Ti
Rivets Failing After 100-200 hr

GP64D22005 cvs

Panel With Exhaust Heating

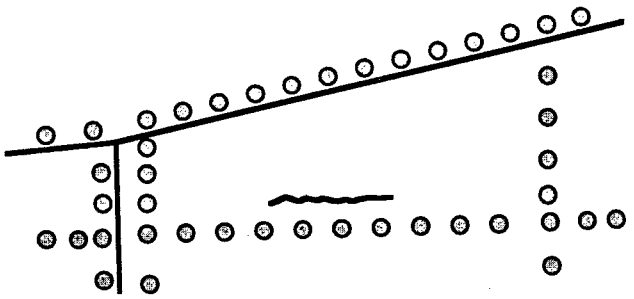

3 in. Crack After 150 hr
Area Subjected to
Engine Exhaust
168 dB, T = 350°F

Stop Drill and
Doubler Repair Crack
Showing After 390 hr

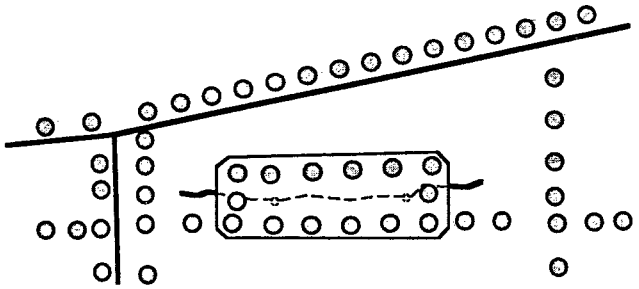

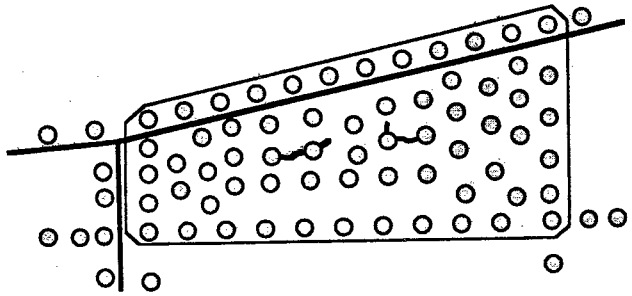

Larger Doubler
With Field Rivets Cracks
Emanating From Rivet Holes

GP64D22006.cvs

Lessons Learned

- Riveted Doublers Over Stop Drilled Cracks Not Effective
  - Adding as Much (or More) Mass as Stiffness
  - Field Rivets Are Crack Initiators

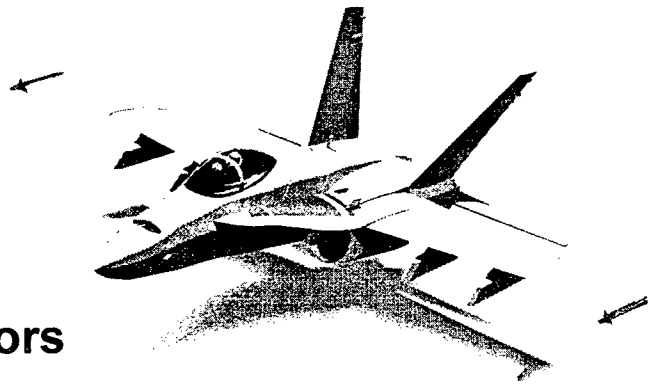

- Selective Stiffening May Make Problem Worse
- Take Static Loads Into Account
- Number of Cycles Very High, Design to Endurance Limit
- Must Match Repair to Structure

PHANTOM WORKS
MCDONNELL DOUGLAS

To Truly Fix the Problem Permanently, One Needs to Know:

- Approximate Acoustic Level, Critical Frequencies
- Temperature Range
- Static Loads

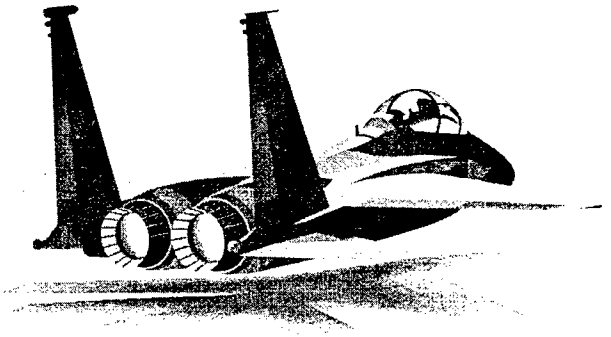

- Flight Condition Causing Problem, Time in Condition
- Structural Response
  - Strain Distribution
  - Critical Frequencies
  - Strain Changes With Possible Modifications

Proper Diagnostic Approach

Flight Test Data Analysis Software for Temperature and Pressure Loads

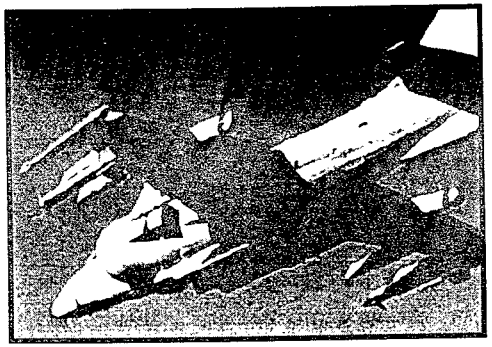

Finite Elements Post Processing Software for Acoustic Analysis

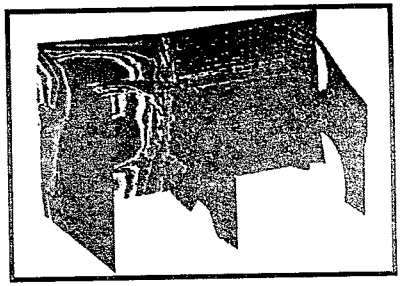

Automated Material Fatigue Property Testing

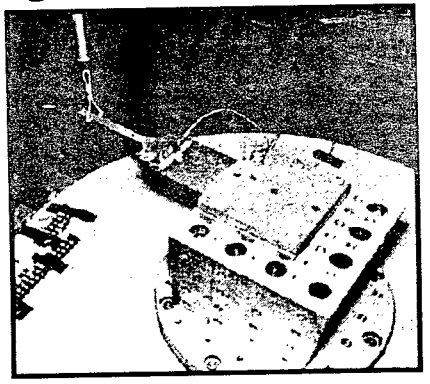

MDA-E Acoustic Fatigue Analysis/Repair Tools

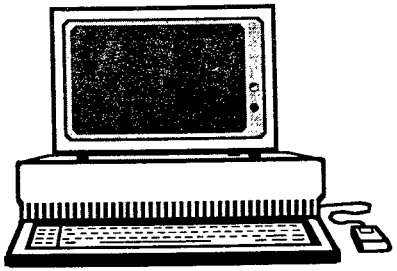

GP64D22009 cvs

PHANTOM WORKS
MCDONNELL DOUGLAS

Possible Solutions

- Modify Structural Stiffness
  - Effective for Resonance Match
  - Effective if One Structural Detail Weaker Than Others

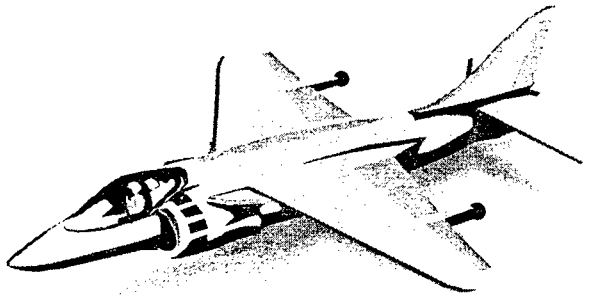

- Add Damping With Bolted Repair
  - Suitable Field Repair for Lightly Loaded Structure
  - Limit Fasteners to Insure Proper Action of Damping Medium

- Develop Damped/Bonded Repairs
  - Eliminates Stress Concentration of Rivets
  - Reduces Added Mass

GP64D22010.cvs

PHANTOM WORKS
MCDONNELL DOUGLAS

Bolted Repair With Damping

PR-1750 Is a Common Sealant in Production and Field Bolted Repairs. When Properly Constrained, It Can Substantially Increase Structural Damping Due to Inherent Damping Properties

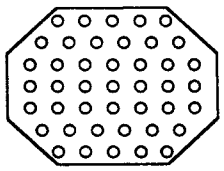

Poor

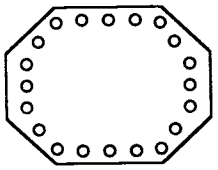

Good

PR-1750 Damping Loss Factor at Room Temperature

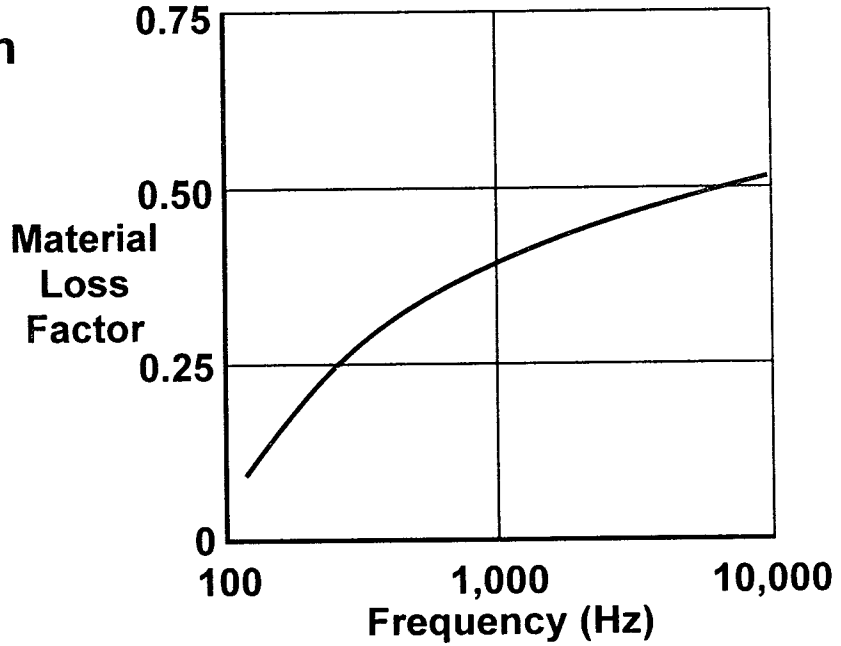

GP64D22011 cvs

PHANTOM WORKS
MCDONNELL DOUGLAS

Damped Stand-Off Treatment

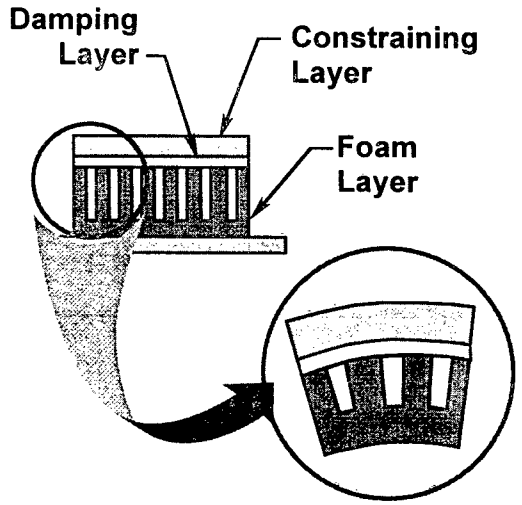

Foam Grid Spreads During Deformation and Amplifies Shear Strains in Damping Layer Damping Increases With Shearing Action of Adhesive Layer

Vibration Test Evaluation

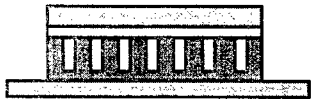

1/10 in. Foam
10 mils Fd-400
20 mils Aluminum

Panel:
- 8 in. x 8 in.
- Clamped Edges

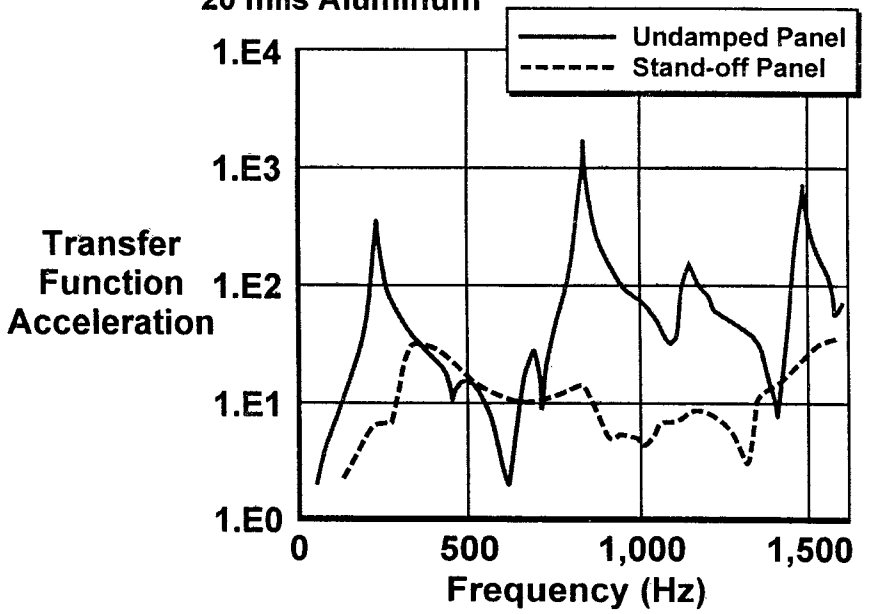

GP64D22013.cvs

Damped Stiffener Treatment

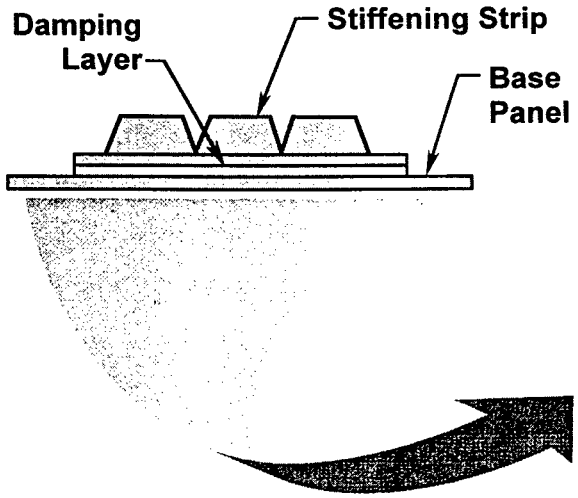

Stiffening Strip Bending Inertia Is Matched to the Base Panel for Best Damping Performance.

Vibration Test Evaluation

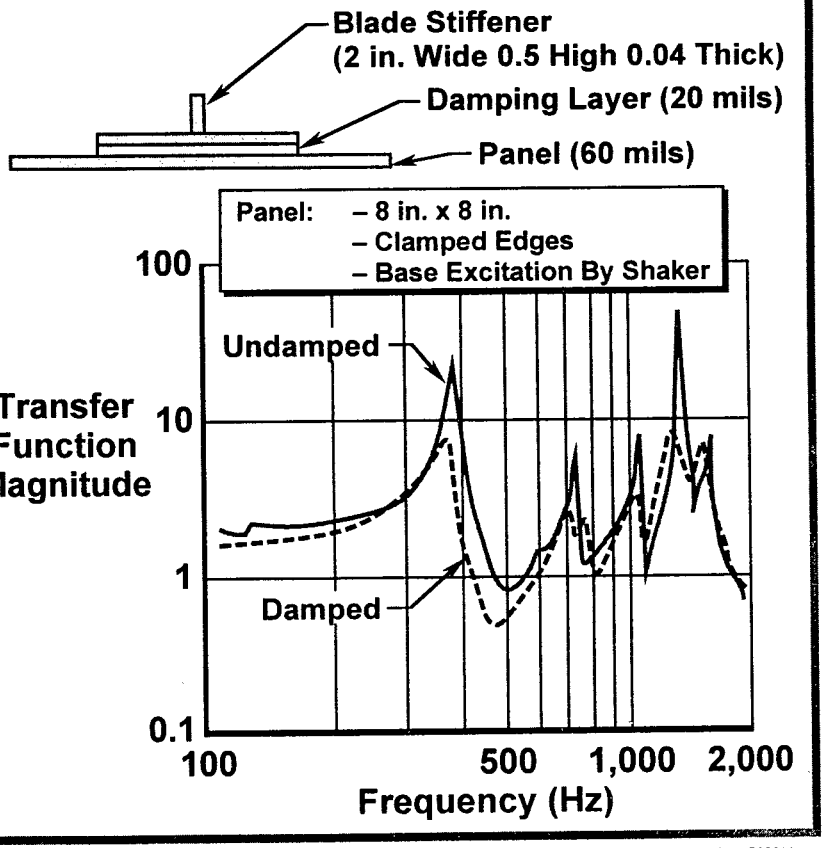

GP64D22014.cvs

Damped/Bonded Repair Development

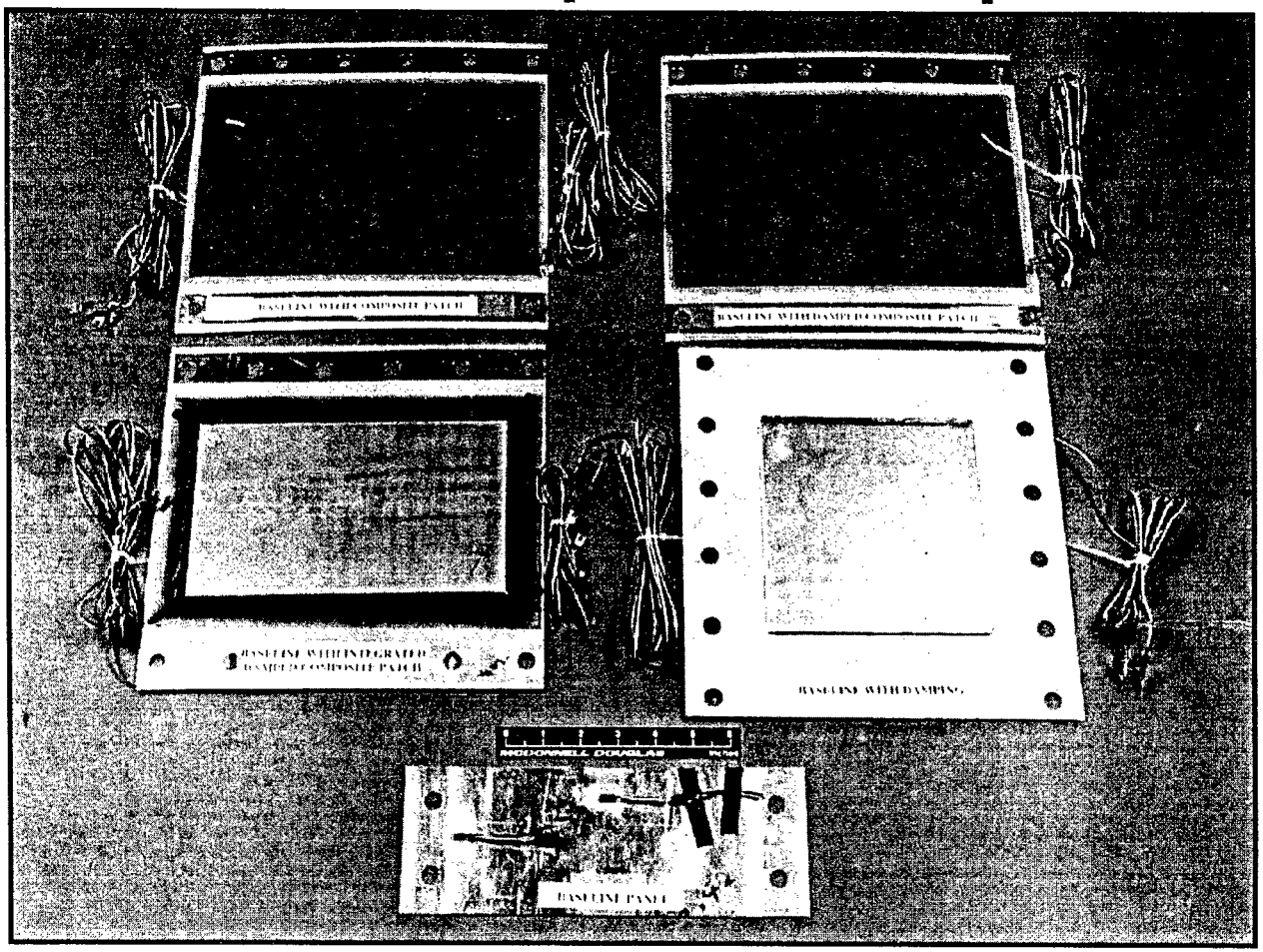

GP64D22012.cvs

Bonded Repairs Development

Task Description	1995	1996	1997	1998
Materials, Coupon, and Sub-Element Testing	• PR-1750 Tests • Damped Stiffener Tests	• Stand-Off Panel • Integral Composite	• High Temperature Damping	
Analysis Tool Development	• Damping Design Software	• RMS Post-Processing	• Combined Loads Analysis	
Damping Designs	• Stiffener Concepts	• Stand-Off Concepts • Integral Composite	• Syntactic Core Panels	
Demonstrations		• Ground Fatigue Tests	• Flight Test Demo	• Flight Line Demo

GP64D22015 cvs

Concluding Thoughts

- Impediments to Damped/Bonded Repairs
  - Specific Kits/Numbered Parts Required, Each Application
  - Elaborate Application Procedure, New Skills Required
  - Lack of Trust in Bonded Damping Material

- Current Engineering Needs
  - Recognition of Sonic Fatigue Damage
  - Tools for Estimating Sonic Loads, Analyzing Structural Response, Designing Repairs; Materials Database

- Recommendations
  - Develop Standard Damped/Bonded Repairs
  - Provide Tools in Addendum to ***Sonic Fatigue Design Guide***

GP64D22016.cvs

APPLICATION OF THE MECSIP PROCESS TO THE B-2 GROUND REFUELING SYSTEM

EDWIN J. WELLS
FUEL SYSTEM ENGINEER
B-2 SYSTEM PROGRAM OFFICE
UNITED STATES AIR FORCE
WRIGHT-PATTERSON AIR FORCE BASE OH

Abstract

This paper discusses the application of the MECSIP process to the design and analysis of a fuel system control valve on the B-2. The ground refuel manifold isolation valve as applied resulted in a single point failure in the fuel system. Failure under high flow conditions could have caused high system surge pressures in excess of the system yield and burst strength. The MECSIP process was employed to assess possible design solutions to prevent this condition. Ultimately, the valve was removed and a man in the loop was used to control the fuel system.

I. Description of the B-2 Fuel System

The B-2 fuel system contains eight integral fuel tanks symmetric about the centerline of the aircraft. The tankage system is categorized as a main and three auxiliary tanks (inboard, aft, and outboard). The total capacity of the system is over 165,000 pounds or about 25,000 gallons. Aerial and ground refueling are accomplished through common transfer lines that connect each tank. Aerial refueling inlets are connected to the transfer system from the aerial refueling receptacle slipway installation (ARRSI) located on the top surface of the aircraft near the aircraft CG. Ground refueling inlets are connected to the transfer system from two single point receptacles (SPR) located in the left hand main landing gear wheel well.

FUEL TANK ARRANGEMENT

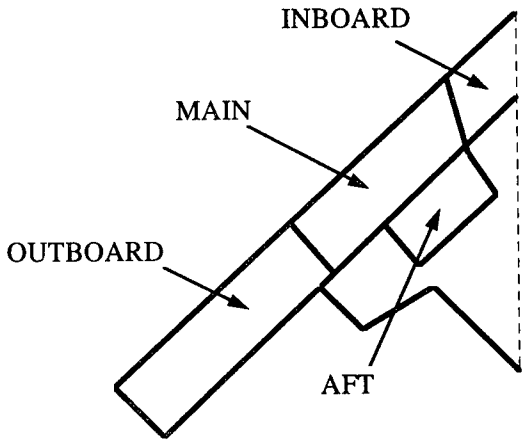

Maximum flow rates for aerial refueling can achieve 1100 gallons per minute (gpm) at 55 psi and ground refuel rates can achieve 950 gallons per minute at 55 psi. Control of fuel into a fuel tank is controlled by two level control valves (LCV) assembled in parallel so that failure of one LCV will not prevent refueling from being completed.

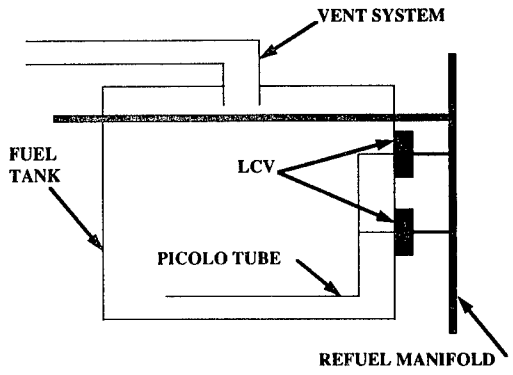

Fuel management is accomplished through the fuel measurement/management system

(FM/MS) computers. There are four general features of the control system and are rank ordered in priority: Feed engines, control CG, keep main tanks full and thermal balance. Fuel is actively transferred during a mission to minimize control surface movement for low observable purposes. The transfer system used for in flight fuel movement is the same system used for aerial and ground refueling. An independent feed system is used for engine feed.

II. Ground Refuel Subsystem

The ground refueling subsystem is capable of accepting ground source fuel at rated conditions of 950 gpm at 55 psig from two independent single point ground refueling receptacles (SPR). Each SPR independently can supply 600 gpm at 55 psig. Non-linear reduced flow capability from both SPRs is caused by the downstream plumbing consisting of tubing and a ground refuel manifold isolation valve (GRMIV). The ground refuel manifold assembly immediately downstream of the SPRs contains a sharp bend at each SPR and the bifurcated flow is combined through another sharp bend. The changes in the velocity vectors create high turbulent flow conditions. Soon after the flow is recombined the fuel is controlled by the GRMIV.

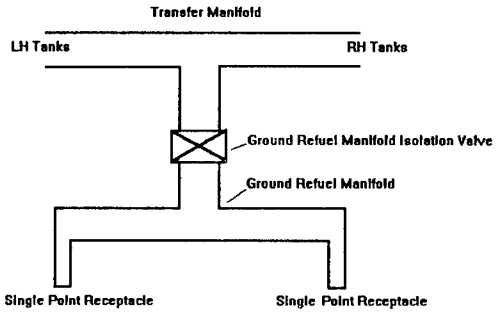

The GRMIV is a butterfly valve configuration that positions the valve disk in the flow stream. Mechanical control of the valve is achieved through a 1/25 HP DC motor connected to a gear assembly and drive shaft. The purpose of the GRMIV is to provide automatic shut down of ground refueling operation in the event of a failed open level control valve (LCV) or other safety critical failures. Open failure of an LCV would allow a fuel tank to fill to capacity and overflow into the surge tank located on the wing tip. The surge tank would then overflow and result in fuel spillage through the vent/dump outlet. A second feature of the GRMIV was to provide a tertiary fuel seal between the fuel system and potential leakage past the SPRs into the landing gear bay. The primary and secondary seals are provided by a check valve and a locking cam in the SPR.

III. Failure of GRMIV

Original design requirements did not account for the high cyclic loads generated by the high velocity flow field. The original requirements were based on a static requirement of nominal (120 psi), proof (240 psi) and burst (360 psi) pressures. The fatigue requirements were established based on the number of cycles the component was expected to encounter. If the valve were operated less than 10 times per flight the valve was qualified to 10,000 unloaded open and close cycles. If the valve were operated ten times per flight or more the valve was qualified to 100,000 unloaded open and close cycles. This type of approach did not consider the system application of the valve. The expected operation of the valve was less than 10 times per flight since the valve was only operated during ground refueling and less than 10,000 cycles were expected. However, because of the cyclic loading due to turbulent flow this design criteria was inadequate. Consequently the valve and drive train assembly were undersized.

The effect of the LCF condition was manifested during testing of the fuel system simulator (FSS) which is a full scale fuel system test article. The FSS simulates fuel tank volume, refuel, engine feed plumbing and components as well as the fuel control system. Although not identical to the air vehicle, correction models could adequately predict operational performance.

The original design was constructed of aluminum alloy materials with a predicted duty cycle based on typical ground refueling missions. The turbulent loads associated with the high pressure drop conditions in the ground refuel manifold were not considered. Tests conducted at 850 GPM/50 PSIG resulted in an expected life of less than 5 minutes.

Cyclic loads caused by the turbulent flow resulted in failure of the drive shaft at a radius location. Without restriction of the valve, the unsteady flow forced the valve disk to rapidly

close. Estimated time of closure was 0.002 to 0.010 seconds. Closure of this rate was judged to be a fast closing valve which creates considerably higher surge pressures than a slow closing valve. Measured surge pressures during the failure were estimated to be above 600 psig. Surge pressures near 1500 psig were estimated at full rated design conditions of 55 psig/1200 gpm. However, the system resistance of the refuel subsystem limited maximum flow rates to about 950 gpm. At these velocities max surge pressures were estimated at 1000 psig, which were still above nominal, proof and burst allowables. The concern about this failure mode was that high surge pressures would cause failure of aircraft components and/or ground support equipment. Likely rupture would occur and result in a hazardous condition for the ground crew.

IV. System Safety Analysis

Formal assessment of the GRMIV failure was accomplished using the System Safety Real Hazard Index (RHI) analysis. This analysis assesses the hazard severity coupled with probability of occurrence. Each hazard category and probability of occurrence is assigned a numerical value that is shown in parenthesis after each . There are four hazard categories:

- Category I: Catastrophic (4)
- Category II: Critical (3)
- Category III: Marginal (2)
- Category IV: Negligible (1)

Probability of occurrence is separated into 6 categories sorted by rough order of magnitude of expected failures per flight hour. These categories are defined as:

- Frequent (1 E-3 flight hour) (6)
- Reasonably Probable (1 E-4 flight hour) (5)
- Occasional (1 E-5 flight hour) (4)
- Remote (1 E-6 flight hour) (3)
- Extremely Improbable (1 E-7 flight hour) (2)
- Impossible (< 1 E-8 flight hour) (1)

For the specific failure of the GRMIV the hazard category was Category I, Catastrophic and the probability of occurrence was remoter. The resultant RHI of I/12 was calculated. The italics in following table defines conditions that are considered Safety Critical. If a Safety Critical condition exists, limitations, workaround or redesign is necessary to prevent the condition from being recurring.

	HAZARD CATEGORY			
PROBABILITY	I	II	III	IV
Frequent	*24*	*18*	*12*	6
Probable	*20*	*15*	*10*	5
Occasional	*16*	*12*	8	4
Remote	*12*	*9*	6	3
Improbable	8	6	4	2
Impossible	4	3	2	1

Workarounds for this condition limited ground refueling to 300 gpm based upon the finding during failure simulations. At flow rates equal to or less than 300 gpm, failure of the GRMIV was unlikely and peak surge pressures would be less than proof pressure in the event of a failure.

V. Failure Simulations

Initial failure mode testing on the fuel system simulator were not conclusive in determining the loading spectrum on failed parts. Failure mode information was necessary to confirm analysis of failed parts as well as for definition of a solution. A test set up was developed that duplicated the aircraft manifold and single point receptacles and simulated the refueling pantograph and refueling sources. Pressures were established at 55 psig and the flow rates were increased incrementally by 50 gpm. Flow conditions were tested for two single point refueling locations as well as one single point refueling location to assess the effects of non-symmetric refueling. Data collected included shaft torque, fluid flow rate, fluid velocity, steady state and transient pressure.

The drive train of the valve was disassembled and replaced with a retaining pin that held the valve disk in a fixed location in the flow stream. Steady flow was established and maximum positive and negative torque values were recorded. Drive shaft failure was simulated by rapidly removing the valve retaining pin.

The failed part on the isolation valve was the radiused section of the drive shaft. Torque and peak surge pressure were recorded during the rapid closure of the valve. Analysis of the weakest section of the GRMIV, radiused shaft section, indicated max allowable torque of 108 in-lbs. Failure mode tests indicate that level of torque was encountered at about 700 gpm

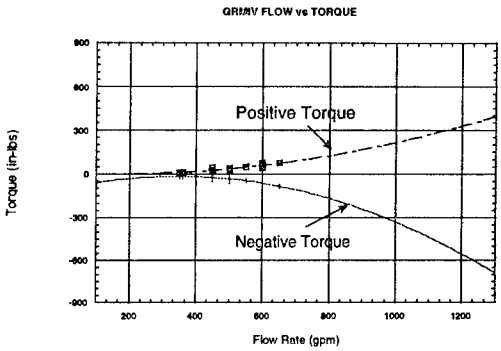

VI. Service Life Assessment

After the failure simulation tests were completed, a duty cycle for the GRMIV was generated. The duty cycle was created by determining the number of hours that would accumulate during the life cycle of a B-2. Most of the loads were generated by the turbulent flow associated with ground refueling, however, additional loads such as fuel system transients during flight, proof pressure checks and mechanical bending from structural movement were also considered. Only the open and close cycle with no fuel flow loads, and dynamic loading associated with the unsteady turbulent flow were included in the design duty cycle.

VII. Redesign Options

Because operation of the valve was considered safety critical, damage tolerance criteria was applied to the design. Material changes from aluminum to SS were evaluated with surface treatment and radius changes. However, predicted loads derived from failure simulations suggested that the loads were excessive for the proposed changes. The physical envelope for the GRMIV was fixed and did not allow any expansion without affecting two castings. For this reason, simple cross section increases of critical areas could not solve the limited life problem without excessive cost.

Process Control: Material and mechanical properties were not considered since a DT approach was not taken. However, control of properties and processes would have been reasonable and straight forward. This would have been economically feasible only because of the limited number of parts that a redesign would have replaced.

Once it was determined that the straight forward (obvious) solutions would not meet requirements, two other options were assessed. The first redesigned the butterfly disk for better hydrodynamic performance. A contoured disk was devised that would reduce the large pressure drop associated with the baseline design. The second option employed a spring-mass-damper.

All three options were deselected for the following reasons:

Option 1: Design of the contoured disk was sensitive to fuel properties e.g., viscosity, density, and shear forces. Because JP-8 had a wide range of these properties around the world worst case conditions for fuel properties were applied and could not meet DT requirements.

Option 2: Design of a spring-mass-damper system presented a high level of technical risk due to the compact envelope requirements. The cost associated with such a high risk design was the basis for rejection.

Option 3: This option applied DT criteria to a design with use of high strength materials and surface finish improvements and applied NDI inspection methods to confirm material flaw size. Since two lifetime requirements could not be met, periodic inspections would have been required. Life cycle costs associated with this option were considered to be too high.

VIII. MECSIP Considerations

Because DT analysis could not be satisfied within the envelope constraints, removal of the valve was selected to resolve the problem. MECSIP considerations were applied to this option before removal was finalized. Several criteria had to be satisfied:

1. Safety critical condition was removed (Safety)
2. Performance was not impacted (Mission)
3. Insignificant impact to LCC (Economic)

Safety Critical Analysis: Removal of the valve eliminated the failure mode of high surge

pressure. However, it also eliminated the automatic shut down feature of ground refueling. This risk was mitigated by requiring ground maintenance personnel to monitor surge tank quantity indications on the ground refuel panel located adjacent to the SPRs. In the event of a failed open LCV, fuel would flow through the vent system and fill the surge tank located in the wing tips. Located in each surge tank is a float switch that is activated at about 10% full quantity. Activation of the float switch extinguishes a light on the ground refuel panel. After extinguishing of the light, the ground crew must stop refueling within about one minute to prevent fuel spillage. This was considered to be adequate to satisfy minimum human factors response time. Operation of the surge tank light can be confirmed with a press to test operation. This effectively required two independent "failures" to occur: hardware failed and human error.

Since the GRMIV provided a third level of redundancy for leakage, the applicability of the valve was reconsidered. Fire protection design criteria for a flammable zone required two levels of redundancy to prevent leakage. Without the valve in place, this criteria could still be met since the single point receptacle provided two levels of leakage protection into the MLG wheel well. The only consideration was fuel spillage on the ground in the event of a failed open level control valve during ground refueling which did not change with removal of the GRMIV.

Mission Critical Analysis: The four inch GRMIV contributed a large percentage of the pressure drop budget for the ground refueling system. Removal of the valve provided a benefit of decreased refueling time, which helped decrease overall mission turnaround times. Additionally, inherently safer operations were encountered based upon the fact that shorter refuel times reduces the exposure for an accident. The failure associated with this accident is fuel spillage during refueling resulting in potential fire.

Economics Analysis: LCC cost benefits were relatively small with this option. Spare provisioning was not required, however, costs were incurred with technical data changes. The majority of savings were recognized by avoiding the contractual changes and procurement of parts associated with a redesign.

IX. Conclusions

FMEA discovered a safety critical failure mode that was analyzed using methods recommended in the MECSIP Guide. MECSIP revealed an error in definition of the GRMIV duty cycle. Open and close cycles were considered to be the only loading of the valve and the number of these applications were clearly understood. However, secondary effects caused by turbulent flow across the valve disk created greater loads and higher number of cycles that became the overriding design condition. Thorough understanding of component duty cycles is necessary for adequate design criteria.

Application of the MECSIP process was reapplied to deletion of the valve to determine the effect on system safety, mission, and life cycle costs. This criteria was evaluated and determined to be too costly for the benefit of the operation of the valve. However, the MECSIP process provided methods to conduct a thorough analysis of failure modes and trade study options to arrive at a decision with a favorable cost/benefit ratio.

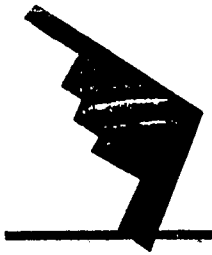

ASIP 96

B-2 SPO

Application of the MECSIP Process to the B-2 Ground Refueling System

EDWIN WELLS
FUEL SYSTEM ENGINEER
B-2 SYSTEM PROGRAM OFFICE
WRIGHT PATTERSON AFB, OH

ASIP 96

B-2 SPO

B-2 Fuel System

Description of Failure

System Safety Assessment

MECSIP Considerations

Lessons Learned

ASIP 96

B-2 SPO

Eight integral composite fuel tanks

Over 165,000 lb capacity

Redundant Tank Sealing

JP-8 Primary fuel

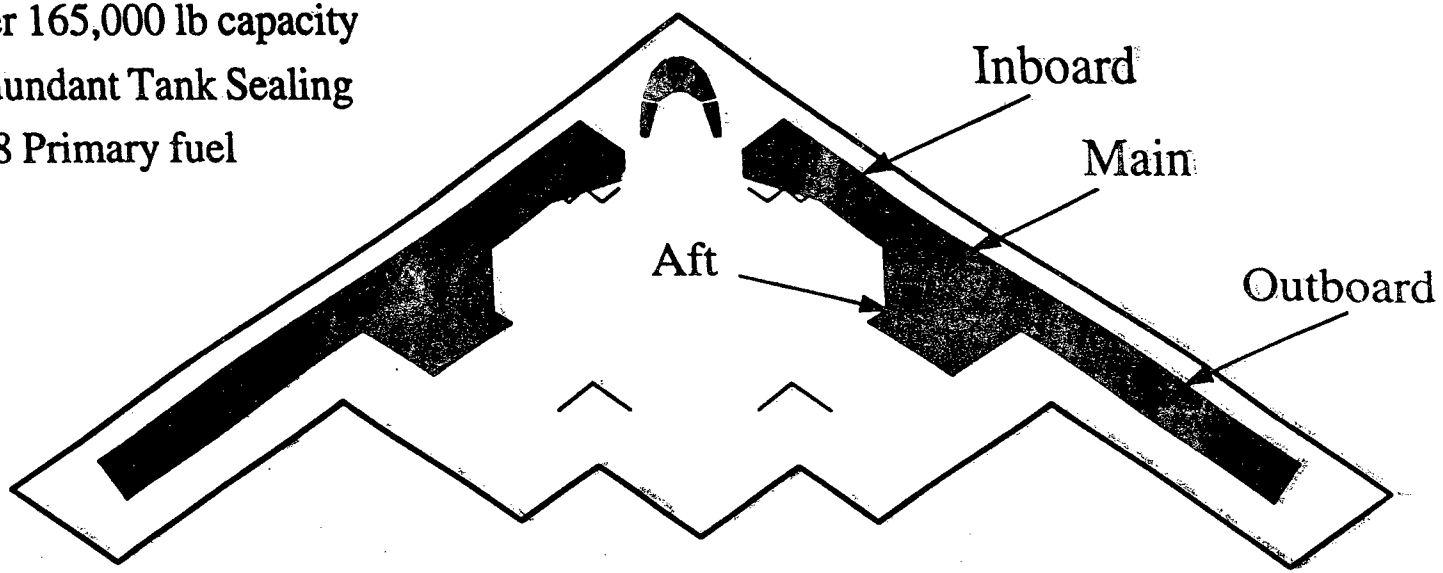

FUEL TANK ARRANGEMENT

ASIP 96

B-2 SPO

Refuel/Transfer Subsystem

- Dedicated subsystem of valves and tubing for tank to tank transfer and refueling
  - Ground and In Flight Refueling
- Independent from engine feed subsystem except for fuel pumps
- Tank to tank transfer used for
  - Aircraft CG management
  - Thermal management

ASIP 96

B-2 SPO

Ground Refuel Manifold Arrangement

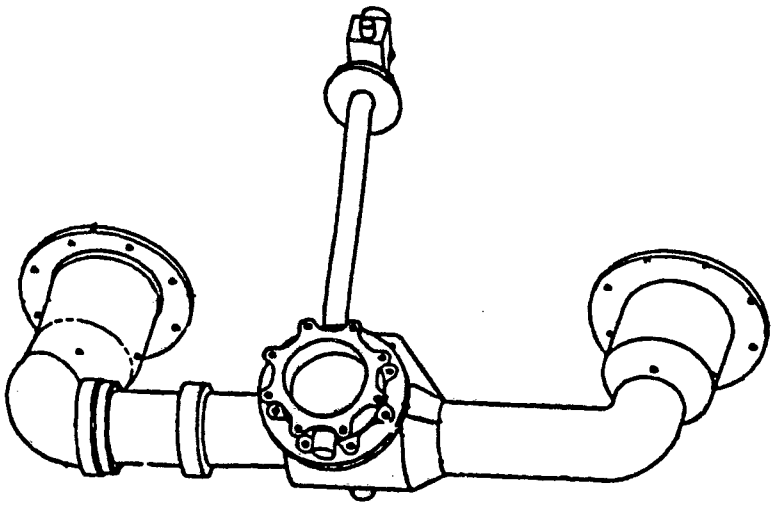

ASIP 96

B-2 SPO

Ground Refuel Manifold Isolation Valve

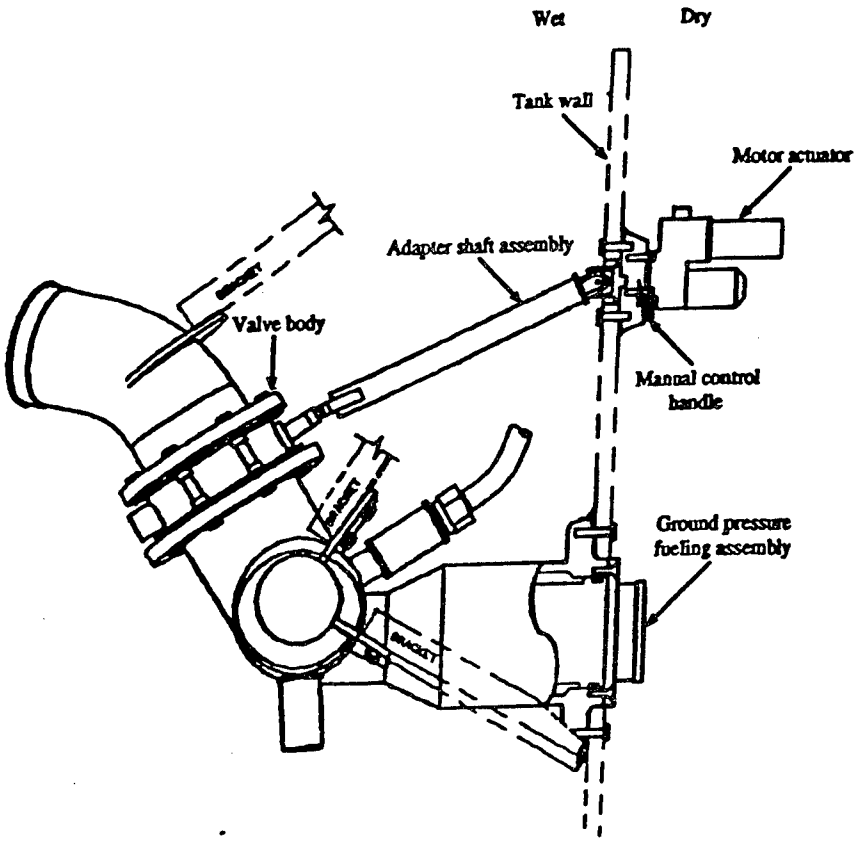

ASIP 96

B-2 SPO

Ground Refuel Manifold Isolation Valve

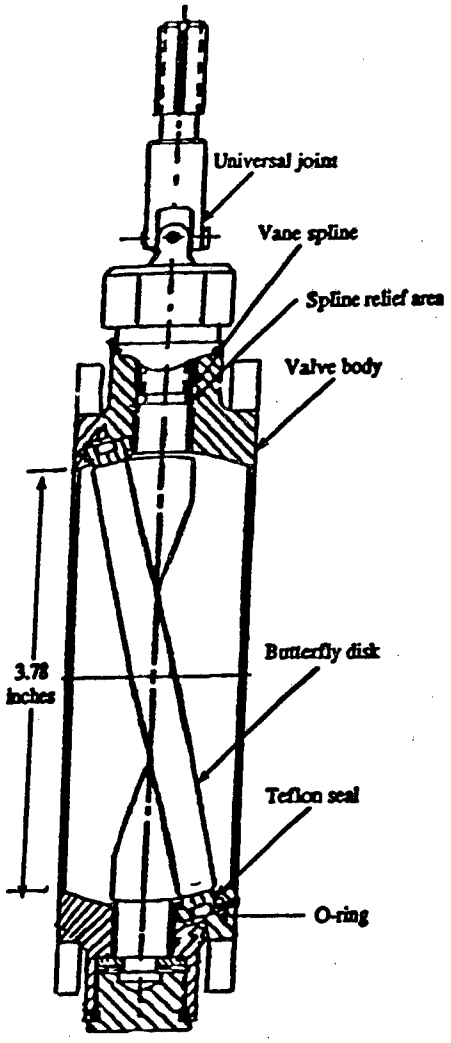

ASIP 96

B-2 SPO

Description of Failure

- Drive train failed allowing free movement of butterfly disk
- High surge pressure generated on closure
- Single Point Receptacle separated from tank wall
- Occurred during Fuel System Simulator testing under high flow conditions
- Not predicted by either analysis or qual test

ASIP 96

B-2 SPO

GRMIV DUTY CYCLE

Dry Cycles (open/close):	500 cycles
Rated Flow 1200 gpm (open close):	200 cycles
Room Temp 1200 gpm (open/close):	5000 cycles
High Temp 1200 gpm (open/close):	2000 cycles
Low Temp 1200 gpm(open/close):	2300 cycles
Endurance 1200 gpm:	500 hrs

- Duty cycle derived from Mil-F-8615
- Straight pipe configuration vs. high velocity bend manifold
- Inaccurately predicted adequate life

ASIP 96

B-2 SPO

SSG Hazard Category

- Category I: Catastrophic
- Category II: Critical
- Category III: Marginal
- Category IV: Negligible

Probability of Occurrence

- Frequent (1 failure per 1000 hrs)
- Reasonably Probable (1 failure per 10,000 hrs)
- Occasional (1 failure per 100,000 hrs)
- Remote (1 failure per 1,000,000 hrs)
- Extremely Improbable (1 failure per 10,000,000 hrs)
- Impossible (Less than 1 failure per 100,000,000 hrs)

ASIP 96

B-2 SPO

	HAZARD CATEGORY			
PROBABILITY	I	II	III	IV
Frequent	*24*	*18*	*12*	6
Probable	*20*	*15*	*10*	5
Occasional	*16*	*12*	8	4
Remote	*12*	*9*	6	3
Improbable	8	6	4	2
Impossible	4	3	2	1

ASIP 96

B-2 SPO

- GRMIV Failure Determined to be Safety Critical
  - Real Hazard Index I/12
  - Catastrophic/Remote
  - Safety critical condition equivalent to fracture critical
- First Application of MECSIP
  - Redesign required to meet damage tolerance requirements
  - Initial Flaw size selected based on B-2 ASIP criteria
  - Aluminum material could not meet requirements as designed

ASIP 96

B-2 SPO

Failure Simulation

- High flow condition using aircraft components
- Test performed to collect Torque vs Flow in 100 gpm increments
  - Valve train assembly exposed to flow generated torque
  - Valve could not survive above about 600 gpm
    - Requirement was for 1100 gpm
  - Data was curve fitted and extrapolated to 1100 gpm to estimate max torque required
  - Estimated to be 300 in-lbs

ASIP 96

B-2 SPO

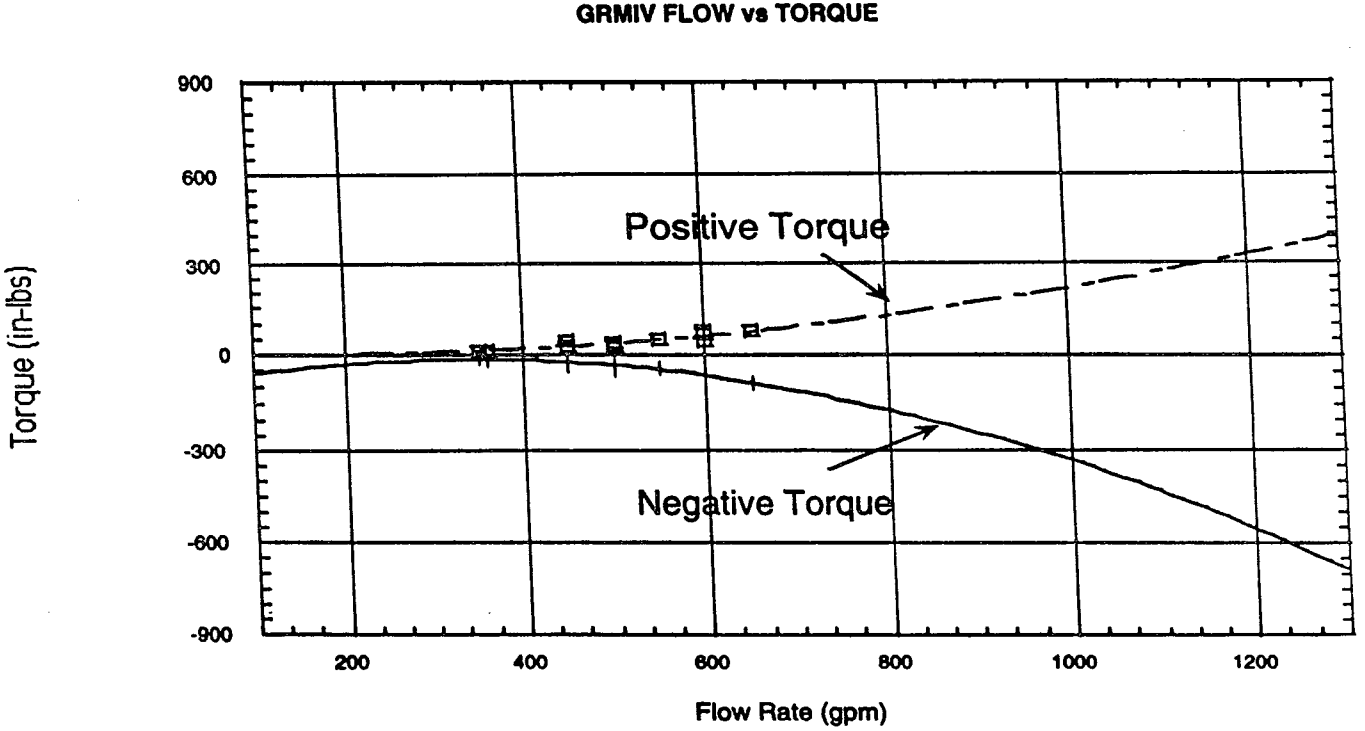

ASIP 96

B-2 SPO

Options to Meet Damage Tolerance Requirements

- Higher strength material unavailable
- Increase cross section
  - Envelope too small
- Modification to valve disk to reduce drag
  - Turbulent flow could not be smoothed by geometry change
- Install damper to reduce torque
  - Damper would become Safety Critical part

ASIP 96

B-2 SPO

Cost/Benefit Analysis

- More than one part in valve drive train resulted in single point failure
- MECSIP analysis suggests all parts that could cause a Safety Critical condition meet damage tolerance requirements
  - Restrictive material properties
  - Management of key production processes
  - Material tracebility
  - Potential periodic inspection in limited access area (fuel tank)
  - Corrosion, wear, fretting difficult to quantify

ASIP 96

B-2 SPO

Second Application of MECSIP

- Since redesign and Life Cycle Costs (LCC) were high, function of valve was challenged

- Would Removal of GRMIV create a Safety, Mission or Economical Critical condition

- Fault Tree Analysis (FTA) used to answer question

ASIP 96

B-2 SPO

Fault Tree Analysis

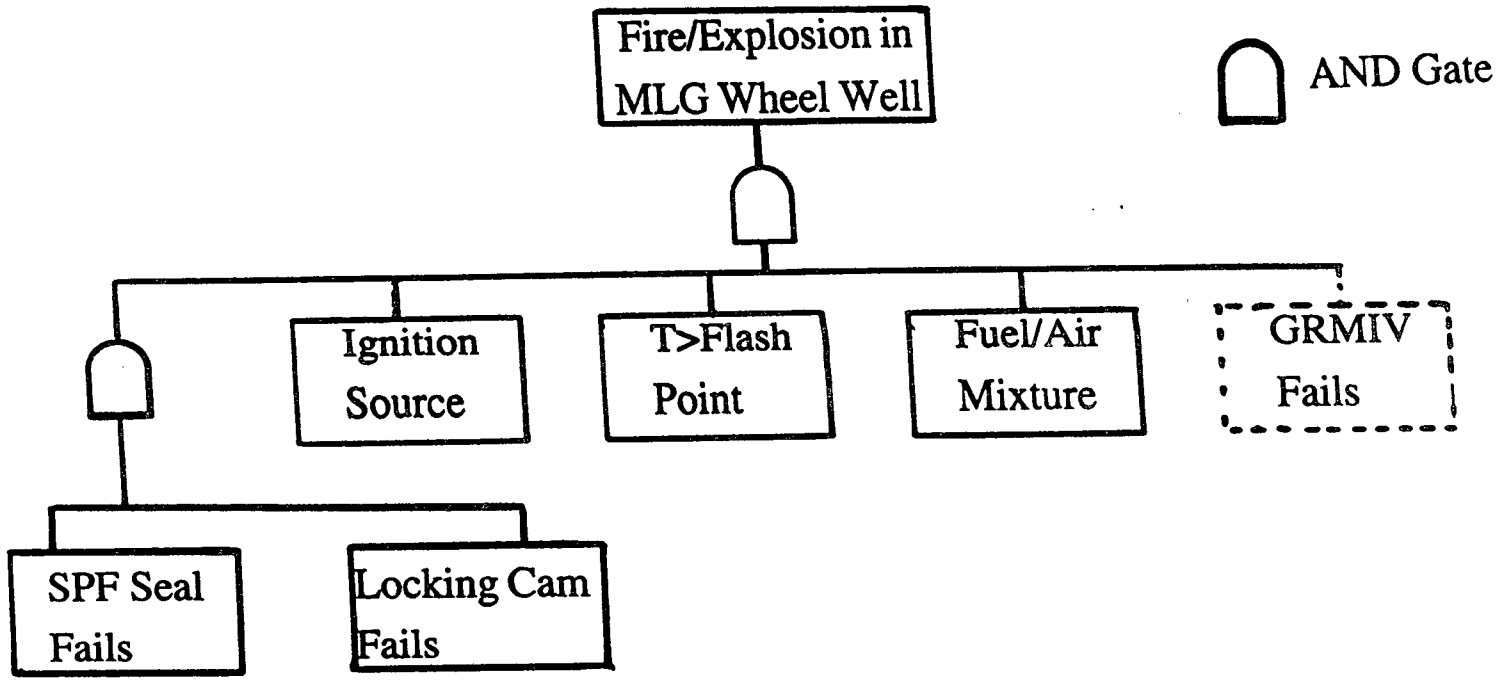

ASIP 96

B-2 SPO

- Lessons Learned
  - Duty Cycle definition critical
    - ON/OFF vs hydrodynamic loading
    - Important to define at early stages of design process
  - Component/Lab mock up must represent system application or correct data with correlation model
  - Material characteristics and key manufacturuing processes must be declared at the beginning of design process
    - Standard QA limits were too broad for adequate definition
    - Standard Acceptance Test Procedure data unusable

ASIP 96

B-2 SPO

- Lessons Learned (cont)
  - MECSIP is not a stand alone process however can be easily integrated into systems engineering process
    - FTA, FMEA, System Safety are complimentary tools
  - Must employ MECSIP at early stages of design process
    - Allows for thorough C/B analysis
    - Allows for proper trade study of redundancy vs weight
  - Butterfly valves in high velocity flow can generate significant cyclic loads

ASIP 96

B-2 SPO

B-2 Team Members

- System Program Office (SPO)
  - Wright Patterson
  - Tinker AFB
- Northrop Grumman
  - Vought
- Boeing
- ITT Aerospace

SESSION VI

WIDESPREAD FATIGUE DAMAGE

Chairman: *T. Swift*, FAA

Controlling Multi-Site Damage by Means of Design and Inspection Trade-Offs

A. Brot
Engineering Division
Israel Aircraft Industries
Ben-Gurion Airport, Israel

Abstract

The results of a parametric study on controlling multi-site damage is reported. The effects of the pitch/diameter ratio, number of fastener rows, NDI method and inspection intervals were considered. The parametric study was performed using the ***INSIM*** computer program which simulates the fatigue and inspection process. Five design configurations are recommended, with the aim of minimizing the probability of failure of a potential multi-site damage structure.

Introduction

Multi-site damage (MSD) represents a particularly dangerous configuration from the standpoint of structural integrity. Small cracks can initiate at several sites and will grow simultaneously. Eventually the cracks will link-up, with failure occurring shortly afterwards. Multi-site damage can be thought of as the prelude to catastrophic widespread fatigue damage.

In order to design a potential multi-site damage structure to have a very low expectation of failure, the important parameters must first be identified. These parameters can be classified as design parameters (material, hole diameter, hole pitch, number of fastener rows, stress level, etc.) and inspection parameters (NDI method and inspection interval). These parameters can then be traded-off in order to achieve the degree of safety required.

One important design parameter is the ratio of hole pitch distance to hole diameter, p/D. As p/D becomes smaller, and the holes are closer together, the

amount of load transferred at each fastener is reduced. As p/D becomes larger, and the holes are further apart, the amount of load transferred at each fastener is increased. For a typical multi-site damage configuration, crack initiation, crack growth and total lives were calculated using strain-life and crack growth analyses respectively, as is shown in Figure 1.

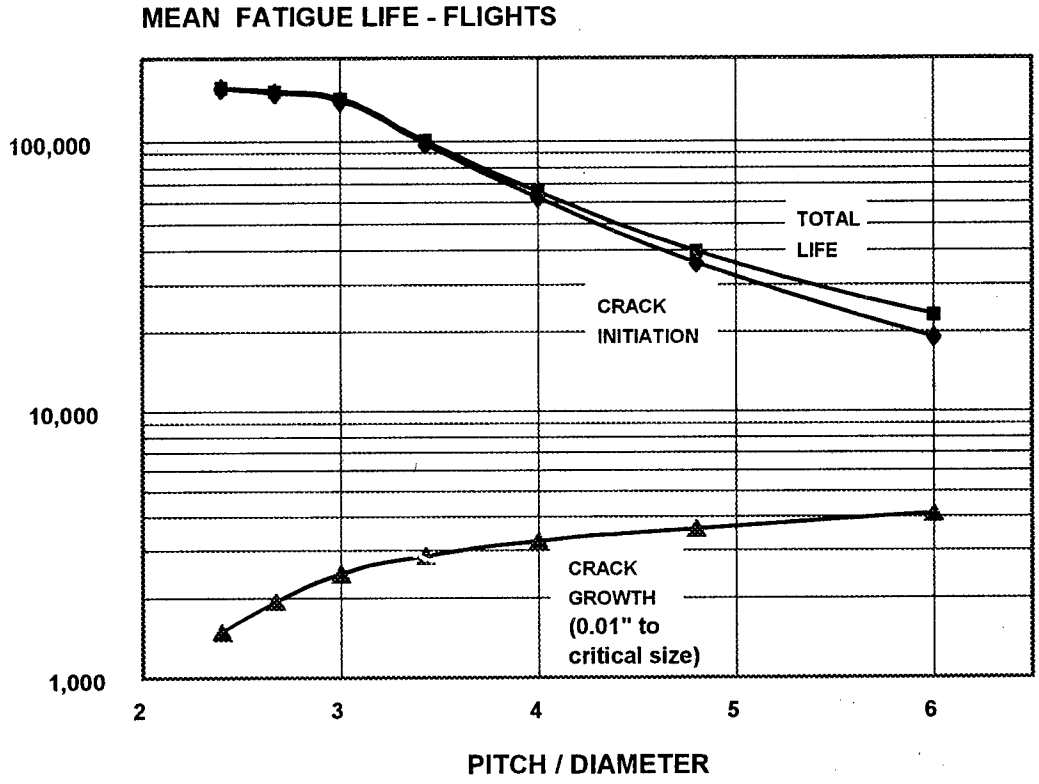

Figure 1: Effect of p/D on crack initiation and growth of an MSD structure

Figure 1 indicates that the crack initiation life and total life are very much affected by the pitch/diameter ratio. Due to the increased load-transfer, the crack initiation life drops by nearly an order-of-magnitude as p/D is increased from 3 to 6. This is consistent with the observation stated in Reference 6, "... *the single most important feature for insuring a long fatigue life in metallic structures is the need for a low bearing stress on all fasteners at critical locations in the structure*".

Figure 1 indicates that the crack growth life *increases* as the pitch/diameter ratio increases. This is due to the longer distance between holes, which allows the

cracks to grow for many more cycles before becoming critical. Figure 2 shows the effect of the pitch/diameter ratio on the critical crack size and indicates that the critical crack size is increased at the larger values of p/D. Figure 2 also shows that the critical crack size increases from a virtually undetectable size at p/D = 2.4 to a readily detectable size at p/D = 6.

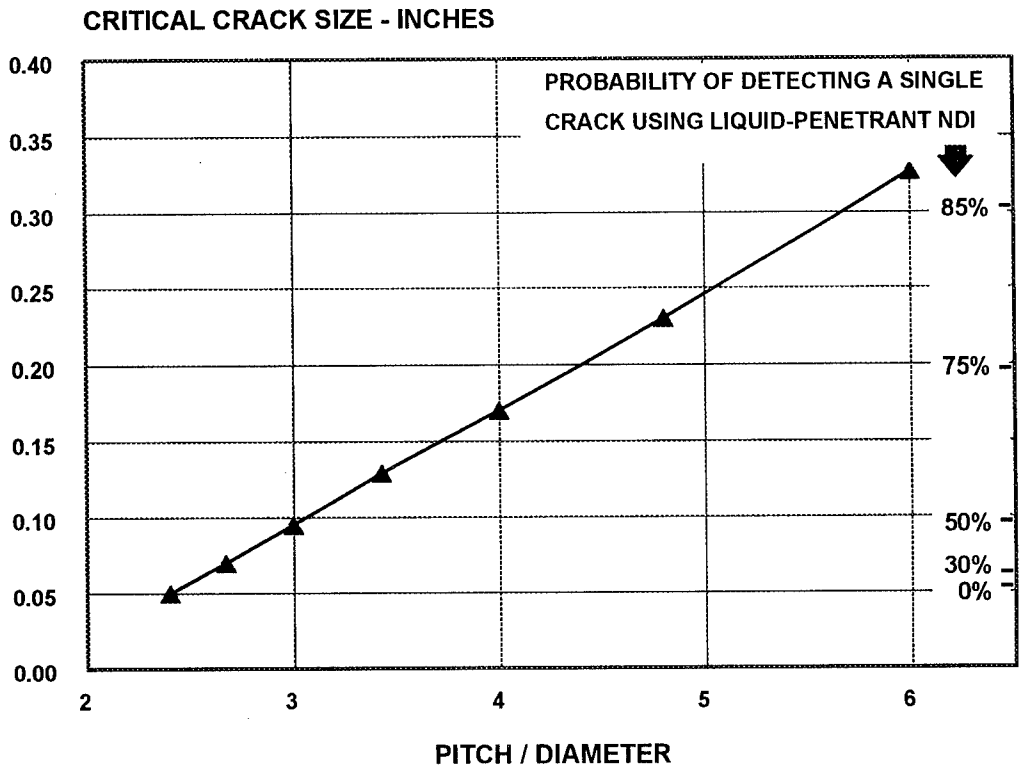

Figure 2: Effect of p/D on critical crack size and crack detectability

Finding the optimum value of p/D, that will insure maximum safety, is not at all straightforward. Should we select a small value of p/D, such as three, and rely on a large crack initiation or total life? Or should we pick a large value of p/D, such as six, and rely on slow crack growth and enhanced NDI capability? In order to help answer this question, a computer simulation method, called ***INSIM,*** was used.

The ***INSIM*** computer program, which is described in detail in References 1–3, has been developed in order to simulate the entire fatigue environment that a

structure must withstand. ***INSIM*** simulates, in a probabilistic manner, service life variation, service load severity, time to crack initiation, crack growth history and NDI detection capability.

Cracks initiate at critical locations of aircraft structures. These cracks propagate and, unless detected and repaired, will eventually result in a failure. There are three, mutually exclusive, outcomes of the fatigue process:

(1) The aircraft may reach the end of its operational life and be retired from service. The retired aircraft may or may not have undetected cracks at critical locations.

(2) A crack may be detected during maintenance operations. The affected part is usually repaired or replaced.

(3) A crack reaches its critical size undetected and the structure fails in service.

INSIM performs a simulation of a single critical location for every aircraft in an entire fleet. Cracks initiate at various times and grow at variable rates in each aircraft. Inspections are performed according to a predetermined schedule, using as many as six different NDI methods. Cracks are detected during these inspections according to the statistical expectation of detection. As the simulation proceeds from aircraft to aircraft, cracks are detected, aircraft are retired from service or failures occur. The computer acts as a scorekeeper, amasses the statistics and summarizes the results. In order to provide statistically significant results, a large number of simulations must be performed. In a typical simulation, 300,000 inspections will be performed for a fleet of 100,000 aircraft, taking less than one minute on a Pentium equipped computer.

Based on these simulations, ***INSIM*** calculates the probability that all the *lines of defense* have been breached, and failure occurs.

Simulation of a Typical Multi-Site Damage Splice

In order to study the various possibilities for trading-off design and inspection parameters, a series of parametric studies were performed on a typical multi-row, multi-site damage splice location. Figure 3 describes the loaded-hole configuration that was studied, with the variations to the hole diameter, hole pitch, holes per row and number of rows noted. In addition, two NDI methods were studied at a variety of inspection intervals. Actually, three separate parametric studies were performed. In the first study, the hole diameter was varied while the splice width

and number of holes were kept constant. In the second study, the hole diameter and number of holes were kept constant while the splice width was varied. In the third study, the hole diameter was kept constant while the splice width and number of holes were varied. All three studies allowed the pitch/diameter ratio to be varied. Obviously, quantitative differences were found in the three studies, but qualitatively, all three parametric studies yielded very similar results. The results quoted in this paper are taken to be representative of all three parametric studies.

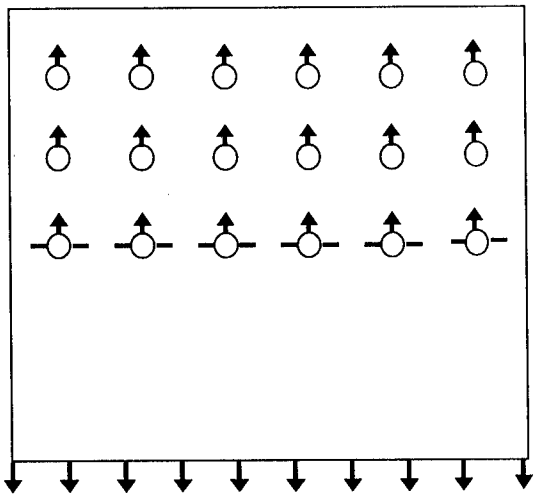

Material: 2024-T3 Aluminum Alloy

Hole Diameter: 0.20 - 0.33 inches

Hole Pitch: 0.6 - 1.0 inches

Number of Fastener Rows: 2 - 5

Number of Holes Per Row: 4 - 10

Remote Stress: 20 KSI, R = 0

Bearing Stress: 0 - 60 KSI

Figure 3: Typical loaded-hole multi-site damage configuration

For each configuration that was analyzed, the mean crack initiation life was calculated using a strain-life analysis. Crack growth of the multi-site damage was calculated using the methodology described in Reference 4. These calculated values were input into ***INSIM***, together with NDI parameters, and the program simulated crack initiation, crack growth and crack detection and finally determined the probability that failure will occur. In reality, each of the many cracks will initiate independently of the others and will begin to grow. Simulating the independent initiation of each crack and tracking its growth was thought not to be necessary because of the following reasons:

(1) Experience has shown that cracks in a multi-site damage configuration are usually very similar in size. This is usually referred to as the "catch-up phenomenon" and is considered to be compatible with the typical characteristics of multi-site damage. (See Reference 5.)

.(2) Since failure in a multi-site damage structure usually occurs as a result of "net-section yield", the worst situation is that when all the cracks grow simultaneously and are of equal size. If this were not the case, the net-section yield failure would be delayed until further crack growth takes place, thereby increasing the crack growth life.

In light of the above, it was decided that ***INSIM*** would treat the transition from crack initiation to crack growth in an approximate way — by assuming that the lives for crack initiation and crack growth refer to the *mean value* of all the cracks. It is believed that this assumption adds only a slight amount of conservatism to the results.

Crack detectability is often modeled by the three-parameter Weibull distribution,

$$P(a) = 1 - e^{-\left(\frac{(a-a_0)}{(\lambda-a_0)}\right)^{\alpha}} \qquad (1)$$

where P(a) is the probability of detecting a crack of length "a". α, λ and a_o are the three Weibull parameters that characterize the statistical distribution and are a function of the NDI method used as well as the characteristics of the cracked location. Figure 4 describes this distribution (curve corresponding to one crack) for a liquid-penetrant inspection method.

When several cracks are present, the laws of probability state that the probability of detecting *at least* one crack is given by,

$$P = 1 - (Q_1 \times Q_2 \times Q_3 \times \ldots\ldots\ldots \times Q_n) \qquad (2)$$

where P is the probability of detecting at least one crack and Q_n is the probability of not detecting the n^{th} crack.

If all the cracks are of equal length, Equation (2) reduces to

$$P = 1 - Q^n \qquad (3)$$

where Q is the probability of not detecting any one crack. Figure 4 has been constructed, based on Equations (1) and (3). Figure 4 indicates that as the number of cracks increase, the probability of detecting at least one crack improves dramatically. For example, a single 0.08 inch crack has only about a 40% probability of detection with liquid-penetrant NDI. However, the probability of detecting *at least one of ten* such cracks is nearly 100%. Thus, the multitude of

cracks, which are so dangerous from the standpoint of structural integrity, makes it possible to achieve very high probabilities of detection.

The *INSIM* computer program models crack detectability in a multi-site damage configuration in accordance with Equations (1) and (3). It allows the study of the interplay between the relatively short critical crack length and the enhanced crack detectability of the MSD configuration.

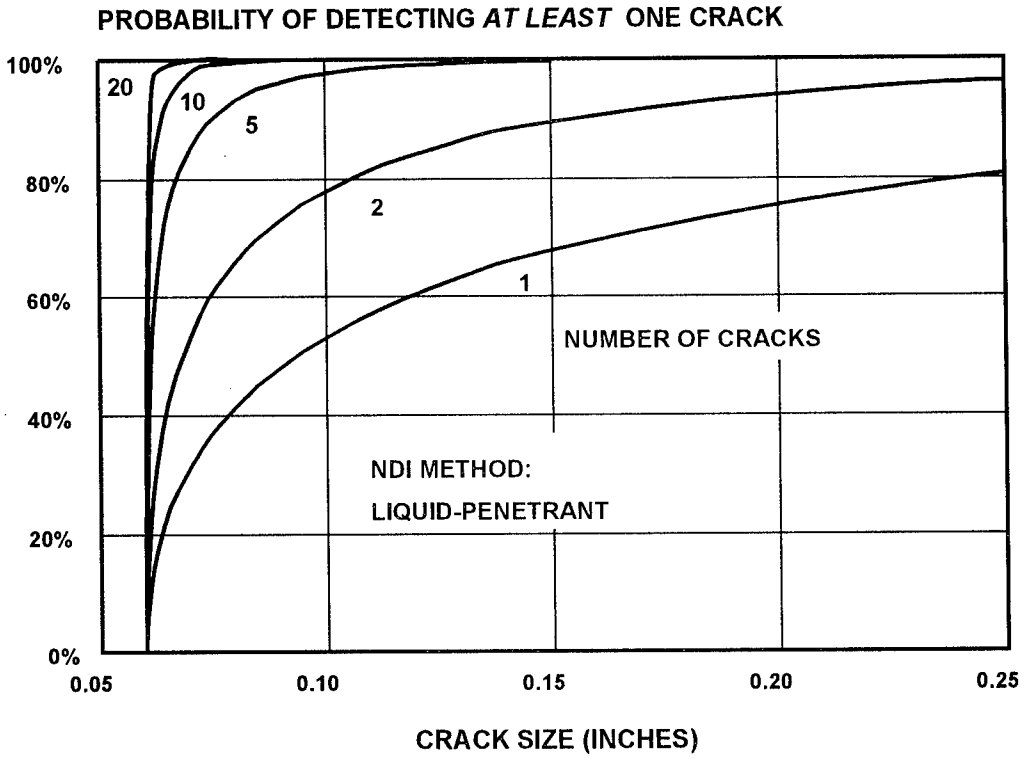

Figure 4: Probability of detecting at least one crack using liquid-penetrant

Effect of Pitch/Diameter and Inspection Interval on the Probability of Failure

As previously described, crack initiation lives and crack growth lives were determined for each configuration that was studied. An aging aircraft scenario was selected which assumed that the mean fleet life has reached the design target life and the high-time aircraft has reached 150% of the design target life. *INSIM* runs were performed for each geometrical configuration for a variety of inspection

intervals using two different NDI method. Figure 5 describes the results for a splice having three rows of fasteners. Figure 5 indicates the probability of failure for various ratios of pitch/diameter and for various liquid-penetrant inspection intervals.

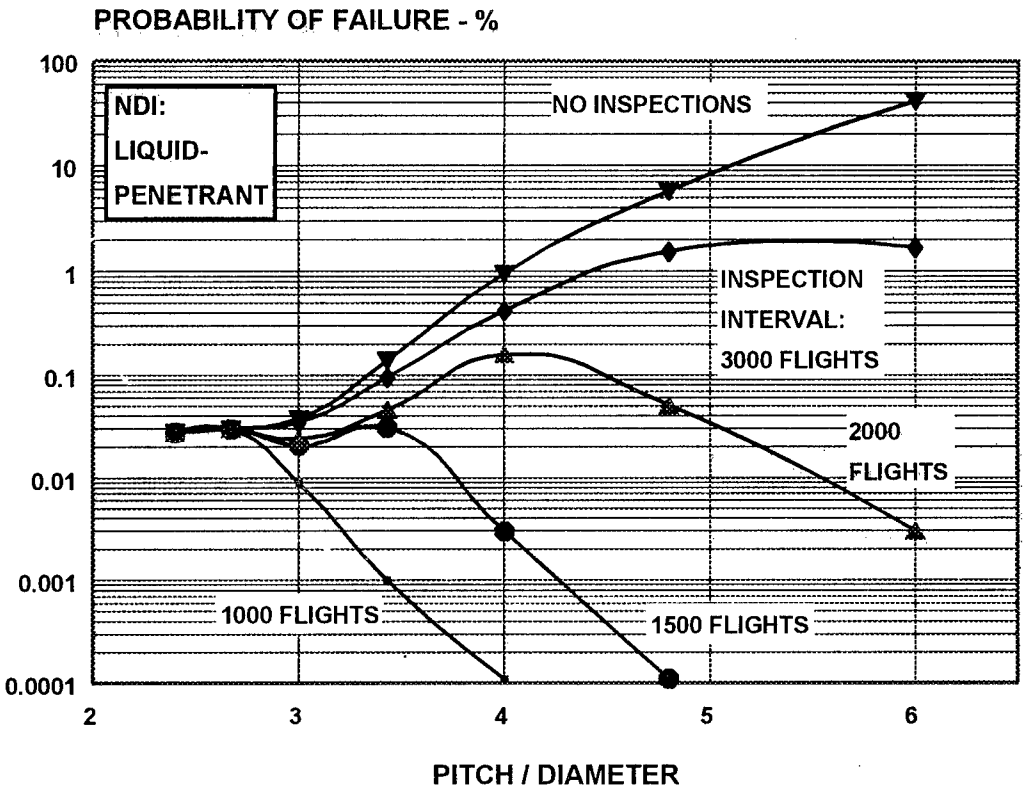

Figure 5: Effect of p/D and inspection interval on the probability of failure

When no inspections are performed, Figure 5 shows that the probability of failure increases rapidly with increased p/D, due to the increase in load-transfer at the large values of p/D. The use of NDI has very little effect in reducing the probability of failure for p/D = 3 but has a major effect at p/D = 6. This is obviously due to the enhanced capability for crack detection corresponding to the relatively large critical crack sizes and slow crack growth corresponding to the large value of p/D. (See Figures 1 and 2.) In fact, for p/D = 6, and a liquid-penetrant inspection at 2000 flight intervals, the resulting probability of failure is calculated to be 0.003% compared to 0.038% for p/D = 3 with no inspections. This means that the minimum probability of failure can be achieved at relatively

large values of pitch/diameter, but at the cost of frequent inspections. It has been calculated from the *INSIM* results that approximately half the fleet will be cracked at aircraft retirement under the p/D = 6 configuration with the 2000 flight intervals. This means that a significant number of repairs will be needed for the fleet if this configuration is adopted.

Figure 5 also indicates, for the 2000 flight inspection interval, the largest probability of failure occurs at a pitch/diameter ratio of four, the value that is commonly recommended by aircraft design manuals.

Effect of the Number of Fastener Rows on the Probability of Failure

Figure 6 indicates the effect of the number of fastener rows on the probability of failure, as determined from the *INSIM* calculations. Figure 6 assumes a liquid-penetrant inspection at 2000 flight intervals, but the results would be valid for all inspection methods and intervals. The effect of additional rows is to reduce the amount of load-transfer in the critical row.

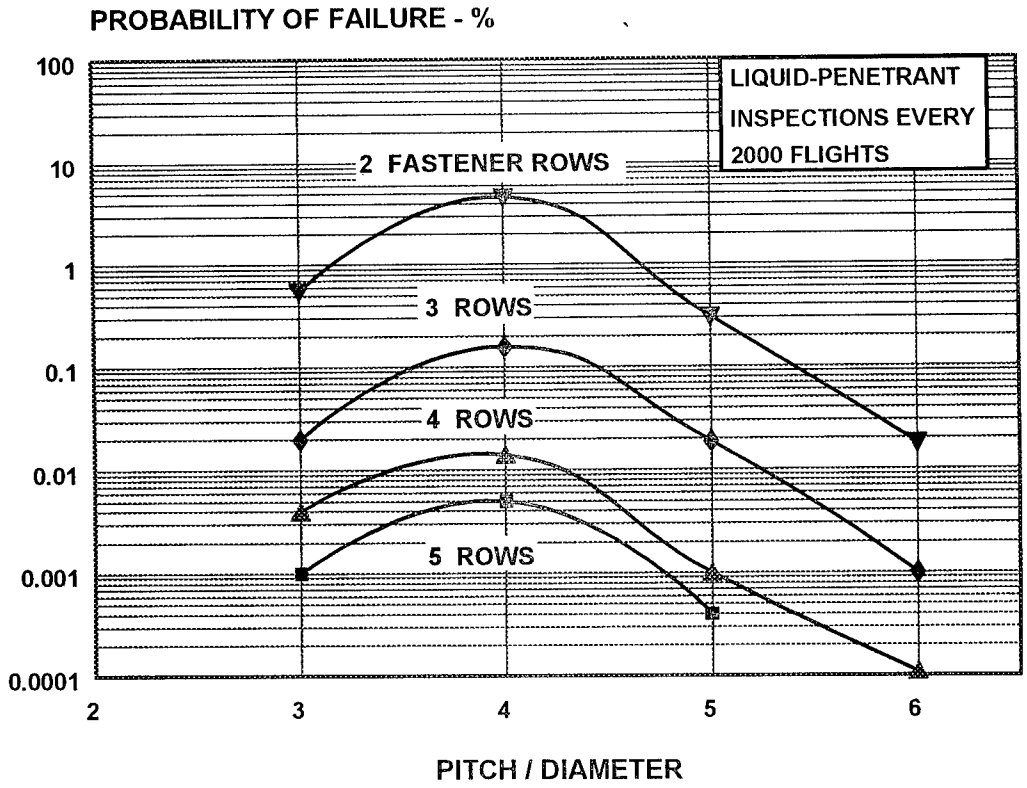

Figure 6: Effect of the number of fastener rows on the probability of failure

Figure 6 clearly shows that additional rows tend to decrease the probability of failure for all values of pitch/diameter. It should be noted that additional rows of fasteners carry with it a weight penalty resulting from the increased overlap of the skins.

Effect of the NDI Method Used on the Probability of Failure

Figure 7 describes the probability of failure for two NDI methods and compares the results to those with no inspections. The results clearly show that the eddy-current method is superior to liquid-penetrant, especially at the larger values of p/D.

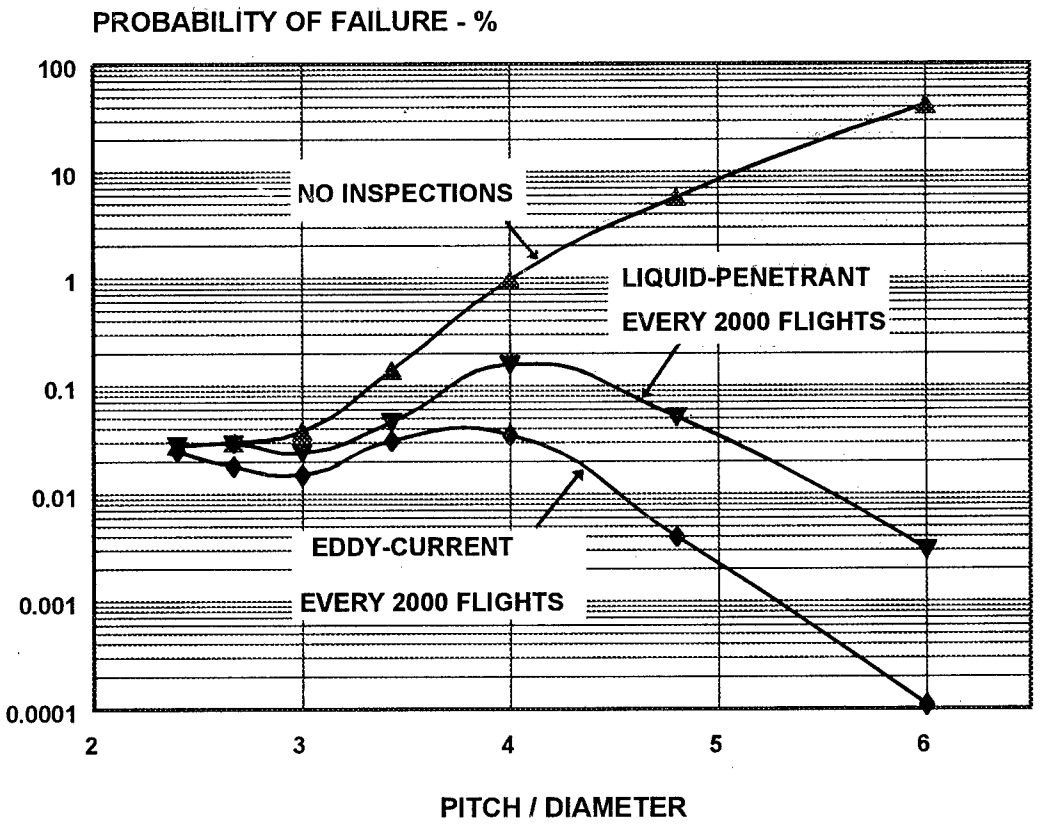

Figure 7: Effect of NDI method on the probability of failure

Design Recommendations for Minimizing the Probability of Failure

Figure 8 presents *five* design recommendations for minimizing the probability of failure for the MSD configuration shown in Figure 3, based on the ***INSIM*** parametric study that was performed. The recommendations refer to a baseline configuration of p/D = 4 and three rows of fasteners, which has a predicted probability of failure of 0.96%. Values of p/D less than three or more than six were not considered. All five recommendations will result in a probability of failure significantly better than the baseline. Solution D, which features cold-working the fastener holes, should be evaluated experimentally, since the amount of life improvement due to the cold-working can be very dependent on stress levels and the degree of load-transfer. No specific recommendations can be given, since each application must be evaluated individually. The recommendations are summarized in Table 1, together with an evaluation of the advantages and disadvantages of each. All five recommended configurations are at a pitch/diameter ratio of three (without inspections) or at a ratio of six (with inspections), instead of the more common ratio of four.

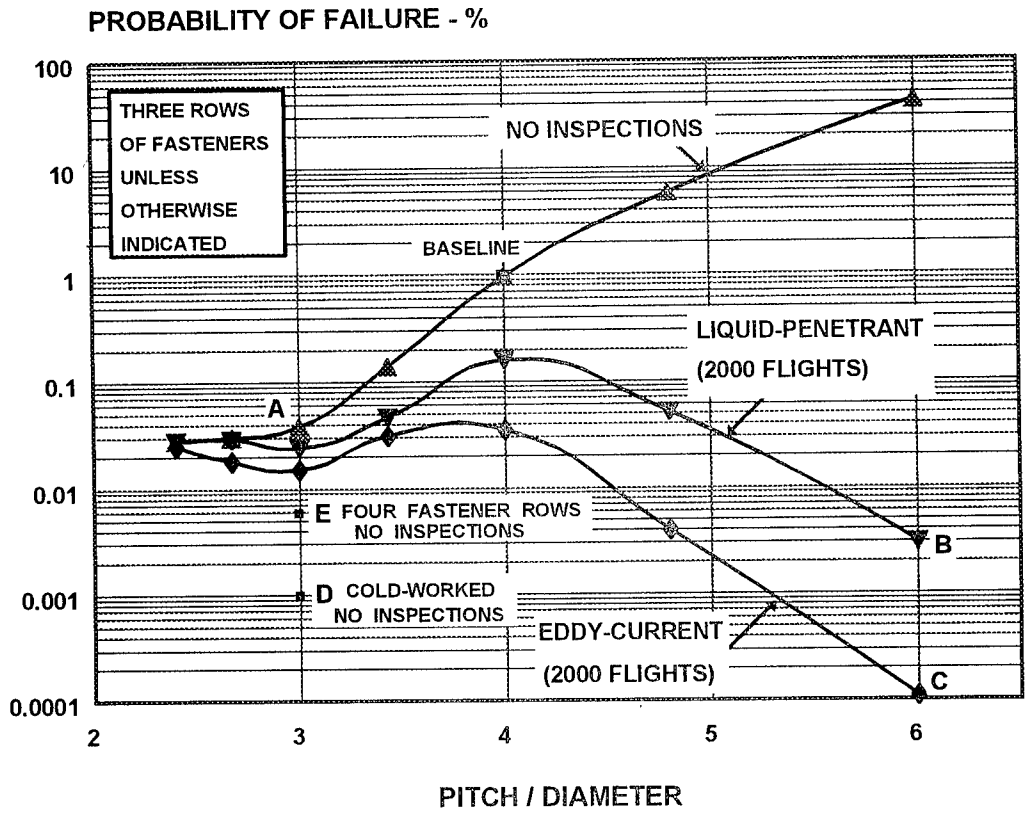

Figure 8: Multi-site damage design recommendations

Table 1: Recommended Configurations for Multi-Site Damage Structures

Recommended Configuration (per Figure 8)	Description	Calculated Probability of Failure	Comments
BASELINE	p/D = 4 3 Fastener Rows No Inspections	0.96%	
A	p/D = 3 No Inspections	0.038%	"Install and Forget"
B	p/D = 6 Liquid-Penetrant every 2000 flights	0.003%	Frequent inspections. Significant fleet cracking can be expected
C	p/D = 6 Eddy-Current every 2000 flights	≈ 0%	Frequent inspections. Significant fleet cracking can be expected
D	p/D = 3, Holes Cold-Worked * No Inspections	0.001%	May be most cost-effective
E	p/D = 3 4 Fastener Rows No Inspections	0.006%	Weight increase is likely

* – Assumes that the crack initiation life and crack growth life have been doubled

Summary

The results of a parametric study on controlling multi-site damage by means of trading-off design and inspection parameters was reported. The effects of the pitch/diameter ratio, number of fastener rows, NDI method and inspection interval on the expected probability of failure were described. The study was performed with the aid of the ***INSIM*** computer program which simulates the entire fatigue process. Five design configurations were recommended, with the aim of minimizing the probability of failure. All five recommended configurations are at either a pitch/diameter ratio of three (without inspections) or at a ratio of six (with inspections) instead of the more common ratio of four.

References

1. Brot, A. "Probabilistic Inspection Strategies – a Key to Controlling Multi-Site Damage", USAF Report No. WL-TR-96-4030, *Proceedings of the 1994 USAF Structural Integrity Program Conference*, San Antonio, TX, December 1994.

2. Brot, A., "Developing Inspection Strategies to Enhance Structural Reliability of MSD Structures", *Proceedings of the 18th Symposium of the International Committee on Aeronautical Fatigue (ICAF)*, Melbourne, Australia, May 1995.

3. Brot, A., "Controlling Fatigue Failures by Means of a Trade-off Between Design and Inspection Parameters", *Proceedings of the FAA-NASA Symposium on Continued Airworthiness of Aircraft Structures*, Atlanta, GA, August 1996.

4. Nathan, A. and Brot, A. "An Analytical Approach to Multi-Site Damage", *Proceedings of the 17th Symposium of the International Committee on Aeronautical Fatigue (ICAF)*, Stockholm, Sweden, June 1993.

5. Horst, P. and Schmidt, H. J., "On the Significance of Probabilistic Parameters for the Assessment of MSD in the Case of Aging Aircraft", *Proceedings of the 19th Congress of the International Council of the Aeronautical Sciences (ICAS)*, Anaheim, CA, 1994.

6. Hart-Smith, L. J.: "Easily Assembled Structurally Efficient Joints in Metallic Aircraft Structures". *Proceedings of the 18th Symposium of the International Committee on Aeronautical Fatigue (ICAF)*, Melbourne, Australia, May 1995..

Analysis of Stiffened Panels with Multiple Site Damage

*Mr. Markus B. Heinimann
Dr. Alten F. Grandt, Jr.
School of Aeronautics & Astronautics
1282 Grissom Hall
Purdue University
West Lafayette, IN 47907-1282

Abstract

This paper investigates the effect of multiple site damage (MSD) on stiffened panels. An analytical model based on displacement compatibility was used to analyze the link up and residual strength behavior of stiffened panels with lead and MSD cracks. Fifteen inch wide stiffened aluminum specimens with various lead and MSD crack lengths and two different stiffener configuration were tensile tested to determine crack link up and panel failure loads. A tip stress intensity reduction factor was verified experimentally through fatigue tests of stiffened panels, and used in two different link up and panel failure criteria to predict the lead crack link up and panel failure loads. The ligament yield criterion, modified for the stiffened panel, was shown to accurately predict the lead crack link up load. The apparent fracture toughness criterion consistently overpredicts link up loads for specimens with MSD. The stiffener failure criterion was shown to be able to predict panel failure to within less than 4 percent for specimens with a true lead crack. The net section failure criteria gives good results for specimens were the lead crack was arrested at a hole.

Introduction

Multiple site damage (MSD) is characterized by the simultaneous presence of several cracks at various sites, such as at different holes in a structural element. MSD may become significant and critical when cracks are of sufficient size and density whereby the structure will no longer meet the present damage tolerance requirements, i.e. it may reduce the lead crack residual strength and fatigue life of a structural component below those based on a single lead crack approach without considering the interaction with the surrounding cracks [1]

Since both military and commercial aircraft, are being increasingly used beyond their designed lifetime, MSD poses a significant challenge to those who must assure the structural integrity of aircraft. Most commercial aircraft are designed and maintained according to the "damage tolerance" philosophy based on the principles of fracture mechanics [2]. This damage tolerance philosophy is based on a single lead crack in a structure. Small MSD cracks, however, can cause a structure to catastrophically fail from smaller lead cracks than those which cause failure when MSD is not present.

Previous research at Purdue University and the Air Force Institute of Technology (AFIT) has examined the applicability of various simple failure criteria to predict crack link up in open hole panels with lead and MSD cracks [3, 4]. The current work aims to expand this model to include stiffeners, stringers and tear straps. Another project is examining the effects associated with lap joints.

An analytical model based on displacement compatibility between the sheet and the stiffener at the rivet locations [5, 6, 7] has been implemented here to quantify the effects of stiffeners on lead crack stress intensity factors. The model was verified by testing 15 inch wide panels with two different stiffener configurations and various lead and MSD crack geometries. The link up and ultimate failure loads were predicted using simple analytical failure criteria.

Open Hole MSD Background

Previous work at Purdue and AFIT [3, 4, 8] has resulted in the development of a model capable of predicting residual strength and fatigue crack growth in open hole panels with MSD. A number of different crack link up criteria proposed in the literature [9, 10] were evaluated and compared to the residual strength tests. The residual strength test specimens were made form Al2024-T3,

0.09 inches thick for the 9 inch wide panels, 0.04 inches thick for the 15 inch wide specimens. The specimens contained various lead and MSD crack configurations, which were fatigue cracks for the 9 inch wide specimens [3], and fine saw cuts in the 15 inch wide panels [4]. The ligament yield criterion proposed by Swift [9] was best able to predict the crack link up leading to sheet failure. Figure 1 shows a comparison of various simple analytical failure criteria and their ability to predict residual strength in 9 inch and 15 inch wide 2024-T3 aluminum panels which contained a row of cracked holes.

Since it is very difficult to precrack wide panels to obtain uniform MSD crack lengths, fine saw cuts or EDM notches often are used to as MSD and lead cracks [11]. In order to verify that the use of saw cuts to model lead and MSD cracks several of Moukawsher's residual strength test [3] were repeated using fine saw cuts (0.013 inches wide) rather than actual fatigue cracks to represent the MSD and lead crack.. For each of the 9 inch wide open hole specimens with fatigue lead and MSD cracks, two identical saw cut panels were tested. The residual strength of the saw cut panels was within 3% of the fatigue crack panel residual strength [4], leading to the conclusion that the use of fine saw cuts to model fatigue cracks in residual strength testing is acceptable. This conclusion is also supported in the literature. Broek reports, for example, that the use of jeweler's saw cuts instead of fatigue cracks in Aluminum alloy sheets does not effect the residual strength results [12]. Recent work by Dawicke, et al [13] indicates that using saw cuts instead of fatigue cracks has a significant effect on stable crack growth, but only a small effect on failure stress.

Stiffened Panel Model

The presence of stiffeners in a cracked panel has two basic effects that need to be modeled. First, the stiffeners reduce the crack tip stress intensity factor by increasing amounts as the crack approaches the stiffener. Second, the presence of the lead crack causes increased loading in the stiffener near the crack plane. The analysis outlined below can be used to determine the magnitude of both of these effects for a given specimen and crack configuration. The analysis of stiffened panels is accomplished using an analytical model. The model is based on displacement compatibility and has successfully been used in the past to analyze stiffened panels containing lead cracks [5, 6, 7]. The analysis employs the theory of elasticity to determine the displacements at the rivet locations, due to the applied remote stress and the unknown rivet forces, in a center cracked sheet and stiffeners. The rivet location displacements v_i in the sheet can be written as:

$$v_i = \sum_j A_{ij}(-Q_j) + B_i\sigma \qquad (1$$

and the corresponding displacements v_i^{st} in the stiffener are given by:

$$v_i^{st} = \sum_j A_{ij}^{st} Q_j + B_i^{st}\sigma \qquad (2$$

The matrix A_{ij} in Eq. 1 represents the displacements at the rivet location i in the sheet due to a unit force at rivet location j, B_i represents the displacement at the rivet location i in the sheet due to the applied remote stress σ. Similarly The matrix A_{ij}^{st} in Eq. 2 represents the displacements at the rivet location i in the stiffener due to a unit force at rivet location j, B_i^{st} represents the displacement at the rivet location i in the stiffener due to the applied remote stress σ. The displacements in the sheet and stiffener match at the rivet locations, therefore, equations 1 and 2 can be equated, and the resulting system can be solved for the unknown rivet forces, Q_i.. Figure 2 shows schematically how the presence of the stiffener is modeled using the rivet forces Q_i. The stress intensity factor for the stiffened sheet can then be obtained using superposition of the stress intensity factor for a center crack subject to applied stress σ, and the stress intensity factor for a center crack subject to the point loads Q_i.

For convenience two non-dimensional parameters are introduced to describe the crack tip stress intensity reduction and the load transfer into the stiffener [7]. The tip stress reduction factor C is defined as the ratio of the stress intensity factor of the sheet with and without stiffeners (equation 3).

$$C = \frac{K_{stiffened}}{\sigma\sqrt{\pi a}} \qquad (3$$

The stiffener load concentration factor L is defined as the ratio of the maximum stringer stress, which occurs in the crack plane, and the stress in the stringer at the end of the panel (equation 4).

$$L = \frac{\sigma_{max}}{\sigma_\infty}\Big|_{\text{stiffener}} \qquad (4$$

Because of symmetry only one quarter of the panel needs to be analyzed. The number of rivet locations that are considered determines the size of the system

of equations that needs to be solved. A computer code was written to determine the unknown rivet forces, tip stress reduction factor C, and load concentration factor L, given the material and geometric properties of the stiffened panel. The code was verified by comparison with the results obtained by Poe [6], using the same analytical method, and Vlieger [7], using finite elements. This comparison showed that using 20 rivet locations per quadrant results in a fully converged solution that matches both Poe [6] and Vlieger [7].

Modeling of MSD

The stiffened panel model outlined above does not include the presence of MSD cracks. Hence the presence of MSD in addition to the lead crack has to be modeled separately. A more complicated stiffened panel model proposed by Nishimura [14] allows for multiple cracks in the sheet.

The presence of multiple cracks in a sheet leads to crack interaction. The interaction between the lead and MSD cracks was modeled here using the Kamei-Yokobori interaction factor [15] as was done in the previous unstiffened panel work. [3, 4]. Figure 3 shows a schematic for the Kamei-Yokobori interaction factor as well as the equations used.

The area loss in a finite sheet due to MSD also has to be considered. It is modeled using appropriate areas in stress intensity factor compounding and load calculations for the failure criteria.

Panel Failure Criteria

Failure criteria in this stiffened panel research refers to criteria that determine the ultimate, and catastrophic failure of the stiffened panels. Two different panel failure criteria were examined in this project.

Stiffener Failure

The stiffener failure criteria predicts panel failure when the stress in the stiffener near the crack plane reaches the stiffener material's ultimate stress. This condition can be expressed by equation 5.

$$P_{stif} = \frac{\sigma_{ult\,st}\ \psi\ A_{st}}{L}\,\frac{A_{st}E_{st} + A_{net}E}{A_{st}E_{st}} \tag{5}$$

where: $\sigma_{ult\,st}$ = stiffener ultimate stress

L = stiffener load concentration (Eq. 4)
ψ = geometry factor
A_{st} = stiffener cross sectional area
E_{st} = stiffener elastic modulus
$A_{net} = (W - 2a - n\,d - 2n_{MSD}a_{MSD})\,t$ = net cross sectional area of sheet (i.e. excluding areas of holes, lead and MSD cracks)
a = lead crack half length
n = number of open holes with or without MSD
d = hole diameter
n_{MSD} = number of holes with MSD
a_{MSD} = MSD crack length
t = sheet thickness
E = sheet elastic modulus

The ratio term with the cross sectional areas and elastic moduli determines how much of the total load is carried by the stiffener, assuming stiffeners and sheet have the same strain away from the crack plane.

Net Section Failure

According to the net section failure criterion, panel failure occurs when the stress in the sheet and the stiffener both reach their respective ultimate stress. The expression for the net section failure criteria is shown in equation 6.

$$P_{section} = \sigma_{ult} A_{net} + \frac{\sigma_{ult\,st}\,\psi\,A_{st}}{L}\frac{A}{A_{lead}} \tag{6}$$

where: σ_{ult} = sheet ultimate stress
A = sheet gross cross sectional area
$A_{lead} = (W - n\,d - 2n_{MSD}a_{MSD})\,t$ = lead crack cross sectional area
W = Sheet width
n = number of open holes with or without MSD
d = hole diameter
n_{MSD} = number of holes with MSD
a_{MSD} = MSD crack length
t = sheet thickness

The ratio between the sheet cross sectional area and the lead crack area accounts for the load concentration in the stiffener due to the MSD area loss in the sheet.

Link Up Criteria

Because of the stiffener's arrest capabilities lead crack extension and link up with MSD cracks is possible without leading to panel failure. The two criteria discussed below are used to determine the loads which cause link up between lead and adjacent MSD cracks. Depending on lead crack length and panel configuration, multiple link-ups can occur before final panel failure.

K apparent

The apparent fracture toughness criterion predicts crack link up when the lead crack stress intensity factor exceeds the materials fracture toughness. The lead crack stress intensity factor is adjusted here using the Kamei-Yokobori factor to account for the presence of the MSD crack. Equation 7 gives the expression for the apparent fracture toughness criterion.

$$P_{K\,app} = \frac{K_c\, A_{net}}{\sqrt{\pi a}\beta_{il}\, C} \frac{A_{net}\, E + A_{st}\, E_{st}}{A_{net}\, E} \tag{7}$$

where: K_c = apparent fracture toughness of sheet
a = lead half crack length
β_{il} = Kamei-Yokobori interaction factor for lead crack
C = Tip stress intensity reduction factor

Ligament Yield

The ligament yield criterion was proposed by Swift [9] and has been used successfully for unstiffened panels [3, 4, 10]. As shown in Fig. 4, crack link up is predicted to occur when the plastic zones ahead of the lead crack and the adjacent MSD crack "touch". Based on work by Cherry et. al. [4] the Irwin plastic zone radius combined with the material yield stress has been used to determine the plastic zone sizes in this project. Hence, the size of plastic zone is estimated to be equal to Irwin's plastic zone radius [9].

$$R = \frac{1}{2\pi} * \left(\frac{K}{\sigma_{ys}}\right)^2 \tag{8}$$

where: R = plastic zone size in front of the crack

K = stress intensity factor at the crack tip
σ_{ys} = yield strength of the sheet material

As the remote stress level increases, the plastic zone sizes of different cracks will increase and will eventually linkup. When the plastic zones of the lead crack meet the plastic zone from the nearest neighboring MSD crack, the ligament has effectively yielded. Therefore, the lead crack effectively extends to the far end of the MSD crack. Figure 4 shows a schematic of this linkup criterion [9]. When the applied load reaches a level that causes the effective ligament between cracks to yield, the ligament will fail.

According to Swift, the predicted failure of a specimen with MSD is a function of the plastic zone size of the lead crack and its nearest neighboring MSD crack, the material's yield strength, and an interaction factor between the MSD crack, and the lead crack.

The stress intensity factor for the lead and MSD cracks are found by the method of compounding. The stress intensity factor for the lead crack then becomes (eq. 9)

$$K_2 = \left[\frac{P}{A_{net}}\right]\sqrt{\pi a}\,\beta_{il} C \frac{A_{net}}{A_{lead}} \tag{9}$$

where: P = applied load

The stress intensity factor for the MSD crack (eq. 10) is based on a fit to the Bowie solution for a cracked hole [16] and includes the appropriate area for compounding as well as the interaction factor for the adjacent crack tips.

$$K_1 = \left[\frac{P}{A_{net}}\right]\sqrt{\pi a_{MSD}}\,\beta_h \beta_{i\,MSD} \frac{A_{net}}{A_{MSD}} \tag{10}$$

where: a_{MSD} = MSD crack length (from edge of hole)
$\beta_{i\,MSD}$ = Kamei-Yokobori interaction factor for MSD crack
$A_{MSD} = A_{net} + (d + 2a_{MSD})t$ = appropriate area for MSD crack compounding
β_h = Bowie factor

$$\beta_h = \left[\frac{F_1}{F_2 + \frac{a_{MSD}}{r}} + F_3 \right] \tag{11}$$

where: r = radius of the hole

F1, F2, F3 = hole configuration constants

for holes with cracks emanating from both sides:	or holes with only one side cracked:
F1 - 0.6865	F1 - 0.8733
F2 - 0.2772	F2 - 0.3245
F3 - 0.9439	F3 - 0.6762

The predicted failure load according to the Swift criterion, then, becomes:

$$P_{swift} = \sigma_{ys} A_{net} \sqrt{\frac{2t}{\left(a_{MSD} \beta_h^{\,2} \beta_{iMSD}^{\,2} \left(\frac{A_{net}}{A_{MSD}} \right)^2 + a \beta_{il}^{\,2} C^2 \left(\frac{A_{net}}{A_{lead}} \right)^2 \right)}} \frac{A_{net} E + A_{st} E_{st}}{A_{net} E} \tag{12}$$

where: t = crack tip separation

For each crack configuration the link up and panel failure loads were calculated using the four criteria described above (Eqns. 5, 6, 7, 12). If the link up load was below the panel failure load, the lead crack was assumed to have linked up with the adjacent MSD crack and the process was repeated. Final panel failure was predicted when the panel failure load exceeded the link up load.

Specimen Geometry and Test Procedures

To verify the stiffened panel model and the failure criteria described above, a series of experiments using wide Aluminum panels was performed. The sheet material for all tests was Al 2024-T3 in the MRS condition, 0.063 inches thick, and all tests were performed with the specimens loaded in the L-T direction. The stiffener material was 0.09 inches thick Al 2024-T3. Stiffeners were riveted to both sides of the specimen to avoid out of plane deformation during testing. Standard aircraft riveting procedures were followed in bucking the MS20470AD-6 rivets using a pneumatic rivet gun [17]. Figure 5 shows the basic dimensions for

the stiffened panel specimens used in the verification program.. Although most of the residual strength tests employed 1.5 inch wide stiffeners, a few residual strength tests were performed using stiffeners that were only 0.75 inches wide. These two stiffener configurations will from here on be referred to as heavy and light stiffeners respectively. The analytical tip stress intensity reduction factors and load concentration factors for both stiffener cases are shown in Figure 6. Table 1 summarizes the lead and MSD crack lengths as well as the stiffener type for the residual strength tests. All residual strength specimens had the same MSD crack lengths at each open hole. Both the lead and the MSD cracks were made using a jeweler's saw with a blade thickness of 0.012 inches. The specimens were tested using a 100 kip servo-hydraulic test machine at the Fatigue and Fracture Test Facility of the Flight Dynamics Laboratory at Wright-Patterson Air Force Base. The loading was a performed at a constant load rate of 0.25 kips per second. Although buckling guides were employed for the unstiffened R-curve tests, they were not used for the stiffened panel residual strength tests Link up and failure loads were recorded during the tests.

The same basic specimen without stiffeners and holes was used to perform three R-curve tests following ASTM E-561 [18]. The R-curve tests were performed in the same WPAFB facility as the residual strength tests. Stable crack extensions were monitored and measured using traveling microscopes. The resulting R-curve for the sheet material is shown in Figure 7.

Two stiffened panels with a lead crack, but without open holes were fatigue tested to experimentally verify the analytical tip stress intensity reduction factors using the backtracking method [19]. The fatigue tests were performed in the Fatigue and Fracture Lab of the School of Aeronautics and Astronautics at Purdue University. Each panel was tested at a different constant amplitude loading, and fatigue crack propagation of the lead crack was measured using traveling microscopes. The crack length versus cycle data was then converted to da/dN versus a using the procedure outlined in ASTM E-647 [20]. Using established baseline da/dN versus ΔK data for Al 2024-T3, an experimental stress intensity factor K_{exp} was then calculated for each crack length.

The results of these tests and comparison with analytical predictions are presented in the next section.

Results

The purpose of the experimental test program was to verify the analytical model for stiffened panels with lead and MSD cracks, and to determine which of the failure and link up criteria were most suitable.

Experimental Tip SIF Reduction Factors

The experimental stress intensity factor obtained from the two stiffened panel fatigue tests can be converted to experimental tip stress intensity reduction factors using equation 13.

$$C_{exp} = \frac{K_{exp}}{\sigma\sqrt{\pi a}\beta_w} \tag{13}$$

where: K_{exp} = experimental stress intensity factor

σ = applied remote stress

$\beta_w = \sqrt{\sec\frac{\pi a}{W}}$ = finite width correction factor

W = width of sheet

The comparison between the experimental and the analytical tip stress intensity reduction factor is shown in Figure 8. As figure 8 shows, the analytical and experimental results agree well with each other.

Reduction of Residual Strength due to MSD

The experimental residual strengths for the stiffened panel specimens are shown in Table 2. After link up all cracks arrested at the stiffener, except for MSD-13, where crack extension past the stiffener and panel failure were nearly simultaneous. Figure 9 shows the reduction in residual strength due to the presence of MSD. Note that the presence of MSD cracks that are only 0.05 inches long reduces stiffened panel residual strength by 24 percent for specimens with 4.5 and 6.0 inch lead cracks.. MSD cracks that are 0.1 inch long lead to a residual strength reduction of 32 percent, and more severe MSD cracks that are 0.15 inches long lead to a reduction in residual strength of 40 percent.

Link Up Criteria Comparison

The apparent fracture toughness and the ligament yield criterion outlined earlier were used to predict crack link up in the residual strength specimens. All specimens had one crack link up before failure, except for MSD-9, MSD-10 and MSD-13 which had two separate crack link ups. The actual and predicted first

link up loads are given in Table 3. The ligament yield criterion cannot be applied to the baseline tests (MSD-1 to MSD-4) because no MSD crack were present. For specimens with MSD, cracks the ligament yield criterion predicts the first link up well, with an average difference of 3.3 percent and no difference larger than 8 percent. The apparent fracture toughness criterion works well for the baseline cases (no MSD), but consistently overpredicts the link up load for specimens with MSD. The actual and predicted link up loads for the three specimens that had a second link up are given in Table 4. Note that for the second link up the apparent fracture toughness criterion gives much better results, while the ligament yield criterion does slightly worse than for the first link up. Neither criteria does very well for the second link up on MSD-13. This was the only specimen that had crack extension past the stiffener load line. The validity of the plastic zone expression across the stiffener load line is debatable and could have influenced the predictions. Comparison of the actual and predicted first and second link up loads are shown graphically in Figure 10.

Failure Criteria Comparison

Total panel failure was predicted whenever the predicted panel failure load was lower than the link up load. The net section failure and the stiffener failure criterion were used to predict panel failure loads. The actual and predicted panel failure loads are summarized in Table 5. The net section failure criteria is able to predict the failure load of the baseline specimens (MSD-1 to MSD-4) and the specimens with MSD and heavy stiffeners (MSD-4 to MSD-10) well with an average difference of less than 4.5 percent, but is very unconservative for the panels with the light stiffeners (MSD-11 to MSD-13). The stiffener failure criterion works well for specimens with MSD (MSD-5 to MSD-13) with an average difference of less than 3.5 percent, but underestimates the failure load of the baseline specimens. This is most likely due to the fact the after lead crack extension in the baseline specimen the lead crack end at a hole, which is a less severe situation than a lead crack of equal length, which is the case assumed by the stiffener failure criterion. Figure 11 summarizes the actual and predicted panel failure loads.

Work to Be Completed

This project brought to light some issues that need further attention. Currently the lead crack is being modeled as a center crack in a sheet. However, when the lead crack links up with the adjacent MSD crack, the crack lengths extending from the hole can be very small (0.05 inches in this work). It is not clear that the center crack model is an accurate representation of the stress intensity factor at the crack tip.

Specimen MSD-13 showed that when crack extension occurs past the stiffener line, neither of the current link-up criteria is able to accurately predict this link up. The ligament yield criterion that was shown to work well for all other cases, was not able to predict the second link up within less than 10 percent. The authors believe that the currently used plastic zone model is not a good approximation for plastic zone extending across stiffener load lines.

Consideration is also given to including stable crack extension before link up or failure in the various link up and failure criteria.

The analytical model was shown to work well for link up and residual strength predictions. Fatigue tests of stiffened panels with MSD and lead cracks will be conducted in the future to evaluate the model for fatigue crack growth calculations.

Summary

An analytical model based on displacement compatibility was used to analyze the link up and residual strength behavior of stiffened panels with lead and MSD cracks. The stiffened panel correction factors were used in two different link up and panel failure criteria to predict the lead crack link up and panel failure loads in 15 inch wide stiffened aluminum specimens. The ligament yield criterion, modified for the stiffened panel, has proven to be able to predict lead crack link up load within 4 percent. The apparent fracture toughness criterion consistently overpredicts link up loads for specimens with MSD. The stiffener failure criteria is been shown to be able to predict panel failure to within less than 4 percent for specimens with a true lead crack. The net section failure criteria gives good results for specimens were the lead crack was arrested at a hole.

Acknowledgments

Portions of this research were supported by the Air Force Office of Scientific Research Grant F49620-93-1-0377 with Dr. W. F. Jones as program monitor. The authors greatly appreciate the assistance of Mr. B. Westerlund of ALCOA, Davenport who provided the sheet material. The authors are also grateful to Lt. D. Conley for making the use of the Fatigue and Fracture Test Facility of the Flight Dynamics Directorate, Wright-Patterson Air Force Base possible.

References

1 Mar, J. W., "Preserving Aging Aircraft," Aerospace America, Jan. 1996, pp. 38-43.

2 Mar, J. W., "Structural Integrity of Aging Airplanes: A Perspective," Structural Integrity of Aging Airplanes, S. N. Alturi, S. G. Sampath, P. Tong, Editors, Springer-Verlag, Berlin, Heidelberg, 1991.

3 E.J. Moukawsher, M.B. Heinimann, A.F. Grandt, Jr., "Residual Strength of Panels with Multiple Site Damage," Journal of Aircraft, Vol. 33, No. 5, 1996.

4 M.C. Cherry, S. Mall, M.B. Heinimann, A.F. Grandt, Jr., "Residual Strength of Unstiffened Aluminum Panels with Multiple Site Damage," Submitted to Engineering Fracture Mechanics, August 1996.

5 Romualdi, J. P., Frasier, J. T., Irwin, G. P., "Crack-Extension-Force Near a Riveted Stiffener," NRL Report 4956, Naval Research Laboratory, Washington, D.C., 1957.

6 Poe, C.C., Jr., "Stress-Intensity Factor for a Cracked Sheet with Riveted and Uniformly Spaced Stringers", NASA TR R-358, 1971.

7 Vlieger, H., "The Residual Strength Characteristics of Stiffened Panels Containing Fatigue Cracks," *Engineering Fracture Mechanics*, Vol. 5, pp. 447-477, 1973.

8 Moukawsher, E. J., Neusel, M.A., and Grandt, A. F., Jr., "Analysis of Panels With Multiple Site Damage," AIAA Paper No. 94-1459, AIAA 35th SDM Conference, April 18-21, 1994, Hilton Head, SC.

9 Swift, T., "Widespread Fatigue Damage Monitoring Issues and Concerns," presented at the *5th International Conference on Structural Airworthiness of New and Aging Aircraft*, Hamburg, Germany, June 16-18, 1993.

10 Jeong, D. Y., and Brewer, J. C., "On the Linkup of Multiple Cracks," Engineering Fracture Mechanics, Vol. 51, No. 2, 1995, pp. 233-238.

11 Broek, D., "The Effects of Multi-Site-Damage on the Arrest Capability of Aircraft Fuselage Structures," FractuREsearch TR 9302, 1993.

12 Broek, D., "The Residual Strength of Aluminum Alloy Sheet Containing Fatigue Cracks or Saw Cuts," NLR TR-M-2134, 1965.

13 Dawicke, D.S, Newman, J.C., Jr., Sutton, M.A., and Amstutz, B.E., "Stable Tearing Behavior of Thin-Sheet Material with Multiple Cracks," NASA Technical Memorandum 109131, July 1994.

14 Nishimura, T., "Stress Intensity Factors of Multiple Cracked Sheet With Riveted Stiffeners," *Journal of Engineering Materials and Technology*, Vol. 113, pp. 280-284, 1991.

15 Kamei, A., and Yokobori, T., "Two Collinear Asymmetrical Elastic Cracks," Report of the Research Institute for Strength and Fracture of Materials, Tohoku University, Vol. 10, Section 1-4, pp. 41-42, December 1974.

16 Grandt, A. F., Jr., "Stress Intensity Factors for Some Thru-Cracked Fastener Holes," International Journal of Fracture, Vol. 5, No. 2, April 1975, pp 283-294.

17 *Standard Aviation Maintenance Handbook*, EA-282-0, IAP, Inc.

18 "Standard Practice for R-Curve Determination," ASTM E561-94, Annual Book of ASTM Standards, Vol 03.01, American Society for Testing and Materials, 1996.

19 James, L. A. and Anderson, W. E., "A Simple Experimental Procedure for Stress Intensity Factor Calibration," Engineering Fracture Mechanics, Vol. 1, April 1969, pp. 565-568.

20 "Standard Test Methods Measurement of Fatigue Crack Growth Rates," ASTM E647-95a, Appendix X1.2, Annual Book of ASTM Standards, Vol 03.01, American Society for Testing and Materials, 1996.

Table 1: Summary of lead and MSD crack lengths and stiffener type for residual strength specimens

Specimen ID	Lead Crack Length (2a) [in]	MSD Crack Length [in]	Stiffener Type
MSD-1	5.982	-	heavy
MSD-2	5.975	-	heavy
MSD-3	4.525	-	heavy
MSD-4	4.520	-	heavy
MSD-5	5.992	0.051	heavy
MSD-6	6.003	0.149	heavy
MSD-7	5.982	0.103	heavy
MSD-8	5.976	0.058	heavy
MSD-9	4.471	0.054	heavy
MSD-10	4.48	0.098	heavy
MSD-11	6.025	0.053	light
MSD-12	6.026	0.048	light
MSD-13	5.975	0.097	light

Table 2: Summary of experimental residual strength of stiffened panels

Specimen ID	Lead Crack Length (2a) [in]	MSD Crack Length [in]	Actual Failure Load [kips]
MSD-1	5.982	-	47.25
MSD-2	5.975	-	49.97
MSD-3	4.525	-	51.36
MSD-4	4.520	-	52.02
MSD-5	5.992	0.051	38.16
MSD-6	6.003	0.149	30.90
MSD-7	5.982	0.103	34.11
MSD-8	5.976	0.058	37.81
MSD-9	4.471	0.054	37.09
MSD-10	4.48	0.098	34.04
MSD-11	6.025	0.053	23.53
MSD-12	6.026	0.048	24.35
MSD-13	5.975	0.097	20.29

Table 3: Actual and predicted first link up loads for stiffened specimens

Specimen ID	Actual First Link Up Load [kips]	App. Fracture Toughness Criterion [kips]	% Difference	Ligament Yield Criterion [kips]	% Difference
MSD-1	35.80	36.76	2.682		
MSD-2	35.60	36.76	3.258		
MSD-3	34.30	35.76	4.257		
MSD-4	34.90	35.76	2.464		
MSD-5	26.80	34.57	28.993	26.10	-2.612
MSD-6	13.60	25.85	90.074	13.85	1.838
MSD-7	20.50	30.19	47.268	19.61	-4.341
MSD-8	26.40	34.10	29.167	26.63	0.871
MSD-9	27.10	31.36	15.720	26.24	-3.173
MSD-10	21.20	27.75	30.896	20.31	-4.198
MSD-11	17.60	22.67	28.807	18.53	5.284
MSD-12	18.10	22.84	26.188	18.85	4.144
MSD-13	14.20	19.55	37.676	13.14	-7.465

Table 4: Actual and predicted loads for second link up for stiffened panel specimens.

Specimen ID	Actual First Link Up Load [kips]	App. Fracture Toughness Criterion [kips]	% Difference	Ligament Yield Criterion [kips]	% Difference
MSD-9	34.80	33.57	-3.534	37.77	8.53
MSD-10	29.50	28.71	-2.678	30.18	2.31
MSD-13	19.80	21.78	10.000	22.05	11.36

Table 5: Actual and predicted panel failure loads for stiffened panel specimens.

Specimen ID	Actual Panel Failure Load [kips]	Net Section Failure [kips]	% Difference	Stiffener Failure [kips]	% Difference
MSD-1	47.25	48.40	2.434	42.66	-9.714
MSD-2	49.97	48.42	-3.102	42.68	-14.589
MSD-3	51.36	54.24	5.607	49.40	-3.816
MSD-4	52.02	54.29	4.364	49.44	-4.960
MSD-5	38.16	40.68	6.604	37.10	-2.778
MSD-6	30.90	28.02	-9.320	30.79	-0.356
MSD-7	34.11	34.20	0.264	33.84	-0.792
]MSD-8	37.81	39.84	5.369	36.71	-2.909
MSD-9	37.09	39.92	7.630	36.77	-0.863
MSD-10	34.04	34.02	-0.059	33.84	-0.588
MSD-11	23.53	29.75	26.434	21.83	-7.225
MSD-12	24.35	30.79	26.448	22.30	-8.419
MSD-13	20.29	25.75	26.910	21.62	6.555

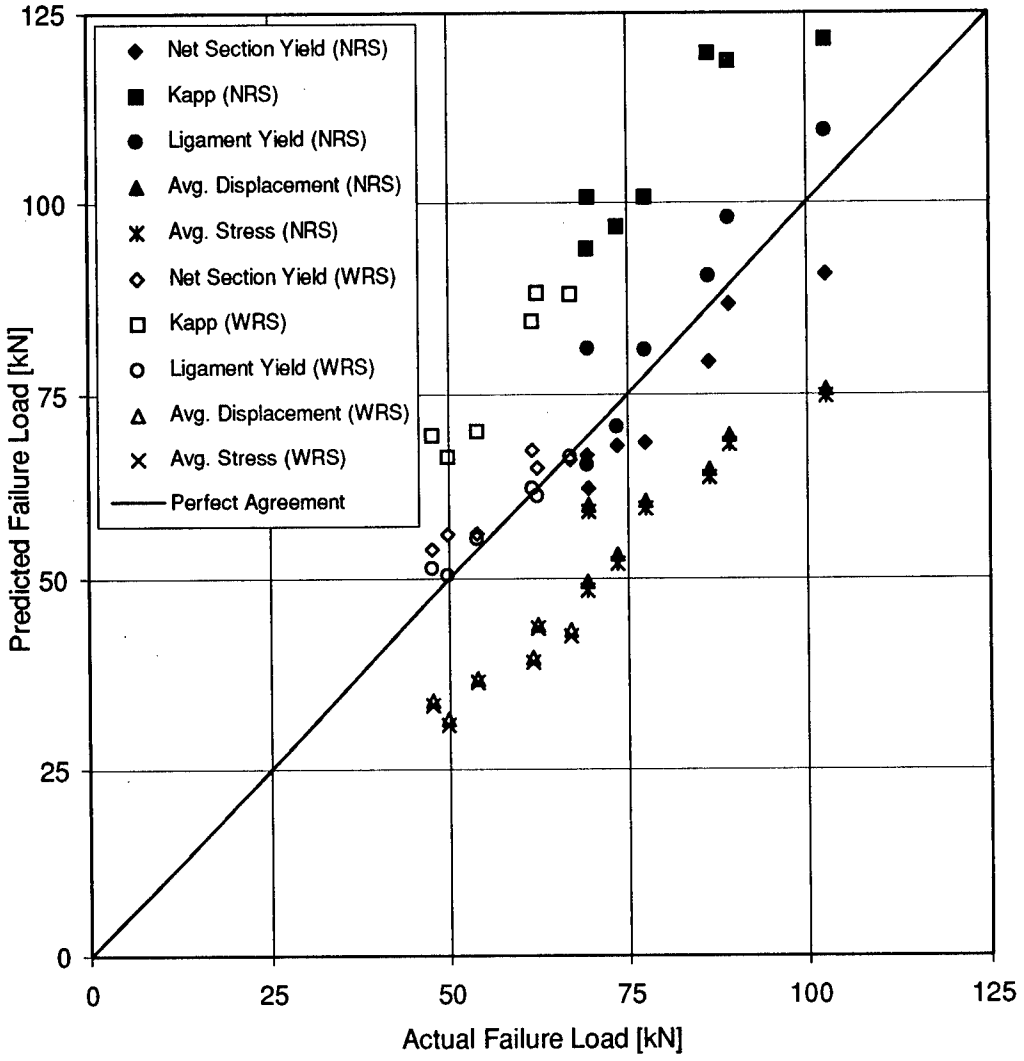

Figure 1: Comparison of actual and predicted failure loads by various analytical failure criteria for residual strength tests with 9 inch (NRS) and 15 inch (PRS) 2024-T3 aluminum panels.

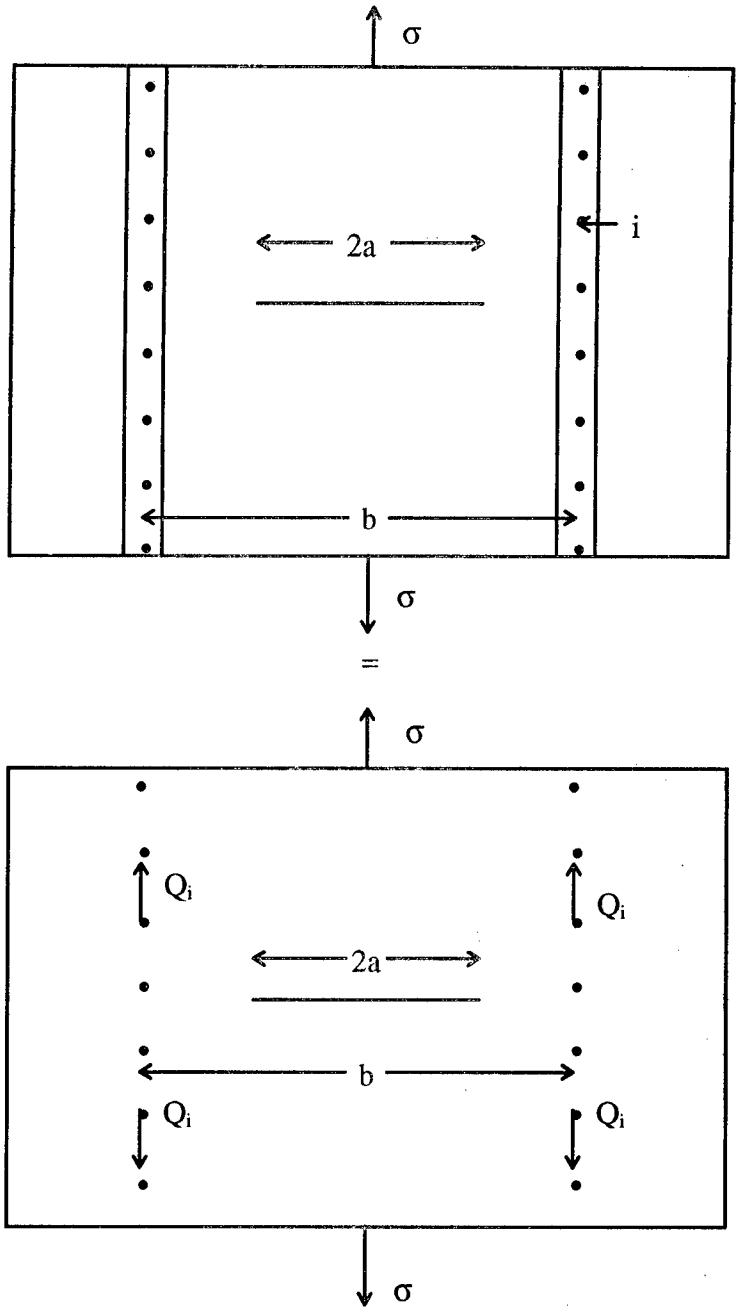

Figure 2: Schematic of stiffened panel model showing the modeling of the effects of the stiffeners using the rivet forces Q_i.

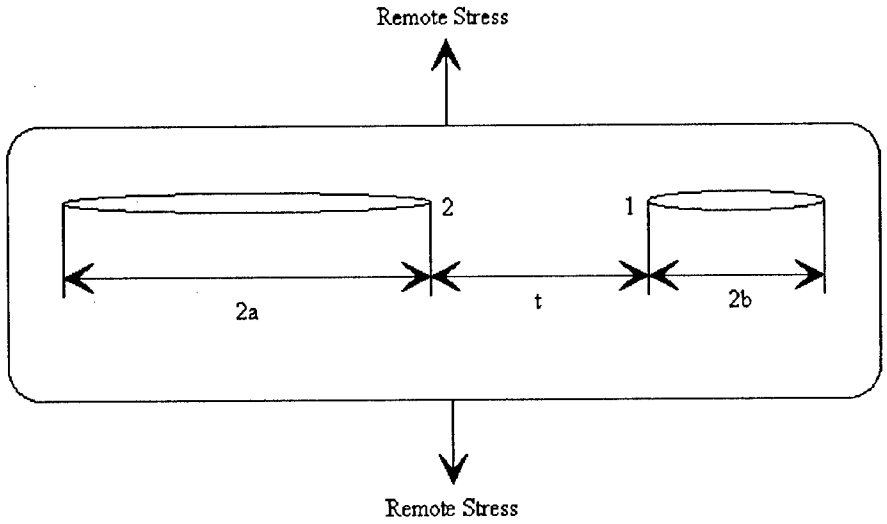

$$\beta_{i1} = \sqrt{1+\frac{2b}{t}}\left[1-\left(1+\frac{t}{2a}\right)\frac{K(k)-E(k)}{K(k)}\right]$$

$$\beta_{i\,MSD} = \sqrt{1+\frac{2a}{t}}\left[1-\left(1+\frac{t}{2b}\right)\frac{K(k)-E(k)}{K(k)}\right]$$

where: $K(k)$ = complete elliptic integral of the first kind
$E(k)$ = complete elliptic integral of the second kind

$$k = 2\sqrt{\frac{ab}{(2a+t)(2b+t)}}$$

Figure 3: Definition of Kamei-Yokobori interaction factor for two planar crack of unequal length in an infinite plate [15].

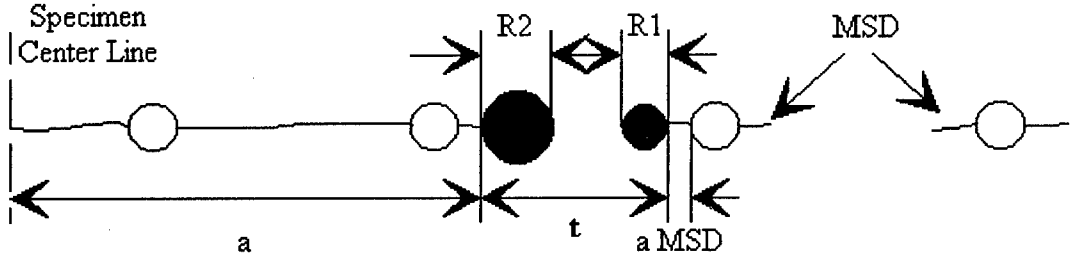

Figure 4: Schematic of the lead and MSD cracks and plastic zones for the ligament yield method [9].

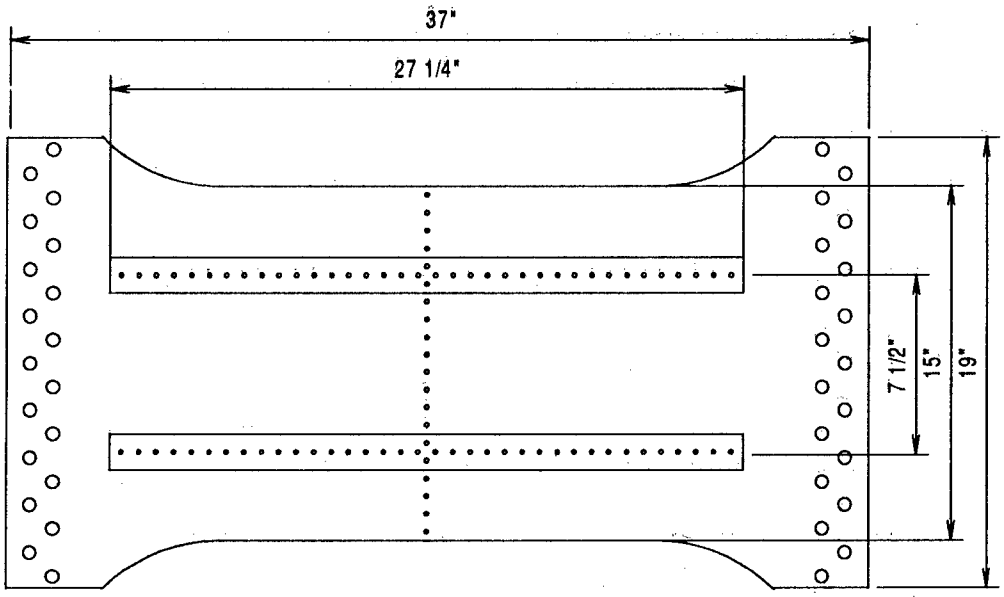

Figure 5: Schematic of stiffened panel specimen used for residual strength testing.

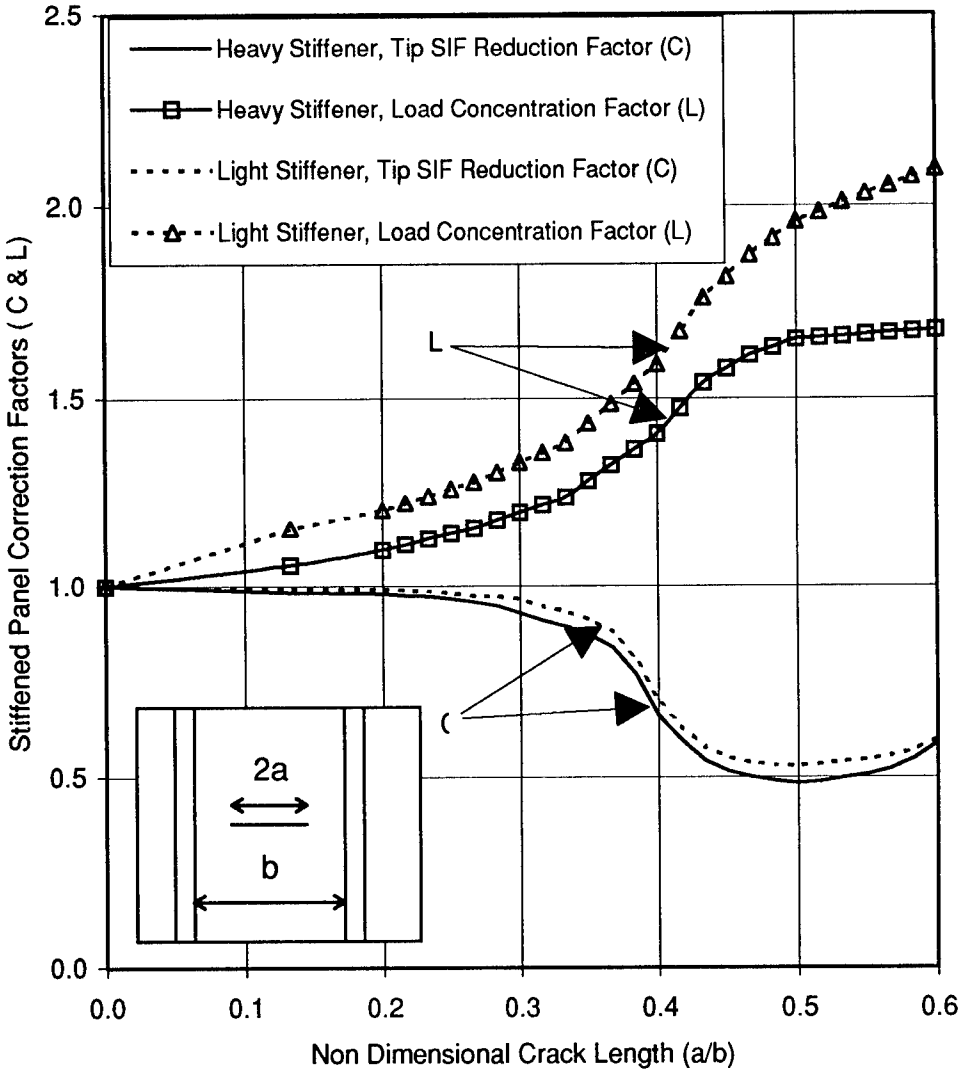

Figure 6: Analytical tip stress intensity reduction and load concentration factors for heavy and light stiffener residual strength specimens.

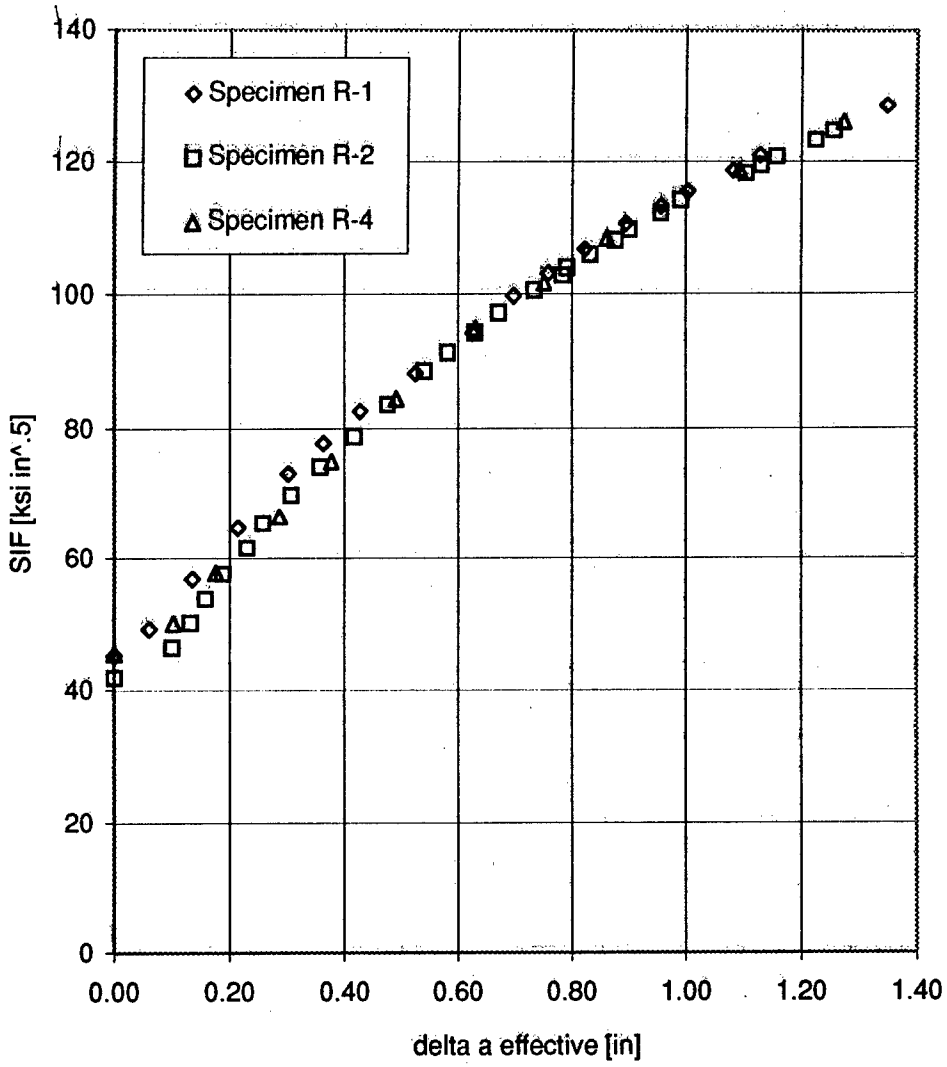

Figure 7: R-curve for Al 2024-T3 MRS in the L-T direction obtained from 15 inch wide specimens.

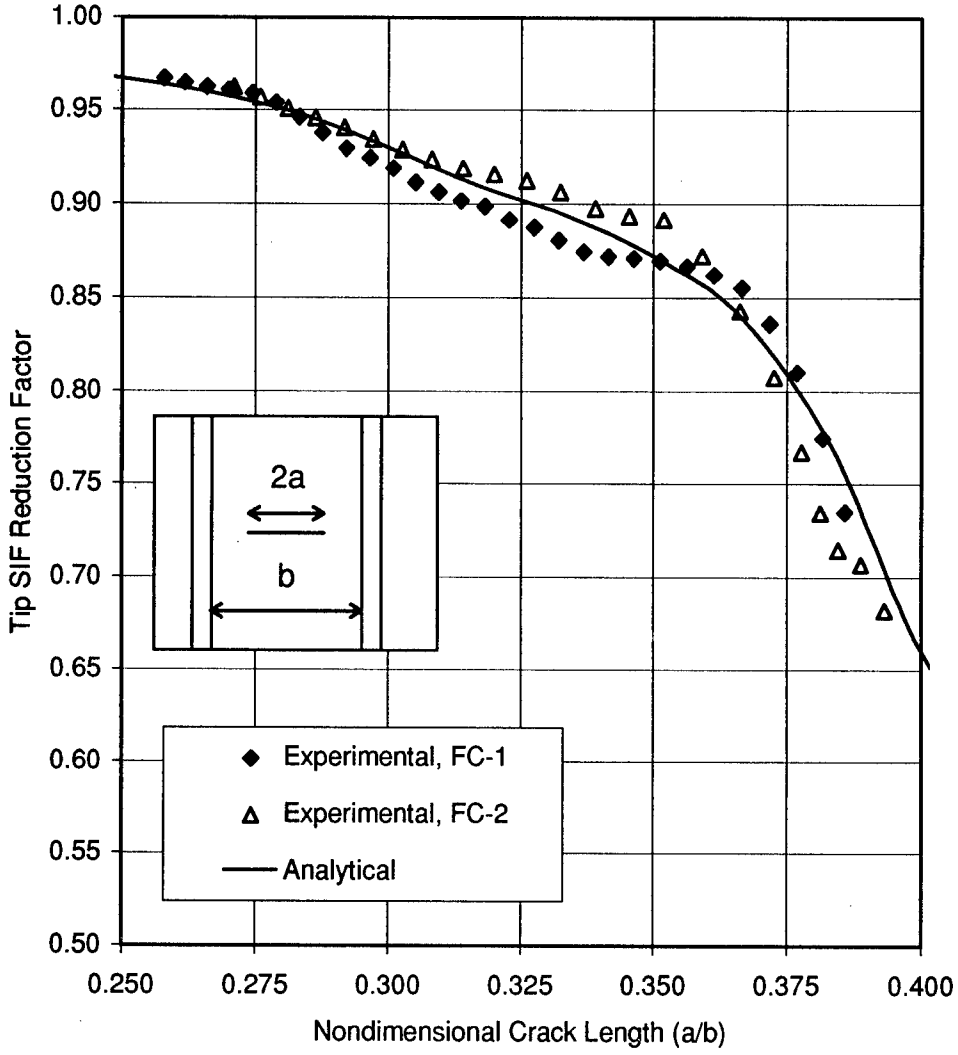

Figure 8: Comparison of analytical and experimental tip stress intensity reduction factors for 15 inch wide panel with heavy stiffeners.

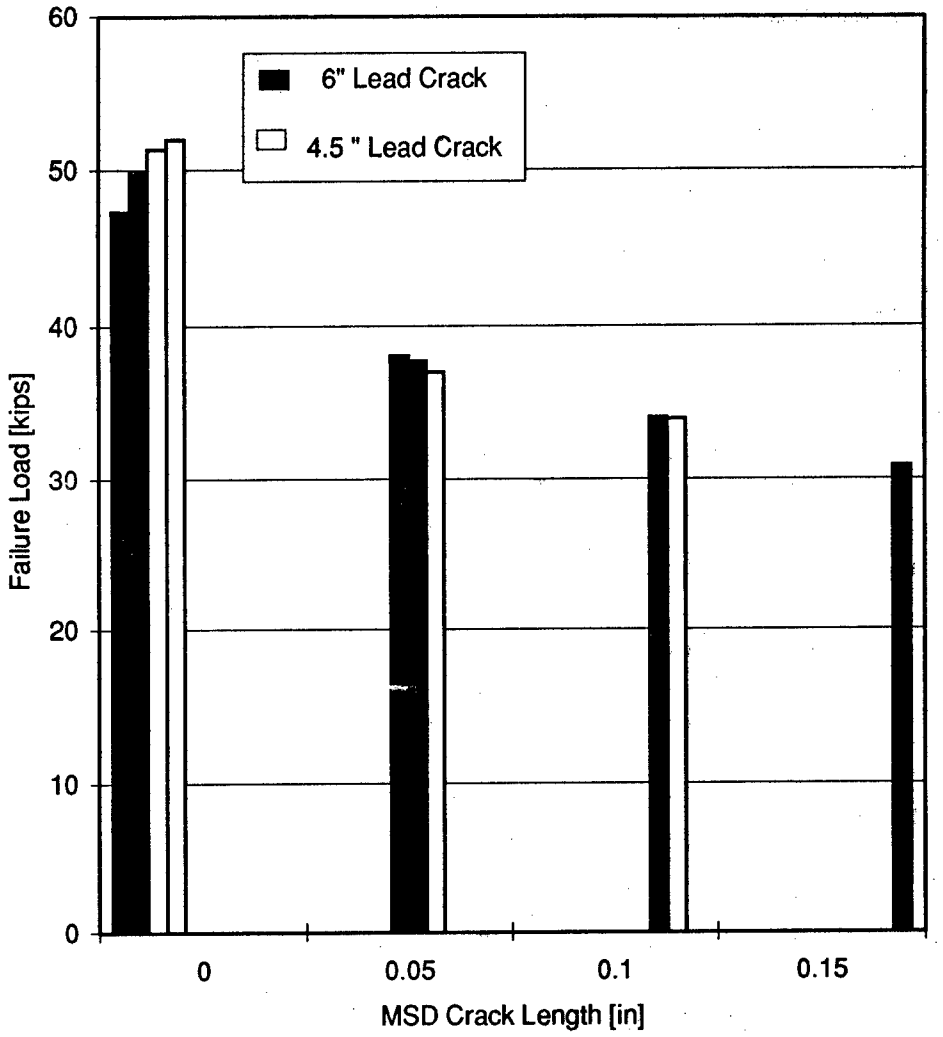

Figure 9: Reduction in residual strength of 15 inch 2024-T3 aluminum panels with heavy stiffeners due to MSD.

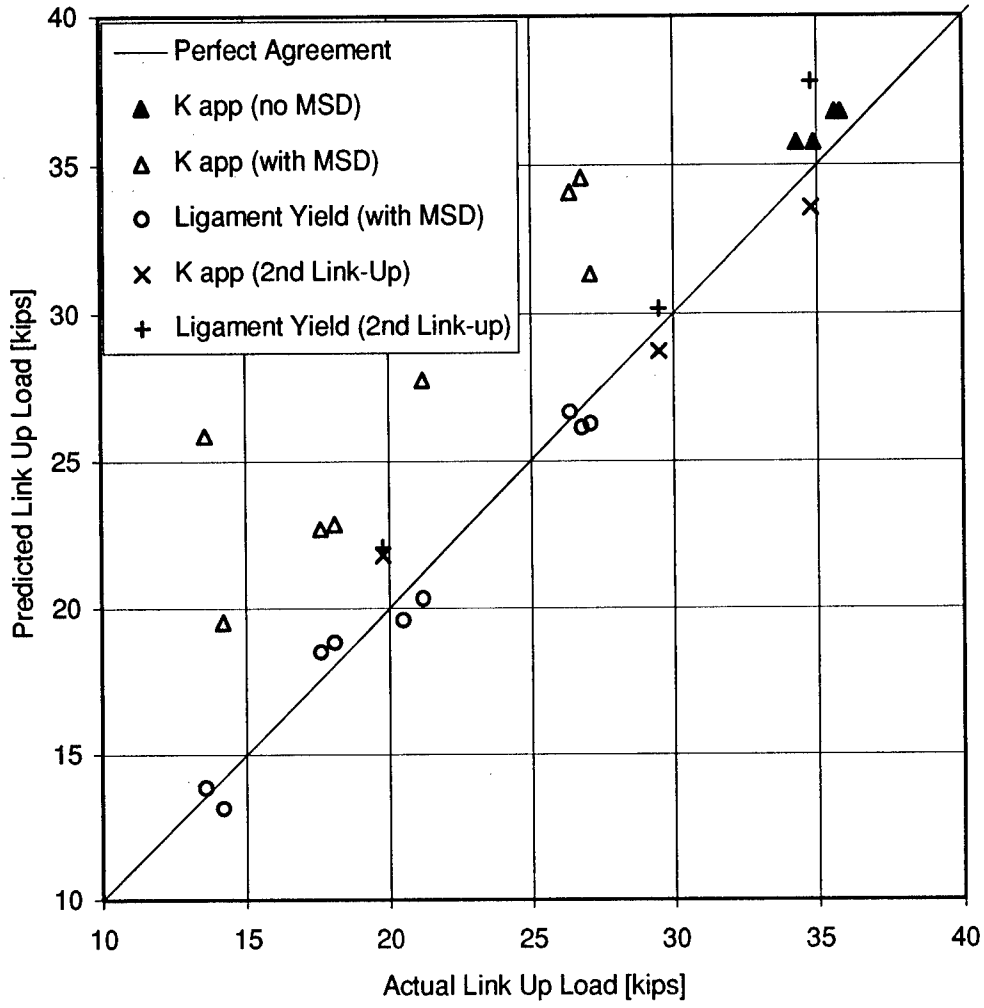

Figure 10: Comparison of actual and predicted link up loads by two different link up criteria for 15 inch wide, stiffened, 2024-T3 aluminum panels containing lead and in most cases MSD cracks.

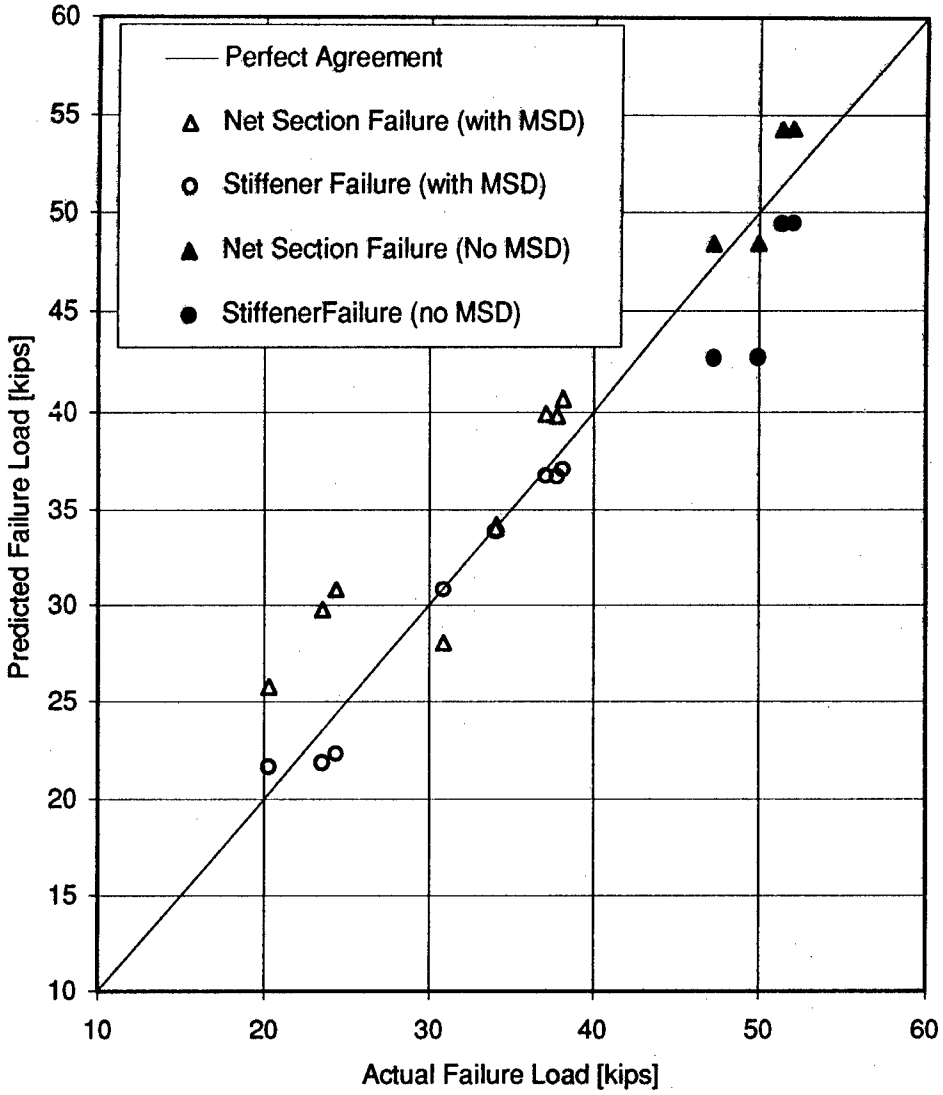

Figure 11: Comparison of actual and predicted panel failure loads by two different failure criteria for 15 inch wide, stiffened, 2024-T3 aluminum panels containing lead and in most cases MSD cracks.

A Proposed Engineering Approach to Assessing the Residual Strength of Aircraft Containing a Lead Crack Interacting with Multiple Site Damage

*Dr. G. Graham Chell
Mr. Matthew Ferrell
Dr. R. Craig McClung
Dr. Stephen J. Hudak, Jr.
Southwest Research Institute
6220 Culebra Road
San Antonio, Texas 78238-5166

Introduction

The loss of structural integrity of aircraft due to fatigue cracking at fastener holes and other stress concentration features is a major concern, particularly in relation to the operation of aging aircraft. An important aspect of this problem is the effect of multiple site damage (MSD) on the residual strength of an aircraft which suffers discrete source damage from, for example, projectiles caused by the disintegration of an engine disk. The effect of MSD on the residual strength of a structure with a lead crack is illustrated in Figure 1. This figure shows that as the applied stress is increased, the lead crack links with MSD to form a longer crack which eventually becomes unstable at a stress level that is below the residual strength of the original lead crack in the absence of MSD.

In this paper, a fracture mechanics model based on the elastic-plastic parameter, J, is proposed to address the problem of how to calculate the reduction in residual strength due to MSD. The objectives of the work are shown in Figure 2. The adopted technical approach utilizes a simplified version of the strip yielding model for a lead crack, modified to incorporate the effects of smaller multiple cracks located near the lead crack tips (Figure 3). This simplified engineering approach can capture most of the salient features of the problem: crack tip plasticity; interactions between the lead crack and multiple site damage; and ductile tearing leading to crack link-up and instability. It will need modification to incorporate aircraft structural details, such as tear straps and

stringers. However, Nilsson and Hutchinson (1993) have shown how such features can be modelled within the strip yielding model.

The developed fracture model has been applied to predicting the results of the wide plate fracture tests performed at NIST on lead cracks interacting with simulated multiple site damage (MSD). The agreement between the theoretical predictions and the experimental results is very good, both qualitatively and quantitatively, providing strong encouragement that the model can be successfully extended to cracking in more complex structures, such as aircraft.

J Estimation

The developed J estimation scheme is based on a modified version of the approach developed under EPRI sponsorship (for example, see Kumar et al., 1981 and Figure 4). In the modified approach the strip yielding model is combined with the reference stress approach to provide a J estimation scheme of the form shown in Figure 5. In this figure, J_{ssy} is a small scale yielding (ssy) estimate for J based on the strip yield solution for an embedded crack with N MSD cracks symmetrically distributed about its center, and J_p is a fully plastic solution based on the reference stress approach which also includes the presence of MSD cracks. The derivation of a J estimation scheme based on the reference stress approach is described by Ainsworth (1984). The meanings of the terms a, d_{MSD}, s_{MSD}, and a_{MSD} are shown in Figure 9. P is the applied load, σ_o the yield stress, α and n the constant and exponent in a Ramberg-Osgood representation of the stress-strain curve which has the form shown in equation (1), where E is Young's modulus and ϵ the strain corresponding to the stress, σ.

$$\epsilon = \frac{\sigma}{E} + \alpha \frac{\sigma_o}{E} \left(\frac{\sigma}{\sigma_o}\right)^n \qquad (1)$$

J_e is the linear elastic value of J for the lead crack and is related to the stress intensity factor under plane stress conditions by the equation

$$J_e = \frac{K^2}{E} \qquad (2)$$

and P_o is the value of P at which net section yielding occurs.

The ssy solution based on the strip yielding model is necessary for the model to capture the interaction of the lead crack-tip plastic zone with the MSD cracks, and the influence of this on J. The advantages of the strip yield model for this problem are that it can be expressed in terms of linear elastic weight functions, W(x,x) (Figure 6), and the model is known to be particularly suitable for through cracks in thin section structures deforming in plane stress. In the present approach, the weight function is simplified by using a form that is only applicable near the crack tip. This can be done because of the assumption of ssy.

The J-integral is related to the crack tip opening displacement, $\Phi(x=a)$, which is calculated using the equation shown in Figure 6. The expression for J_{ssy} is too complicated to present here; its evaluation involves an iterative procedure for determining the plastic zone size. However, the key equations are presented in Figure 6.

Crack instability occurs in ductile materials when the applied value of J becomes tangent to the toughness of the material expressed in terms of a J-resistance curve, $J_R(\Delta a_t)$, where Δa_t is the amount of ductile tearing (Figure 7).

Validation of Fracture Model

The proposed J estimation scheme has been applied to predicting the NIST wide plate test results (DeWit et al., 1995). A schematic of the test specimen used is shown in Figure 8. The plates were made of 2024-T3 aluminum alloy. The plates were 90 inches wide and 0.04 inch thick. Simulated MSD, in the form of flaws, were machined in the plates so that they were symmetrically located either side of the lead crack. The test matrix is summarized in Figure 9. The cracked plates were loaded to failure under remote tension and the applied load and extension of the lead crack recorded. Figure 10 summarizes the observed failure modes. In all but one case, MSD-9, the lead crack ran unstably through the MSD cracks after linking with the second MSD crack. In test MSD-9, lead crack instability occurred simultaneously with the lead crack linking with the first MSD crack.

The steps followed in the validation analysis were (Figure 11):

(1) Using the J estimation scheme a J-R curve was derived based on the load versus crack extension data for the NIST fracture tests MSD-1, MSD-2 and MSD-3, which were carried out on plates containing single cracks with no simulated MSD. The resulting J-R curve (Figure 12) was fitted by a power law (equation (3)) for tear lengths Δa_t<1.4",

$$J_R = 0.319+0.828\ (\Delta a_t)^{0.54} \quad (ksi\text{-}inch) \tag{3}$$

(2) The tensile stress-strain curve of the material was fitted by a Ramberg-Osgood law of the form shown in equation (1) where E=10,500 ksi, α=0.852, σ_o=53.3 ksi and n=15.4. This fitted curve is shown in Figure 13.

(3) The load versus crack extension curve was predicted by finding the value of load P which satisfies the equality (Figure 11).

$$J(a+\Delta a,\ d_{MSD},\ s_{MSD},\ a_{MSD},\ N,\ P) = J_R(\Delta a_t) \tag{4}$$

In performing the calculations, both yielding and potential ductile tearing at the MSD crack tips were ignored. A "local" instability for the lead crack is predicted from equation (4) when P attains a maximum as Δa_t increases for a given value of a. At local instability, the lead crack was assumed to link with the first MSD crack and its crack length was increased accordingly and the value of N reduced by 1. The recharacterized lead crack was then allowed to advance by ductile tearing at constant load P until equation (4) was again satisfied, when the lead crack was assumed to arrest. The load was then further incremented and a similar procedure followed to determine the load at which the next linkage between the lead crack and the next MSD crack occurred.

A typical calculated result showing the variation of J for NIST test MSD-4 which had three MSD cracks either side of a lead crack of half length 7 inch (see Figure 9) is shown in Figure 14. The behavior in Figure 14 was derived according to step (3). It can be seen that arrest is predicted after the lead crack links with the first MSD crack because the value of J falls as a consequence of the linkage. Additional load is required before the re-characterized lead crack simultaneously links with the second and third MSD cracks. After this link-up, the crack again arrests, and additional load is required to cause more ductile crack extension.

The reason why a lead crack can arrest after linking with an MSD crack is explained by reference to Figure 15. This figure shows calculated J solutions for the MSD-4 lead crack as a function of applied stress and assuming no ductile crack extension. As the applied stress increases the initial lead crack plastic zone spreads across the ligament between the first MSD crack and as this MSD crack is engulfed by the zone the value of J abruptly increases (curve A). As the applied stress continues to increase, further abrupt increases in J occur as the

second and third MSD cracks are engulfed by the plastic zone. Also shown in Figure 15 are the J solutions for two single cracks with no MSD. These solutions correspond to half crack lengths equal to the initial lead half crack length (curve B), and a half crack length equal to the initial crack linked to all three MSD cracks (curve C). Interestingly, after the plastic zone of the initial lead crack engulfs the first MSD crack its J value exceeds that for the deeper crack (curve C) evaluated at the same stress level. Hence, propagation of the initial lead crack to link-up with all three MSD cracks will cause a reduction in J and possible ductile crack arrest, depending on the J-resistance curve of the material. This was observed in the NIST test MSD-4. Figure 15 also displays the J values for the lead crack after it has linked with the first MSD crack and has two remaining MSD cracks (curve D), and when it has linked to the second MSD crack and has only one remaining MSD crack (curve E). Since curve A falls above curve D for all stress levels after the plastic zone engulfs the first lead crack, the results in Figure 15 predict that the lead crack will always arrest after the initial lead crack links with the first MSD crack. Furthermore, since curve E is either nearly equal to curve D (at high stress levels), or falls above it (at lower stress levels), the results in the figure also predict the simultaneous failure of the second and third MSD cracks, and the arrest of the resulting lead crack (curve C falls below curve E at high stress levels) after the plastic zone engulfs the first lead crack.

The results of applying steps (1) through (3) to the NIST results are shown in Figures 16 to 21 for tests MSD-4, MSD-5, MSD-7, MSD-8, MSD-9 and MSD-10, respectively. These figures show the predicted and observed applied loads plotted against half the instantaneous lead crack length. It can be seen that the SwRI J estimation scheme is in very good agreement with the experimental data in all cases.

Conclusions

The main conclusions of this work are shown in Figure 22. It is worth emphasizing that the fracture model developed at SwRI does not require elastic-plastic finite element computations. It is therefore computationally very quick (only a few seconds of computational time was needed on a 486 PC to analyze a single NIST test) and ideally suited for use in a probabilistic calculation. The strip yield model requires only linear elastic fracture mechanics solutions for its implementation, and the only additional information needed to implement the reference stress approach is the yield load, P_0, and the stress-strain curve. The model is easily extended to include a random distribution of MSD cracks, and can be modified to include the influence of reinforcing structural details, such as tear

straps and stringers, by linking the J estimation module to an appropriate structural analysis computer program.

Acknowledgements

We gratefully acknowledge Dr Roland DeWit at NIST who kindly made the detailed results of the NIST wide plate tests available to the authors.

References

R. A. Ainsworth, "The Assessment of Defects in Structures of Strain Hardening Material," Eng. Fract. Mechs., Vol. 19, pp. 633-642, 1984.

V. Kumar, M. D. German, C. F. Shih, "An Engineering Approach for Elastic-Plastic Fracture Analysis," EPRI NP 1931, July, 1981.

K.-F. Nilsson and J. W. Hutchinson, "Crack Arrest Capability of Tear Straps in Presence of Multi-Site Damage," Proc. 5th Int. Conf. Structural Airworthiness of New and Aging Aircraft, Hamberg, Germany, June, 1993.

R. DeWit, R. J. Fields, S. R Low III, D. E. Harne and T. Foecke, "Fracture Testing of Large-Scale Thin-Sheet Aluminum Alloy," Federal Aviation Administration Report DOT/FAA/AR-95/11, Office of Aviation Research, Washington D.C., 1995.

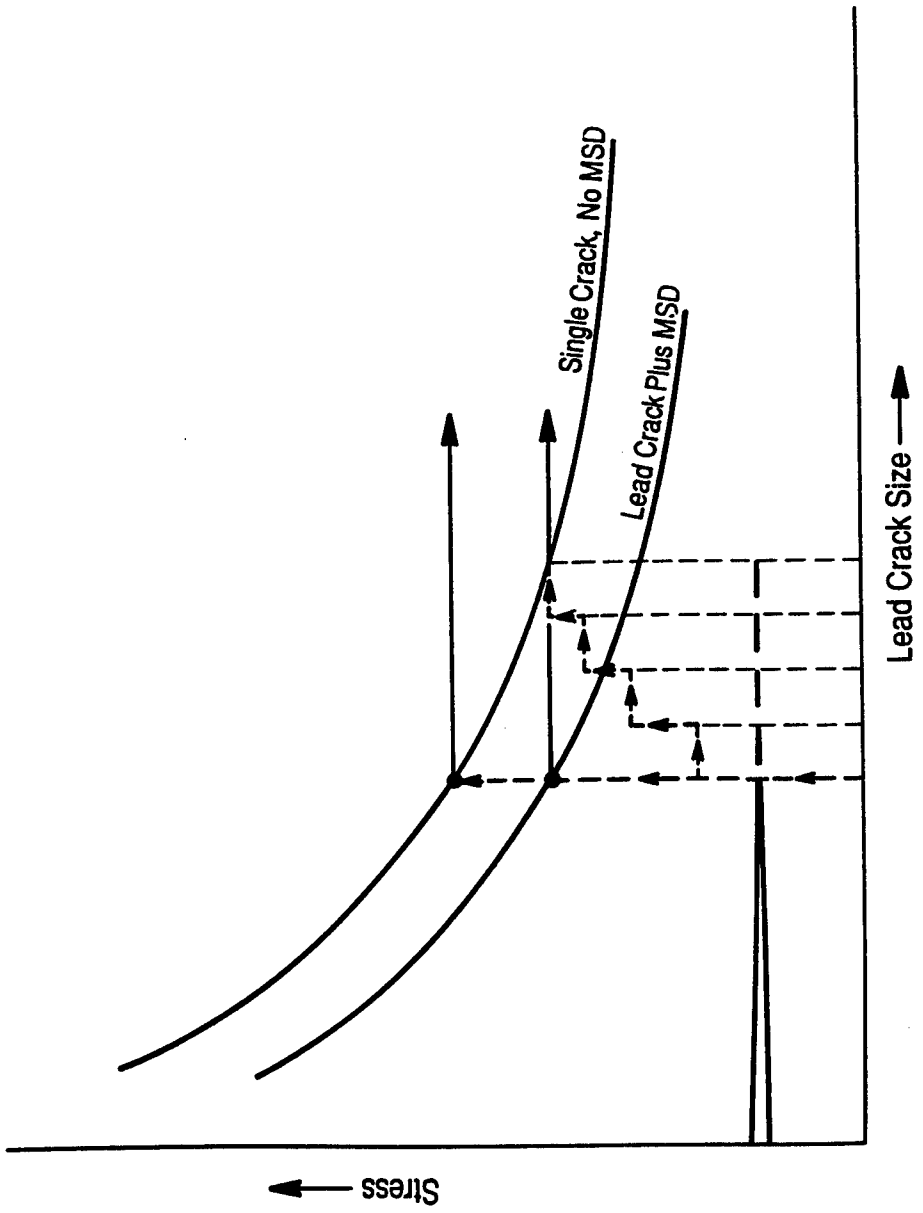

Figure 1: Residual strength diagram showing deleterious effect of MSD cracks.

- **Develop engineering approach to assess the residual strength**
- **Capture major aspects of the problem:**
  - **include crack tip plasticity and interaction with MSD cracks**
  - **include lead crack ductile instability criterion**
- **Develop relatively simple and computationally efficient fracture model**
- **Validate fracture model against NIST wide plate test data**

Figure 2: Objectives of the current work.

- **Use the elastic-plastic fracture mechanics parameter, J**
- **Estimate J using a modified version of the ERPI J estimation scheme**
- **Use strip yielding model to evaluate influence of MSD cracks on J in small scale yielding regime**
- **Use reference stress approach to evaluate influence of MSD cracks in large scale yielding regime**
- **Assume yielding and ductile crack extension occurs only at the lead crack tips**
- **Initially ignore detailed fracture behavior of MSD cracks (yielding and ductile tearing)**

Figure 3: The technical approach.

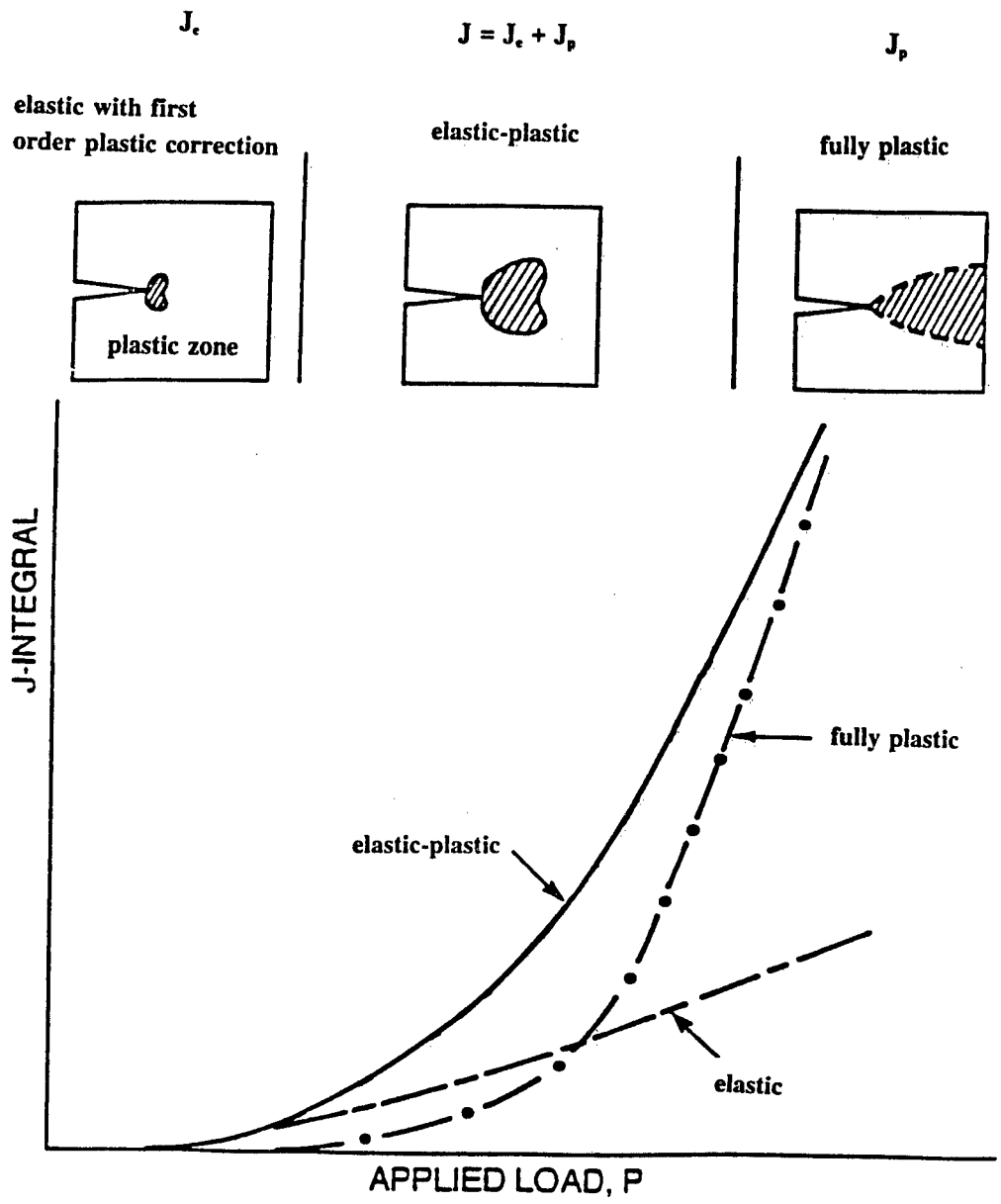

Figure 4: Schematic showing EPRI J estimation scheme.

$$J = J_{ssy} + J_p$$

$$J_{ssy} = J_{strip\ yield}(a, d_{MSD}, s_{MSD}, a_{MSD}, N, P, \sigma_o)$$

$$J_p = \alpha\ J_e(a)\ \left(\frac{P}{P_o}\right)^{n-1}$$

$$P_o = t\ \sigma_o\ (W - 2a - 2N \times 2a_{MSD})$$

Figure 5: SwRI J estimation scheme for lead crack interacting with MSD cracks.

$$J_{strip\ yield} = \sigma_o \ \Phi(x-a)$$

$$\Phi(x) = \frac{2}{E} \int_{x}^{a+s} W(x',x) \ [K(a+s,x',\sigma) - K(a+s,a,x',\sigma_o) \ dx'$$

$$K(a+s,\sigma) = K(a+s,a,\sigma_o)$$

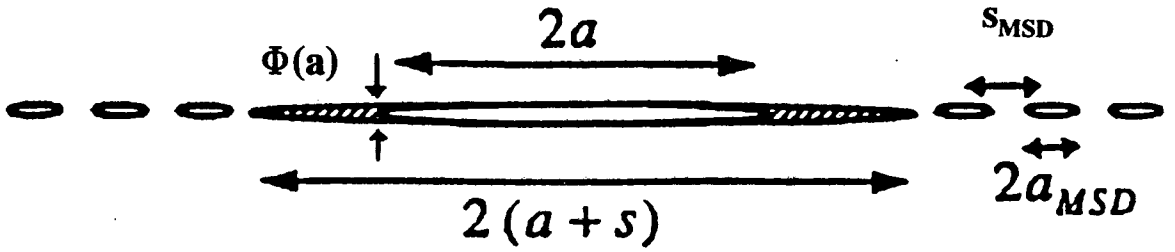

Figure 6: J estimated using the strip yielding model.

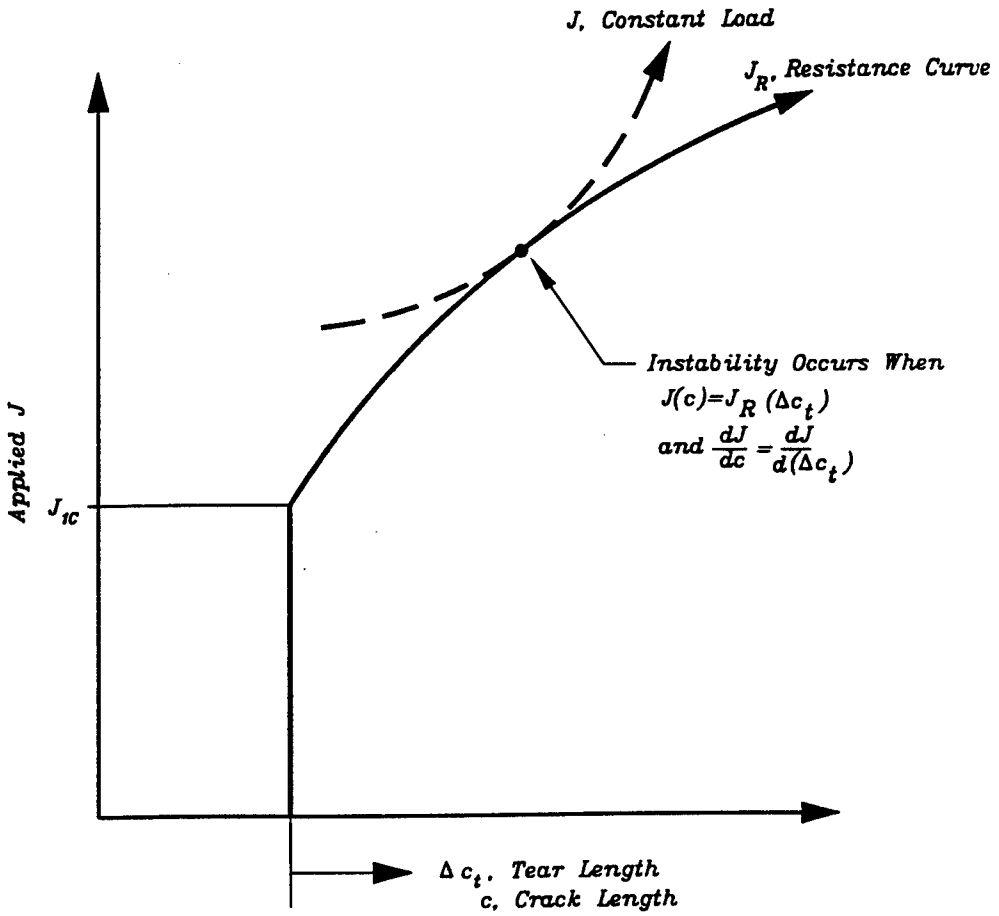

Figure 7: J-based ductile fracture criterion.

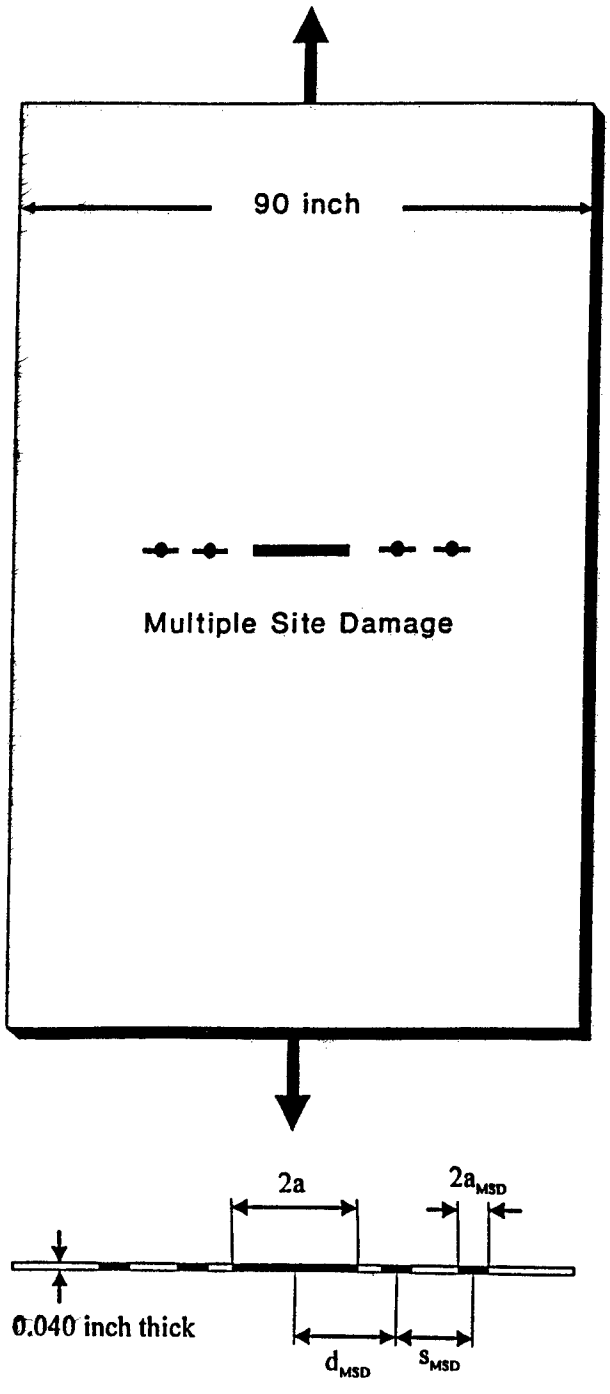

Figure 8: NIST wide-plate test set-up.

Test Number	Crack length 2a (inch)	d_{MSD} (inch)	s_{MSD} (inch)	$2a_{MSD}$ (inch)	Number per side
MSD-4	14	7.5	1.0	0.4	3
MSD-5	5.6	3.5	1.5	0.6	3
MSD-7	20	10.5	1.5	0.5	5
MSD-8	19	10.5	1.5	0.5	10
MSD-9	10	6.5	1.0	0.4	10
MSD-10	20	10.5	1.5	0.5	5

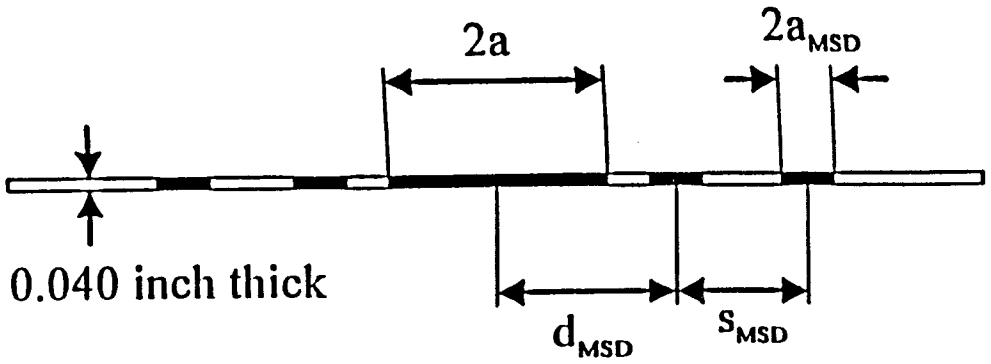

Figure 9: NIST test matrix.

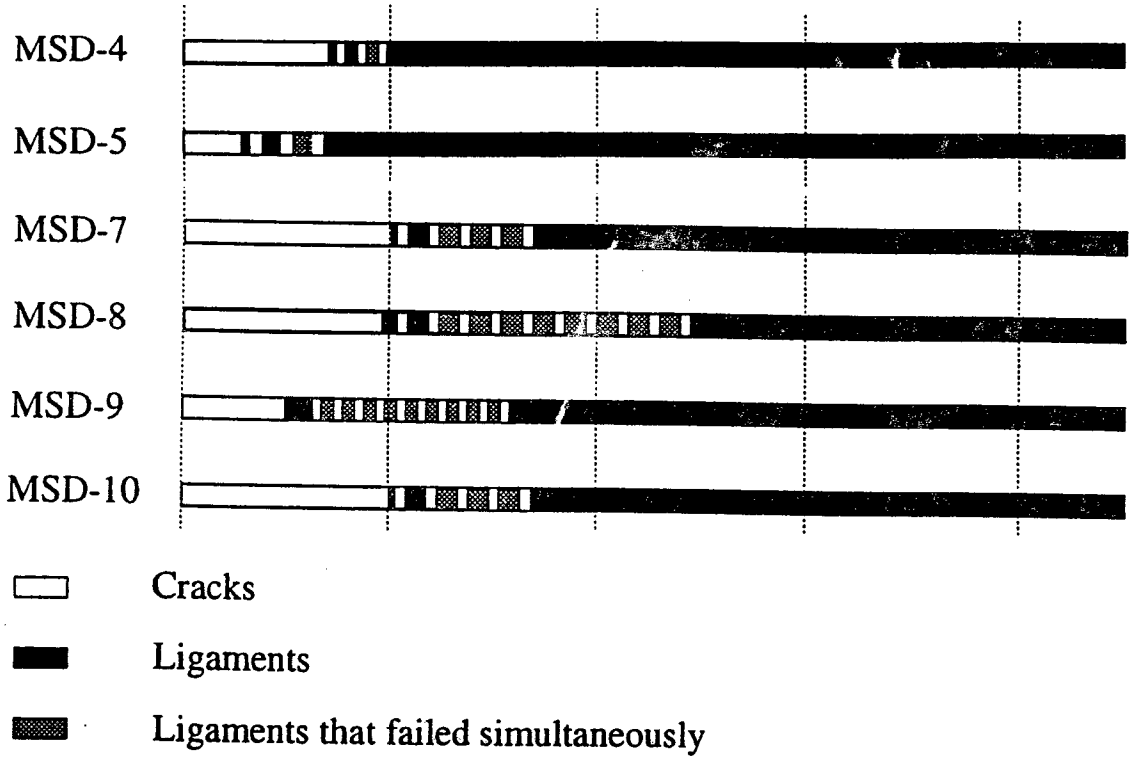

Figure 10: Ligament failure modes for the NIST tests analyzed.

- Determine J-resistance curve from NIST load versus crack length data for single cracks without MSD
- Fit Ramberg-Osgood law to stress-strain data for 2024-T3 aluminum alloy
- Determine applied load, P as a function of Δa_t by solving

$$J(a+\Delta a_t,\ d_{MSD},\ s_{MSD},\ a_{MSD},\ N,\ P) = J_R(\Delta a_t)$$

- Local instability occurs at a Δa_t where P attains a maximum value, P_{max}
- At P_{max}, lead crack and first MSD crack link-up and N reduces by 1
- Determine P as a function of Δa_t for the re-characterized lead crack and search for new P_{max}

Figure 11: The validation procedure.

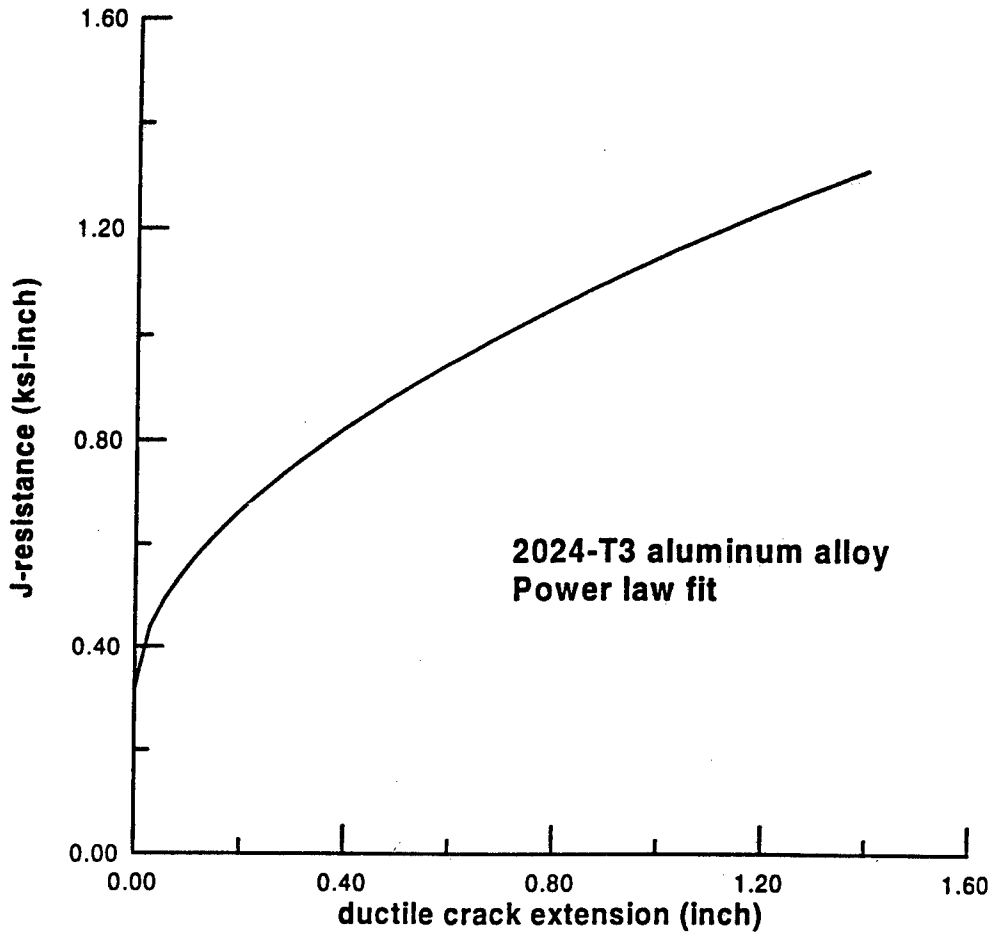

Figure 12: Fitted J-resistance curve for 2024-T3 aluminum alloy tested by NIST.

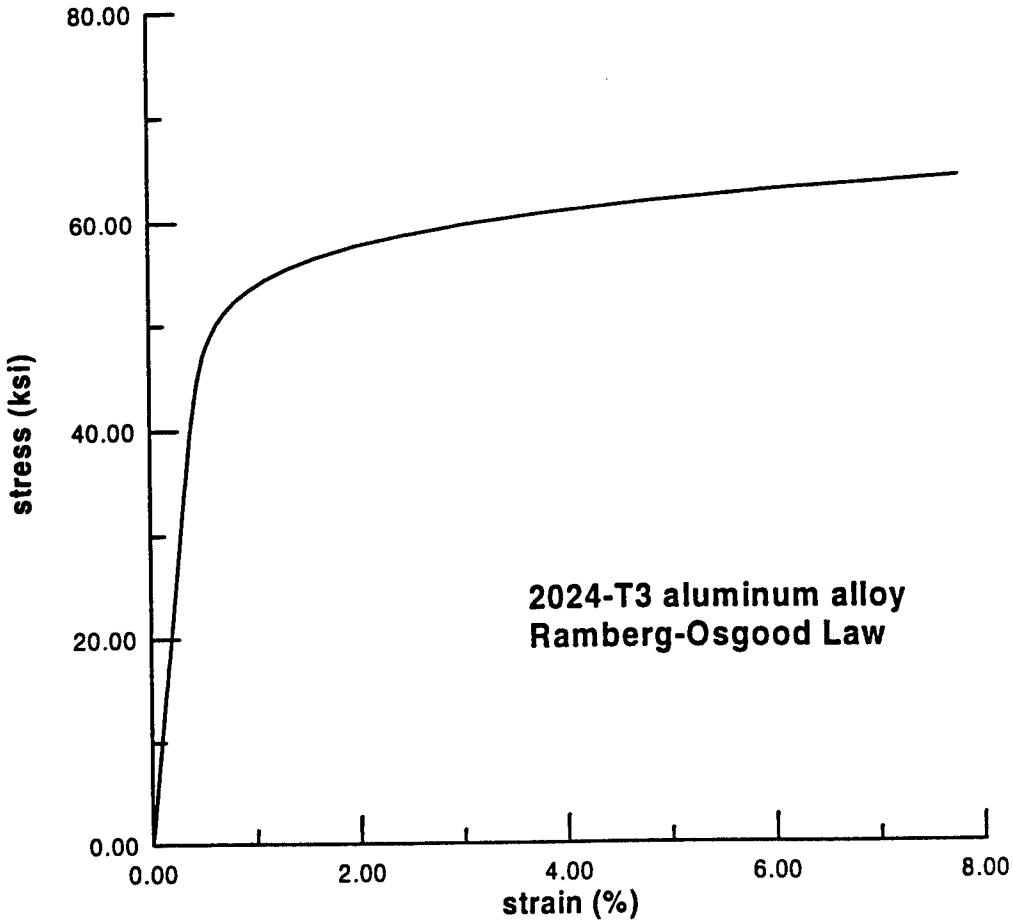

Figure 13: Fitted stress-strain curve for 2024-T3 aluminum alloy tested by NIST.

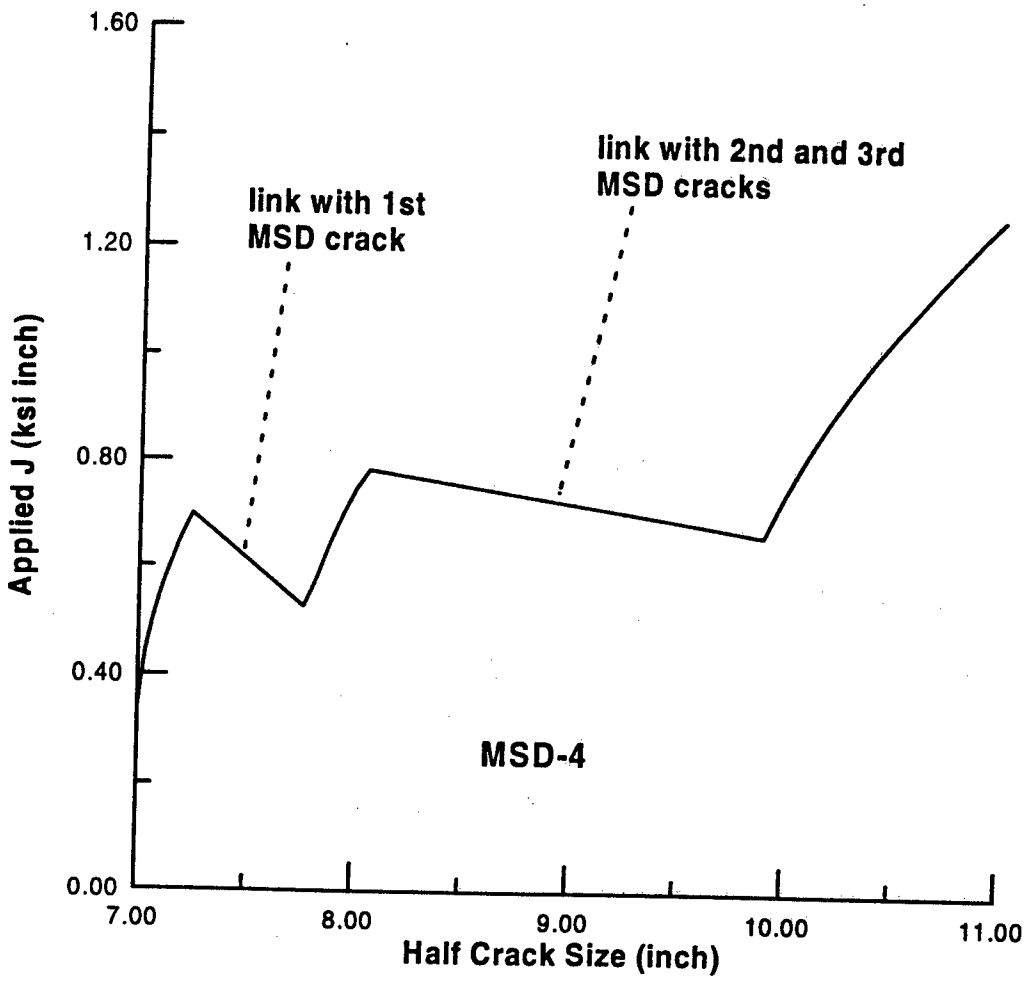

Figure 14: Predicted variation of J for NIST test MSD-4.

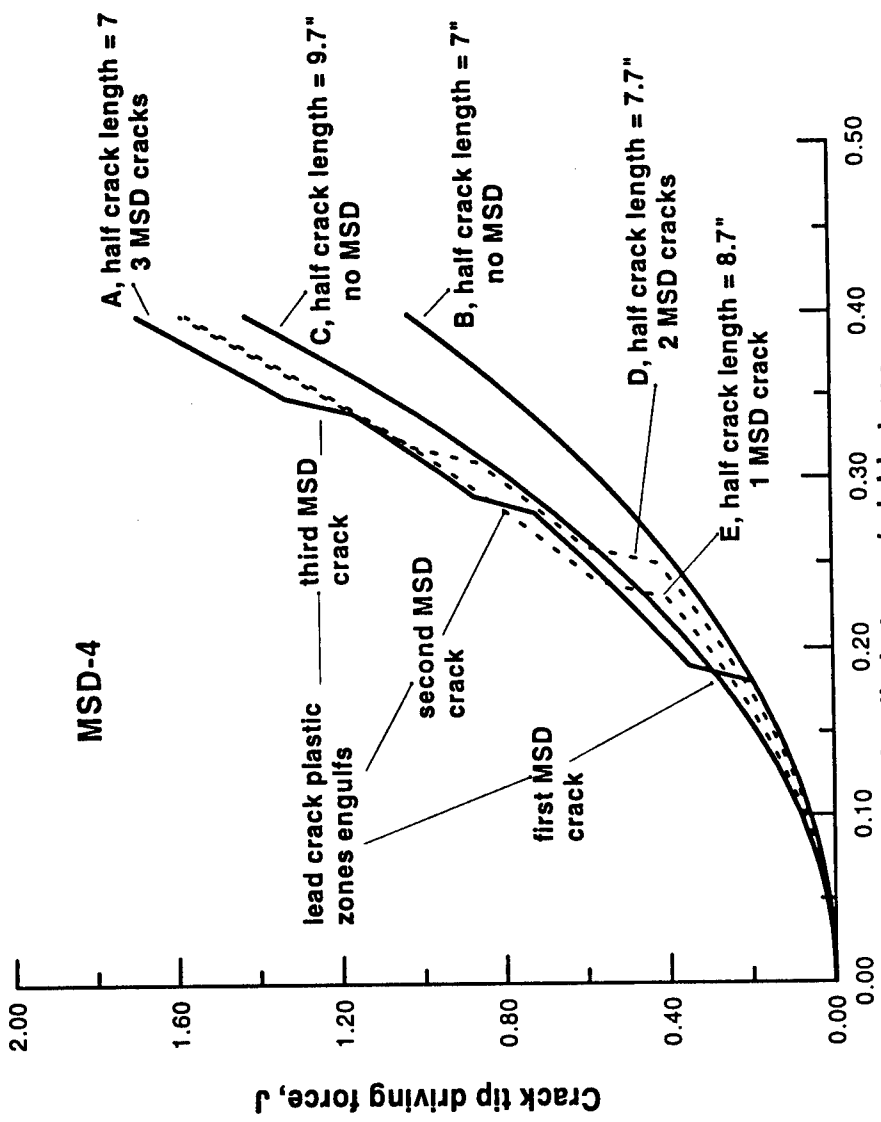

Figure 15: Variation of J with applied stress for different lead crack and MSD crack configurations demonstrating the predicted crack arrest capability of NIST test MSD-4.

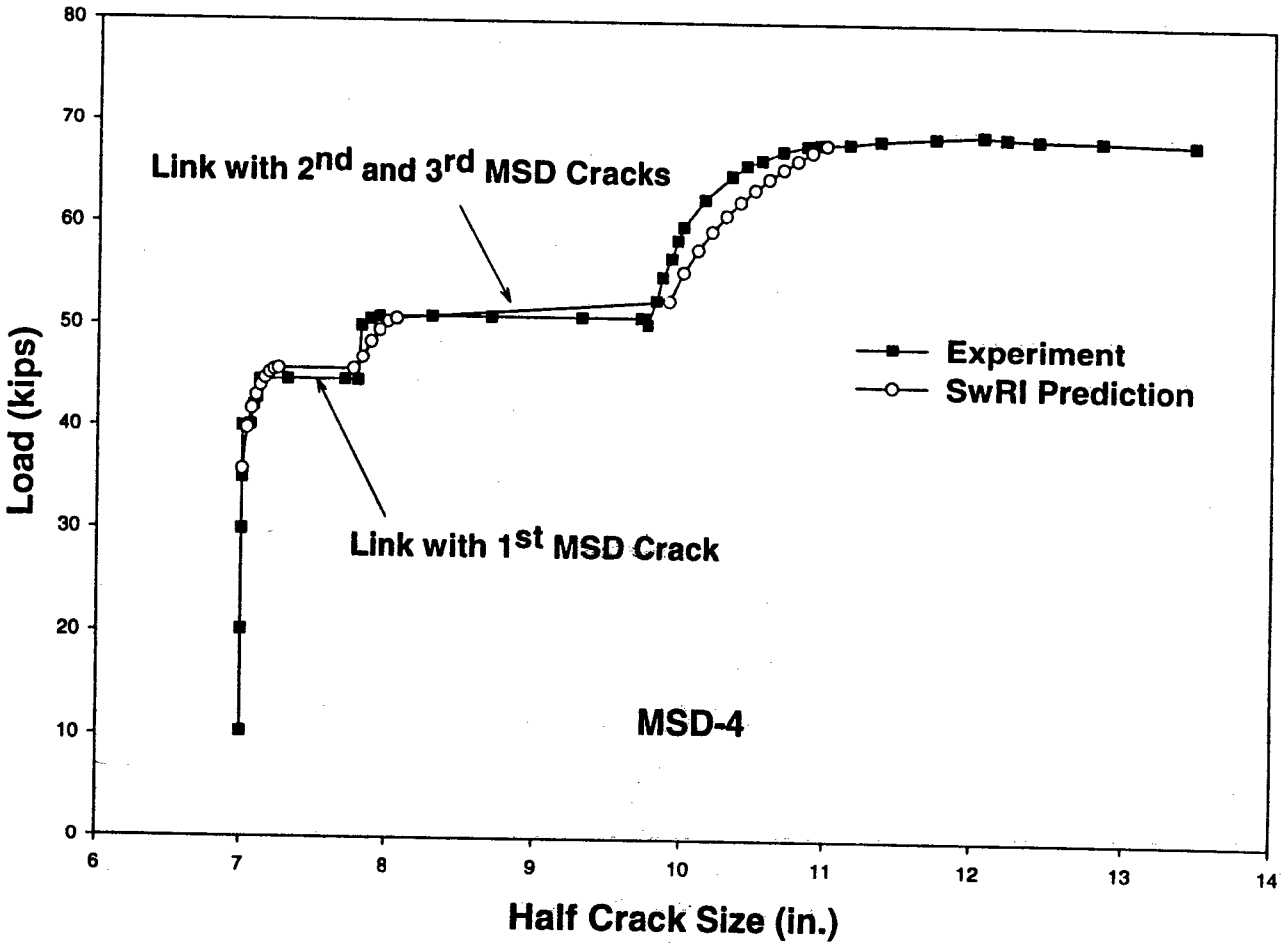

Figure 16: Comparison of predicted and observed fracture behaviors for NIST test MSD-4.

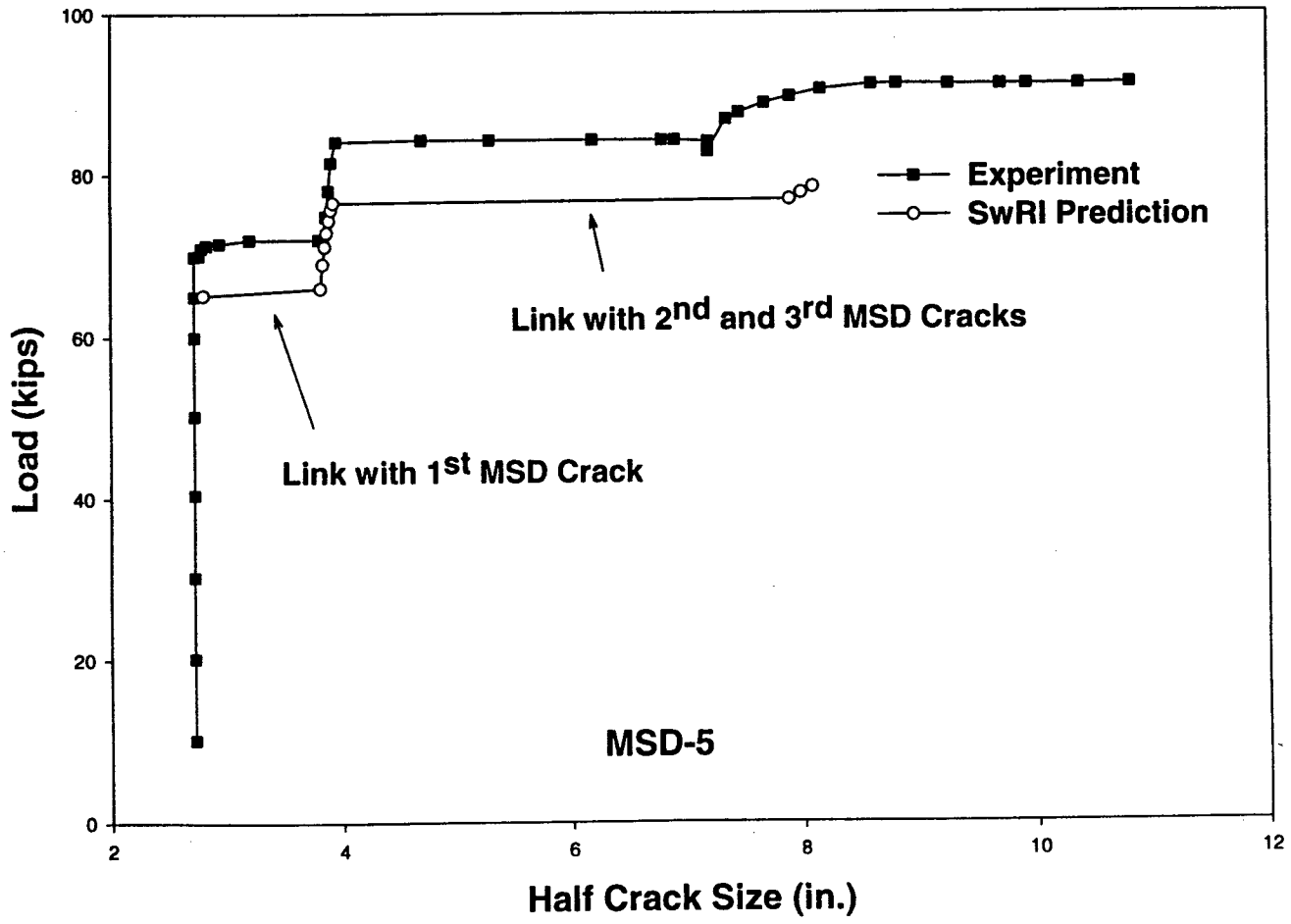

Figure 17: Comparison of predicted and observed fracture behaviors for NIST test MSD-5.

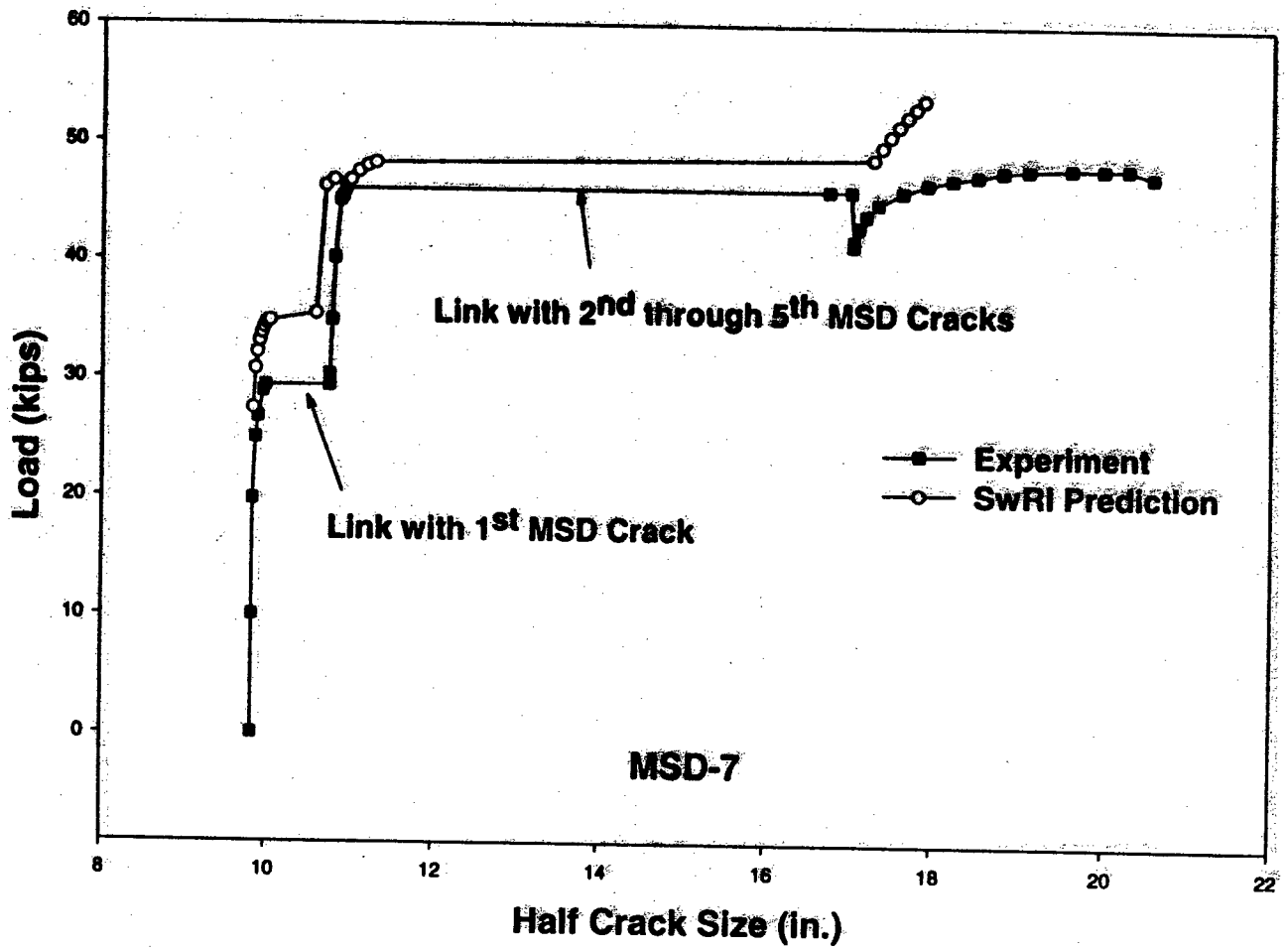

Figure 18: Comparison of predicted and observed fracture behaviors for NIST test MSD-7.

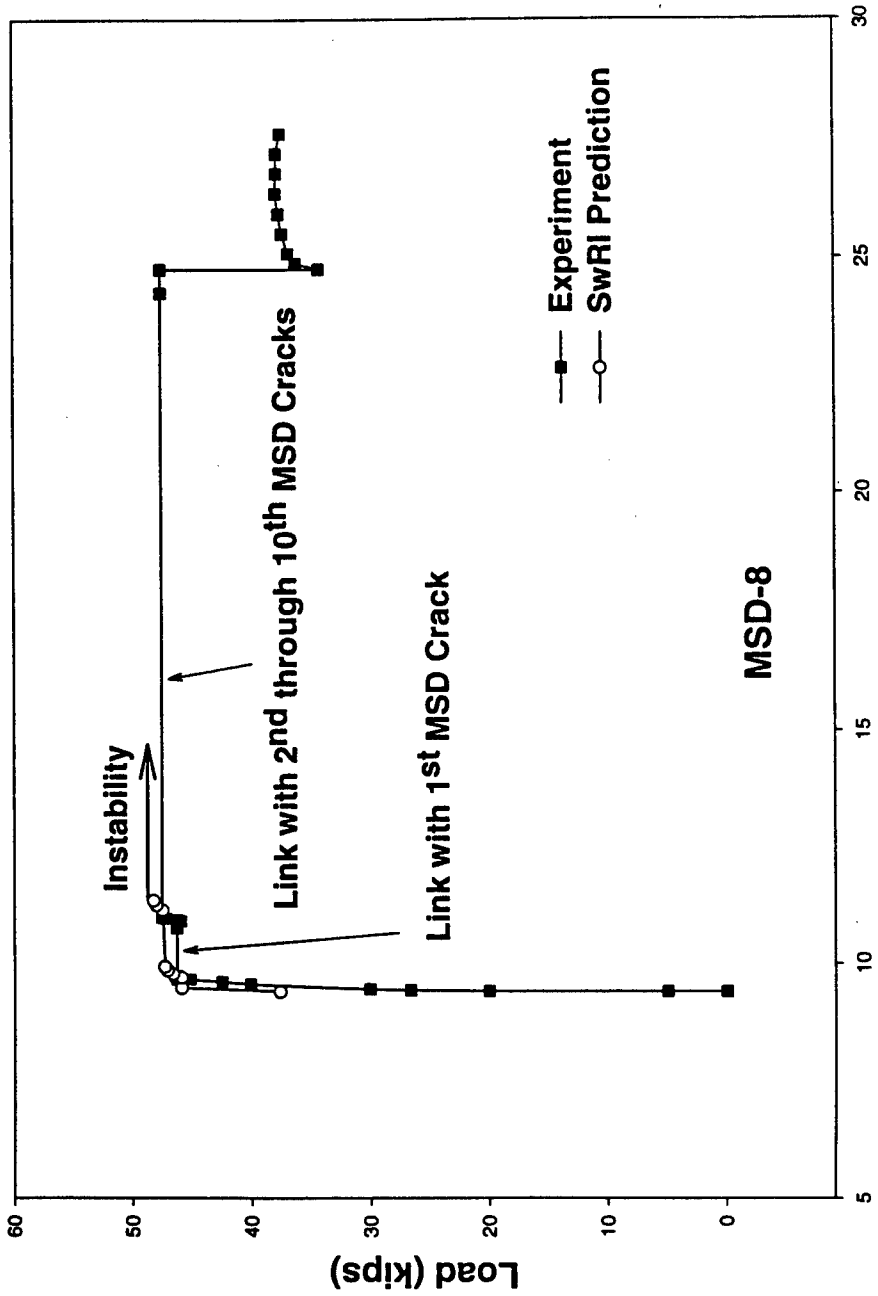

Figure 19: Comparison of predicted and observed fracture behaviors for NIST test MSD-8.

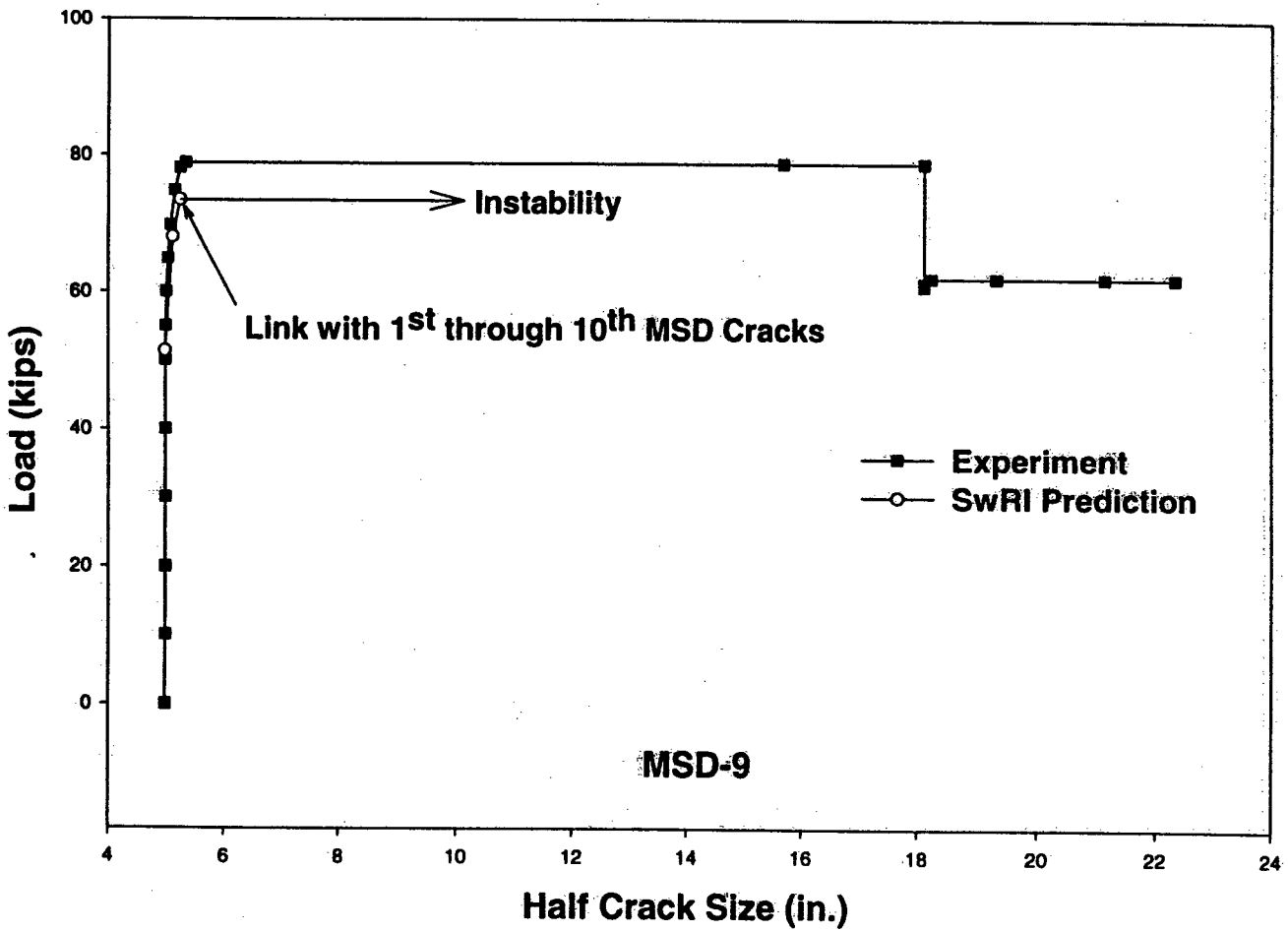

Figure 20: Comparison of predicted and observed fracture behaviors for NIST test MSD-9.

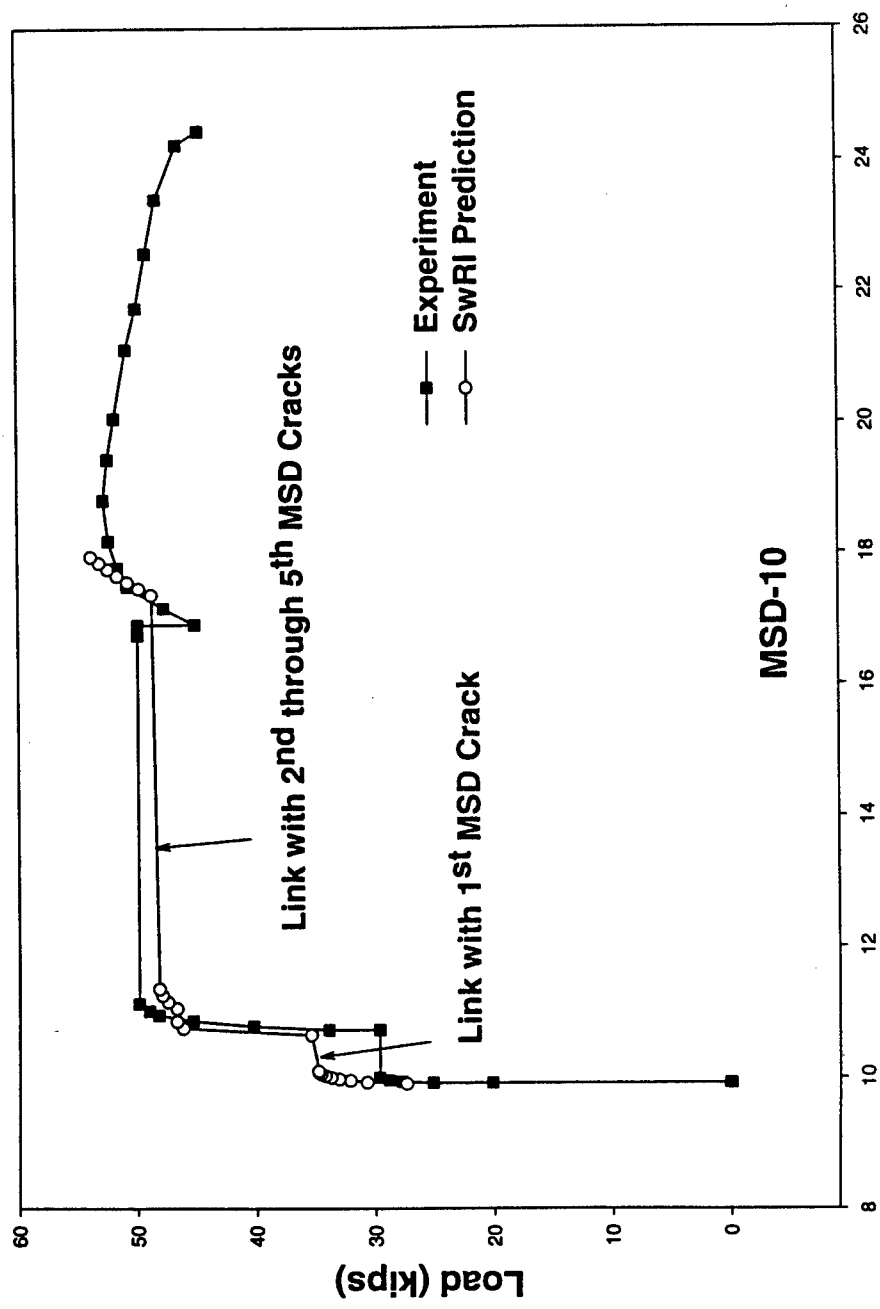

Figure 21: Comparison of predicted and observed fracture behaviors for NIST test MSD-10.

- A relatively simple elastic-plastic fracture mechanics model has been developed to describe the ductile fracture behavior of a lead crack interacting with MSD cracks
- The model is computationally efficient and avoids the need for elastic-plastic finite element fracture mechanics calculations
- In the model, the influence of the MSD cracks on the lead crack is due to the reduction in load bearing area produced by the MSD cracks in the plastic zone of the lead crack
- The model has been successfully validated against the NIST wide plate test results
- The model can be extended to address random distributions of MSD cracks and shell reinforcements, such as tear straps and stringers.

Figure 22: Conclusions.

Enhanced *R*epair *A*ssessment *P*rocedure and *I*ntegrated *D*esign *(RAPID)*

Jin Yu
C. C. Chen
Miles Nomura
Ching Hsu
Mary Kubo
MCDONNELL DOUGLAS

John G. Bakuckas, Jr.
Catherine A. Bigelow
Paul V. Nguyen
Paul W. Tan

Richard Blauvelt
Alan Copeland
NORTHROP GRUMMAN

USAF ASIP Conference
San Antonio, Texas
December 3, 1996

1

Outline

- Objective
- RAPID Overview
- Damage Tolerance Methodology
  - Fastener Load Calculation
  - Initial Flaw Configuration and Subsequent Growth
  - Stress Spectrum Development
  - Crack Growth Calculation
  - Residual Strength Calculation
  - Inspection Schedule
- Test Validation
- Summary

Objective

Develop A ***R***epair ***A***ssessment ***P***rocedure And ***I***ntegrated ***D***esign (***RAPID***) Tool To Perform Static Strength and Damage Tolerance Analyses Of Aircraft Structural Skin Repairs

3

Repair Assessment Procedure and Integrated Design (RAPID)

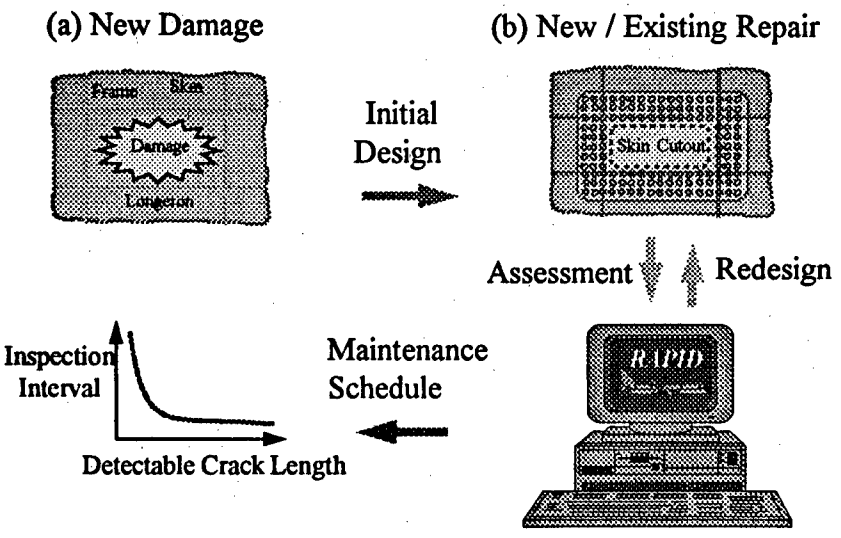

RAPID Repair Configurations

Type I

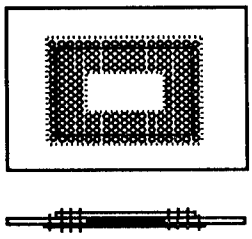

Type II

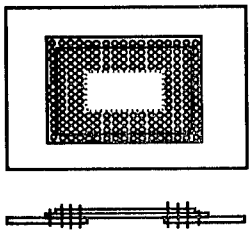

Type III

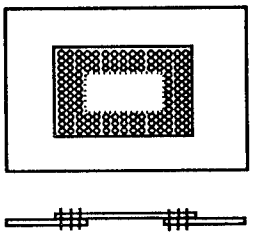

5

RAPID Repair Configuration

Complex Repairs:

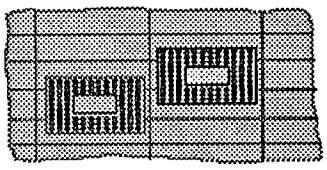

Repairs Near Other Repairs

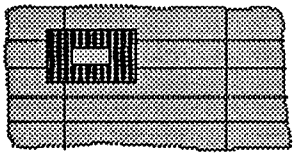

Repairs Over Stiffeners

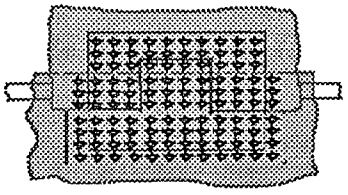

Repairs Over Joints

RAPID - Sponsorship

- Phase I (June 1993 - March 1995)
  - Technical Manager: Paul Tan (FAA-TC)
  - Originator: Tom Swift (FAA-NRS)
  - Sponsors:
    - Bobby Sexton (FAA-ACE)
    - Rich Yarges (FAA-ANM)
- Phase II (April 1995 - January 1997)
  - Technical Manager: Paul Tan/John Bakuckas (FAA-TC)
  - Originators:
    - Tom Swift (FAA-NRS)
    - Mark Wilson/Debbie Bailey (USAF)
  - Sponsors:
    - Bobby Sexton (FAA-ACE)
    - Jack Lincoln (USAF)

RAPID - Development Team

- McDonnell Douglas Aerospace
  - Jin Yu
  - C. C. Chen
  - Miles Nomura
  - Ching Hsu
  - Mary Kubo
- Northrop Grumman Corporation
  - Richard Blauvelt
  - Alan Copeland
- FAA-TC
  - John G. Bakuckas
  - Catherine A. Bigelow
  - Paul V. Nguyen
  - Paul W. Tan

RAPID System Architecture

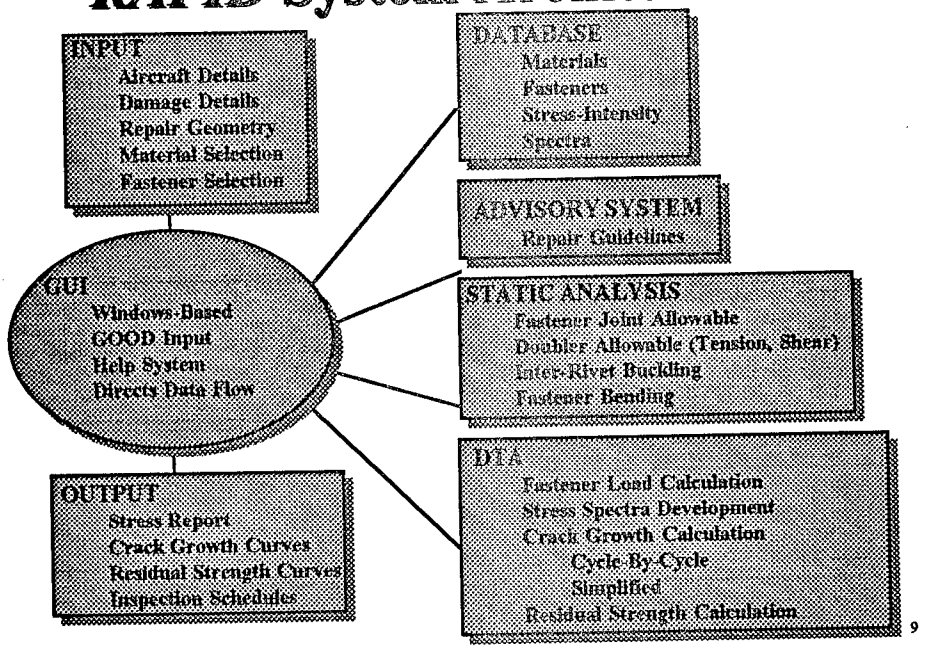

9

RAPID Graphical User Interface

Multi-Document Interface

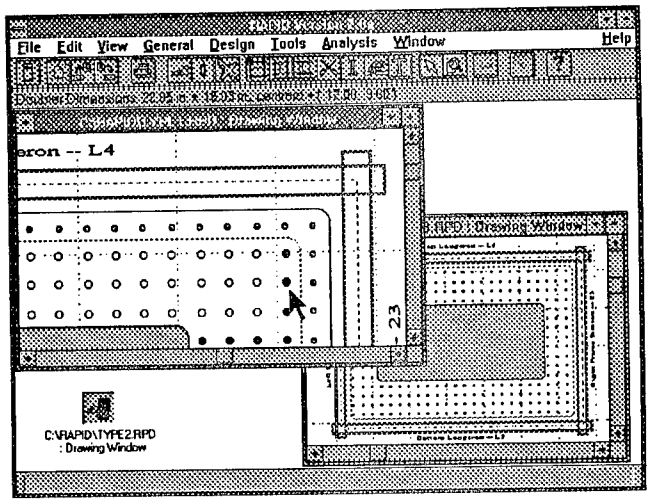

10

Product Delivery Schedule

◆ Prototype	Simple Fuselage Repairs	July 1994
◆ Beta Version I	Simple Fuselage Repairs	September 1995
◆ *RAPID* Version I	Simple Fuselage Repairs	March 1996
◆ Beta Version II	Complex Repairs	January 1997
◆ *RAPID* Version II	Complex Repairs	March 1997

11

RAPID Industry Demographics

Industry	# Reps.	Major Companies		
Major Airlines	30	• American • Continental • Delta • Northwest	• TWA • United • USAir • KLM	• Canadian Airlines • Quantas • Swissair
Regional and Cargo Airlines	20	• RAA • American Flagship • Continental Express	• Piedmont • Simmons • UPS	• USAir Express • Federal Express
Modifications and Repairs	15	• Chrysler • E-Systems	• Dee Howard • Ameriflight	• Flight Structures • Tramco
Manufacturer	42	• Airbus • Boeing • Douglas • Lockheed-Martin	• Jetstream • Embraer • Raytheon • Cessna	• SAAB • Gulfstream • Canadair
Certification/ Consultants	100	• FAA ACO (LA, Seattle, Atlanta, NY) • Structural Integrity Engineering	• Atlantic Aviation • Foster-Miller Inc,	• Blue Sky Aviation
Government, DOD	48	• USAF (WP, Tinker, Kelly, Robins) • US Navy	• NASA • Royal Air Force	• DSTO

12

RAPID Damage Tolerance Analysis

- Fastener Load Calculation
- Initial Flaw Configuration and Subsequent Growth
- Stress Spectra Development
- Crack Growth Calculation
- Residual Strength Calculation
- Inspection Schedule Determination

13

Fastener Loads

◆Determine Fastener Loads at The Center and Corner Fastener in Critical Row:

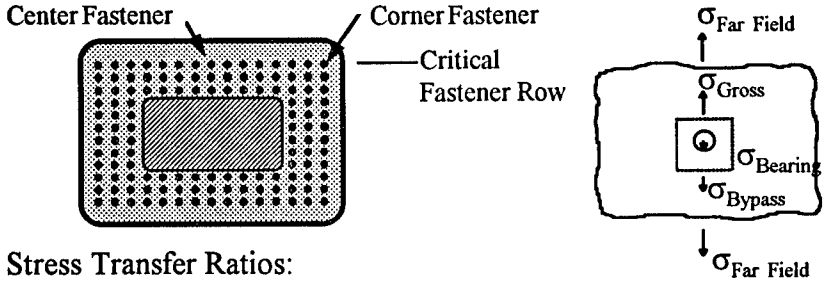

◆ Stress Transfer Ratios:

Stress Scale Factor (SSF) = σ_{Gross} / $\sigma_{Far\ Field}$

Bearing Factor (BRF) = $\sigma_{Bearing}$ / σ_{Gross}

Bypass Factor (BPF) = σ_{Bypass} / σ_{Gross}

14

Initial Flaw Geometry and Growth

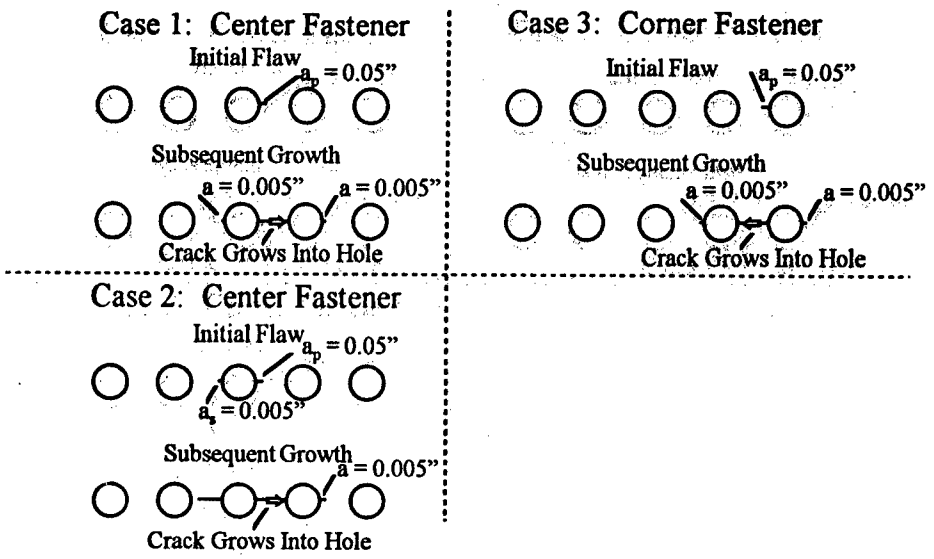

15

Stress Spectra Development

- **Generic Wide Body**
- **Generic Narrow Body**
- **User Defined**
- **Equivalent Stress**

16

RAPID Generic Stress Spectra Development

- Mission Profile
  - Aircraft Parameters
  - Usage Parameter
- C. G. Load Spectra
  - Flight Loads: Maneuver, Gust, Pressure
  - Ground Loads: Taxi, Takeoff, Landing
- Load-Stress Transfer

17

Aircraft and Usage Parameters

Parameters	NB	WB
Flight Distance (Miles)	712	3500
Operation Empty Weight (lbs)	78,500	300,000
Maximum Payload (lbs)	44,000	135,000
Average Payload Factor	70%	70%
Cruise Altitude (ft)	35,000	39,000
Fuel Consumption Rate (lbs/hr)	5,600	15,500
Reserve Fuel Weight (lbs)	8,500	23,000
Takeoff Speed (Mach)	0.22	0.22
Cruise Speed (Mach)	0.76	0.80
Landing Speed (Mach)	0.20	0.20
Climb Duration (hr)	0.40	0.40
Descent Duration (hr)	0.40	0.40

18

Generic Mission Profile

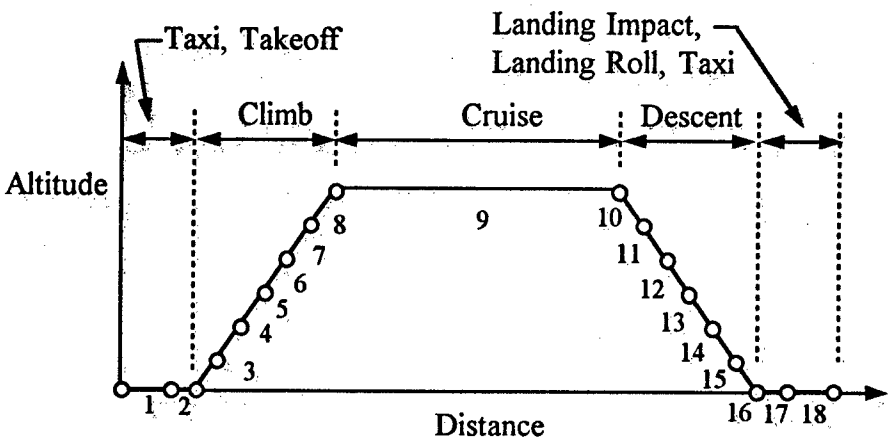

19

Typical Load Sequence

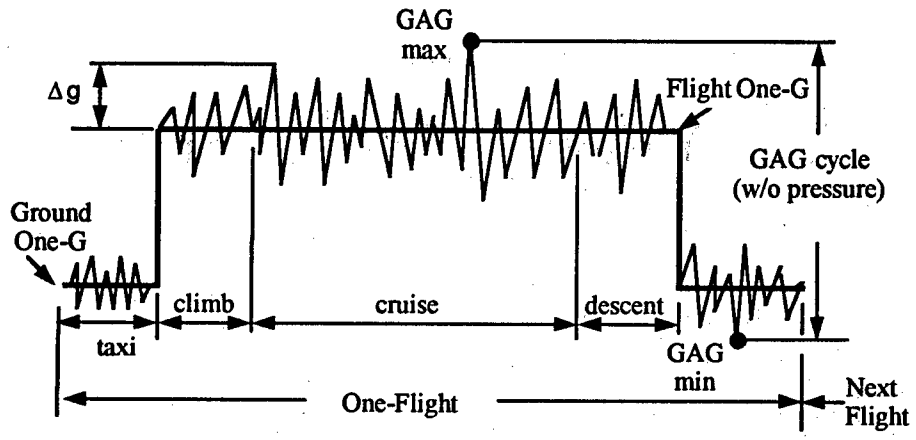

20

Stress Spectra Development

Fuselage is Divided Into Four Zones

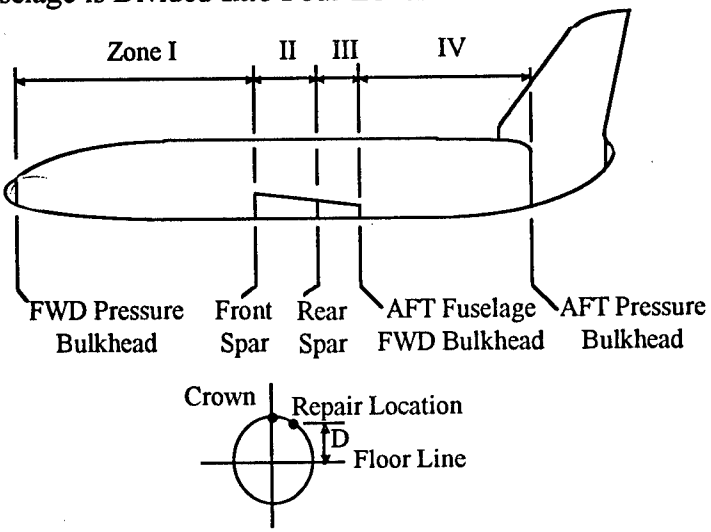

21

Stress Spectra Development

Longitudinal Stress Distribution at Crown Area

GAG maximum stress = $pR / 2t + \alpha \sigma_{1g}$ $(1.3 < \alpha < 1.5)$

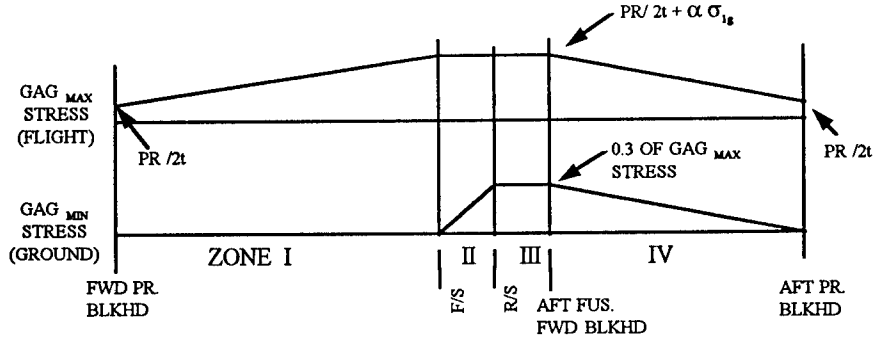

One-G Stress (σ_{1g}) is Estimated Based on Material Allowable, Design Limit Load and Payload Factor

22

Stress Spectra Development

Longitudinal Stress Distribution at Floor Line Area

$$\sigma_{GAG\ Max.} = \frac{pR}{2t}$$

Linear Interpolation Used Stress Between Crown and Floor Line

23

Stress Spectra Development

Circumferential Stress Distribution

- **GAG Maximum Stress**

$$\sigma_{GAG\ Max.} = \frac{pR}{t}$$

- **GAG Minimum Stress**

$$\sigma_{GAG\ Min.} = 0$$

24

Crack Growth Model

- Simplified Crack Growth Model

$$\frac{da}{dN} = C\left\{(1-R)^q K_{max}\right\}^p$$

- Cycle-By-Cycle Crack Growth Model
  - Crack Growth Data Look-Up
  - Retardation, Generalized Willenborg Model

25

Crack Growth Model:
Cycle-By-Cycle Validation

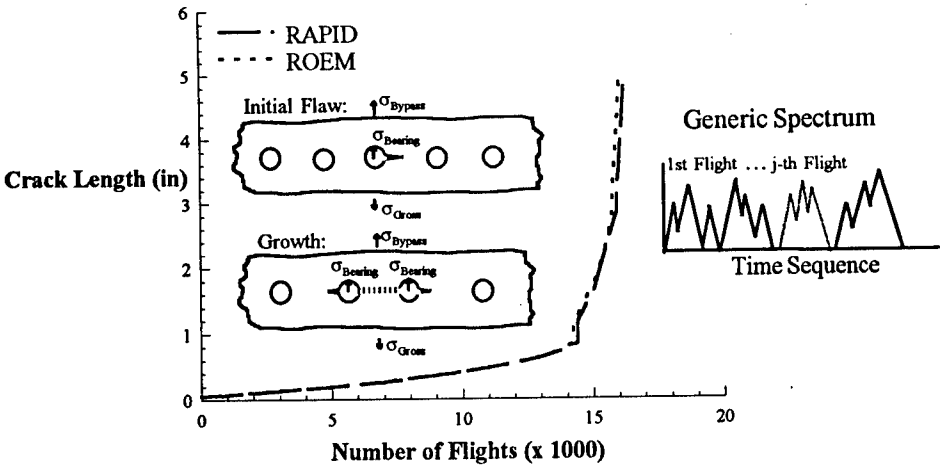

26

Crack Growth Model:
Simplified Analysis Validation

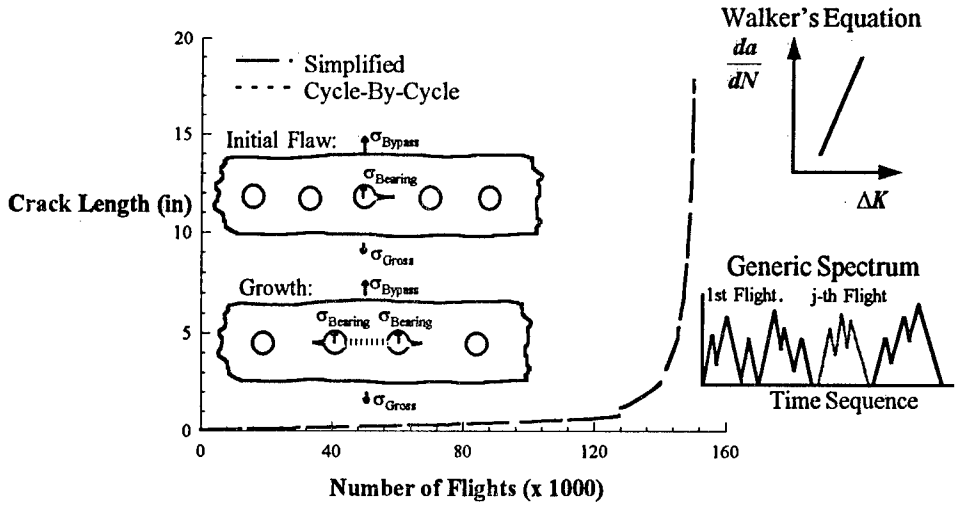

27

Crack Growth Model:
Simplified Analysis Validation

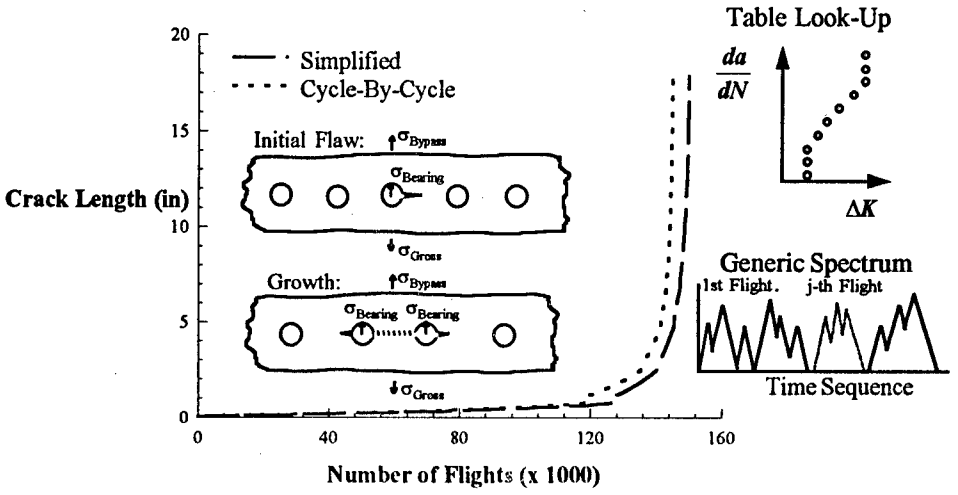

28

Residual Strength

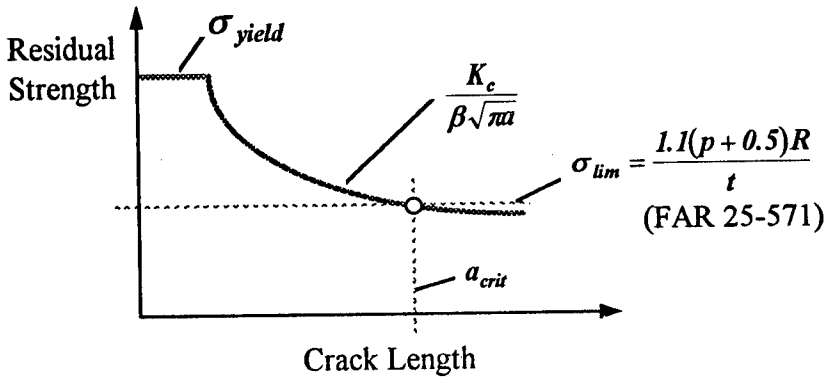

Inspection Schedule

- **Inspection Threshold:**

$$N_{thres} = \frac{N_{crit}}{2}$$

where N_{crit} is the number of flights for the crack to grow from initial flaw size to the critical size, a_{crit}

- **Inspection Interval:**

$$N_{int} = \frac{N_{crit} - N_{det}}{2}$$

where N_{det} is the number of flights to reach the detectable crack size for a specific inspection method

Test Validation

- Testing Conducted By Sandia National Labs
- Specimen Configuration and Loading:

Skin:
- Thick: 0.04"
- Height: 34"
- Width: 12"

Doubler:
- Thick: 0.05"
- Height: 7.75"
- Width: 8.5"

Cut-Out:
- Height: 2.75"
- Width: 3.5"

Fastener Arrangement:
- Countersunk Angle: 100°
- Diameter: 0.15625"
- Pitch: 0.75"
- Edge Dist.: 0.5"

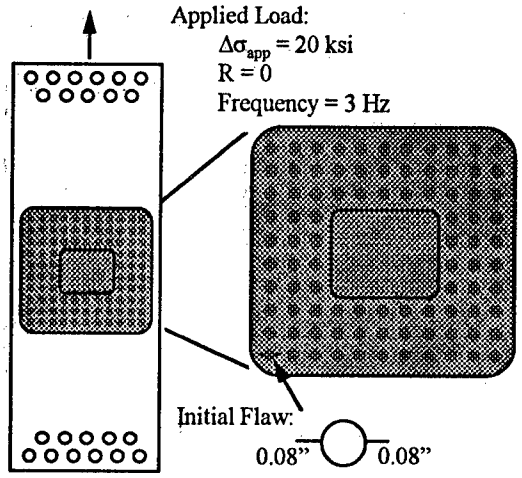

31

Test Validation

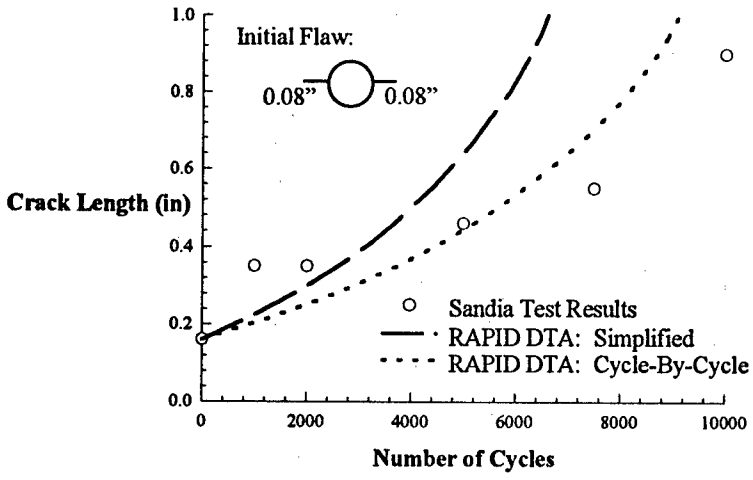

32

Summary

- ***RAPID*** is a Simple, User-Friendly PC-Based Repair Tool:
  - Windows™-Based Graphics User Interface
  - Both Static and Damage Tolerance Analyses to Evaluate Fuselage Skin Repairs
  - Advisory System to Provide Repair Procedure Guidelines
  - Extensive Database Accessible For Additions
- Software Availability:
  - Prototype, Fuselage Skin Repairs - July 1994
  - Version I, Fuselage Skin Repairs - March 1996
  - Version II, Complex Repairs - March 1997
- Over 300 Requests For ***RAPID*** 1.2

33

Summary

- Enhancements Include:
  - Two Dimensional Model To Calculate Fastener Loads
  - Generic Stress Spectra
    - Wide Body
    - Narrow Body
    - User Specified
    - Equivalent Stress
  - Crack Growth Models Include Simplified and Cycle-By-Cycle
    - Circumferential and Longitudinal Crack Growth
    - Retardation Effects (Generalized Willenborg Model)
- ***RAPID*** Home Page For Internet Access:

  http://www.asp.tc.faa.gov/RAPID
- ***RAPID*** Results In Reasonable Agreement With Sandia Experimental Results

34

The Onset of Multiple Site Damage and Widespread Fatigue Damage in Aging Airplanes

David Y. Jeong
U.S. Department of Transportation
Volpe National Transportation Systems Center
Cambridge, MA 02142 USA

and

Pin Tong
Hong Kong University of Science and Technology
Clear Water Bay, Kowloon, Hong Kong

ABSTRACT. This paper presents a methodology for predicting the thresholds of multiple site damage and widespread fatigue damage in fuselage lap splices. Widespread fatigue damage is a type of multiple cracking that reduces the airframe residual strength to a level below the damage tolerant requirement. The MSD threshold refers to the point in the lifetime of an airplane when two adjacent collinear fatigue cracks can linkup at the allowable stress. The WFD threshold is the point in time when linkup of a primary crack created from accidental damage and secondary cracks created from fatigue can result in a catastrophic failure. The methodology presented in this paper combines results from residual strength analysis and fatigue crack growth testing to determine these thresholds. In particular, a displacement compatibility approach is adopted to calculate residual strength in curved stiffened panels tested in the laboratory. The laboratory experiments also include fatigue testing of full-scale panels containing a debonded lap splice. Based on this methodology, the threshold of widespread fatigue damage for these laboratory panels, adjusted for zero minimum-stress cycling, is between 32,300 and 43,500 cycles, and the threshold of multiple site damage is about 70,600 cycles.

1.0 INTRODUCTION

The foremost technical challenge related to aging aircraft is the problem of widespread fatigue damage (WFD). Widespread fatigue damage is a type of multiple cracking that reduces the airframe residual strength to a level below the damage tolerant requirement. Two sources of widespread fatigue damage have been identified [1]. They are characterized by the simultaneous presence of fatigue cracks in the same structural element (referred to as Multiple Site Damage or MSD), and in adjacent structural elements (called Multiple Element Damage or MED). Since current procedures have been established from assuming damage in the form of a single crack only, research on WFD is necessary and prudent. Moreover, multiple cracks emanating from rivet holes along fuselage lap splices have been found in aging airplanes. The work described in this paper is concerned with the effects of such cracking on the damage tolerant capability of airplane fuselages.

Analysis of MSD in aircraft structures must address two issues. The first issue is to determine the size of cracks adjacent to primary damage that will degrade the residual strength below the allowable level. Experiments on flat panels [2] have demonstrated that cracks as small as 0.05 inch ahead of a 14-inch lead crack can reduce the residual strength by more than 30%. Analyses by Swift [1] have shown that residual strength can be degraded below required levels in a fuselage containing a long lead crack and 0.032-inch MSD-type cracks, but without crack stoppers. In both works, the MSD-crack length was measured from the edge of the rivet hole. This point is noteworthy because Tong [3] has noted that uncracked rivet holes ahead of a long lead crack can reduce the residual strength by similar orders of magnitude. The second issue regarding MSD is to predict when such cracking will occur in the operational life of the airplane. In this paper, we shall make a distinction between the time when these cracks can linkup in operation and the time when multiple cracking becomes WFD. The first point in time is referred to as the onset or threshold of MSD, and the second point in time is called the onset of WFD. Establishing these thresholds is the subject of study in this paper.

Previous research has been conducted to understand the failure mechanisms associated with MSD [1,4, and 5]. Particular attention has been given to examine damage in the form of a lead crack with smaller collinear cracks. This cracking scenario represents damage produced by penetration of an engine fragment (lead crack) and by fatigue (MSD-type cracks). Swift [6] and others [7] have hypothesized that a lead crack will linkup with smaller collinear cracks when the average stress in the ligament between crack tips equals the yield strength of the material. Testing and analysis of flat and curved panels have supported this hypothesis [8]. In addition, full-scale testing has been conducted by Foster-Miller, Inc. (FMI) using curved stiffened panels containing lap splices. Several residual strength [9,10] and fatigue tests [11] were performed to determine static strength and crack growth behavior.

In this paper, a methodology is presented to predict the thresholds of MSD and WFD. The methodology makes use of results from previous research efforts. As an application of the methodology, the thresholds of MSD and WFD are predicted for cracks emanating from rivet holes along the lap splices in the Foster-Miller full-scale panels.

2.0 THEORETICAL CONSIDERATIONS

The theoretical framework to predict the threshold of WFD is based on residual strength analysis and fatigue crack growth data from a curved stiffened panel with a lap splice (Figure 1). In the panel, a lead crack spans along the lap splice over two bays with the center stiffener broken. Secondary collinear or MSD-type cracks are adjacent to the primary or lead crack. The secondary cracks can reduce the residual strength of the stiffened panel, as shown schematically in Figures 1(a) and 1(b).

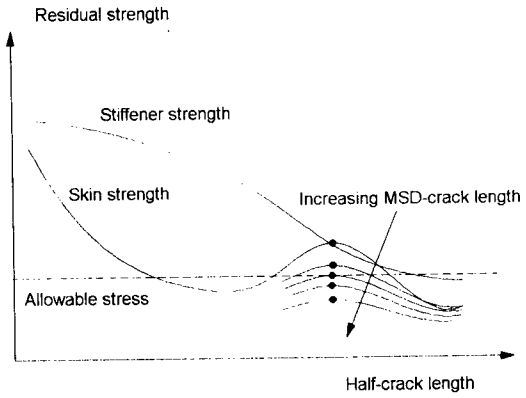

(a) Lead crack residual strength curves.

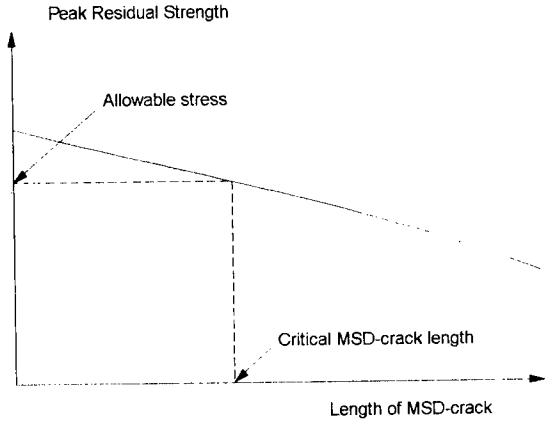

(b) Effect of MSD on lead crack residual strength.

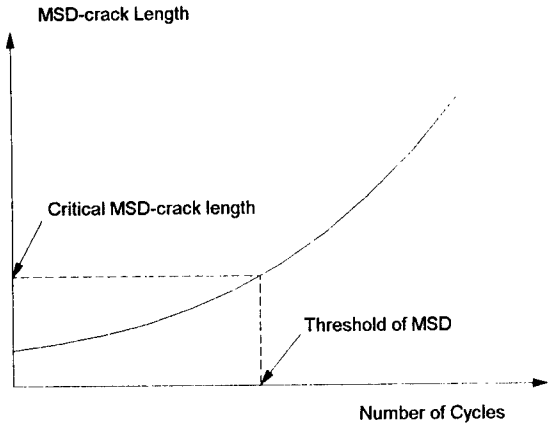

(c) MSD-crack growth curve.

Figure 1. Outline to determine threshold of WFD.

Two definitions for the critical size of secondary cracks are considered in this paper. One critical size is the length of the adjacent collinear fatigue cracks at which they can linkup at the allowable stress level. Another critical size is defined as the length of the secondary crack at which the residual strength of the panel equals the allowable stress level. The former definition is used to determine the threshold of MSD, and the latter is used to determine the threshold of WFD. In the latter case, the linkup of a lead crack with such a secondary crack could result in a catastrophic failure at the allowable stress level.

Crack growth data and analysis can then be used to calculate the number of cycles to produce cracks equal to the critical sizes. These numbers of cycles are considered as the thresholds of MSD and WFD. In this study, we are concerned with multiple cracks emanating from rivet holes of lap splices. Therefore, we shall use crack growth data associated with holes only in which the crack length is measured from the edge of the hole.

2.1 Residual Strength Analysis

The residual strength in stiffened panels can be determined through several analytical approaches. An engineering-mechanics approach was developed by Swift [12] that is based on the principle of displacement compatibility. The application of the finite element methods to determine residual strength in stiffened structure has also been the focus of previous research. For example, Tong *et al.* [7] have developed a hybrid finite element technique in which the linear elastic crack-tip stress singularity was imbedded into the finite element solution. The effect of stiffening from frames, tear straps, and stringers was also included in the hybrid finite element formulation. In addition, Nikishkov and Alturi [13] have developed a finite element approach that combines elastic-plastic analyses with the Schwarz-Newmann alternating method.

In the present work, the displacement compatibility method has been adopted to analyze the full-scale panels tested by Foster-Miller because it is convenient to conduct parametric studies. The first objective in this method is to determine the loads carried by the stiffeners which is accomplished by matching the difference in skin and stiffener deflection to the fastener shear deflection at each fastener location. The total stress intensity factor is the sum of the contributions from the stiffener loads and the remote stress. This total is normalized by the stress intensity factor without stiffeners, and is denoted as β_S. Therefore, for a panel containing a single crack, the residual strength is calculated by

$$\sigma_{SKIN} = \frac{K_C}{\beta_S \beta_B \sqrt{\pi a \sec\left(\frac{\pi a}{W}\right)}} \tag{1}$$

where a is the half-length of the crack, W is the width of the panel, and K_c is the plane stress fracture toughness of the skin material. Another correction factor called the bulging factor, β_B, is used to account for curvature. The strength of the stiffener or tear strap is calculated from

$$\sigma_{STIFF} = \frac{\sigma_{ult}}{\psi} \tag{2}$$

where σ_{ult} is the ultimate tensile strength of the stiffener material and ψ is the stiffener load concentration factor. Table 1 lists the dimensions of the laboratory panel tested by Foster-Miller, Inc.

Table 1. Panel Dimensions.

Parameter	*Value*
Radius of curvature (inches)	75
Skin thickness (inch)	0.036
Tear strap spacing (inches)	10.0
Frame spacing (inches)	20.0
Cross-sectional area of tear strap (in^2)	0.054
Rivet spacing (inch)	1.00
Rivet shank diameter (inch)	0.158
Rivet head diameter (inch)	0.250
Panel width (inches)	120

2.1.1 Plastic Collapse Criterion

The role of plasticity in the context of multiple site damage can be explained by calculating the size of the plastic zone ahead of a long crack in aircraft aluminum. At the onset of rapid crack propagation for the stress level given by equation (1), this size can be as much as 2 inches for 2024-T3 aluminum, which is greater than the typical rivet spacing of 1 inch. The material between the edge of a rivet hole and a neighboring crack tip or between adjacent crack tips is called a ligament. Calculations reveal that the ligament plastically yields before it fractures. Consequently, equation (1) would overestimate the residual strength of panels containing cracks in a row of rivets. Therefore, separate analyses were developed for cracks within a row of rivets which are representative of cracks in the lap splice of a fuselage. Residual strength calculations were performed on the assumption that failure occurs when the entire ligament yields plastically. This failure mechanism, referred to as plastic collapse, implies that the critical parameter is the yield strength of the material, and not the fracture toughness. Table 2 lists the material properties for 2024-T3 aluminum assumed in this paper. In principle, the residual strength of the panel is the lower of the two values calculated from the fracture and the plastic

collapse criteria. For the cases considered in this paper, linkup of multiple cracks is governed by plastic collapse.

Table 2. Assumed Material Properties for 2024-T3 Aluminum.

Property	*Value*
Modulus of elasticity, E (msi)	10.5
Poisson's ratio, ν	0.33
Yield strength, σ_p (ksi)	50.
Ultimate tensile strength, σ_{ult} (ksi)	64.
Plane stress fracture toughness, K_C (ksi-in$^{1/2}$)	120.

Plastic Collapse Criterion for a Single Crack in a Row of Rivets

The plastic collapse criterion has been applied to predict the residual strength of panels containing a single crack within a row of rivets [3]. Failure was assumed to occur when the ligaments between the tips of the single crack and the edge of the adjacent holes yield plastically. Thus, for a single crack within a row of rivets (Figure 2), Tong [3] derived the following equation to predict the remote stress at linkup:

$$\sigma_o = \frac{\sigma_p}{\beta_B \beta_S} \frac{\left[\sqrt{1+\frac{L}{2a}}+\sqrt{\frac{L}{2a}}\right]\left[\sqrt{\frac{2L}{a}}\right]}{1+\frac{1}{\beta_B \beta_S}\sqrt{\frac{2L}{a}}\left[\sqrt{1+\frac{L}{2a}}+\sqrt{\frac{L}{2a}}\right]} \tag{3}$$

where σ_p is the yield strength of the material and L is the ligament length which in this case is the distance between the crack tip and the edge of the neighboring fastener hole. For the crack configuration in Figure 2, the ligament length is the rivet spacing (1.00 inch) minus the diameter of the rivet hole (0.25 inches), or 0.75 inch.

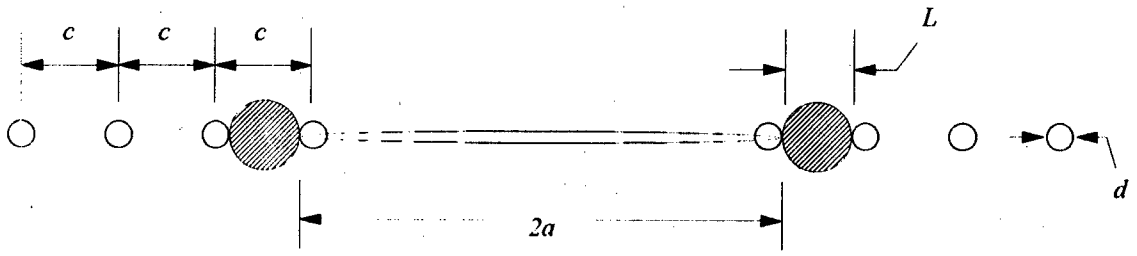

Figure 2. Schematic of plastic zones ahead of a crack in a row of rivets.

Plastic Collapse Criterion for a Lead Crack with Adjacent MSD-Type Cracks

The plastic collapse criterion was originally hypothesized for the case of a lead crack with smaller collinear or MSD-type cracks [6]. For this crack configuration (Figure 3), the remote stress at linkup is predicted by [7]

$$\sigma_o^2\left[\frac{(\beta_S\beta_B\beta_a)^2 a}{\sigma_p-\sigma_o(1-\beta_S\beta_B\beta_a)}+\frac{(\beta_H\beta_b)^2 b}{\sigma_p-\sigma_o(1-\beta_B\beta_b)}\right]=2L(\sigma_p-\sigma_o) \tag{4}$$

where a is the half-length of the lead or larger crack, b is the length of the adjacent MSD-type crack measured from the edge of the rivet hole, and L is the distance between crack tips. In equation (4), β_a and β_b are stress intensity correction factors to account for the interaction of cracks. From Tada *et al.* [14], these correction factors are

$$\beta_a=\sqrt{1+\left(\frac{2b}{L}\right)}\left\{1-\left[1+\left(\frac{L}{2a}\right)\right]\left[1-\frac{E(k)}{K(k)}\right]\right\} \tag{5}$$

$$\beta_b=\sqrt{1+\left(\frac{2a}{L}\right)}\left\{1-\left[1+\left(\frac{L}{2b}\right)\right]\left[1-\frac{E(k)}{K(k)}\right]\right\} \tag{6}$$

In equations (5) and (6), $E(k)$ and $K(k)$ are the complete elliptic integrals of the first and second kind:

$$E(k)=\int_0^{\frac{\pi}{2}}\sqrt{1-k^2\sin^2\phi}\,d\phi \qquad K(k)=\int_0^{\frac{\pi}{2}}\frac{d\phi}{\sqrt{1-k^2\sin^2\phi}} \tag{7}$$

where k depends on the lengths of the cracks and the distance between crack tips

$$k=\sqrt{\frac{4ab}{(L+2a)(L+2b)}} \tag{8}$$

Equation (4) also includes a correction factor to account for the stress concentration at the edge of an open hole produced by the remote loading [15]:

$$\beta_H=1+\frac{1}{2\left(\frac{2b}{d}\right)+1.93\left(\frac{2b}{d}\right)+0.539}+\frac{1}{2\left[\left(\frac{2b}{d}\right)+1\right]} \tag{9}$$

where b is the length of the crack emanating from the edge of the rivet hole and d is the rivet hole diameter.

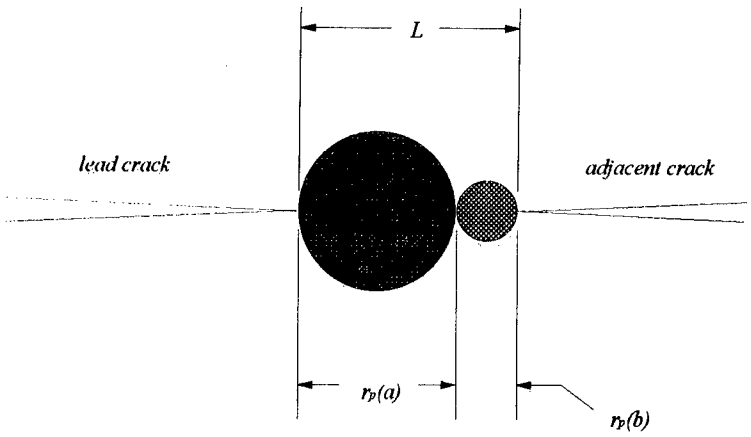

Figure 3. Schematic of plastic zones ahead of a lead crack and an MSD-type crack.

Equations (3) and (4) were derived from the exact distribution of stress ahead of a crack which includes nonsingular terms [7]. The plastic-zone size predicted by these equations is larger than that predicted by the Irwin equation which includes only the singular term in the asymptotic expression for stress. For cases where the yield strength, σ_p, is much greater than the remote stress, σ_o, the present models are equivalent to those based on the Irwin equation. In most practical cases, however, the yield strength and the remote stress have the same order of magnitude, and equations (3) and (4) are more applicable than those derived from the Irwin equation.

The effect of stable tearing can be included in equations (3) and (4). Stable tearing increases the total crack length and decreases the ligament length. Thus, predictions of residual strength with stable tearing will be lower than those without the effect. An iterative solution procedure is required to include the effect of stable tearing. The effect has not been included in the calculations to determine the MSD and WFD thresholds.

Other criteria have also been proposed to predict the linkup of a lead crack with smaller collinear cracks. Specifically, two alternative criteria are the critical crack tip opening angle (CTOA) [16] and the T_ε*-integral [17]. In applying these criteria to predict residual strength, however, elastic-plastic finite element analyses are required.

Residual strength predictions for flat panels with a variety of multiple-crack configurations based on the T_ε*-integral criterion in conjunction with the elastic-plastic finite element alternating method have been presented by Pyo *et al.* [18]. Among these results were linkup predictions for 20-inch-wide panels containing a lead crack with 2 MSD-type cracks, one ahead of each tip of the lead crack (Figure 4). Linkup stresses

based on the plastic collapse criterion (as presented in this paper) and the T_ε*-integral criteria (as presented in Reference [18]) are compared in Table 3 for the panel geometry as shown in Figure 4. As a first-order estimate, the linkup stresses based on plastic collapse assumed an unbounded or infinite panel. When compared to linkup stresses calculated using the T_ε*-integral criterion, the difference in the two predictions increases as the lead-crack size increases, suggesting an influence due to the finite width of the panel. Therefore, Table 3 also lists plastic-collapse predictions where a finite-width correction was included in equation (4). The following equation was used to account for finite width [14]:

$$\beta_W\left(\frac{a}{W}\right) = \left[1 - 0.1\left(\frac{a}{W}\right)^2 + 0.96\left(\frac{a}{W}\right)^4\right]\sqrt{\sec\left(\frac{\pi a}{W}\right)} \tag{10}$$

where W is the panel width. When this finite-width correction factor is included in equation (4), the linkup stresses from both criteria are within reasonable agreement. The effect of finite width on the smaller MSD-type cracks has been neglected in the predictions based on plastic collapse. In these comparisons, the effect of stable tearing was included in the calculations using the plastic collapse criterion. Stable tearing affects the linkup calculations via a reduction in ligament length, L, by the amount of stable growth which, in turn, increases the magnitude of the stress intensity factors. In these calculations, stable growth is governed by a crack resistance curve of the form

$$K_R = K_o \cdot \Delta a^q \tag{11}$$

where K_o and q are material constants which are equal to 103.4 ksi-in$^{1/2}$ and 0.14, respectively.

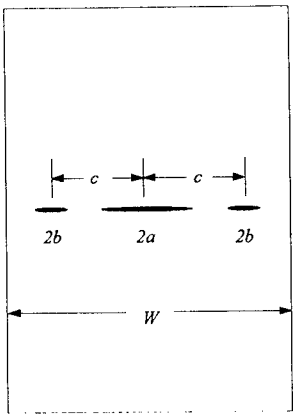

Figure 4. Finite-width panel with a lead crack and two MSD-type cracks.

Table 3. Comparison of Predicted Linkup Stresses.

a (inches)	*Linkup Predictions (ksi)*		
	Plastic Collapse (Infinite Panel)	*Plastic Collapse (Finite Width)*	T_ε* *Integral*
3.75	23	22	20
5.25	20	17	15
6.75	18	13	11

NOTES:
Results for plastic collapse include the effect of stable tearing.
Referring to Figure 4, the panel configuration for these calculations is characterized by the following dimensions:

a = half-length of main or lead crack
b = half-length of the MSD cracks = 0.25 inch
c = center-to-center crack spacing = a + 1.25 inches
W = width of panel = 20 inches

Plastic Collapse Criterion for Adjacent MSD-Type Cracks

Linkup of two adjacent secondary or MSD-type cracks is assumed to occur when the net section stress equals the yield strength (Figure 5):

$$\sigma_o = \sigma_p (c - d - 2b) / c \tag{12}$$

where c is the rivet spacing, d is the diameter of the rivet hole, and b is the length of the secondary crack emanating from the edge of the rivet hole. Thus, the critical length of secondary cracks at the onset or threshold of MSD can be calculated by setting equation (11) equal to the allowable stress.

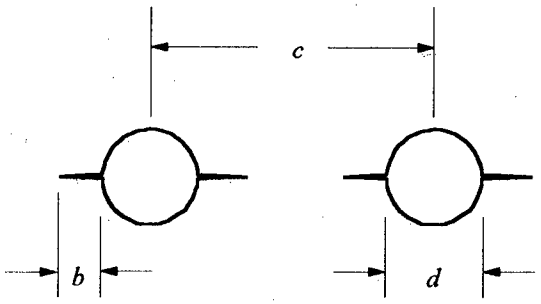

Figure 5. Secondary cracks emanating from adjacent rivet holes.

2.1.2 Nonlinear Bulging Factor

To account for curvature in the residual strength analyses, the stress intensity factor is multiplied by the bulging factor. Previous work has shown that the bulging factor may be nonlinear with respect to the applied stress [19]:

$$\beta_B = \sqrt{1+\alpha\left[\left(\frac{E}{\sigma_o}\right)\left(\frac{a}{R}\right)^2\right]^{2/3}} \tag{13}$$

where E is the modulus of elasticity, R is the radius of curvature, and α is an empirical constant. For the FMI panels, the value of the empirical constant is assumed to be 0.671.

2.2 Crack Growth Analysis

Crack growth data were collected during fatigue testing of a curved, stiffened panel [11]. This panel contained a debonded lap splice with 100 rivets in each of the three rows in the joint. Twenty-two (22) rivet holes were cracked as a result of cyclic pressurization at constant amplitude. Figure 6 shows crack growth curves from selected rivet hole locations. In addition, two curves are drawn in the figure. One curve represents "average" crack growth data that was derived by calculating the arithmetic mean of all the crack lengths measured at each cycle increment. The other curve is an approximation of the fastest crack growth observed in the experiment which represents the "worst" case. The crack lengths shown in Figure 6 were measured from the edge of the rivet hole. These data, however, represent crack growth behavior for a particular set of loading conditions: maximum pressure of 9.5 psi, minimum pressure of 1.0 psi, and a frequency of 0.2 Hertz.

In the full-scale fuselage panels, the stress amplitudes or stress ranges at each rivet hole depend on the locations of the holes. To simplify the analysis, we divided the data into two groups; namely, those for holes near a stiffener and those away from it. We assumed that the stress amplitudes of each group were the same. Moreover, we shall use a Paris-Walker-type crack-growth model [20] to extrapolate these data to other loading conditions. The assumed crack-growth model has the following functional form

$$\frac{da}{dN} = C\frac{\Delta K^m}{(1-R)^n} \tag{14}$$

where ΔK is the stress intensity factor range and R is the ratio of minimum to maximum applied stress, called the stress ratio. Also, C, m, and n are empirical constants. In the current analyses, the exponents in equation (14) were assumed to be m =4 and n =1 [21]. A crack growth constant, C, was chosen to fit the data of each curve. We found that C =3.6×10^{-10} for the worst-case data for the holes near the stiffener, and C = 3.3×10^{-10} for

the group of holes away from the stiffener. The "average" crack growth constant for all holes is $C=2.6\times10^{-10}$.

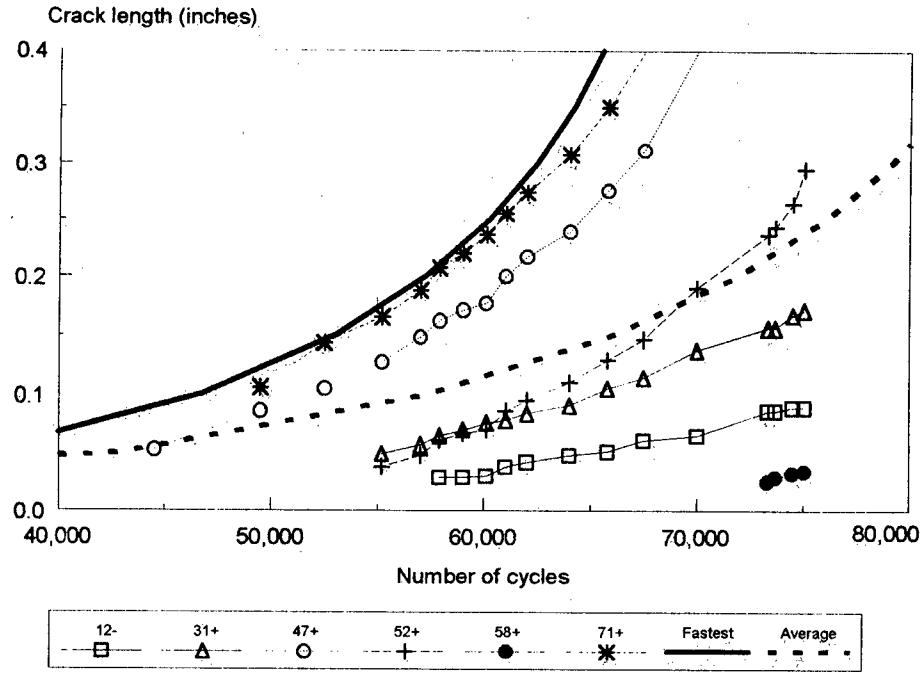

Figure 6. Crack growth data from FMI panel tests at selected rivet holes.

The stress intensity factor was assumed to be

$$\Delta K = \Delta\sigma\beta_H\sqrt{\pi a} \tag{15}$$

where a is the length of the crack measured from the edge of the hole, $\Delta\sigma$ is the stress range (14.52 ksi assumed), and β_H is the correction for the stress concentration at the edge of the rivet hole that was defined in equation (9) for open holes. Thus, equation (15) is a first-order approximation to the actual stress intensity factor because the data were obtained from holes containing rivets that carried load. Moreover, the foregoing crack-growth analysis is used only to adjust for different levels of mean stress.

According to the damage tolerant requirement, the residual strength of a fuselage panel with a two-bay crack must be above an allowable stress level (normally the design limit load). If multiple cracking is confined within two bays, a linkup of cracks will simply result in a larger crack within two bays, and therefore, has no effect on the residual strength. If multiple cracking occurs near a stiffener, however, and if the lead crack is located in the two bays adjacent to the stiffener, the panel will have a lower residual strength [5]. Therefore, we must examine the fatigue crack growth at that midbay

location and near the stiffener. In general, the hoop stress at midbay is higher than near the stiffener which results in a higher crack growth rate.

3.0 EXAMPLE CALCULATION

To demonstrate the methodology, the thresholds of MSD and WFD were predicted for the Foster-Miller panels. In the displacement compatibility analysis, the flexibility of the fastening system between the skin and the tear straps must be known to determine the load transfer from the skin to the stiffeners. In the FMI test panels, however, the flexibility of the fastening system was unknown. Therefore, two cases of flexibility were considered to establish bounds on the MSD threshold for the FMI panels. In one calculation, the fastening system was assumed to be infinitely stiff, meaning that the relative displacement between the skin and stiffener is zero. From this assumption, an upper bound estimate was established. In a separate calculation, the load was assumed to be carried entirely by the rivets implying that the adhesive bonding was ineffective. In this case, the rivet flexibility was calculated from an empirical formula derived by Swift [22]. This calculation was considered as a lower bound because the tear straps in the actual panels were both riveted and adhesively bonded to the skin. Results from the displacement compatibility analysis of the Foster-Miller panels are summarized in Table 4. The analyses assumed that the center tear strap and frame in the panel were broken. The correction factors for stress intensity and the stiffener load concentration factor for the tear straps near the lead crack tips are listed in the table for both cases.

Table 4. Results from Displacement Compatibility Analysis of FMI Panels.

Half-crack length, a (inches)	*Lower Bound Rivet flexibility = 5.48 μin/lb.*		*Upper Bound Rivet flexibility = 0 μin/lb.*	
	β_S	ψ	β_S	ψ
2	1.170	1.030	1.172	1.034
4	1.109	1.112	1.110	1.125
6	1.074	1.278	1.073	1.312
8	1.033	1.610	1.029	1.685
10	0.843	2.567	0.766	2.909
12	0.687	3.965	0.610	4.507
14	0.692	4.839	0.635	5.427

The residual strength of panels containing a skin crack was calculated using equation (1). Similarly, residual strength of panels containing a crack within a row of rivet holes was calculated from equation (3). Equation (4) and the results from the displacement compatibility model were used to calculate the residual strength for panels containing a lead crack with various sizes of MSD-type cracks. These residual strength curves are

shown in Figure 7 for the lower bound results, and in Figure 8 for the upper bound estimates.

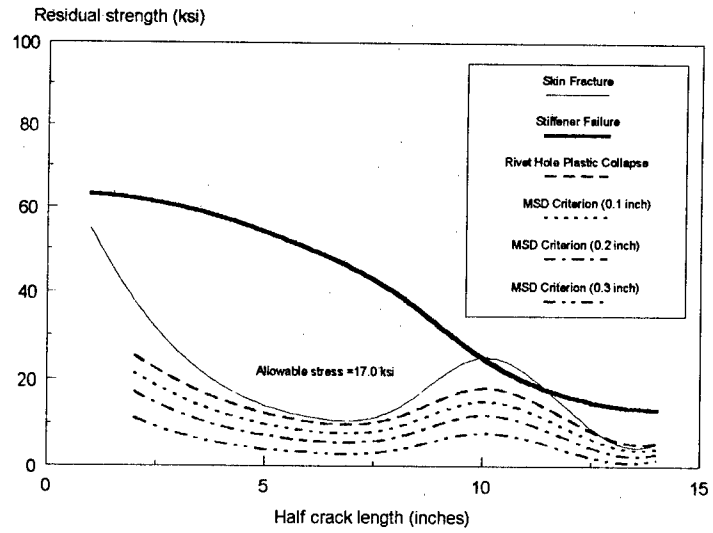

Figure 7. Residual strength diagrams for lower bound estimate.

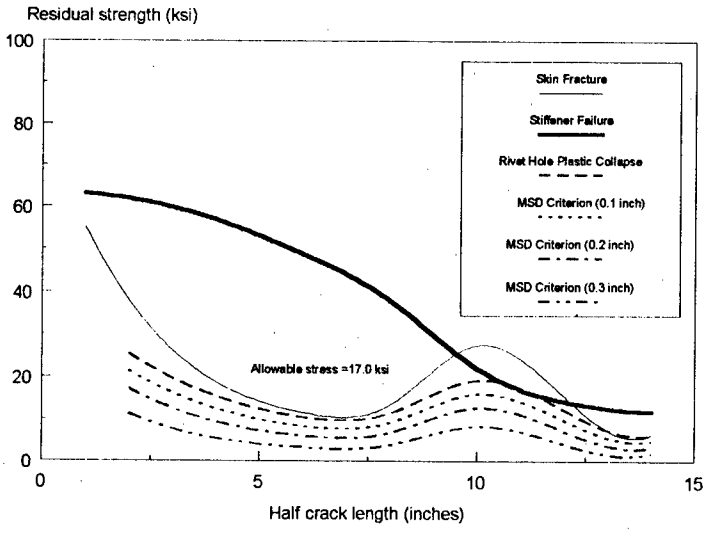

Figure 8. Residual strength diagrams for upper bound estimate.

The peak value or local maximum of the residual strength curve near the location of the stiffener or tear strap is considered to be the residual strength of the panel. These peak values are listed in Table 5. Thus, the residual strength of a panel with a crack within a row of rivets is 28 to 31% lower than a panel with a skin crack. When MSD-type cracks

are present, the residual strength of the panels is decreased further. This result is shown in Figure 9 which is a plot of the data listed in Table 5.

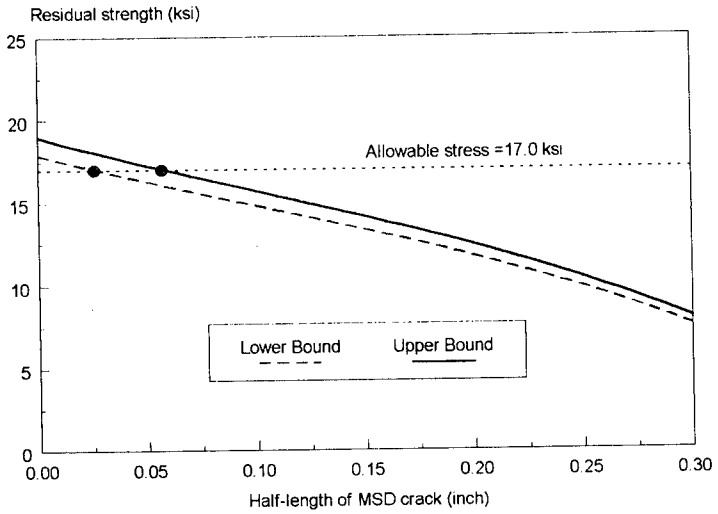

Figure 9. Effect of MSD on lead crack residual strength.

Table 5. Results of Residual Strength Analysis for FMI Panels.

	Lower Bound Estimate	*Upper Bound Estimate*
Skin Fracture Criterion (ksi)	25.0	27.6
Rivet Hole Criterion (ksi)	17.9	19.0
MSD Criterion for 0.1 inch (ksi)	14.8	15.7
MSD Criterion for 0.2 inch (ksi)	11.7	12.4
MSD Criterion for 0.3 inch (ksi)	7.5	8.0

The allowable stress level is assumed to be 1.33 times the operating hoop stress which is calculated as 82% of the thin-walled cylinder estimate, or

$$\sigma_{ALL} = 1.33 \times 0.82 \times \frac{pr}{t} \tag{16}$$

where p is the nominal operating pressure (7.5 psi assumed), r is the radius of the cylinder, and t is the skin thickness. The 82% factor was used in previous calculations by Swift [1] to approximate the hoop stress at midbay, and was later confirmed by strain gage testing on a retired Boeing 737 airplane during ground pressurization tests [23]. From equation (16), the allowable stress level is 17.0 ksi.

By interpolating values of residual strength for the allowable stress level of 17.0, the lower and upper bound estimates for the critical size of secondary cracks are 0.03 and 0.06 inches (see Figure 8). Applying the worst-case crack growth data from the FMI data for rivet holes near the stiffener, the threshold of WFD is between 28,900 and 38,900 cycles. The WFD threshold represents the point in time when accidental damage may result in linkup of the primary crack with secondary cracks. These estimates for the WFD threshold should be adjusted to account for actual loading conditions. In the FMI laboratory tests, the ratio of minimum to maximum stress was 0.105. In an actual airplane, the minimum stress is zero. When the crack growth curve is adjusted accordingly using equation (14), the WFD threshold varies between 32,300 and 43,500 cycles. As a point of reference, the FMI panel failed after 75,263 cycles[1]. Therefore, the threshold of WFD for this panel occurred between 0.43 and 0.58 of its total life. The results of the WFD threshold calculation are summarized in Table 6.

Table 6. Estimates for WFD Threshold in FMI Panels.

	Lower Bound Estimate	*Upper Bound Estimate*
Critical Size of WFD (inch)	0.03	0.06
WFD Threshold (cycles)	28,900	38,900
Adjusted WFD Threshold	32,300	43,500

The previous calculation assumed that the primary or lead crack and the broken center stiffener in the panel were the result of accidental damage from penetration of an engine fragment, as an example. Another scenario should also be assumed where all rivet holes contain fatigue cracks with the center stiffener is intact. Assuming all cracks have the same length and grow at the same rate, equation (12) can be used to calculate the critical length of fatigue cracking at which linkup will occur at the allowable stress. This damage scenario is an oversimplification because the actual stress distribution across each bay of the fuselage is not uniform. The simplifying assumptions, however, are useful to demonstrate the concept and to perform a first order estimate. A critical length of 0.21 inch was calculated from equation (12). From the worst-case FMI data for rivet holes away from the stiffener, such cracking will occur after 63,200 cycles. Adjusting for in-service loading (i.e., minimum stress equal to zero), this value becomes 70,600 cycles. This number of cycles is referred to as the threshold of MSD, and represents the point in time when linkup of multiple cracks can occur from fatigue loading only. Additional analysis should be performed to predict this new fatigue threshold more accurately. Modeling of fatigue cracks emanating from rivet holes has been developed by Park and Atluri [24] which appears to be appropriate for this damage scenario. << Such analyses were recently performed using an elastic-plastic finite element alternating method [25].>>

[1] "Failure" as used here means that the size and density of multiple site damage was such that proper loading could not be maintained to continue testing.

A scatter factor is usually applied to fatigue calculations in order to account for the variability in fatigue data. In other words, the number of cycles calculated from the crack growth analysis should be divided by a scatter factor. Thus, the application of the scatter factor adds conservatism to the predictions. In the MSD and WFD threshold predictions, a scatter factor was not applied because the crack growth analysis assumed the worst-case data which is already a conservative assumption.

4.0 DISCUSSION

Two different points in the lifetime of an airplane were defined in this paper. The threshold of MSD refers to the point when two adjacent collinear fatigue cracks can linkup at the allowable stress. The threshold of WFD is the point when a crack less than two bays in length created from accidental damage may lead to catastrophic failure. Calculations based on residual strength analysis and crack growth data showed that the threshold of WFD for laboratory panels containing a debonded lap splice was between 32,300 and 43,500 cycles. The threshold of MSD was about 70,600 cycles.

It may appear counter-intuitive that the WFD threshold is less than the MSD threshold. The reasons are twofold. The critical secondary-crack length for WFD is much smaller than that for MSD linkup (0.03 and 0.06 inch versus 0.21 inch). In addition, the worst-case data from the FMI data for rivet holes near a stiffener had a higher crack-growth rate than that for holes away from stiffeners. Therefore, less time is required for fatigue cracks near a stiffener to initiate and grow to the critical size than those away from it.

After the WFD threshold has been reached, small fatigue cracks near a stiffener are critical only if there is a long lead crack adjacent to the stiffener. Such a long lead crack can be created from either accidental damage or linkup of secondary cracks near the stiffener. The probability that accidental damage will create a lead crack of sufficient size near the stiffener with fatigue cracks may be small. Linkup of secondary cracks can only occur after the MSD threshold has been reached. Thus, the probability of catastrophic failure is likely to be small after the WFD threshold. On the other hand, after the number of flight cycles has reached the MSD threshold, multiple cracks near the stiffeners with sizes larger than the critical WFD length are likely to exist. A linkup of two adjacent fatigue cracks can lead to a subsequent linkup with other cracks and result in a catastrophic failure. Therefore, the risk of catastrophic failure can be much higher after the MSD threshold has been reached. Estimating the risk of failure, however, is beyond the scope of this study.

Estimates for the MSD and WFD thresholds are useful in developing guidelines for inspection programs. Special inspection procedures can be implemented to detect MSD-type cracks after an airplane has reached the MSD or WFD threshold. Based on the lower bound estimates, these inspections must detect cracks between 0.03 and 0.06 inch at the

rivet holes near the stiffeners. At midbay, the critical crack-length is larger and is relatively more detectable.

Another benefit of these threshold estimates may be in developing guidelines for full-scale testing. For example, it may be easier to verify that multiple site damage will not occur within a prescribed lifetime than it would be to actually verify the threshold value through fatigue tests. Based on the calculations presented in this paper, the total life of the FMI panel was between 1.7 and 2.3 times its WFD threshold. Therefore, in fatigue testing of an actual airplane, two lifetimes should be sufficient to ensure that WFD or MSD will not occur.

The estimates for the MSD and WFD thresholds presented in this paper appear to be reasonable and conservative. The largest source of conservatism is that the fatigue were collected from a panel containing a completely debonded lap joint. In an actual aircraft fuselage, the skins in the lap splice are joined together with an adhesive bond as well as with rivets. If the bond remains effective throughout the life of the airplane, the thresholds of MSD and WFD will be much higher than those predicted in this paper. Also, if the rate of debonding in the lap joint depends on location (i.e., midbay versus near a stiffener), the relative difference between the MSD and WFD thresholds will be different from the predicted difference. These actual differences, however, cannot be quantified without further testing and analysis. Ultimately, these thresholds must be established through full-scale fatigue testing followed by tear-down inspections.

Another source of conservatism in the threshold estimates is the use of the worst-case fatigue data for all rivet holes. After the MSD threshold has been reached, an adjacent pair of collinear fatigue cracks of critical size may not exist. Even if such a pair of cracks were present, the rivet holes adjacent to these cracks may not be cracked or may have cracks less than the critical size. In these scenarios, the linkup of multiple cracks would not lead to catastrophic failure.

Design variables such as rivet spacing and stiffener strength can greatly affect residual strength of panels containing multiple cracking [1]. Thus, it appears that the risk of MSD and WFD can be mitigated through appropriate design. The methodology presented in this paper can be useful to evaluate such designs.

Acknowledgments - This work was supported by the Research and Grant Council of Hong Kong and by the Federal Aviation Administration Technical Center in Atlantic City, NJ, USA.

REFERENCES

[1] Swift, T., "Widespread fatigue damage monitoring - issues and concerns," *Proceedings of the 5th International Conference on Structural Airworthiness of New and Aging Aircraft*, DGLR-Bericht 93-02, 1993, pp. 133-150.

[2] Maclin, J.R., "Performance of fuselage pressure structure," *1991 International Conference on Aging Aircraft and Structural Airworthiness*, NASA Conference Publication 3160, 1992, pp. 67-74.

[3] Tong, P., "Influence of fastener holes on residual strength," *International Journal of Fracture 67*, 1994, pp. 351-324.

[4] Jeong, D.Y., and J.C. Brewer, "On the linkup of multiple cracks," *Engineering Fracture Mechanics* 51, 1995, pp. 233-238.

[5] Tong, P., R. Greif, and L. Chen, "Residual strength of aircraft panels with multiple site damage," *Computational Mechanics 13*, 1994, pp. 285-294.

[6] Swift, T., "Damage Tolerance Capability," *Specialists Conference on Fatigue of Aircraft Materials*, Delft University of Technology, October 1992.

[7] Tong, P., R. Greif, L. Chen, and D.Y. Jeong, "Damage tolerance of fuselage panels with widespread fatigue damage," *17th Symposium of the International Committee on Aeronautical Fatigue*, Stockholm, Sweden, June 1993.

[8] Broek, D., D.Y. Jeong, and D. Thomson, "Testing and analysis of flat and curved panels with multiple cracks," *FAA/NASA International Symposium on Advanced Structural Integrity Methods for Airframe Durability and Damage Tolerance*, NASA Conference Publication 3274, Part 1, 1994, pp. 85-98.

[9] Samavedam, G., and D. Hoadley, "Fracture and Fatigue Strength Evaluation of Multiple Site Damaged Aircraft Fuselages - Curved Panel Testing and Analysis," Final Report, DOT/FAA/CT-94/10, DOT-VNTSC-FAA-93-8, January 1994.

[10] Samavedam, G., D. Hoadley, and D. Thomson, "Full-Scale Testing and Analysis of Curved Aircraft Fuselage Panels," DOT/FAA/CT-93/78, DOT-VNTSC-FAA-93-10, December 1993.

[11] Samavedam, G., D. Thomson, and D.Y. Jeong, "Evaluation of the fuselage lap joint fatigue and terminating action repair," *FAA/NASA International Symposium on Advanced Structural Integrity Methods for Airframe Durability and Damage Tolerance*, NASA Conference Publication 3274, Part 2, 1994, pp. 653-664.

[12] Swift, T., "The effects of fastener flexibility and stiffener geometry on the stress intensity in stiffened cracked sheet," *Prospects of Fracture*, Noordhoff International, Leyden, The Netherlands, 1974, pp. 419-536.

[13] Nikishkov, G.P. and S.N. Atluri, "An analytical-numerical alternating method of elastic-plastic analysis of cracks," *Computational Mechanics 13*, 1994, pp. 427-442.

[14] Tada, H., P. Paris, and G. Irwin, *The Stress Analysis of Cracks Handbook*, Second Edition, Paris Productions, Inc., 1985.

[15] Schijve, J., "Stress intensity factors of hole edge cracks, comparison between one crack and two symmetric cracks," *International Journal of Fracture 23*, pp. R111-R115, 1983.

[16] Newman, Jr., J.C., D.S. Dawicke, M.A. Sutton, and C.A. Bigelow, "A fracture criterion for widespread cracking in thin-sheet aluminum alloys," *17th Symposium of the International Committee on Aeronautical Fatigue*, Stockholm, Sweden, June 1993.

[17] Atluri, S.N., "Energetic Approaches and path-independent integrals," *Computational Methods in the Mechanics of Fracture*, edited by S.N. Atluri, North Holland Publishers, 1986, pp. 123-165.

[18] Pyo, C.R., H. Okada, and S.N. Atluri, "An elastic-plastic finite element alternating method for analyzing widespread fatigue damage in aircraft structures," *Computational Mechanics 16*, 1995, pp. 62-68.

[19] Jeong, D.Y., and P. Tong, "Nonlinear bulging factor based on R-curve data," *FAA/NASA International Symposium on Advanced Structural Integrity Methods for Airframe Durability and Damage Tolerance*, NASA Conference Publication 3274, Part 1, 1994, pp. 327-338.

[20] Walker, E.K., "The effect of stress ratio during crack propagation and fatigue for 2024-T3 and 7075-T6 aluminum," *Effects of Environment and Complex Load History on Fatigue Life, ASTM STP 462*, American Society for Testing and Materials, Philadelphia, PA, 1970, pp. 1-14.

[21] Anon., "Damage Tolerance Assessment Handbook, Volume I," Final Report, DOT/FAA/CT-93/69.1, DOT-VNTSC-FAA-93-13.1, October 1993.

[22] Swift, T., "Development of the fail-safe design features of the DC-10," *Damage Tolerance in Aircraft Structures, ASTM STP 486*, American Society for Testing and Materials, Philadelphia, PA, 1971, pp. 164-214.

[23] Jeong, D.Y., D.P. Roach, J.V. Canha, J.C. Brewer, and T.H. Flournoy, "Strain Fields in Boeing 737 Fuselage Lap Splices: Field and Laboratory Measurements with Analytical Correlations," Final Report, DOT/FAA/CT-95/25, DOT-VNTSC-FAA-95-10, June 1995.

[24] Park, J.H., and S.N. Atluri, "Fatigue growth of multiple cracks near a row of fastener holes in a fuselage lap joint," *Computational Mechanics 13*, 1993, pp. 189-203.

[25] Wang, L., W.T. Chow, H. Kawai, and S.N. Atluri, "Predictions of Widespread Fatigue Damage Threshold," *Proceedings of the FAA/NASA Symposium on Continued Airworthiness of Aircraft Structures,* Atlanta GA, August 1996.

SESSION VII

ENGINES

Chairman: *C. Pomfret*, RAF (Retired)

A PROBABILISTIC APPROACH TO AIRCRAFT TURBINE ROTOR MATERIAL DESIGN

G. R. Leverant, D. Littlefield, R. McClung,

H. Millwater, and J. Wu

1996 USAF Aircraft

Structural Integrity Conference

San Antonio, Texas

December 5, 1996

TURBINE ROTOR MATERIAL DESIGN

Sponsor: Federal Aviation Administration
FAA Technical Monitor: Mr. Bruce Fenton
SwRI Program Manager: Dr. Gerald Leverant

Program Team:

AlliedSignal Aerospace
Allison Engine Co.
General Electric Aircraft Engines
Pratt & Whitney Aircraft
Southwest Research Institute

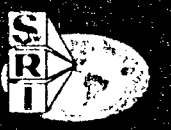

PROGRAM OBJECTIVE

TO DEVELOP A PROBABILISTICALLY-BASED DAMAGE TOLERANT DESIGN CODE TO AUGMENT THE CURRENT SAFE-LIFE PHILOSOPHY FOR LIFE MANAGEMENT OF COMMERCIAL AIRCRAFT GAS TURBINE ROTORS AND DISKS

BACKGROUND

Periodic adverse events have been associated with microstructural anomalies in titanium compressor and fan disks in aircraft gas turbines during the past 25-30 years

A commercial DC-10 airliner crash-landed at Sioux City in 1989 as a result of an uncontained titanium fan disk failure attributed to a hard alpha inclusion

In 1990, the *FAA Titanium Rotating Component Review Team Report* recommended consideration of incorporating risk management and damage tolerance concepts into design procedures for critical components in commercial engines

BACKGROUND (Cont'd)

The AIA Rotor Integrity Subcommittee was asked to respond to this challenge and has been developing defect distribution curves and preparing advisory circulars for the FAA since 1991

Southwest Research Institute, in collaboration with certain members of the AIA Rotor Integrity Subcommittee, submitted a proposal in 1995 in response to an FAA *Grants for Aviation Research Program* solicitation

Grant cooperative agreement awarded in August, 1995

CHARACTERISTICS OF HARD ALPHA

- Abnormally High Nitrogen Content
- Very Hard (R_c 55-80)
- Brittle
- Usually Associated with Void(s) and Crack(s)
- Variable Size

TURBINE ROTOR MATERIAL DESIGN

- The current safe-life philosophy for life management of commercial aircraft gas turbine rotors does not account for undetected material and manufacturing anomalies.
- A probabilistic damage tolerance design code is needed to augment the safe-life approach such that opportunity inspections can be done only on rotors that are shown to exceed certain risk levels.

VALUE TO PUBLIC

- Reduction of uncontained rotor events due to melt-related defects in titanium by up to a factor of 10.
- Avoidance of one Sioux City-type incident results in:
  - Over 100 lives saved
  - In excess of $1.0 billion saved
- Opportunity inspections increase surveillance of high risk disks with no increase in required shop time or delay time.

TURBINE ROTOR MATERIAL DESIGN

PROGRAM GOAL

To improve the safety of the commercial airliner fleet by developing a generic, probabilistically-based damage tolerance design code to augment the current safe-life approach for design and life management of gas turbine rotors.

INITIAL PAYOFF

For new airliners that join the fleet over the next 20 years, a significant reduction in the 1984-1989 uncontained disk failure event rate due to titanium melt defects (1.4×10^{-8} per engine cycle).

STEERING COMMITTEE

- Funded Members
  - AlliedSignal
  - Allison
  - General Electric
  - Pratt & Whitney
- Other engine company members
  - MTU
  - Rolls Royce
  - SNECMA
  - Sunstrand
  - Williams
- Engine Titanium Consortium (ETC)

SUBCONTRACTOR PARTICIPANTS

Allied Signal

Craig Balis

Chet Date

Allison

Nick Provenzano

Charles Teague

General Electric

Jon Tschopp

Pratt & Whitney

Gary Peters

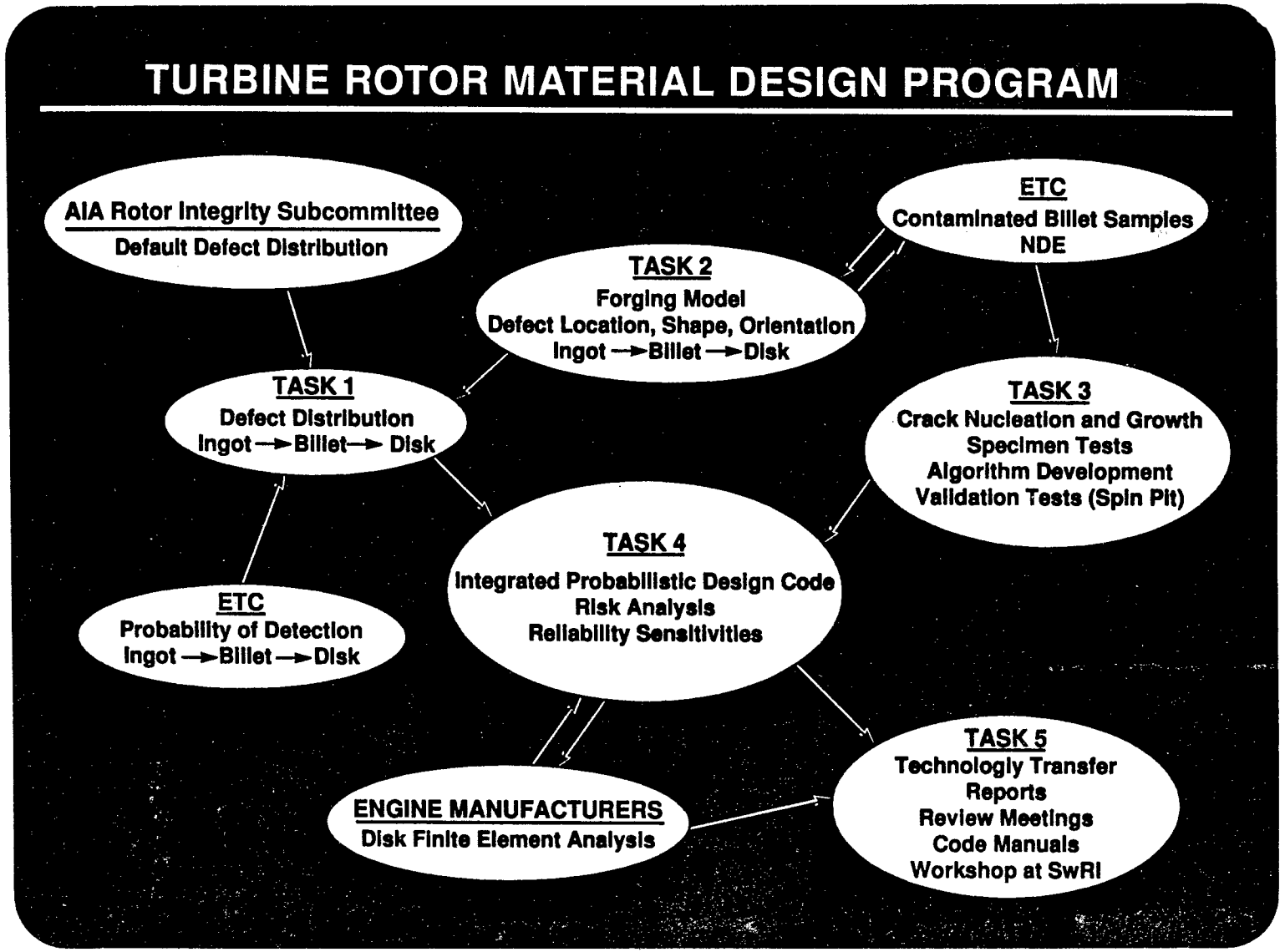
TURBINE ROTOR MATERIAL DESIGN PROGRAM
AIA Rotor Integrity Subcommittee
Default Defect Distribution
ETC
Contaminated Billet Samples
NDE
TASK 2
Forging Model
Defect Location, Shape, Orientation
Ingot → Billet → Disk
TASK 1
Defect Distribution
Ingot → Billet → Disk
TASK 3
Crack Nucleation and Growth
Specimen Tests
Algorithm Development
Validation Tests (Spin Pit)
TASK 4
Integrated Probabilistic Design Code
Risk Analysis
Reliability Sensitivities
ETC
Probability of Detection
Ingot → Billet → Disk
ENGINE MANUFACTURERS
Disk Finite Element Analysis
TASK 5
Technologly Transfer
Reports
Review Meetings
Code Manuals
Workshop at SwRI

TASK 1 -- MATERIAL AND MANUFACTURING ANOMALY DISTRIBUTIONS

- Establish POD and defect distribution curves for titanium and nickel disk alloys
- Initial emphasis is on titanium melt defects (hard alpha)
- Will build on defect distribution curves developed by the AIA Rotor Integrity Sub-committee
- A new defect distribution will ultimately be developed based on operational experience provided by the engine companies, the forging code developed in Task 2, and POD data developed by the ETC from a new multizone UT inspection system.

Final Distribution
Early 1980's Triple Melt Hard Alpha Inclusion Distribution
#3/#3 FBH Billet/Forging Inspection

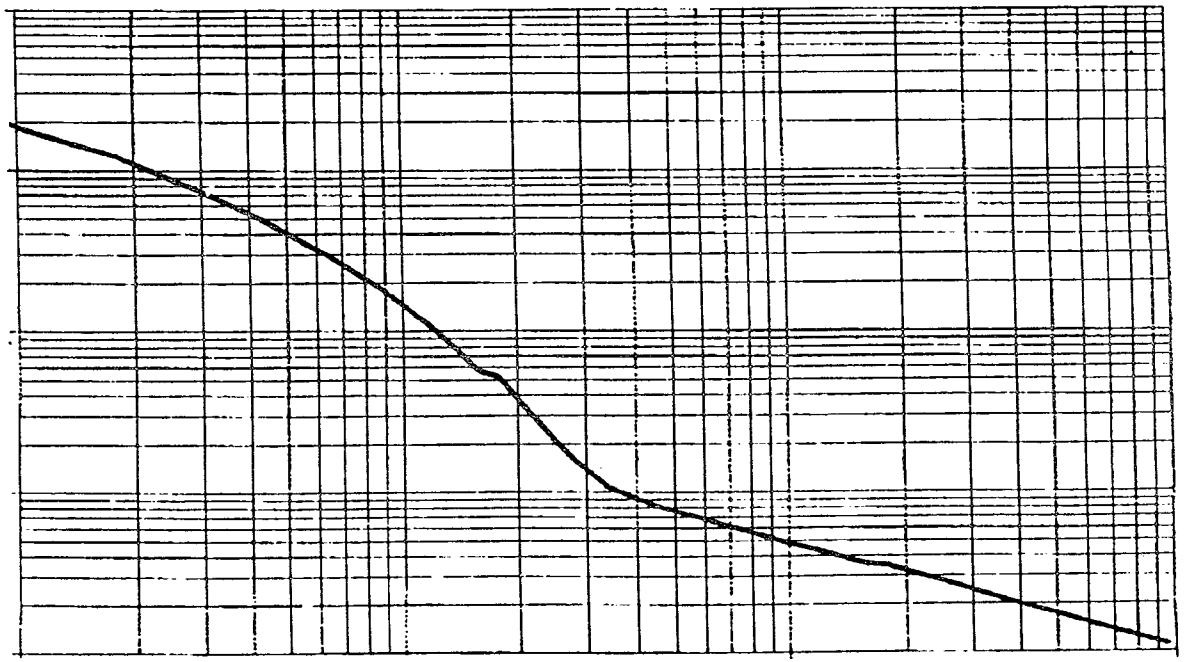

TASK 2 -- EFFECT OF FORGING ON DEFECT MORPHOLOGY

- The shape, orientation and location of a hard alpha defect is altered during ingot breakdown to a billet and during forging of a mult to a disk.
- A code is being developed to predict the movement as well as shape, orientation, and fragmentation of hard alpha during forging.
- The orientation of a mult during forging to a disk will be dictated by the forging code analysis in conjunction with the defect distribution and service stress distribution for the particular disk geometry.
- Should a defect be present, this will ensure that it will have a high probability of being benign.

TASK 2 - EFFECT OF FORGING ON DEFECT MORPHOLOGY (cont'd.)

- Constitutive properties data for Ti-64, Ti-6242, and Ti-17 have been provided by General Electric.
- Constitutive properties data for hard alpha of various nitrogen contents will be generated in this program.
- Validation forging tests will be run on Ti-64 blocks containing hard alpha seeds and on a contaminated heat of Ti-64 containing hard alpha defects. Periodic NDE will be done by the ETC.
- Parametric benchmarking will be conducted on four selected disk geometries.

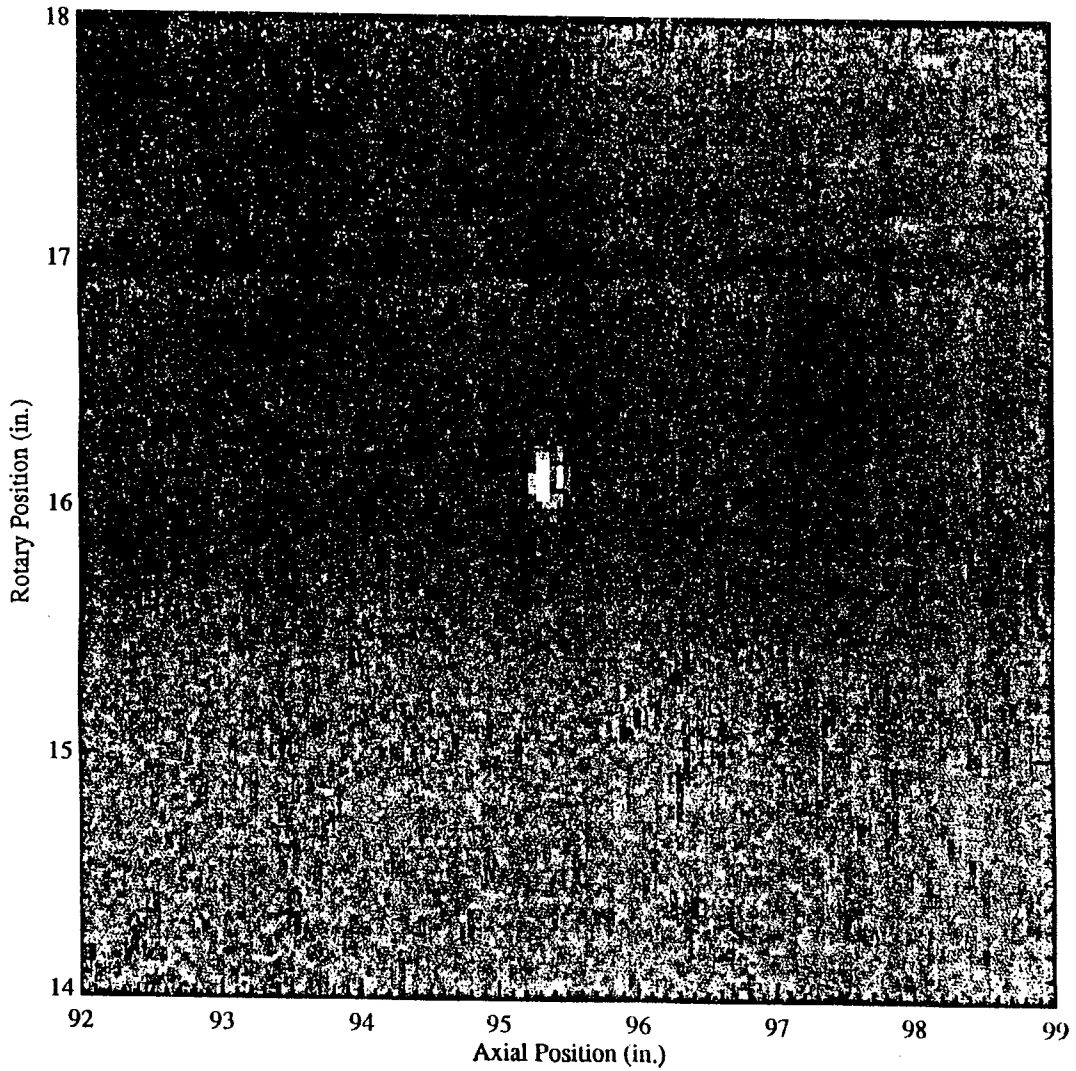

File : D:\DATA\RMI\883588\B1AW

Heat Number : 883588
Billet ID : B1AW1

Zone: 1

B1AW1 Indication "E"
Amplitude +4 dB, SNR 4.47
Depth 0.61"

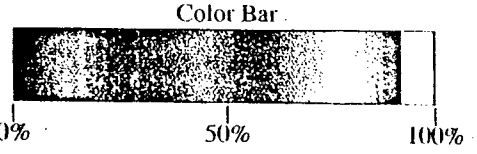

NUMERICAL MODEL

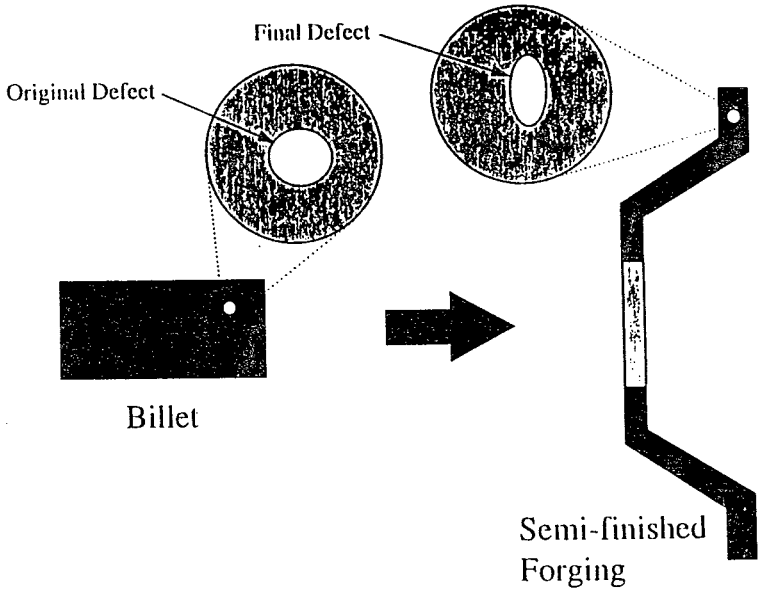

- **"Microcode" performs calculation in a control volume that moves along with defect.**
- **Boundary conditions needed for "microcode" are provided by "macrocode" (DEFORM2D).**
- **"Microcode" approach is the most efficient manner to calculate the change in size, shape and orientation of defect.**

Radial Compression

- **Geometry:**
  - » Nugget Diameter = 160 mils
  - » Diffusion Zone Diameter = 320 mils
  - » Microvolume Size = 2 in x 2 in

- **Microvolume Inputs:**
  - » Inital radius = 3 in
  - » Inital axial location = 1 in (not needed to run calculation)
  - » Radial velocity = -0.1 in/sec
  - » Radial strain rate = v_r/r
  - » Axial velocity = computed
  - » Axial strain rate = computed
  - » Shear strain rate = 0

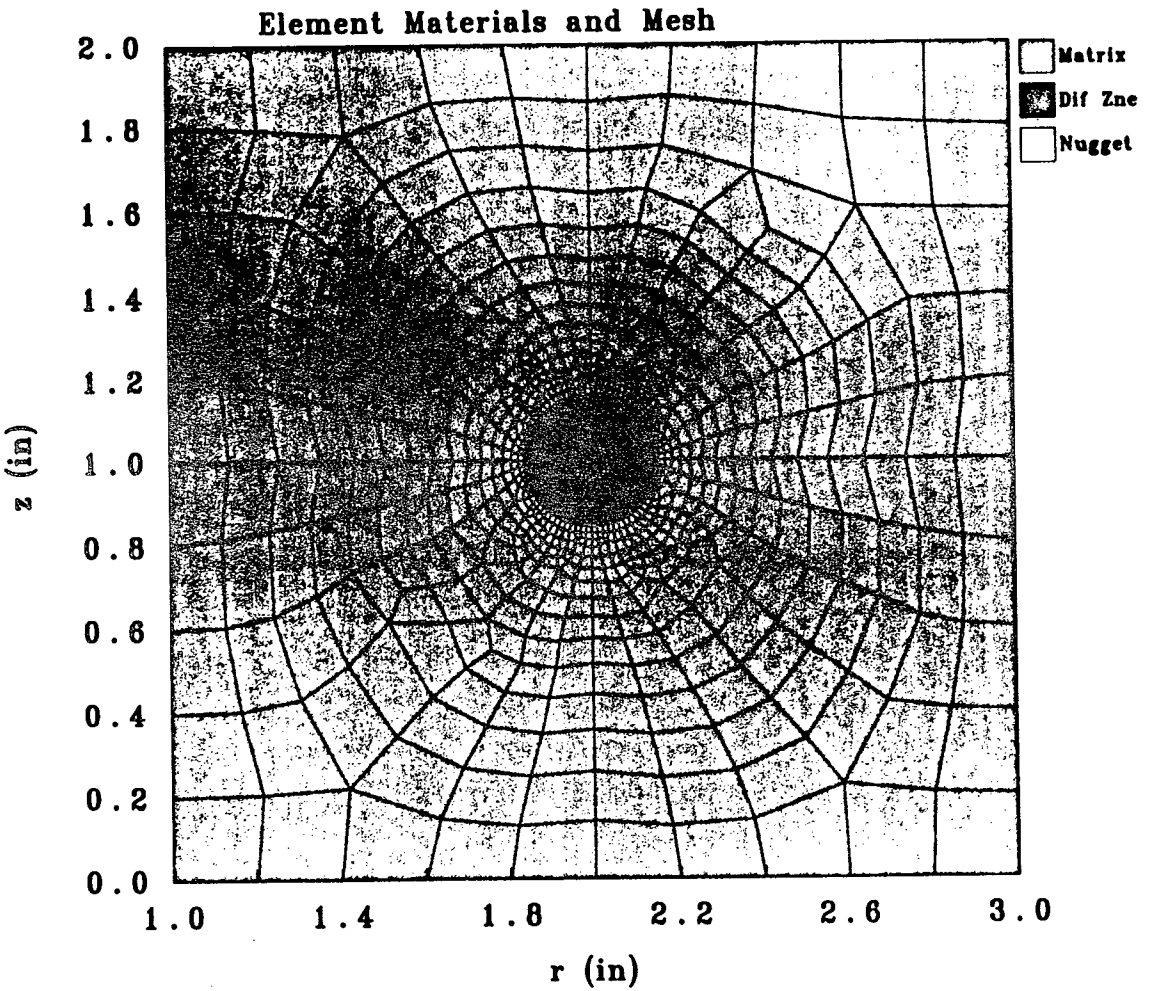

160 mil HA nugget in Ti Matrix, MAAP2D (8/10/96)
Time = .000

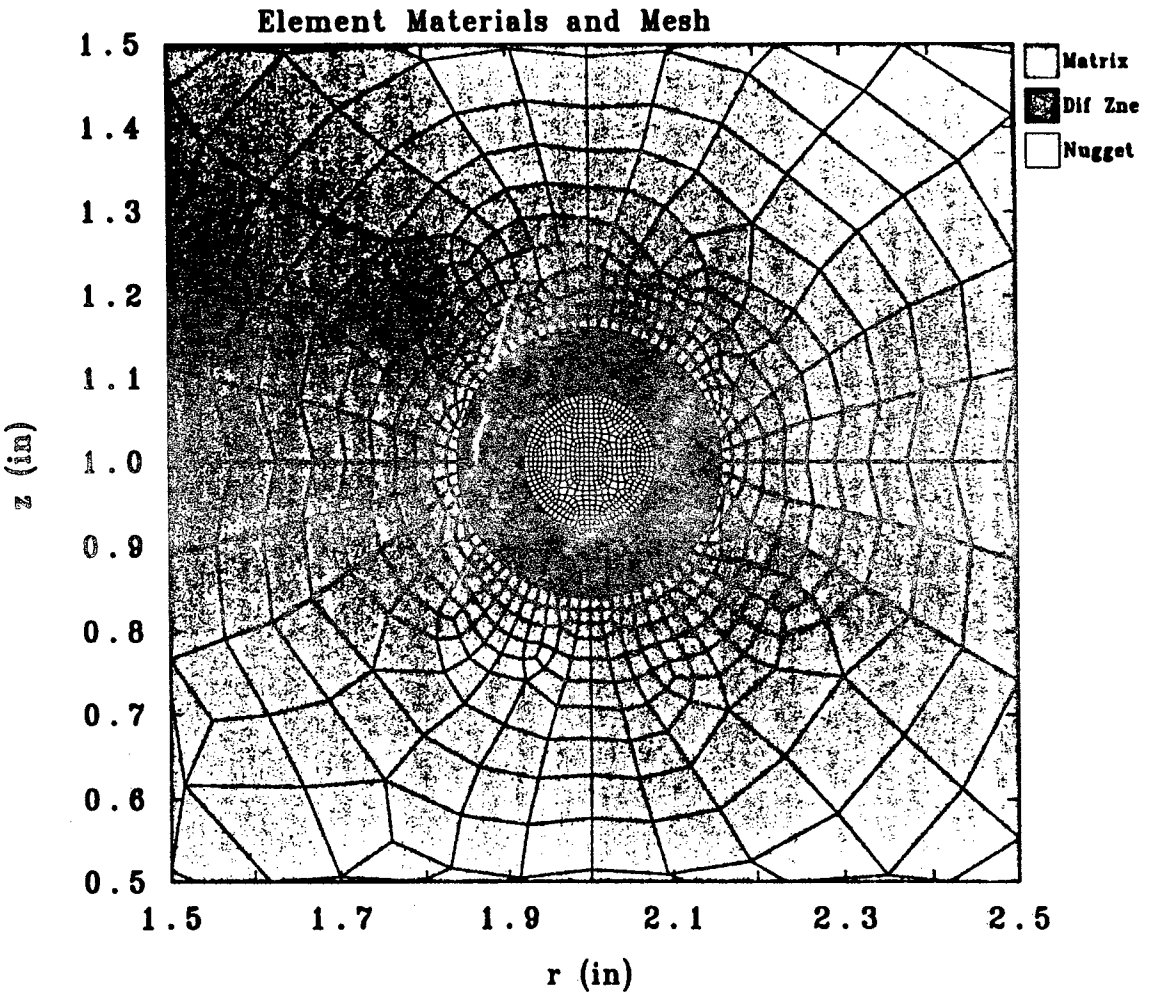

160 mil HA nugget in Ti Matrix, MAAP2D (8/10/96)
Time = .000

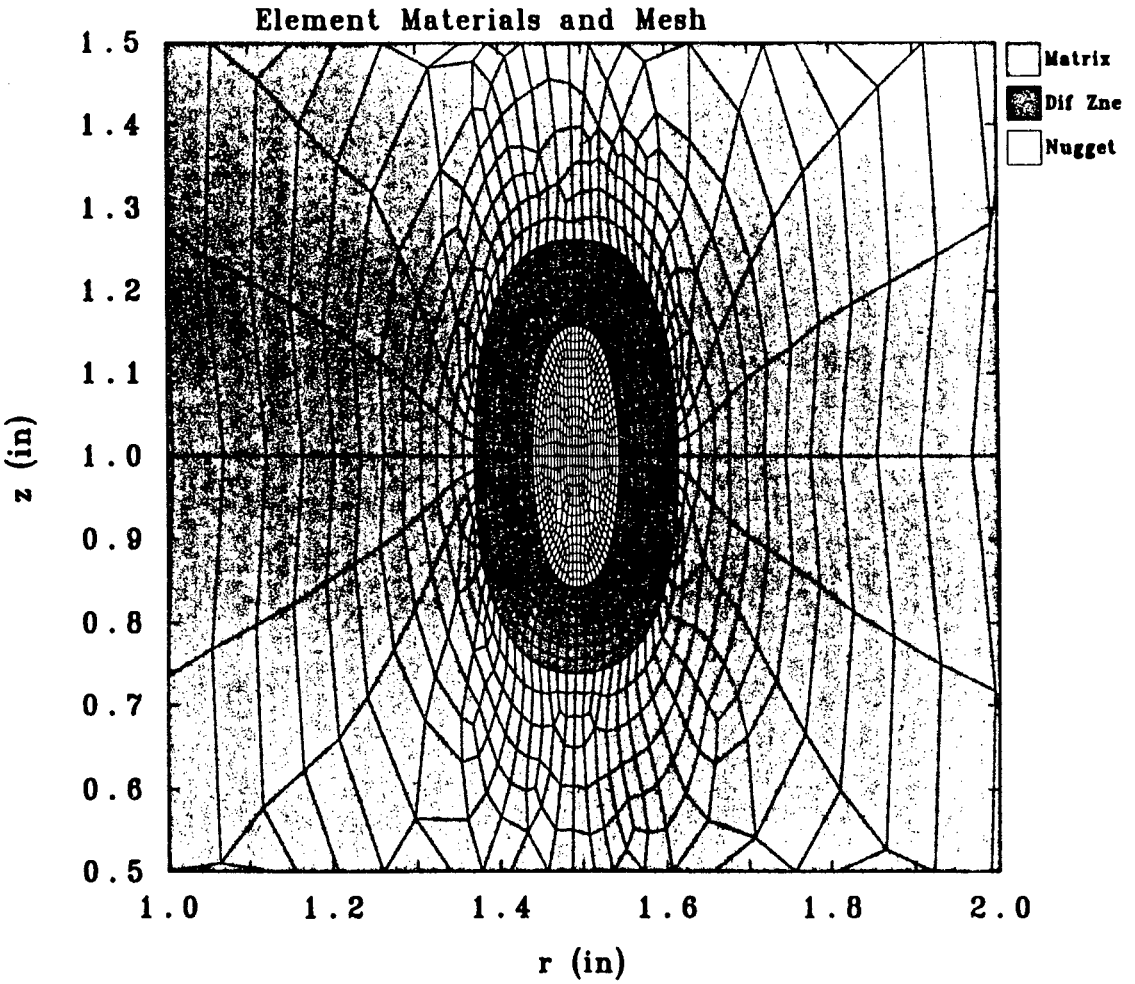

160 mil HA nugget in Ti Matrix, MAAP2D (8/10/96)
Time = 5.100

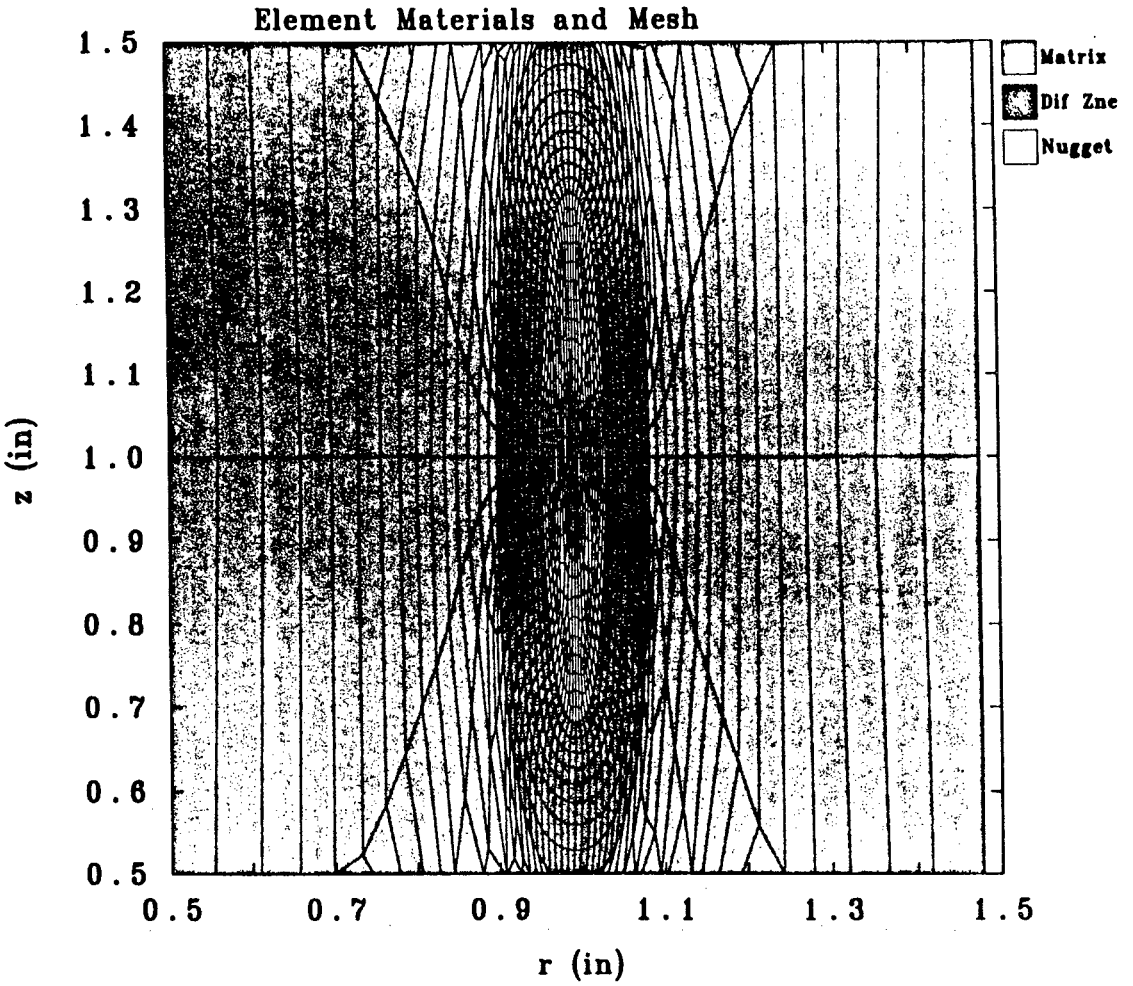

160 mil HA nugget in Ti Matrix, MAAP2D (8/10/96)
Time = 10.100

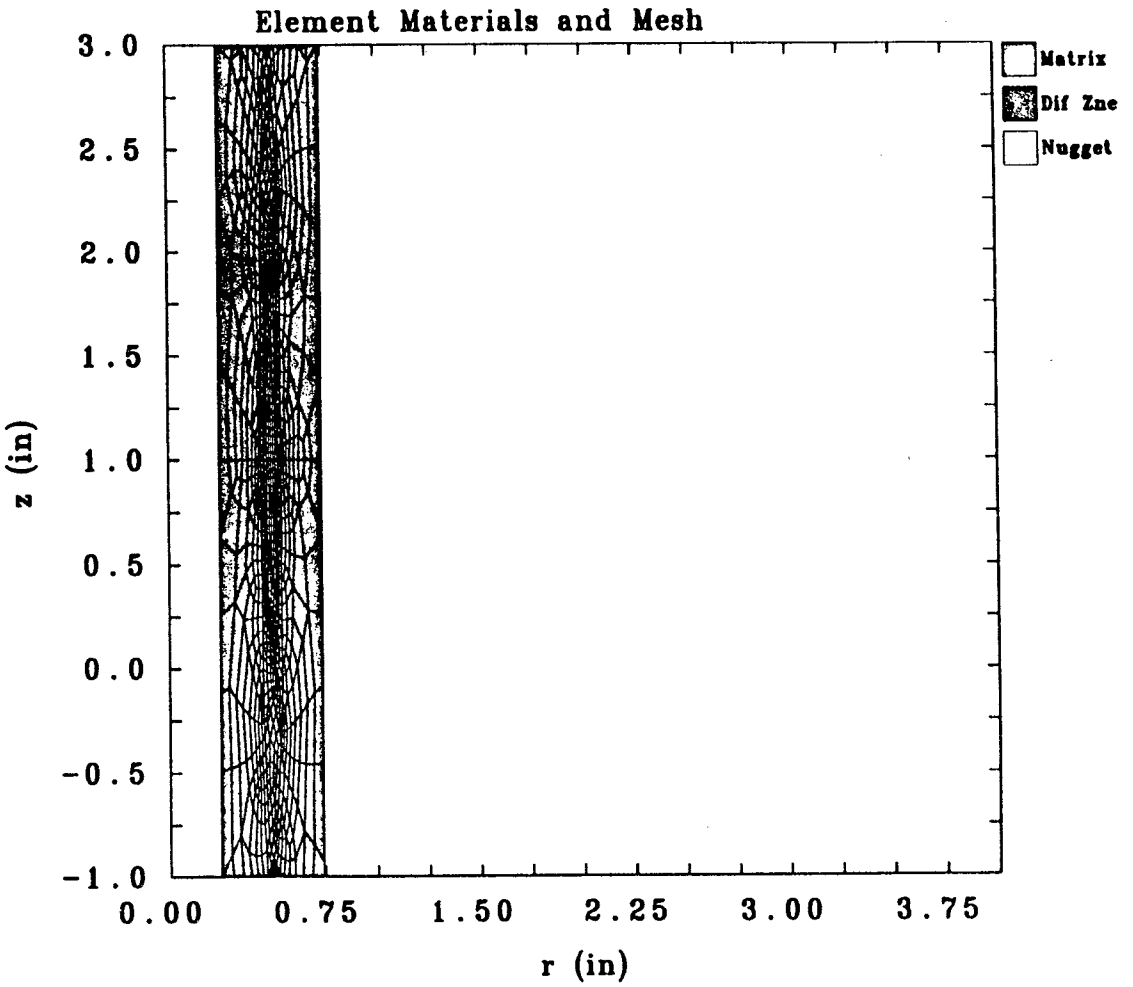

160 mil HA nugget in Ti Matrix, MAAP2D (8/10/96)
Time = 15.100

Combined Shear and Compression

- **Geometry:**
  - » Nugget Diameter = 160 mils
  - » Diffusion Zone Diameter = 320 mils
  - » Microvolume Size = 2 in x 2 in

- **Macrovolume Inputs:**
  - » Inital radius = 3 in
  - » Inital axial location = 1 in (not needed to run calculation)
  - » Radial velocity = 0.1 in/sec
  - » Radial strain rate = v_r/r
  - » Axial velocity = computed
  - » Axial strain rate = computed
  - » Shear strain rate = 0.1 sec^{-1}

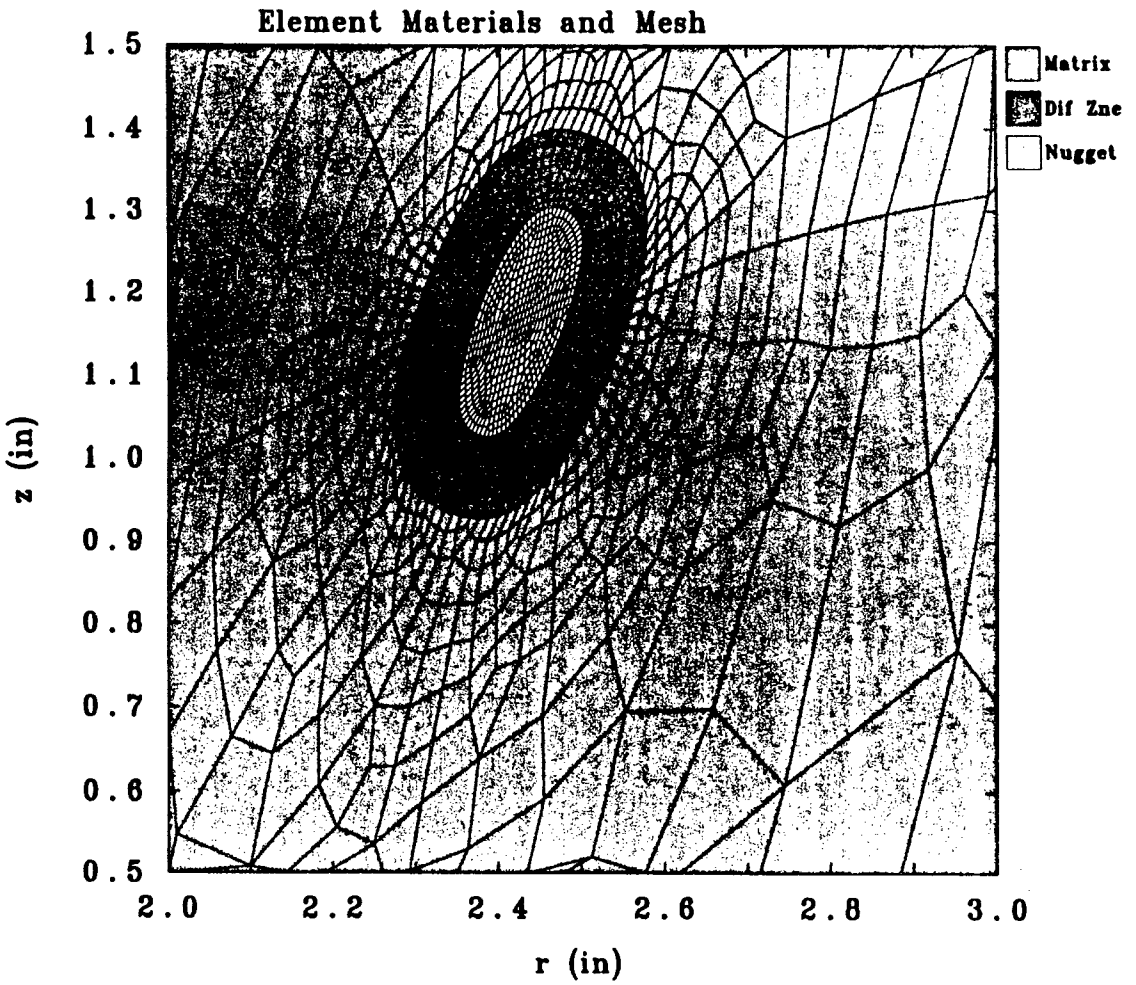

160 mil HA nugget in Ti Matrix, MAAP2D (8/10/96)
Time = 6.000

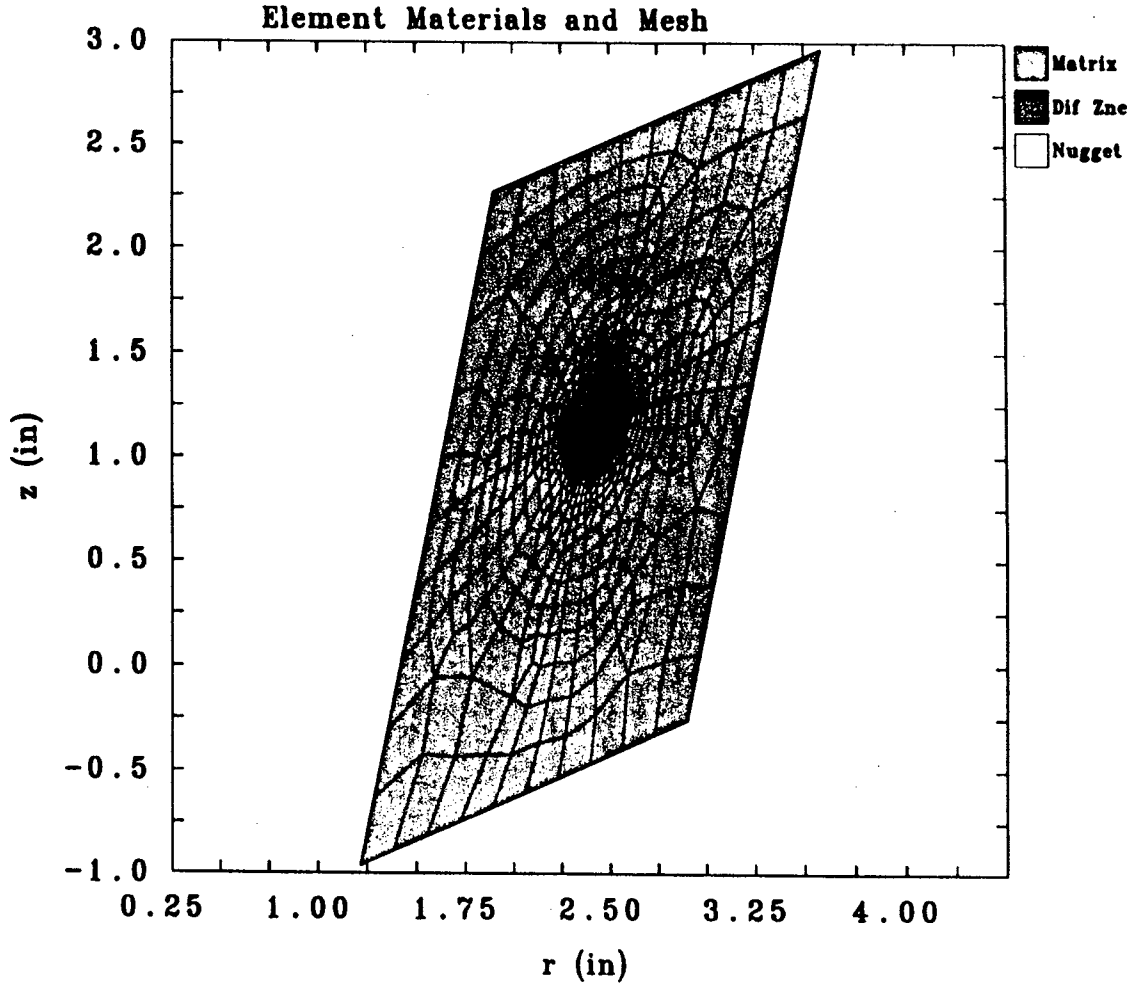

160 mil HA nugget in Ti Matrix, MAAP2D (8/10/96)
Time = 6.000

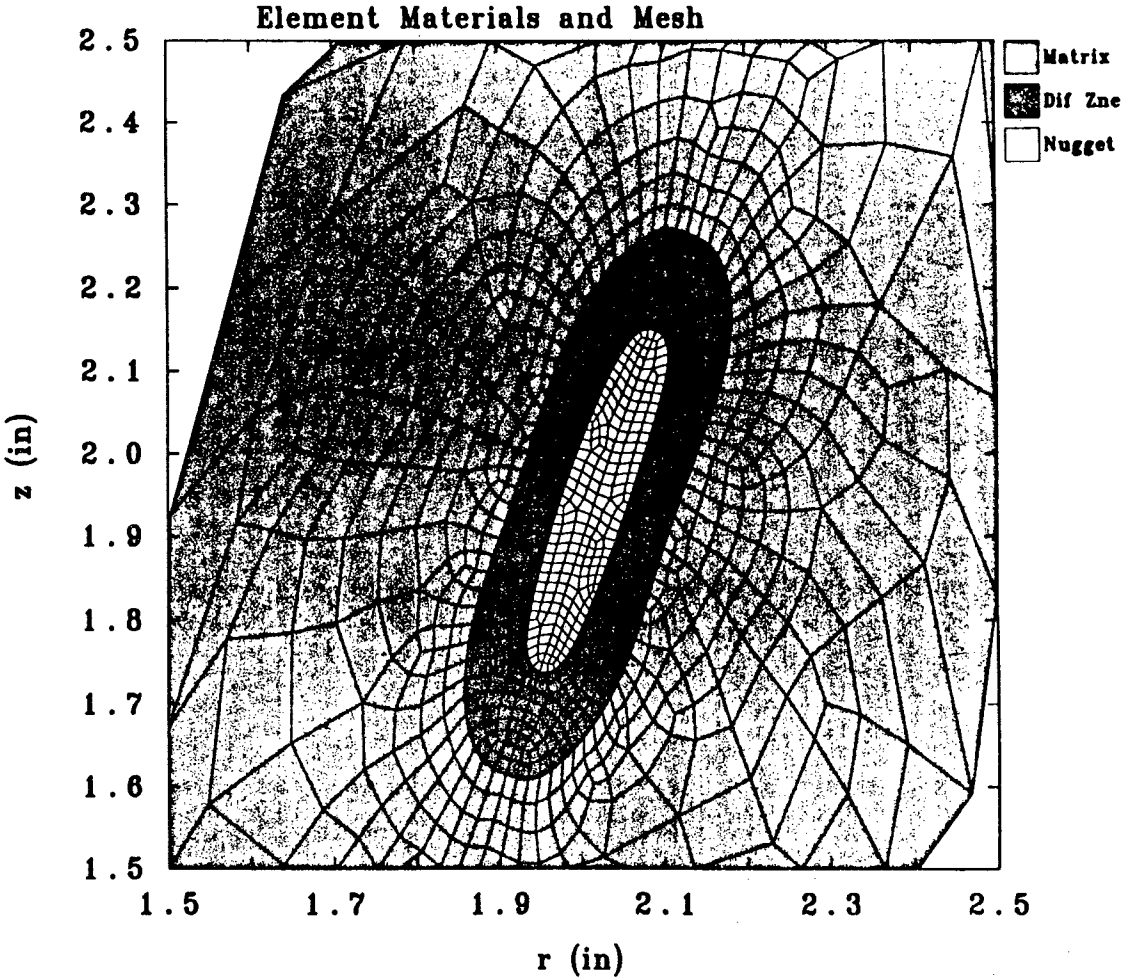

160 mil HA nugget in Ti Matrix, MAAP2D (8/10/96)
Time = 12.200

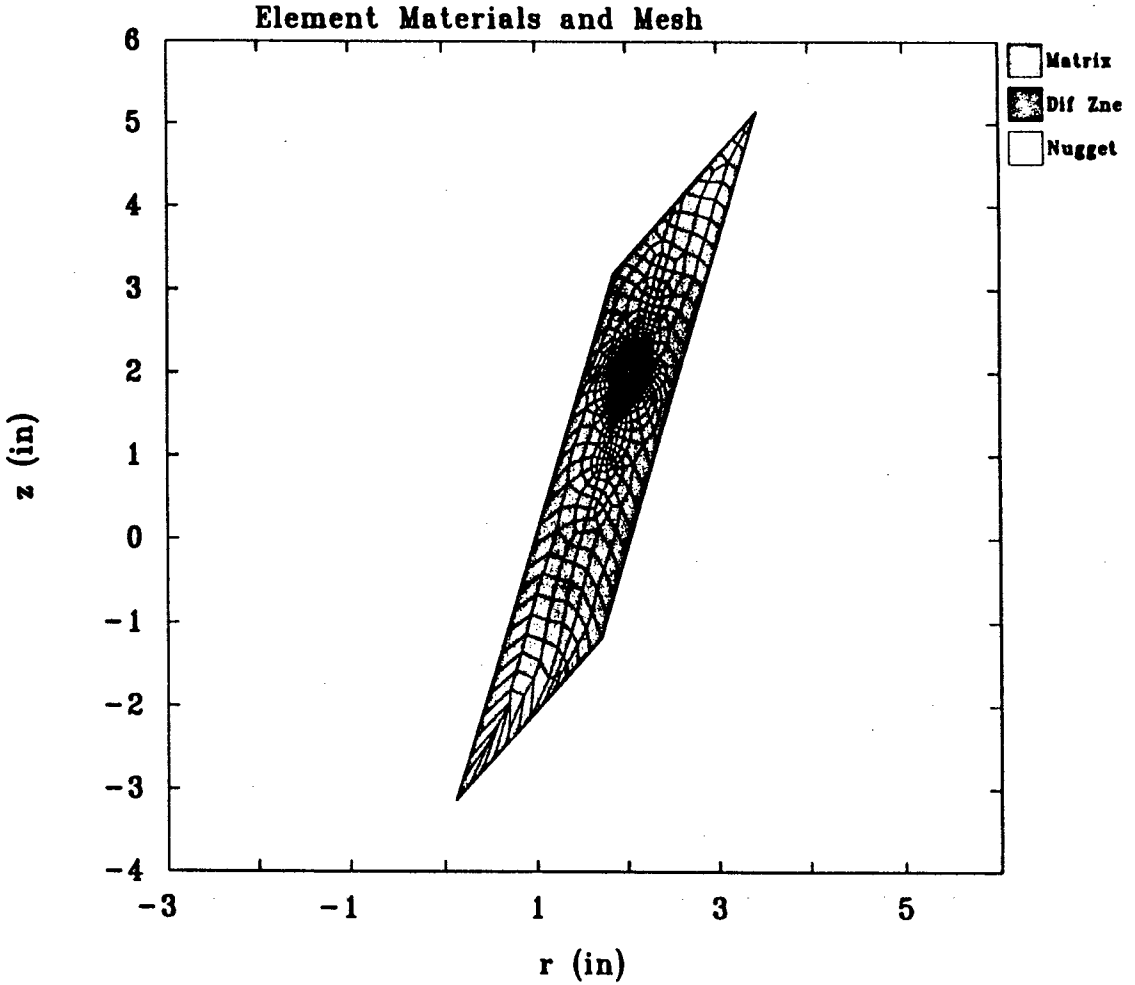

160 mil HA nugget in Ti Matrix, MAAP2D (8/10/96)
Time = 12.200

Constitutive Model Test Matrix
Compression Tests

Strain Rate	Nitrogen Content				
	2.5%	3.85%	6.6%	9%	12%
0.01 sec^{-1}		X		X	X
1 sec^{-1}	X	X	X	X	X

Effect of nitrogen content and strain rate (T=1750°F)

Temperature	Strain Rate	
	0.01 sec^{-1}	1 sec^{-1}
1700°F		X
1750°F	X (Table 1)	X (Table 1)
1800°F		X

Effect of temperature (12% Nitrogen)

TASK 3 -- CRACK NUCLEATION AND GROWTH DATA AND MODELING

- Eighty percent of cracked or burst titanium rotors with defects had the crack originate at subsurface locations, i.e., in a virtual vacuum.
- Fatigue crack growth data is being generated in vacuum for three titanium disk alloys.
- Monotonic and cyclic crack initiation data is being developed for artificially-seeded and, perhaps, natural hard alpha defects.
- Deterministic and probabilistic fatigue crack growth algorithms are being developed for incorporation into the design code.

PHASE I CRACK INITIATION TESTS ON Ti-64 CONTAINING HARD ALPHA SEEDS

Hard-α Diameter	*Number and Type of Test for each Described Condition*			
	Surface-breaking Defect		**Subsurface Defect**	
	Low (2%) Nitrogen	**High (6%) Nitrogen**	**Low (2%) Nitrogen**	**High (6%) Nitrogen**
small (2/64")				1 monotonic 1 cyclic
large (5/64")		2 monotonic 2 cyclic 1 TBD		1 TBD

VACUUM FATIGUE CRACK GROWTH TESTS

Materials: Ti-64, Ti-6242, Ti-17 (5A1-2Sn-2Zr-4Mo-4Cr)
(All 3X VAR and alpha/beta forged)

Source of Material: Ti-64 (G.E. CF6 disk)
Ti-6242 (AlliedSignal TFE 731 impeller)
Ti-17 (G.E.)

R-ratios: 0.05, 0.5, 0.75

Temperatures: Ti-64 (70, 200, 400°F)
Ti-6242 (70, 500, 1000°F)
Ti-17 (70, 750°F)

Data Obtained: ΔK_{th} and region II da/dN

Ti-64 SPECIMEN CUT-UP PLAN

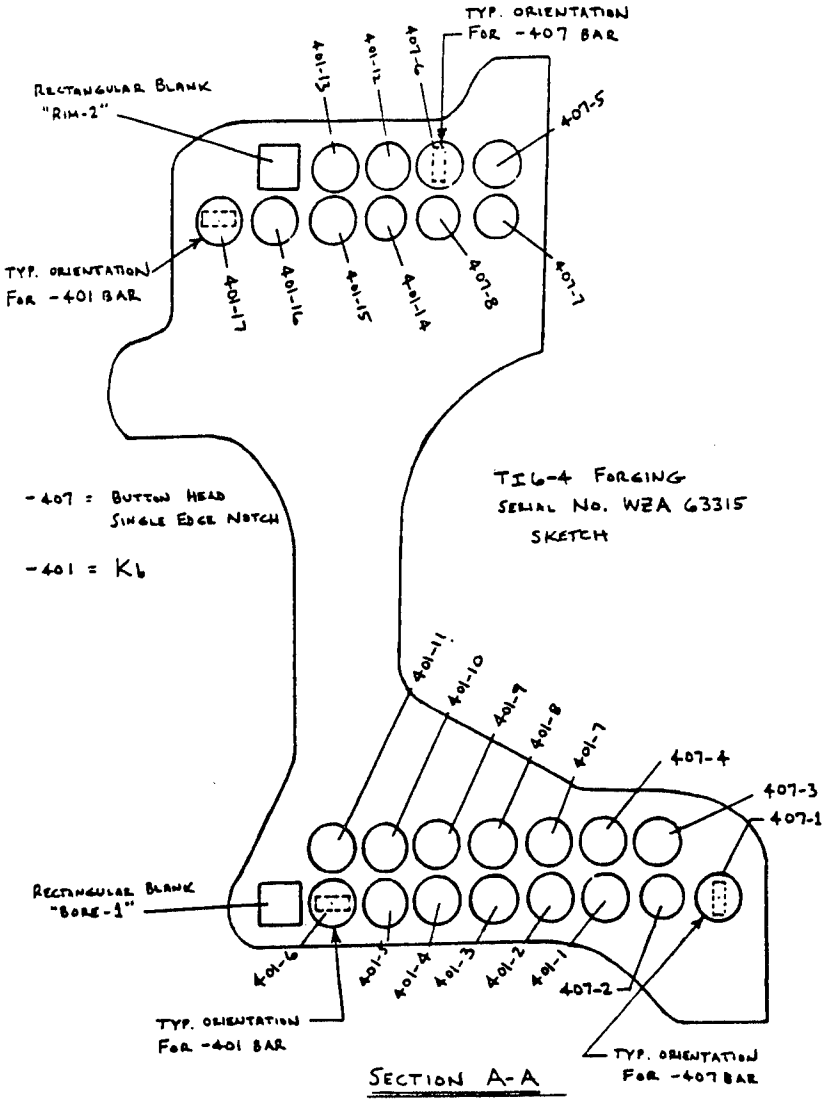

AGARD Fatigue Crack Growth Rate Data

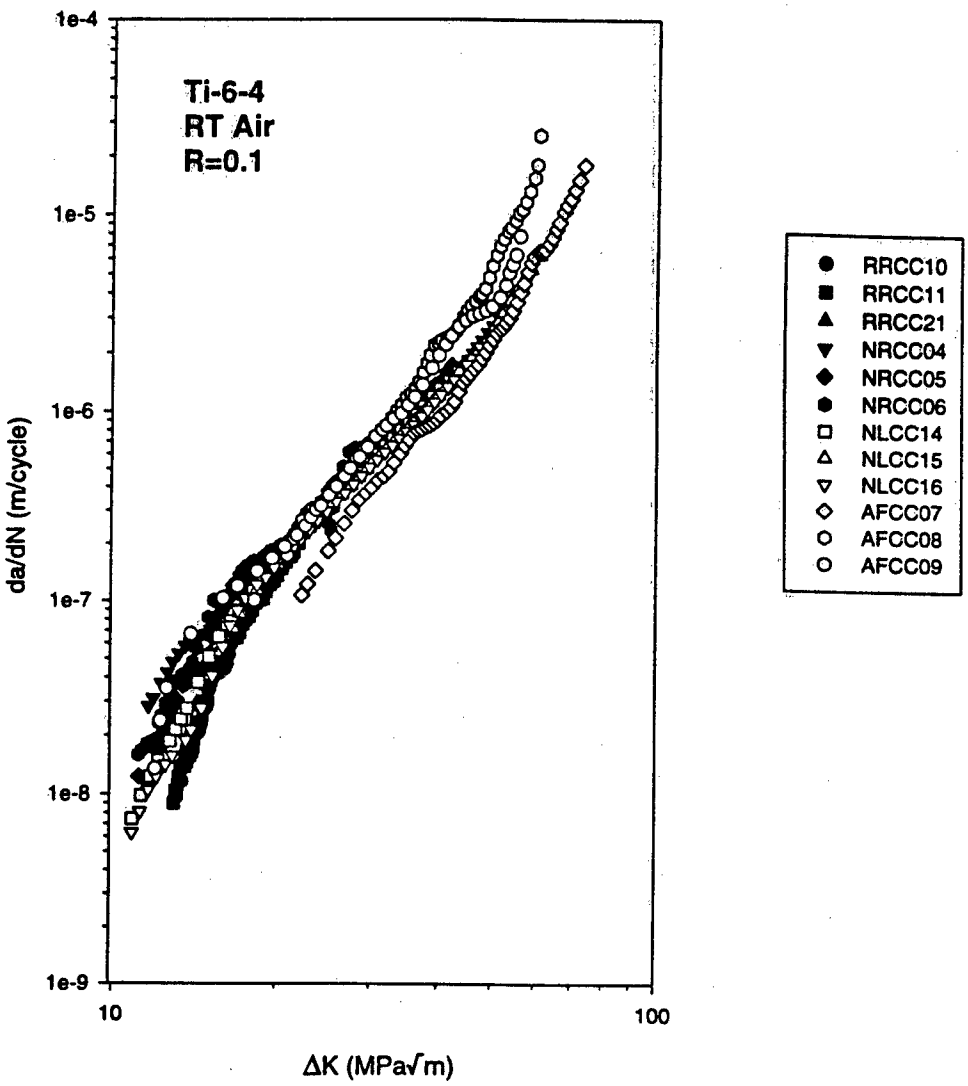

TASK 4 -- PROBABILISTIC INTEGRATION DESIGN CODE DEVELOPMENT AND SENSITIVITY STUDIES

- Development of a generic, damage tolerance rotor design code to augment the current safe-life approach.
- Will incorporate advanced, computationally efficient probabilistic algorithms developed at Southwest Research Institute.
- Development of sensitivity and parametric design curves that identify the relative importance of random input variables.
- The code will be interfaced with the general purpose finite element codes used by the jet engine manufacturers.

Probabilistic Rotor Design Computer Code

Random Variables

- Defect occurrence
- Defect distribution
  - Size, shape, orientation
  - Built in defaults, user-defined
- Fracture toughness
- Fatigue crack growth constant
- Shop visit time
- Mission variations
- Geometrical variations
- Expandable to others
- Distribution library built in, expandable by user

Probabilistic Methods

- System reliability approach
  - Define approx. iso-risk zones
  - Sum risks from all zones
- Monte Carlo simulation
  - Restart capability
  - User-specified confidence/error
- Tailored, more efficient method
- Limit state approach coupled with adaptive life approximation method and adaptive importance sampling method

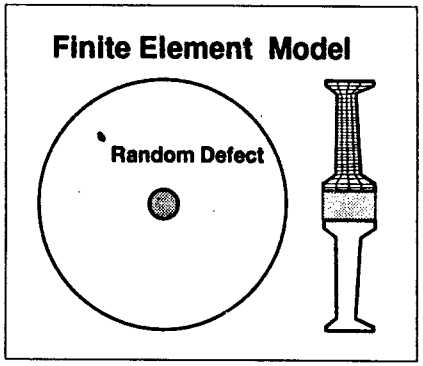

Reliability/Risk & Reliability Sensitivity Analysis

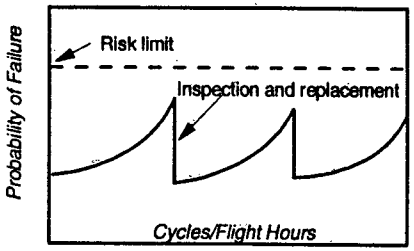

Failure Modes

- Fatigue and fracture due to hard alpha defects in titanium
- Expandable to others

Crack Growth

- Surface and subsurface
- Interface with NASGRO or user supplied code or tabular a vs. N input
- Stress gradient effects

Stress Analysis

- Finite element analysis
- Axisymmetric models
- 3D stress effects through stress modification (e.g., stress concentration factors)
- Neutral file for other FE codes
- Overspeed

Inspection Features

- Different POD's for different regions
- Different POD's for initial and field inspection
- POD library built in, expandable by user
- Multiple inspection schedules

Computer Operation

- Graphical user interface
- Text input file interface
- HP Unix-based workstations

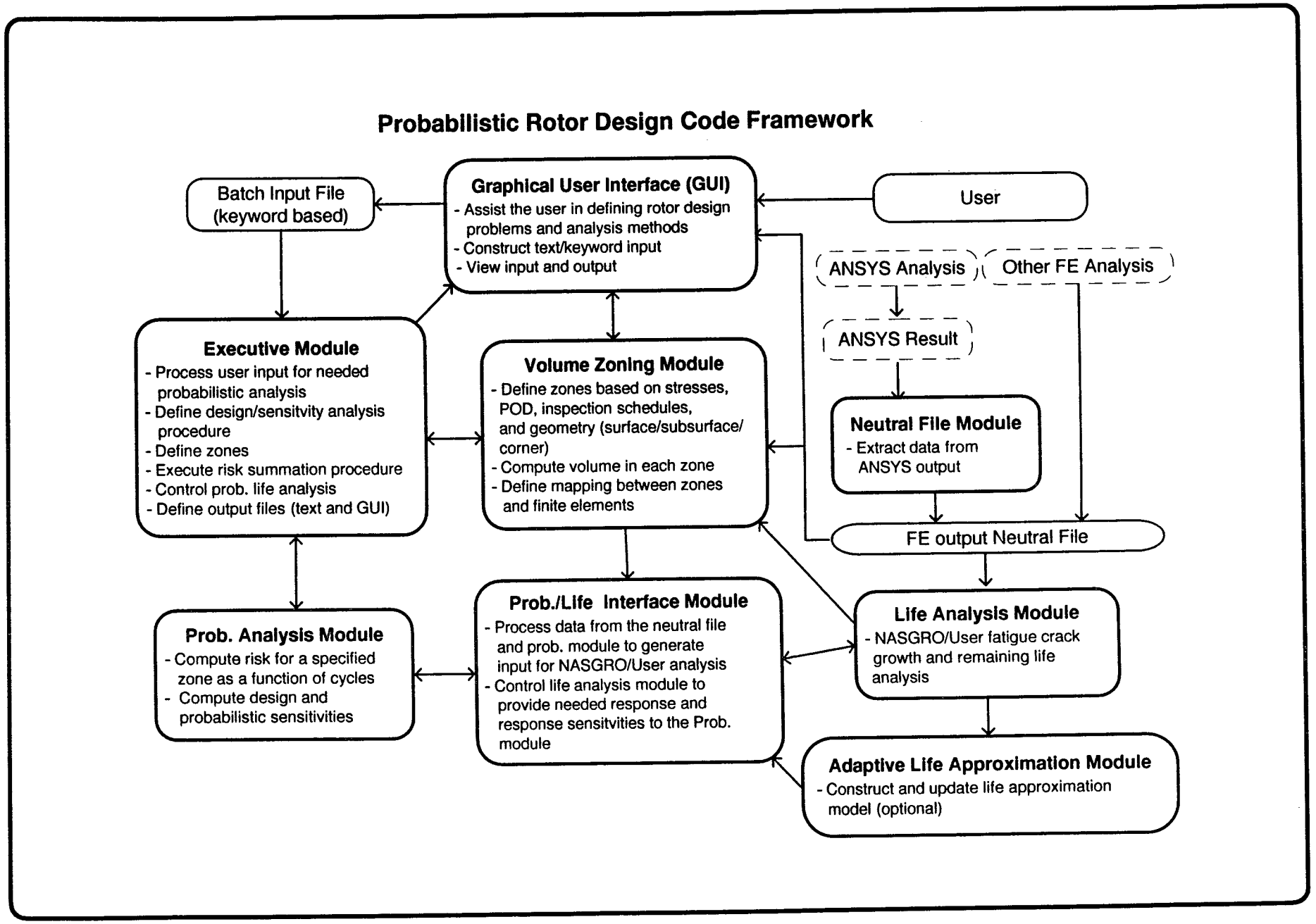
Probabilistic Rotor Design Code Framework
Batch Input File (keyword based)
Graphical User Interface (GUI)
- Assist the user in defining rotor design problems and analysis methods
- Construct text/keyword input
- View input and output
User
ANSYS Analysis
Other FE Analysis
ANSYS Result
Executive Module
- Process user input for needed probabilistic analysis
- Define design/sensitvity analysis procedure
- Define zones
- Execute risk summation procedure
- Control prob. life analysis
- Define output files (text and GUI)
Volume Zoning Module
- Define zones based on stresses, POD, inspection schedules, and geometry (surface/subsurface/corner)
- Compute volume in each zone
- Define mapping between zones and finite elements
Neutral File Module
- Extract data from ANSYS output
FE output Neutral File
Prob./Life Interface Module
- Process data from the neutral file and prob. module to generate input for NASGRO/User analysis
- Control life analysis module to provide needed response and response sensitvities to the Prob. module
Life Analysis Module
- NASGRO/User fatigue crack growth and remaining life analysis
Prob. Analysis Module
- Compute risk for a specified zone as a function of cycles
- Compute design and probabilistic sensitivities
Adaptive Life Approximation Module
- Construct and update life approximation model (optional)

Engine Health Monitoring System for Gas Turbine Engines

*Dr. Michael J. Roemer
Dr. Neville F. Rieger
Stress Technology Incorporated
1800 Brighton-Henrietta Town Line Road
Rochester, New York 14623

Abstract

Accurate component life measurement and integrated diagnostics that reflect component design principles is critical to optimizing the structural integrity of gas turbine engine components once installed in an engine. State-of-the-art technologies such as "virtually sensing" currently unmeasured engine parameters such as turbine entry temperature (TET) are now being used in critical component lifing algorithms to enhance structural integrity assessments in a timely manner. In addition, complex finite-element and empirical models of structural and performance related engine areas can now be accessed in a real-time monitoring environment. Integration and implementation of these proven technologies presents a great opportunity to significantly enhance current engine health measurement capabilities and safely extend engine component life.

A strategy adopted by the USAF to develop a modular, comprehensive engine health monitoring system is presented. An R&D program whose ultimate aim is to develop and test an engine health monitor (EHM) capable of component life measurement, performance and mechanical diagnostics, sensor validation, trending, and anomaly detection is discussed. Engine data currently sensed and recorded for post flight processing will be analyzed in a continuous real-time mode.

The measured data will be used as inputs to "virtual sensing" modules that will predict non-measured parameters needed in the life measurement module. Hence, life usage algorithms will determine critical component remaining life more accurately based on actual mission severity. For fault detection and accommodation, extensive knowledge of how a healthy engine operates under given conditions will be analyzed, and any deviation from this "normal" pattern of expected parameters will be detected and further analyzed. Faults resulting from sensor failure modes will be promptly isolated and more complex faults will be identified by pattern recognition schemes and fuzzy logic. The system under development is designed for the Rolls-Royce F405 engine (Adour) which is fitted to the Navy's T45 trainer, and a full-scale demonstration of the technology will ultimately be conducted on this engine.

EHM System Architecture

The Engine Health Monitoring system under development consists of four modules that will perform sensor validation/recovery, trending, diagnostics, prognostics, and life usage functions. The four modules are named (1) data management, (2) health, (3) diagnostic and (4) engine life and operate simultaneously, transferring real-time, trended, diagnostic, and component life data between the modules as needed. The basic block diagram illustrating the functionality of each module is given below in Figure 1.

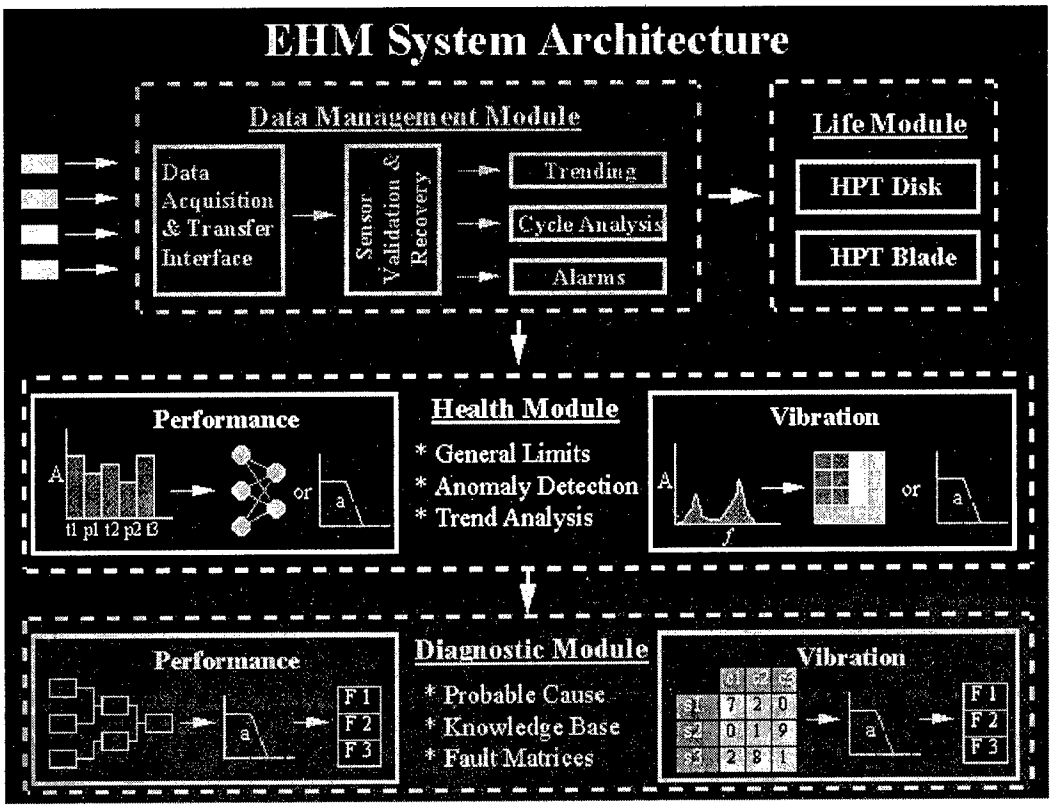

Figure 1 EHM System Architecture

Data Management Module

The first responsibility of the Data Management Module is to acquire the real-time, sensed engine data. Next, the module utilizes a neural network predictor architecture to perform several quality control checks to ensure the integrity of the sensed data. Details on the sensor validation scheme are given later in this paper. Once the data is thoroughly checked, additional engine parameters are predicted in real-time from the directly sensed engine parameters using a standard back propagation network architecture trained by "engine performance synthesis" models. Hence, currently unmeasured engine parameters such as turbine entry temperature (TET) can be predicted and utilized in real-time just as the directly sensed parameters. These "virtually sensed" engine parameters are then used in the engine life module to obtain more accurate and realistic measures of hot component life parts. An engine duty monitor is also present in the data

management module. Engine life is accumulated for both the HP turbine blades and disk based on LCF, creep, and thermal cycles and is presented as a fraction of total available life. The final function to be performed in this module is overall system data storage and retrieval. Raw sensed data, trended data, diagnosis results and engine life accumulation reports are all stored in this sub-module.

Sensor Validation and Recovery System

An advanced sensor validation scheme capable of detecting failed sensor hardware without sensor redundancy and during non-steady state monitoring conditions is a necessary "front end" to the EHM system. The developed approach utilizes neural networks and fuzzy logic to accomplish the desired goal. Neural networks are used to recognize the non-linear, inter-relationships between the different types of sensors used in a transient or steady-state measurement environment. Fuzzy logic is used to pre- and post-process the measurement data in order to determine general characteristics about the state of the process being monitored.

A block diagram of the sensor validation system architecture is given in Figure 2. The speed/power sensor data is first accepted by two parallel fuzzy logic modules. The first module determines the state of the speed/power condition (i.e., increasing, decreasing, or steady-state) and the second verifies the validity of speed/power sensor itself. The output of the speed/power condition module triggers a particular neural network module that was specifically trained to know the sensor relationships for either increasing, decreasing or steady power output. Only one neural network module is triggered at a time, depending on the outcome of the prior fuzzy logic decisions. The sensor confidence values predicted by the neural networks are trended over time and passed through another fuzzy logic module to interpret the results. These extra steps are used to ensure that false alarms do not occur.

For the gas turbine engine application discussed in this paper, there are four primary performance related sensors (along with LP and HP rotor speeds) that are measured during turbine operation. These sensors include; fuel flow (Wf), HP compressor delivery pressure (P3), LP compressor delivery temperature (T2), and Jet Pipe temperature (T6). The outputs of the neural networks yield a confidence factor associated with the

probability of a failed sensor. A confidence factor near one represents proper sensor operation, while a confidence factor near zero indicates a faulty sensor mode. A fuzzy logic module is used at the output of these neural networks to decide whether the sensor is good, bad, or somewhere in between. For instance, if a hard decision was utilized to alert the crew when a sensor confidence factor reached a level less than 0.80, false alarms would likely occur even though a sensor confidence factor of 0.78 might still indicate a properly working sensor.

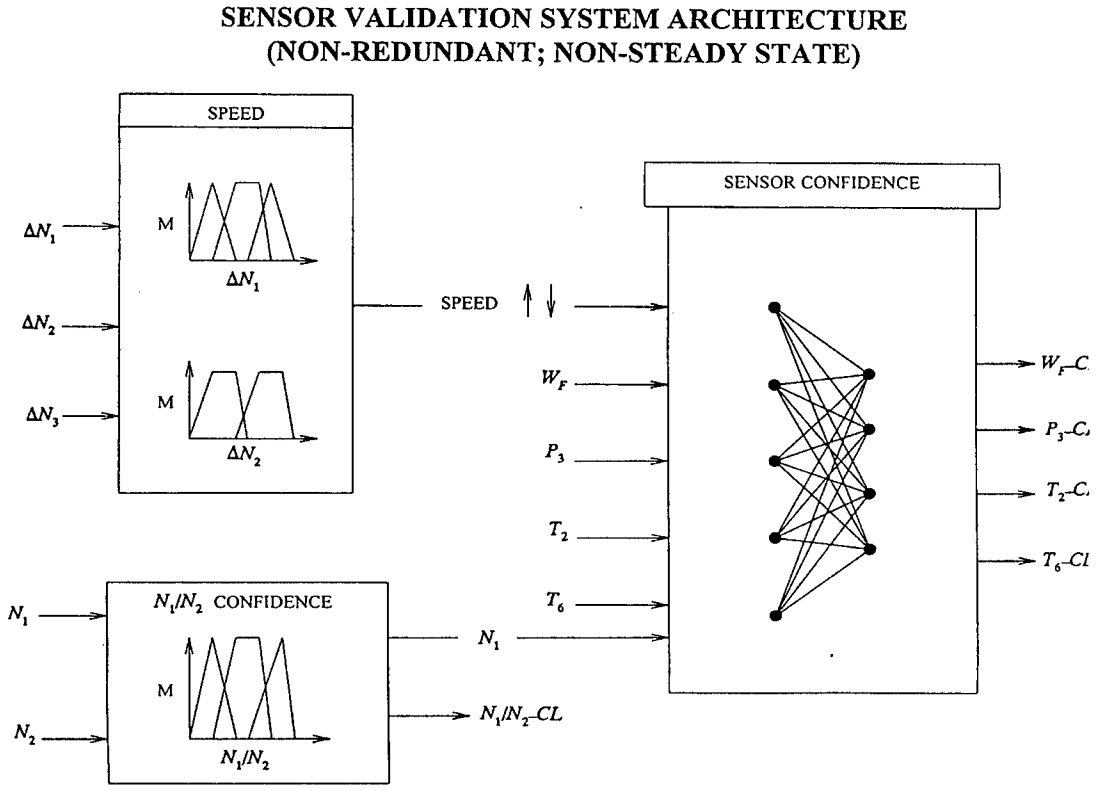

Figure 2 Sensor Validation Scheme

Health Module

The Health Module is dedicated to examining the real-time engine parameter data set and detecting any engine anomalies that exist with respect to the normal engine's operating signature. This function is performed for both the performance parameters and vibration data. First,

the measured performance parameters are examined within pre-determined speed bands during the entire mission to ensure consistent and accurate performance patterns scans. When a set of acquired engine performance parameters trigger an anomaly being detected, the current real-time performance data is forwarded to the diagnostic module for detailed examination. Based on the trended data and fault pattern recognized, the severity and duration of the recognized fault can be determined.

Engine performance anomalies are detected by comparing normal "engine signatures" with a set of current measured engine data. Normal engine signatures are obtained for each engine during the standard production pass-off tests. Each measured parameter (T1, P1, T2, P3, T6, Wf, NL, NH) on the engine is plotted against the HP rotor speed to yield a "normal" range of operation for that specific engine. Any deviations from "fuzzy" bands encompassing these parameter plots will trigger the anomaly detection routines. The "fuzzy" bands are implemented with a dedicated fuzzy logic routine that contains membership functions that are specifically related to the particular engine being monitored.

In addition to the performance anomaly detection described above, vibration anomaly detection and diagnostics is also performed within the real-time monitoring environment. Vibration spectrums from the available engine installed accelerometers are gathered at particular engine operating speeds to form a "current" database of the engine's vibration characteristics. The speed ranges at which the spectrums are stored for the F405 engine are 80%, 85%, 90%, 95%, and 100% maximum NH rotor speed. Figure 3 is an illustration of the vibration anomaly detection and diagnostic scheme showing the spectrums gathered for the starboard tangential and port radial accelerometers.

Once the acceleration power spectral densities are organized into their respective bins, the peaks of the NL and NH rotor speeds are examined for overall amplitude and location (in terms of the % max NH speed) of the peaks. This information is used by the fuzzy logic diagnostic algorithms to determine if the vibration is coming from either the compressor or turbine and if it is associated with the HP or LP shaft. Once the basic location of the vibration source is determined, a more detailed diagnosis of the vibration problem is predicted. Currently, the system has been trained to recognize vibration fault patterns including; 1.)

Unbalance/Misalignment, 2.) Rotor Rub and Mechanical Looseness, and 3.) Deteriorated Bearing Conditions.

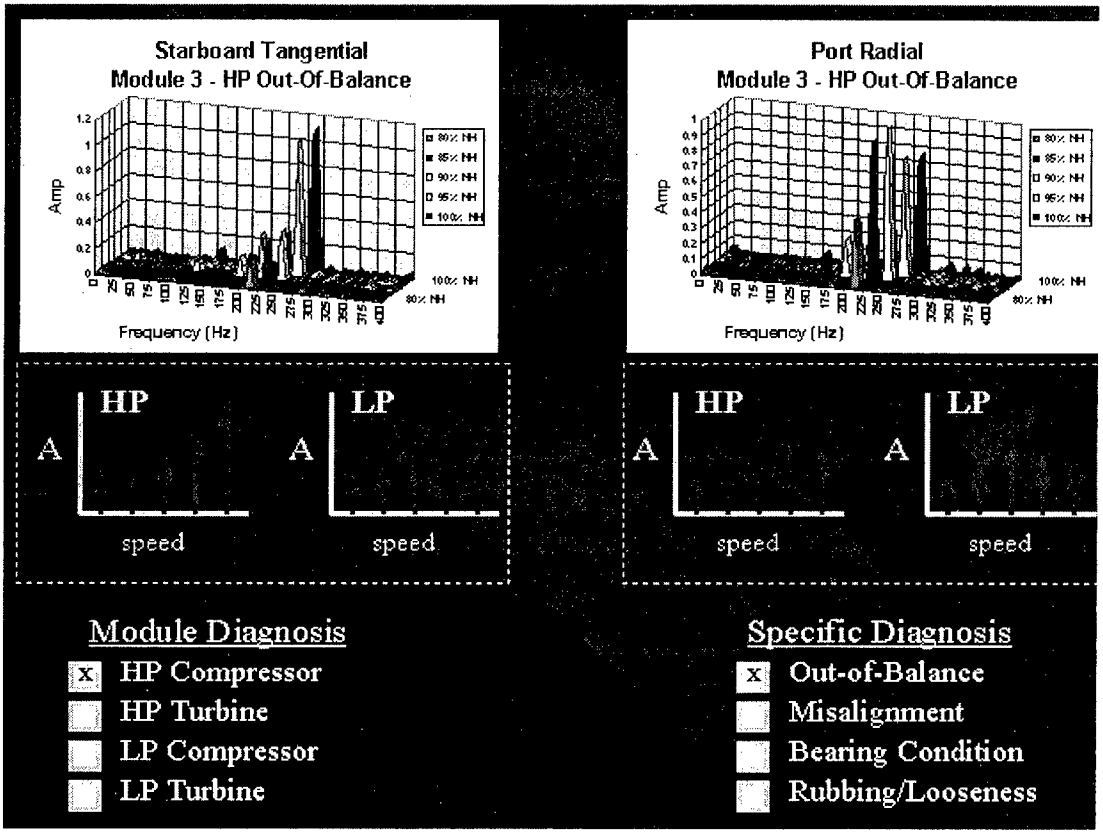

Figure 3 Vibration Anomaly Detection and Diagnostics Scheme

Diagnostic Module

Once an anomaly is detected and the current data is transferred to the Diagnostic Module, dedicated neural network fault classifiers determine the probable cause of the fault or degraded performance. A block diagram of the performance diagnostic procedure is given in Figure 4 shown below.

The underlying design of this model-based, fault diagnostic module lies in the determination of changing conditions appearing in engine sensory data due to the existence of particular faults. These observed

changes are compared with the "normal" operating engine process to recognize error residuals. These residuals and associated patterns are then analyzed for failure detection and diagnosis by comparing them with known failure signatures associated with a failed component on the operating engine.

Engine fault signatures, which illustrate the effect of a failure on particular engine parameters, are generated from both historical engine data and engine synthesis models of the engine. In fact, a combination of these approaches is utilized in this EHM system. In the end, the failure diagnosis is accomplished with a neural network classifier to recognize the patterns of respective failure signatures. The performance diagnostic module in this program utilizes both self organizing neural network maps (to cluster and identify similar patterns) and trained network classifiers for specific problem diagnosis.

The real-time engine data for a particular speed-band is first compared with the corresponding "normal" operating patterns to determine measured parameter changes. These error patterns are then normalized with respect to the maximum measured parameter change and passed to a self organizing neural network map (Kohonen network) for initial pattern clustering. Figure 5 illustrates the results of Kohonen self-organizing map under noisy pattern conditions. Error pattern clustering was used as an initial diagnostic step because of its high robustness with respect to pattern noise. After the error pattern has been organized into a particular location on 10x10 interpretive Kohonen map, a trained back-propagation network classifies the coordinate location on the map into a specific diagnosis.

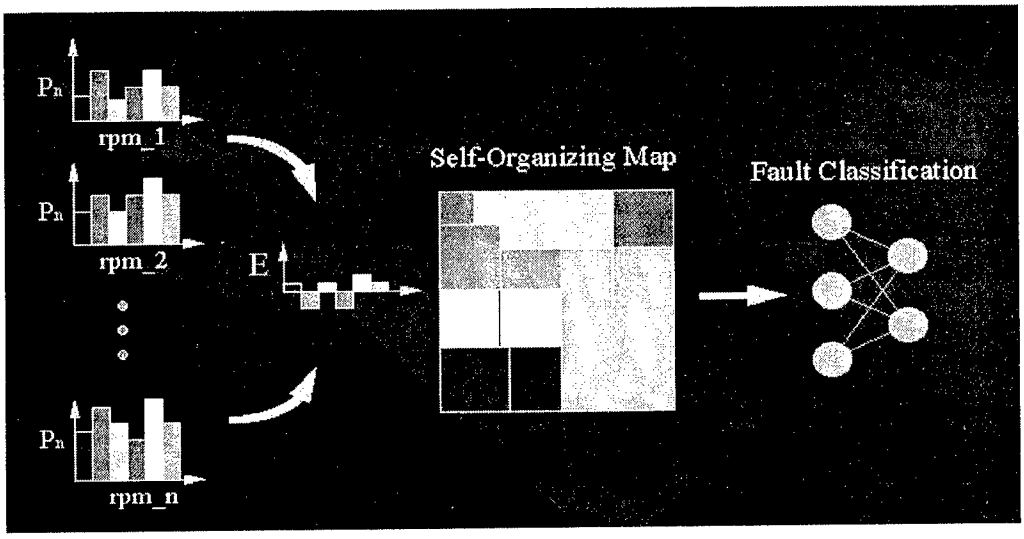

Figure 4 Performance Diagnostics Scheme

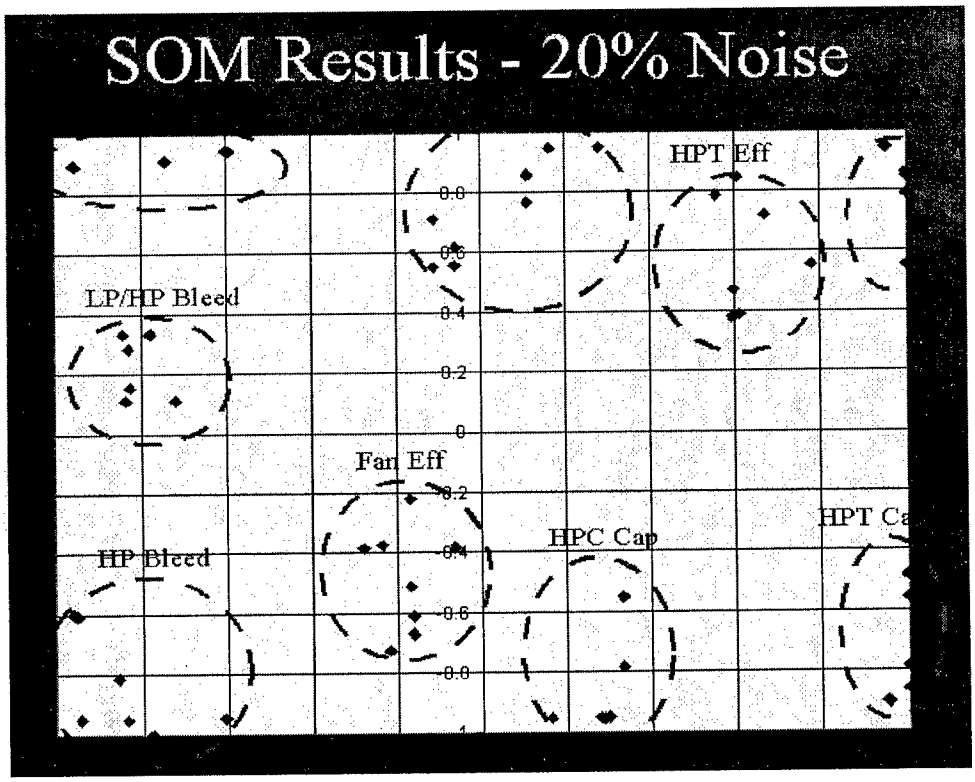

Figure 5 Kohonen Map Diagnostics

Engine Life Module

During the mission, data from the engine duty monitor within the Data Management Module is continuously being transferred to the Engine Life Module so that "mission representative" life may be accumulated. The life accumulation algorithm will include the engine specific parameters tracked throughout the entire mission. Hot section temperatures and stresses will be estimated in real-time based on a neural network architecture trained from engine synthesis models and BLADE-GT finite element models. Corresponding material creep and thermo-mechanical fatigue will therefore be more accurately determined based on actual mission severity. At the end of the mission, critical component life accumulated during that mission is reported and transferred back to the data management module for overall accumulation of each components life usage.

A significant advancement will be made in monitoring the life of HP turbine blades and disks by utilizing state-of-the-art BLADE-GT finite element models in real-time to predict the blade's critical stresses. The process for obtaining "virtual stress measurements" is accomplished by training neural networks with data that is generated by exercising the BLADE-GT model over a full range of engine operating conditions. This process has already been proven in several other applications with FE and engine synthesis models, with predictive virtual sensor results having an average error of less than 0.5%. Currently, the EHM system developed for the F405 engine on the Navy Trainer "virtually senses" SOT, T3, T4, and W1A.

Once the network is trained from the off-line model results, the network is ready to be accessed in real-time to produce the most accurate estimates of stresses and temperatures without actually having strain gauges or RTDs in place. This procedure has wide application in other areas of the engine where accurate models can be used to predict unmeasured parameters.

The discussed EHM system incorporates LCF, material temperature/creep, and thermo-mechanical fatigue aspects into a comprehensive damage accumulation algorithm. This represents a significant enhancement over the current life monitoring systems. Primarily, increased emphasis will be placed on "hot" components where these

mechanisms play a large role in the failure process. The proposed approach of *individually tracking the total life of each critical component* will allow for a more representative and less conservative estimate of component life consumption.

The engine life module developed for the F405 engine concentrated on the HP turbine disk and blades Other components can easily be added to the system if the necessary life algorithms are available. Engine life usage algorithms for creep and low cycle fatigue of critical parts are already included in the Aircraft Data Recording system on the T45A Goshawk aircraft. The algorithms for the HP disk will be refined to use the more specific data available from the Data Management module to record accumulated life usage.

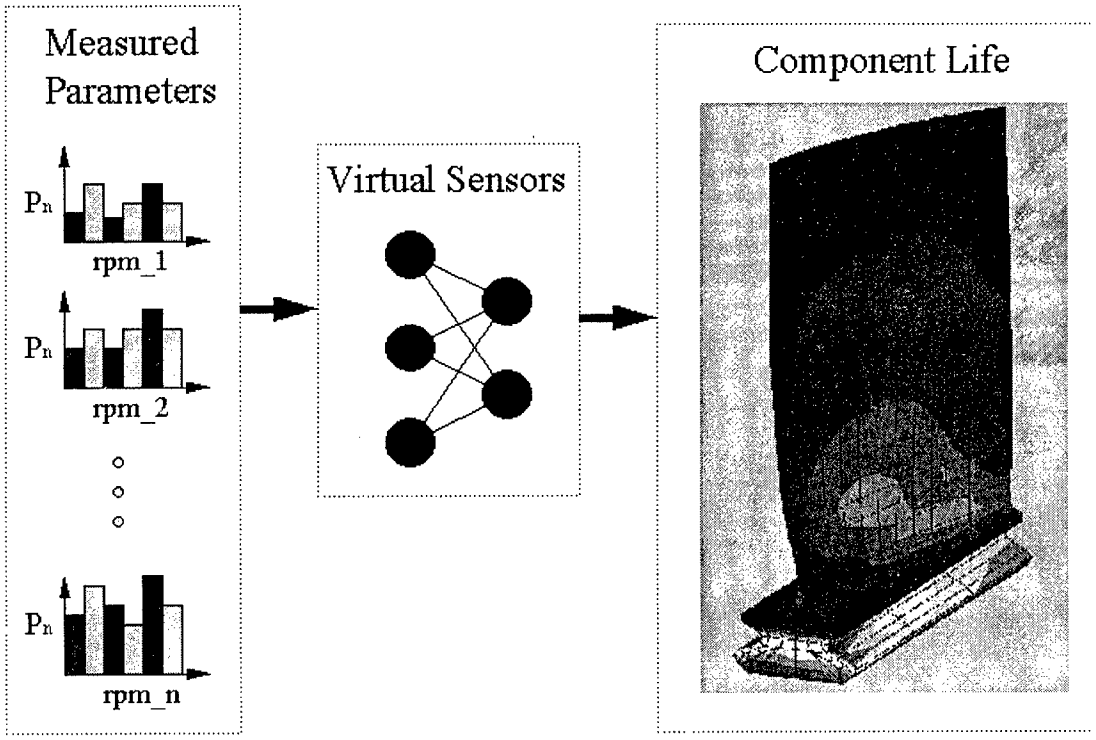

Figure 6 Engine Component Life Monitoring Scheme

EHM Ground Test System Software

A dedicated EHM software interface has been designed to aid in the development and testing of the real-time monitor. Specific user interface modules have been developed so that all monitoring aspects of the system can be examined during the testing stages of the program. Each of the engineering modules and corresponding software interfaces are discussed in this paper with examples of Adour engine data that have been processed by the EHM. The main "front end" EHM software screen is given in Figure 7.

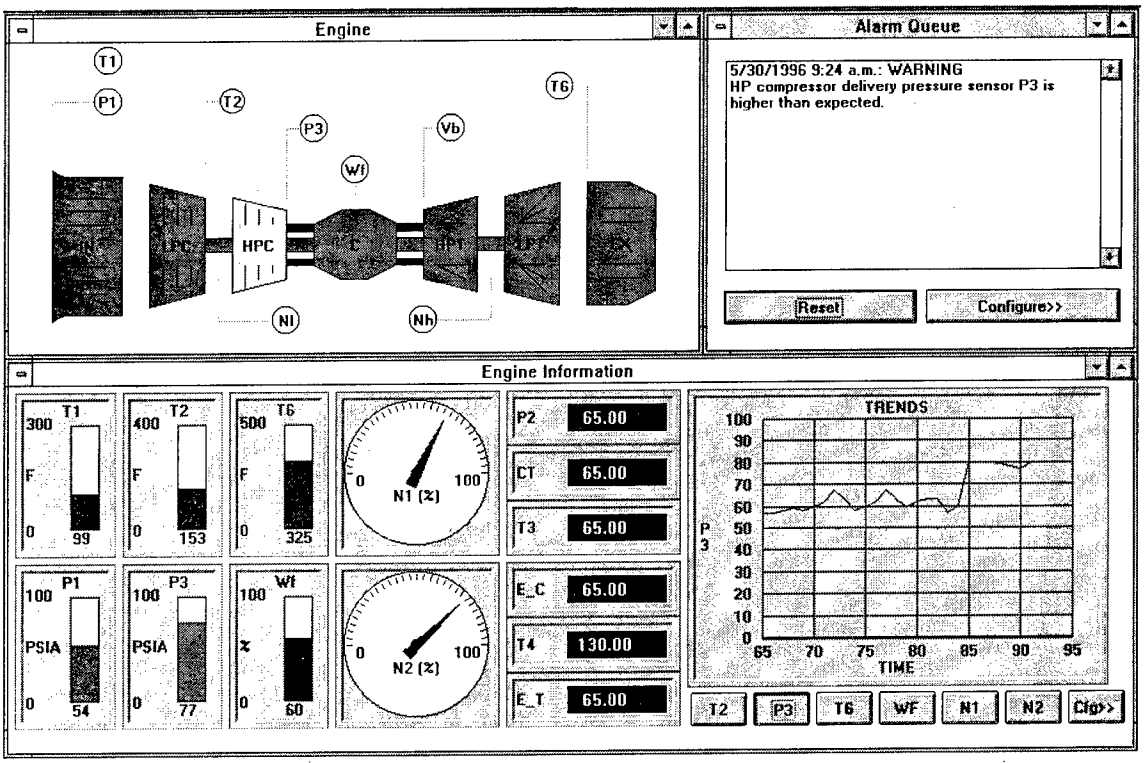

Figure 7 EHM Software "Main Screen"

Conclusions

With the application of artificial intelligence to real-time engine diagnostics and more mission representative lifing algorithms, current

engine health monitoring systems can be improved significantly. In particular, the incorporation of neural networks and fuzzy logic into the diagnostic process will yield great benefits in terms of processing speed, robustness, knowledge acquisition, and adaptability. A list of some important technical benefits of applying AI and advanced life prediction schemes to condition monitoring, diagnosis, and life usage are as follows:

1. Enhanced ability to capture, organize, and utilize all relevant data, experience, and rules within a massively parallel, interconnected processing unit.

2. Provides an automated procedure for incorporating data from several knowledge sources including; analytical FEM models, aerothermal performance models, empirical/trended test data, and heuristic (rules based) experience.

3. Neural network system architectures are well suited for processing large quantities of non-linear, multidimensional, coupled parameters such as temperatures, pressures, etc. that occur within a gas turbine engine.

4. Utilizing artificial intelligence results in a process that is less dependent on human experts and more automated to facilitate quick decision making.

5. Incorporating more accurate information into the proposed life accumulation algorithms will provide a more accurate outlook on the remaining life of critical engine components.

References

1. Walker, N. D. and G. F., Wyatt-Mair, "*Sensor Signal Validation Using Analytical Redundancy for an Aluminum Cold Rolling Mill,*" Control Engineering Practice, Vol. 3, No. 6, June 1995, pp.753-760.

2. McAvoy, T. J., "*Sensor Data Analysis Using Autoassociative Neural Nets,*" World Congress on Neural Networks, Vol. 1, 1994, pp.161-166.

3. Holbert, K. E., A. S., Heger, and N. K., Alang-Rashid, "*Redundant Sensor Validation by using Fuzzy Logic,*" Nuclear Science and Engineering, Vol. 118, No. 1, Sept. 1994, pp.54-64.

4. Harrison, P. R., and P.A., Harrison, *"Validating an Embedded Intelligent Sensor Control System,"* IEEE Expert, Vol. 9, No. 3, June 1994, pp. 49-53.

5. Ahmadi-Echendu, J. E., and Zhu Hengjun, "*Detecting Changes in the Condition of Process Instruments,*" IEEE Transactions on Instrumentation and Measurement, Vol. 43, No. 2, April 1994, pp.355-358.

6. Lee, S. C., "*Sensor Value Validation Based on Systematic Exploration of the Sensor Redundancy for Fault Diagnosis,*" IEEE Transactions on Systems, Man and Cybernetics, Vol. 24, No. 4, April 1994, pp. 594-605.

MJR:jah

d:\roemer\ASIP96.doc

The Role of Residual Stress in Low Cycle Fatigue of Gas Turbine Engine Disks

*Mr. E.F. Bradley
Mr. S.G. Berkley
Fatigue Management Associates
1000 N. US Highway 1, Suite 615, Jupiter, FL 33477-4481

Mr. R. J. Fairbank
United Airlines
San Francisco International Airport
San Francisco, CA 94128-3800

Low Cycle Fatigue (LCF) is the mechanism that defines the ultimate life of fracture-critical aircraft engine disks. Given the potential Airworthiness implications of LCF cracking, it is extremely important to understand the mechanism and it's interaction with other mechanical, metallurgical, and structural conditions.

Low Cycle Fatigue is cumulative fatigue damage associated with that part of the standard strain range versus cycles to failure curve which includes cycles to failure of up to about 10^4 cycles, see Figure 1. Low Cycle Fatigue involves both mechanically and thermally induced strains according to Bradley et al. *(Reference 1)*. Since it is the normal wearout mechanism in gas turbine engine disks, LCF has a profound effect on engine structural integrity and flight safety.

The technical mechanism of LCF has been exhaustively studied and it is agreed that the strain range and frequently the plastic strain range, is more significant than the stress range in the LCF of metals. Tavernelli and Coffin (*Reference 2*) have suggested that the plastic strain range is directly related to endurance in LCF. The correlation between total strain range and cycles-to-fracture shows that surface damage can greatly influence component life as revealed by crack growth rate studies. The work of S. Manson and Hirschberg (*Reference 3*) has established the basic relation between cyclic life and total strain

range. In the low life range the elastic component is almost negligible compared to the plastic component. At higher cyclic lives, however, the plastic strain rapidly diminishes to negligible values while the elastic strain range remains relatively high. Thus the total strain slope approaches tangency to the elastic strain slope. According to Manson, the crossover point is about 10^3 cycles. Figure 1 shows the total strain amplitude vs. life curve obtained from the superposition of the elastic and plastic strain amplitudes vs. life curves. Therefore, in short fatigue lives, plastic strain amplitude is more dominant than the elastic strain amplitude so that LCF life is controlled by the material's ductility. At long fatigue lives, the elastic strain amplitude is more significant than the plastic strain amplitude, and the fatigue life is determined by fracture strength (*Reference 4*).

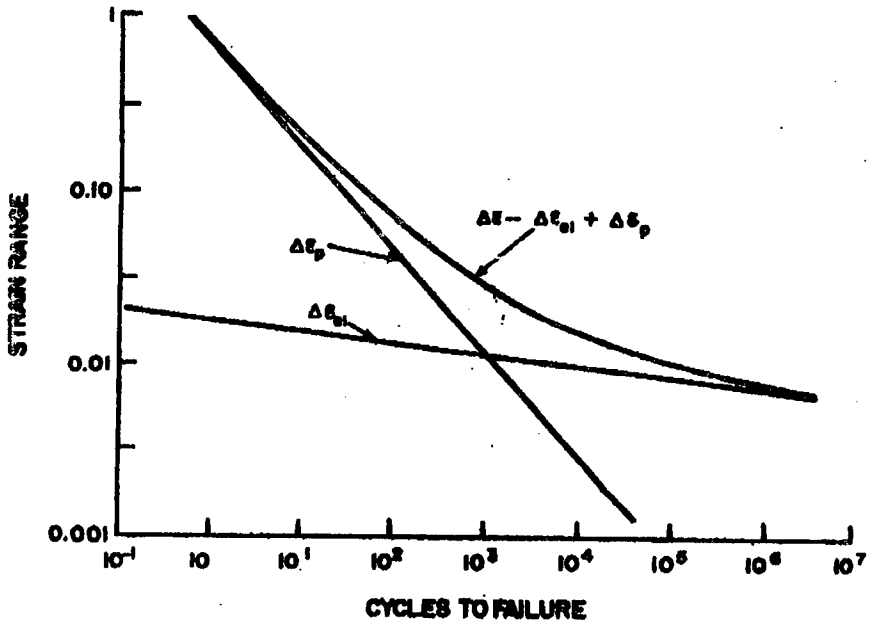

Figure 1. Strain Range versus Cycles to Failure Curve

It is generally accepted that the free surface of a component is the common site for nucleation of fatigue cracks. Further, it is well known that fatigue cracks originate in surfaces that are stressed in tension. Therefore the manner in which the surface is prepared during manufacture has a decisive role in dictating the time of initiation of fatigue cracks. Consider shot peening for example, which is widely used to improve the fatigue life of many engine structural parts. In the shot peening process, a stream of small hard spheres (typically around 1 mm diameter) is impinged on the surface being treated. Depending on the diameter of the shot, the velocity of their impact on the surface, and the duration of the process, the

maximum compressive residual stress generated by the localized plastic deformation of the surface layer can measure approximately 75% of the typical yield strength of the material. The compressive residual zone spans a depth of about $^1/_4$ to $^1/_2$ the diameter of the shot. This compressively stressed surface layer significantly enhances the total part fatigue life by reducing the damaging effect of the tensile portion of fully reversed cyclic loads (*Reference 5*).

Because LCF is the primary degradation mechanism in aging engine disks, aircraft engine manufacturers have acquired broad semi-empirical knowledge of the LCF mechanism. Experience has shown that LCF failures are characterized by multiple cracking in highly stressed areas experiencing general surface degradation. This differs from high frequency fatigue failures which are generally singular, initiating at precise defect sites with the crack propagating by stress concentration. The effects of metallurgical structure, material processing, environment, mechanical properties, defects and surface treatments have been evaluated for many alloys. Aircraft engine metallurgists and engineers, therefore, are very familiar with the many complex interactions that affect LCF. These include crack initiation and propagation, crack mode (intergranular or transgranular), grain size and grain boundary effect, microstructure, environment (temperature and applied stress), mechanical properties (strength, ductility, fracture toughness), and the very important condition of residual stress.

Engine disks are carefully designed to resist the onset of LCF as well as for the projected cumulative service conditions. This may require trade offs between cross-section thickness and weight, proper selection of material and processing (i.e. heat treatment, surface treatment, etc.) with adequate combination of LCF resistance, service temperature strength (i.e. creep, stress-rupture, yield, etc.), ductility and fracture toughness. On top of all this it is very important to provide exacting control on the part's manufacturing procedures. Residual stress is produced by normal manufacturing processes, such as machining, and can be beneficial to the LCF life of a disk if compressive, or detrimental if tensile. Mechanical working, which causes nonuniform plastic deformation, may be used to impart favorable residual stress distribution. Shot peening and surface rolling of fillets are two examples. Deleterious residual stress patterns may also arise from mechanical working as, for example, in the development of tensile stresses due to cold straightening or abusive machining. Furthermore, common machining operations such as grinding, polishing and milling cause different degrees of surface roughness. The valleys in rough surfaces serve as areas of stress concentration which, in turn, induce different levels of resistance to fatigue crack nucleation. Also, changes in mission mix, mission profiles and operating

environment can significantly alter residual stress thus affecting LCF life. But these residual stresses are not normally measured and have not been related to cycles.

Aircraft engine manufacturers utilize this knowledge together with experience gained from engine performance of similar parts in sophisticated modeling techniques to establish life limits for rotating components (disks, shafts, hubs). In determining these life limits very conservative assumptions and safety factors are incorporated. For commercial engines, Federal Aviation Administration regulations provide guidance for the lifing process and regulators review and approve all life limits. The LCF life prediction is based on a minimum life criterion. This means that in a large population of parts, the system pertains only to the life forecast of the weakest component of that population (less than one in a thousand parts). Only minimum materials properties are used in the part design. The majority of life limited parts reach their maximum life and are retired without in-service difficulties. Occasionally, lifelimited parts develop LCF cracks prior to reaching their maximum life. Low Cycle Fatigue cracks are found either during post engine disassembly inspection or in rare occurrences by in-service failures. The detection of LCF cracks usually results in mandated programs that increase part inspections and/or implement specific localized non-destructive inspection procedures. The intent of these programs is to prevent in-service failures by detecting cracks before they progress to failure. In this frame of reference, detection of LCF cracks is a warning of potential part failure.

Obviously, processing and surface treatments for disks are of great significance. Yet in the design of these critical components and the setting of a conservative life prediction system the effect of the important shot peening surface treatment has not been considered on most disks in service. Metal part fabrication and surface treatment confer on components a strain history which should be taken into account in relation to subsequent LCF resistance. This resistance is important in engine operation because component stresses may exceed the yield strength of the material in the vicinity of stress risers. This explains the interest with which cold working surface treatments like shot peening, barrel finishing and honing, are viewed in regard to the augmentation of fatigue resistance. Compressive residual stresses are a product of these treatments. It has been amply demonstrated that fatigue cracking (LCF or high frequency) initiates on surfaces stressed in tension. For this reason, providing surface residual compression stresses by operations such as shot peening is beneficial from the standpoint of fatigue resistance. Fatigue life is improved because service applied stress and temperature conditions must overcome the residual compressive stress and build up sufficient tensile stress before fatigue cracks can start.

It is important here to recognize that total stress equals the sum of applied stress and residual stress. Compressive residual surface stress acts negatively, detracting from the applied tensile loading. It is total stress that finally causes the part to crack. This does not mean that fatigue cracking will initiate as soon as the residual compressive stress has been dissipated, since the part has been designed to resist the onset of LCF under the service conditions without regard to the beneficial effects of shot peening. This is partly because of the conservative nature of the life prediction system, but also due to the fact that up to this time there was no convenient way to determine the actual surface residual stress. Thus the fatigue life improvement due to shot peening is, in effect, an uncredited bonus. Other beneficial manufacturing processes include chemical milling, honing, polishing and burnishing. All of these enhance the surface by removing defects and stress risers that can be produced by other previous manufacturing operations. Properly controlled shot peening, however, is the most appropriate method to ensure the surface is in residual compressive stress. The surface compressive stress will gradually be decreased due to the imposed service applied tensile loading and operation at elevated temperature, and in time the onset of LCF will occur if the part remains in service.

As long as the surface remains residually stressed in compression, fatigue failures will not initiate. Therefore, if the part is periodically measured for surface residual stress using a newly developed Fatigue Management Associates (FMA) non-destructive inspection method, an accurate and safe prediction can be made relative to continuing part use, need for rework, or part retirement. These predictions consider that disk usage produces hoop stresses and LCF takes the form of multiple cracking at blade slots and other highly stressed locations such as disk bores. FMA's basic concept is that as disks age in service, the original surface compressive stress condition will degrade (Figure 2), and in time become tensile. Periodic residual stress measurement of disks, therefore, will provide an indication of remaining life and early warning of potential LCF cracking. The benefits of such a process are substantial, and can be measured in terms of increased safety margins and reduced maintenance costs. Safety margins are increased by reducing the potential of in-service failures, and economics are improved by reducing the number of forced engine removals and disassemblies to inspect specific parts for the presence of LCF cracks and provide a basis for extended usage.

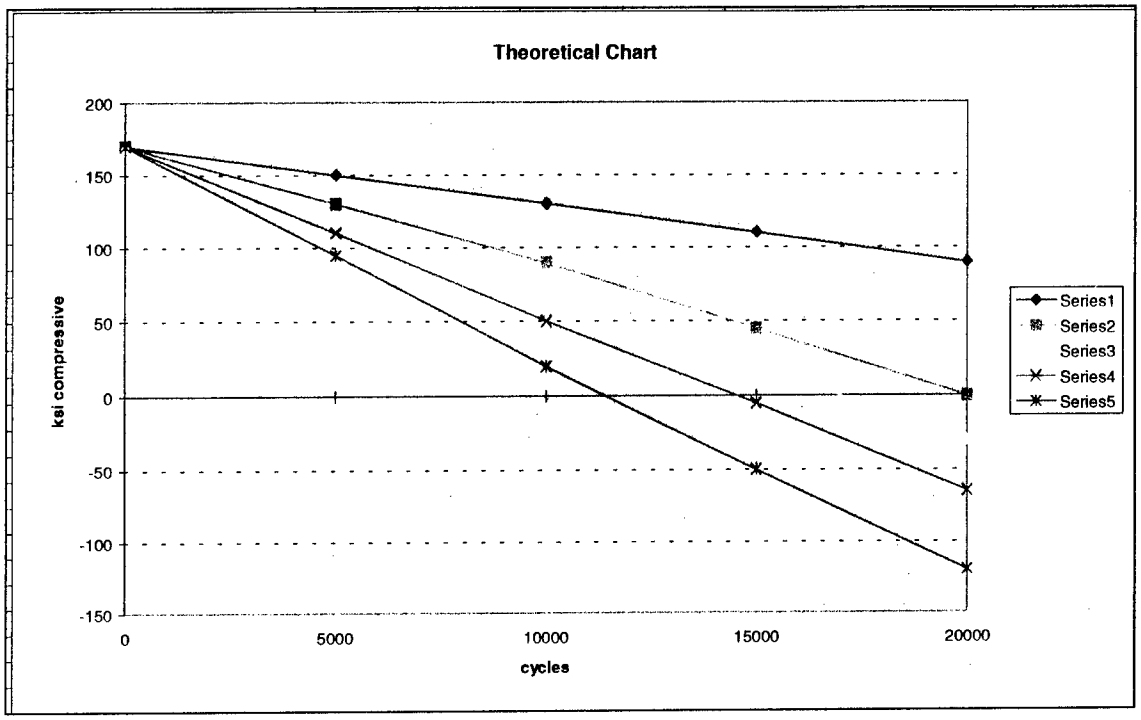

Figure 2. Residual Compressive Stress versus Cycles (Theoretical Curve)

In addition, mandated reduced cyclic life is a high cost to the Original Equipment Manufacturer (OEM) in terms of original life guarantees and to the user by requiring shorter periodic Non-Destructive Testing (NDT) inspections. For example, Airworthiness Directives (AD) can significantly reduce cyclic life or hours on disks. These amendments may be prompted, in part, by new temperature data from engine testing or experience that result in different recalculated stress levels. These data can cause a change in the calculated cyclic service life. The actions specified by these AD are intended to prevent disk failures, which may result in an uncontained engine failure and possible damage to the aircraft.

FMA's new, patented process (*Reference 6*) to quantify the surface residual stress condition of metal parts uses X-Ray diffraction for measuring the residual stresses. Stresses are determined by measuring the strain in the atomic lattice and by relating the strains to stresses through the elastic theory. Combining advanced computer technology with the X-Ray diffraction equipment allows the complex residual stress analysis to be quickly and accurately made. Of the various techniques for measuring residual stresses, the X-Ray diffraction method is most developed and widely used. It is the only technique, applicable to all crystalline

materials, that can measure absolute stress in a material without the need for measurement of a sample in the unstressed state, and that is capable of making measurements in localized regions as small as one millimeter in diameter. In addition, current X-Ray diffraction equipment is portable, mobile and reliable.

Initial feasibility of the FMA process was demonstrated on a limited basis by residual stress measurements of three retired 12th stage Pratt & Whitney F100 Waspaloy compressor disks supplied by the U.S. Air Force. These results showed a linear degradation in stress vs. cycles but might have been fortuitous since these data were determined using X-Ray diffraction equipment with a chromium anode X-Ray tube.(Figure 3) It was later discovered during a U.S. Air Force Phase I SBIR contract that use of a manganese tube rather than a chromium one in the X-Ray unit significantly improved equipment measurement reliability.

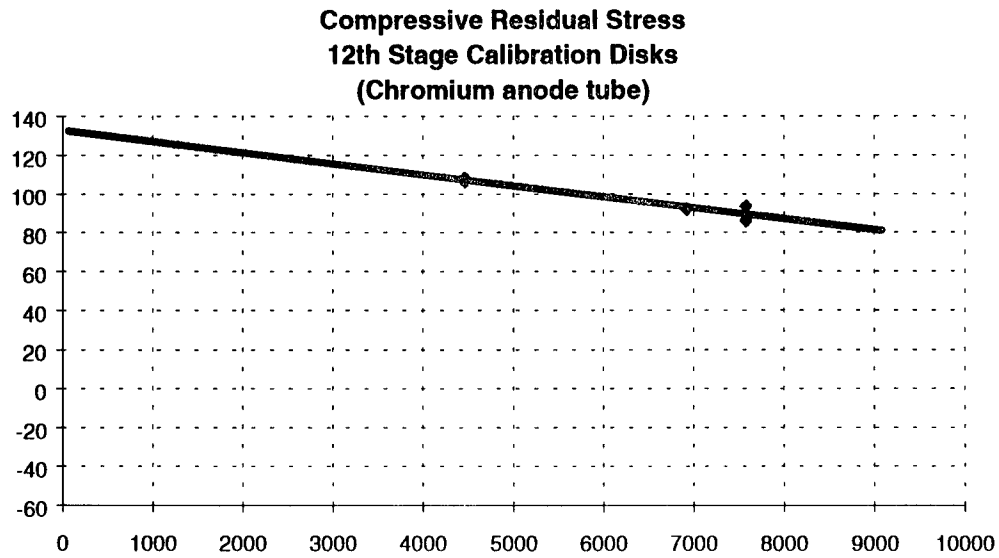

Figure 3. Residual Compressive Stress vs. Cycles (Chromium anode tube)

The Air Force, impressed by these results, awarded FMA a Phase I SBIR project to further demonstrate feasibility of the process. This work was hampered by the small number of disks supplied by the Air Force for measurement . Only 22 disks of the planned 80 disks were received by FMA during the Phase I project. Consequently the limited number of data obtained were inadequate for quantitative statistical analysis, but did permit qualitative conclusions to be drawn. The most important of these is that residual compressive stress, does indeed decline with increasing number of cycles. It was further established that the relationship is

linear. Thus the results of the Phase I study (*Reference 7*) demonstrated that the FMA original concept is valid . In fact a reasonable degradation slope was constructed, plotting residual stress vs. service cycles (Figure 4).

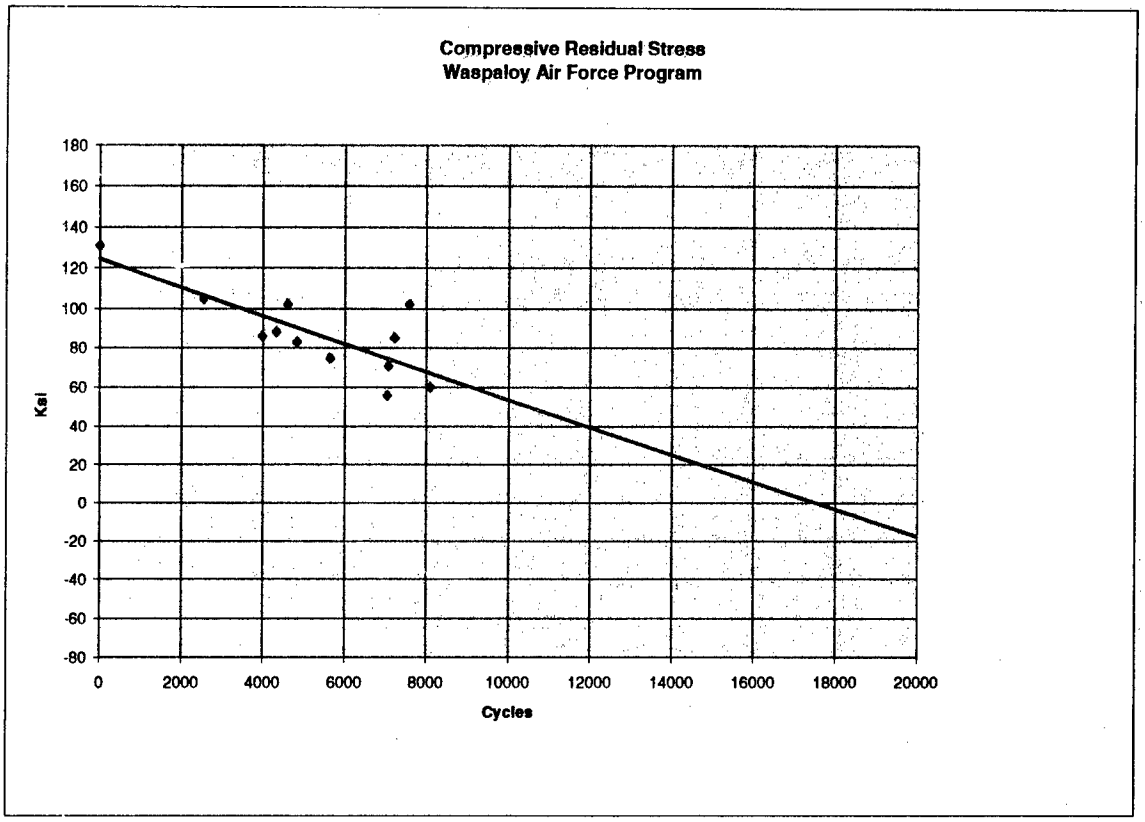

Figure 4 Phase I residual stress vs. service cycles Mn anode tube

Since the completion of the Air Force phase I project, several United Airlines Pratt & Whitney JT9D and JT8D Waspaloy and Inco 901 engine disks have been examined by the FMA procedure. Measurement results of nine Waspaloy disks were added to FMA's database (see Table 1). United Airlines advised that three additional disks had been rejected for LCF cracks and were not available for measurement. One Waspaloy JT9D 4th stage turbine disk showed 102 LCF cracks in the fir tree slots after 8,861 cycles and two Waspaloy JT9D 14th stage compressor disks had multiple LCF cracks in the bore area after 7,036 and 11,089 cycles respectively. The presence of cracks, occurring below the 15,000 cycle life limit for these parts, confirms the multiple cracking mode of LCF. Two JT8D Inco 901 turbine disks were also measured for residual stress.

TABLE 1

Compressive Residual Stress in Hoop on Waspaloy Disks

Part #	SERIAL	DATE	TUBE	STAGE	CYCLES	AVG. KSI
USAF						
4068810	H18207	12/22-AST	Mn	F-100 10	5641	75
4068810	H18402	12/22-AST	Mn	F-100 10	4593	102
4022610-N	H18406	12/22-AST	Mn	F-100 10	7211	85
4022610-S	K23583	12/22-AST	Mn	F-100 10	4832	83
4022610	*N80051* *	12/22-AST	Mn	F-100 10	0	131
4069910	N98460	12/22-AST	Mn	F-100 10	3982	86
4022612-J	5A3080	12/22-AST	Mn	F-100 12	7577	102
4022612-N	G97186	12/22-AST	Mn	F-100 12	7059	71
4022612	J37976	12/22-AST	Mn	F-100 12	4322	88
4068812	N99403	12/22-AST	Mn	F-100 12	2553	105
4022612	*K35332* *	4/9/96-AST	Mn	F-100 12	8078	60
4022612	*G03131* *	4/9/96-AST	Mn	F-100 12	7038	56
United						
587501	N44592	7/31/96AST	Mn	JT8D T-1	17,056	26
672915	8A3360	7/31/96AST	Mn	JT9DC-15	5,663 bore	45
672915	8A3360	7/31/96AST	Mn	JT9DC-15	5,663	17
718904	H94972	6/14/96AST	Mn	JT9D T-4	2626 bore	-24
718904	H94972	6/14/96AST	Mn	JT9D T-4	2626	42
758104	G49651	Cracks slots		JT9D T-4	8861 est.	-73
758303	8X4113	6/14/96AST	Mn	JT9D T-3	14,332	12
789614	3Y0118	6/14/96AST	Mn	JT9DC-14	14,307	28
789614	8X6777	7/31/96AST	Mn	JT9DC-14	13,562 bore	62
789614	8X6777	7/31/96AST	Mn	JT9DC-14	13,562	22
789614	IA7649	7/31/96AST	Mn	JT9DC-14	13,754	65
789614	IA7649	7/31/96AST	Mn	JT9DC-14	13,754 bore	90
790014	K95888	Cracks bore		JT9DC-14	11,089 est.	-80
792003	S17222	7/31/96AST	Mn	JT9D T-3	2402	25
5000814-01	J31288	Cracks bore		JT9DC-14	7036 est.	-60
5000815-01	N/A	7/31/96AST	Mn	JT9DC-15	11,116 bore	110
5000815-01	N/A	7/31/96AST	Mn	JT9DC-15	11,116	85

FMA residual stress measurements taken at United Airlines on retired and active commercial engine disks can be separated into the following categories.

1. Retired Waspaloy disks measured on 14 June 1996.

2. Retired Waspaloy disks measured on 31 July 1996.

3. Inservice Waspaloy disks measured on 31 July 1996.

4. Miscellaneous measurements on two JT8D 4th stage Inco 901 turbine disks, one new and one with 8,419 cycles, taken 31 July, 1996.

The residual stress measurements of disks at United Airlines overhaul shop, were made with portable X-Ray equipment (Figures 5 & 6).Despite the necessity of make-shift fixturing, all residual stress readings were meaningful.

Measurements taken on 14 June, 1996 (category 1 above) show that two disks retain normally expected residual compressive stress levels (12 KSI at 14,332 cycles and 28 KSI at 14,307 cycles) based on the projected Air Force baseline relaxation and intercept curve. The third disk was found to have 24 KSI tensile residual stress in the bore after 2,626 cycles and 11,087 hours which is well below the projected Air Force relaxation slope. Thus the retired status of this disk appears prudent (Figure 7).

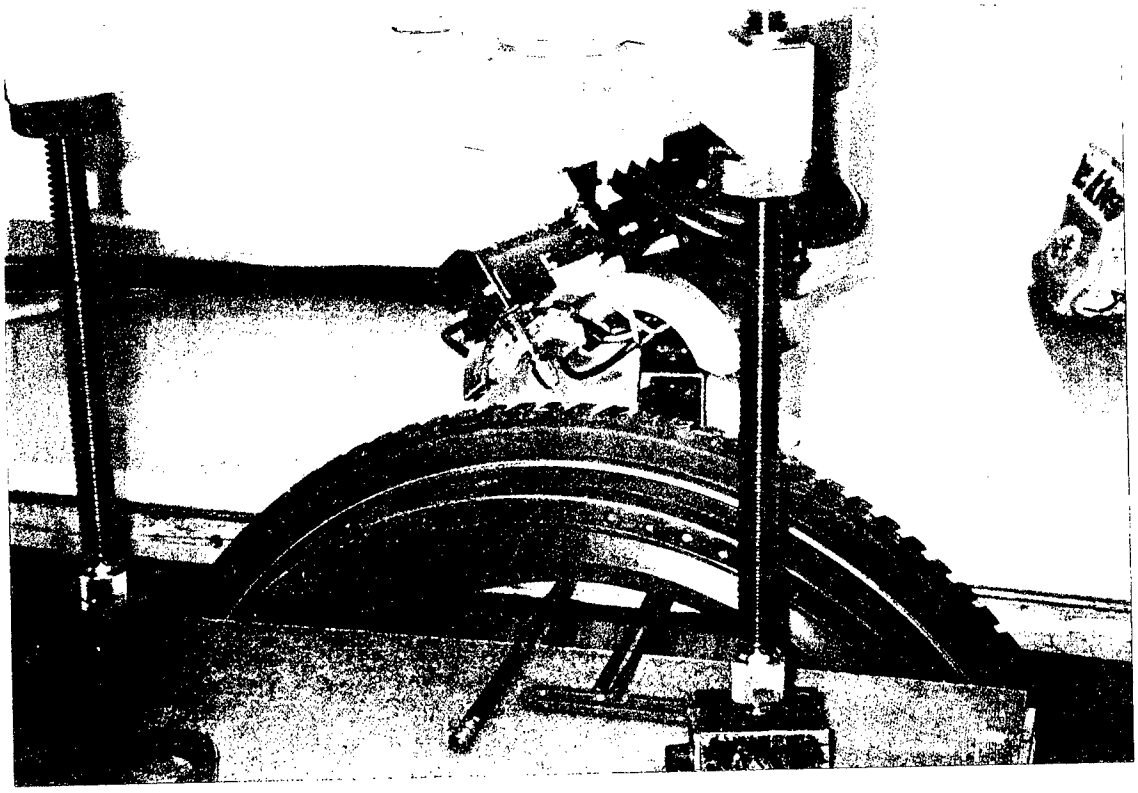

Figure 5 & Figure 6 at United Airlines makeshift fixturing photos

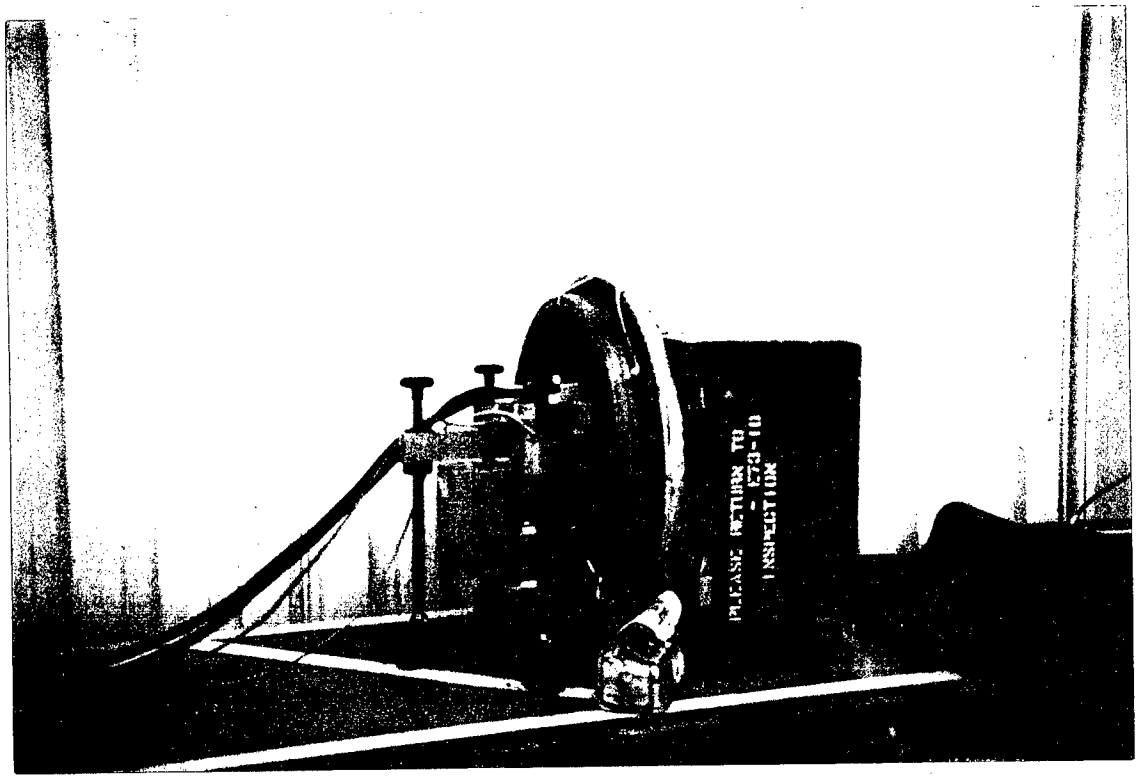

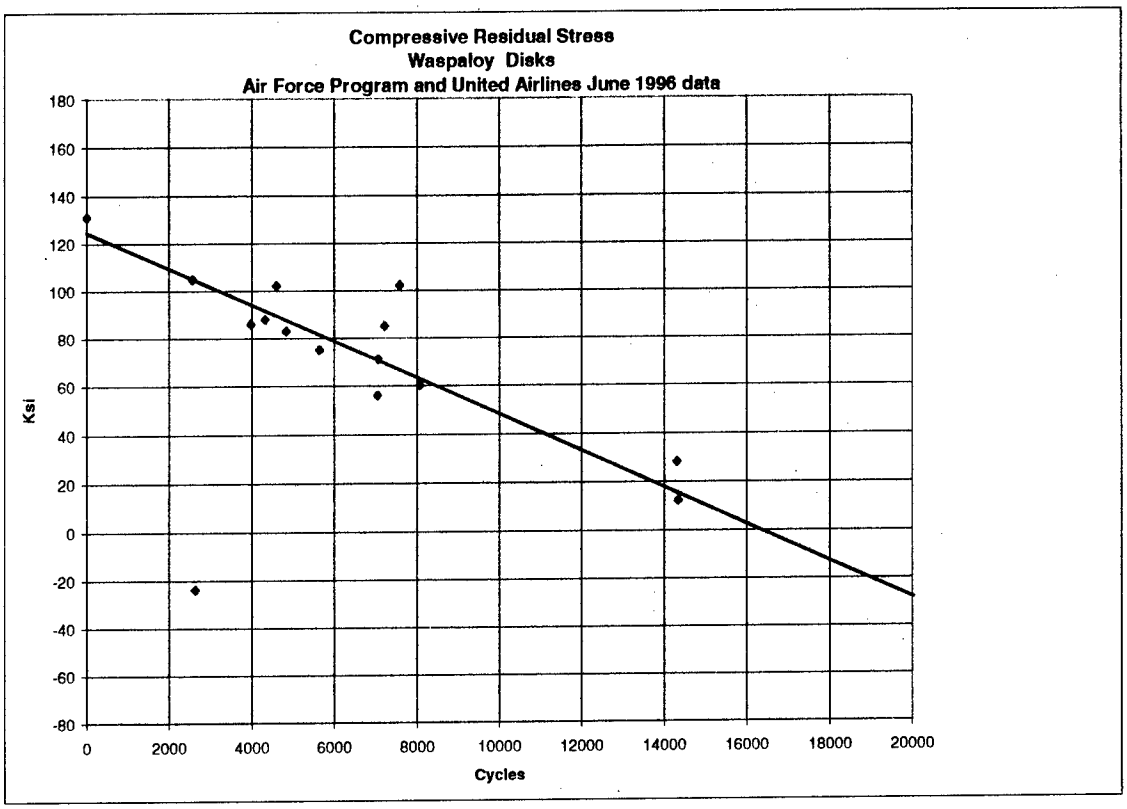

Figure 7 First three United Airlines data points on Air Force baseline curve

Measurements of retired Waspaloy disks on 31 July, 1996 (Category 2 above) show three of these retain compressive stresses that are in reasonably good agreement with the projected Air Force baseline relaxation slope (28 KSI at 14,307 cycles, 22 KSI at 13,562 cycles and 26 KSI at 17,056 cycles). One disk has a residual compressive stress of 65 KSI at 13,754 cycles that is much higher than the projected Air Force slope, which would suggest that this disk may have been re-shot peened at a previous overhaul or started its life with an above average residual compressive stress.

Results of measuring in-service Waspaloy disks on 31 July, 1996 (category 3 above) show one JT9D 15th stage compressor desk with 85 KSI compression at 11,116 cycles which is considered above the projected Air Force slope. This suggests that the disk may have been recently re-shot peened or entered service with above average residual compressive stress. The other in-service JT9D 3rd stage turbine disk which is at a lower compressive stress level (25 KSI at 2,402 cycles and 15,981 hours) than the projected Air Force baseline relaxation slope,

suggesting that it should be retired or reworked before continuing in service. Although there is no direct correlation between the United Airlines results and the standard degradation slope established in the Air Force Phase I project, it is non-the- less of interest to make the comparison which shows reasonable agreement (Figure 8).

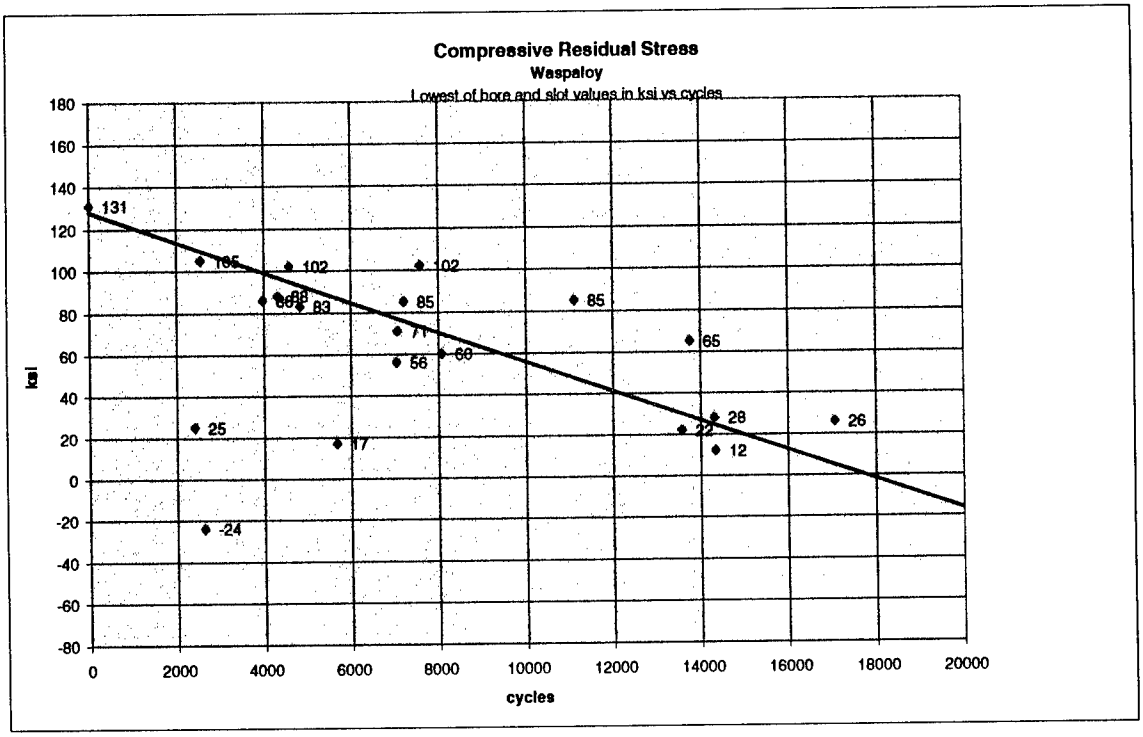

Figure 8 Additional United Airlines data points slots & bores

Review of these initial FMA residual stress measurements indeed shows some variations. However, until the original shot peening and/or disk finishing process is controlled and measured in terms of residual stresses on new parts, there will be variations in in-service measurements as a consequence of manufacturing variations and operating environments. It has already been shown that equipment scatter can be reduced by use of the manganese tube and appropriate selection of measurement location.

All residual stress data from United Airlines' Waspaloy disks including estimated values for cracked disks are shown in Figure 9.

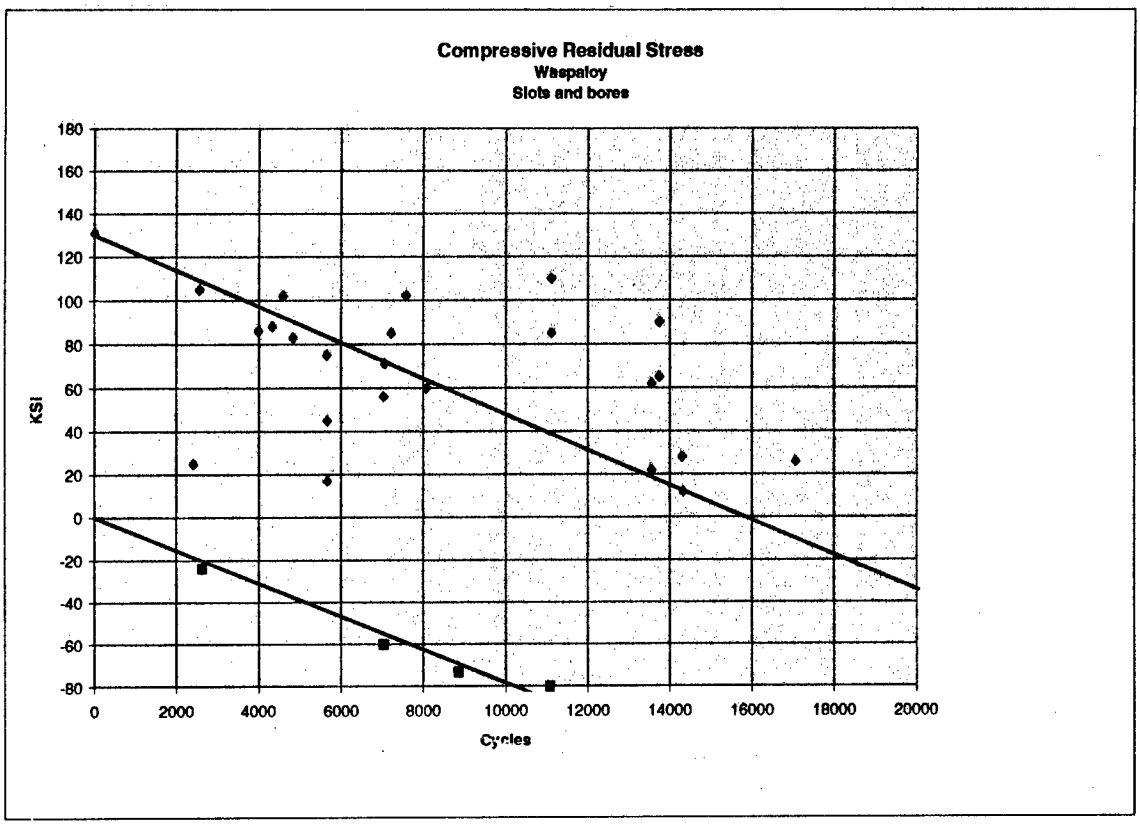

Figure 9. All values in Table 1 including estimate of cracked disks.

Miscellaneous measurements taken in two areas on two JT8D 4th stage Inco 901 turbine disks, one new and one with 8,419 cycles (Category 4 above) showed the expected degradation from the new part to the used part. The remarkable nature of these limited data is that the stress percentage degradation inferred in both areas is the same 57 percent (Table 2) suggesting a general systemic degradation of the stressed surfaces.

TABLE 2

Comparison of Measurements on New and Used Inco 901
4th Stage JT8D Turbine Disks

Residual Compressive Stress in average psi

Area of Measurement	New Disk	Used Disk	Percentage Loss
Web, near OD	57,900	24,700	57
Corner of ID and web	28,600	12,222	57

SUMMARY

LCF, cumulative fatigue damage with cycles to failure up to 10^4, is the common mode of engine disk failures and features widespread surface degradation and multiple cracking. The fact that fatigue cracks originate in metal surfaces that are stressed in tension is a well known engineering axiom. For this reason great care is taken in the manufacture of critical aircraft engine disks to ensure that fatigue limited surfaces are stressed in compression. Shot peening is presently the most appropriate method to leave these surfaces so stressed.

Historically the management procedure used with turbine engine disks is the conservative " safe life" approach which is based on an estimated part fatigue life through analysis, testing and comparable experience by engine manufacturers. This approach attempts to estimate the point at which the shortest lived part in the total population could be expected to fail. After allowing for suitable safety margins, an arbitrary retirement life, usually in cycles and sometimes in hours, is adopted. The conservative nature of this system is heightened by the facts that minimum materials properties are used and the beneficial effect of shot peening is not usually credited in the disk design values for total stress.

More recently, the U. S. Air Force has instituted, for some parts, a less conservative system, the " retirement for cause" concept, (RFC). Using this philosophy parts are periodically examined non-destructively for cracks. Once a crack is observed that particular part is removed from service. Other parts which may have service lives equal or greater than the retired part continue in use until they developed cracks. The danger of this system is that parts may fail because of

an undetected crack, since crack detection may not always occur in a timely fashion.

The limitations of the two procedures are obvious. An economic loss is associated with the safe life retiring of parts that have significant life remaining. The retirement for cause procedure may decrease flight safety due to continued service of parts with potentially undetected cracks.

The newly developed FMA X-Ray diffraction inspection method has been shown to have technical merit by the initial, but limited, test evaluations. The process provides a means of periodically measuring the surface residual stress of fatigue limited metal components before crack initiation has begun. On the basis of these residual stress measurements one can determine whether or not a crack is imminent in a qualitative manner and then estimate the remaining service life. For example, disks approaching their cyclic life limits, but still retaining a sufficient level of compressive residual stress in the fracture critical areas could continue in service based on extrapolation of their individual or population stress life trendline. On the other hand, a disk which has been excessively or harshly treated during service, but is still within it's cycle limit, could be retired early or be reworked because the residual stress had become tensile.

This paper discusses the role of component residual stress and examines its relationship with LCF service cycles. Portable X-Ray diffraction equipment combined with computer technology quantifies residual stresses with accuracy and reliability. A recent semi-empirical study of retired military engine disks compared residual surface stress measurements with the corresponding component cyclic service life and determined a definite relationship. Finally, the paper discusses the potential use of residual stress measurements in ENSIP and the RFC program.

CONCLUSIONS:

1. LCF, if allowed to progress to failure, is characterized by widespread surface degradation and multiple cracking in highly stressed areas. This is the common mode in the occasional in-service disk failure.

2. Fatigue cracks initiate in surface areas that are stressed in tension. Thus surface areas with residual compressive stresses are invariably free of low cycle fatigue cracking.
3. Residual compressive stress condition of engine disk surfaces declines with service cycles and / or hours.

4. The relationship of residual surface stresses with cycles is linear.

5. Initial residual stress measurements of disks confirm the validity of the original FMA concept which is that as disks age in service the residual compressive stress gradually decreases until tensile stresses form. Periodic stress measurements of disks provide quantitative part serviceability data.

6. Variations in initial stress measurements are caused, in part, by equipment capability (although use of a manganese to rather than a chromium tube significantly reduced scatter), but also by manufacturing and part- to- part statistical differences. Improved shot-peening control by way of residual stress measurements of new parts will minimize such variations.

7. Disks should be measured for residual stresses on the highly stressed areas, both in blade slots and bore surfaces.

8. Degradation of compressive residual stress occur on critical surfaces during service and could degrade at different rates.

9. Re-shot peening of disks at overhaul changes the residual stress and has a significant effect on interpretation of the measurements.

10. Degradation of the entire part appears to occur uniformly during service based upon limited data percentage change.

11. The FMA process quantifies disk residual stress conditions and clearly identifies above average, average and below-average disks. This provides the industry with a qualitative tool to cull out the below-average disks (weak links) before cracks initiate.

12. Commercial Waspaloy disks are assigned a service limit of as much as 20,000 cycles but military F-100 disks, degrading at comparative rates, are retired at only 8,000 cycles.

13. FMA' s residual stress measurements could allow the Air Force retirement for cause program to safely continue and the engine manufacturers to recommend increased disk life limits based on semi empirical data collected on a statistically valid program.

REFERENCES

(1) E.F. Bradley, R.C. Boettner, M.J. Donachie, R.A. Sprague Problems in Low Cycle Fatigue, Pratt & Whitney, 9/15/67

(2) J. Tavernelli, L. Coffin: A compilation and Interpretation of Cyclic Strain Fatigue Tests on Metals, Trans. ASM, V 51, 1959

(3) S. Manson, M. Hirschberg: Fatigue Behavior in Strain Cycling in the Low and Intermediate Cycle Range, FATIGUE, Syracuse University Press.

(4) S. Suresh: Fatigue of Materials, Cambridge Solid State Science Series, 1994, page 139

(5) S. Suresh: Fatigue of Materials, Cambridge Solid State Science Series, 1994, pages 134-5

(6) S.G. Berkley: United States Patent Number 5,490,195 and U.S. and foreign patents pending.

(7) S.G. Berkley Non-destructive Residual Stress Analysis Inspection Method for Critical Engine Parts, CLIN 0001AF, AF 95-162, Jan 1996

Quantification of Process Margin for Robust Engine Components

*Dr. Paul A. Domas
Mr. Herbert G. Popp
GE Aircraft Engines
P.O. Box 156301, One Neumann, Way, M/Z Q105
Cincinnati, OH 45215-6301, USA

1. ABSTRACT

Engine Structural Integrity Programs have long promoted and, through military standards and guidance documents, provided methodologies for increased engine component reliability. Recently, new concepts and terms such as "6-sigma", capability index (C_{pk}), process yield, "defects per unit (DPU)" are being adapted from the manufacturing environment and more widely used to describe desired system and component robustness.

A fairly extensive series of replicate, elevated temperature, low cycle fatigue (LCF) tests on powder metal, nickel-base superalloy material test samples, containing round and shaped holes manufactured with "best practice" (BP) and alternate practice (subject to special cause) hole making processes, followed by BP shot peen, provides an opportunity to quantitatively illustrate some of these possible alternate measures of fatigue reliability margin in engineering terms.

The potential detrimental influence of processing induced special and common cause surface damage on LCF life and the increased life margin provided by hole surface post-finishing (honing or abrasive flow) to remove as little as 25μ (0.001") of material is discussed. Process influenced life variation is expressed in terms of LCF life differences, "X-sigma", C_{pk} parameter, and process yield to facilitate comparison among potential robustness criteria.

2. INTRODUCTION/BACKGROUND

The term "6-sigma" is increasingly being used to describe quality and reliability initiatives across various industries[1,2] including the gas turbine engine industry[3,4]. In simple terms the concept utilizes data collection and statistical data

analysis to quantitatively establish process capability and margins in relation to specification limits. Most often this type of quality measurement is discussed in connection with manufacturing issues such as tolerances or scrap rates. However, the concepts are potentially useful in assessing "design margins" or other possible engineering measures of component robustness.

An important reliability and customer satisfaction metric is component fatigue life. The useful fatigue life of rotating components is often limited by stress concentrating features such as holes, fillets, or slots. The fatigue capability of these features is influenced by the manufacturing process used to make them. Common and special cause process perturbations lead to variation in component fatigue life. Quantification of this variation is a needed step in establishing product robustness.

3. OBJECTIVE

Obtaining multiple test points for several hole making processes tested at nominally identical test conditions provides an opportunity to assess the influence of hole making process variation on component fatigue life. The margin between lower limit (specification) life and expected (mean) life can be quantified using several potential measures. Traditional measures such as fatigue life ratio (minimum life divided by mean life) can be compared to the alternate robustness and margin measures currently being advocated as part of the 6-sigma movement.

A key objective of this paper is to illustrate the potential use of these collective margin measurements in assessing critical rotating part engine component reliability.

A second objective is to present test data indicative of the potential significant robustness gain to be realized by removing even a small surface layer of disturbed material from finish machined holes in nickel-base superalloy materials at nominal operating conditions.

4. LOW CYCLE FATIGUE TESTING

An extensive integrated material development test program described in general terms elsewhere[5,6] provided a large number of LCF test results for use in this study.

The material tested is a powder metallurgy, extruded and isothermally forged, nickel-base superalloy used for turbine and compressor disk and seal components. The two hole rectangular test specimen and hole making process is shown in Figure 1. The holes were manufactured by a variety of hole making processes including drill-bore, drill plus ream, drill plus peripheral mill. The drill-bore and drill plus ream holes were round while the peripheral milled holes were shaped.

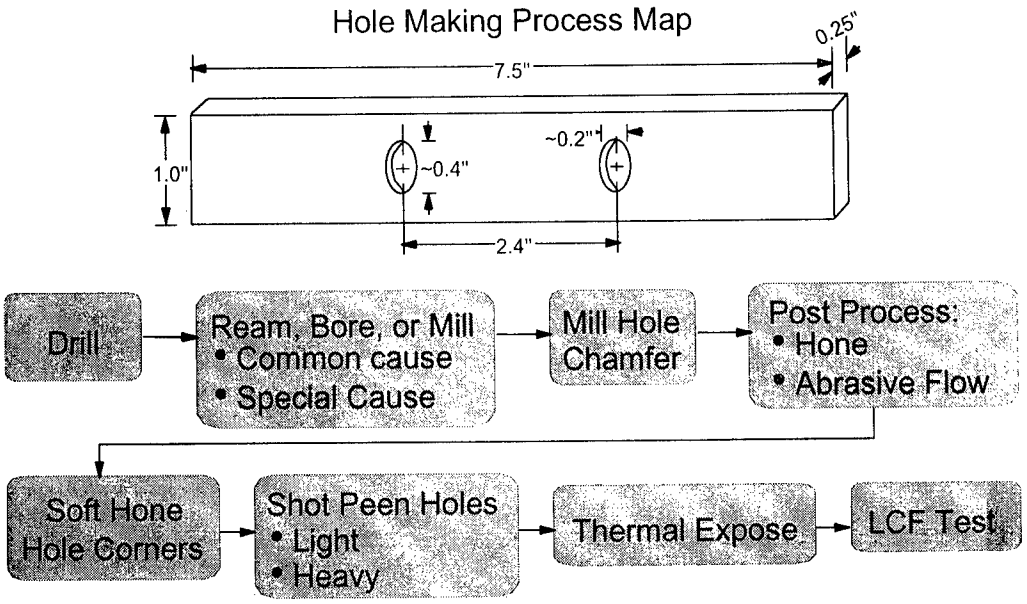

Figure 1: Test specimen and processing routes.

Several types of processing were considered. Best practice (BP) processing utilized parameters (e.g., chip load and feed rate) well within defined processing windows. "Special cause" processing utilized parameters beyond defined processing windows. Some of the specimens received additional post-finishing (PF) treatment, either honing (round holes) or abrasive flow (shaped holes), to remove approximately 25μ (0.001") of surface layer from the hole. The finished specimens were all BP shot peened and thermally exposed[4]. The load control tests were conducted using induction heating under continuously cycled, triangular wave form, 30 cpm, $R \cong 0.0$ conditions. Test temperature was 650C (1200F) for most tests with a few tests run at 590C (1100F).

5. TEST RESULTS

5.1 Stress versus Life (S-N)

Figure 2 depicts the LCF results on a conventional S-N plot. The feature test data from this program are compared to "nominal" material behavior data obtained from low stress ground (LSG) and polished cylindrical bar strain controlled tests at nominally the same conditions. The range of nominal data between mean and minimum (-3σ) is shown in the figure.

Several things are apparent from this data representation. First, for the non PF holes, there is a large amount of scatter in resultant fatigue life. For like processing there can be more than an order of magnitude range of results. Taken

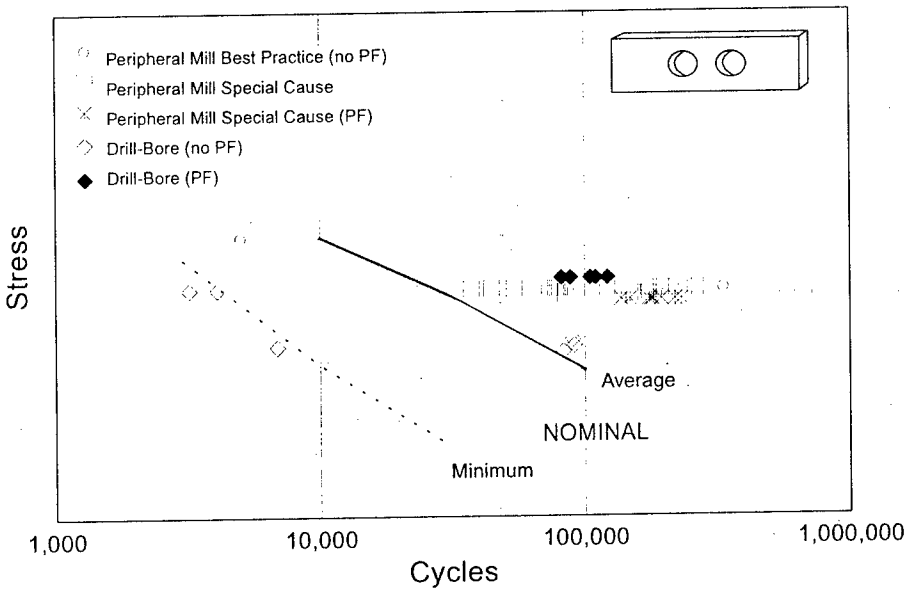

Figure 2: LCF of machined and peened holes - Nickel base superalloy, 650C. Significant scatter with out post-finish. 25μ (0.001") surface removal reduces scatter, increases life.

in the entirety, accepting that hole geometry and processing route differ, LCF lives ranging over two orders of magnitude were observed.

Other studies have shown this scatter to be related to the periodic occurrence of detrimental surface layer regions associated with rubbing or smearing of entrapped machining chips and a concurrent build up of excessive heat and surface cold work[4,6].

Removal of the potentially overly deformed surface layer through a PF process leads to the second observation from Figure 2. The PF processed holes have much reduced scatter and exceptional LCF life capability.

Another, less obvious observation is that even designated BP hole making (reference the peripheral mill process in Figure 2) without final PF has the potential for common cause variation that could yield less than desired LCF capability, if subjected to sufficiently high stress. The apparent stress dependence of these results suggests the potential to utilize a fracture mechanics model and associated threshold concepts to further quantify the behavior. This is a subject under study.

5.2 Standard Deviation as a Measure of Margin

The traditional S-N diagram clearly reflects the presence of scatter in the test data. But it does not provide a very good means of quantifying the scatter or its

significance (beyond the fact that results range over orders of magnitude). Figure 3 is an alternative data depiction. Probability density distributions (assuming log-normal LCF behavior) are shown as a function of the number of standard deviations (σ) from the nominal (LSG + polish) mean. [Further details of the procedure for obtaining these curves are given in the next section.] For reference, a cyclic life scale is superimposed at the top of the figure.

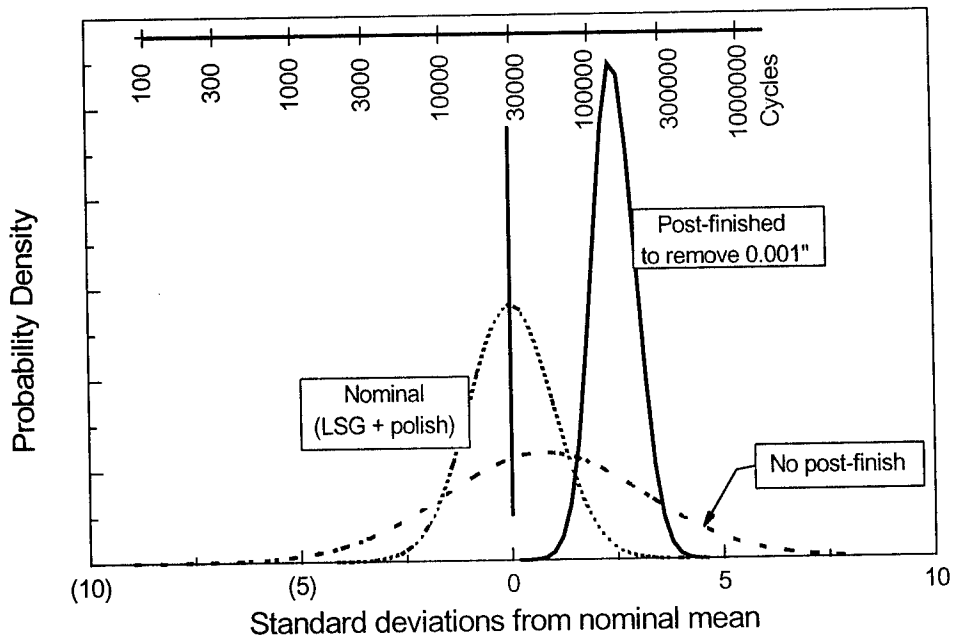

Figure 3: Distributions of hole making data with and without post-finishing. Shape and location of normal curves illustrates margin and scatter.

Figure 3 more intuitively illustrates the overall differences in the processing routes. The nominal material behavior expectation has a "bell shape" log-normal distribution centered at zero σ and decaying symmetrically toward very low probabilities at $\pm 3\sigma$ from the mean. The results without PF are more widely spread with a mean somewhat above the nominal mean. The PF results are centered well above the nominal with a comparatively much more narrow spread. The number of standard deviations between the several means is a potential measure to quantify the amount of fatigue life margin for a given processing route.

5.3 Fatigue Life as a Measure of Margin

Figure 4 presents test results on log-normal probability paper. The fatigue life of each test (expressed in terms of the number of nominal behavior σ's from

nominal mean at the test condition) is plotted versus the probability of attaining or exceeding that life. The specimens from several processing routes are combined into two groups: PF (solid symbols) and non-PF (open symbols). When constructed in this way, the nominal behavior is always represented by the heavy straight line through the two points: [zero σ, 50% probability (nominal mean)]; and [-3σ, 0.135% probability (nominal -3σ)]. The parameters (mean, slope)

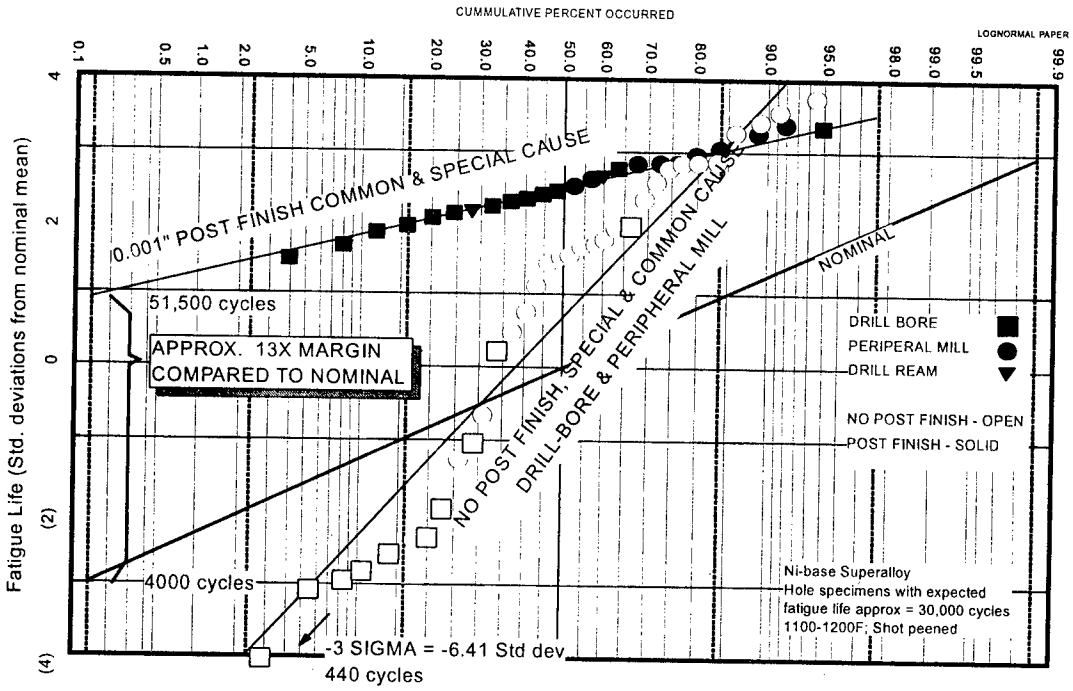

Figure 4: Distributions of hole making data with and without post-finishing. Data on probability paper illustrates LCF margin and use of standard deviations from nominal mean.

describing the straight line data regression fits can be used to construct the distribution plots of Figure 3.

Non-PF results have more scatter (steeper slope) than nominal, PF results have less scatter (more shallow slope). The mean life of each group is readily read from the 50% probability crossings.

An advantage of this depiction is that quantitative statements can be made and test conditions with slightly different stresses or at different temperatures can be collected into one common format, facilitating comparisons. Obviously this

combining must be done with caution to avoid inappropriately lumping differing mechanistic behaviors.

Another potential measure of robustness (margin) is to compare the minimum LCF life obtained using the desirable (i.e., PF) processing to a lower specification limit (LSL). Typically the LSL would be taken as the minimum (-3σ) nominal life, which for this 650C (1200F) example is 4,000 cycles. The minimum PF feature life would be projected to be about 51,500 cycles, providing a margin of approximately thirteen-fold between the specification lower limit and the expected minimum life for holes made using this process route. This "LCF life margin" is perhaps most typical of historical margin measures.

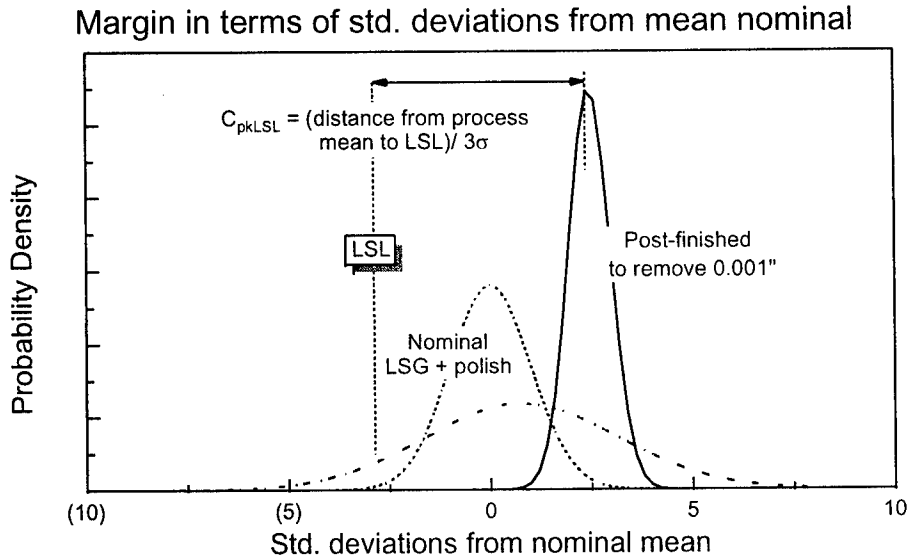

Figure 5: C_{pk} and 6-sigma measures illustrated. C_{pkLSL} is defined as distance from process mean to lower specification limit (LSL) divided by 3σ. $C_{pkLSL} = 2$ for a 6 sigma process.

5.4 Cpk and "6-Sigma" Measures

The burgeoning discussion of Six Sigma Processes[1] and Six Sigma Quality[2,3] prompts one to attempt to consider the process margins discussed above in the context of these measurement systems and this jargon. Figure 5 illustrates definitions of the "sigma" of a process and the capability index C_{pk} as referenced to the LSL. The LSL is again taken as the minimum (-3σ) of the nominal (LSG + polish bar) behavior. For a given process the mean and standard deviation (σ_p) of

the resultant LCF behavior is established by replicate testing. The capability index (C_{pkLSL}) is defined as the difference between the process generated mean life and the LSL (expressed in number of σ_p's) divided by $3\sigma_p$. Hence a "3-sigma" process is one in which $C_{pkLSL} = 1.0$. A "6-sigma" process has $C_{pkLSL} = 2.0$.

In addition, it is appropriate to recognize inherent process variation by acknowledging the likely presence of process drift. If unknown, one could consider, for example, that the long term capability of the process under study drifts over time by some amount, say $\pm 1.5\sigma_p$ from the short term mean. If this occurs, a 6-sigma process in the short term would become a 4.5-sigma process in the long run and would more appropriately be categorized as having a C_{pkLSL} of 1.5.

Hole Making Process	CpkLSL	"X - Sigma"
Process with no PF + peen	0.5	1.6
Nominal (target LSL)	1	3
"6-Sigma" process (reference)	2	6
Process with 25μ PF + peen	3.6	11
Process with PF + peen with assumed $\pm 1.5\sigma$ drift	3.1	9.5

Table 1: Process comparisons in "6-sigma" terms.

Table 1 compares the various hole processing routes in terms of C_{pkLSL} and the "sigma" of the process. The desired quality level in this scheme is at least 6-sigma ($C_{pkLSL} = 2$). A quality level consistent with the nominal behavior used to establish the LSL would be 3-sigma. Processing without PF, under the conditions studied, delivers only 1.6-sigma ($C_{pkLSL} = 0.5$) capability. PF removal of the surface layer raises the process capability to ~11-sigma. Even if an assumed drift of $\pm 1.5\sigma_p$ on the process mean was to occur, the capability would still be at ~9.5-sigma.

5.5 Margin in Terms of Process Turns

Yet another potential measure of margin is the number of "process turns" without violating the LSL. That is, for a given hole making process, how many holes exceeding design target (fatigue life > -3σ nominal) can be made before

making a less than target capability (fatigue life < -3σ nominal) hole? Table 2 summarizes the process capability in these terms.

A 3-sigma process has a process yield of 741 holes and a probability of yielding a hole with less than design target (LSL) life of 0.00135. The non-PF process in this study, a 1.6-sigma process, yields only 18 holes, while the PF process could deliver more than 1 billion high quality holes even if a long term drift of $\pm 1.5\sigma_p$ is included.

6. RELIABILITY ILLUSTRATION

A way to illustrate the relative significance of some of these measures of margin is to consider a probabilistic analysis, using the previous data for PF or non-PF holes, applied to an analytical (not an actual component) disk. This conceptual component is envisioned to contain 160 holes manufactured using one of several potential processes and to operate at 650C (1200F) in a continuously cycled manner. It is assumed that the manufacturer of this component makes 500,000 holes of this type in a year.

Figure 6 shows the results of such an analytical study in the form of probability of fracture as a function of the number of mission cycles for various process capability scenarios. If the process was as robust as the PF process in this study and yielded no abused holes the probability of encountering a hole with less than the expected nominal mean life (~30,000 cycles) would be much less than 1 in a billion. If, in contrast, there was no PF applied and (as an extreme) every hole made was abused (at least to the special cause extent observed in this study) there would be ~ 1% chance of failing the disk at about 2,000 cycles. Clearly actual processing is more capable than this pessimistic assumption. However, even if

Hole Making Process	"X-sigma"	Probability of Life < Design Target (LSL)	No. of Holes Before a Low Life (-3σ) Hole
Process with no PF + peen	1.6	0.0548	18
Nominal (target LSL)	3	0.00135	741
"6-sigma" process	6	9.9 e-10	1 billion
"6-sigma" process with 1.5 σ_p drift	4.5	0.0000034	294,000
Process with 25μ PF + peen	11	>> 9.9 E-10	>> 1 billion
Process with 25μ PF with 1.5σp drift + peen	9.5	> 9.9 E-10	> 1 billion

Table 2: Process capability in terms of process turns.

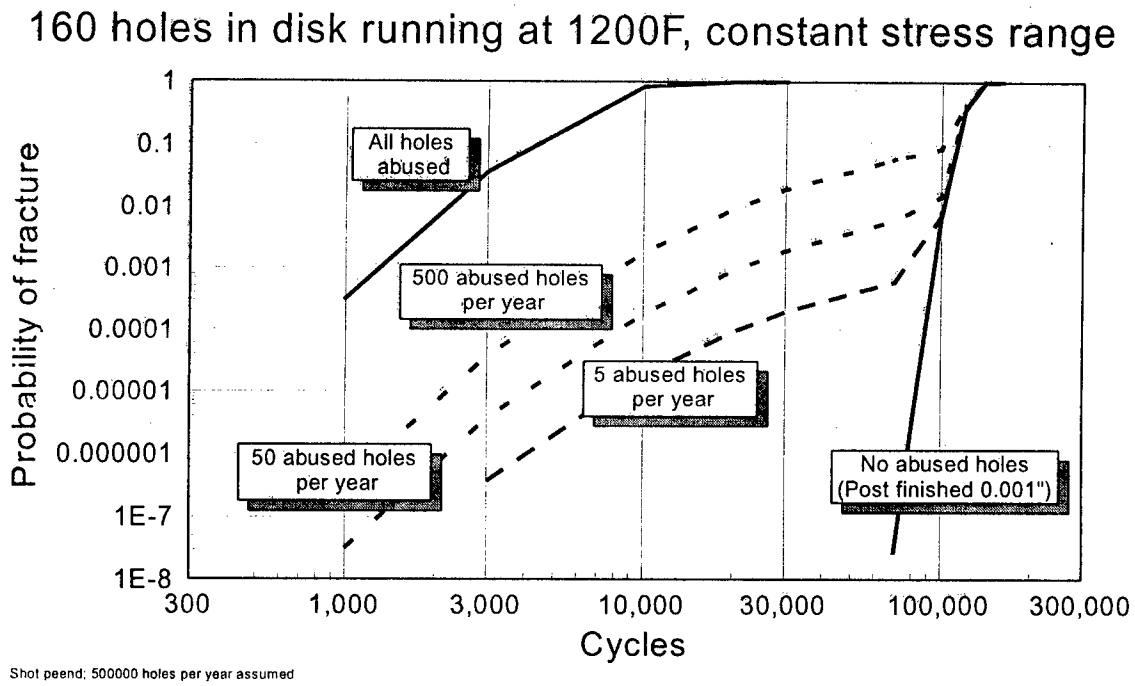

Figure 6: Illustration of reliability differences for an analytical disk. Conceptual design only, stresses higher than typical design stress. Post-finishing provides much greater robustness even when potential for abusively made holes is low.

the particular process were to deliver only 5 abusively made holes a year (0.001%) the reliability (probability of fracture), though considerably improved over the worst case assumption, is orders of magnitude less than the best case assumption. PF processing clearly provides the highest reliability.

7. SOME CONSTRAINTS

The test series providing the data discussed in this paper were not originally designed to demonstrate with rigor the margin metrics discussed here. The results provided an opportunity to explore, to a first order, the 6-sigma margin concepts in terms of component fatigue life. There are caveats to be noted:

- Results from peripheral mill, drill-bore, drill plus ream and drill+mill processing have been combined to provide approximately 60 tests, most at 650C (1200F) a few at 590C (1100F). Similar trends were observed for ~150 tests at 204C (400F)[7].
- To accentuate the anticipated behavior, the tests were run at stress levels above those typically expected in actual components.

- In this study no attempt was made to assess the statistical potential for special cause events nor the actual process drift.

8. SUMMARY

Replicate LCF testing allowed quantified hole making process margin comparison. A variety of inter-related measures of margin can be used, from traditional LCF life factor to 6-sigma capability indices.

For the processes studied, post-finishing to remove 25μ (0.001") surface layer provided the most robust process by any of various measures. These are summarized Table 3.

Measure	Value
LCF life margin	13 times
Capability Index	C_{pkLSL} = 3.1 - 3.6
Process Sigma	9 - 11 sigma
Process Yield	> 1 billion holes

Table 3: Various process robustness comparisons.

Such quantified measures lead naturally to consideration of potential life limit increases (raised LSL) for post-finished holes. However, other quantification would be necessary to enable this, including, for example: determination of actual process drift, analysis of the influence of other component life variables, further consideration of confidence intervals and development of first principle mechanistic models.

9. ACKNOWLEDGMENTS

Numerous General Electric Company teams contributed to the results discussed by the authors. The especial contributions of: P. Bailey, G. Geverdt, R. Meese, and W. Ross are gratefully acknowledged.

10. REFERENCES

1. Harry, Mikel, J., "The Vision of Six Sigma: A Roadmap for Breakthrough", 4th Ed., Sigma Publishing Co., Phoenix, 1994.

2. Squires, T., and Clingerman, D., "Six Sigma and Robustness", presented at Second Annual Workshop on the Application of Probabilistic Methods to Gas Turbine Engines, Dayton, OH, 8-9 October, 1996.
3. Welch, John, F., Jr., "GE Quality 2000: A Dream with A Plan", Presented at the GE Company 1996 Annual Meeting, Charlottesville, Virginia, April 24, 1996.
4. Welch, John, F., Jr. "Jack Welch's Encore - How GE's chairman is remaking his company again" Business Week, Oct. 21, 1996.
5. Domas, P.A., "Elevated Temperature Component Fatigue Robustness - An Holistic Approach", Thermal Mechanical Fatigue of Aircraft Engine Materials, AGARD-CP-569, March, 1996.
6. Domas, P.A., "Substantiating Powder Metal Life Methodologies for Engines," Impact of Materials Defects on Engine structures Integrity, AGARD-R-790, April, 1993.
7. GE Aircraft Engines, New Product Introduction teams., Unpublished research.

Structural Integrity of Composite Containment Structures

Dr. Pascal K. Gotsis and Dr. Christos C. Chamis*
National Aeronautics and Space Administration
Lewis Research Center, Cleveland, Ohio 44135-3191

and

Dr. Levon Minnetyan
Clarkson University, Potsdam, NY 13699-5710

Prepared for the
1996 Aircraft Structural
Integrity Program
San Antonio, Texas
December 3-5, 1996

Structural Integrity of Composite Containment Structures

Dr. Pascal K. Gotsis and Dr. Christos C. Chamis*
National Aeronautics and Space Administration
Lewis Research Center, Cleveland, Ohio 44135-3191

and

Dr. Levon Minnetyan
Clarkson University, Potsdam, NY 13699-5710

Abstract

Structural integrity of composite containment structures is evaluated by using computational simulation of progressive fracture during the containment process. An integrated computer code (CODSTRAN) was modified to simulate the progressive damage, containment and/or penetration of composite containment structures under impacting loading. The objective of this investigation is to evaluate the containment process of fiber composite structures impacted by an escaping blade. The simulation traces the history of damage initiation, growth, accumulation, progression and propagation to containment or penetration. Results show that for specified initial velocity of the escaping blade the containment damage sustained decreases approximately quadratically with containment structure thickness.

Introduction

Concerns for safety and survivability of critical components in engine structures require a quantification of the composite structural integrity or damage tolerance during overloads. Characteristic flexibilities in the tailoring of composite structures make composites more versatile for fulfilling structural design requirements for example, containment of escaping blades. However, these same design flexibilities render the assessment of composite structural integrity and durability, in overload situations, more complex, prolonging the design and certification process and adding to the cost of the final product.

It is difficult to evaluate the resistance of composite containment structures because of the complexities in predicting their overall congruity and performance, especially when structural degradation occurs by damage propagation. The evaluation of damage initiation, damage growth, and propagation to fracture are important in quantifying the impacting load carrying capacity, damage tolerance, safety, and reliability of composite containment structures. The most effective way to obtain this quantification is through integrated computer codes that couple composite mechanics with dynamic

structural analysis and damage progression modeling. One such code is the COmposite Durability STRuctural ANalysis (CODSTRAN) computer code [1] which has been developed for this purpose.

In a previous article [2] CODSTRAN was used to evaluate the penetration resistance of a containment composite shell with specified thickness and different initial blade velocities.

The present paper investigates the response of a containment fiber composite thin shell structure impacted by an escaping blade with specified initial velocity of the blade but with different shell thicknesses.

Brief Description of CODSTRAN

CODSTRAN is an integrated computer code (Fig. 1) that was written in FORTRAN 77 computer language and currently runs in unix operating system at NASA Lewis Research Center. CODSTRAN was developed by coupling the following modules: (1) ICAN [3], (2) MHOST [4] and (3) progressive fracture tracking [1]: ICAN is a computer code that provides the composite mechanics simulation starting with constituent material properties and accounting for hygrothermal environments.

MHOST is a finite element computer code [4] for the solution of structural analysis problems. The code has the capability to perform linear or nonlinear static and dynamic analysis. MHOST has a library with a variety of elements; for the present work the four node shell element was used. When supplied by the boundary conditions, the desired type of analysis, the applied loads and the laminate properties (via ICAN) MHOST performs the structural analysis. In addition MHOST provides the computed nodal resultant stresses to ICAN which computes the ply stresses for each ply and checks for ply failure and respective fracture modes.

The damage progression keeps track of composite degradation through ICAN for the entire structure and provides input to ICAN and MHOST for the iterative analysis steps. ICAN uses failure criteria (Fig. 2) for the detection of ply failures as follows: a) maximum stress criterion, according to which failure occurs when the individual ply stress s_{Lij} for i,j = 1,2,3, exceeds the corresponding ply strength S_{Lij} for i,j=1,2,3; and b) a modified distortion energy criterion, in which the combination of the ply stresses is taken into account. In both criteria ply stresses are referred to the material axes 1, 2, 3, with the direction of the 0° fibers along the material 1-axis.

The integrated architecture of CODSTRAN simulation cycle is shown in Fig. 1. In this figure, from the left side along the clockwise direction the material properties of the constituents (fiber and matrix) are provided by ICAN's database, subsequently the ply properties are computed by using the micromechanics theory,

and following the laminate properties are computed using the laminate theory. These properties in conjunction with the finite element mesh, the loads and the boundary conditions are input into MHOST. MHOST performs the structural analysis and provides the nodal resultant stresses to ICAN (on the right side of Fig. 1); after that, ICAN computes the ply stresses using the laminate theory and checks for ply failure.

In MHOST the nonlinear structural analysis is performed in conjunction with an incremental load algorithm. The load is increased in small increments and within each load increment a number of iterations are performed, (Fig. 3). In each iteration the structure is checked for ply failure. If damages are detected in the structure, the laminate properties of the structure are updated and a new finite element analysis is performed. Iteration continues until no further damage occurs and global equilibrium is reached within a load increment. Afterwards the load is increased and the above procedure is repeated until the containment or penetration of the structure by the impacting object. Impact damage progression and penetration of the structure are assessed via the incremental iterative computational simulation method described above.

Summary of CODSTRAN Modification for Impact Response

The escaping blade has a mass m, an initial velocity u_o, and a contact velocity u_b when it hits the containment. The impulse law is:

$$m u_o - m u_b = \int_{t_o}^{t} F dt \tag{1}$$

where F is the impact force. The difference of the kinetic energy of the escaped blade before and after the impact is equal to the external work done by the impact force. From the first law of thermodynamics, the loss of the kinetic energy is equal to the work done by the impact force, therefore

$$\frac{1}{2} m u_o^2 - \frac{1}{2} m u_b^2 = W_{external} \tag{2}$$

The equations of dynamic equilibrium are written for the combined containment structure and the impacting escaped blade dynamic system from the time of initial contact that starts the impact.
The system dynamic equations in matrix form are:

$$[M]\{\ddot{u}\} + [D]\{\dot{u}\} + [K]\{u\} = 0 \tag{3}$$

where [M] is the mass matrix of combined containment plies blade finite element model, [D] is the damping matrix, [K] is the stiffness matrix, and {u}, {u}, {u} are the displacement, velocity, and acceleration vectors of the system.

During impacting blade contact the time is short and the inertial response of the shell is negligible. Therefore equation (3) reduces to:

$$[K]\{u\} = \{F_i\} \tag{4}$$

Equation 4 may be solved via computational simulation for displacements and damage as a function of the impact force. The instantaneous velocity u_b of the impacting blade is obtained from equation (2) in which the right hand side is evaluated by computing the work done by the impact blade force

$$W_{external} = \int_0^{u_b} [F]du \tag{5}$$

where u_b is the current displacement of the impacting blade.
Finally from equation (1), the time interval Δt (or the impact time) is computed by discretizing the force integral using the trapezoidal rule. From equation 4 the displacement vector {u} is computed for different load increments. Consequently the $W_{external}$ is computed by multiplying the displacement vector by the impact force vector and from equation (2) the final velocity (or impact velocity) is computed. From equation (1), discretizing the integral using the trapezoidal rule we compute the time interval Δt for the various load increments.

The subsequent dynamic response of the shell and the shell-blade combination can be computed from equation (1). That response is not included in this investigation since we are evaluating only the containment and onset of penetration. The dynamic response is being evaluated and will be reported at a future structural integrity conference.

Structural Integrity of Composite Containment Structures Through Progressive Fracture

The sample case, composite containment structure is a thin cylindrical shell made of graphite/epoxy laminate. The shell is impacted by an escaping blade as shown in Fig.4. The laminate configuration is $[0/\pm45/90]_s$ which consists of uniform thickness plies with different thickness varying from (0.05 to 0.35 in.)The boundary conditions of the cylindrical shell are one end fixed and the other free. The direction of the 0° fibers are in the axial direction of the shell and the direction of the 90° fibers are in the circumferential direction of the shell as shown in Fig. 5. The fiber volume ratio is $V_f = 0.60$ and the void volume ratio is $V_v = 0.01$. The

temperature was T = 20° C (70° F). The composite containment shell was made from high strength AS-4 graphite fibers (TABLE 1) in a high-modulus, high-strength epoxy matrix HMHS (TABLE 2). The fiber and the matrix properties were obtained from a databank of composite constituent material properties resident in CODSTRAN. The AS-4/HMHS ply strengths were computed by ICAN, and the results are shown in TABLE 3

The length of the cylinder is 310 cm (124 in.) and the inner diameter was 300 cm (120 in.) (Fig. 5). The angular velocity considered is 4000 rpm and the blade weight is 9 kg or 20 lb. The finite element model contained 934 nodes and 898 uniformly sized rectangular shell elements as shown in Figure 6. An expanded view of the local impact conditions are shown in Figure 7.

Sample Case - Typical Results and Discussion

The results obtained from the investigation of the sample case include: (1) the effects of thickness on impact velocity, maximum radial displacement, impact force, and damage sustained; (2) damage progression and respective fracture modes; and (3) graphical representation of displacement patterns for undamaged and damaged composite containment structures.

Effects of Thickness - The effects of thickness on the impact velocity is shown in Figure 8 as a function contact time. The effects of five thicknesses are shown in this figure. It is seen that the contact time varies inversely with the thickness. It is also seen that the blade impact velocity becomes zero for all thickness except the 0.5 in. The interpretation is that the impacting blade was contained for those thicknesses where the blade velocity became zero and penetrated where the blade had a residual velocity beyond the contact time.

The effect of thickness on the maximum radial displacement of the shell at the impact site is shown in Figure 9 as a function of contact time. Note the radial displacement at containment varies inversely with the thickness for the containment (cases line through end points). An approximate design guideline from this behavior is that a mill of containment thickness reduces the containment time by 3 milli-seconds. Note also that the radial displacement varies nonlinearly with time for the containment cases but varies practically linearly for the penetration case.

The effects of thickness on the impact force is shown in Figure 10. As can be seen, the impact force increases with containment thickness and the force-time history is nonlinear for the containment case but almost linear for the penetration case (0.05 in.). Connecting the end points of the containment cases it is observed that the impact force sustained increases linearly with containment thickness. Note further that the impact force is relatively small for the penetration case.

The effect of the thickness on the damage sustained is shown in Figure 11. As can be seen, increasing the thickness decreases the damage almost

proportionally for the three thicknesses (0.15, 0.25 and 0.35 in.). The 0.10 in. shell sustains less damage than the 0.15 in. shell. It is noted that the blade was contained just at the onset of penetration for the 0.10 in. shell. Note also the damage jump at penetration time for the 0.05 in. which sustained the least amount of damage. The afore observations lead to the following significant points which are relevant for the structural integrity of composite containment structures:

1. CODSTRAN-like capability can be used to evaluate the damage sustained .

2. It is not apriori obvious which thickness will sustain the least damage. That can be only determined after the thickness for the onset of penetration has been found (0.10 in. for the sample case).

3. Full penetration (escaping blade) causes the maximum local damage but the least amount of overall damage.

Sequence of Local Fracture Modes - The sequence and type of local ply fracture modes are summarized as they occurred during the containment/penetration process for each thickness. They are listed as a fraction of the fracture load (maximum impact load) for the node that had exhausted all its resistance in each of its plies fracture mode, for the containment thickness investigated. The summary for the 0.05 in. thickness is shown in Table 4. Node 4 exhausted its plies fracture modes first (see Fig. 7 for location). Note that fracture is initiated by ply transverse ply fracture and progresses through the ply thickness by longitudinal tensile and compressive fractures. Comparable results for the other thicknesses are summarized in Tables 5 to 8. Since the nodes that fracture are adjacent to the contact nodes (Fig. 7), local fracture and/or penetration occurs by local bending as the blade pushes the composite through in front of it. It appears from these summaries that laminates with 0/90 plies at the mid-thickness are most effective for containment.

Displacement Patterns - The displacement pattern for the composite containment shell during the impact event is shown in Figure 12. This is for the shell with 0.25 in. thickness and at a force of 37 klb. The displacement pattern just before containment with some local fractures is shown in Figure 13. Note the impact load for this displacement pattern is almost double. It indicates that the shell contained the blade even though it sustained partial local damage. The displacement patterns for shells with other thickness (0.10, 0.15 and 0.35 in.) are similar. Those for the 0.05 in. shell (blade penetration) shows similar damage patterns but much more pronounced locally indicating the blade penetration. Note the pronounced local bending (hoop and axial adjacent to the contact site) in both of those figures. It is important to note that local bending forces causes the near mid-thickness plies to resist the impact force primarily by membrane action. Plies at 0°/90° at that location will provide effective containment resistance.

Generalized Approximations

The afore described results, observations and significance respectively, lead to the following generalized approximations which may be useful in designs.

- A mill of containment thickness reduces the containment time by about 3 milli seconds.
- The containment structure maximum radial displacement decreases linearly with containment thickness beyond containment.
- The containment force increases linearly with containment thickness.
- The containment structure damage sustained decreases quadratically with containment thickness.
- Laminate configuration with 0°/90° plies near the laminate mid-thickness provide the most effective containment resistance.

Summary

The salient finding of an investigation to evaluate the structural integrity of a composite containment structure are:

- Damage initiates by transverse tensile ply fracture in the inner and outer plies at about 70% of the fracture load.
- Damage progresses by longitudinal compressive ply fracture in the inner plies shortly thereafter.
- Damage continues to grow rapidly by combinations of ply fracture modes through the inner plies.
- Penetration occurs where all through-the-thickness plies have fractured by longitudinal tension or compression.
- Penetration occurs by near field bending as the blade pushes the material through.
- Subsequent dynamic response being evaluated.

References

1. C. Chamis, P. L. N. Murthy and L. Minnetyan, Progressive Fracture of Polymer Matrix Composite Structures: A New Approach, NASA TM - 105574, January 1992.

2. P.K. Gotsis, C. C. Chamis and L. Minnetyan: Progressive Fracture of Composite Containment Structure, submitted for publication.

3. P. L. N. Murthy and C. C. Chamis: ICAN (Integrated Composite Analyzer) computer code, NASA TP 2525, 1986.

4. Nakazawa, J. B. Dias and M. S. Spiegel: The MHOST Finite Element Program: 3-D Inelastic Analysis Methods for Hot Section Components: Volume II, User's Manual, NASA CR-182235, July 1989.

Table 1: A-4 Graphite Fiber Properties:

Number of fibers per end = 10000
Fiber diameter = 0.00762 mm (0.3E-3 in)
Fiber Density = 4.04E-7 Kg/m^3 (0.063 lb/in^3)
Longitudinal normal modulus = 227 GPa (32.9E+6 psi)
Transverse normal modulus = 13.7 GPa (1.99E+6 psi)
Poisson's ratio (n_{12}) = 0.2
Poisson's ratio (n_{23}) = 0.25
Shear modulus (G_{12}) = 13.8 GPa (2.E+6 psi)
Shear modulus (G_{23}) = 6.9 GPa (1.E+6 psi)
Longitudinal thermal expansion coefficient=1.E-6/°C (-0.55E-6/°F)
Transverse thermal expansion coefficient=1.E-6/°C (-0.56E-6/°F)
Longitudinal heat conductivity = 43.4 J-m/hr/m^2/°C
= (580 BTU-in/hr/in^2/°F)
Transverse heat conductivity = 4.34 J-m/hr/m^2/°C
= (58 BTU-in/hr/in^2/°P)
Heat capacity = 712 J/Kg/°C (0.17 BTU/lb/°F)
Tensile strength = 3,723 MPa (540 ksi)
Compressive strength = 3,351 MPa (486 ksi).

Table 2: HMHS Epoxy Matrix Properties:

Matrix density = 3.4E-7 kg/m^3 (0.0457 lb/in^3)
Normal modulus = 4.27 GPa (629 Ksi)
Poisson's ratio = 0.34
Coeffient of thermal expansion = 0.72/°C (0.4E-4/°F)
Heat conductivity = 1.25 BTU-in/hr/in^2/°F
Heat capacity = 0.25 BTU/lb/°F
Tensile strength = 84.8 MPa (12.3 Ksi)
Compressive strength = 423 MPa (61.3 Ksi)
Shear strength = 148 MPa (21.4 Ksi)
Allowable tensile strain = 0.02
Allowable compressive strain = 0.05
Allowable shear strain = 0.04
Allowable torsional strain = 0.04
Void conductivity = 16.8 J-m/hr/m^2/°C (0.225 BTU-in/hr/in^2/°F)
Glass transition temperature = 216 °C (420 °F)

Table 3 - AS-4/HMHS Ply Strengths

S_{L11T} = 1930.30 MPa (280 ksi)
S_{L11C} = 1475.85 MPa (210 ksi)
S_{L22T} = 91.38 Mpa (13 ksi)
S_{L22C} = 228.27 MPa (33 Ksi)
S_{L12} = 65.57 MPa (9.5 Ksi)
S_{L23} = 59.98 MPa (8.7 ksi)

where 1, 2, 3 are the material axes of the ply. The direction of the fibers are parallel to 1-axis. T is for tension and C is for compression.

Table 1: AA-4 Graphite Fiber Properties:

Number of fibers per end = 10000
Fiber diameter = 0.00762 mm (0.3E-3 in)
Fiber Density = 4.04E-7 Kg/m^3 (0.063 lb/in^3)
Longitudinal normal modulus = 227 GPa (32.9E+6 psi)
Transverse normal modulus = 13.7 GPa (1.99E+6 psi)
Poisson's ratio (n_{12}) = 0.2
Poisson's ratio (n_{23}) = 0.25
Shear modulus (G_{12}) = 13.8 GPa (2.E+6 psi)
Shear modulus (G_{23}) = 6.9 GPa (1.E+6 psi)
Longitudinal thermal expansion coefficient=1.E-6/°C (-0.55E-6/°F)
Transverse thermal expansion coefficient=1.E-6/°C (-0.56E-6/°F)
Longitudinal heat conductivity = 43.4 J-m/hr/m^2/°C
= (580 BTU-in/hr/in^2/°F)
Transverse heat conductivity = 4.34 J-m/hr/m^2/°C
= (58 BTU-in/hr/in^2/°P)
Heat capacity = 712 J/Kg/°C (0.17 BTU/lb/°F)
Tensile strength = 3,723 MPa (540 ksi)
Compressive strength = 3,351 MPa (486 ksi).

Table 2: HMHS Epoxy Matrix Properties:

Matrix density = 3.4E-7 kg/m^3 (0.0457 lb/in^3)
Normal modulus = 4.27 GPa (629 Ksi)
Poisson's ratio = 0.34
Coeffient of thermal expansion = 0.72/°C (0.4E-4/°F)
Heat conductivity = 1.25 BTU-in/hr/in^2/°F
Heat capacity = 0.25 BTU/lb/°F
Tensile strength = 84.8 MPa (12.3 Ksi)
Compressive strength = 423 MPa (61.3 Ksi)
Shear strength = 148 MPa (21.4 Ksi)
Allowable tensile strain = 0.02
Allowable compressive strain = 0.05
Allowable shear strain = 0.04
Allowable torsional strain = 0.04
Void conductivity = 16.8 J-m/hr/m^2/°C (0.225 BTU-in/hr/in^2/°F)
Glass transition temperature = 216 °C (420 °F)

Table 3 - AS-4/HMHS Ply Strengths

S_{L11T} = 1930.30 MPa (280 ksi)
S_{L11C} = 1475.85 MPa (210 ksi)
S_{L22C} = 228.27 MPa (33 Ksi)
S_{L22T} = 91.38 Mpa (13 ksi)

S_{L12} = 65.57 MPa (9.5 Ksi)
S_{L23} = 59.98 MPa (8.7 ksi)

where 1, 2, 3 are the material axes of the ply. The direction of the fibers are parallel to 1-axis. T is for tension and C is for compression.

Table 4 - Damage Progression Through the 0.05 in. Composite Containment at Node 4 (Fig. 7) (Graphite/Epoxy 0.6 FVR 0.01 VVR)

		impact load/fracture load, (fracture load = 6.7 kips)				
ply	angle	0.69	0.70	0.706	0.713	0.786
1	0		σ_{122T}	σ_{111C}		
2	–45			σ_{111C}		
3	45				σ_{111C}, σ_{112+}	
4	90				σ_{122C}, σ_{112-}	
5	90				σ_{122T}	σ_{111T}, σ_{112-}
6	45				σ_{112+}, σ_{111T}	
7	– 45			σ_{122T}	σ_{111T}	
8	0	σ_{122T}	σ_{111C}			

Table 5 - Damage Progression Through the 0.10 in. Composite Containment at Node 5 (Graphite/Epoxy 0.6 FVR 0.01 VVR)

		impact load/fracture load, (fracture load = 28.3 kips)		
ply	**angle**	**0.419**	**0506**	**0.596**
1	**0**		σ_{122T}	σ_{111T}
2	**–45**		σ_{122T}	σ_{111T}
3	**45**	σ_{122T}		σ_{111T}
4	**90**		σ_{122T}	σ_{111C}
5	**90**		σ_{122T}	σ_{111T}
6	**45**			σ_{112+} , σ_{111C}
7	**–45**			σ_{112-}, σ_{111C}
8	**0**			σ_{111C}

Table 6 - Damage Progression Through the 0.15 in. Composite Containment at Node 1) (Graphite/Epoxy 0.6 FVR 0.01 VVR)

		impact load/fracture load, (fracture load = 28.3 kips)			
ply	**angle**	**0.267**	**0340**	**0.640**	**0.690**
1	**0**	σ_{122T}		σ_{111T}	
2	**–45**		σ_{122T}		σ_{111T}
3	**45**			σ_{122T}	σ_{111T}
4	**90**			σ_{122T}	σ_{111C}
5	**90**				σ_{111T} , σ_{122C}
6	**45**				σ_{112+} , σ_{111C}
7	**–45**				σ_{112-}, σ_{111T}, σ_{122T}
8	**0**				σ_{111C}, σ_{122T}

Table 7 - Damage Progression Through the 0.25 in. Composite Containment at Node 7 (Graphite/Epoxy 0.6 FVR 0.01 VVR)

		impact load/fracture load, (fracture load = 69.3 kips)		
ply	angle	0.435	0.506	0.512
1	0	σ_{111T}		σ_{122T}
2	–45	σ_{122T}		σ_{111T}
3	45	σ_{122T}		σ_{111T}
4	90		σ_{122T}	σ_{111C}
5	90			σ_{111T}
6	45		σ_{112+}	σ_{111C}
7	–45			σ_{111C}, σ_{112+}
8	0		σ_{111C}	

Table 8 - Damage Progression Through the 0.35 in. Composite Containment at Node 7 (Graphite/Epoxy 0.6 FVR 0.01 VVR)

		impact load/fracture load, (fracture load =113.2 kips)			
ply	**angle**	**0.147**	**0.37**	**0.39**	**0.402**
1	**0**	σ_{122T}	σ_{111T}		
2	**–45**		σ_{122T}		σ_{111T}
3	**45**		σ_{122T}		σ_{111T}
4	**90**			σ_{122T}	σ_{111C}
5	**90**				$\sigma_{111T}, \sigma_{122T}$
6	**45**			σ_{112-}	σ_{111C}
7	**–45**			σ_{112+}	σ_{111C}
8	**0**			σ_{111C}	

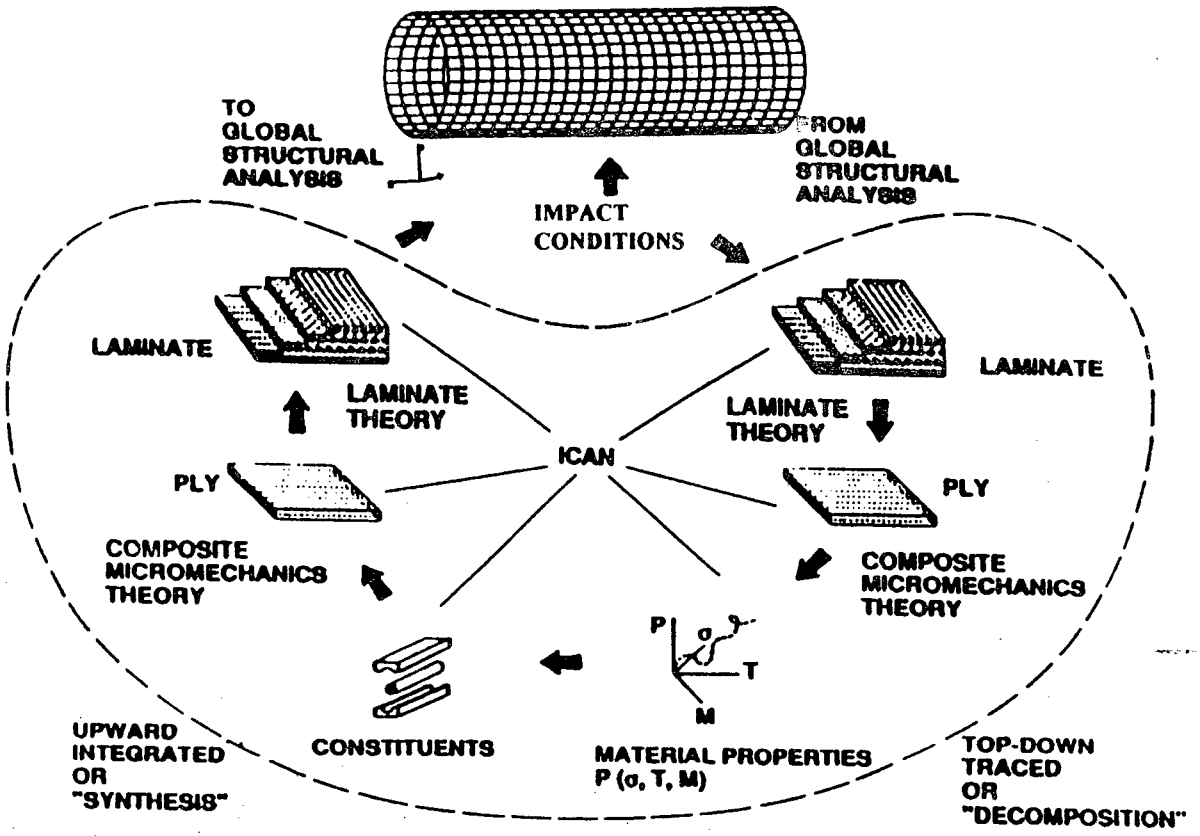

Figure 1 - Schematic of CODSTRAN computational simulation cycle (lower part - composite mechanics, upper part - general finite element structural analysis).

♦ MAXIMUM STRESS FAILURE CRITERION.

THE SIX PLY STRESS COMPONENTS ARE ALONG THE MATERIAL AXES .

$$S_{L11C} < \sigma_{L11} < S_{L11T}$$

$$S_{L22C} < \sigma_{L22} < S_{L22T}$$

$$S_{L33C} < \sigma_{L33} < S_{L33T}$$

$$S_{L12(-)} < \sigma_{L12} < S_{L12(+)}$$

$$S_{L23(-)} < \sigma_{L23} < S_{L23(+)}$$

$$S_{L13(-)} < \sigma_{L13} < S_{L13(+)}$$

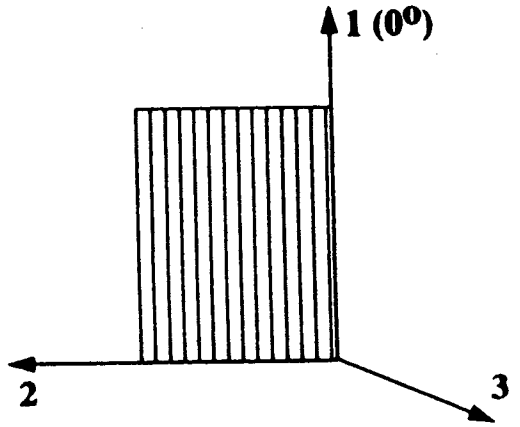

♦ MDE COMBINED STRESS FAILURE CRITERION.

$$F = 1 - [\ (\sigma_{L11a}/S_{L11a})^2 + (\sigma_{L22b}/S_{L22b})^2 - K_{L12ab}(\sigma_{L11a}/S_{L11a})(\sigma_{L22b}/S_{L22b}) + (\sigma_{L12S}/S_{L12S})^2\ ].$$

Figure 2 - ICAN ply fracture modes criteria for progressive fracture tracking.

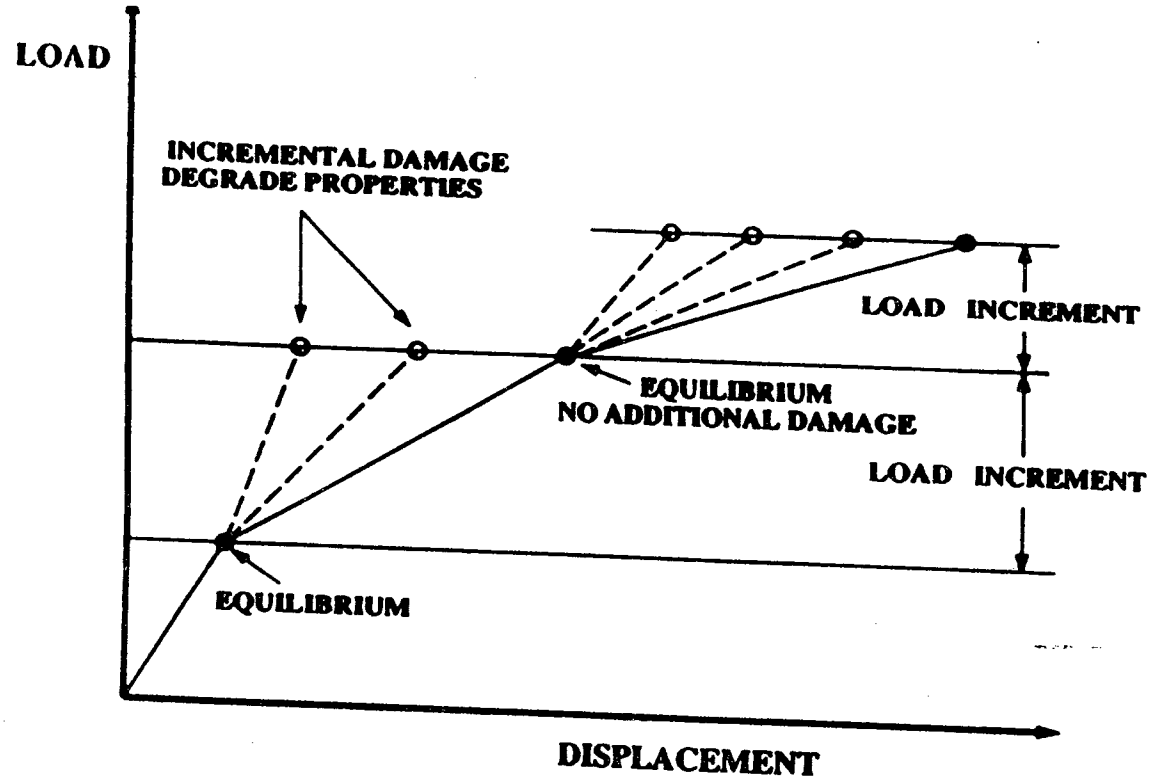

Figure 3 - Schematic of CODSTRAN load incrementation and damage progression tracking.

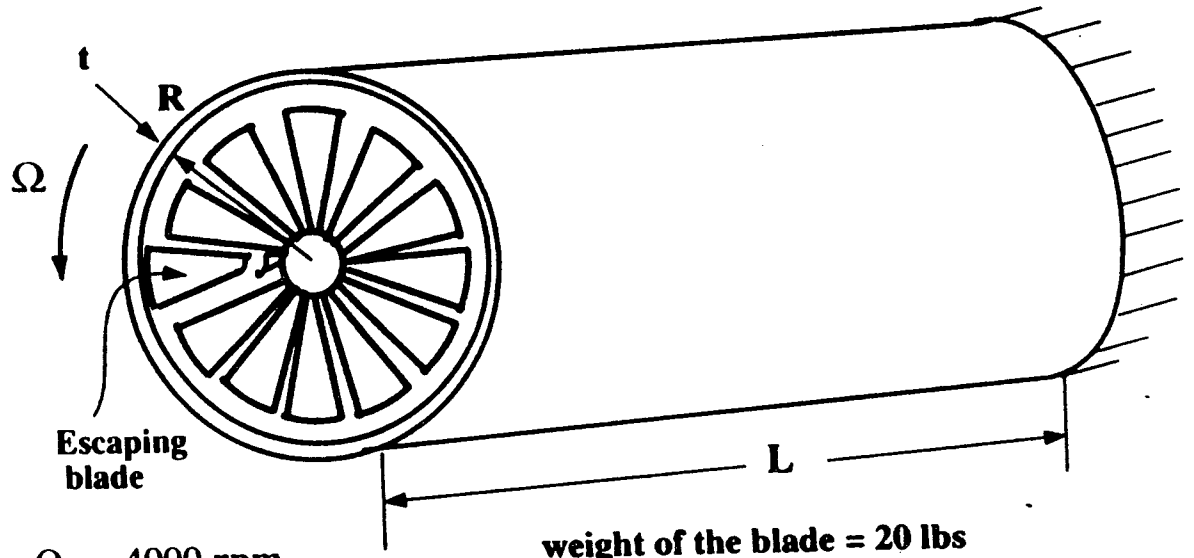

Ω = 4000 rpm

weight of the blade = 20 lbs

L = 124. in, R = 60. in, t = 0.05 in, 0.10 in, 0.15 in, 0.25 in, 0.35 in.

Graphite/Epoxy, (0/±45/90)s , 8 uniform plies.

FVR = 60%, void volume ratio = 1%

Figure 4 - Schematic of sample case evaluated - geometry, loads, and composite.

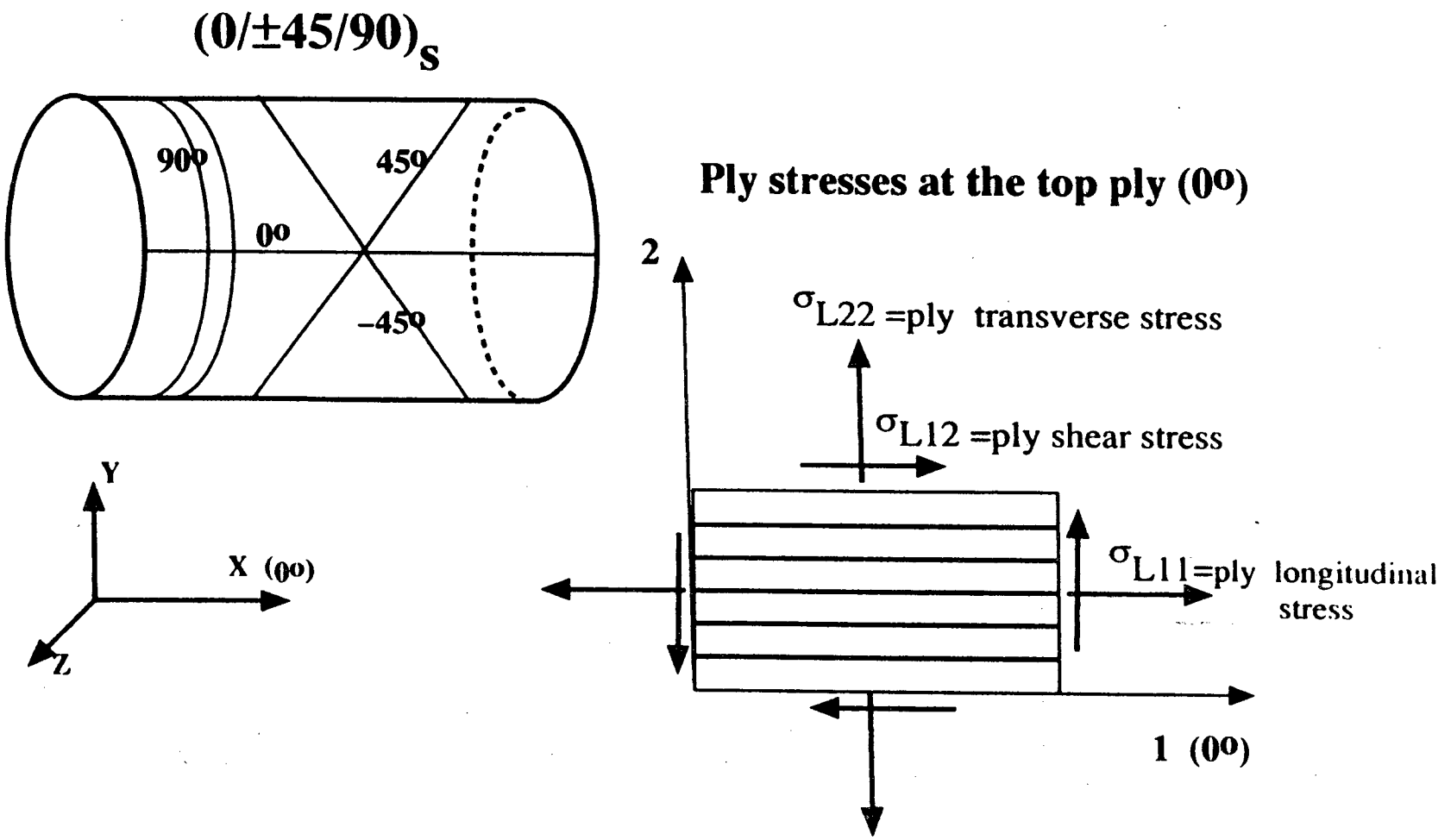

Figure 5 - Schematic of composite containment shell laminate configuration and ply stress definition.

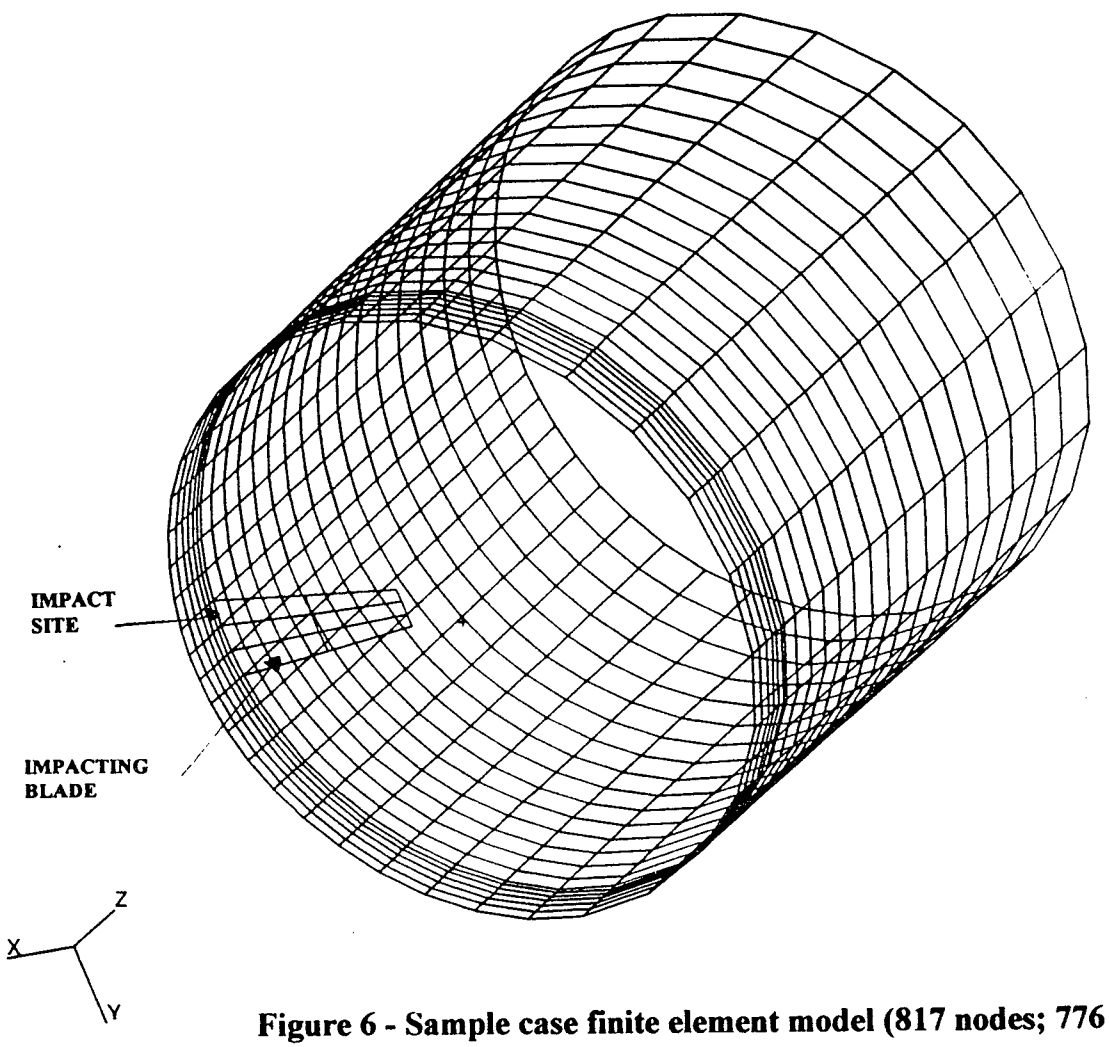

Figure 6 - Sample case finite element model (817 nodes; 776 quad elements, 4632 FDOF).

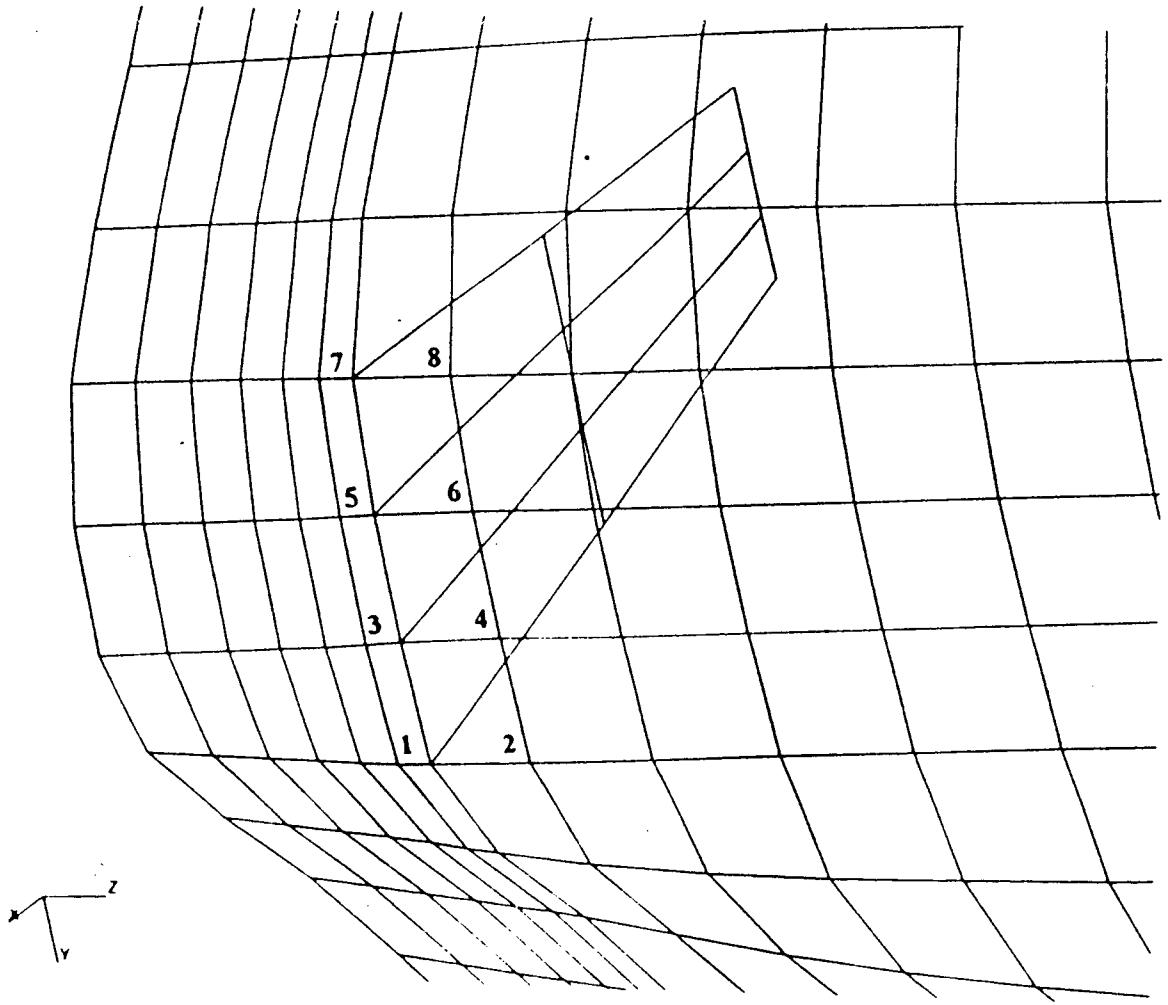

Figure 7 - Expanded finite element model of impact site - nodes at which damage tracking is presented.

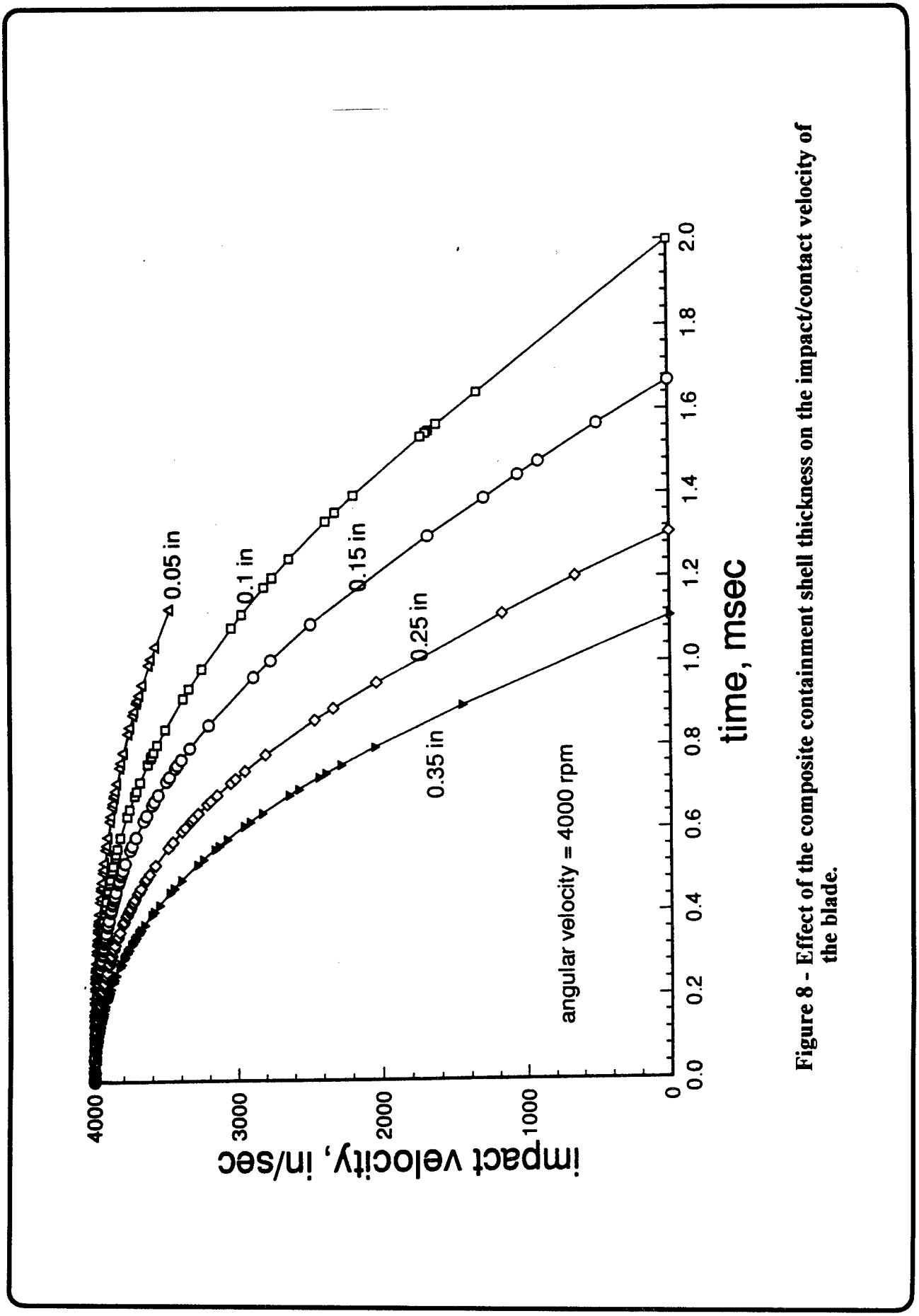

Figure 8 - Effect of the composite containment shell thickness on the impact/contact velocity of the blade.

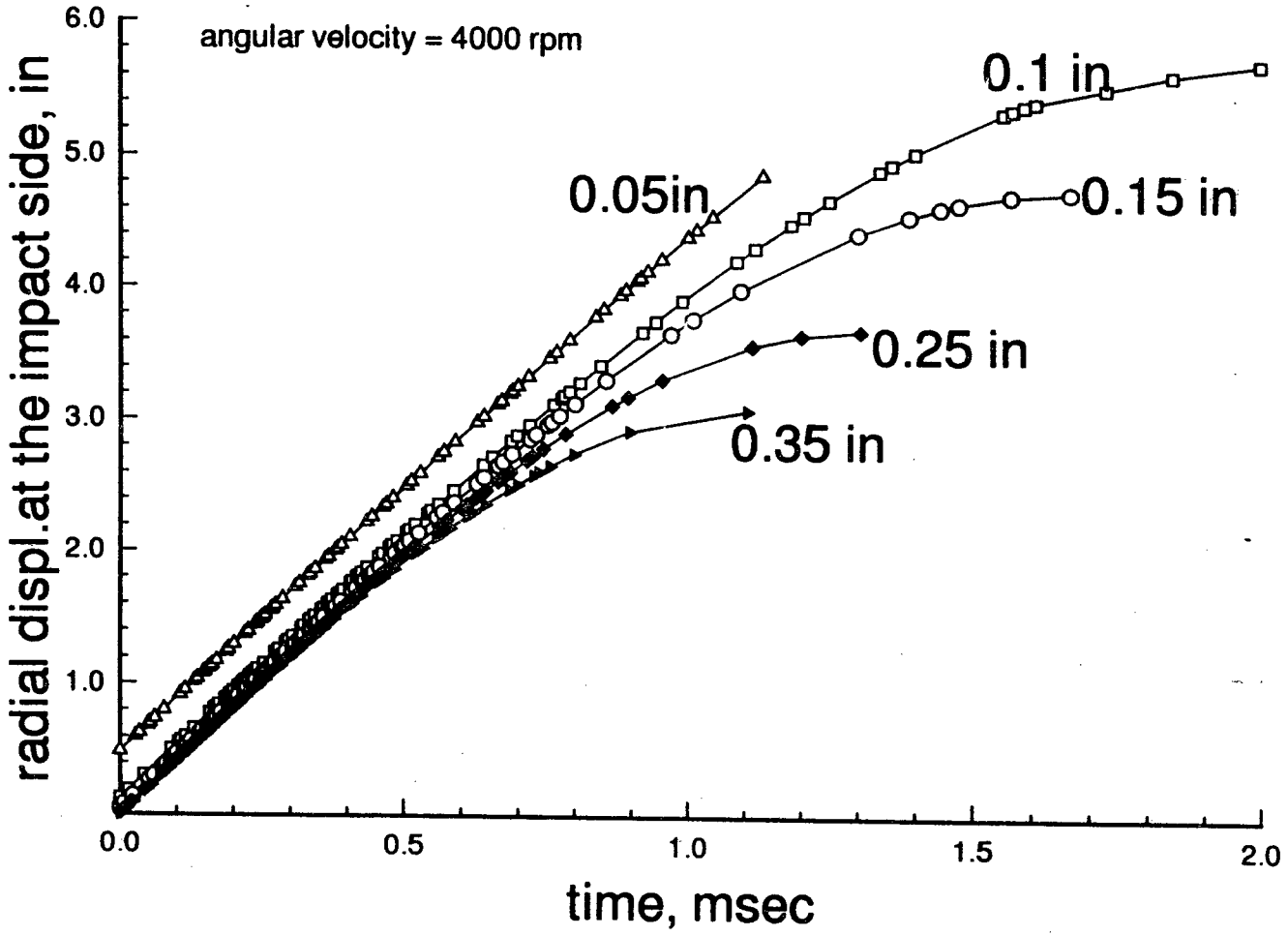

Figure 9 - Effect of the composite containment shell thickness on the radial displacement at impact site.

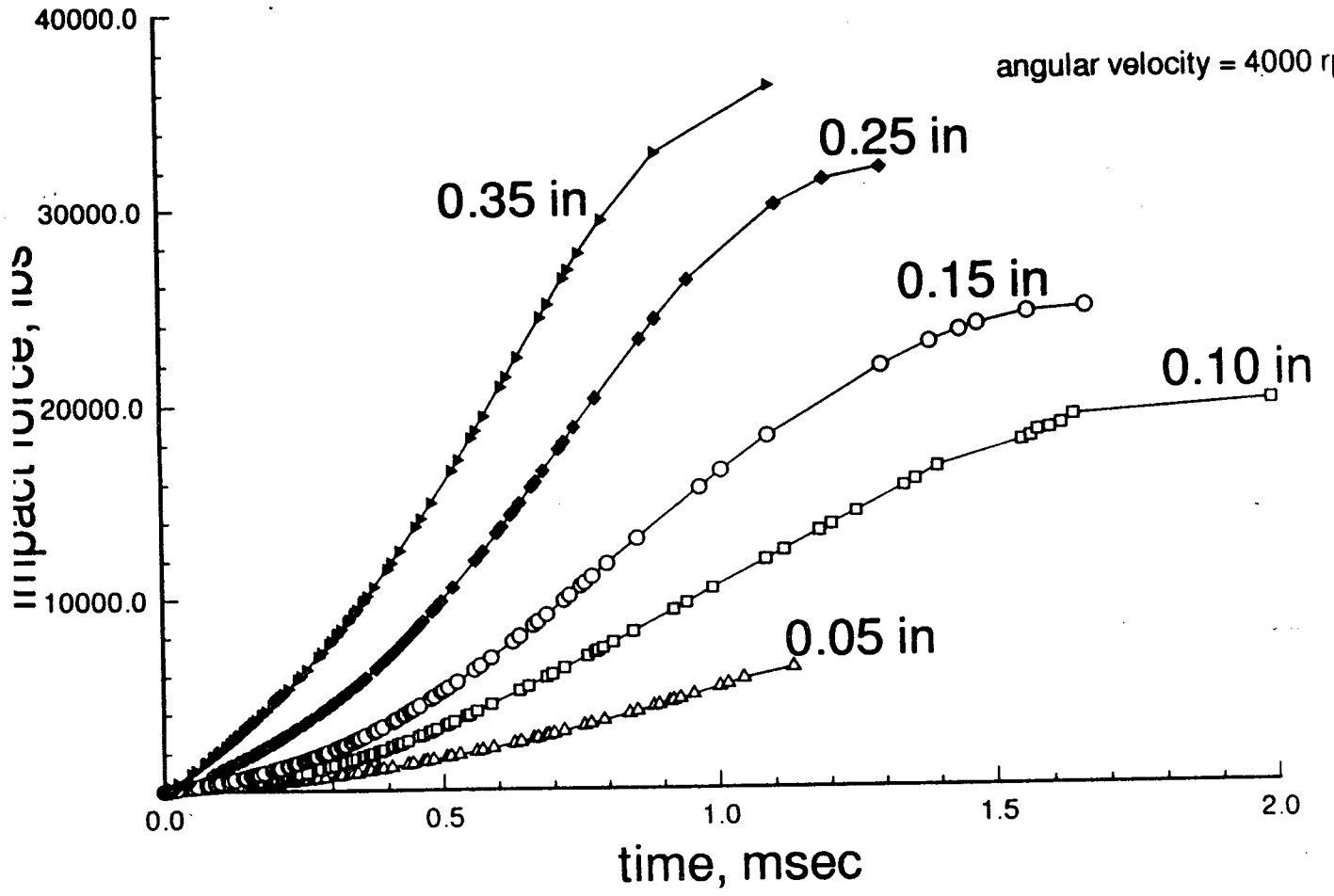

Figure 10 -Effect of composite containment shell thickness on the impact force.

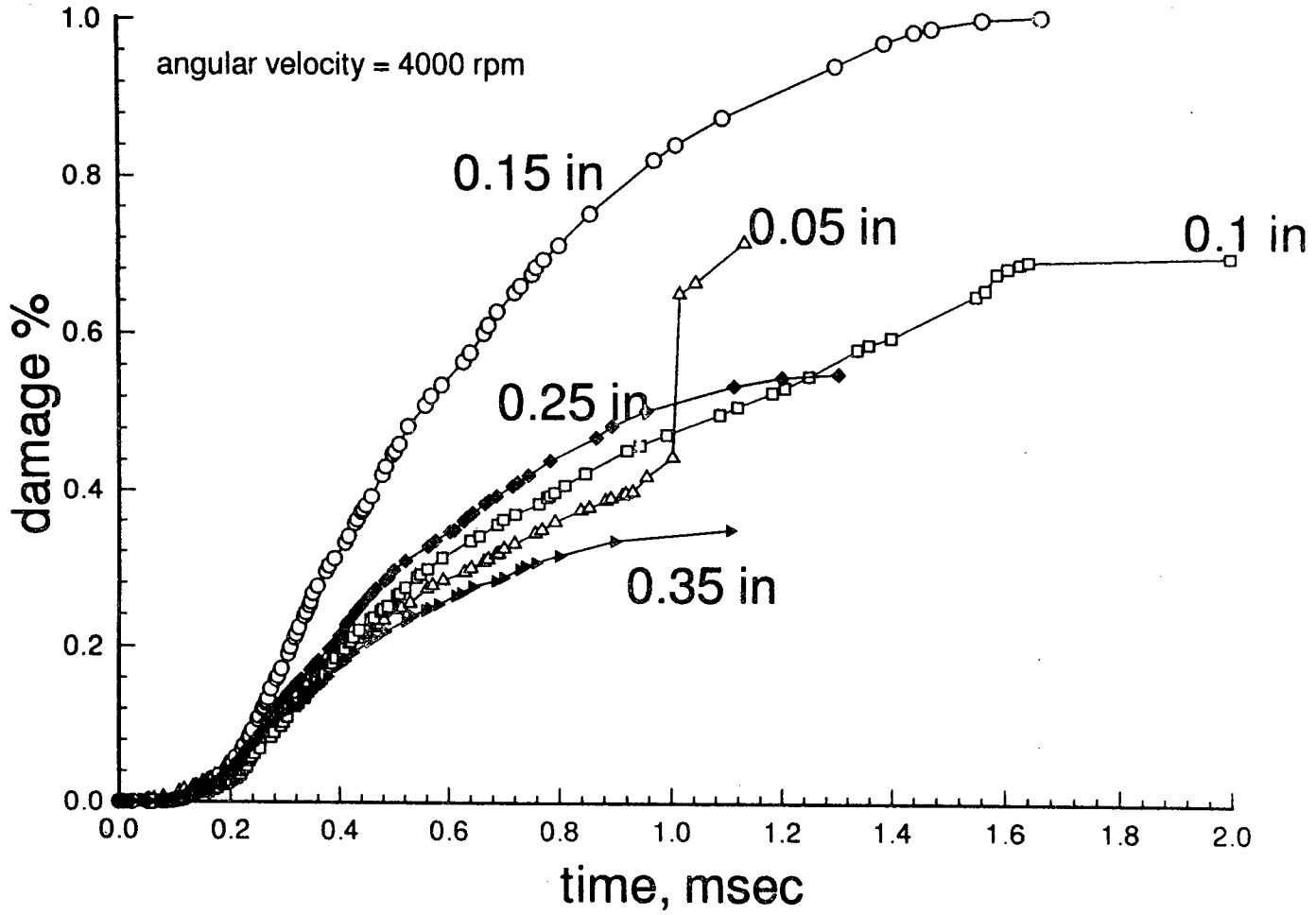

Figure 11 - Effect of the composite containment shell thickness on the cumulative damage sustained.

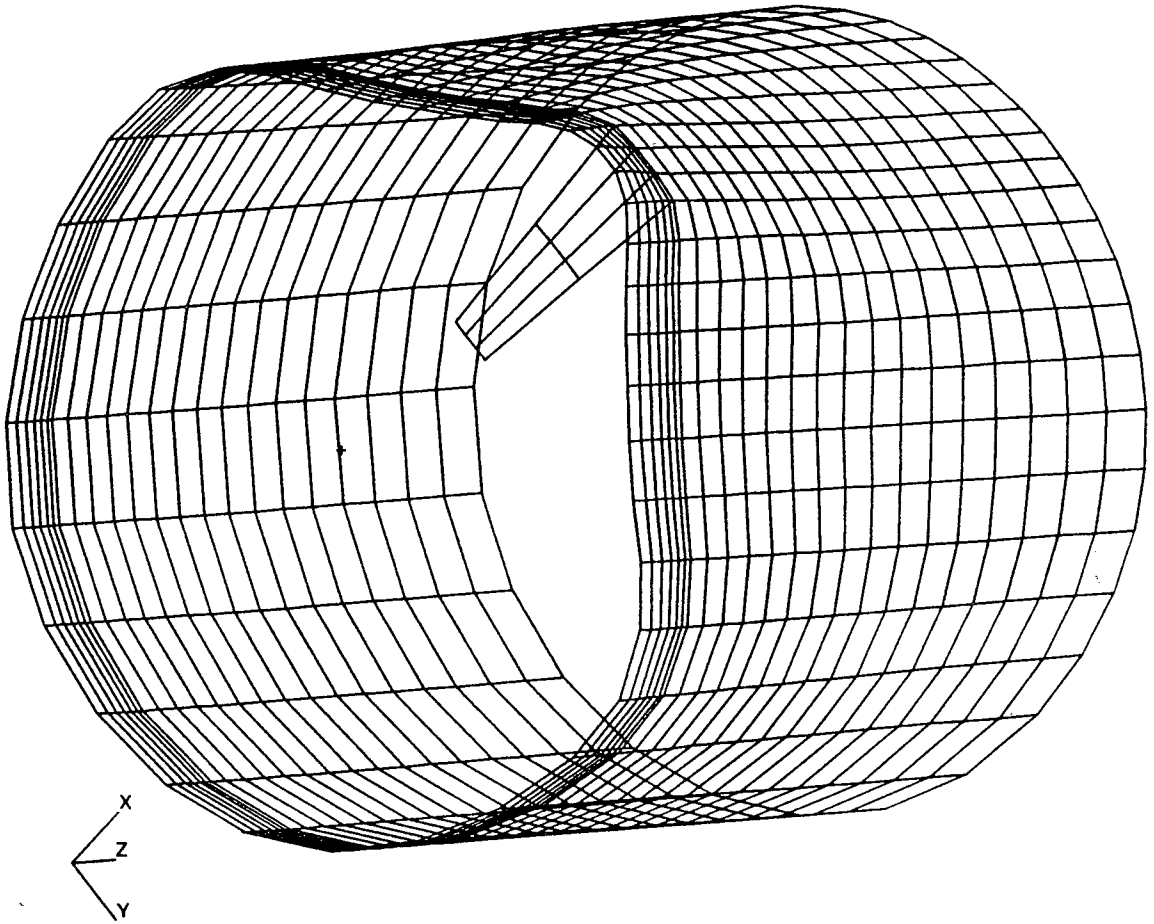

Figure 12 - Typical impact displacement patterns of a 0.25 in thick composite containment shell prior to initial damage (37 klb impact force; see Figure 4 for other parameters).

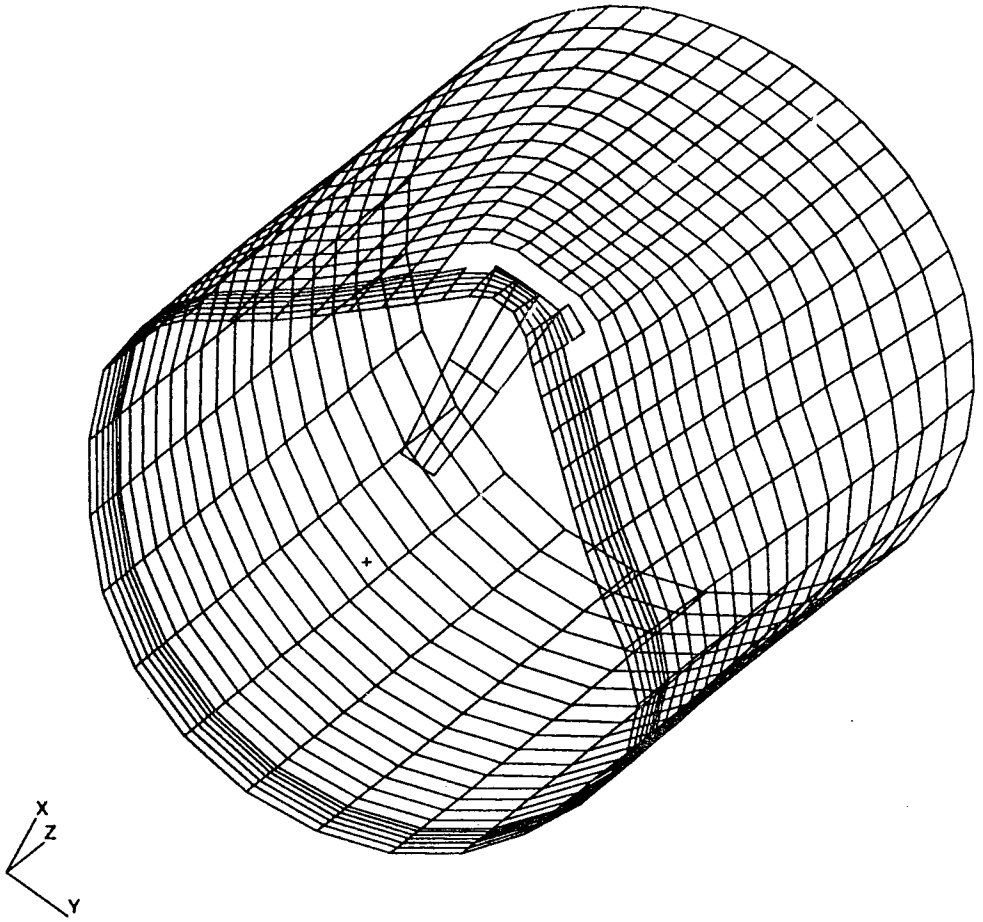

Figure 13 - Typical impact displacement and damage patterns of a 0.25 in. thick composite containment shell (66 klb impact force; see Figure 4 for other parameters).

A Probabilistic Life Method for a Two-Lobed Turbine Disk Attachment

Dr. Chetan Date
Mr. Craig Balis
*Dr. Dan Greving
Mr. Jan Musgrave
Mr. Dennis Langefels
Mr. Kurt Richardson
AlliedSignal Engines
111 S. 34th St., Phoenix, Arizona 85072-2181

Abstract

The fatigue life of a gas turbine disk attachment is affected by several variables such as surface finish, material fatigue property, blade and disk attachment tolerances, temperature, and stresses. The traditional life prediction approach generally treats all variables except the material fatigue property as invariants which are established at certain design parameters. The design parameters are usually fixed at some probable level or at some conservative value. Because the traditional approach ignores the effects of most variables on fatigue life, it results in component designs with inconsistent risks. That is, some component designs may be overly conservative when compared to others in the same engine. This inadequacy of the traditional method can be eliminated by treating the dominant variables probabilistically.

A probabilistic method was used to evaluate the fatigue life of T800-LHT-801 gas generator turbine (GGT) disks two-lobe attachments. Disk and blade attachment tolerances and material fatigue properties were established as the two dominant variables on attachment life. Manufacturing tolerances for disk and blade attachments were monitored with an Automated Disk Slot Inspection System (ADSIS). Results show that disk and blade attachment tolerances are well controlled in a narrow band smaller than allowable values. A comprehensive research program was conducted to determine the fatigue property distribution for the disk attachment material, wrought nickel base alloy Udimet 720LI. An emphasis was placed on the effects of surface condition produced by the

attachment broach machining operation. A significant quantity of configured notch fatigue specimens were manufactured with production broach tooling and shot peened according to required specifications. A resultant bi-modal fatigue life distribution was used in the life analysis. A Monte Carlo simulation method was used to couple the material fatigue property distribution with the tolerance distribution to produce an outcome distribution of disk attachment lobe life.

Background

The firtree slots of gas turbine disks serve as attachment points for inserted blades. The Light Helicopter Turbine Engine Company's (LHTEC) T800-LHT-801 gas generator turbine disks use a two-lobed attachment design. The disk material is a nickel base wrought alloy, Udimet 720 Low Inclusion (LI), and the blades are single crystal (SC) 180.

The criteria for establishing a minimum service life for attachment regions on turbine disks is based on customer requirements. A widely accepted minimum life design requirement is based on a "-3σ minimum". Turbine disk attachment lives must be assessed accordingly and risk should remain consistent from one location to the next. For example, the bore should be analyzed with the same level of risk as the attachment. Disk attachment cycle life calculations are traditionally based on deterministic approaches which treat material fatigue properties probabilistically while other variables are held constant at specified design levels. If the variables are treated as invariants held at overly conservative values, a rate of occurrence well below -3σ can occur.

Disk Attachment Variables

Variables such as operating speeds and temperatures, friction between the disk and blade attachment, disk and blade attachment profile tolerances, surface finish, and material fatigue properties influence turbine disk attachment life. For the T800-LHT-801 gas generator turbine disks, material fatigue property and tolerances were established as the dominant variables which influence disk attachment life. All other influences (speed, temperature, friction) are held constant at appropriate design values. The effects of material fatigue properties and tolerances are described in the following subsections.

Material Fatigue Properties: Effect of Surface Condition

Broaching is a material removal process that is used to produce attachment slots in turbine disks. Fatigue crack initiation in broached attachments is predominantly a surface phenomenon that is dependent upon broaching parameters

and surface treatments. Figure 1 shows a 500X photograph of a broached surface in a disk slot. The broach machining grooves are detrimental to fatigue life since they act as local stress concentrations. Shot peening is a surface treatment that is applied to improve fatigue life. The shot peening process produces compressive residual stresses near the surface of a part. Shot peening also acts as a method to reshape and blend the machining grooves produced by broaching.

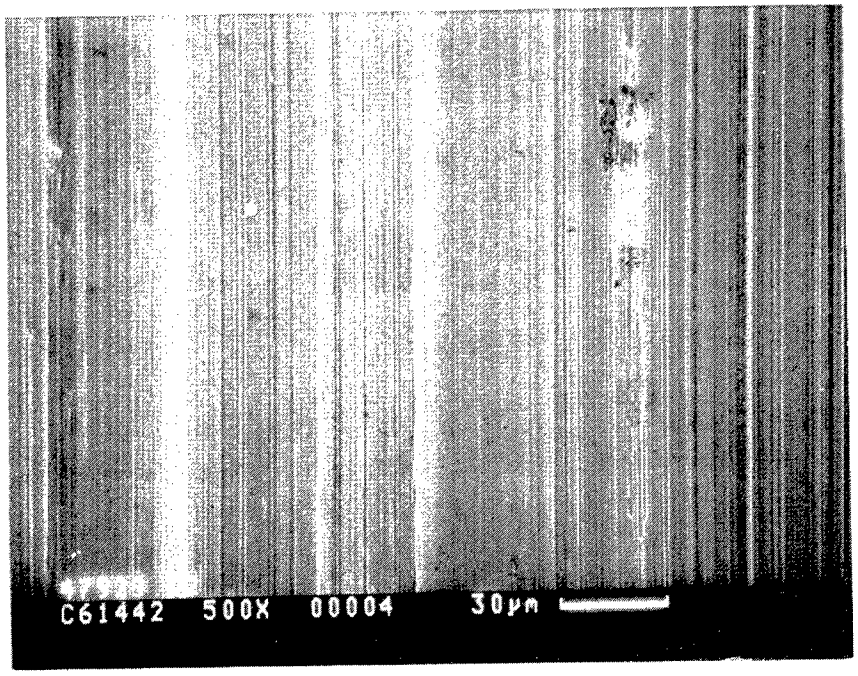

Figure 1. 500X photograph of broach machining marks in a turbine disk attachment slot.

A test program was developed to evaluate the effects of surface condition on the low cycle fatigue (LCF) life of Udimet 720LI. Specimens were removed from disk forgings and broached with the tools used for manufacturing T800 gas generator turbine disks. Figure 2 shows an illustration of a broached specimen. The slot bottom notch is the critical location on the specimen. A test matrix based on a design of experiment (DOE) approach was used in this study. Conditions such as as-broached (without shot peening) and variations in the shot peening process were studied. Results for the conditions used to manufacture production disks are presented here.

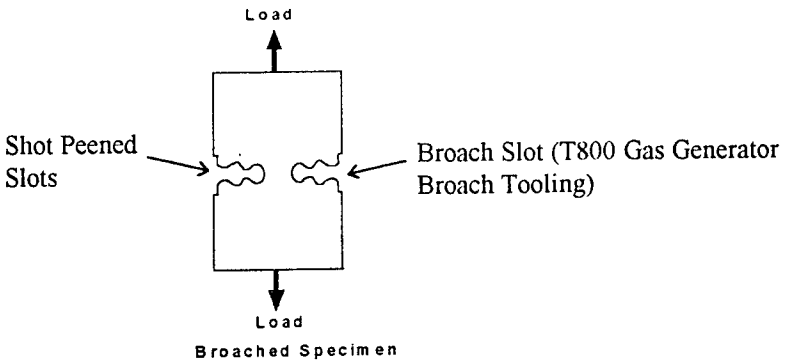

Figure 2. Illustration of configured specimen (Double notch, LCF, load controlled)

Shot peening was applied according to component specifications. A significant quantity of specimens were tested at a single stress and temperature that simulates engine operating conditions. Figure 3 shows a Weibull probability plot of the fatigue specimens tested at one condition. The x-axis in Figure 3 represents cycles to crack initiation and the y-axis represents the cumulative number of occurrences. Crack initiation cycles were based on a typical detectable flaw size for an elliptical surface crack.

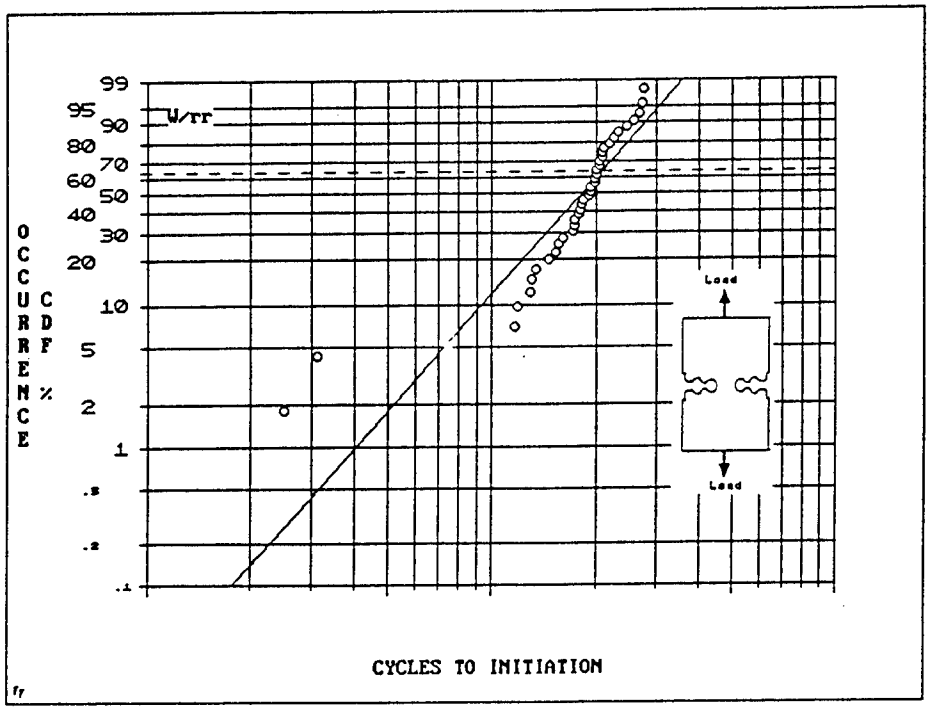

Figure 3. Weibull plot of broached Udimet 720 LI fatigue specimens with shot peen.

Figure 3 shows a distinct separation of failure mechanism for shot peened data. Two of the shot peened specimens experienced a substantially lower life than the other specimens in the sample. The low-life specimens were examined in detail and no indication of surface anomaly was found. Fractography shows that the low-life shot peened specimens initiated cracks at the surface where the remaining samples initiated cracks at subsurface crystallographic sites. Since two modes of failure (surface versus subsurface) occurred, a bi-modal fatigue property distribution exists.

These results show that shot peening has a certain amount of inherent scatter resulting from low-life dropouts. A dropout is described as a specimen with a low life and an uncharacteristic surface initiation while the majority of the other samples have subsurface initiations. The two specimens with a low life and a surface initiation represent approximately 5% of the specimen sample.

Effect of Tolerance:

Three dimensional finite element analysis shows that disk to blade tolerance has a significant influence on attachment stresses. Tolerances can result in uneven load sharing for the two attachment lobes. Worst case tolerances result in maximum lobe stresses. Figure 4 shows an illustration of the tolerances associated with a two-lobed disk and blade attachment. Figure 4 also shows how tolerances combine to produce a gap. Gap is a measure of the difference in tolerance when the disk and blade are coupled. A gap on the inner lobe results in higher loading on the outer lobe and a gap on the outer lobe results in higher loading on the inner lobe.

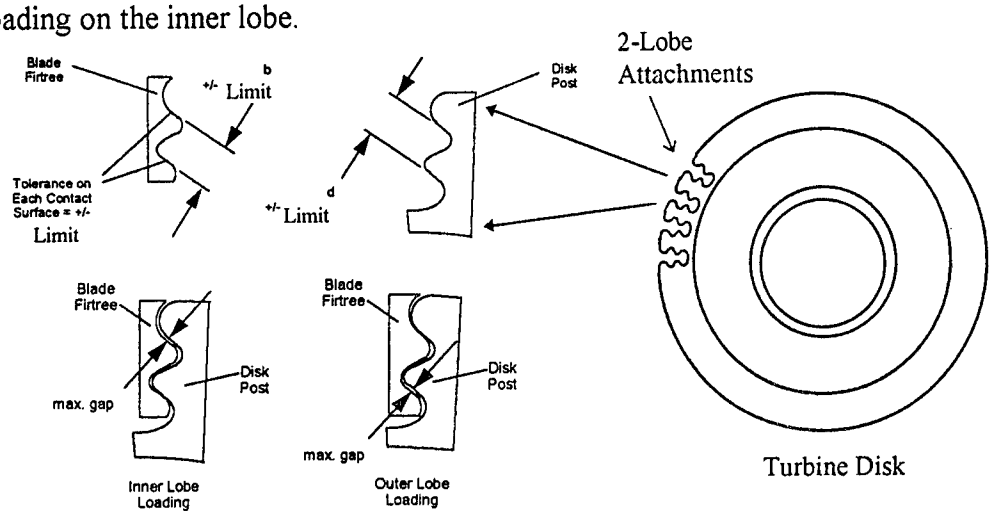

Figure 4. Illustration of disk and blade tolerances and resulting gap and load split.

Figures 5 and 6 show actual tolerances measured for gas generator turbine disks and blades. The inspections were performed with an automated disk slot inspection system (ADSIS). There are 28 disks from two separate lots represented in Figure 5. Five slots were measured from each disk. These results show that disk and blade tolerances are well within the current print limits.

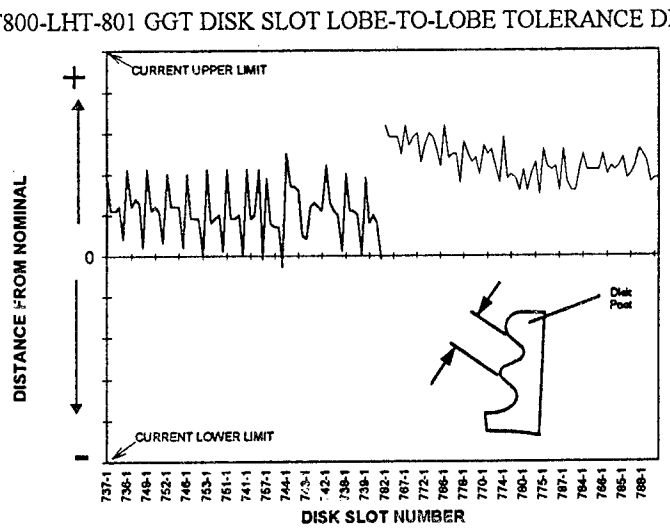

Figure 5. Actual disk attachment tolerances measured with an automated disk slot inspection system (ADSIS).

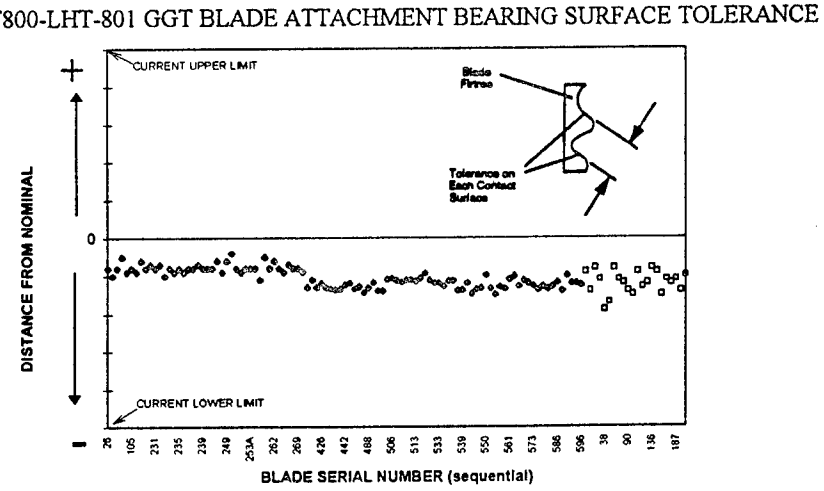

Figure 6. Actual gas generator turbine blade attachment tolerances.

Monte Carlo Simulation

A Monte Carlo simulation was used to assess the combined influence of the input variables (fatigue data and tolerances) on attachment stresses and disk attachment life. The simulation proceeds by generating independent random values for each input variable. The resulting input values are used to establish the output values based on parametric relations. These steps are repeated for a large sample (i.e. 100,000 disk simulation) and the distribution of the output is established. Figure 7 illustrates the simulation process.

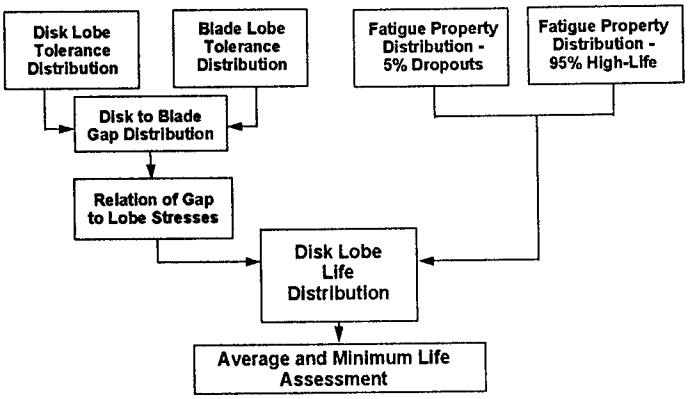

Figure 7. Illustration of the Monte Carlo simulation process which includes variation in tolerance and material fatigue property.

Variables and Distributions

Specimen Fatigue Data: Specimen data was used to establish the material fatigue life input distribution. The material fatigue life distribution was generated from the bi-modal fatigue property presented in Figure 3. The material fatigue property distribution was based on the Weibull parameters for 95% high life (no dropouts) and 5% low life data. Figure 8 shows a 100,000 fatigue specimen distribution simulated in the Monte Carlo process.

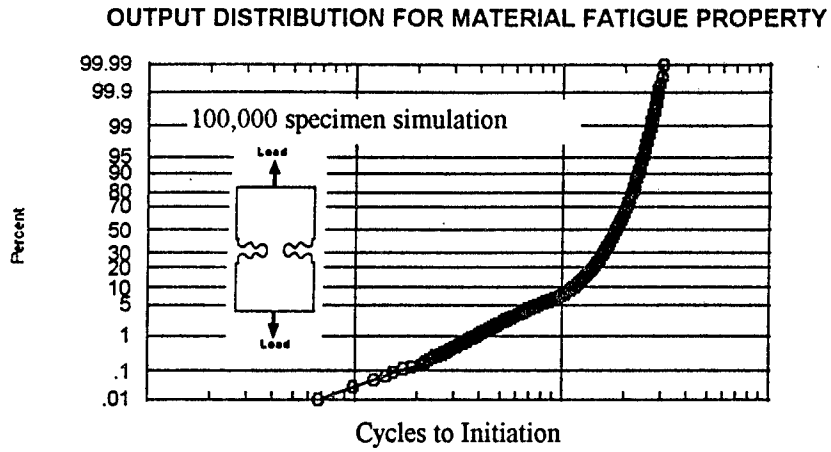

Figure 8. Probability plot of output distribution for material fatigue property based on a Monte Carlo simulation of shot peen data with 5% dropout rate.

Gap: The dimensional tolerances of the disk attachment are based on the nominal or mean dimensions of the broach slots and the standard deviation or scatter associated with the machining operation. The mean dimensions of the broach are assumed to be a uniform or random distribution while the standard deviation or scatter associated with the machining operation is assumed to be a normal distribution about the mean. The tolerance mean can vary anywhere between the upper and lower tolerance limits. The data displayed in Figures 5 and 6 was used to establish broach and blade attachment scatter. For simulation purposes, the mean tolerance for both the disk and blade is allowed to be at the upper or lower limit. Figure 9 shows an illustration of the tolerance distribution assumed for the disk and blades.

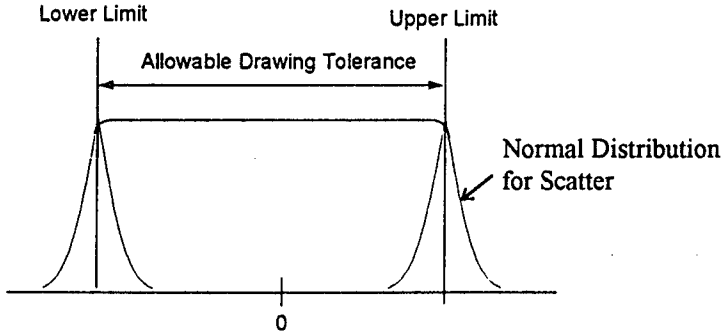

Figure 9. Illustration of the disk and blade tolerance distribution assumed for the Monte Carlo simulation.

The total gap is a combination of the tolerances for the disk and blade. Figure 10 shows the resulting Monte Carlo distributions for disk and blade tolerances and the combined gap. The distributions in Figure 10 were based on a 100,000 disk simulation. Note that disk and blade tolerances resemble a uniform distribution between the upper and lower tolerance limits. For the purpose of the simulation only, scatter allows tolerance limits to be exceeded. The Monte Carlo distributions resemble the illustrated distribution shown in Figure 9.

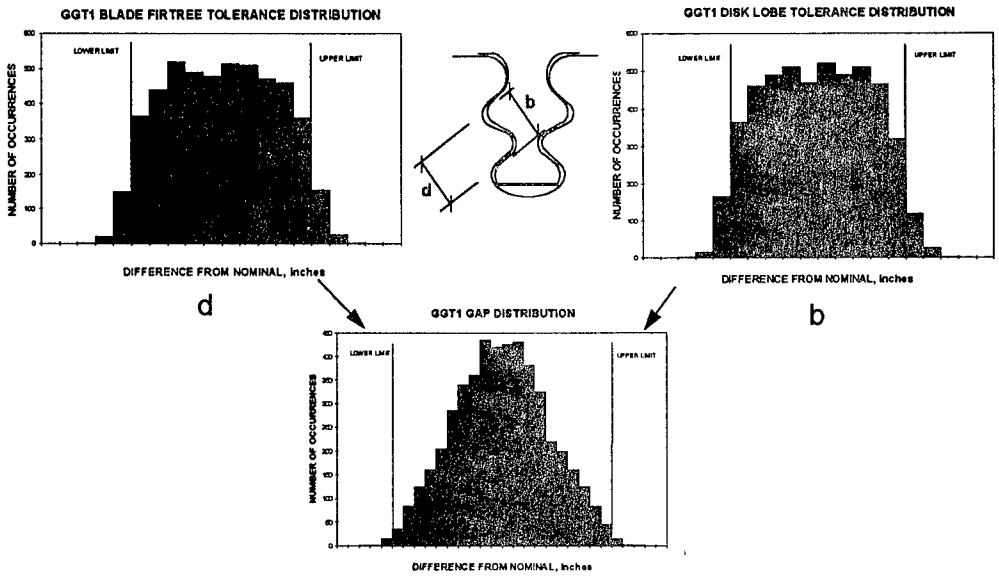

(d-b)

Figure 10. Disk and blade tolerances and resulting gap produced by the Monte Carlo simulation (100,000 disk simulation).

Figures 5 and 6 showed actual plots of lobe to lobe tolerance variation for disks and blades. Figures 5 and 6 show that tolerance is well within the print limits. Most tolerances did not exceed ±40% of the limits. This indicates that the distributions used in the Monte Carlo simulation are conservative since mean tolerances are allowed to vary from ± print limits and scatter allows limits to be exceeded.

Parametric Relations

Once the tolerance and gap distributions have been established, a parametric relation between stress and gap must be developed. Parametric relations are a set of equations that present the output variables in terms of input variables. The load distribution in the attachment region is dependent upon the magnitude and sign of the gap. If the disk and blade for a particular attachment

are both positive, the gap will be positive and the majority of the load will be applied to the inner lobe. If the total gap is negative, the majority of the load will be applied to the outer lobe. The parametric relations were established from 3-dimensional (3D) and 2-dimensional (2D) finite element analysis. Figure 11 shows a plot of the stress versus gap relation for the inner and outer lobes of a gas generator disk.

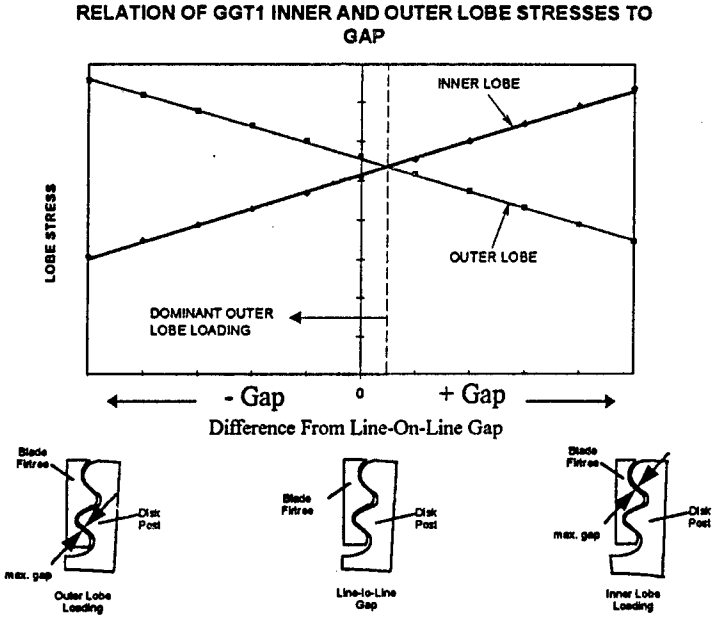

Figure 11. Relation of lobe stress to gap for the gas generator disk inner and outer lobes.

Output Distribution and Minimum Life Assessment

After establishing the variables and parametric relations, the Monte Carlo simulation can be applied. Disk life is the final output distribution and is found by relating the gap stresses to the material fatigue properties. Schemes for interpolating between different temperatures and stresses are also included. The lives are sorted and assessed for -3σ or 0.135% minimum and 50% average life. Figure 12 shows an example output distribution for a gas generator disk inner lobe.

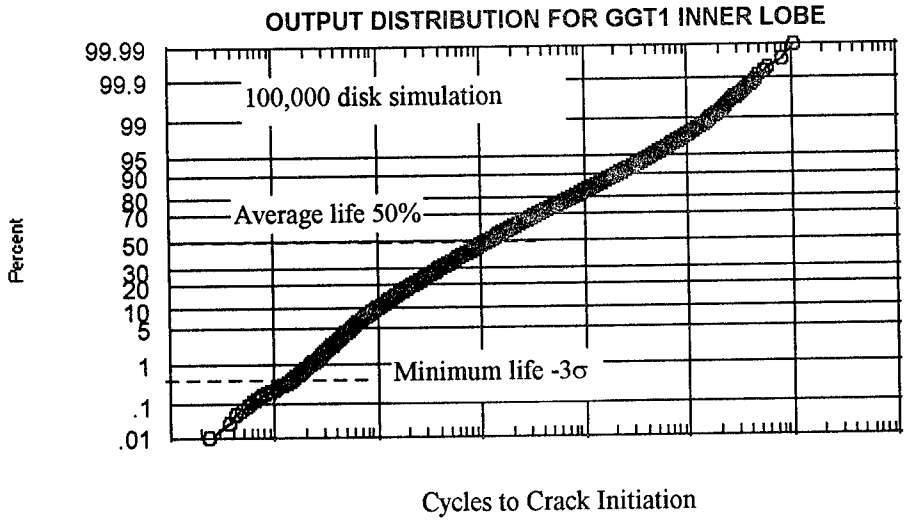

Figure 12. Probability plot showing output distribution of inner lobe lives based on Monte Carlo simulation with material fatigue property and tolerance variation included.

Summary and Conclusions

- A Monte Carlo simulation was used to couple the material fatigue property distribution and the tolerance distribution to produce an outcome distribution of disk attachment lobe life.
- Broached specimens with shot peening resulted in a bi-modal fatigue property distribution. Shot peening on average improves fatigue life but low-life scatter at a rate of approximately 5% occurred.
- Inspections of actual hardware show that worst case tolerances rarely occur. Inspected tolerances were well within print limits.
- Tolerance distributions were established by allowing disk and blade tolerances to vary uniformly between print limits. Tolerance scatter was established from actual inspection data.
- Finite element analysis was used to establish the relation of tolerances to disk lobe stresses.
- The results from the traditional method provide an overly conservative risk that is impractical for design considerations. A comparison of the minimum life calculated by the traditional method to the disk life distribution from the

probabilistic method shows that the traditional method produces a risk well below the -3σ design requirement. For the gas generator inner lobe, the minimum life determined by the traditional method using worst case tolerances and -3σ material fatigue properties would provide a risk of approximately -4.5σ (1 in ≈ 300,000 disk failures) when compared to the probabilistic disk life distribution.

- The probabilistic method that includes tolerance variation and material fatigue properties provides a method where the -3σ design requirement can be met. The probabilistic method provides the appropriate life method for evaluating the T800-LHT-801 disk attachment lobes.

Acknowledgments

The authors would like to acknowledge the Light Helicopter Turbine Engine Company (LHTEC) and the Aviation Troop Command (ATCOM) for their support. The authors would also like to thank Dr. Tim Gabb of NASA for his input to this project.

PT6A-68 JPATS ENGINE STRUCTURAL INTEGRITY PROGRAM

Bill Wilkinson
Pratt & Whitney Canada
December 5, 1996

Pratt & Whitney Canada
A United Technologies Company

PT6 INSTALLATIONS

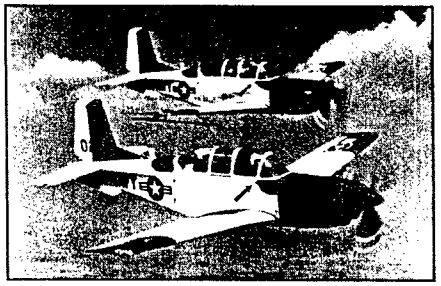

Beech T34C

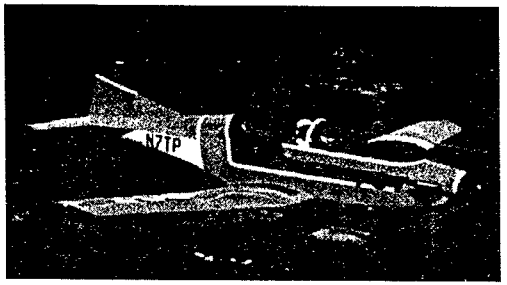

Pilatus PC7

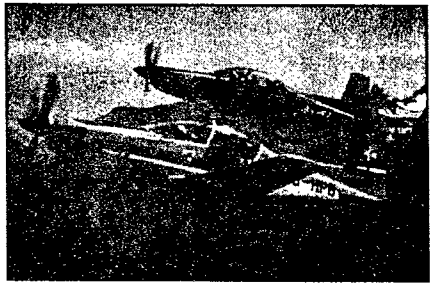

Pilatus PC9

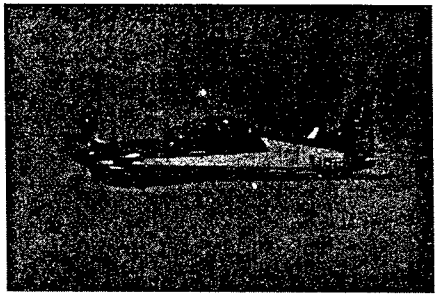

Northrop/Embraer Tucano

Piper Cheyenne III A

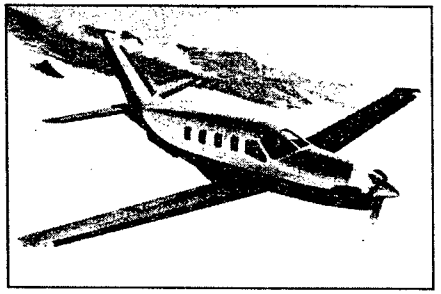

TBM 700

209044 2

880

ENSIP ACTIVITY FOR TOMORROW'S PRIMARY TRAINER

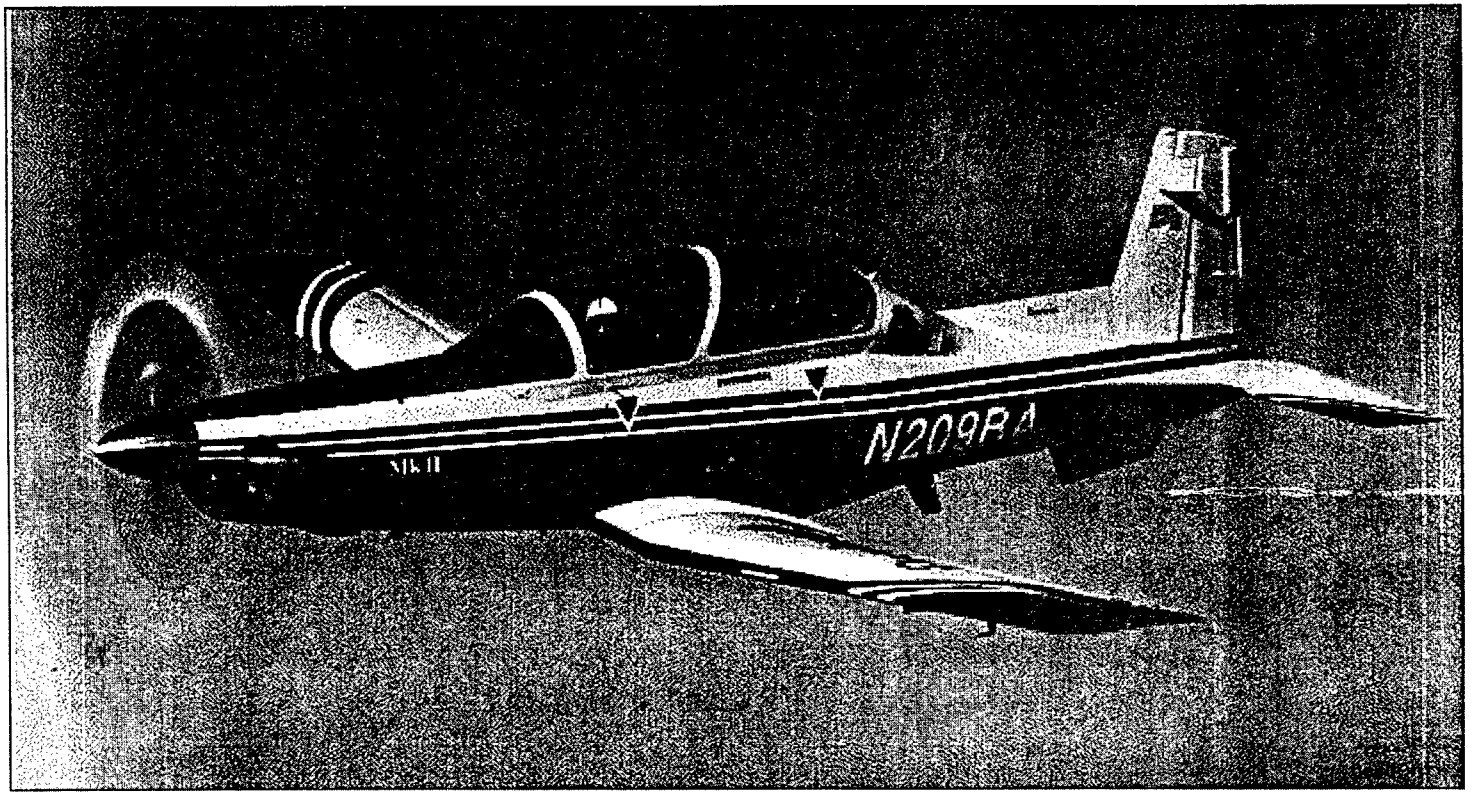

PT6A-68 ENGINE FOR JPATS

- Single engine
- Turboprop
- Primary trainer

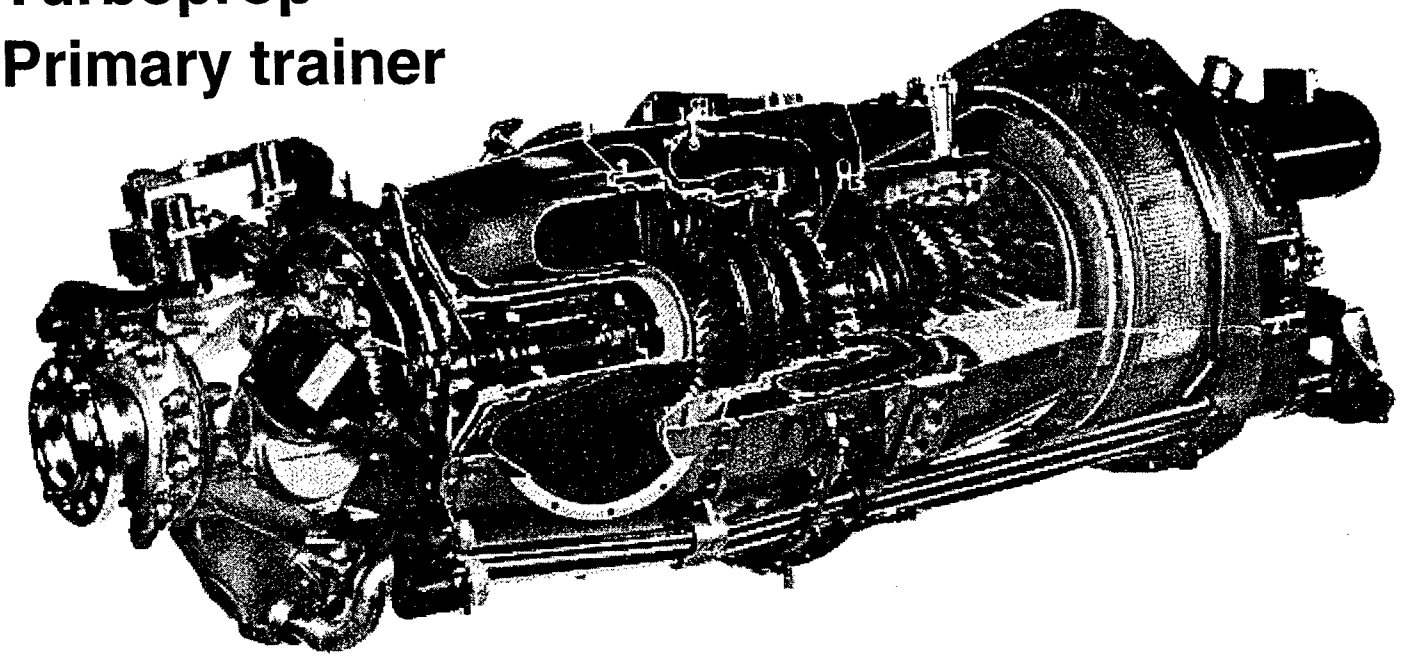

209044 4

PT6 ENGINES

- Demonstrated structural integrity in 110 different applications
- Over 187 million operating hours and 30 years of experience
- Over 13 million hours in single engine applications
- Almost 6 million hours in military trainers (T34, Tucano, PC7, PC9)
- Over 3 million hours in T34 application

ENSIP APPLIED TO PT6A-68

- Structured approach (based on MIL-STD-1783)
  - Tasks I to V
- Experience
  - Pratt & Whitney - Government Engines & Space Propulsion (GESP)
  - T-1A Jayhawk (JT15D-5B)

CRITICAL PARTS SELECTION PROCESS

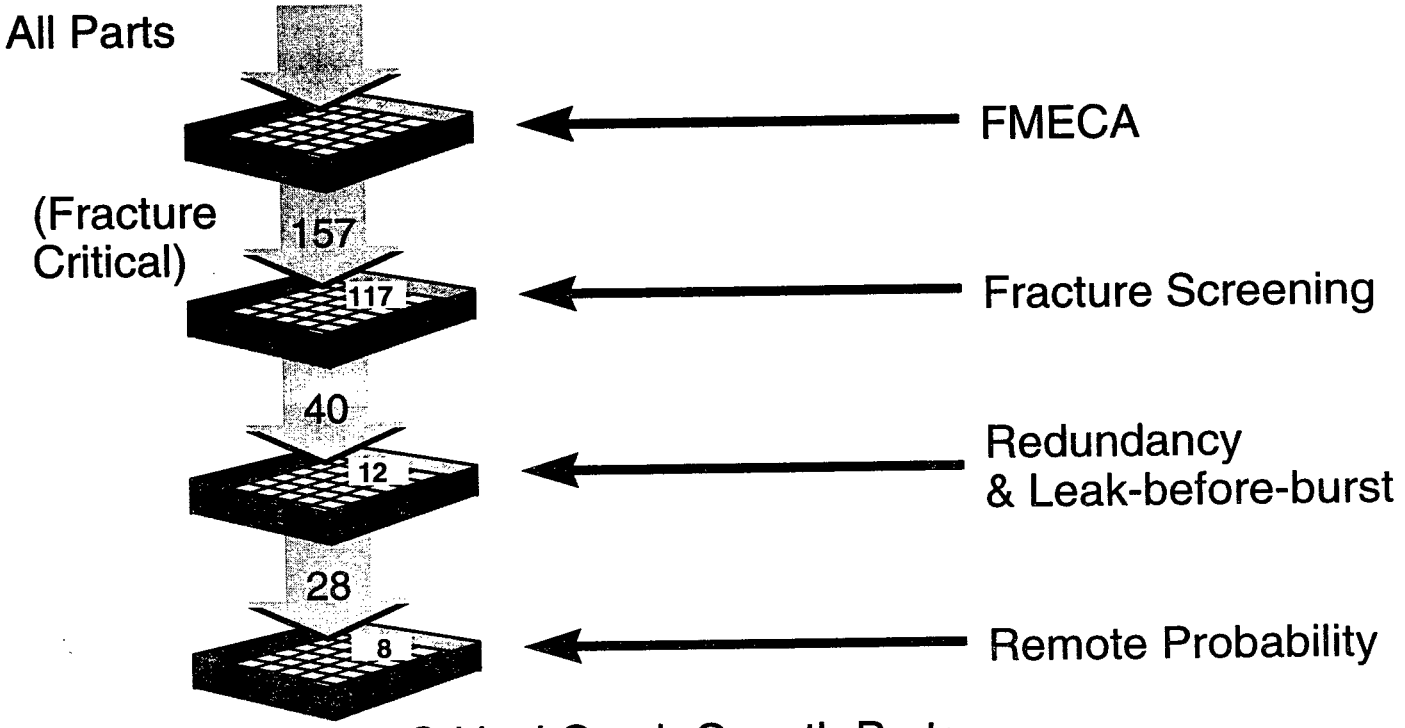

20 Critical Crack-Growth Parts
+ 2 Durability-Critical Parts

22 Parts to be tracked

209044 7

COMPONENTS REQUIRING REDESIGNS

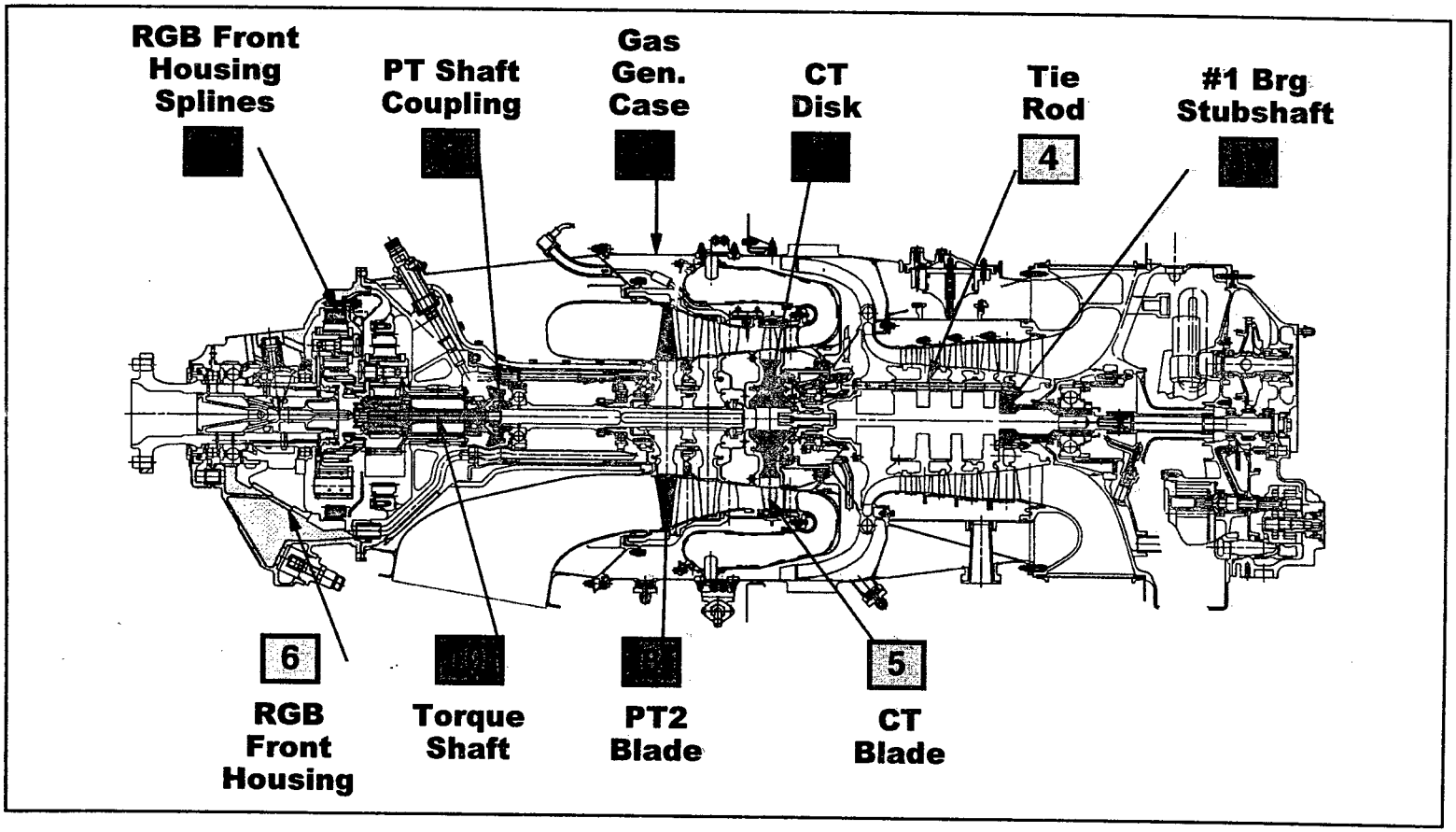

209044 8

MINOR GEOMETRY MODIFICATIONS

1 No. 1 bearing stubshaft
- light weight outer rim
  - controlled crack growth

2 Gas generator case
- thickened diaphragm wall
  - controlled crack growth

3 PT shaft coupling
- optimized fillet radius
  - controlled crack growth

209044 9

MATERIAL CHANGES

4 Tie rods
- from AMS 6322 to AMS 5708
  - corrosion resistant

5 CT blade
- from PWA 1422 to PWA 1480
  - improved LCF and creep properties

6 RGB front housing
- from AMS 4215 to AMS 4219
  - fracture screening

888

REDESIGNS

7 CT disk
- – wider rim, reduced blade count
  - • LCF improvement

8 PT2 blade
- – reduced platform overhang and optimized blade lean
  - • LCF and crack growth improvement

9 RGB front housing splines
- – case thickened, stiffer
  - • durability improvement

10 Torqueshaft
- – alternate torque path provided
  - • damage tolerance compliant through 'redundancy'

STATE OF THE ART ANALYTICAL TOOLS

- 3-D FE modelling
- Linear elastic fracture mechanics
  - Nascrak (BIGIF)
  - Surck
  - CGRMOD (Crack Growth Rate Modelling system)
- Explicit crack growth modelling
  - FRANC2D/3D
- Probabilistic risk analysis
  - RBRISK (rotor buried flaw life)
  - RKRISK (probabilistic risk analysis)

DURABILITY (LCF)

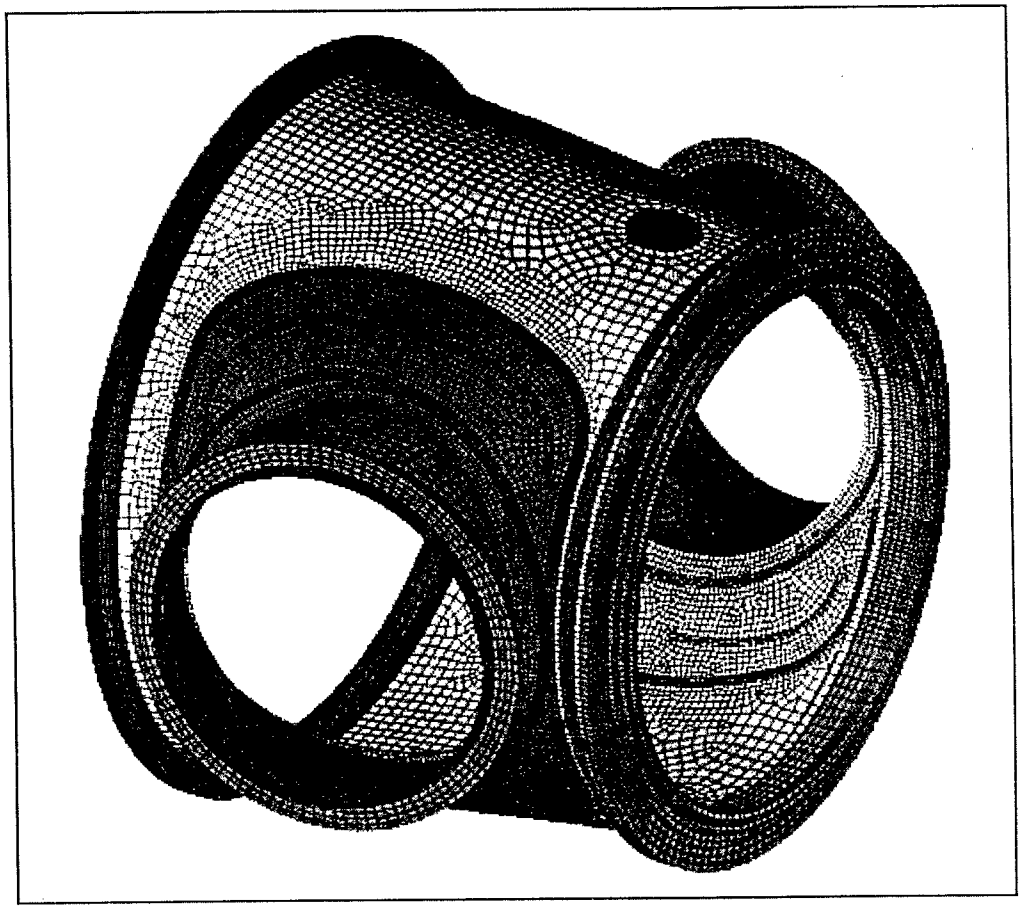

209044 13

FRACTURE MECHANICS ANALYSIS

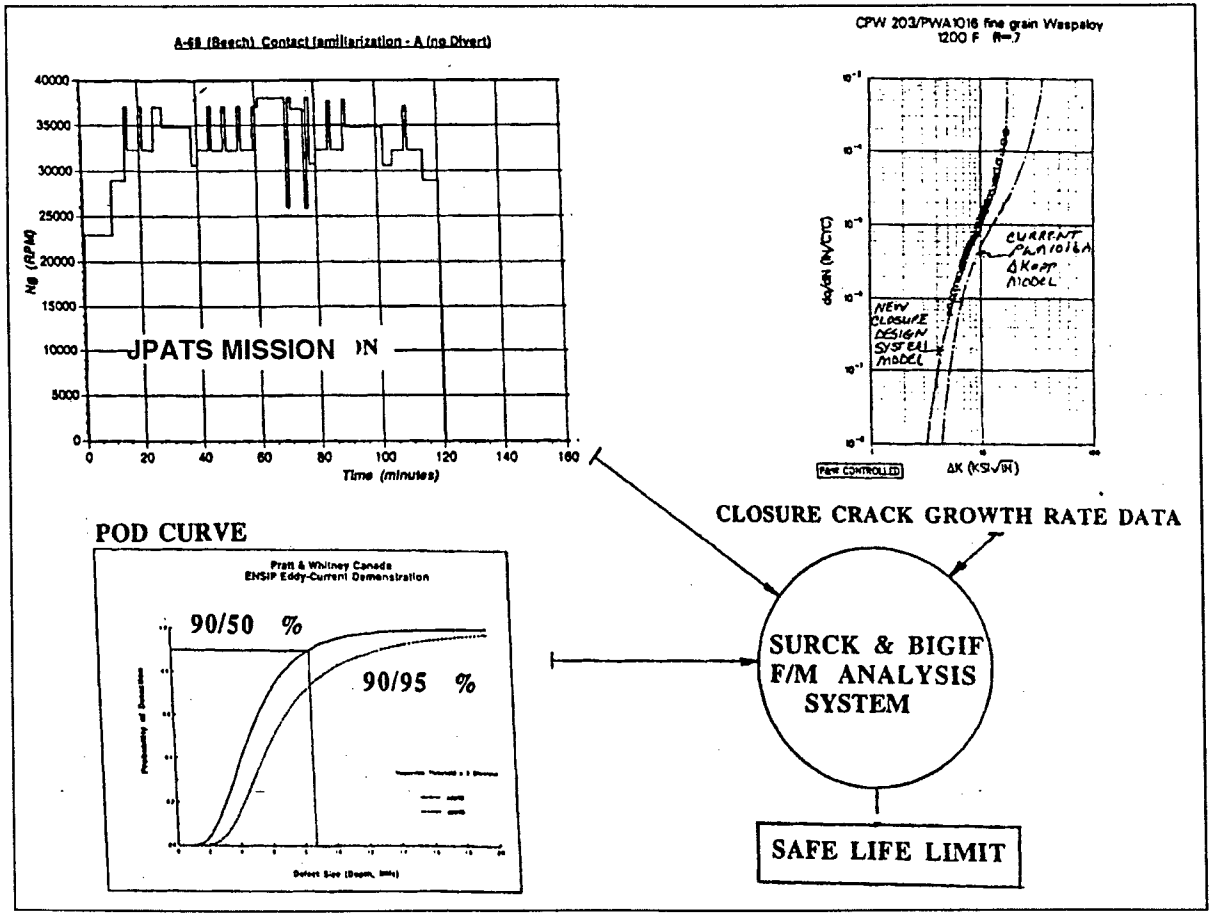

ROTOR BURIED FLAW ANALYSIS

- Rotor buried flaw lifing system
- Probalistic method (Monte Carlo)

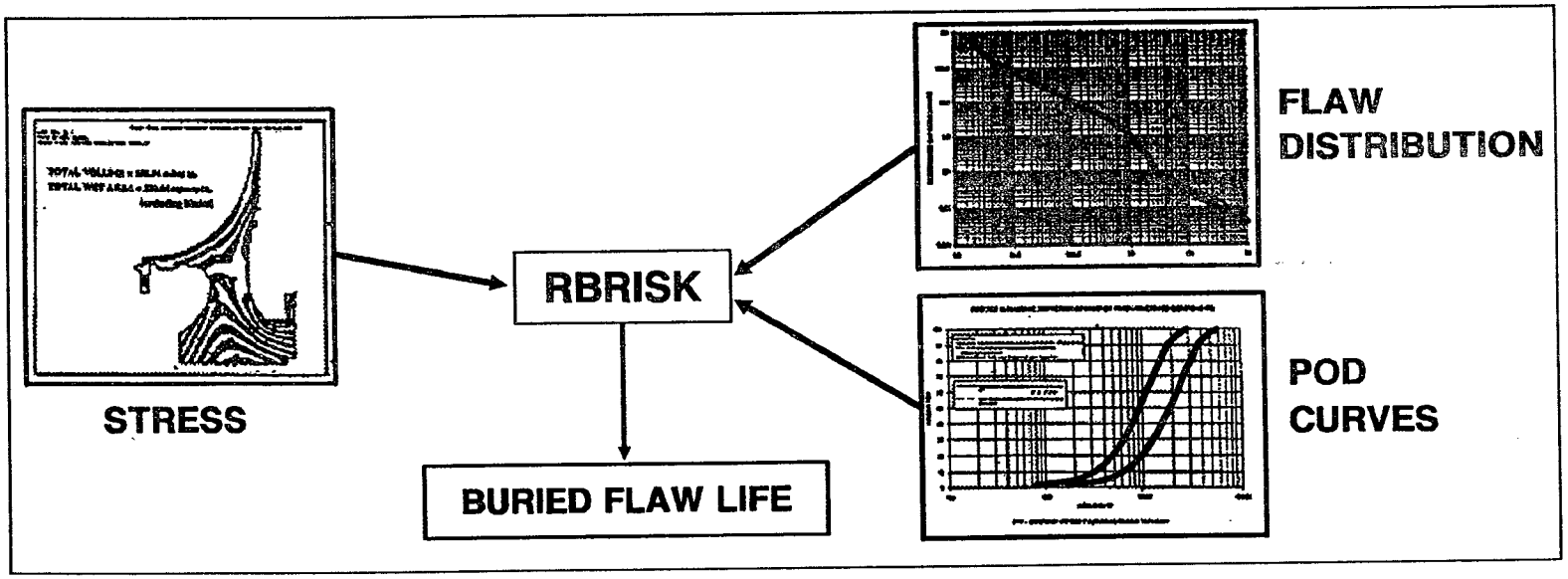

MATERIAL CHARACTERIZATION

- 9 materials to characterize
  - full (2)
  - partial (5)
  - spot check (2)
- Remaining da/dN available through T-1A and PWA-GESP database

NDE AND QUALITY CONTROL

- NDI proven capability at P&WC
  - automated eddy current inspection system
  - automated FPI facility
  - POD capability demonstrated for T-1A
    - ultrasonic, fluorescent penetrant inspection, eddy current
- Additional demonstrations
  - 3 ultrasonics
  - 4 eddy current

209044 17

COMPONENT DAMAGE TOLERANCE TESTING

- 3 spin pit tests
  - integrally-bladed rotor
  - No. 1 bearing stubshaft
  - disk/ blade assembly (CT)
- 3 rig tests
  - gas generator case
  - PT coupling
  - 2nd stage carrier

ACCELERATED MISSION TEST

- Reflects defined missions - including predicted throttle excursions
- Represents one overhaul interval (4500 hours)
  - non-damaging dwell times eliminated
  - actual run time: 41% of TBO (1850 hours)
- Demonstrate tracking systems algorithms and software

LIFE MANAGEMENT PROCESS

RAYTHEON AEROSPACE

P&WC

EMUT

REPORT

CPTS

DATABASE

REPORT

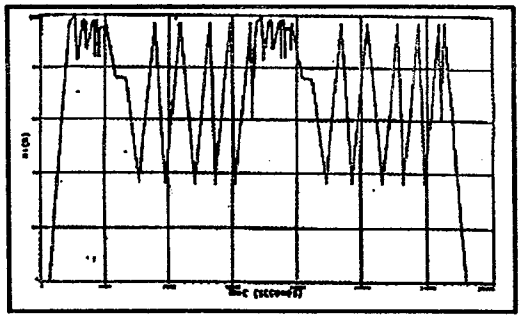

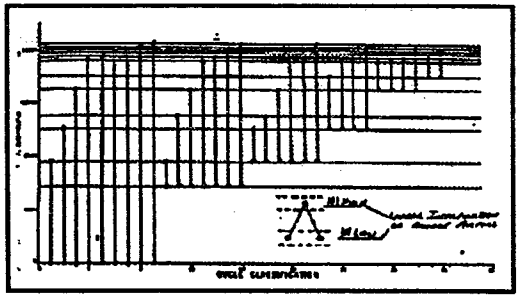

Algorithms calibrated during AMT

SUMMARY

ENSIP REQUIREMENTS WELL-UNDERSTOOD

- Analyses of components complete
  – state of the art analytical tools
- Minimal design changes
- Material characterization underway
- Enhancing proven NDE capability
- Component damage tolerance testing planned
- AMT to be conducted
- Tracking systems being developed

The Future Direction and Development of Engine Health Monitoring (EHM) Within the United States Airforce

Sqn Ldr Andrew J. Green

Wright Laboratory
Wright Patterson Air Force Base
Dayton, Ohio 45433-7251

ABSTRACT

1. The ability to trend an engine's performance has been possible ever since James Watt fired-up his first steam engine; however, the development of the ability to monitor and predict an engine's life, health and performance has not kept abreast with technology. Advancements like model based digital engine control management and the use of data management buses have enabled us to obtain considerable sensed data whilst the engine is running. With major advances in computer science and production control technologies we can now realize a true cognitive (awareness), ontogenetic (learning organism) engine health monitoring (EHM) system.

2. The DOD's engine development towards increased power to weight goals and the need to show improved reliability will obligate major advances in control and diagnostic technologies. The acquisition of real time engine data is already achievable, however the interpretation and utilization of such data is difficult. Thus by actively advancing technology we can realize a true cognitive and ontogenetic (CO)EHM system that will trend and predict the performance, life consumption and health of an engine in real time. The USAF's/DOD's research & development activities are firmly assisting in the development work that is required to provide a future COEHM system that can be truly called artificial intelligence (AI) based. These activities will bring about technologies to make accurate predictions and provide technical solutions so as to reduce engine life cycle costs and enhance operational capabilities.

THE ENGINE MONITORING (EM) GOALS

3. The increasing emphasis on improved affordability, availability and safety prompted has prompted an investment in improved embedded engine diagnostic technologies; this approach has been called 'Autonomics'. The focus of this investment was to select the "low hanging fruit," i.e. the relatively high value low risk problems.

Although extensive improvements in diagnostic capability for controls, accessories and lubrication system components have been incorporated in the latest generation engines, the diagnostic coverage for gas path does requires further development. Problems with gas path structures relate to approximately 30% of current fighter engine in-flight shutdowns.

4. The DOD's/USAF's Integrated High Performance Turbine Engine Technology (IHPTET) goals for performance, weight reduction, reliability and life cycle costs will need accurate and timely data. These objectives will only be achieved through an EM system that provides real time monitoring and health information. Therefore IHPTET needs a COEHM system that will monitor, trend, diagnose, predict and inform. This paper addresses some of the research and development programs and the required methodologies that will help achieve real time AI EM.

EM DEVELOPMENT

5. The development of an AI EM system will need to use tools such as data filters, polynomials, fuzzy logic, expert systems, probabilistics and neural networks. This list is not exhaustive and will require the application of novel approaches to give the system the ability to make accurate prediction before the event it is monitoring happens. A COEHM system will provide fast and accurate diagnostic and prognostic information to reduce maintenance times, no fault founds and turn round times. The improved critical life management aspect will reduce engine life cycle costs. Therefore the development of a COEHM system will considerably reduce engine cost of ownership, enhance operational capabilities and overcome loss of technical experience due to personnel downsizing.

COEHM METHODOLOGY

6. The COEHM Methodology approach (pictorially shown at fig 1) requires an integrity check through a Data Integrity Module for all data inputted and will compare this to imperial data as well as real time model data from the Engine Model Module. The Engine Model Module feeds accurate data for real and derived parameters into the Life Control, Alerts and Diagnostic Modules. The Health Module will be able to make comparisons between the data coming from the engine, those derived from the model and those performance curves that were obtained during engine pass off and are now contained within the Individual Engine Model Module. The system feeds life, alerts and health data directly to maintenance staff or can be feed through an Ontogenetic Prognostic (i.e. true AI) Module that will improve the probability of identifying the outcome of current or future events; this final module will give the maintainer a true diagnostic and prognostic capability that is accurate and fast. As a modular approach the

system concept can be modified to meet the needs of the user and as such can be applied to aging aircraft as well as those currently in service and planned for the third millennium.

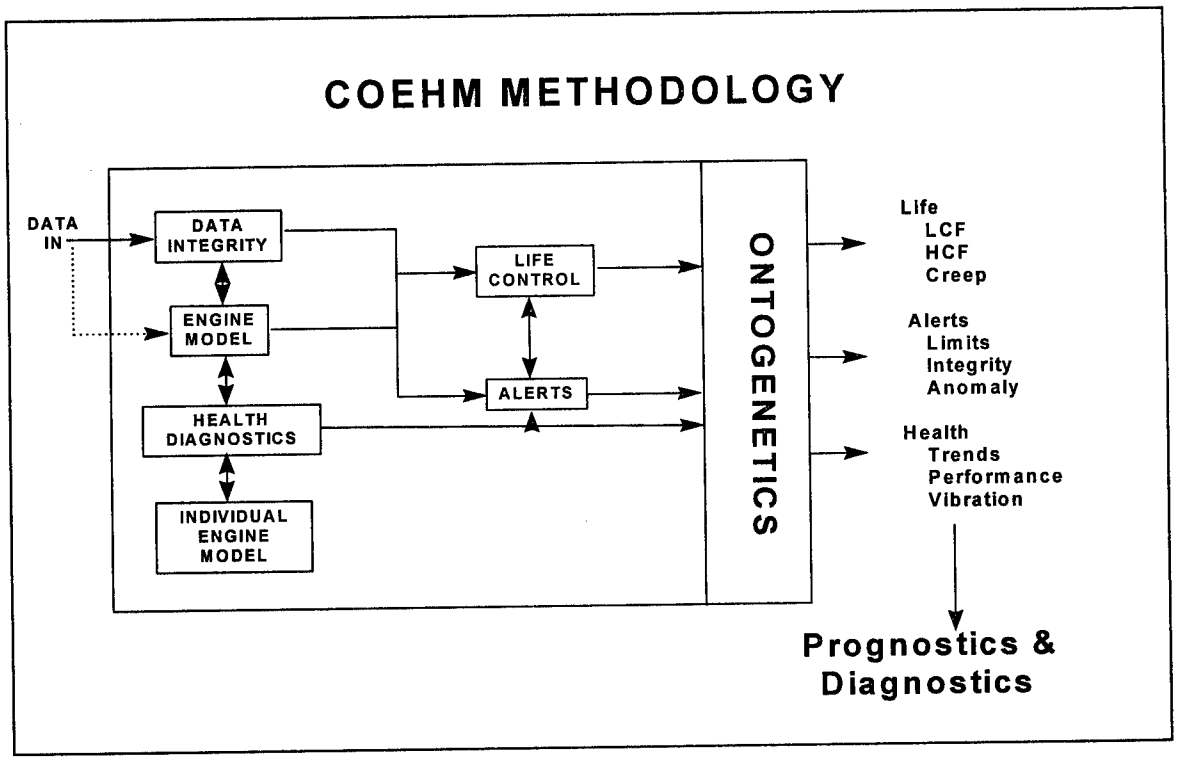

Fig 1

7. **COEHM Model Based Diagnostic & Performance Algorithms**. The Engine Model Module is a model based diagnostics system, which can be used to improve performance, increase reliability and sortie generation rate, and so reduce maintenance costs. This system features a real-time, nonlinear, physics based, dynamic model of the engine embedded in the engine controller (FADEC) or as part of the EM system. This model is updated in real-time using a tracking filter to match actual engine characteristics. Model computed values can then be passed to the Health & Diagnostic Module. Some gas path structural failures occur with significant precursors identifiable in performance parameters. To date normalizing performance parameters sufficiently to detect and isolate these precursors has been difficult. The advent of adaptive on-board performance simulations has provided normalized gas path performance parameters that are proportional to changes in engine module performance. This methodology utilizes these parameters and a neural network to improve detection accuracy.

8. **COEHM Health & Diagnostics Approach**. Advancing the USAF's capabilities in engine life measurement, diagnostic and prognostics capability of critical engine components is necessary to improve engine availability, minimize performance degradation, and reduce life cycle costs. Engine data currently sensed and recorded for post flight processing can be analyzed in a continuous real-time mode within the Health & Diagnostic Module. Proven AI technologies such as neural networks, fuzzy logic and expert systems present an opportunity to significantly enhance current trending and diagnostic capabilities in a real-time monitoring environment. For fault detection and accommodation, extensive knowledge of how a healthy engine operates under given conditions will be analyzed, and any deviation from this 'normal' pattern of expected parameters will be detected and further analyzed. The same sensed data will be used as inputs to life usage algorithms in the Life Control Module and will determine critical component remaining life based on actual experienced severity.

9. **Probabilistic Method (PM) for Life Management and Diagnostics**. The use of PM for the development of improved design and life sensitivities has been achievable for some years, and we can now more accurately design and life a component. The growth in computing power has freed this statistical tool and allows the application of resolving tools such as Monte Carlo, Second Order, Taylor Expansion, Orthogonal Array etc. The extension of PM for the production of generic High Cycle Fatigue (HCF) codes will require validation and verification (V&V) of the sensitivities that were applied. The function of a PM V&V tool would be ideally suited to run concurrent with the component, so as to assure that the real time experience reflects the one assumed at the design stage.

10. The ability of a PM code to apply sensitivity to data will further increase the chances of identifying the cause of an engine's fault (diagnostics) or deducing the most likely health or performance outcome (prognostics). Probabilistic as a real-time diagnostic, prognostics and life management tool will be an important contributor to producing a COEHM as well as to help meet the IHPTET goal of reducing maintenance costs. The application of a global genetic 'optimization' probabilistic tool will improve the sensitivity for diagnostic and prognostic speed and accuracy. The use of P M for V&V, fault isolation, identification and prediction still needs further development.

DATA NEEDS FOR A COEHM SYSTEM

11. **'Total System' Sensing**. The need for data integrity is a corner stone of an effective COEHM approach, and the ability to model real time data or virtual data (Reference 1) are major steps towards a true understanding of the engine's health. However there is a need for a more 'total system' approach to sensing data and this is

pictorially shown at fig 2. A 'total system' approach to data sensing will require the application of new advances in sensing technology. The concerns about any sensing expansion is weight and reliability and so the approach must be towards function

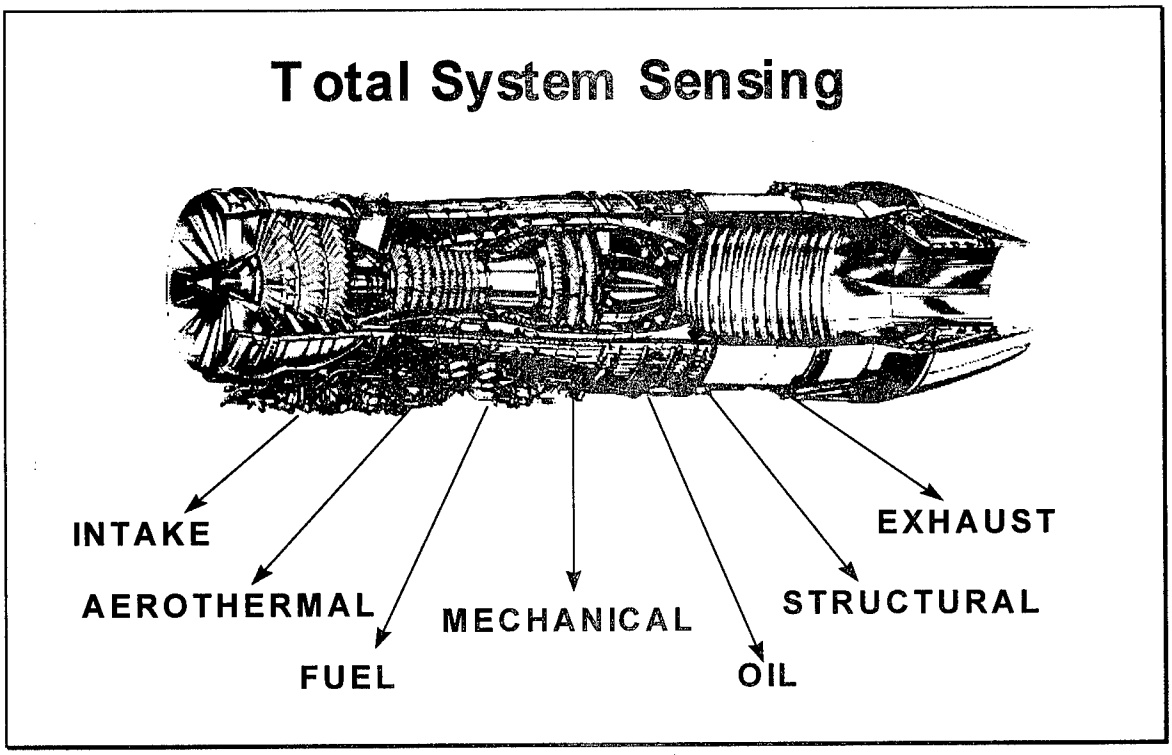

Fig 2

amalgamation and simplification, e.g. we will develop sensors and methodologies that will perform both vibration and speed or temperature and speed monitoring. The development of more passive sensors will improve reliability in that they only need to detect changes in amplitude or frequency.

12. **FOD Detection & Exhaust Emissions Analysis** . The increasing complexity of modern aircraft inlet structures will increase the maintenance burden for routine inspections for Foreign Object Damage (FOD). FOD detection technology (acoustic, radar or electrostatic) will reduce the maintenance burden by providing an automatic FOD detection capability; it does require detailed signature profiles of events to be effective. The systems are:

a. **Acoustic.** The acoustic approach utilizes close coupled high response pressure transducers and advanced signal processing to detect the acoustic energy emitted when a engine fan blade is impacted by a damaging foreign object. This concept focuses

on the characterization of the acoustic signal generated by impact and the detectability of that characteristic within the normal engine background noise environment. Laboratory and engine testing demonstrated that this detection technology is practical with high accuracy for cases of blendable FOD.

b. **Radar**. The radar approach was initially designed to detect blade damage. The system uses a low power radar emission and detection system within the inlet; this approach has already been able to detect 1mm defects in blades as far back as the compressor's third stage. The system goal is to determine the type and characteristics of all possible FOD ingested by an engine. The technology can already derive velocity and relative mass and can determine the difference between a split pin and other metallic objects.

c. **Electostatic**. The electrostatic approach monitors both the inlet and outlet gas path. It employs an electro-magnetic detector in the inlet as well as one in the outlet. The system monitors the change in ionization of the gas path and is more complex than the approaches detailed above and as such requires a high rate of data acquisition and considerable computer power to perform diagnostic and prognostic evaluations. Electrostatic Engine Monitoring (EEM) has been a technology that has shown promise since the early 1970s. Many evaluations from laboratory, to engine and flight testing have shown that material within the engine gas path is detectable as charge particles either entering or exiting the engine gas stream. The early attempts to employ this technology were troubled by false indications and problems in setting thresholds for normal versus abnormal signatures. New sensing electronics and signal processing software promise to overcome these problems.

13. **Non Synchronous Vibration - HCF**. The failure of an aircraft's gas turbine engine can be catastrophic. Similarly, millions of aviation industry maintenance man-hours are spent each year inspecting for the precursors to HCF damage. HCF is caused by resonance, and whilst its effects in a gas turbine can be reduced by avoiding/eliminating resonance at the design stage, changes in usage or configuration can unknowingly introduce HCF. HCF differs from Low Cycle Fatigue (LCF) in that the fatigue mechanism from varying loads of smaller amplitude but much higher frequency. This will cause rapid propagation of a crack and lead to failure in a short time. The combinations of parameters which generate HCF are much more difficult to define and predict, than the well characterized conditions which are associated with LCF. An accurate and effective means of monitoring HCF damage and diagnosing it would be essential for COEHM system.

14. **Real-Time Vibration Monitoring & Improved Vibration Analysis**. The need to measure true individual blade vibration is essential to any active vibration control system or to accurately deduce where a component is on its life to failure curve.

The current technology of using accelerometers is adequate for determining out of balances or identifying a pump malfunction, but they have application and environmental limitations. Therefore new approaches are required to the measurement, in real time, of vibrational forces being experienced inside an engine. The technologies that could be used are almost limitless, but some of the current thinking is towards:

a. **Acoustic**. Required only to pick up the acoustic changes in a passing blade, but does require an expert interpretation of the resolved frequencies. The sensor is passive in that it only receives and has no emit requirement. The rotational speed as well as pressure can also be easily monitored.

b. **Blade Tip Deflection Sensors**. This system uses time measurement to determine the dynamic tip deflection. The optical probes are located over the blades being monitored and laser light is used to detect changes in the position of a blade, and as such can be directly related to vibration (Reference 2). The reflected light process is more complex than an acoustic sensor but can provide rotational speed as well as thermal data when used in conjunction with thermographic phosphors.

c. **Eddy Current**. With a eddy current probe mounted on the shaft then any changes in an electro-field can be resolved directly into a vibration. The system can also deduce rotational speed and torque. The inherent property of a rotating mass is that it vibrational signature changes dramatically if it has a defect, and as such this approach could also detect blade or disc cracks.

d. **Oil Monitoring**. The use of in line real time oil monitoring (Reference 3) will identify the mass and density of any bearing material in the oil system. As bearing break-ups follow a characteristic burn out curve the comparison of vibrational data and bearing debris data will help identify more accurately incipient bearing failures.

15. **Real-Time Crack Detection**. The ability to accurately design and so predict a defect free component is driven by the need to control life cycle costs within technology constraints. The greater the need to produce a defect free component then the greater are the potentials to gain additional cost or performance benefits (design and manufacturing cost reductions, weight reductions, life extension and improved damage tolerence). This approximation of events is shown at fig 3. However there will never be a point of zero failure and so we must consider the need for a real-time crack detection system. The current technologies would lend to the development of a system to detect cracks using eddy currents or X-Ray Tomography (Reference 4).

IMPROVED LIFE ALGORITMS

16. The effectiveness of monitored data depends on how it is interpreted. The used of

life algorithms are well understood to equate a total life as well as deduce a life used. To

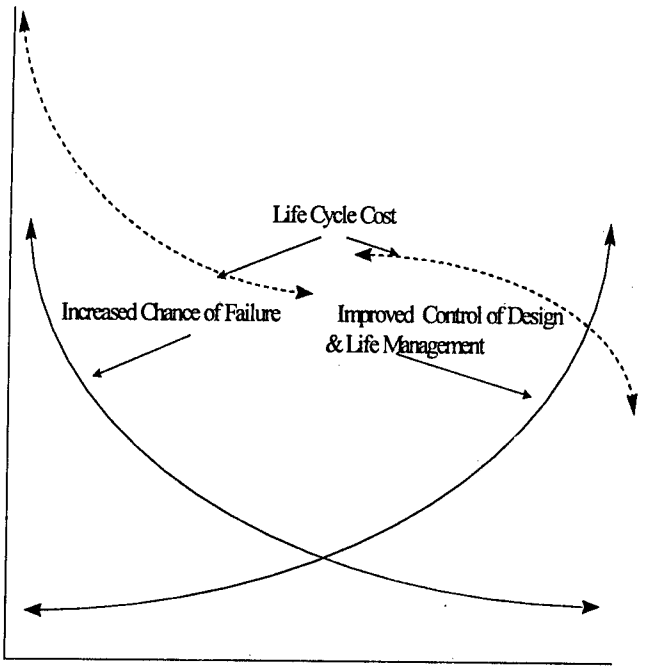

Fig 3

date the accuracy of these algorithms have been adequate, but a more precise approach is now required. The tracking of engine usage has progressed from manually recorded engine operating time to today's standard of total accumulated cycles based on monitoring of speed gates. Even today's approach, however, is a rough approximation of actual life consumption during normal engine operation. These rough approximations result in considerable uncertainty in setting inspection intervals, and can result in inspections occurring too late, impacting safety or too early, impacting availability. The development of advance life algorithms rely on design structural analysis equations and on-board measurements to improve accuracy. The use of Probabilistic as a design and life tool was defined at para 9 and reflects the current thinking on more accurate life predictions.

CONCLUSION

16. The USAF has set itself goals for capability, performance and reliability standards that it must achieve if it is to maintain air superiority. The advent of novel design

methodologies and materials has put the spot light on engine diagnostics and prognostics as an essential element to achieve those goals. The development and implementation of the COEHM Methodology will help meet the set Autonomics goals and the needs of the third millennium. The development of a totally sensed engine (real or virtual) that provides exact and accurate data will help a COEHM system perform the AI function that is required to derive fast and accurate answers; this will enable the maintainers to quickly regenerate an aircraft for it next mission. The COEHM is more than just an approach but an asserted effort to produce a range of compatible EM systems for 2001 and beyond.

References:

1. Roemar, M. J. and Atkinson, B. "Real-Time Engine Health Monitoring and Diagnostics for Gas Turbine Engines." SAE Aerospace Atlantic Conference, May 22-23 1996, Dayton, Ohio.

2. Stange, A. W. "Non-Intrusive Sensing Techniques for Advanced Turbine Engine Structures." SME Gas Turbine and Aeroengine Congress and Exposition, June 11-14 1990, Brussels, Belgium.

3. Muir, D. and Howe, B. "In-Line Oil Debris Monitor". SAE Aerospace Engineering Oct 96, p9 to 12.

4. Kirchner, T. Burstein, P. and Youngberg, J. "Spin Synchronous X-Ray Sinography for Nondestructive Imaging of Turbine Engines Under Load." U.S. DOT/FAA Final Report # DOT/FAA/94/01 June 94.

SESSION VIII

NDE/I

Chairman: *R. Paglia*, AF NDI Program Office, WL/MLS-OL

Computer Monitored Shot Peening, An Update

James R. Harrison: Manager Technical Services, Metal Improvement Co., Inc.
Wichita, KS 67211

1996 USAF Aircraft Structural Integrity Conference

Abstract

Shot peening has been used by industry for more than 50 years. The significant increases in resistance to fatigue, fretting, galling, and stress corrosion are well known, yet engineers have been reluctant to use shot peening in design allowables due to a lack of confidence in the reproductibility of the process. AMS 2432 SHOT PEENING, COMPUTER MONITORED was written by the Society of Automotive Engineers, Inc. so that the performance enhancement of peening could be taken into account in the initial design. It tightens the requirements on the media and the equipment to the maximum extent practicable. Of most importance, the peening of subsequent parts even years later will be a duplicate of the original part that was fatigue tested. *Peenstress*™ is a new software program capable of predicting the residual stresses that are introduced by shot peening in most metals. This new program allows engineers to optimize the basic peening parameters so that the first peening selection is correct.

AIRCRAFT HARDWARE, because of the overriding necessity to save weight under dynamic loading condictions, are usually designed to fatigue criteria rather than to ultimate strength. Metal fatigue is caused by cyclic tensile stresses, usually highest at the surface and concentrated by notches, holes, physical damage, etc. Metal fatigue is further aggravated by the effects of environment (corrosion fatigue), by residual tensile stresses caused by welding or grinding, for instance, or by localized wear (fretting fatigue.) Metallurgical coating such as plating or flame deposition can cause a severe reduction in fatigue strength. Metal fatigue most often initiates as a microscopic crack at the surface after many load cycles and propagates until the part fails. Another stress-related mode of failure of great concern to the designer is stress corrosion cracking. The combination of environmental conditions (airborne salt or a leaky toilet, for instance), a susceptible material and a surface static tensile stress (residual or applied) can also cause failures.

In all the modes of failure mentioned above, the common denominator is tensile stress, which in effect pulls the surface apart in a propagating crack. Compressive stress which can be thought of as causing the surface to push together will prevent surface cracks from initiating or propagating. Shot peening is the most economical and practical method of ensuring surface residual compressive stresses. A recent test by an airframe manufacturer on a wing attach fitting showed the development of a crack at 60% of predicted life. The flaw was removed, then the same area on the part was shot peened. The fitting was then fatigue tested to over 300% life without further cracking. Flight critical components like this require shot peening controls that insure quality processing. Other components such as a turbine blisk; see figure 1, require complex machine setups because the contour of the blades can be changed by incorrect peening.

Computer Monitored Shot Peening

The procedure is as follows. The engineer designates on the drawing the critical Almen intensity verification locations. An Almen fixture preferably made from a scrap part or a fixture duplicating the proper geometric areas is fabricated. See figure 2. Then shot peening machine setups are made with tooling designed to hold the part to insure proper placement of it in the machine. The Almen test fixture is then processed to verify intensity and saturation curves for each location.

The first part is then processed by applying a fluorescent tracer dye to verify complete coverage. The computer monitors shot flow, air pressure, part movement, and shot stream movement over the part. If any of the parameters vary out of tolerance the computer will abort the cycle

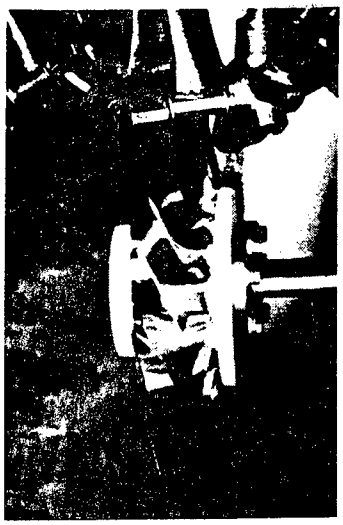

Fig. 1 - Titanium turbine blisk with peening nozzles welded in fixed location.

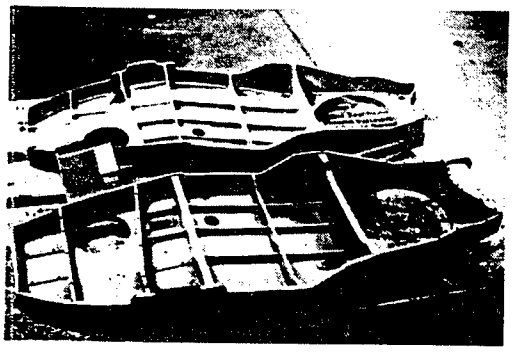

Fig. 2 - Tip rib for V-22 Osprey at rear. In front is a fabricated Almen fixture made from plastic.

telling the operator where the problem is so he can fix the problem and then finish the cycle. See figure 3.

Upon successful completion of the first part, the nozzle fixture is fabricated freezing the setup (permanently welding the nozzles in place) and part numbered so that it is only used for that particular part. The next part is processed using the fluorescent tracer to verify the nozzle rack holding fixture. All parts processed to this procedure are approved by the manufacturer's quality assurance source. The procedure is then frozen, recorded in hard copy, and retrieved any time a lot of this part number is to be shot peened, therefore exact duplication of the process is assured.

Shot Peening, Computer Monitored

AMS 2432/5	SAE	AMS 2432/6
Paragraph	Parameter	Units	Process Tolerance Shutdown Limit Plus or Minus
3.2.5.1 (R)	Shot Flow (for each nozzle)	Pounds/minute (kg/minute)	10%
3.2.5.2 (R)	Air Pressure (for each nozzle)	psi (kPa)	10%
3.2.5.3 (R)	Wheel Speed (for each wheel)	RPM	20 RPM
3.2.5.4 (R)	Nozzle or Wheel Translation Speed	inch/minute (mm/minute)	10%
3.2.5.5 (R)	Deflector Speed	inch/minute (mm/minute)	10%
3.2.5.6 (R)	Nozzle and/or Wheel Shut Down	Seconds	1
3.2.5.7 (R)	Turntable Speed	RPM	10%
3.2.5.8 (R)	Part Speed	RPM/inch/minute (mm/minute)	10%
3.2.5.9 (R)	Conveyor Speed	inch/minute (mm/minute)	10%
3.2.5.10 (R)	Peening Cycle Time	Seconds	1
3.2.5.11 (R)	Nozzle/Wheel Position	inch/degree (mm/degree)	0.062 inch (1.57 mm)/ 5 degrees
3.2.5.12 (R)	Table/Part Indexing	inch/degree (mm/degree)	0.062 inch (1.57 mm)/ 5 degrees

Calibration or measuring devices used in the peening system shall be performed in accordance with ISO-10012-1.

Fig. 3 - Peening parameters for computer monitored shot peening per AMS 2432B.

Because of the confidence in the repeatability of computer monitored shot peening, The Department of the Navy's Naval Air Systems Command (NAVAIR) allowed the benefits of shot peening to be used in the original design of the Bell/Boeing V-22 aircraft. NAVAIR Instruction 4870.2 states; "peening required during repair or rework to attain fatigue life will be by computer controlled and monitored processes or will conform to the same specifications and standards used for original manufacture." The controlling document will be AMS 2432B. A significant weight savings was obtained on the V-22 utilizing the beneficial compressive stresses from shot peening to attain required fatigue life.

Computer Optimization of Shot Peening

A software program, *Peenstress*™, has been developed to optimize the effects of shot peening by predicting the residual stresses derived from the process. The careful selection of shot size, hardness, and shot composition, the Almen intensity (which determines the depth of the compressive layer) and the percent of coverage are possible.

The many possible combinations of these factors without this program make the correct choice difficult. There are over 70 materials in MIC's *Peenstress*™ library from which to choose. To use the program, we first choose the type and size of shot as well as the Almen intensity which experience would indicate should be best for the application. *Peenstress*™ will then calculate the shot velocity, using the material behavior laws for the material selected to determine the residual stress created. The *Peenstress*™ program will then print out a stress curve that shows both the magnitude of the residual stress distribution and the depth profile beneath the surface. The benefits of this program are best understood using an example where the program has been used to help an engineer call out a shot peening parameter to get the best choice for a given problem.

Full scale fatigue testing of a new design landing gear fitting indicated a low cycle fatigue crack in a fillet, figure 4, on an attach lug. The company's in-house shot peening specification suggested an Almen intensity of 5 to 9 A using MI 230R shot for 7075-T73 aluminum. Finite analysis revealed tensile stresses to .008in. depth in the critical area.

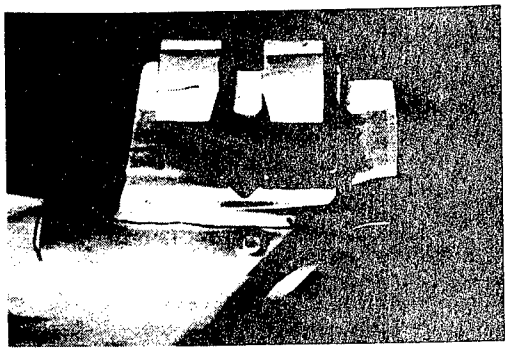

Fig. 4 - Landing gear trunion fitting being prepared for processing. Cracks were initiating in the fillet of the lugs before peening, which improved fatigue life by 400%.

As can be seen in figure 5, using the low end of the call out, Almen 5 A, a residual compressive stress of .006 in. depth is possible. This is a compressive stress of .002 less than needed with a tensile stress of +5 ksi at .007 in., far from ideal. Figure 6 shows that by using a larger diameter shot, MI 330R, at a higher intensity, 10 A, the surface compressive stress was improved from -17 ksi to -30 ksi due to an improved surface finish. The depth of the beneficial compressive stress is now .011 in. or .003 in. deeper than the stress to the component. Testing on the fitting peened to an Almen intensity of 10 to 14 A showed a 400% increase in fatigue life!

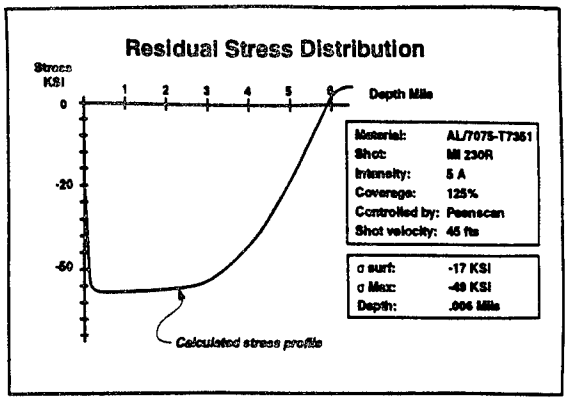

Fig. 5 - Residual stress distribution of 7075-T73 aluminum calculated by *Peenstress*™. There is residual tensile stress where finite analysis showed applied tensile stress.

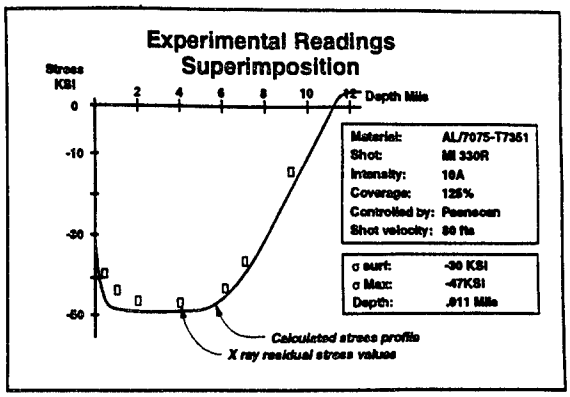

Fig. 6 - *Peenstress*™ calculates that by shot peening at a higher intensity 10A, the compressive stress is now deeper than the loading of the part. The rectangles are actual measurements by x-ray defraction.

Conclusion

Shot peening is a recognized method of improving the fatigue strength and damage tolerance of a piece part. Large magnitudes of improvement are possible, yet no non-destructive method to verify the quality has been developed. Computer monitoring of the shot peening process however assures repeatability of the process, allowing the use of the beneficial residual stresses to attain required fatigue lives. The ability to predict the residual stress using computer software is a very effective tool in the selection of peening parameters. *Peenstress*™ gives the designer the ability to optimize the shot peening process.

References

1 Daly, James J. and Daniel E. Johnson, COMPUTER-ENHANCED SHOT PEENING

2 Metal Improvement Company, Inc., SHOT PEENING APPLICATIONS

3 Gassner, R. H., CN's Inc., SHOT PEENING, COMPUTER MONITORED, presentation notes

4 Department of the Navy, NAVAIR Instruction 4870.2

5 LeGuernic, Y., MIC France, IMPACT, *Peenstress*™ Software Selects Shot Peening Parameters

Freeze-Frame Imaging of Operating Turbine Engines Using Synchronous Multiplane Tomography (SMT)

*Mr. Ted E. Kirchner
Foster-Miller, Inc.
195 Bear Hill Road
Waltham, MA 02154-1196

Dr. P. Burstein
Skiametrics, Inc.
Winchester, MA
Dr. F. Séguin
Boston Physics
Boston, MA

Dr. J. Youngberg
Mr. L. Nuttall
Perceptics, Inc.
Sandy, UT

Dr. M. Barker
Lockheed Martin Missiles & Space Co.
Palo Alto, CA

Abstract

Synchronous Multiplane Tomography (SMT) provides a series of freeze-frame X-ray cross-sectional pictures of the interior of a turbine engine while it is running and under load. SMT allows users to detect and monitor crack growth in turbine disks and other critical components long before they become dangerous. Many of these cracks, which would be closed under non-rotating conditions, open under engine operation and are thus visible to freeze-frame SMT imaging. SMT can also measure interior clearances and other difficult-to-obtain operating parameters.

In the first phase of a USAF-sponsored SBIR program, the interior of a rotating automobile turbocharger was imaged, demonstrating that SMT could detect calibrated cracks having thicknesses of 0.0003 in. and areal extents of 0.01 square inches. In the second stage of the program, a full-scale SMT system has been demonstrated on a T-53 turboshaft engine which contains calibrated cracks in its first stage turbine disk. The demonstration, completed in early October 1996 at the Navy China Lake facility yielded excellent data. First images and preliminary analysis are presented in this paper.

This successful demonstration will be followed by an end-to-end scan of an operating F-404-100 engine and on a flawed turbine disk rotating at 10,000 rpm in early 1997 also at NAWC/China Lake.

1. Introduction

Turbine disk cracks can lead to catastrophic engine failure, destroying an airplane and possibly killing the crew. Synchronous Multiplane Tomography (SMT) is an X-ray imaging device that produces highly detailed cross-sectional pictures of the insides of a turbine engine while the engine is hot, running, and under load. Under these conditions, cracks at the center of turbine disks - especially those on the bore - are expected to open due to the high centrifugal forces and be detectable by synchronous X-ray computed tomography imaging methods. Other internal features that can lead to engine failures, e.g., blade root cracking, can also be imaged with this technique.

Normally, such turbine disk cracks - buried deeply within a turbine engine - are impossible to detect without complete dismantling of the engine. Thus, the impetus to find small, incipient cracks on routine engine teardowns before they grow to potentially catastrophic size is high. Today's methods of inspection require dismantling the engine and removing the disk from the engine for a bench test. For such small, closed, or nearly-closed cracks these methods include total immersion ultrasonics, eddy current, and dye penetrant. Even when the inspection *is* conducted, any incipient crack is usually closed and the two sides of the crack are in intimate contact, perhaps even under some pressure. Under these conditions, these inspection techniques can and do fail.

The trend in modern turbine engine life extension programs is in pushing the intervals between routine engine teardowns to much longer periods. The two major enabling mechanisms for such extensions are the greater consistency of materials performance data and the availability of remote sensing instrumentation that yield preliminary warnings of engine failure. SMT falls in the latter category. The major reasons for avoiding teardown are cost and the complexity of engine teardown and re-assembly. Hard cost numbers are difficult to find in the military engine world, because the total cost is a highly variable function of engine type and perceived cost of the labor component. According to industry sources, the cost of a teardown and re-assembly operation for a typical military turbine engine is at least $250K. (In the civilian aerospace market, the Engine Economics Group at Boeing estimates the cost at $500K to $850K.) Moreover the probability of an engine's being incorrectly re-assembled is high. For these reasons, an alternative to engine teardown is highly desirable, from both economic and flight safety points of view.

2. Conventional Computed Tomography (CT) as an Inspection Approach

From a naive perspective, CT appears to fulfill most of the requirements for flaw detection and mensuration of anomalies hidden deep within the engine. The truly seductive aspect of CT is that it provides a visual image of a virtual cross-sectional plane of the test specimen. There is a 1:1 correspondence between each picture element seen in the image and the corresponding volume element in the real object. In addition, CT provides a quantitative measure of quality: Discrepancies in measured X-ray density. Conventional CT, unfortunately, has three requirements that make its use extremely difficult on engines:

1. A test specimen, only parts of which are moving rapidly, is not a rigid unchanging scene, a necessity for conventional CT.

2. Every volume element in the test specimen line of reconstruction must be examined from all directions, even if we wish to inspect only the region near the center. This effectively precludes examination of all but the smallest of engines with conventional CT.

3. Conventional CT requires that X-ray absorption data be acquired in a plane perpendicular to the spin axis. In a large turbine, this path may require X-ray penetration of 20 to 30 in. of metal - too large an attenuation to result in a useful measurement.

While conventional CT fails to inspect spinning turbine engines, CT-derivative technologies can be utilized with existing hardware to circumvent such difficulties and produce diagnostically useful images. SMT, our implementation of this approach is spin-synchronous to the engine, and it allows an anomaly to trace a unique sinusoidal pattern in successive inspection positions of the engine.

3. SMT as a Viable Inspection Approach

SMT is a second generation synchronous X-ray CT imaging system for turbine engines. The SMT concept is based on a previous system, the FAA-sponsored Spin-synchronous X-ray Sinography (SXS) that was designed to do much of the same thing, albeit with different detection technology. Both SXS and SMT produce cross-sectional images of the interior of the turbine engine. The main difference is in the speed of data acquisition, and in the increased spatial resolution that will be attainable with SMT. SXS produces a single cross-sectional

image at a time, while SMT produces an entire series of multiplanar images simultaneously.

4. How SMT Technology Works

The main concept of synchronous CT imaging is shown in Figure 1. As the "turbine" is rotated, the point source of X-rays to the left of the rotating engine is pulsed at a predetermined rotation angle to produce an instantaneous X-ray shadow of the pin, as shown. At each angle the X-ray source is pulsed so that finally, the pattern at the right side of the figure is generated, with the position of the pin forming a sinusoidal pattern. The original SXS approach used a single linear array of detection elements to gather data in this manner. Thus SXS

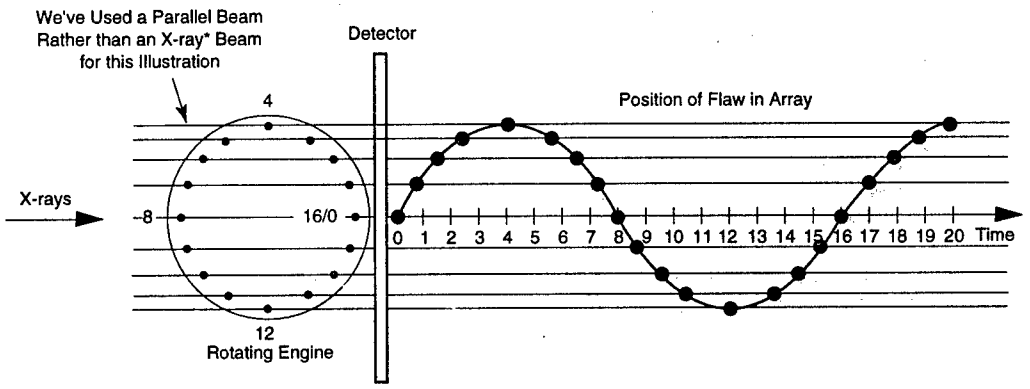

Figure 1. This figure shows sinography within a single plane. The X-ray source is to the left, and a one-dimensional X-ray sensitive of detector records the appearance of a point flaw as the disk is rotated. Within the detector, the flaw begins at the middle, moves up to the top, then descends to the bottom, and then moves to the middle before it begins the cycle again. If we rotate the disk at constant time and plot the position as a function of time (or alternatively, as a function of disk phase angle), we get the curve on the right, which is simply a sine curve. A knowledge of the sinography pattern for each point at each position in time (or, equivalently, angular position) allows us to reconstruct the interior of the disk. The sinogram of a complex object contains the superposition of the sinograms of each individual feature. Moreover, for the SMT, the measurements are no longer constrained to a single plane, but are taken simultaneously over many oblique (with respect to the spin-axis of the test specimen) planes .

gathered only a single slice or plane of data at a time. SMT gathers data with an area detector so that an entire volume, equivalent to many slices or planes can be inspected simultaneously.

Synchronous X-ray CT Imaging Technology is different from conventional CT in three ways, as shown in Figures 2 and 3.

1. SMT is synchronized to the rotary motion of the engine so that the rotation itself substitutes for the necessity for moving the X-ray beam generator and detection system around the engine (Figure 2).

2. SMT uses proprietary algorithms that do not require that all data are taken around the periphery of the test specimen. The algorithm also rids the image of stationary clutter, co-rotating clutter, and the artifacts that those extraneous regions produce.

3. SMT uses a skewed form of data collection (Figure 3) that allows non-orthogonal slices to be reconstructed, and hence the long attenuating path through the center of the disks is avoided.

5. SMT Inspection Advantages

The data acquisition sequence illustrated in Figure 2 is the same for SXS and SMT. The difference between the two is shown in Figure 4, which is a top view

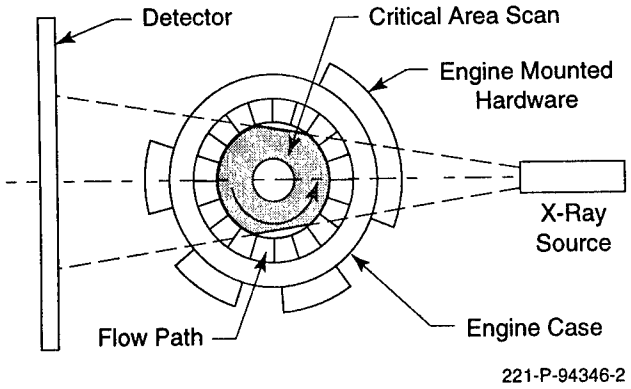

Figure 2. SMT technology is synchronized to the rotary motion of the engine with the CT rotation provided by the engine itself. The proprietary algorithms developed by the SMT team permit data acquisition only in the area of interest and do not require a much larger data set for the entire rotating part as in conventional CT.

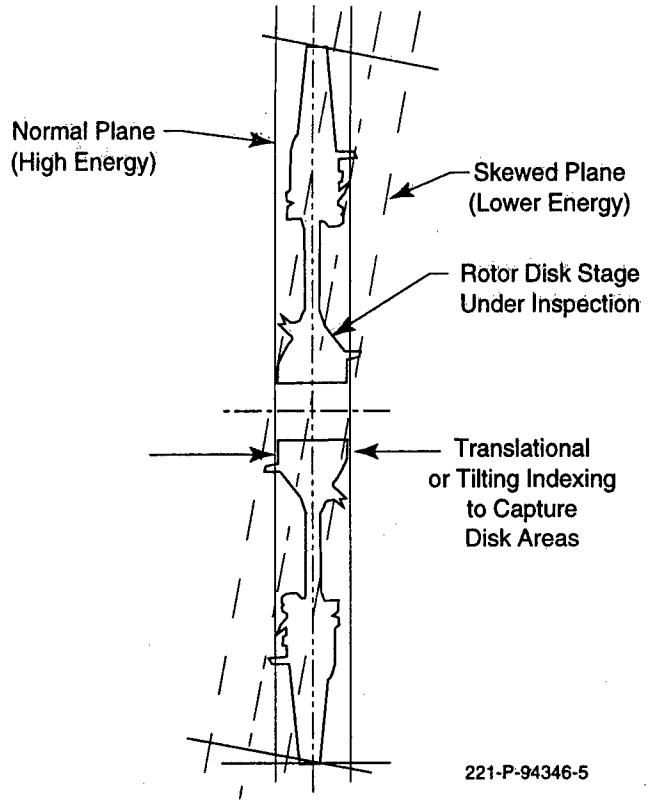

Figure 3. SMT technology gathers X-ray attenuation data slightly off-axis to the orthogonal plane typical to conventional CT, thereby avoiding the unacceptably high attenuation of X-rays that would have to pass through the entire diameter of the turbine disk.

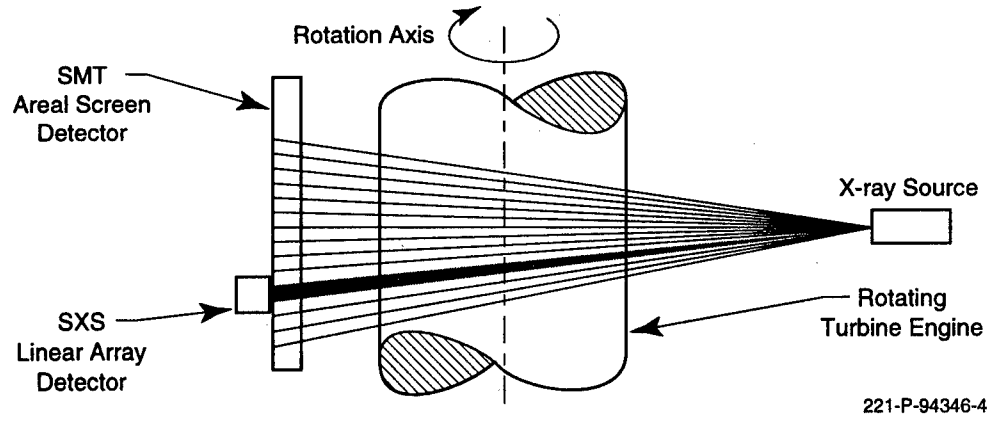

Figure 4. Top view of Figure 2 showing how SMT simultaneously gathers many data sets of planes or slices while SXS gathers only a single plane of data in the same data run or time period.

of Figure 2. As the turbine rotates, the X-ray source is strobed to obtain the X-ray shadow of the turbine at a particular engine phase angle. This single frame of data is called a view. An entire sequence of views is gathered, each at an appropriate engine phase angle, and a sequence of cross-sectional images can be reconstructed. What distinguishes SMT from the cross-sectional imaging that we accomplished in the earlier SXS program is in the detector and reconstruction algorithm. The SXS approach uses a one-dimensional linear array which can gather data on only one cross-sectional "slice" at a time. The SMT approach measures the entire region along the axis simultaneously.

SXS presents spatial resolution in radial and axial directions of approximately 0.02 and 0.06 in. respectively. SMT is able to present much higher spatial resolutions, as high as 0.005 in. in either direction. (Spatial resolution is typically much coarser than defect detection capability. Thus, while spatial resolution is 0.005 in., the defect detection capability might be 0.0003 in.) SMT should be able to acquire data in a much shorter time interval than SXS.

6. SMT Phase I Results

In the USAF-sponsored SBIR Phase I SMT program, we accomplished experimental verification of the principles of the technique, performance predictions of the full-up system, and provided a conceptual design and cost-benefit and use plan for SMT. The main results from the Phase I program are:

- The SMT system will detect cracks as small as 0.0003 in. in thickness, having areal extents of 0.01 $in.^2$.

- Complete data can be acquired on a single engine in a time of approximately an hour or less; meaningful data and its analysis and interpretation can be completed very shortly thereafter.

- The SMT concept is useful not only for turbine disks, but for blades and other rotating members as well. In addition, SMT may find use in applications outside aerospace, e.g., massive turbines in electricity-generating equipment, and anywhere else where failure or downtime in high-cost capital equipment or critical components can justify the initial investment costs in SMT technology.

- A cost/benefit analysis shows that introduction of SMT technology can pay for itself rapidly — probably within six months after deployment at a major air logistics center.

An image produced in this Phase I program is shown in Figure 5. The image is a 2 in. square section of a fiducial disk that was mounted adjacent to the compressor section of an automobile turbocharger. As the compressor/fiducial disk of the turbocharger was rotated, shadowgraph X-ray images of the central region of the turbocharger were obtained. Artificial separations of sizes ranging from 0.020 in. to 0.0003 in. were inserted in the fiducial disk; they can all be detected in these images. If these data were to be obtained on an actual SMT system, the acquisition time for the entire component/assembly would be less than a minute.

7. SMT Phase II Initial Demonstration

A prototype SMT system was assembled in the Air Force sponsored Phase II SBIR program. This system, as shown in Figure 6, used an X-ray source (9 MeV Linatron) provided by NAWC/CL, an X-ray camera developed by Lockheed and the data acquisition, control and processing electronics (HR3DCT Breadboard Workstation) on loan from the Air Force.

The demonstration specimen for the initial demonstration was the turbine section of a T-53 turboshaft engine with a calibrated crack disk bolted directly to the turbine disk. The test configuration is shown in Figure 7 with a close-up of the crack calibration disk shown in Figure 8. A drawing of the crack calibration disk is shown in Figure 9 with the six 1/8, 1/4 and 3/8 in. diameter "crack stacks" shown in their relative positions.

Experiment Demonstration Results

The first overall image that was reconstructed from these data is shown in Figure 10. We emphasize that this is an early result, and that there has been no special processing or tinkering done with the image beyond our standard algorithmic approaches. We have not yet begun any artifact compensation work. The stainless steel disk image reveals the three holding bolts spaced at 120 deg intervals, about halfway in radius between the center of the disk and its outside edge.

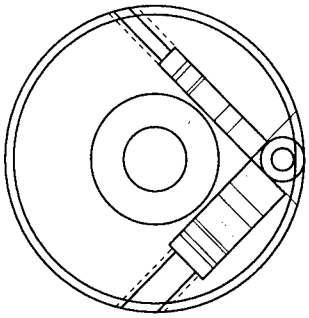

271-AFW 95002-1

a) Drawing of crack phantom disk. The entire disk is 1.5 inches in diameter and was rotated within its 6" diameter housing while all data were acquired. Two sets of crack anomalies were utilized, 1/4" and 1/8" in diameter. The section shown in the drawing is through the plane perpendicular to the axes of the crack anomalies. The sizes of these anomalies vary from 0.020" to 0.0003".

b) Reconstructed image of the phantom disk showing artificial calibrated anomalies that were inserted into the disk.

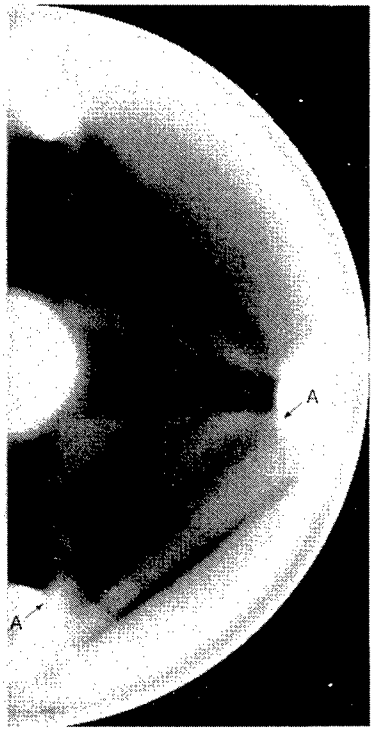

c) An enlargement of the region in the lower right hand quadrant showing the anomalies at higher contrast.

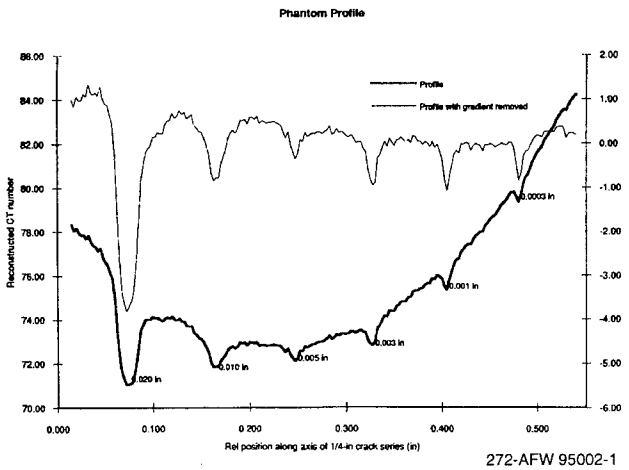

272-AFW 95002-1

d) A density profile across line A-A' (in figure 1c) containing the anomalies. All anomalies, including the 0.0003" thick crack, were seen. As described later in sections 2.4 and 2.5, the actual sensitivity was in fact higher than this figure - in the 0.00015-0.0002" range.

364-M96-081-3

Figure 5. SMT Phase I results

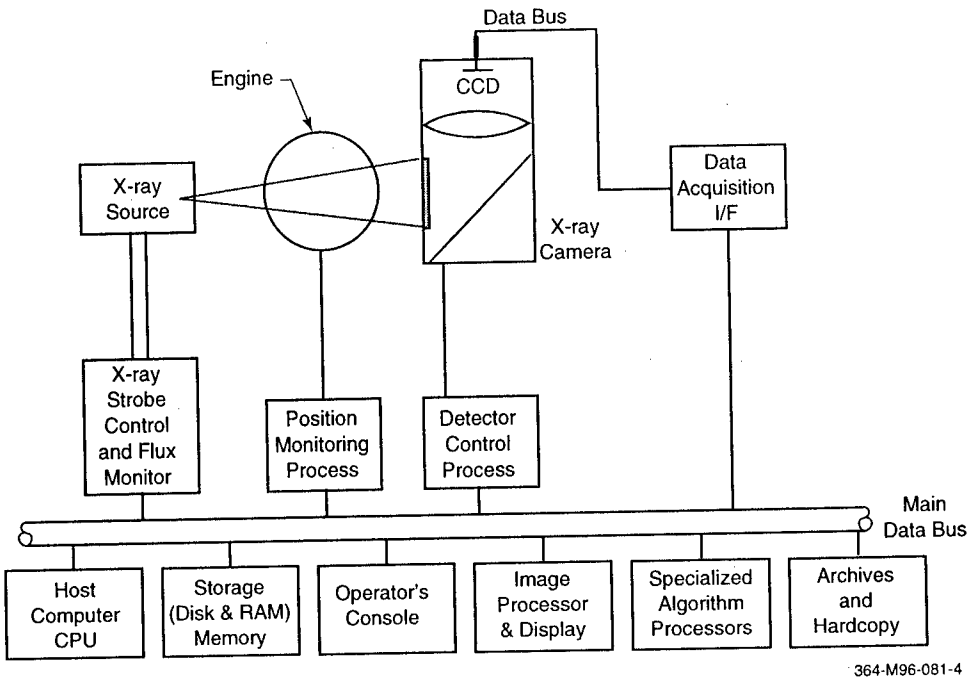

Figure 6. SMT block diagram

In addition, the six sets of calibrated crack simulants are seen. The circumferential cracks, i.e., those that run along the circumferential direction, are located at positions of approximately 1 o'clock, 5 o'clock and 9 o'clock. (The circumferential cracks are arranged so that the gross appearance of each family of cracks appears radial. Inside each band of features, the individual cracks may be seen.) The radial cracks, i.e., those cracks whose major features run in a radial direction, are at positions of approximately 12, 4, and 8 o'clock. The major cracks can be seen in all groups.

Figure 11 shows an expanded view of the section near the circumferential set of 1/4 in. long cracks located at 9 o'clock. These are arranged radially, and at least four and possibly five of the cracks are seen. A profile of the density as a function of radial position is shown in Figure 12, where the different cracks are seen. Starting from the inside and working out, we see that the 0.020 in. thick crack, the 0.010 in. crack, and the 0.003 in. crack are seen very clearly. The 0.005 in. crack, while seen on the image, is not so prevalent in the profile as the 0.003 in. crack. We believe that the 0.005 in. shim material may be somewhat denser than the others, and hence more X-ray opaque. There is also a strong visual indication that the 0.001 in. thick shim is present in the image, but that is due to the fact that the observer knows where to look for it. (The bright mark at

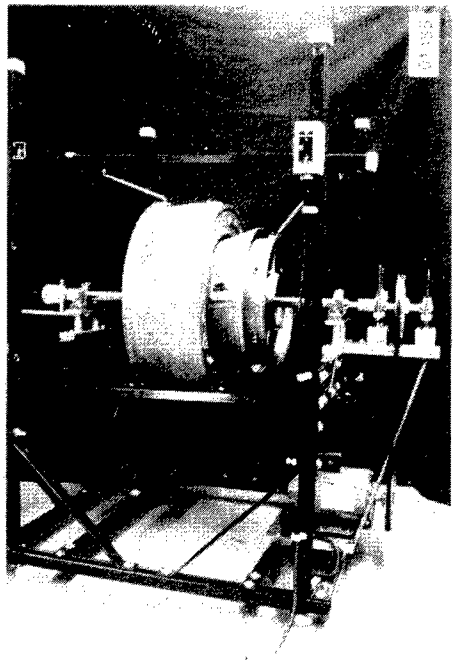

Figure 7. Turbine section of T53 turboshaft engine shown on test stand with its electrical drive system on right and shaft position encoder on left. The cowling is approximately 2 ft in diameter.

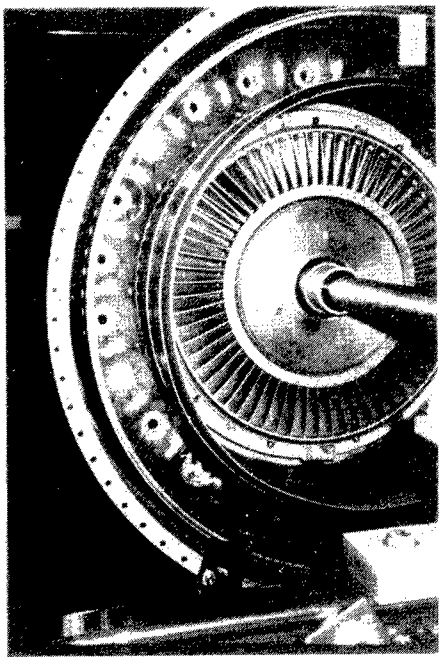

Figure 8. A close-up view of the interior of the T53 engine showing the crack calibration disk held by three screws to the turbine disk, interior to the blades. The diameter of the supplementary disk is about

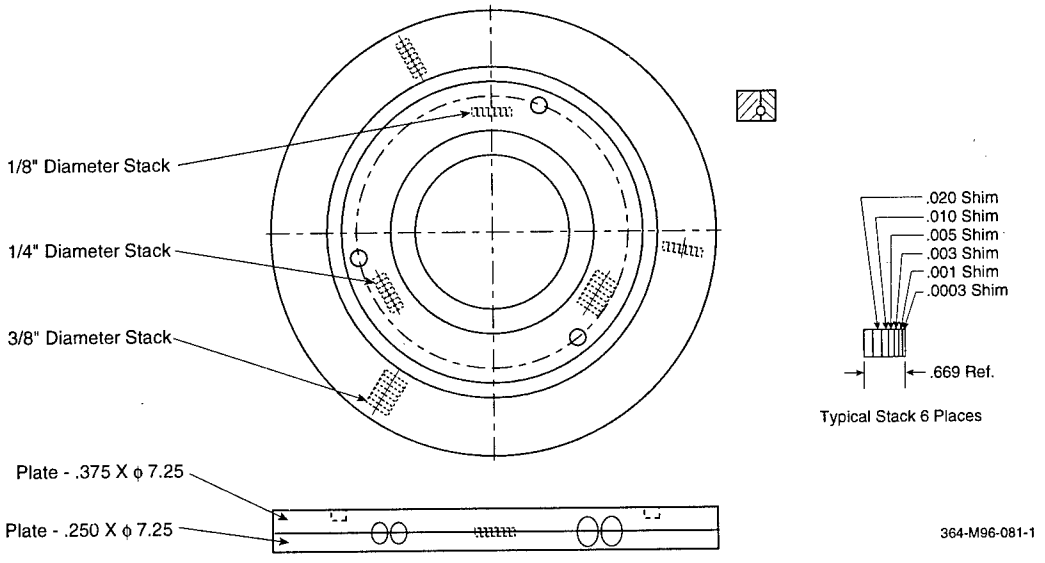

Figure 9. Crack calibration disk

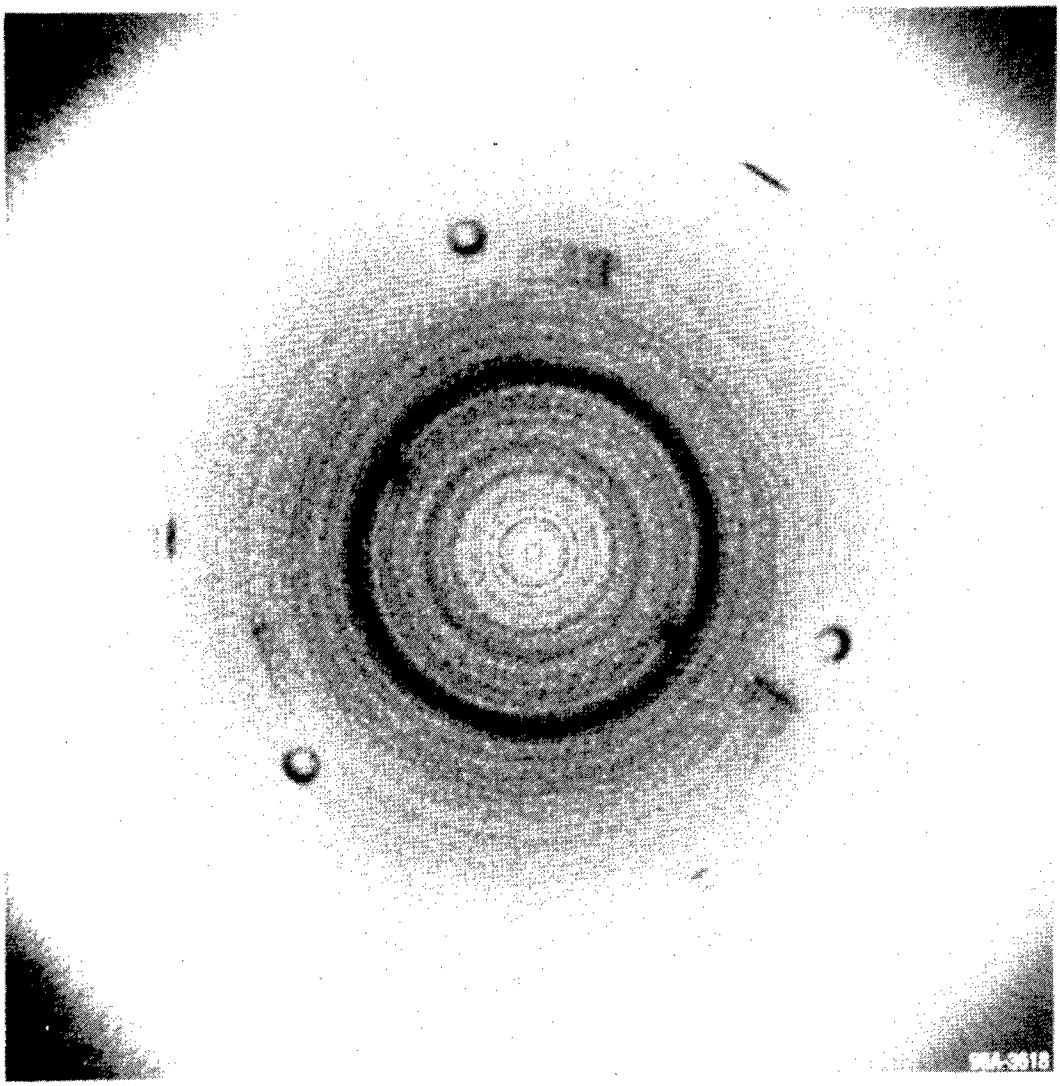

Figure 10. The first reconstruction of the stainless steel disk phantom having calibrated crack-simulants. See text for discussion.

the larger radius end of the pattern is the position where the last spacer meets the plate.)

We will return to the field in the spring to produce images on a production fighter engine. Based on these initial results, we are very optimistic about producing images that are suitable for both mensuration and diagnostic NDT information.

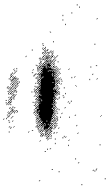

Figure 11. An expanded view of the 1/4 in. diameter crack simulants reconstructed in the image. The cracks of sizes 0.020, 0.010, 0.005 (less contrast, as discussed in text), and 0.003 are easily seen. In addition, the 0.001 in. crack can be seen, but not with as much contrast as the others.

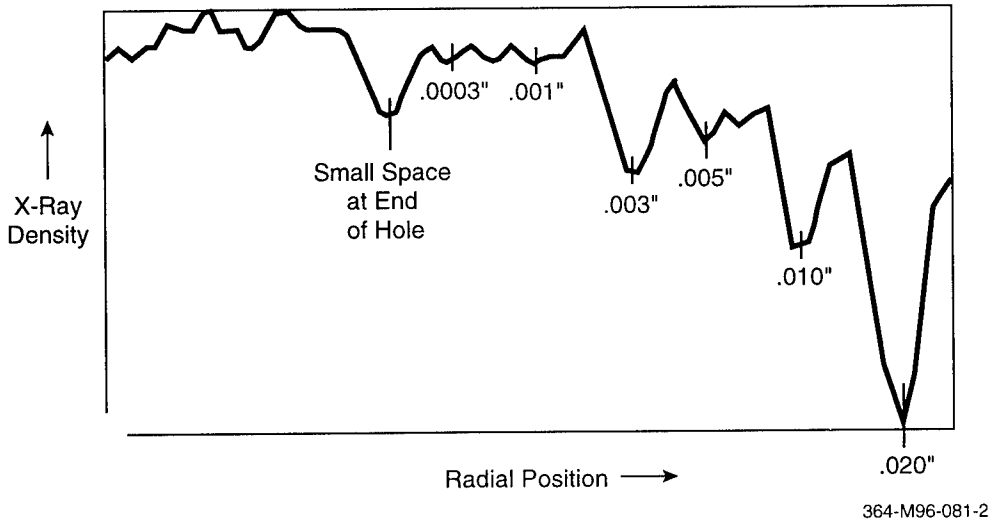

Figure 12. A radial density profile of the region shown in Figure 11. The overall gradient is an artifact of the first reconstruction process. This will be removed in much the same way that the previous Phase I results shown in Figure 5 were. The crack positions are shown in the figure.

8. Acknowledgment

The SMT team consisting of Foster-Miller, Skiametrics, Perceptics, Lockheed and GE wish to acknowledge the excellent support we received from Jon Rogerson of NAWC - China Lake in the conduct of the initial SMT demonstration at the Navy's China Lake facility.

ORTHOGONAL-AXIS EDDY CURRENT PROBES FOR HIGH SENSITIVITY/HIGH PRODUCTIVITY INSPECTION OF AIRCRAFT STRUCTURES

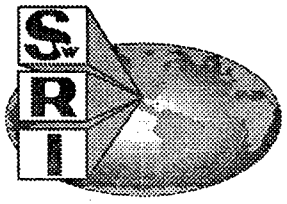

Gary L. Burkhardt
Jay L. Fisher
Jeffrey S. Stolte
Southwest Research Institute

E-Systems
A Raytheon Company

Steven R. Kramer
Kevin L. Cobble
Raytheon E-Systems
Greenville Division

PROBLEM

- Detection of hidden cracks and corrosion in thick, multi-layer structures of P-3, RC-135, and other aircraft
- Structure thickness up to 0.3-inch thick.
- High productivity inspection required

APPROACH

- Develop eddy current probes based on orthogonal-axis design
- Probes provide high sensitivity to subsurface flaws and low liftoff noise
- Perform inspection with McDonnell Douglas MAUS III
  - Portable, single-person operation
  - High-speed raster scanning
  - C-scan imaging

PROBE DESIGN

- Probe configuration consists of exciter and sensor coils with axes orthogonal to each other.

- Orthogonal coil orientation minimizes direct electromagnetic coupling because magnetic flux from exciter does not link with the sensor. This significantly reduces signals caused by liftoff variations as probe is scanned.

PROBE DESIGN (CONT'D)

- Exciter and sensor coils can be optimized for their individual purposes to enhance overall probe performance.
- Probe design is compatible with MAUS III scanner and instrumentation.

PROBE CONFIGURATION FOR CORROSION (MATERIAL LOSS) DETECTION

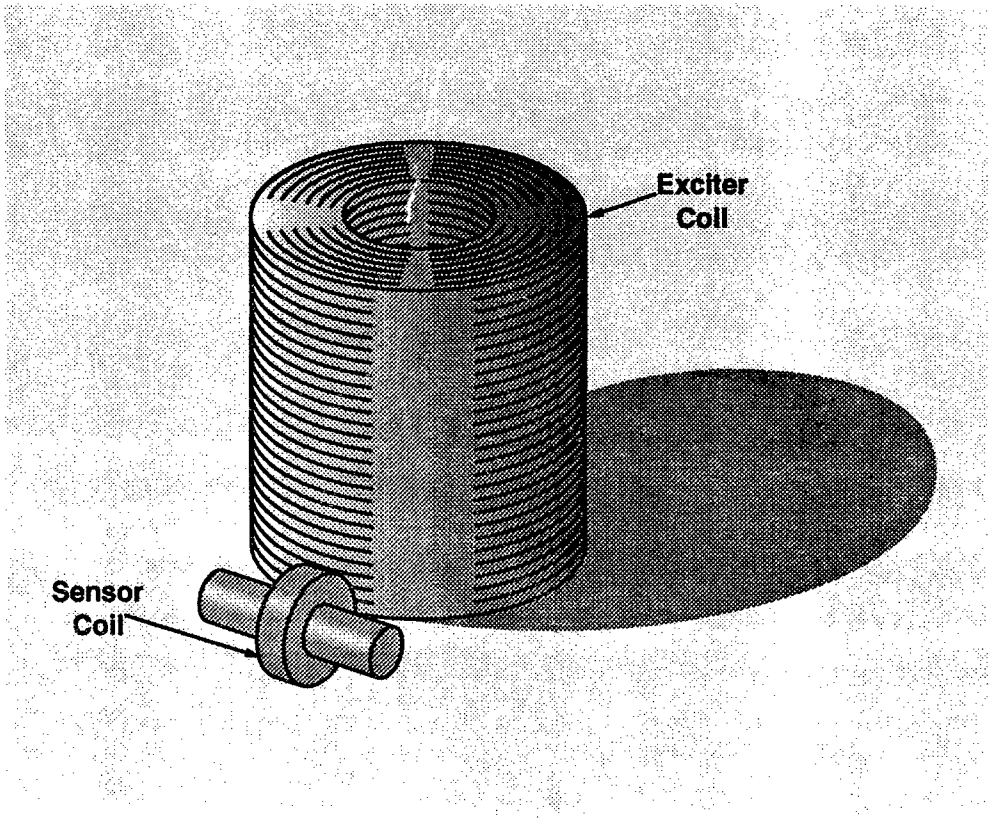

PROBE CONFIGURATION FOR DETECTION OF CRACKS AROUND FASTENERS

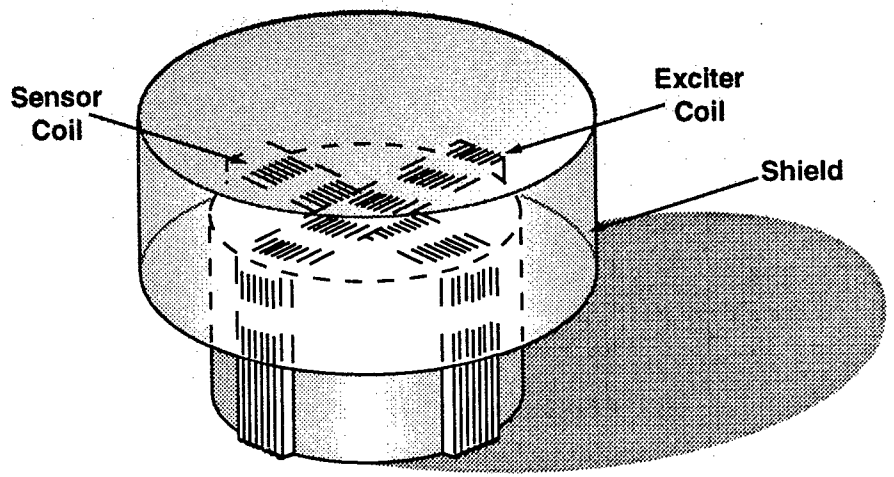

MAUS SYSTEM

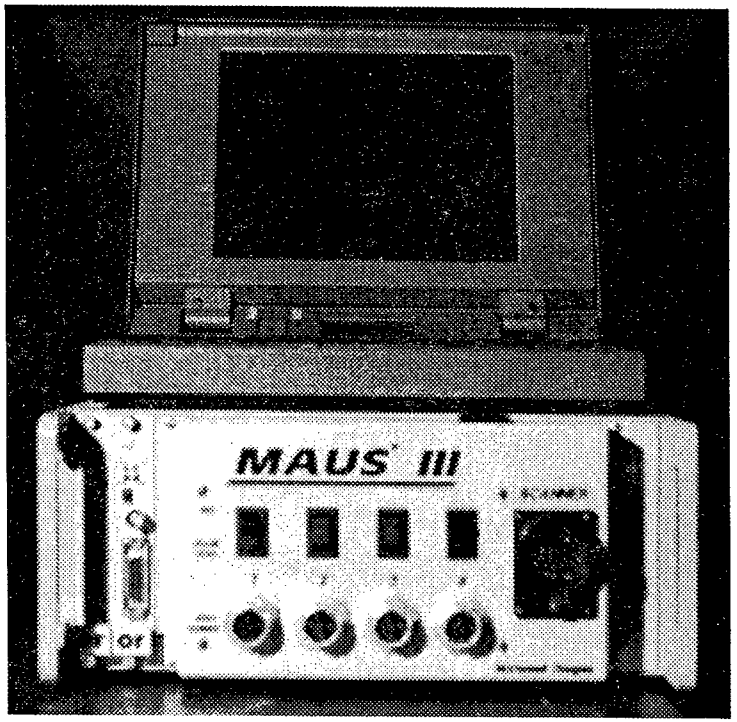

System Computer and Electronics

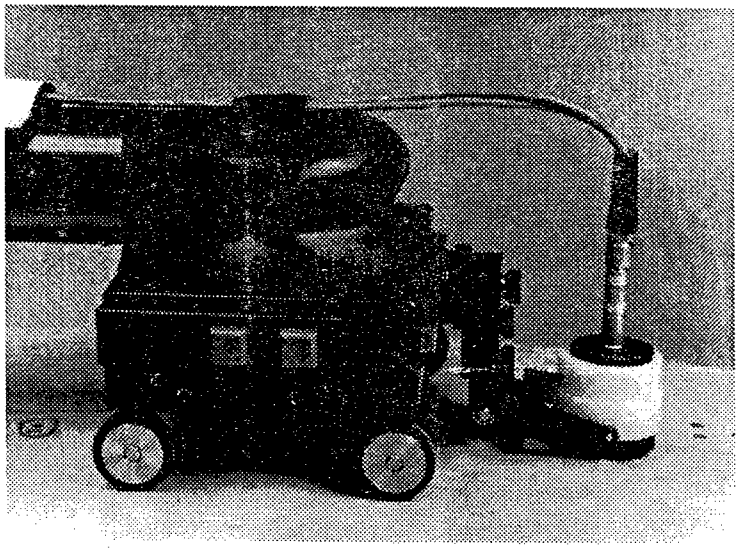

Scanner with Eddy Current Probe

CORROSION SPECIMEN

- Corrosion simulated by flat-bottom holes with rounded edges in bottom layer
  - 1.7 percent to 15 percent of total specimen thickness for total thickness up to 0.15 inch
  - 1 percent to 10 percent of total specimen thickness for total thickness up to 0.3 inch

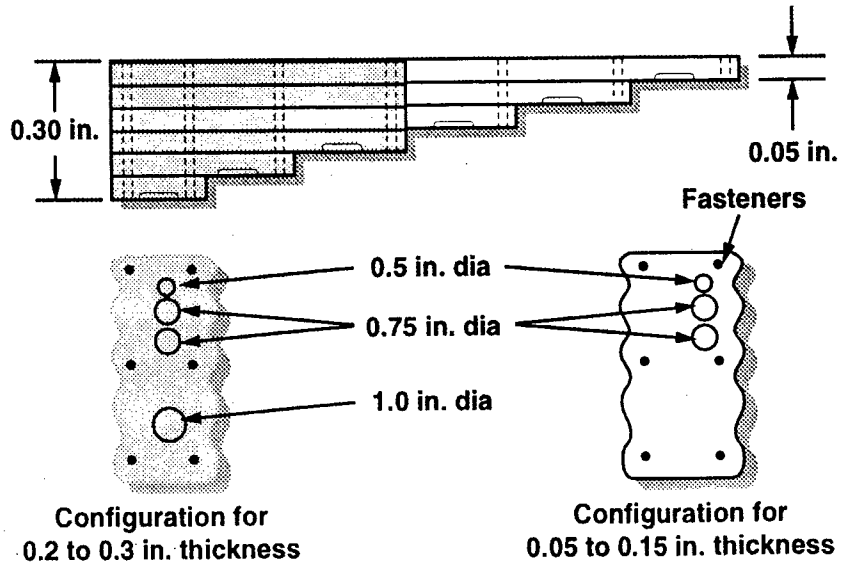

CORROSION DETECTION RESULTS ORTHOGONAL-AXIS PROBE

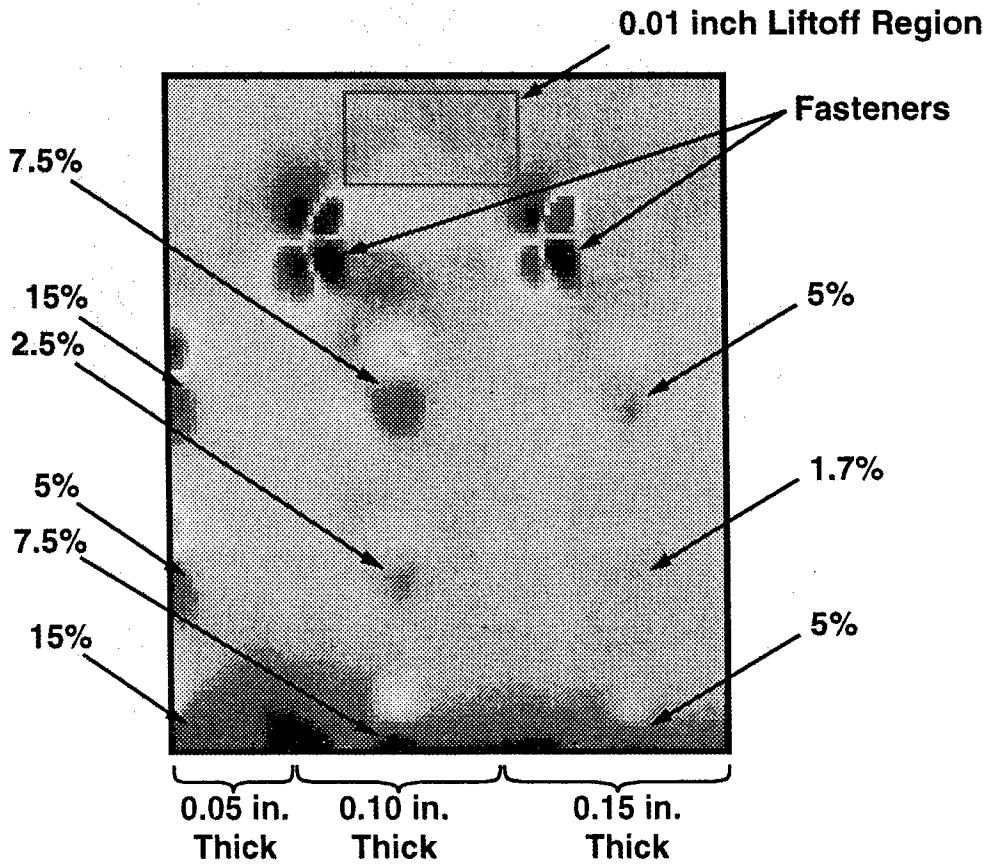

CORROSION DETECTION RESULTS ABSOLUTE COIL

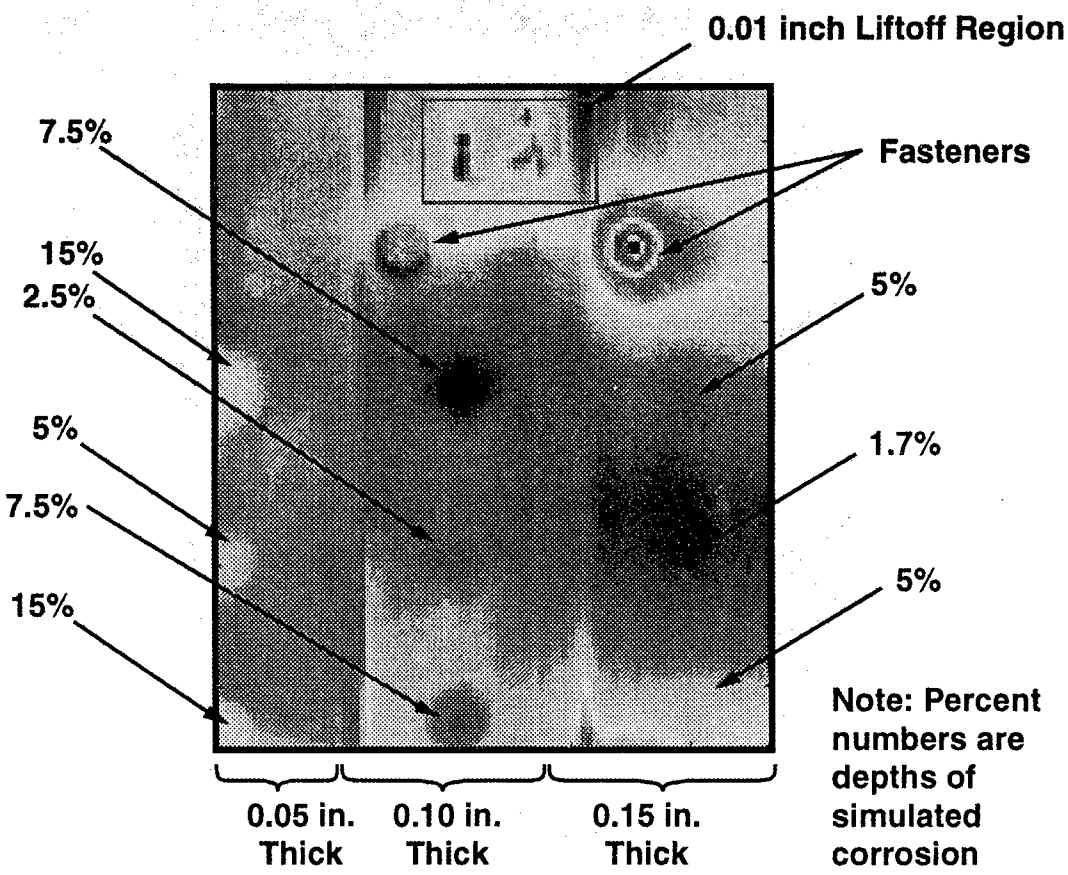

CORROSION DETECTION RESULTS ORTHOGONAL-AXIS PROBE

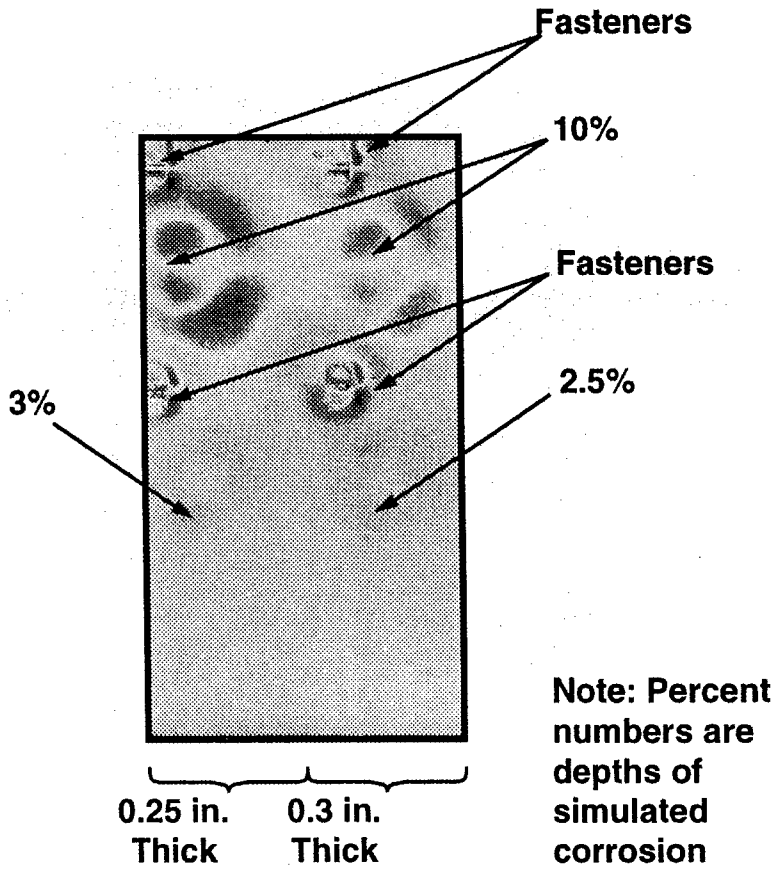

Note: Percent numbers are depths of simulated corrosion

CORROSION SPECIMEN NO. 2

- Corrosion simulated by flat-bottomed holes around fasteners in 2nd layer
- Specimen also contained notches in 2nd layer

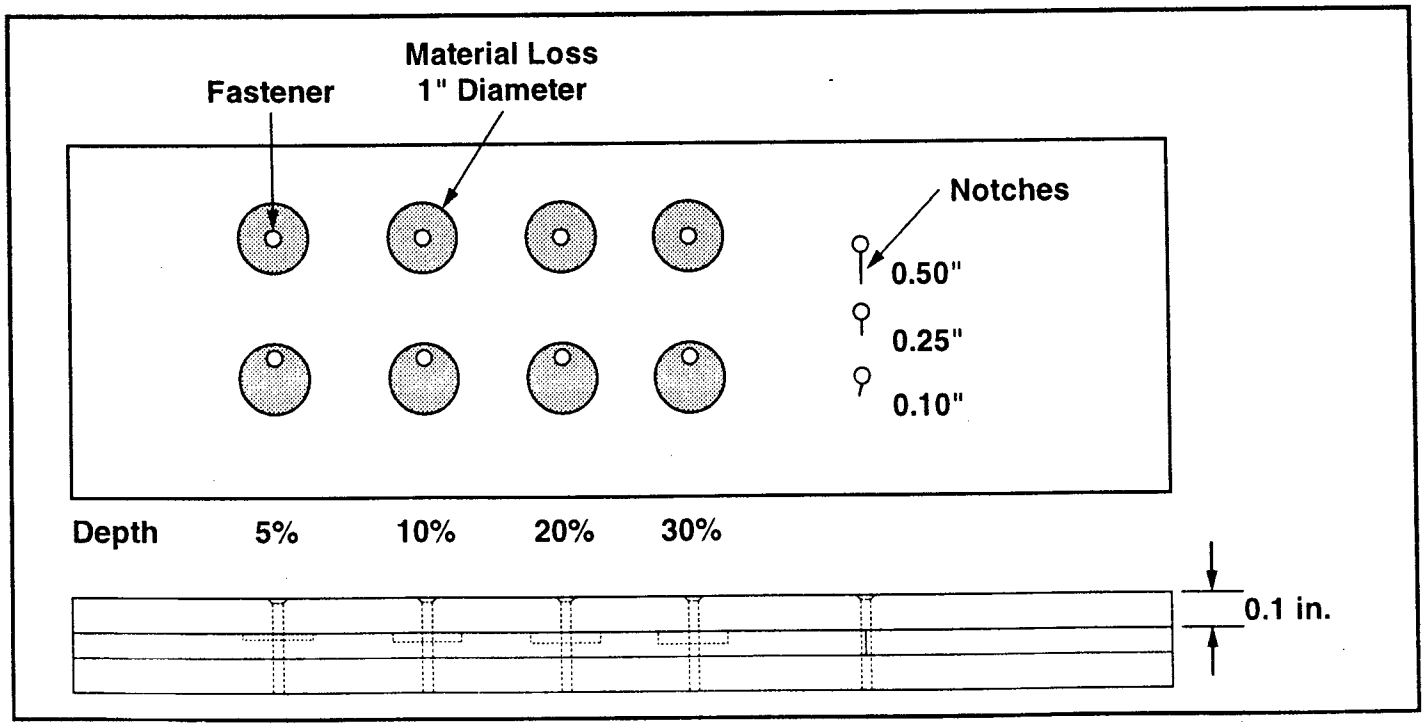

CORROSION DETECTION RESULTS
ORTHOGONAL-AXIS PROBE, SPECIMEN NO. 2

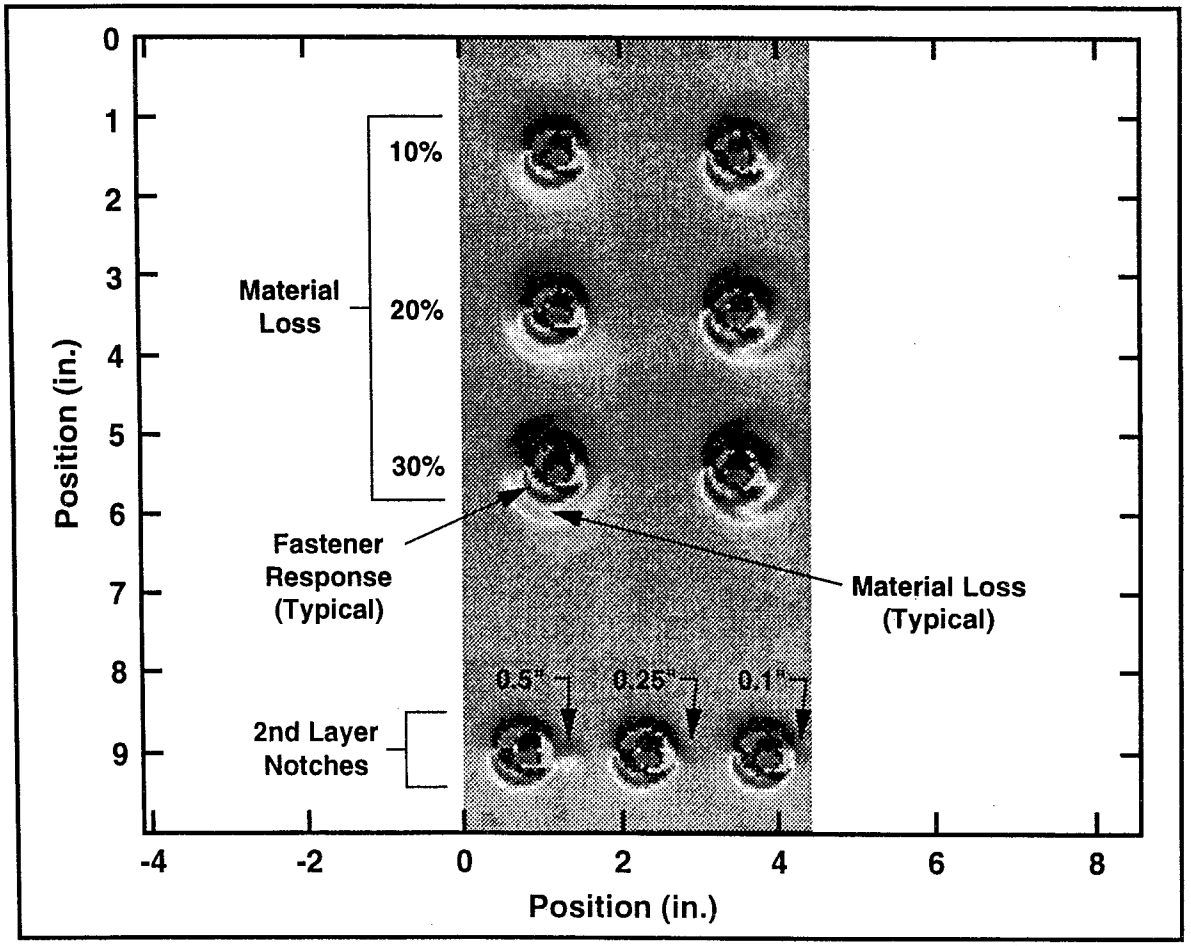

CRACK SPECIMEN

- 0.125 inch thick layers
- 0.25 inch long simulated fastener-hole crack in second layer

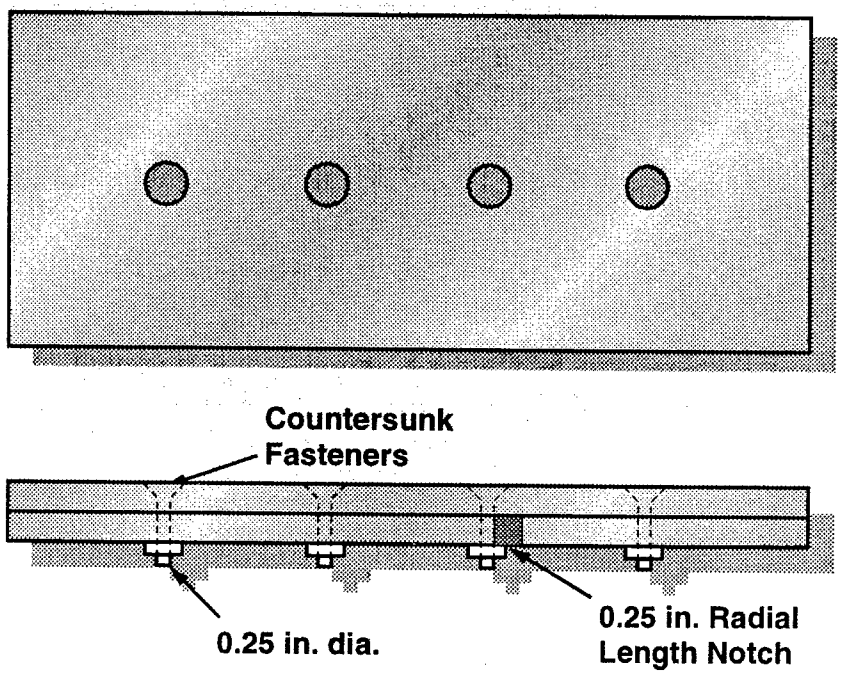

CRACK DETECTION RESULTS

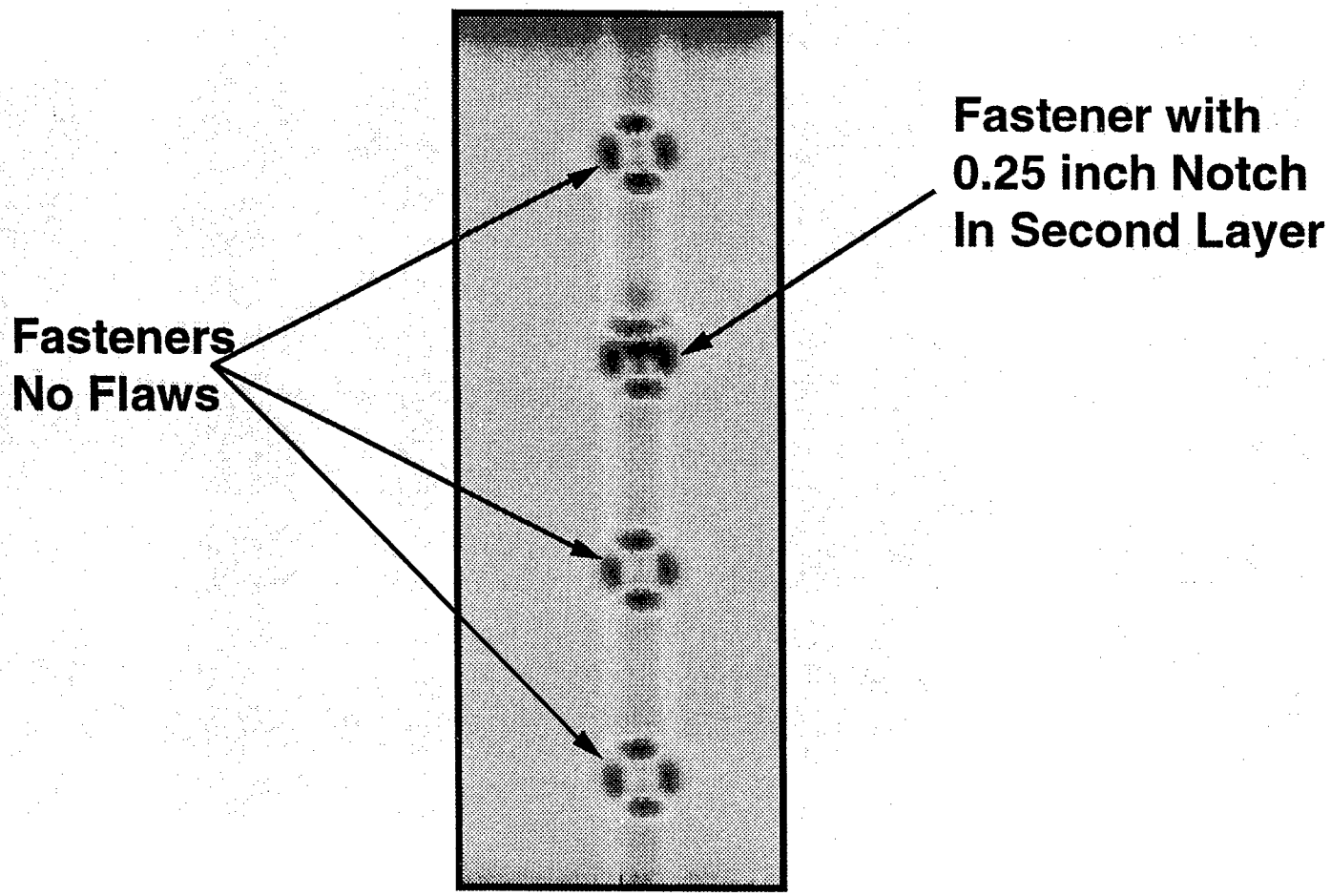

CONCLUSIONS

- Orthogonal-axis probes are effective for detection of corrosion and cracks in thick aircraft structures having multiple layers.
- The probes provide significant improvement compared to conventional MAUS-compatible probes:
- Flaw detection sensitivity is greater.
- Sensitivity to liftoff noise caused by variations in probe-to-specimen spacing is reduced.

CONCLUSIONS (CONT'D)

- Orthogonal-axis probes, in combination with the MAUS III, provide a high-sensitivity, high-productivity inspection for aircraft structure.

FUTURE PLANS

- Probes will be optimized to improve spatial resolution.
- Inspection will be implemented on actual aircraft.

Eddy Current Inspection of Engine Blade Slots

Mr. Wally Hoppe
Systems Research Laboratories
An Operation of Calspan SRL Corporation
2800 Indian Ripple Road
Dayton, Ohio 45440-3696

Sponsor - USAF through several contracts:
F33657-93-C-0075, F41608-91-G-0005, DOE03317 (GE PO#)

Background

- GE's side-mounted coil technique
- P&W's swivel head sewing stitch probe research
- SRL's hole probe with gating
- GE's sewing stitch technique
- Dr. Marchand's potential drop technique
- P&W's eddy current perturbation technique
- SRL's sewing stitch technique
- P&W/SRL/Uniwest's Wide Field Coil

Requirements

- Geometry/coverage
  - To edge
  - Defined by picture
- Flaw Size/Orientation
  - .005 - .010 inch depth
  - Corner - 1 X 1 axial
  - Surface - 2 X 1 axial
- Throughput Rate
- False Calls/Rework
- RFC system application

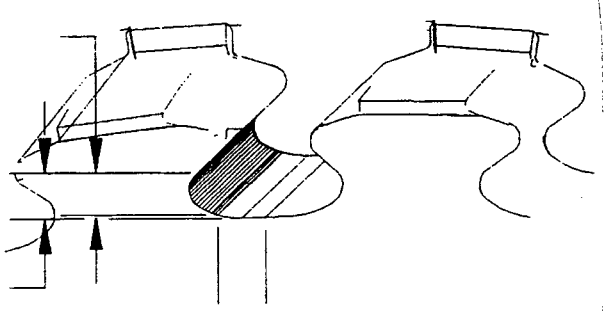

The Challenge of the Feature

- Inspection requirement includes the edge of the slots
- Each slot is chamfered - possibly hand chamfered
- Some of the slots are slanted - possibly in two directions
- There is galling in some areas of the slots due to fretting
- The slots may have broaching irregularities

The Challenge of the Inspection

- Geometry signals - produced by scanning across the edge
- Coil design
  - Diameter, shape, orientation, frequency
- Probe design
  - Shoe, compliance, manipulation
- Data acquisition
  - Scan speed, sampling rate, index step size
- Signal processing

Sewing Stitch - Perpendicular Coil Orientation

- Coil
  - Split-D, ferrite core, differential, reflection
  - Core 0.020" diameter
  - 0.030" Outer dia.
  - Split of coil perpendicular to shaft of probe tip
  - 6 MHz

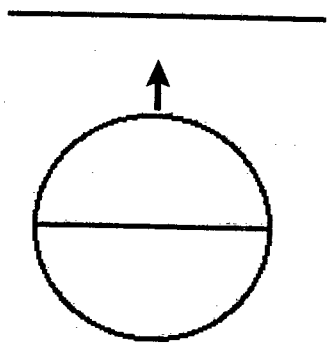

Sewing Stitch - Perpendicular Coil Orientation

- Probe/shoe
  - Long needle type probe tip
  - Coil mounted in small shoe
  - 0.003" Teflon tape applied to shoe
  - Shoe runs in contact with engine part
  - Single axis of compliance
    - Spring loaded
    - Ball slides for parallel displacement
    - Micromanipultor for coil position

Sewing Stitch - Perpendicular Coil Orientation

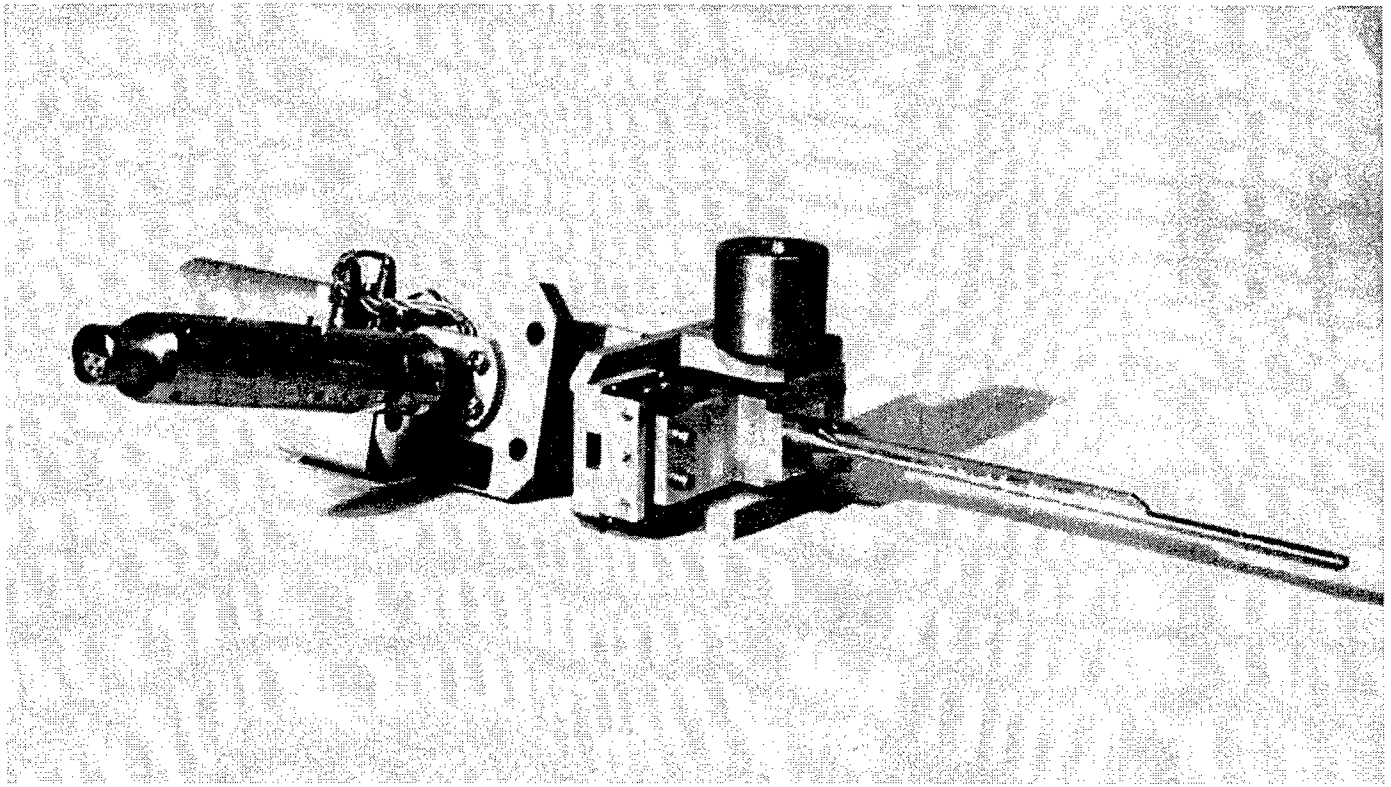

Sewing Stitch - Perpendicular Coil Orientation

- **Data Acquisition**
  - **Scan through the length of the slot**
  - **Scan coil from above top edge to below bottom edge**
  - **Data is digitized by 12 bit A-D at 2500 samples/sec**
  - **Scan Speed is 1.25 inch/sec**
  - **Dynamic range is important**
  - **Index 1/4 of coil diameter**

Sewing Stitch - Perpendicular Coil Orientation

- Signal Processing
  - Concept is to subtract every other waveform
  - Account for DC offset shifts
  - Account for time shifts (discreet plus interpolation)
  - Scaling to compensate for coil/probe misalignment
  - Least-squares best-fit of one waveform to another, with DC offset, time alignment, and scaling
  - Subtract fit from reference to remove geometry signal
  - Threshold residual to detect flaws

Sewing Stitch - Perpendicular Coil Orientation

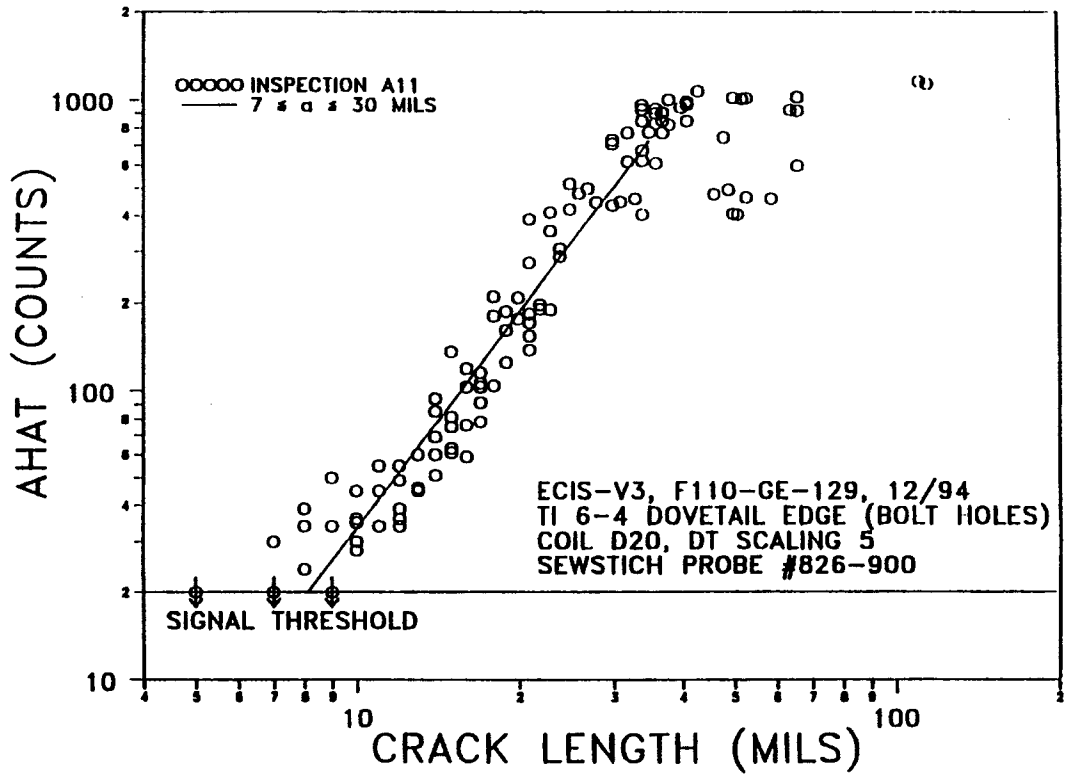

Sewing Stitch - Perpendicular Coil Orientation

- Challenges to this technique
  - False calls
  - Flaw size limited by large dynamic range required
  - Slow inspection

Sewing Stitch - Parallel Coil Orientation

- Coil - same except split of coil parallel to shaft of probe
- Probe/shoe - same
- Data acquisition - same
- Signal processing
  - Adaptive modeling
  - Fit model to data, constrain, subtract, filter, and threshold

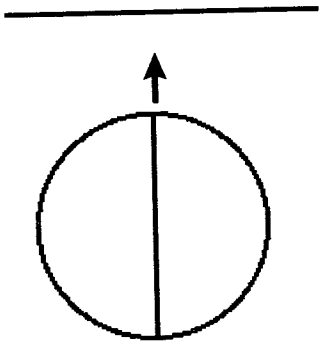

Sewing Stitch - Parallel Coil Orientation

- **Signal processing - continued**
  - **Form of Model:**
  - ***M*** **= magnitude**
  - ***C*** **= DC offset**
  - ***Xave*** **= time position**
  - β **controls steepness**
  - ***X*** **= independent variable**
  - **Optimize parameters**

Step Function

$$\left[\frac{M}{1+\left(\frac{X}{Xave}\right)\beta}\right]+C$$

Sewing Stitch - Parallel Coil Orientation

0.007 Inch Corner Crack

Edge Signal and Model

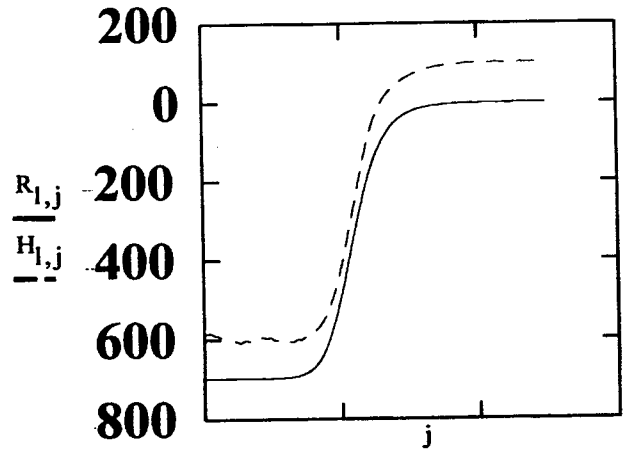

Residual Signal

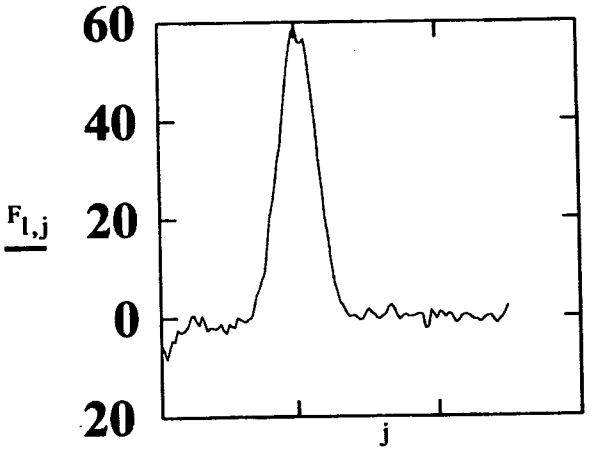

Sewing Stitch - Parallel Coil Orientation

Clean Edge

Edge Signal and Model

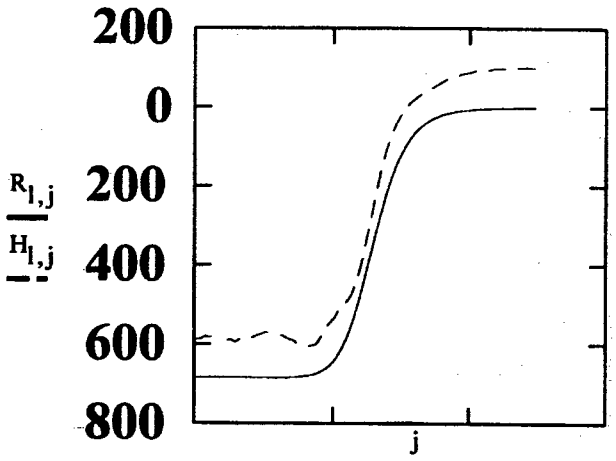

Residual Signal

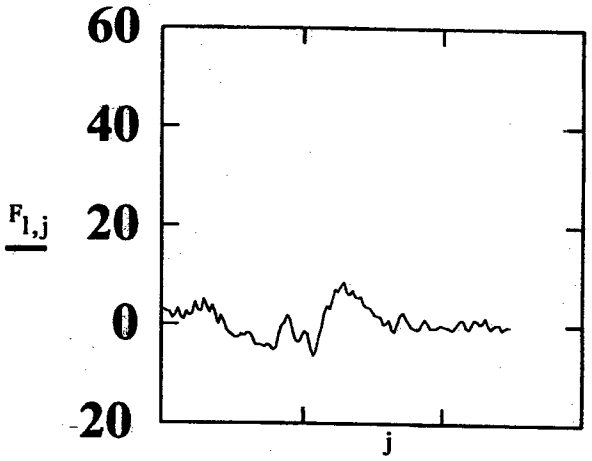

Sewing Stitch - Parallel Coil Orientation

Broach Edge Reliability data

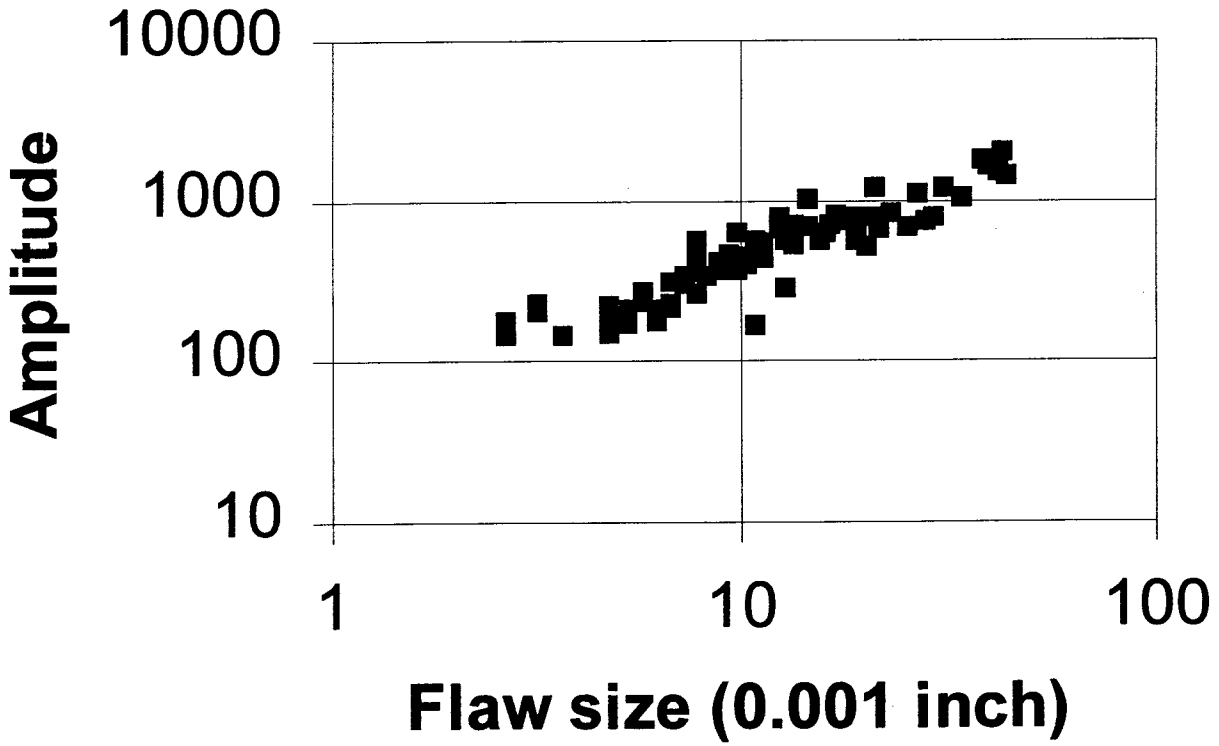

Sewing Stitch - Parallel Coil Orientation

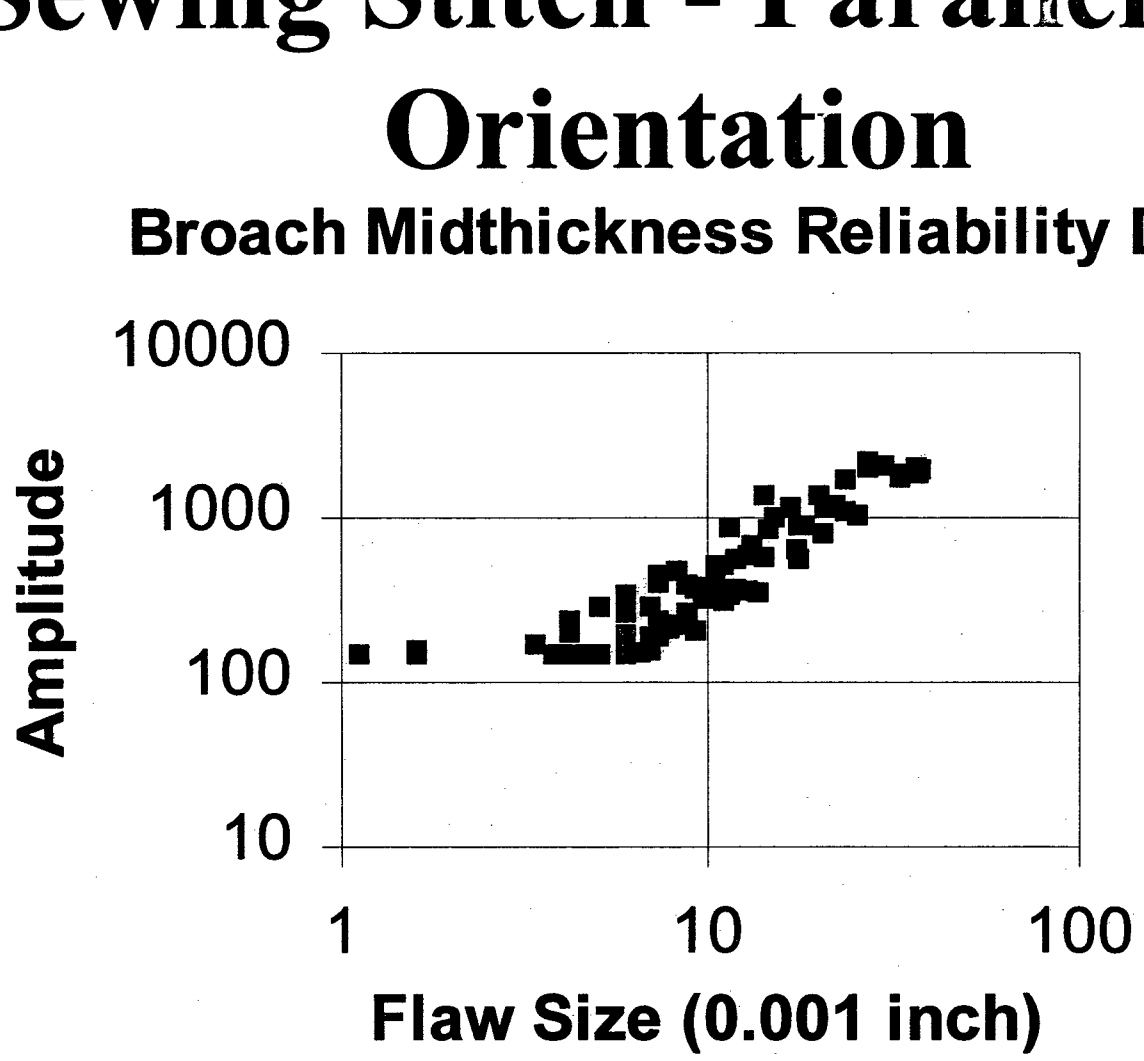

Sewing Stitch - Parallel Coil Orientation

- Challenges to this technique
  - Small flaw sizes
  - Cracks too far into chamfer are hard to find
  - False calls - no rework allowed
  - Throughput - slow inspection (eg. 20 min/slot)
  - Tilted slots require preprocessing to eliminate monopolar pulse at edge - less effective during processing (more false calls due to geometry signal)

Shaped Coil - Parallel Approach

- Coil
  - Shaped like blade slot
  - Coil windings parallel to edge (bobbin like)
  - Axis of coil parallel to axis of slot
  - 3 MHz
  - Differential - Reflection

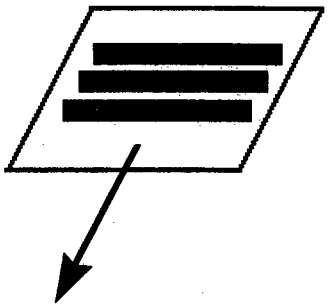

receive
drive
receive

Shaped Coil - Parallel Approach

- Probe
  - Delron shoe (contact)
  - Double compliance
  - Spring loaded
- Data Acquisition
  - Scan up and down
  - No need to index
  - 12 bit A-D, 1000 samples/second

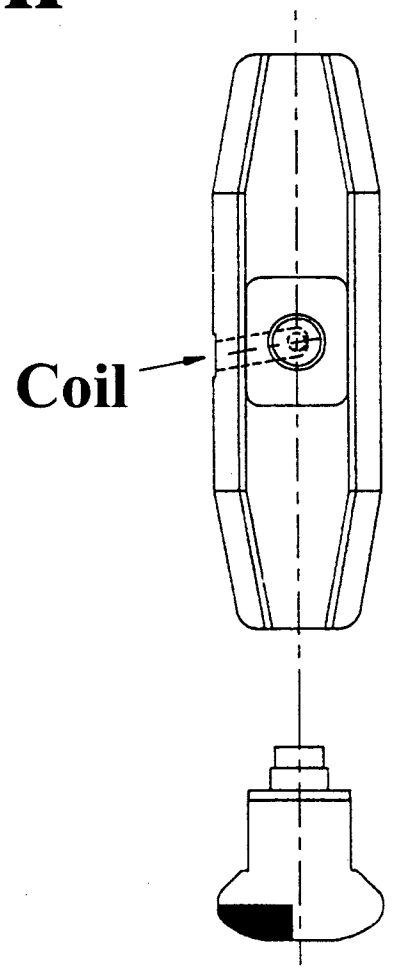

Shaped Coil - Parallel Approach

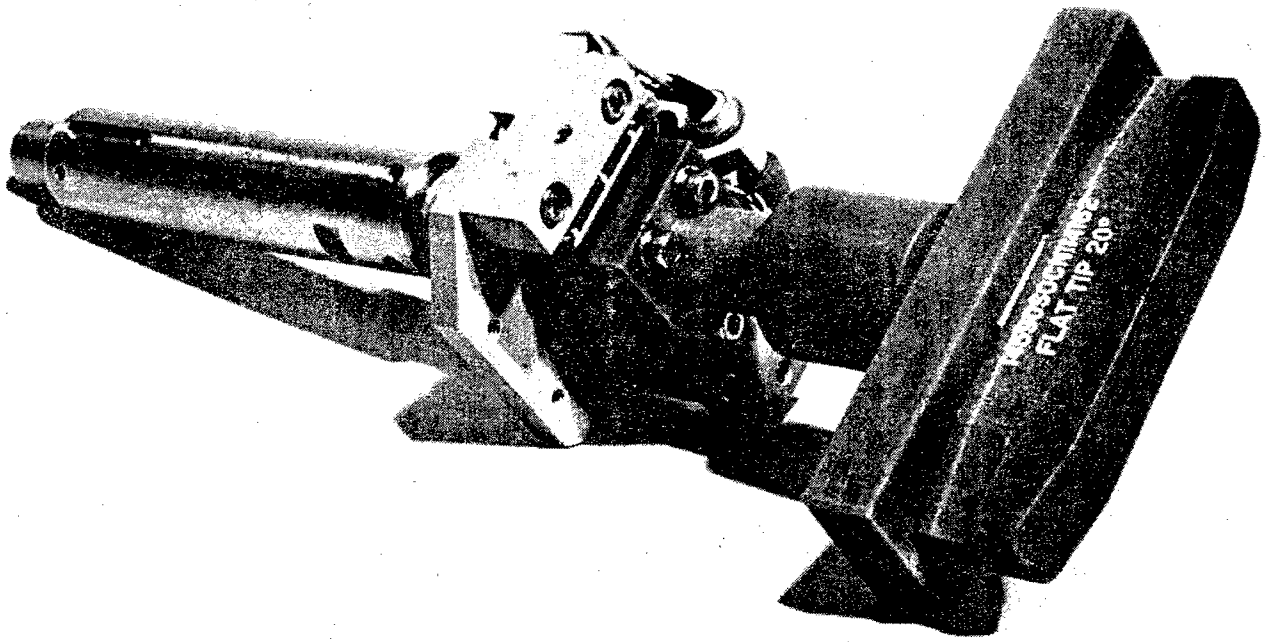

Shaped Coil - Parallel Approach

- Signal Processing
  - Edge signal at same frequency as flaw, so can only inspect to within ~0.070 inches from edge
  - Need to gate out the edge signal

Shaped Coil - Parallel Approach

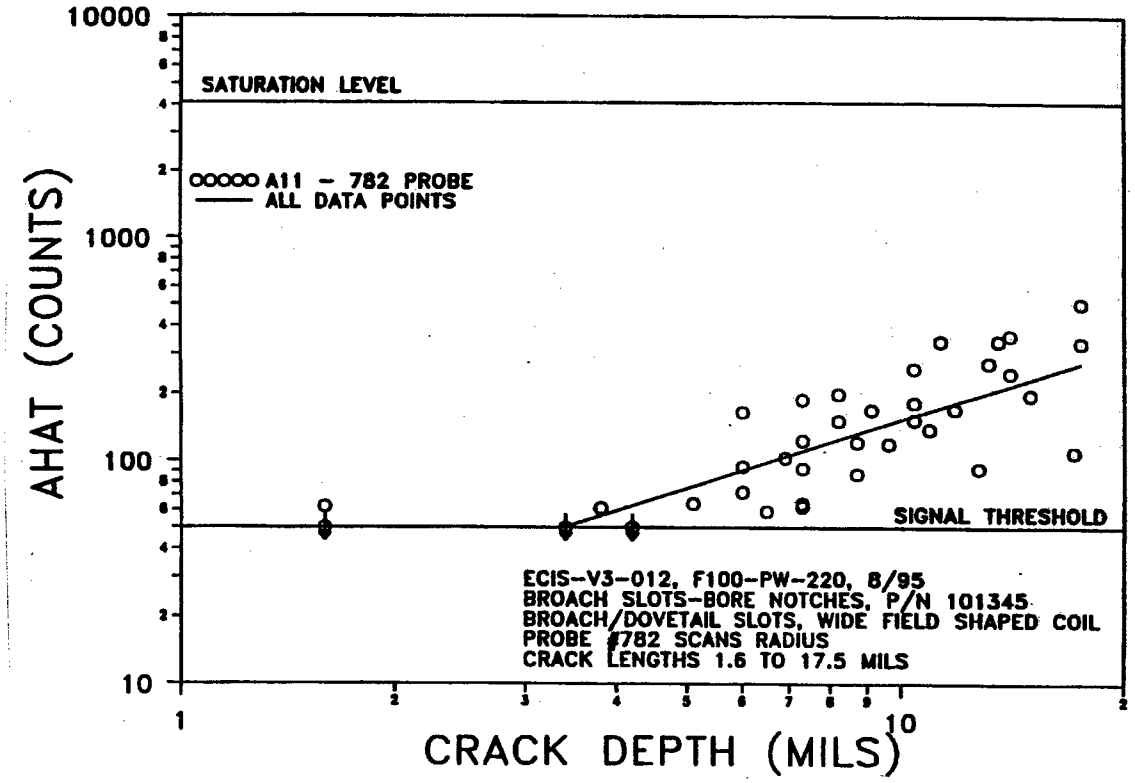

Shaped Coil - Parallel Approach

- Challenges to this technique
  - Cannot inspect slot edges
  - False calls when gate is too close to edge
  - Slot tolerances for fixed shoe/coil shape can cause liftoff and reduced sensitivity

Shaped Coil - Tilted Approach

- Coil
  - Essentially the same except tilt coil for ~25 degree angle to slot edge
- Probe/shoe
  - Same
- Data acquisition
  - Same

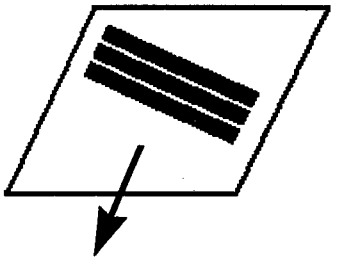

receive
drive
receive

Shaped Coil - Tilted Approach

- **Signal Processing**
  - **"Tilting" the coil produces a frequency separation between edge and crack**
  - **High pass filtering can now reduce edge signal**
  - **Signal to noise ratio can be improved by as large as a factor of ten**
  - **Subtraction of waveforms can improve signal even more (eg. subtract reference)**
- **Reliability data**
  - **None yet**

Shaped Coil - Tilted Approach

- Challenges to this technique
  - Small flaw sizes in the edge
  - Slot tolerances may provide unwanted liftoff
  - Broaching indication?

Summary

- Four techniques have been discussed
  - Sewing stitch - perpendicular coil orientation
  - Sewing stitch - parallel coil indication
  - Shaped coil - parallel approach
  - Shaped coil - tilted approach
- Challenges yet to overcome
  - Small flaw sizes in edges
  - False calls
  - Throughput
  - Tolerances in the slots

SESSION IX

FORCE MANAGEMENT

Chairman: *J. Turner*, SA-ALC/LADD

F-14 FATIGUE TRACKING METHODOLOGY AND LESSONS LEARNED

Richard H. Dalrymple
Timothy M. Fallon
Naval Air Warfare Center Aircraft Division

USAF Aircraft Structural Integrity Program Conference
Hyatt Regency Hotel on the Riverwalk
San Antonio, Texas
December 5, 1996

OUTLINE

- Overview
- Fatigue Tracking Methodology
  - Flight data recorders
  - Fatigue tracking algorithm
  - Feedback / Reporting
  - Results
- Lessons Learned
  - Data Recording
  - Fleet Interface
- Summary

OVERVIEW

- **Historical Tracking**
  - **Flight hours**
  - **CAG (counting accelerometer group)**
- **F-14 Tracking**
  - **Parametric based system**
  - **Refined conservatism**
    - » **Point-in-the-sky effects**
    - » **Sequence accountable**

– One of the most simplistic ways to track aircraft fatigue is by flight hours, which generally is done in a very conservative manner.

– To improve on this, systems were installed on aircraft with CAG's, or counting accelerometer groups, which provided ways to count up the number of times that certain 'g' limits are exceeded. This method gives a much better accounting of the general usage of the aircraft, but many conservative assumptions about the critical location fatigue damage must be made.

– The F-14 fatigue tracking system improves on that methodology by using a multi-channel flight data recorder to capture structurally significant events when they occur. This refines the conservatism in the fatigue damage computation by taking advantage of point-in-the-sky and sequencing effects.

– The F-14 system is a parametric based system, which differs from a strain-gage based system in that it primarily uses existing aircraft instrumentation already available. This reduces the need to maintain separate instrumentation, and the data is not tied to any specific location on the aircraft. Additional locations on the aircraft can be tracked when the need emerges as the fleet ages.

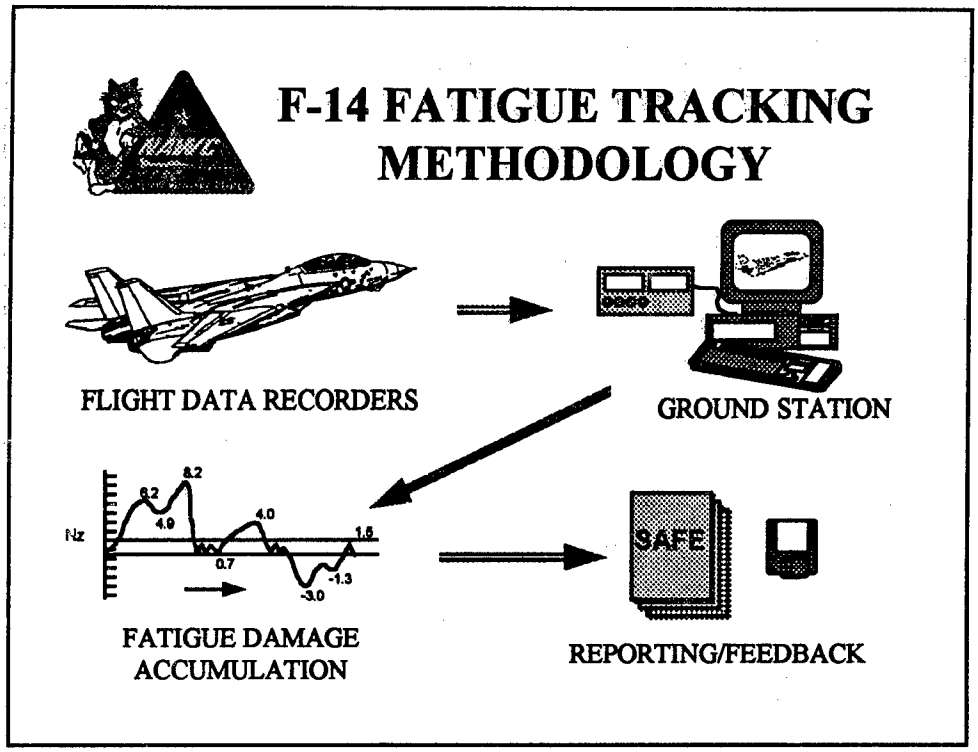

- Like most modern fatigue tracking system, the major components of the F-14 tracking system are the flight data recorder, the ground station, fatigue damage algorithms for tracking locations, and reports and feedback to the fleet.
- In the F-14 community there are 2 different flight data recorders. The first is the Fatigue and Engine Monitoring System (FEMS) on F-14 B and D aircraft, which is a system that was developed and installed integrally with the aircraft. The F-14A has a retrofit system for structural parameters only called the Structural Data Recording Set (SDRS).

FLIGHT DATA RECORDERS

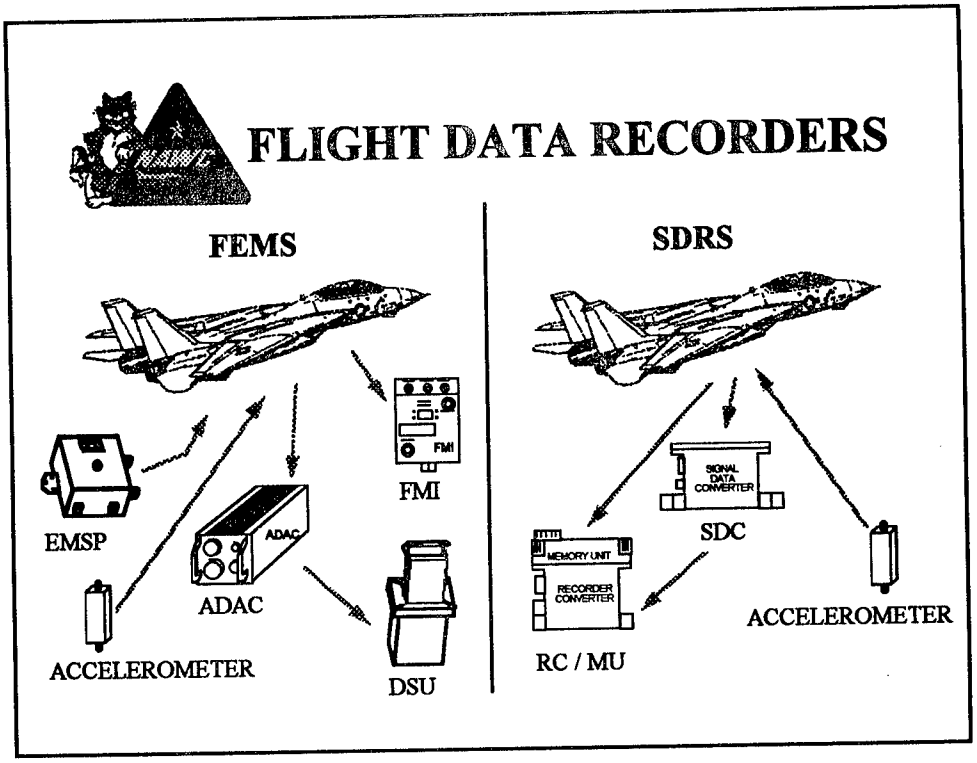

- The heart of the FEMS flight data recorder is the Airborne Data Acquisition Computer. It takes information from the existing aircraft parameters as well as the Engine Monitoring Signal Processor and the linear accelerometer and records the pertinent data to the Data Storage Unit, which is removed from the aircraft and brought to the ground station. The Fault Maintenance Indicator relays any aircraft problems recorded by the FEMS system at the end of each flight.
- Similarly, the SDRS takes information from the existing aircraft parameters as well as the accelerometer. It passes this information through the Signal Data Converter, and using the Recorder Converter, writes the pertinent information to the Memory Unit. The MU is removed from the aircraft for transfer to the ground station.
- List of acronyms:
  - FEMS
    - » Airborne Data Acquisition Computer (ADAC)
    - » Engine Monitoring Signal Processor (EMSP)
    - » DSU (Data Storage Unit)
    - » Fault Maintenance Indicator (FMI)
    - » linear accelerometer for Nz (g) at c.g. of aircraft
  - SDRS
    - » Signal Data Converter (SDC)
    - » Recorder Converter / Memory Unit (RC/MU)
    - » Accelerometer (Nz, Nx and Roll Acceleration)

EVENT TRIGGERS

PEAK/VALLEY TRIGGER	RANGE	DEAD BAND		RISE / FALL VALUE
•Normal Acceleration (Nz)	-3.0g to 10.0g	0.0 g to 2.0 g		1.0 g
•Roll Rate (P)	±250 deg/sec	±30 deg/sec		20 deg/sec
•Differential Stabilizer (left horizontal stabilizer - right horizontal stabilizer)	±24.0 deg	WS < 30°	±3.0°	2.0 deg
		WS 30°-50°	±4.0°	1.0 deg
		WS > 50°	±2.0°	0.5 deg

WS = Wing Sweep Angle

AIRBORNE DISCRETE TRIGGERS
•Angle of Attack Increases through 6, 8, 10, 12, and 14 deg
•Maneuver Flap Position (SDRS)
•Continuation Records (regular intervals)
•Transition Events (to / from ground mode)

GROUND EVENT TRIGGERS
•Takeoff
•Landing
•Touch-and-go

- For the F-14 tracking system, data is recorded only when structurally significant events occur. There are three basic type of events that trigger data recording. In airborne mode, there is "peak/valley" triggering and "discrete event" triggering. And there are ground event triggers.
- The most critical structural event for fatigue tracking is Nz peaks and valleys. The F-14 uses a deadband of 0 to 2.0 g's and a rise/fall criteria of 1.0 g to trigger data recording.
- In addition, there are maximum left and right roll rate triggers and maximum left and right delta between horizontal stabilizers triggers.
- The airborne "discrete events" that trigger data recording include
  - the transition of Angle of Attack (AOA) through 6, 8, 10, 12 and 14 deg,
  - a change in maneuver flap position,
  - continuation records at regular intervals,
  - and transition to and from ground mode conditions.
- Angle of attack triggers are required because peak load at a critical location can develop before peak Nz. This is due to wing stall which can occur because of the unique swing wing configuration of the F-14.

RECORDED PARAMETERS

KINEMATICS

- NORMAL ACCELERATION (Nz)
- WING SWEEP ANGLE
- ALTITUDE
- ANGLE OF ATTACK
- MACH NUMBER
- FUEL REMAINING
- LEFT HORIZONTAL STABILIZER
- DIFFERENTIAL HORIZONTAL STABILIZER
- RUDDER POSITION
- PITCH RATE
- ROLL RATE
- ROLL ACCELERATION

DISCRETES

- Maneuvering Flaps
- Main Landing Gear
- Weight on Wheels

STORES

- Recorded in FEMS
- None in SDRS

- These are the structurally significant parameters recorded with every airborne record written to the storage unit, with the Nz being the most important.
- The data is transferred to an engineering facility via ground station.

FATIGUE ALGORITHM

- **Data Quality Control**
- **Sequential Load History**
  - **External loads**
  - **Transfer functions for critical location strains**
- **Grumman local strain method**
  - **Cyclic stress/strain curves, strain cycling**
  - **Neuber's equation**
  - **Rainflow method of cycle counting**
- **Residual stresses and rainflow across flights**

- When the data is received at the engineering facility, it first goes through a series of quality control procedures. Data that is deemed correctable is fixed, usually in a conservative manner.
- Then the data is converted to a sequential load history for that flight. This is done by first converting the recorded parameters for each event into external loads on the aircraft. External loads, which include wing pivot shear, bending and torsion and aft fuselage bending, are formulated by computing the inertia portion of the load separately from the air load and adding them together.
- The external loads are then converted into a strain using a quasi-regression technique that calculates strains at discrete wing sweep positions and interpolates between wing sweeps.
- In this manner a sequential strain history file is created for each tracking location. The Grumman local strain method is then used to convert these histories into fatigue damage for the given flight. This method incorporates cyclic stress/strain curves with strain cycling concepts and uses Neuber's equation. The rainflow method of cycle counting is used and residual stresses and rainflow counting is maintained between flights.

TRACKING LOCATIONS

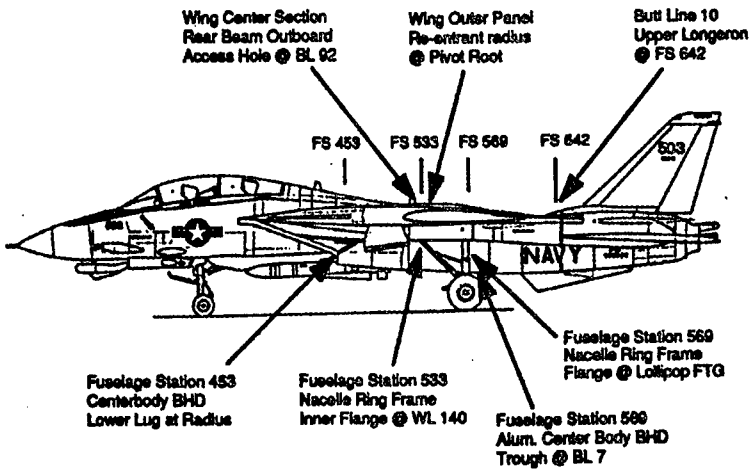

- These are the locations that are currently tracked on the F-14 aircraft. They are primarily wing interface and aft fuselage locations.
- These locations were determined from an extensive Fatigue Life Evaluation and Enhancement Team (FLEET) effort. They are derived from fatigue test article cracks, known fleet cracks, or are analytically determined from finite element model results in conjunction with flight test loads.
- The locations are tracked for scheduled maintenance activities and inspections and major structural life enhancements as well as aircraft retirement. The most critical location can vary with differing aircraft usage.

FEEDBACK / REPORTING

- **Feedback**
  - **Data recovery rates**
  - **Monthly aircraft usage**
- **Usage Studies**
- **Structural Appraisal of Fatigue Effects**
  - **Defines structural life**
  - **Issued quarterly**

- The final aspects of the fatigue tracking system are feedback to the fleet and reporting of results. Monthly reports of data recovery rates and individual aircraft usage are supplied to fleet representatives.
- Because the flight data is stored in a database for easy access, usage studies can be performed on aircraft, squadrons, time periods, etc.
- The final outcome of the tracking system is the SAFE report. Issued quarterly, it is the document which defines the fatigue life expended on each aircraft. This is the document that the fleet uses to schedule aircraft structural modifications and retirements.

RESULTS

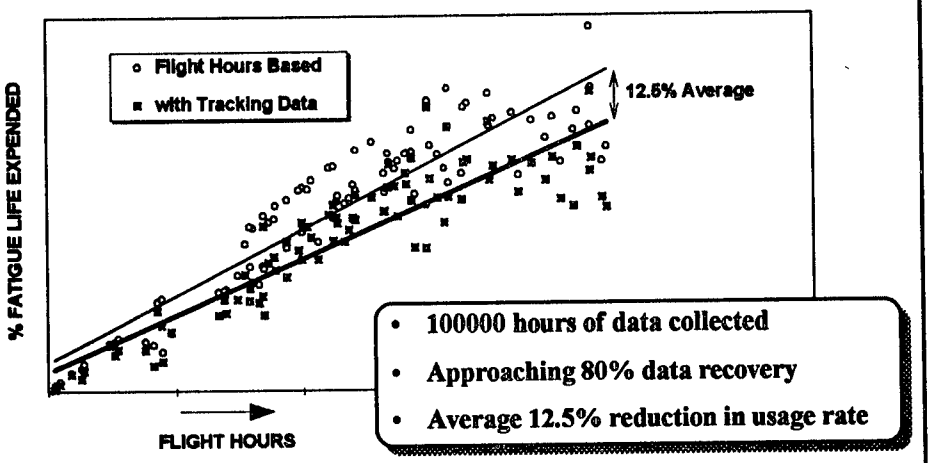

- The primary thrust of the F-14 fatigue tracking system is to obtain as much flight data as possible, reducing the need to replace untracked aircraft flights at conservative statistical levels. The F-14B and D community is now recovering near 80% of the flight hours flown. Dick will discuss the many steps we have taken to achieve this data recovery in his lessons learned.
- Through these efforts, the F-14 community has been able to significantly improve the useful life of our fleet. Through collecting over 100000 hours of data on the F-14B and D aircraft, we have increased the available flight hours for each aircraft an average of 12.5% so far. This translates into an additional 1 1/2 to 2 years of operational use for each aircraft saving many hundreds of millions of dollars in new aircraft costs.

F-14 FATIGUE TRACKING - LESSONS LEARNED

Lessons Learned in Improving Data Recovery

- Fatigue Data Recorders
  - Avionics
  - Ground Stations
- Fleet Interface
  - Aircrew
  - Maintainers
- Summary

AVIONICS

- **We have found advantages and disadvantages to built-in and retrofit Flight Data Recorders (FDR's). Recall that the F-14 program has both:**
  - **FEMS is built into the F-14B/D**
  - **SDRS is retrofit into the F-14A**
- **When tempo of flight operations restricts maintenance, the built-in systems are better maintained since some parameters are mission essential.**
- **One significant disadvantage to built-in systems is that upgrades are very expensive.**
- **Piratization of computing or storage capacity can occur.**

- We have found advantages and disadvantages to built-in and retrofit FDR's. Recall that the F-14 program has both:
  - FEMS is built into the F-14B/D
  - SDRS is retrofit into the F-14A
- When tempo of flight operations restricts maintenance, the built-in systems are better maintained since some parameters are mission essential.
  - Engineering requirements do not always coincide with operational commitments.
  - However, if you can provide something back, like identifying overstresses, then those sensors are better maintained.
- Upgrades on retrofit systems are less programmatically complicated, so it's easy to modify characteristics of individual channels.
  - A distinct disadvantage to built-in systems is that upgrades are very expensive, and take a long time to field. Consequently, a cost-benefit analysis for something simple to improve data recovery and data quality may show the change is cost prohibitive.
- Be wary of piratization of computing or storage capacity.
  - By virtue of being on the aircraft, you are vulnerable to other systems sharing your computing or storage capacity.
  - More likely to happen on a built-in system, as has happened with our FEMS system.

GROUND STATIONS

- **It is impossible to develop ground stations that keep pace with technology.**
  - **NAWCAD Lakehurst suggests planning for hardware obsolescence every 6-7 years, and on-board software changes every 3 years.**
  - **Design with the best technology available, by time system is ready for release, the hardware is affordable.**
  - **Don't lock system design to prevent upgrades and enhancements.**

- It is impossible to develop ground stations that keep pace with technology.
  - NAWCAD Lakehurst suggests planning for hardware obsolescence every 6-7 years, and on-board software changes every 3 years.
    - » The problem is not that the existing ground station cannot meet it's requirements, it's that there comes a time when you cannot get spare parts to keep the machines running
    - » Software support is a continuing requirement for the ground station since on-board software changes are inevitable.
  - Consequently, when you are developing a new system, design it with the best technology available, by time system is ready for release, the hardware is affordable.
    - » There is always that reluctance to use state-of-the-art hardware at the outset of a program.
  - Don't lock system design to prevent upgrades and enhancements.
    - » We've seen where obsolete hardware and operating systems have to be maintained because of the expense of porting to new systems. This means we have to live with work-arounds, which degrades performance and ultimately the data recovery suffers.
    - » One thing that will help is to use commercial off-the-shelf (COTS) hardware and software that is upward compatible where practical, which was not an option 10 years ago.

GROUND STATIONS
Man/Machine Interface

- **Design the system to give the operator the minimum amount of work and training required, while still giving enough information to correct instrumentation problems.**
  - **Assignments are generally collateral duty in a variety of environments.**
  - **Training should be developed, but the best systems can be learned through pass down and on-the-job training.**
  - **Best systems have routine procedures.**
  - **Quality control should be built in to flag aircraft instrumentation problems, and provide data to aid troubleshooting.**

- Design the system to give the operator the minimum amount of work and training required, while still giving enough information to correct instrumentation problems.
  - Assignments are generally collateral duty in a variety of environments.
    - » It is difficult to get manpower dedicated to one system with current budgetary constraints.
    - » The system must go on detachments and deployments, so it must be either portable or transportable.
  - Training can be developed, but the best systems can be learned through pass down and on-the-job training.
  - Best systems have routine procedures.
    - » FEMS data is downloaded at the end of the fly-day.
    - » SDRS data download is tied to 10-hour engine oil sample maintenance action.
  - Quality control should be built in to flag aircraft instrumentation problems, and provide data to aid troubleshooting.
    - » Avionics built-in-test will not catch all of the problems.
    - » Use technical manuals to troubleshoot the problem based on the data provided by the ground station.

AIRCREW

- **Operation of the FDR's are transparent to the aircrew.**
- **What is important is have a working knowledge of aircrew regulations, procedures, routines, and rituals.**
  - **The FDR should be designed with normal operating procedures in mind.**
  - **Knowing the normal operating procedures can help in performing quality control on the recorded data.**

- Operation of the FDR's are transparent to the aircrew.
  - The only exposure to the FDR is a pilot-initiated "data save" for recording engine events on FEMS, and overstresses.
- What is important is for the systems engineers to have a working knowledge of aircrew regulations, procedures, routines, and rituals.
  - The FDR should be designed with normal operating procedures in mind.
    - » We had a problem early on with FEMS where we did not capture flights where they were practicing landings and not raising the landing gear.
  - Knowing the normal operating procedures can help in performing quality control on the recorded data.
    - » The best example of this is we use a neural network to replace invalid wing sweep angle data.

MAINTAINERS

- **Maintainers are a critical element to a successful fatigue tracking system.**
  - **They operate the ground station, they check to see that the data is correct, and they correct instrumentation problems when they occur.**
- **The tools they need are:**
  - **Logistics -- training, publications, supply support, etc.**
  - **Tech Reps -- technical representatives provide training and assistance in troubleshooting.**
  - **Feedback -- we provide data receipt feedback to provide visibility and to correct deficiencies.**

- Maintainers are a critical element to a successful fatigue tracking system.
  - They operate the ground station, they check to see that the data is correct, and they correct instrumentation problems when they occur.
- The tools they need are:
  - Logistics -- training, publications, supply support, etc.
  - Tech Reps -- technical representatives provide training and assistance in troubleshooting.
    - » Tech reps are subject matter experts on the aircraft and FDR's.
    - » They provide continuity with large turnover typical of military environment.
  - Feedback -- we provide data receipt feedback to provide visibility and to correct deficiencies.
    - » Since fatigue tracking is more important at higher levels than squadrons, visibility up the chain of command encourages squadron support.

THE FOCUS...

The critical element to data recovery can change with program maturity. For the F-14 experience,

- **In Infancy, the focus is on:**
  - **Updating hardware and software to correct problems, then maintaining supply support of updated hardware.**
  - **Developing procedures, training, and technical publications.**
- **Later, the focus is on:**
  - **Keeping up with training and fleet feedback.**
  - **Keeping ahead of hardware and software obsolescence.**

The critical element to data recovery can change with program maturity. For the F-14 program, we have that experience in bringing an infant system to to maturity --

- We've done it with FEMS
- We're doing it with SDRS

- In Infancy, the focus is on:
  - Updating hardware and software to correct problems, then maintaining supply support of updated hardware.
  - Developing procedures, training, and technical publications.
- Later, the focus is on:
  - Keeping up with training and fleet feedback.
  - Keeping ahead of hardware and software obsolescence.

SUMMARY

- **The basis of the F-14 Fatigue Tracking Program is a parametric based system that gives point-in-the-sky, sequence accountable information that allows us to safely maximize the life of each aircraft.**
- **We've realized an increase in aircraft life through a high data recovery rate.**
  - **Intense scrutiny on design and upkeep of the avionics and ground stations.**
  - **Close contact with fleet administration, the Tech Reps, and where practical, the maintainers themselves.**

- We tried using an approach where there is little to no impact on the maintainers.
  - An agreement on the A-6 SDRS development was for a once per month download.
    - » SDRS replaced the Counting Accelerometer Postcard, which was a once-a-month odometer-style reading.
    - » Introducing a more labor-intensive FDR was a tough sell when squadron resources were dwindling.
- We rely on total involvement of the whole team. Once they learned the value of FDR's for enhancing the fatigue life of their airframes, they came to us with suggestions to improve data recovery in spite of the increased manpower requirements. They keys are:
  - Close contact with fleet administration, the Tech Reps, and where practical, the maintainers themselves.
  - The maintainers are a critical member of the team.
    - » Give them the tools to effectively do their job.
    - » Remind them that their efforts are important.

CAE

ACHIEVING AN INTEGRATED USAGE BASED MAINTENANCE PROGRAM FOR THE CANADIAN FORCES C-130

by
Mr. Tim Padfield
CAE Aviation Limited
&

Captain Arnold van den Hoeven
DTA 3-3-2
Department of National Defence

1996 USAF ASIP Conference - 3-5 December 1996

CAE

Presentation Outline

- **CF C-130 Fleet**
- **C-130 ASIP**
- **CF C-130 Management Challenges**
- **Current ASIP Initiatives**
  - SSI Database
  - DART and DAM
  - Data Analysis System
- **IAM**
- **Conclusions**

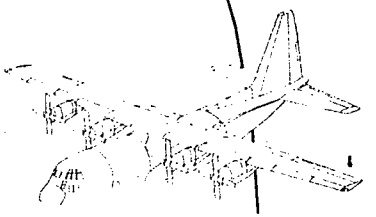

CAE

CF Fleet

- **Current fleet consists of 6 subfleets : E, H, H73, H84, H90, H30**
  - **Age: new H-30 to 35 year old E models**
  - **AF hours : from 0 to 40 000**
  - **Role: transport, SAR,tanker**
  - **Environment: salt water, UN humanitarian aid (unpaved runways)**

CAE

C-130 ASIP

- First DADTA report prepared by Lockheed for CF in 1981 for E Model Outer Wings
- Subsequent DADTA's prepared for Fuselage & Empennage (1983), Center Wing (1984) and H-Model Outer Wing (1989)
- CF collected registering accelerometer exceedance data from 1966 - 1994
- CF began collecting OLM/IAT data in January of 1996

CAE

C-130 ASIP (Cont)

- **CAE Aviation Ltd provides the ASIP contractor support**
- **Current ASIP related initiatives include:**
  - Continued development and updates to Structurally Significant Item database
  - 3rd line damage and repair tracking initiatives
  - Data Analysis and Mapping tools
  - OLM/IAT data reduction and Data Analysis System development

Current Fleet Management Challenges

CAE

- Management of mixed fleet inspection requirements, spares and configurations
- Varied Role by Model (eg. SAR E-Model)
- Single inspection program for fleet.
- Economic Life Expectancy currently planned for 2010 (?????)
- Long term parts supportability issues ie, T56 and APU etc.

HISTORY OF OUTER WING LOWER SURFACE SEVERITY FACTORS

CAE

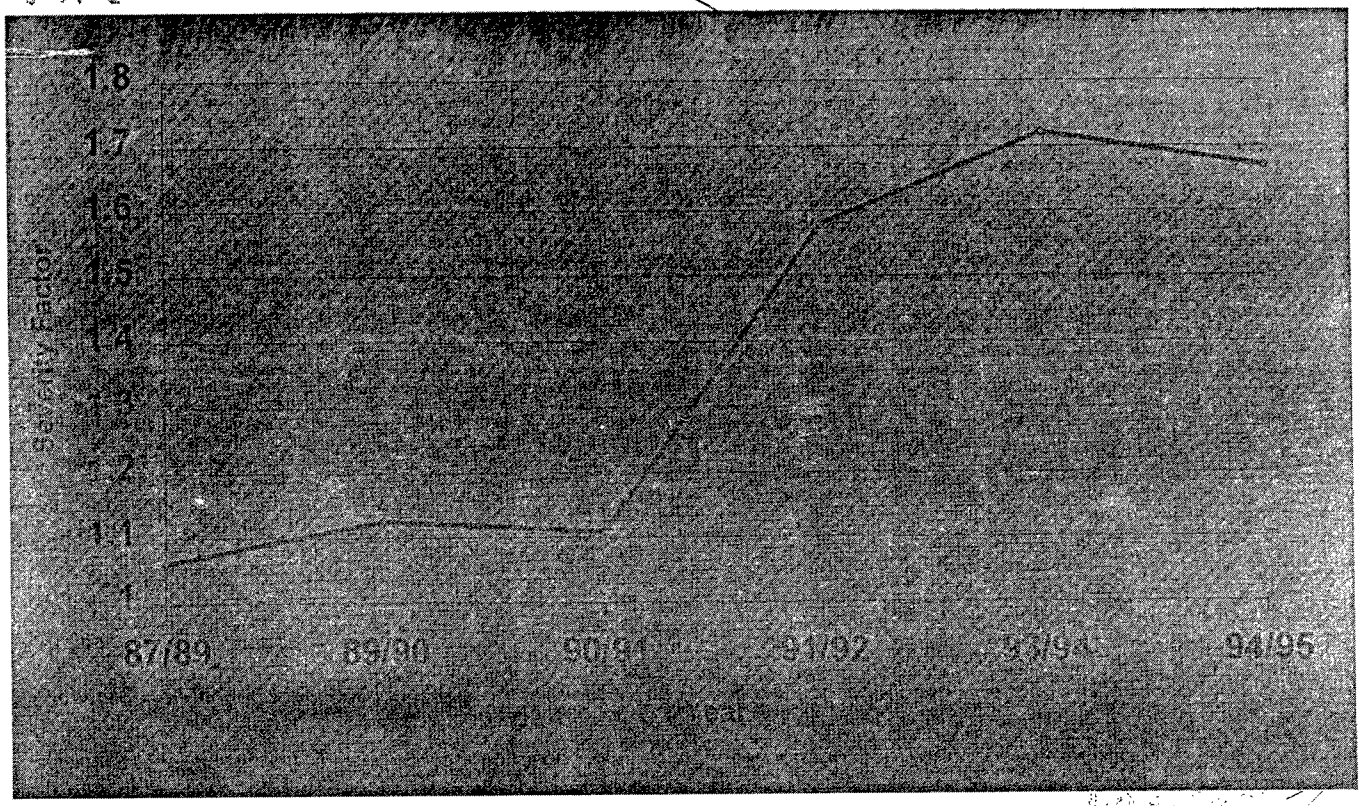

Structurally Significant Item CAE Management

- **Aging aircraft require accurate historical engineering data**
- **SSI database organized to present**
  - critical location details and effectivities
  - fully rationallized inspections and effectivities
  - parts information, background and effectivities
- **allow greater flexibility to manage mixed fleet spanning over 4 decades of C-130**

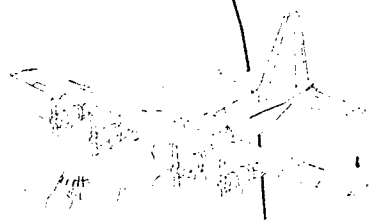

CANADIAN FORCES

PERIODIC AND PROGRESSIVE STRUCTURAL INSPECTION TABLES

CARD NUMBER:
CARD DECK:
PHASE:
LACATION:
INSPECTION ITEM:
AREA
WORK UNIT CODE:
WUC DESCIPTION:
GUIDELINE
NOTE
FREQUENCY:

MAPPING CO-ORDINATES

X1 · X2
Y1 · Y2
Z1 · Z2

PREDECESSOR CARDS | ITEM

SUCCESSOR CARDS | ITEM

CONCURRENT CARDS | ITEM

RATIONAL

SOURCE ID	SOURCE REF.	INSP TYPE	FREQUENCY	DETAILS
SOURCE 1:				
SOURCE 2:				

DRIVING CRITERIA

MAINTENANCE SPECIFIC: ☒
USAGE: ☒
SEVERITY: ☒
FLIGHT TIME: ☒
BASELINE HOURS:
CALENDAR: ☒
CALENDAR INT.:

CONFIGURATION SPECIFICS

NO ☒

YES ☒
TAIL NUMBER:
PART NUMBER:

A/C TYPE

E ☒ H73 ☒ H ☒
H84 ☒ H90 ☒ L100 ☒

GENERAL NOTES:

DIAGRAM

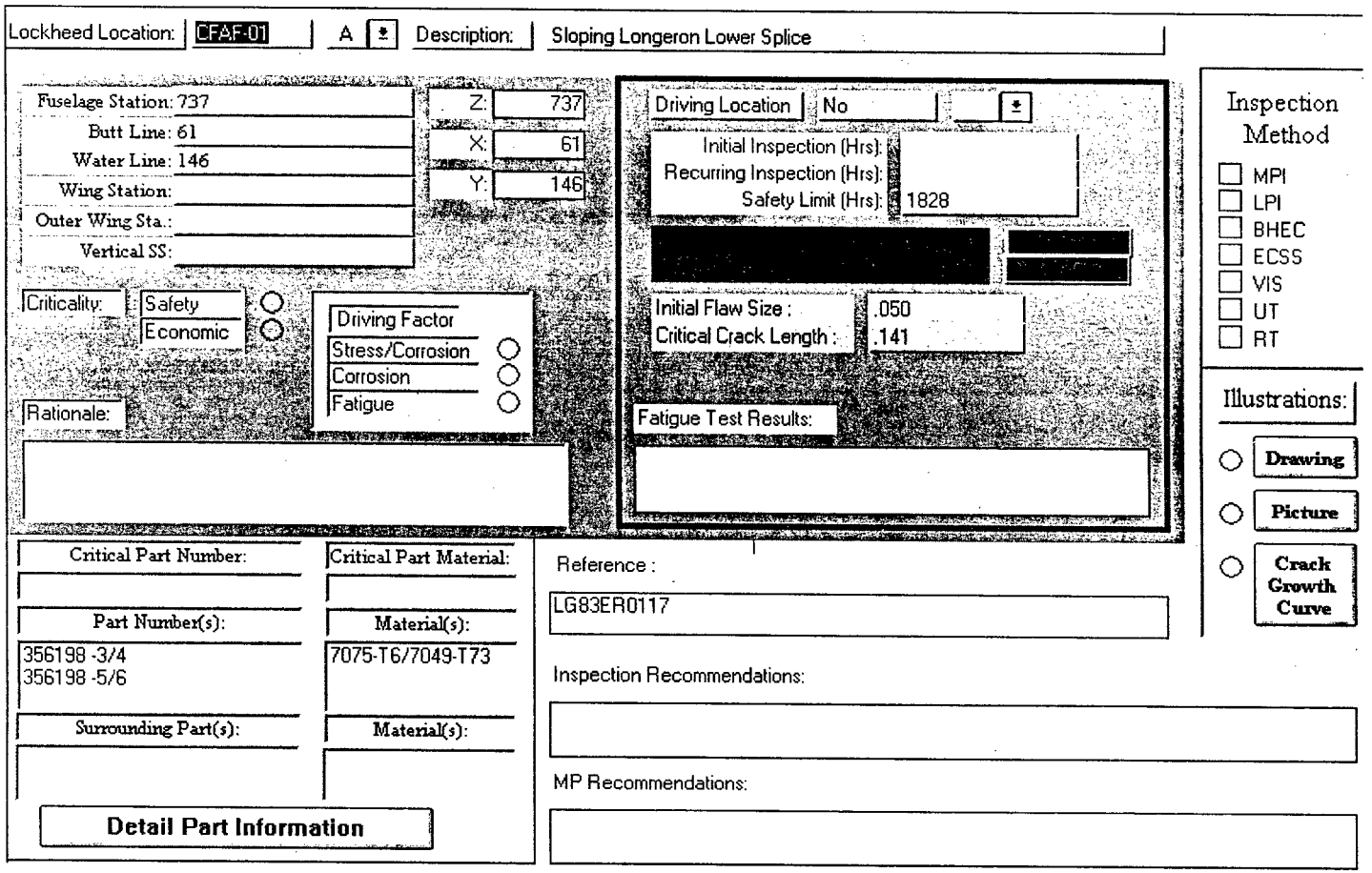
Lockheed Location: CFAF-01
A
Description: Sloping Longeron Lower Splice
Fuselage Station: 737
Butt Line: 61
Water Line: 146
Wing Station:
Outer Wing Sta.:
Vertical SS:
Z: 737
X: 61
Y: 146
Driving Location No
Initial Inspection (Hrs):
Recurring Inspection (Hrs):
Safety Limit (Hrs): 1828
Initial Flaw Size : .050
Critical Crack Length : .141
Fatigue Test Results:
Criticality:
Safety
Economic
Driving Factor
Stress/Corrosion
Corrosion
Fatigue
Rationale:
Inspection Method
MPI
LPI
BHEC
ECSS
VIS
UT
RT
Illustrations:
Drawing
Picture
Crack Growth Curve
Critical Part Number:
Critical Part Material:
Part Number(s):
Material(s):
356198 -3/4
356198 -5/6
7075-T6/7049-T73
Surrounding Part(s):
Material(s):
Detail Part Information
Reference :
LG83ER0117
Inspection Recommendations:
MP Recommendations:

In-Service Structural Data

CAE

- CF has been collecting maintenance data for over 25 years - Highest time military C-130 operator
- *Challenge:* Rapid manipulation and interpretation of data to enhance fleet management decisions
- Under the auspices of the ASIP, tools have been developed to query and display archived structural data
- Fostering International cooperation through universal protocols

Damage and Repair Tracking

CAE

- Captures all relevant data uncovered during depot level maintenance
- Provides details necessary for engineering analysis ie location/severity/images etc
- Includes primary, secondary, tertiary structure, repair or replacement costs etc.
- Serves as the primary data source in CF Data Analysis and Mapping program
- Planned to include 1st and 2nd Line data

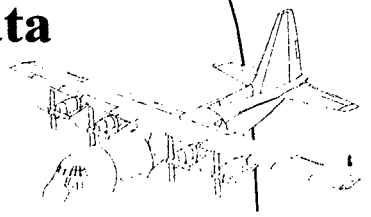

CAE CAE Aviation Ltd.

Damage and Repair Data Entry

Tail No: 324 | AC Hours: 34408.0 | Entered By: Sunitha Zacharia

Tag Number: 12-021-10-3 | Inspection Date: 01-Jun-95 | Date: 28-Jun-95

Damage Type: Pitting/Surface corrosion | Severity: Minor

Locations

FS: 0517
WL: 0146
BL: 0061R

- [x] Part info completed
- [x] Illustration included
- [x] NDT required
- [x] NDT completed

X: 61
Y: 146
Z: 517

Part Number: 389692-2

Depot Card Number: AF-132

Serial No. :

Field Card Number:

Serial Hours:

Classification Of Structure: Primary

Description Of Problem: End bulkhead fitting has several areas of pitting corrosion on the aft face of the fitting. Mating parts were also found corroded. All the parts were not wet installed originally which contributed to the corrosion.

Resolution: Aft face of the fitting was blend out to remove corrosion and surface was kept planar . Blendout limits were within the values specified by CFTO C-12-130-000/VC-001. Reference shop query C130-PSI-047-95

Rectification: Repair / Replace

Replacement Part Number:

Replacement Part Serial Number:

Related Tech Data: C-12-130-000/VC-001, Fig 4-3-8.

Tranform to (X,Y,Z)

CAE

Data Analysis

- **Data Analysis & Mapping**
  - Uses CF maintenance and various engineering data
  - Can include other user data for comparitive analyses
  - Allows visual representation for MSD, WFD and corrosion
  - Integrates failure data, FST results, inspection requirements, DADTA results into a single 3D relational environment
  - Capitalizes on current object oriented technology

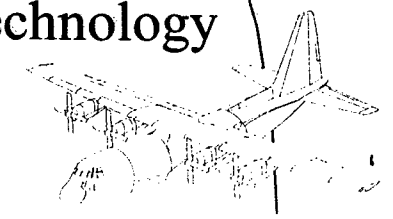

CAE

Data Analysis & Mapping

- **Couples 3D mapping tool & database technologies**
- **Essential that 3d coordinates, P/N and damage categories be used and be consistent!!!!**
- **Gives the user a powerful tool that can be used to quickly perform**
  - Comparitive searches
  - Statistical investigations
  - 3 dimensional mapping for trend analysis or inspection effectiveness evaluation

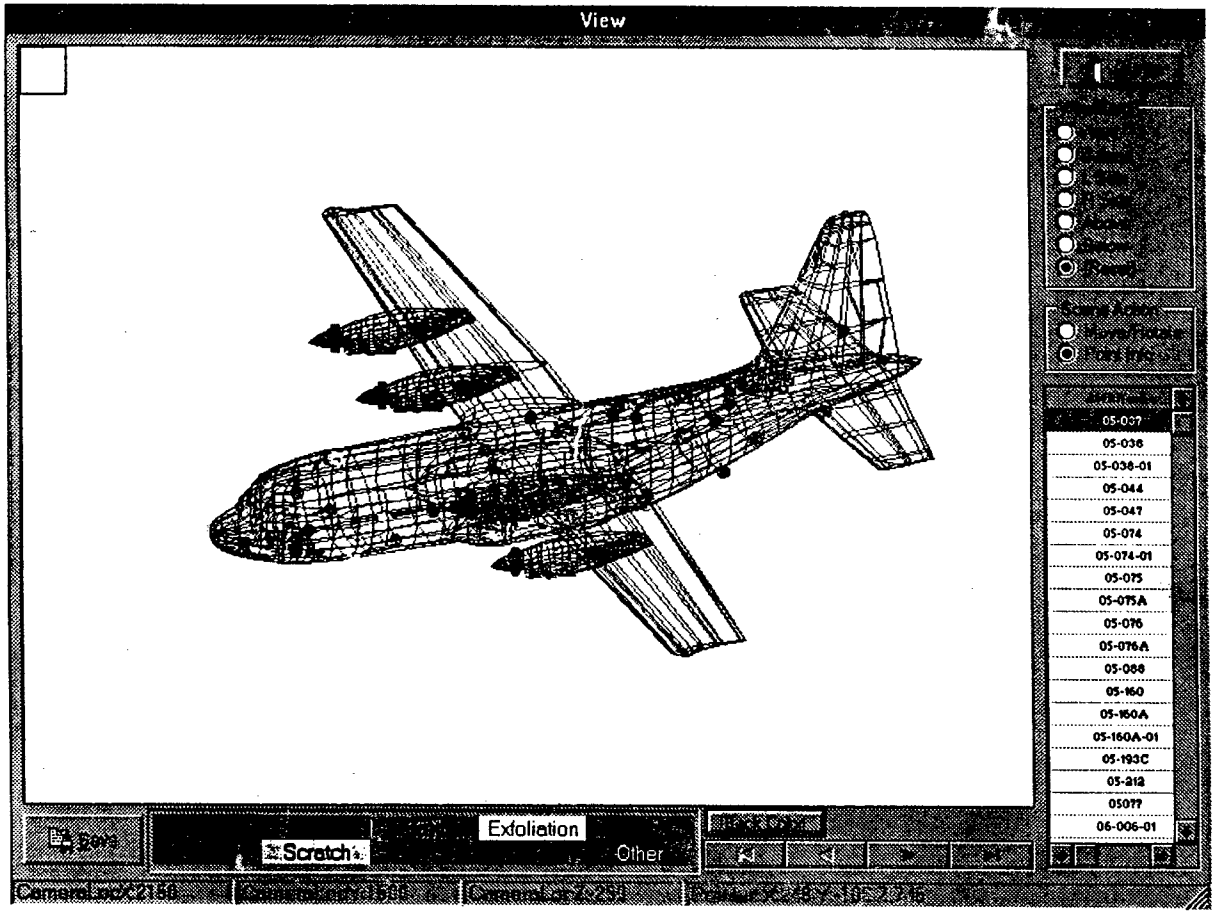
View
05-037
05-038
05-038-01
05-044
05-047
05-074
05-074-01
05-075
05-075A
05-076
05-076A
05-088
05-160
05-160A
05-160A-01
05-193C
05-212
06-006-01
Exfoliation
Other

CAE

DAS

- **Data Analysis System**
  - analyse OLM/IAT flight files
  - present fleet management information
  - allow IAM management
- **Data Input and Sources**
  - VGH (entire fleet)
  - strain gauges (5 locations - 8/30 aircraft)
- **Ouput Features and Capabilities**

CAE

DAS Modules

- **File Processing**
  - Mission Mix, Data Integrity, Data Screening, Mission Profile Validation
- **Loads**
  - Spectra Development, FE, VGH transfer fn
- **Crack Growth**
  - Comparitive incremental crack growth to evaluate severity factor from Lockheed derived baseline

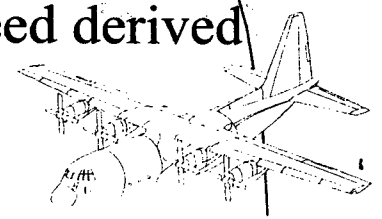

CAE

DAS Modules (Cont)

- **Usage Severity and Mission Data Modules**
  - Usage severity will be tracked by equivalent baseline hours
  - Inspection requirements adjusted for SSI database based on individual aircraft effectivity
  - Flight files mission mix used to evaluate crack growth model approach and assess retroactive aircraft severity tracking programs

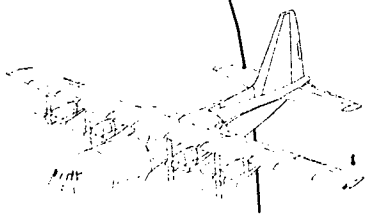

CAE

DAS Modules (Cont)

- **Fleet Management Modules**
  - Provides a comprehensive tool to evaluate current inspection requirements and trends based on OLM/IAT data
- **Integrate with other Fleet Manager Information Sources**
  - DAM
  - SSI

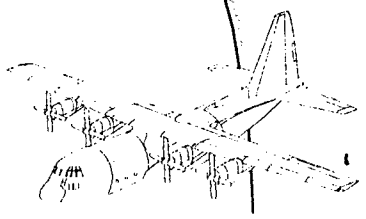

CAE

Individual Aicraft Maintenance

- Tailoring inspection reqmts to sub fleets (model)
- Implementation of Structural Usage Severity factor from DAS to adjust inspection intervals
- Automated inspection card deck (inter-relationships and effectivities)
- Comprehensive tracking system to ensure compliance and evaluate effectiveness

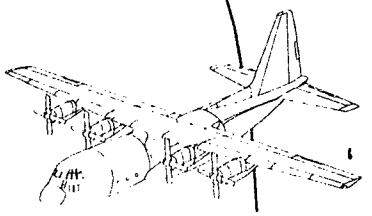

CAE

Conclusions

- **Active ASIP to maximize CC130 ELE**
- **Focus on real time analysis of actual damage data to balance analytical predictions**
  - OLM/IAT
  - DAS
- **Current technology allows low cost tool development**
- **IAM achievable in near term (with management flexibility to implement)**

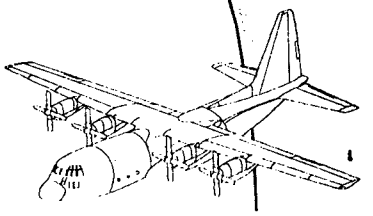

Ageing Aircraft Usage Monitoring in the Royal Australian Air Force

Squadron Leader Mark Wilkin
Flight Lieutenant Doug Keesing
Flight Lieutenant Kim Buhler*
Royal Australian Air Force
Aircraft Structural Integrity Section
Logistics Systems Agency
RAAF Williams
LAVERTON VIC 3027
AUSTRALIA

Synopsis

This paper will describe recent work that the Royal Australian Air Force (RAAF) has undertaken on improving usage monitoring on its fleet of ageing aircraft. The paper briefly outlines where usage monitoring fits into the RAAF Aircraft Structural Integrity Program (ASIP) and why usage monitoring is now the subject of increased attention. The paper then provides cases studies based on P-3, F-111 and B707 aircraft.

For each aircraft type, the following elements are discussed:

a. the basis of ASIP management,

b. how usage monitoring fits into the ASIP,

c. the short comings of the existing usage monitoring program, and

d. improvements to the usage monitoring system.

Introduction

The Royal Australian Air Force (RAAF) has developed a range of programs to manage the structural integrity of aircraft in both RAAF and Australian Army inventory. The specifics of each program are generally unique to an aircraft type, however, each program does accord to the same generic principles. The Aircraft Structural Integrity Program (ASIP) subsumes the individual aircraft programs and is aimed at managing the structural airworthiness of aircraft such that operations can safely continue until the planned withdrawal dates (PWDs) for the aircraft are reached. This ASIP mission can be viewed in terms of the following constituent elements:

a. To constrain the risk of structural failure, particularly for structure the failure of which would have safety of flight (SOF) ramifications.

b. To implement and assist with asset preservation measures to achieve PWD.

c. To achieve the safety and longevity goals without imparting undue operational or logistical constraints.

Pursuit of the above ASIP goals is accomplished via a range of initiatives, the major foundations of which are as follows:

a. Establish, evaluate and substantiate the structural integrity (airframe strength, rigidity, damage tolerance and durability) of the aircraft structure.

b. Acquire, evaluate and utilise operational usage and aircraft structural condition data to provide continual assessment of the in-service integrity of individual aircraft structure.

c. Provide a basis for determining logistics and RAAF and Army planning requirements (maintenance, inspections, spares, rotation of aircraft, weapon system replacement and future requirements).

d. Provide a basis to improve structural criteria and methods of design, evaluation and substantiation for future aircraft structure.

Consequently, usage monitoring (UM) programs are an integral part of the ASIP and provide feedback on the usage of individual aircraft, and the fleet of an aircraft type, to:

a. assess if each individual aircraft is being operated within the fleet's defined usage spectrum and hence, assess if its certification basis remains valid;

b. enable structural life assessments to be based on actual individual aircraft usage; and

c. provide historical data on which to base predicted usage spectra for future acquisitions.

For aircraft approaching or passed their substantiated life limit, accurate UM is particularly important. Accurate usage data enables accurate determination of the rate of damage accumulation. This can facilitate the calibration of aircraft usage to that used in fatigue test work thereby refining safe-life limits or it can help to accurately define inspection requirements for those aircraft that are managed under the safety-by-inspection (SBI) methodology.

The depth of UM varies from simple parametric approaches, rudimentary on-boards monitoring systems utilising N_z meters, to highly advanced digitally based recording systems with on-board processing capabilities. Historically, the level of UM employed in the management of an aircraft was a function of what technology was relevant to the era of manufacture. Some aircraft were retrospectively fitted with N_z meters and others had parametric based systems developed for their management. However, in recent times, economics has driven the RAAF to revisit UM requirements.

Aircraft structural integrity has been assured in the past through the application of management procedures appropriate to the level of capability of the UM system. Accordingly, there has been a degree of conservatism required when implementing the results of rudimentary recording systems. However, with better recording (whether based on improved systems or simply enhancements to current systems), many of the conservatisms can be relaxed. This provides economic benefit in terms of making full use of available aircraft life. Recognition of this, coupled with the cost and robustness of new UM systems, has prompted the RAAF to upgrade the UM systems on the P3C and F-111 and better integrating UM work on B707 aircraft.

P3 Usage Monitoring

The P3 structure is currently managed on a safe life basis in accordance with the Lockheed developed Service Life Evaluation Program (SLEP). This program was developed as part of a Service Life Extension Program which considered the life limiting aspects of the US Navy P3A aircraft. The study examined both fatigue and corrosion aspects of the ageing P3A. The SLEP was considered successful for the P3A and subsequently extended to include the other P3 models operated by the US Navy (P3B (L&H) and P3C).

The SLEP is a unique structural fatigue life management method that incorporates both safe life (SL) and safety-by-inspection (SBI) management. The SL is based on a Miner's cumulative damage analysis method and the SBI component is based on analytical crack growth calculations. The RAAF SLEP only requires hours, flights and landing values for each mission type flown to calculate the SL; Nz data is not required. The SLEP recommends initiation of a SBI program at 75% of the SL but the inspection program is only valid to the SL. Once the SL is reached, a different inspection program must be developed. Thus the SLEP is only useful up to the SL of the aircraft even though it instigates a SBI program. Although, at the SL the structural condition of the safe life components will be known and a decision to continue operation or retire the structure can be made.

In 1981 the RAAF tasked Lockheed to develop a SLEP for the RAAF P3C aircraft. The RAAF SLEP was based on RAAF Nz data and the US Navy SLEP program. Adjustments were made to account for differences in usage between the two fleet, based on mission profiles and Nz data. By 1989, the RAAF usage had changed such that the SLEP was no longer appropriate. Lockheed was tasked to conduct a second SLEP; named SLEP II. SLEP II only considered the SL analysis component of the SLEP and adjusted the program to account for the changes in usage.

Current usage predictions indicate that the SLEP II SL will be exceeded before the P3C PWD of 2015 and, for operations beyond the SL, structural integrity will be assured using a SBI program. The SBI program will begin with the SLEP SBI program but only to the SLEP II SL. After this, SBI will continue but the program will include all SLEP II safe life structural items and all non safe life structural items that may impact on structural integrity.

Present usage indicates that the SLEP II may be inappropriate for future RAAF P3 structural life management because usage has changed since the development of SLEP II. Consequently the SLEP SBI is also considered inappropriate. To further complicate the issue, the RAAF fleet is about to undergo a significant configuration change that will alter the aircraft center of gravity and usage. The uncertainty in the SLEP, the proximity of the SL, the intention to operate the aircraft to 2015 and the unknown effect of the configuration changes, highlight the need for an omniscient through life fatigue life management system for the RAAF P3 aircraft. This need has resulted in the development of a comprehensive P3 structural life strategy that addresses all the structural integrity concerns associated with the use and operation of the P3 beyond the SLEP II SL. The strategy is made up of three distinct phases:

a. Usage monitoring and SL analysis before the configuration change,

b. Usage monitoring and SL analysis after the configuration change, and

c. Usage monitoring and SBI program development for continued operations.

Phase one will involve the installation of advanced monitoring equipment in two aircraft to record wing strain and flight parameters. The data will be used for mission profile development and SL analysis. All historic data held by the RAAF will be reviewed and combined with the wing strain and flight parameter data to produce a complete structural load history for SL analysis of each aircraft. The SL analysis is expected to be based on a Miner's rule analysis and will follow the SLEP analysis approach.

Phase two will involve the installation of an advanced monitoring system, similar to that of phase one, which will remain installed for phase three and the remainder of the aircraft life. The equipment will be installed in a sample of the fleet such that there will always be four operational aircraft monitored. The equipment will record wing, fin and horizontal tail strains, and flight parameters. The data will be used for SL analysis using the program developed in phase one but modified to account for the configuration changes.

Phase three will involve the development of a complete structural SBI program. The analysis will begin with the identification of all structurally

significant areas and include a structural Durability and Damage Tolerance Assessment (DADTA) to all the SL locations.

To date, the functional specification for the hardware of phases two and three has been developed and the equipment will be installed during the configuration modification program. The functionality of the phase one equipment has also been identified and installation is expected early in 1997. The software and analysis methods for the DADTA have not yet be finalised. The phase three SBI program is anticipated to be fully operational in approximately five years.

F-111 Usage Monitoring

The structure of the F-111 aircraft is managed on the basis of assuring integrity through repeated inspections. This SBI methodology requires the determination of inspection requirements through assessment of the rate of damage accrual. Some assessment is possible via the recording of inspection results, however, predictive methods (for fatigue related damage) are largely based on carrying out crack growth calculations. This necessitates developing stress histories in critical structural locations which, in turn, requires details of aircraft usage.

The current inspection requirements for the F-111 are largely based on the results of a DADTA program based on 1980s operational usage. The UM system employed to collect and collate UM data was comprised of three levels. The first level of recording consisted of manual recording of mission parameters such as flight time, weights, profiles and stores. The second level of recording was based on N_z data collected from meters installed on each aircraft. The third level of recording was accomplished via a broad parametric multi-channel recorder (MCR). This MCR recorded a wide range of parameters that were determined to impact upon structural loads; such as altitude, mach number, wing sweep, etcetera. The MCR was only fitted to four aircraft for a limited period of time (that is, on a survey basis) and the first two levels of recording were required to assemble the MCR data such that it was representative of fleet operations.

The first two levels of UM have continued unabated since the 1980s and these have been used to assess whether there has been significant changes in operations since the DADTA spectra were developed. Indications are that changes have occurred (for example, due to Pavetack operations) and, consequently, the validity of the DADTA results needs to be revisited. To accomplish this, an on-board

parametric recording system is again required, however, the MCR system is no longer supportable and an alternate system is required.

Significant progress was made on acquiring and installing Smiths Industries' Standard Flight Data Recorder, however, a funding shortfall forced the cancellation of the project and funds were redirected elsewhere. Shortly afterwards, the RAAF issued and funded a requirement for all aircraft to be fitted with crash data recorders (CDRs). There is a great deal of commonality with the parameters required by the CDR system and that required by a comprehensive parameter based UM system. Accordingly, and at a fraction of the cost of the SFDR system, a UM system is under development that will 'piggy-back' the CDR. The simplicity of the solution is benefited by the upgrade of RAAF F-111 aircraft to digital based systems and there are only a few analogy signals that require conversion prior to storage on a stand-alone memory unit. At this stage, the UM system will only be fitted to a fleet sample and on-board data compression will be limited. This reflects a staged approach to implementation in which initial costs are being minimised by focusing on the minimum requirements necessary to achieve a capable UM system. This is based on the precept that a limited UM system is better than no UM system.

Concurrent with this work, the RAAF, with the assistance of Aeronautical and Maritime Research Laboratories, is developing and refining methodologies for the use and integration of a strain based UM system. The system consists of ten strain gauges and one N_z channel and is fitted to approximately 30 percent of the fleet. Strain data is currently stored on a unique stand alone recording system, however, the new UM memory unit will be capable of storing strain data thereby facilitating the integration of strain data into the UM system for the F-111 aircraft.

B-707 Usage Monitoring

The RAAF operates a fleet of five B-707-300C aircraft in the passenger and cargo transport roles, for both domestic and international travel. Over 1988 to 1992 four aircraft were fitted with removable wing-tip refuelling pods to provide an air-to-air refuelling (AAR) capability. The AAR role increases the fatigue damage accumulation rate to the wing structure compared to non AAR flights, and the RAAF removes the wing-tip pods when they are not in use. The five aircraft have each accumulated between 19 000 to 22 800 flights and 28 600 to 55 600 air-frame hours. The RAAF plans to retain the B-707s in service until

2010, although this is subject to review pending a life cycle cost review and an investigation into noise abatement.

The RAAF B-707 ASIP relies on compliance with the Boeing system of maintenance together with the Boeing ageing aircraft maintenance requirements. These encompass threshold and repeat inspections in accordance with the Supplemental Structural Inspection Program/Document (SSIP), corrosion prevention and control, maintenance program review, and repair quality assessment. Overlaying these requirements is a RAAF unique management system to account for the impact of AAR on aircraft structural integrity. Additional inspections are made to a set of fatigue critical locations that are unique to the AAR modified structure, and adjustments are made to the SSIP inspection requirements for a group of baseline configuration structural locations that are affected by AAR usage. A separate DTA performed by the AAR modification contractor supports the associated inspection requirements. Other key elements of the RAAF B-707 ASI management philosophy include recording and monitoring the structural condition, monitoring aircraft usage and keeping abreast of world-wide B-707 structural activities.

Historically the B-707 usage monitoring system has recorded limited data (flight hours, full stop and touch and go landings) to support the scheduling of SSIP inspections, as well as recording missions that carry the AAR pods to allow adjustments for the pods affected critical structure based on the actual pods-on usage. Considerable other data has also been recorded (such as take-off weight, fuel weight data, and mission duration), however, it has mostly been used for operational purposes and was not well integrated into the structural management program. In recent years the RAAF has revisited the B-707 structural condition monitoring and aircraft usage monitoring programs. This was considered particularly important for the RAAF B-707s which will soon be amongst the world-wide fleet leader population and which are of a unique configuration (fitted for AAR). Particularly, additional usage data was sought to assess the RAAF usage in comparison to the commercial usage that underlies the inspection program mandated by the SSIP. The data is necessary to validate the adequacy of the SSIP for RAAF operations, and also to provide a basis to rationalise the SSIP inspection requirements according to RAAF usage. Particular differences between RAAF B-707 operations and commercial operations include a higher proportion of aircrew training, different operating weights and air-to-air refuelling tasks.

In early 1996 a contractor was tasked to recommend a service life monitoring program (SLMP) for the RAAF B-707 fleet which encompassed updated usage monitoring and integrated structural condition monitoring. The contract assessed the structural build state of each aircraft, recent usage patterns, existing data recording systems and the adequacy of the AAR structural management system. The outcomes from the investigations proposed a manual entry parametric type recording system to satisfy the flight data and maintenance inspection recording requirements, in conjunction with a computer database information management support system. The latter will likely be provided by an existing third party defence contractor who provides data management services for other RAAF aircraft. The studies also highlighted deficiencies in the AAR management system, particularly in the area of the assumed analytical stress spectra used for the DTA, as well as significant changes to the AAR usage patterns that were not automatically accounted for with the current structural management program. Follow-up activities to instigate the proposed SLMP are current RAAF tasks. The following paragraphs describe the RAAF direction for future B-707 flight data usage recording and structural condition recording, and these changes are expected to be made within the next twelve months.

Flight Data Usage Recording. For structural integrity UM support, RAAF B-707 operations will be categorised into five mission profiles based on flight duration, training, and AAR operations. The five profiles comprise short range transport (less than three hours), long range transport (greater than three hours), training, AAR with fuel transfer and AAR ferry. These profiles will be coupled to a fatigue damage model that will allow the RAAF to relate usage to fatigue damage. It is yet to be decided whether a customised damage model will be developed to suit RAAF B-707s, or whether fatigue damage assessments will be referred to the OEM. An existing Flight Engineer's Log form, which is currently used to record take-off weight and fuel data, flight duration and landing information, will be expanded to include altitude/time data, fuel offload weights, and additional landing data and this document will then become the primary UM recording form. The advantage of using this form is that an new system does not need to be introduced to satisfy the operational data recording requirements. The data from the Flight Engineer's Log will be managed using a computer database and six monthly reports will be raised showing periodic usage results, trends, predictions and variations that are likely to impact upon structural integrity. The data will also allow revisions to the inspection intervals in accordance with individual aircraft usage. Furthermore, the information will make comparative studies with other military B-707 operators feasible.

Structural Condition Recording. Considerable structural maintenance data is already recorded by the RAAF and the primary B-707 depot level maintenance (DLM) contractor (QANTAS); however, this data is not well managed or used. Condition reports are raised after each DLM visit and the intention is that these reports will be enhanced to more clearly report corrosion and fatigue defect and repair data. Furthermore, a manual entry recording system will be introduced to record the inspection results from the ageing aircraft program. Positive and negative defect findings will be recorded. These reports will form the basis for on-going structural condition assessments.

Conclusion

The RAAF in the process of enhancing ASIPs for ageing aircraft each aircraft through incorporating improvements to usage monitoring. The objectives of this effort are to support safe, efficient operations until the aircraft PWDs, as well as providing data for new aircraft acquisition. There are various levels and types of UM systems employed in each aircraft type depending upon the associated structural integrity management programs. They range from simple manual entry parametric systems to fully automated flight parameter and strain based systems. The P3C, F-111 and B-707 aircraft are examples of ageing aircraft in the RAAF inventory that are receiving considerable attention and enhancement in usage monitoring. These initiatives are expected to mature on these aircraft within the next few years to better support the life management for each aircraft fleet.

L. Molent
Task Manager
Airframes and Engines Division
Defence Science and Technology Organisation
Aeronautical and Maritime Research Laboratory
PO Box 4331, Melbourne Victoria
Australia 3001

SYNOPSIS

A REVIEW OF A STRAIN AND FLIGHT PARAMETER DATA BASED AIRCRAFT FATIGUE USAGE MONITORING SYSTEM

In the current environment of decreasing budgets, the need for an accurate and reliable fatigue usage monitoring system is of ever increasing importance to ensure the safe and economical utilisation of aircraft, which are now expected to last much longer than first envisaged. Strain based in-flight data recorders are perceived to provide an increase in accuracy over the conventional fatigue *g* meter, and have thus been implemented worldwide by many military fleet operators. Although this may be the case, these new generation recorders and the systems required for fatigue damage interpretation are complex, and many problems can arise with their use.

The Royal Australian Air Force use a system which utilises seven strain sensors and multiple flight parameters to monitor the usage of their F/A-18 fleet. A review of the integrity of the fatigue monitoring system has resulted in several suggestions for improving its accuracy.

This paper addresses the generic findings of this review and presents lessons learnt which should be considered in the implementation of fatigue monitoring systems. Areas covered include problems associated with the positioning of the strain sensors, in-flight sensor calibration and drift, sensor bi-linearity, calibration of damage models against durability test results, and data validation. The reliability of strain sensors and the effects of overloads on life predictions are also considered. The findings discussed in this paper can significantly effect the fatigue damage calculation procedure, regardless of the quality and type of the recorder in use.

1. Introduction

In the current environment of decreasing budgets, the need for an accurate and reliable fatigue usage monitoring system is of ever increasing importance to ensure the safe and economical utilisation of aircraft, which now are expected to last longer than ever. Strain based in-flight data recorders are perceived to provide an increase in accuracy over the conventional fatigue *g* meter, and have thus been implemented worldwide by many military fleet operators. Although this may be the case, these later generation recorders and the systems required for fatigue damage interpretation are complex, and many problems can arise with their use.

In common with other F/A-18 operators, the Royal Australian Air Force's (RAAF) principal tool utilised for managing the life of the F/A-18 aircraft, is a system developed by the aircraft's manufacturer, McDonnell Douglas Aerospace (MDA), known as the Maintenance Signal Data Recording System (MSDRS). The MSDRS utilises seven strain sensors and multiple flight parameters to monitor the usage of individual F/A-18 aircraft. The MSDRS also performs other functions including engine health monitoring. The system used to interrogate the data and calculate individual aircraft fatigue accrual has undergone several iterations since its conception. These iterations have evolved from improvements suggested by MDA and the aircraft's structural integrity managers.

As part of this evolution, a recent intensive review of the integrity of the current fatigue monitoring system was conducted by DSTO's Aeronautical and Maritime Research Laboratory for the RAAF and several suggestions were made to further improve its reliability and accuracy.

In-addition to the primary system based on the MSDRS, the RAAF have also developed an alternative method based on Nz or strain exceedances and simple Miner's Rule known as the Mission Severity Monitoring Program (MSMP). In-addition to these two systems the RAAF's F/A-18 fleet is also equipped with a Range-Pair Count (RPC) recording system, manufactured by British Aerospace Australia, known as the Aircraft Fatigue Data Analysis System (AFDAS), which utilises an additional eleven strain sensors. Currently the AFDAS data is not processed routinely.

This paper addresses the generic findings of the review of the fatigue monitoring system and presents lessons learnt which should be considered in the implementation of any fatigue monitoring system. Areas covered include problems associated with the positioning of the strain sensors, in-flight sensor calibration and drift, sensor bi-linearity, calibration of damage models to durability test results, and data validation. The reliability of strain sensors and the effects of overloads on life predictions are also briefly considered. The issues presented can have a significant effect on the fatigue damage calculation procedure, regardless of the quality and type of the recorder in use. Further the lessons, derived from F/A-18 experience, are applicable regardless of the aircraft structural integrity management philosophy, namely safe life or damage tolerance.

2. Background

The design specification for the F/A-18 required that the aircraft be designed to achieve a 6000 hour (safe) Life of Type (LOT) to a predefined USN manoeuvre and operational environment. To assist the fleet manager in achieving the required LOT the design authority (USN's NAVAL AIR SYSTEMS COMMAND-referred to as NAVAIR) and the prime contractor (MDA) developed a system of fatigue life monitoring tools. This system has been adapted for use by the RAAF and is known as "the Hornet Maintenance Data and Service Life Monitoring System (MD&SLMS)". The MD&SLMS includes the aircraft's on-board data acquisition system, the MSDRS, the data collection and storage functions, and analysis software derived from the NAVAIR F/A-18 "Structural Appraisal of Fatigue Effects (SAFE)" program. The MSDRS is an omnibus system which records time based data from the aircraft's data bus and strain sensors located such as to be representative of fatigue critical locations in significant structural items throughout the aircraft. The strain sensor locations were chosen to be predominantly sensitive to each component's bending load. Strain data is filtered by a discrimination and deadband criteria before it is recorded in Peak/Valley (PV) format. When a "trigger" PV criteria is met for a particular gauge/sensor, that gauge along with all other gauges, and a limited number of flight parameters, are simultaneously recorded.

The fatigue life monitoring program (SAFE) implemented for the aircraft, compares the usage of an individual aircraft to that of a representative fatigue test article. The test spectrum should be similar to that of operational aircraft spectra. As the aircraft was designed and certified to a safe life philosophy, when the damage accumulated on a particular aircraft matches that calculated to have been imparted to the test article at the completion of testing, with appropriate scatter factors applied, the aircraft is said to have consumed its safe life. The duration of all fatigue tests incorporate an appropriate scatter factor on design life which depends on the design specifications.

The SAFE process calculates a Fatigue Life Expended Index (FLEI) for individual aircraft in the fleet. The FLEI is defined as:

$$\Sigma \text{ (Calculated Aircraft Fatigue Damage) } / SF_1$$

and when

FLEI = Σ(Damage Accrued on Fatigue Test Article at Demonstrated Life)*SF_2 = 1.0, the aircraft is said to have consumed its safe life. Where:

Σ	cumulative sum
SF_2	scatter factor applied to fatigue test result as mandated in the test specification
SF_1	scatter factor applied by the fleet operator (if different to SF_2) For the F/A-18 the relevant fatigue substantiation test is designated as the MDA FT01/ST16/FT93 (referred to here as ST16)

As the structure which primarily governs the safe (or economical) life of the aircraft as currently demonstrated on ST16 test is one of the three centre fuselage aluminium wing

attachment bulkheads, the FLEI calculated from the strain sensor placed at the wing root (WR) titanium lug at fuselage station FS470 (the central bulkhead), to monitor the fatigue usage of the centre fuselage and inner wing, is of primary concern.

In-addition to the primary system based on the MSDRS, the RAAF have also developed an alternative method based on Nz and strain exceedances, and a unit damage matrix based on simple Miner's Rule fatigue damage calculation, known as the MSMP. This is available at squadron level to enable the fleet commander to have ready access to flight usage severity information, to enable them to manage flying severity against a planning limit. The MSMP results are also periodically compared to those from the SAFE system.

In conducting the review, both the SAFE and MSMP systems were investigated.

As indicated the F/A-18 was designed and certified to a safe life philosophy. At the core of the SAFE software, is the MDA sequence accountable fatigue crack initiation module, CRACKI, which includes the use of Neuber's notch stress algorithms, equivalent strain equations[1], hysteresis effects and material fatigue data (for $R = \sigma_{max}/\sigma_{min} = -1$). CRACKI is used to calculate the FLEI. The SAFE and CRACKI processes are described in detail in Ref 1 and 3.

As with other high strength aluminium alloys, the 7050-T74 material used in many F/A-18 components has a critical crack size[2] close to the detectability limits of current NDI techniques and are not manageable on a safety by inspection basis. As such, the aircraft operators require a reliable and accurate fatigue monitoring tool to ensure that the LOT is not exceeded.

The major findings of this review included limitations or deficiencies in the MSDRS parameter data checking routines, in the strain based sequence accountable cumulative fatigue damage model, and in the available coupon test and material data. The findings and the results were documented in Ref 1 and 2. Some of the lessons learnt from this investigation form the basis of this paper, but other observations from F/A-18 related activities are also discussed.

This paper does not distinguish between safe life or damage tolerant philosophies, as both are still used by design authorities and play a role in the fatigue monitoring process. The lessons learnt are applicable to both structural integrity management philosophies.

3. Basis of a Fatigue Tracking System

Once the type of in-flight recorder, the position of strain gauges, and the flight parameters to be recorded have been determined and installed for a given aircraft type, there is still much processing to be conducted before the in-flight data can be used to assess the fatigue usage of an aircraft. It is considered that after data retrieval a fatigue tracking system requires the following capabilities:

[1] Converts cycles at any R ratio, to the equivalent cycle for R = -1

[2] The USN define failure to be when a crack on a critical component/location reaches 0.254 mm

1. Pre-processing of collected data:

A code is required that formats aircraft unique data so that it can be processed. It should provide the capability to identify active sensors, identify missing sensor initialisation and determine data hours (generally from landing and take off codes). It should also provide an option to deal with data recorded out of order.

2. Data Checking Module, which should provide the following functions:

- Extracts strain, flight parameter and Nz data;
- Validates data and eliminates bad data by checking flight parameters;
- Creates PV strain files or other appropriate forms;
- Determines inoperative sensors (by comparing recorded against calculated strain) and creates a sensor log;
- Checks gauge initialisation values;
- Checks for strain data spikes;
- Provides the capability to "fill-in" or compensate for missing or corrupted strain data;
- Calculates *cg* and weight of aircraft accounting for stores configuration and fuel usage;
- Normalises Nz (to test article basic configuration);
- Performs sensor calibration;
- Initialises other flight parameter variables (eg angle of attack);
- Tabulates Nz, velocity and altitude exceedance data;
- Identifies mission types.

3. Sequence Counting Module:

The module is required to build a Rain Flow Counted[3] (RFC) spectrum. Depending on computing capability it may also discretise and block the sequence to optimise processing time.

4. Fatigue Damage Module, which;

Calculates damage and fatigue indices for each strain sensor, based on crack initiation or growth algorithms. It also updates the cumulative "all time" damage database for each aircraft, and should check if the accumulated damage equals FLEI, and warn if the damage rate per 1000 flight hours exceeds a predefined design rate.

[3] Otherwise known as range-pair or hysteresis loop counting

5. Post-processor Module, which;

Updates the database file for each aircraft processed, and updates the documentation file of the current software run. Produces a summary report, which includes all detected data anomalies.

Each of these nominated steps are critical to the estimation of fatigue damage accumulated. The review of the RAAF fatigue monitoring processes identified improvements for each of the above steps, some of which are discussed below.

4. Notes on Strain Sensor Characteristics

4.1 Gauge locations

It can be demonstrated that strain gauge based data recorders have the potential to provide a more accurate assessment of fatigue accrual, than conventional Nz based systems, for high performance aircraft. This is principally achieved because judicious placement of the strain gauges can automatically account for aircraft weight and stores effects, and the variation of principal loads, such as Wing Root Bending Moment (WRBM), at various Points In The Sky (PITS) constituting the flight envelope.

To achieve this benefit the location of the gauges must be carefully chosen. In particular, care must be taken to ensure that the location of the sensor:

- is dominated by the principal damage inducing load (eg WRBM);
- is in an area of low stress gradient;
- can be directly related[4] to the stress at critical structural locations;
- is not prone to gauge "drift" (varying response to a nominal load over time[5], see section 4.3);
- is accessible such that the sensors are readily replaceable; and
- is positioned as close as practicable to a backup sensor in the advent that the primary sensors fails.

Further consideration should also be given to the asymmetric manoeuvres, such as rolls, as these will produce differential loading on the main flying surfaces. This manoeuvre asymmetry is demonstrated in
Figure *1*, where data from four rolling manoeuvres, two rolling pullouts (RPO) and two 1g 360° rolls (ROL), taken from F/A-18 flight trials data reported in Ref 4, are shown.

[4] Preferably providing a linear relationship for both positive and negative loads
[5] F/A-18 WR lugs are an example of this

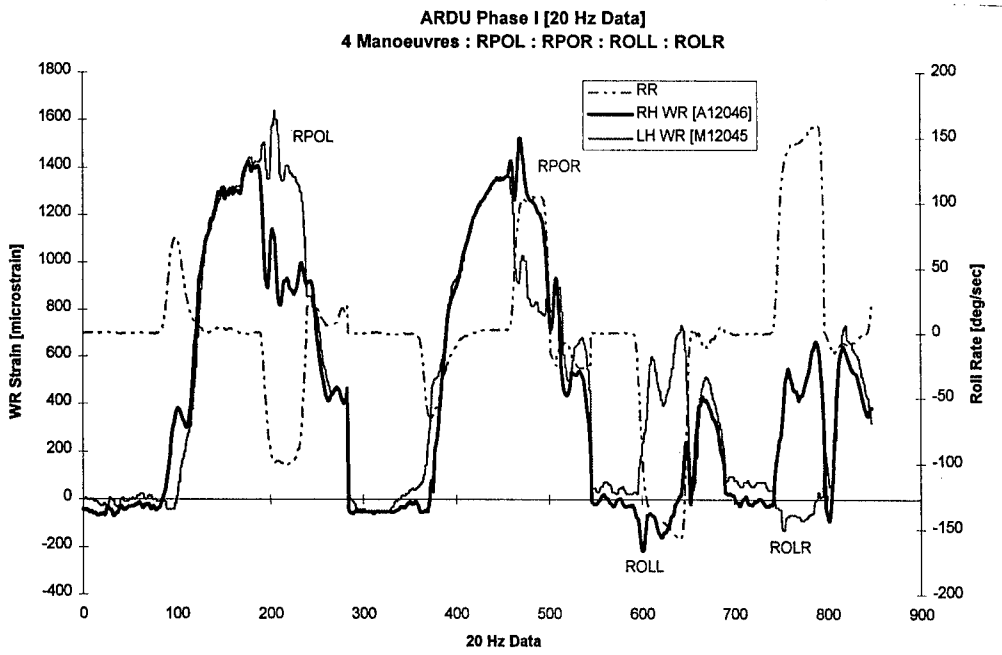

Figure 1: Flight Test WR Strain Time History for Selected Manoeuvres

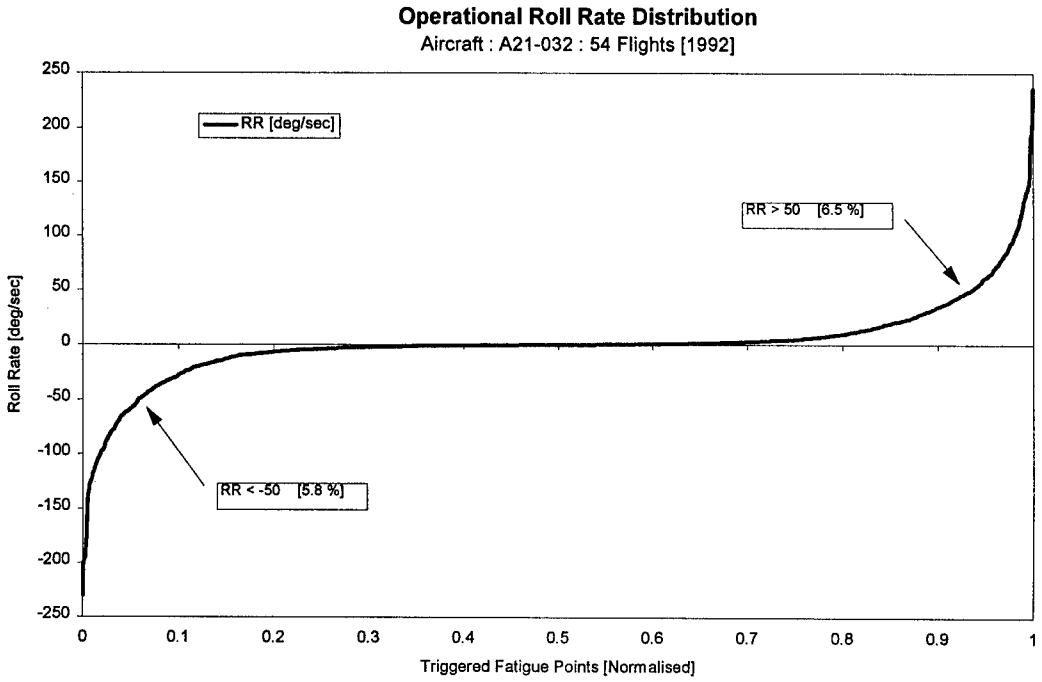

Figure 2: Roll Rate Distribution [Operational MSDRS Data]

From
Figure *1* it can be seen that the right and left wings experience significantly different load maxima and minima during the manoeuvres. A gauge solely on one wing may be acceptable if it can be demonstrated that over time the usage of the wings balances out, for example as

shown for distribution of roll rate from the limited flight trials data (from RAAF A21-032, Ref 4) in Figure 2.

4.2 Sensor Calibration

The fatigue usage of a military aircraft is normally monitored against the damage accumulated on a fatigue test article. Before the strain sensors can be used to assess an aircraft's usage, they must be calibrated such that loading derived from these can be related directly to the equivalent load on the fatigue test article. To verify the fatigue test loading the test article gauges may also have been calibrated against the response of a loads development aircraft. The reasons two gauges placed at nominally identical locations, but on different airframes, may produce varying responses to nominally identical loading, can include slight differences in airframe build quality, slight gauge alignment differences and variations in gauge factors or gauge sensitivity. Multiple load paths in redundant structure may also cause varying gauge response, where differences between aircraft may be "built-in" before delivery.

Great care must be taken when relating the loading from strain measurements from these different airframes. Differences will also arise due to differences in zero strain setting, ie. 1g level flight or pre-take off ground condition, or due to sensor drift or sensor non-linear response.

As it is often impractical to physically ground calibrate every sensor in the fleet, it is normal to rely on in-flight recorded data to relate gauge response between aircraft to the loads on calibrated aircraft. To do this, data recorded at unique PITS which give reproducible values of the principal loading actions are required. For some sensors, namely for gauges on the wing, this is a relatively simple procedure. For the F/A-18, PITS have been identified at which the strain sensor has maximum response to WRBM and is also directly proportional to Nz. These are:

Nz:	3.5, 4.5 and 5.5g ± 0.2g
Altitude:	5000 or 10000 ft ± 1000 ft
Mach No.:	0.80 ± 20 KCAS

From these, PITS relationships between Nz and strain can be determined, which in turn can then be used to scale between WR sensors on different airframes.

In other instances, for example vertical and horizontal tails, the calibration process requires more parameters in order to define unique PITS. Thus a monitoring system which records parameters other than strain is essential to enable scaling factors to be determined. In the case of the F/A-18 Horizontal Tails (HT) and Vertical Tails (VT), analytical techniques have been determined (eg. Ref 5). In order to obtain robust solutions for these structures an order of magnitude increase in the number of data points over that for the wing was required. PITS close to symmetrical conditions are required to provide the data, and these are more difficult to define for the tails than for the wing. The task of identifying these data points would be

assisted if parameters[6], such as rudder and HT deflection, were recorded simultaneously with the sensor strains. However the current MSDRS[7] does not provide this. This requirement would involve an increase in data storage demands, but the benefits would be significant.

Ideally any analytical calibration techniques such as those discussed above should be validated by conducting aircraft ground calibrations on a sample of aircraft prior to routine use.

The recorded Nz is also required to be normalised or corrected with respect to the reference (basic design) gross weight to match the fatigue test configuration.

The lack of parameter information on RPC systems like AFDAS is seen as their major limitation, as it makes the sensor scaling and data validation based on in-flight data alone difficult. An example of a potential method developed for RPC data is described in Ref 6.

4.3 Sensor Drift

Compounding the problem of sensor calibration, is the phenomena experienced by the F/A-18 WR sensors, whose response to specific loads varies over time. This situation is particularly relevant when sensors are placed on lugs.

In the early 1990's *Rider* of AMRL noted a phenomenon occurring to the response of the F/A-18 WR sensor. It was noted when comparing the response of the WR sensor at a "reference" WRBM over different periods of flying for a given aircraft, that it gave different strain values. It was further noted that the response increased over a period of time until a plateau was reached after which point the response remained constant. This became know as WR "drift". This behaviour was subsequently confirmed by MDA and the USN, indicating that it was a "fleet" problem. It is believed that the phenomena is a local effect (in the vicinity of the sensor only) and is due to migration and wear of the bushing within the lug (changes in the lug hole bearing stress). This phenomenon effectively invalidated the calibration values calculated from initial flight data. In turn, the "fatigue life expended" calculated from the WR sensor response was compromised, in many cases conservatively so.

To address this, MDA developed a drift / calibration analytical process[8] (Ref 7), to be used prior to calculating the fatigue life expended. The process can be summarised as follows:

> Once the data files are obtained the strain PV information and flight parameters are extracted at PITS similar to those described earlier. In addition a limitation is also placed on the roll rate allowed, in order to obtain symmetrical manoeuvres.

---

[6] Although beyond the scope of this paper, the HT and VT of the F/A-18 (and other modern fighter aircraft) are affected by high frequency buffet loading. Currently for the F/A-18 the damage induced by buffet is assessed by monitoring time spent at pre-defined angle of attack and dynamic pressure regimes. This further highlights the need for a monitoring system which also records flight parameter in addition to strains.

[7] It does however record these, amongst other parameters, every 5 secs, which is insufficient for this purpose.

[8] An alternative technique was developed in Ref 1.

The expected WRBM is obtained for those selected PITS utilising calibrated flight loads data (requires: weight, altitude and Mach No.). From the WRBM an expected strain is calculated using nominated reference relationship between WRBM and strain. In the F/A-18 case the loads demonstration aircraft data was used.

The ratio between the actual measured strain to expected calculated strain is then the calibration factor for the period represented by the data. Each recorded strain peak and valley are then factored by this value.

Note the above technique simultaneously calculates the amount of gauge drift and its scaling relative to the loads verification aircraft. An example of the WR drift is shown in Figure 3, where the calibration factors were calculated at different cumulative Airframe Hours (AFHRS). Note that the factors are simultaneously calculated for a group of flights, from which the results for the valid PITS are shown at the mean value of AFHRS for these flights in Figure 3.

Ref 1 also documents a discrepancy in the load data used in the above process, in which the maximum WRBM was assumed to corresponded to the maximum Nz. It was shown for the F/A-18 that the two maxima can lag one other by as much as 2 seconds, possibly due to fuselage lift contributions. This discrepancy conservatively effected the calculated fatigue damage by overestimating the sensor drift. Systems in modern military high performance aircraft that rely solely on Nz would experience a similar discrepancy.

Sensor drift is also likely to occur in conventional mechanically fastened aircraft structures where the stiffness is likely to decrease over time as a function of fastener fretting and hole elongation.

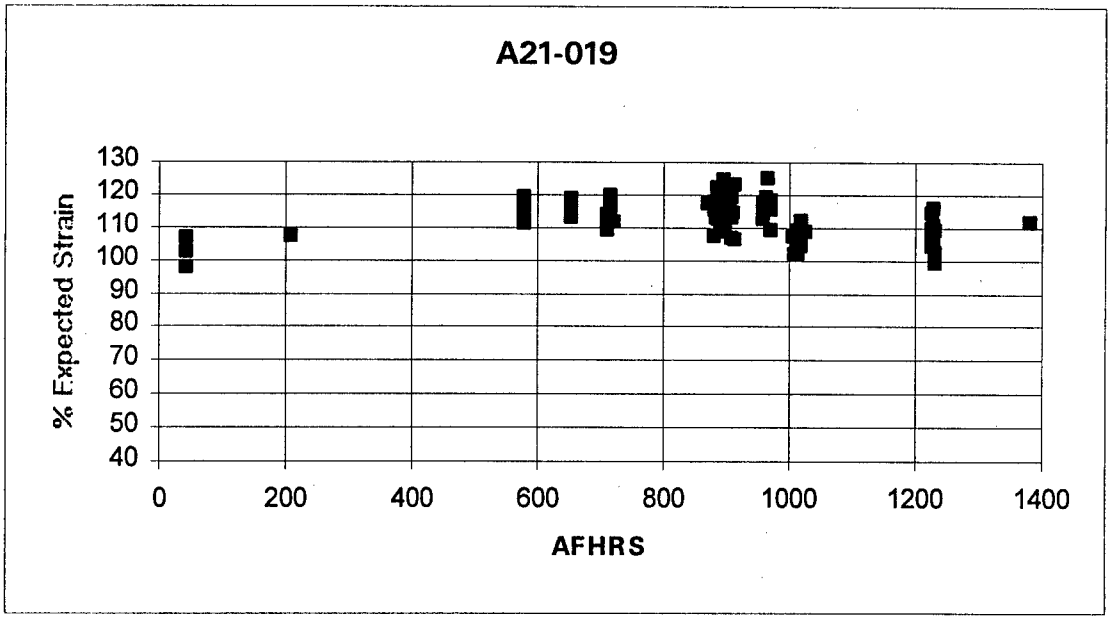

Figure 3: Calculated WR Drift

4.4 Sensor Bi-linearity

The sensor location should be chosen such that the sensor provides a good representation of the principal loading influencing the structural components of interest. Subsequently this gauge can be used to monitor specific locations which are effected by the same loading action.

In the case of the F/A-18 fatigue tracking, it had been assumed in the process that the WR sensor related linearly to strains at critical locations on the centre fuselage bulkheads. Thus strain transfer function relating the WR strain to critical location strains were not specifically needed, as the spectrum normalisation process (described in the following section) would produce the same sequence regardless of the transfer functions used. However, in investigating this relationship between the WR sensor and the bulkhead locations, it was determined that the WR sensor to WRBM response produced a bi-linear ratio between the positive and negative strain ranges and this was reflected in the relationship between the WR strain and the strain at the critical location. An example is shown in Figure 4, using drift corrected ST16 test data for the FS488 bulkhead. When assessing particular locations this bi-linearity must be accounted for, especially when dealing with spectra which contain a significant number of negative load cycles.

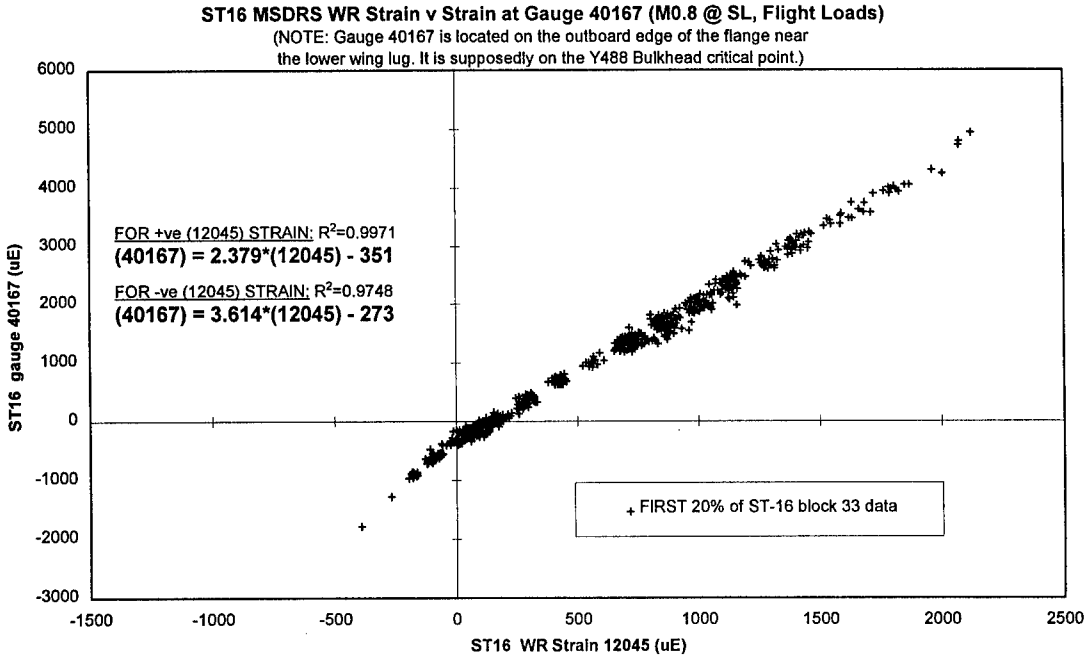

Figure 4: WR MSDRS To Critical Point Strain on FS488 Bulkhead

4.5 Data checking

There are numerous data checks that should be conducted before the recorded fleet data can be used with confidence. Examples include:

- Strain initialisation

- Out of range data
- Sensor health or serviceability
- Missing data
- Strain spiking
- Strain data validity

Of these only strain data validation will now be discussed. In general, when validating strain data, the recorded strain is compared to a calculated value that relies on the PITS flight parameters associated with that strain. In general, simple linear relationships, such as between strain and Nz will not suffice for modern combat aircraft, as loading varies considerably with PITS.

In Ref 8, multiple parameter least squares multiple order equations were developed[9] for the F/A-18 sensors (this was only possible due to the availability of a substantial amount of flight data generated by IFOSTP). The aim of these equations was to predict the strain response of the sensors for a target aircraft to an accuracy of ±5% for all fatigue damaging PITS. For example, the equation developed (from Ref 8) for the WR sensor (valid data range not shown) is:

Positive Nz[10] *(clean stores configuration)*

$$\begin{aligned}\text{Strain} = \; & -134233 + 55.59\times AoA - 7.137\times AoA^2 + 0.2455\times AoA^3 - 0.002954\times AoA^4 \\ & + 39239.9\times CG - 2813.4\times CG^2 + 89.33\times CG^3 - 1.0607\times CG^4 \\ & + 248.9\times Nz + 4.733\times Nz^2 - 0.7931\times Nz^3 \\ & - 228.13\times Q + 30.047\times Q^2 - 1.648\times Q^3 + 0.0312\times Q^4 \\ & + 0.6227\times RR - 0.0152\times RR^2 + 4.372e\text{-}6\times RR^3 + 1.9404e\text{-}7\times RR^4 - 7.8\times GW \\ & + 0.0003242\times GW^2 - 5.926e\text{-}9\times GW^3 + 4.0145e\text{-}14\times GW^4\end{aligned}$$

Where: AoA = angle of attack, CG = centre of gravity position, Q = compressible dynamic pressure, RR = roll rate and GW = gross weight including stores.

From the validation conducted in Ref 8, it was demonstrated that all these flight parameters were required to achieve the required accuracy. The situation is even more complex for empennage sensors, as the following equation indicates (from Ref 8) for a gauge positioned at a vertical tail attachment stub which showed, for a similar level of accuracy, that a fourth order equation of sixteen flight parameters was required:

Strain = *function*[*AoA, CG, LStab, Nz, Q, RR, RRud, RStab, W, RTef, LTef, YR, PR ,M, LAil, RAil*]

Where: L/RStab = left/right stabilator deflection, RRud = right rudder deflection, L/R Tef = trailing edge flap deflection, YR = yaw rate, PR = pitch rate, M = Mach No., L/R Ail = aileron deflection.

---

[9] MDA also developed a series of equations, Ref 3, and have produced load trend "look up tables" for the WR which can also be used.

[10] Number of significant figures shown are considered necessary

As can be seen a significant number of parameters is necessary to achieve the required accuracy. These parameters are available on the MSDRS but not at the required frequency (ideally synchronous with the strain). This currently limits the validation of recorded strains at these locations using this method.

These, or similar techniques, can be used to validate the recorded strain. The importance of achieving good accuracy between measured and predicted values is particularly important with damage models which account for hysteresis effects, such as the Neuber Notch analysis, as unrealistically large strains (data *spikes*) can lead to unrealistic fatigue damage suppression (see material selection, section 4.6.3). This situation can lead to an unconservative estimate of fatigue usage. The techniques can also be used to fill-in for missing or corrupted data. A review of missing data in the RAAF fleet, see Ref 1, indicated that a significant amount, approximately 12%, of data used in the fatigue assessment was based on fill-in techniques. Data fill in options are limited with RPC systems which do not record flight parameters.

A further use of parametric equations is in the gauge scaling process. As the equations are derived for a specific flight trials aircraft, when valid data from another aircraft is input, the difference between the predicted and measured strain is a reflection of the scaling between the two aircraft.

Strain gauges do become unserviceable and their replacement is a significant maintenance burden to the RAAF and other operators. If sufficient flight parameters were recorded at a sufficient frequency by the on-board recorder, then parametric equations of the type shown above could provide a potential alternative to strain based systems.

5. Damage model calibration

The primary purpose of a fatigue tracking system is to compare an aircraft's accumulated damage against the fatigue damage imparted to the test article in the reference fatigue substantiation test. Therefore the fatigue model utilised in the monitoring system must be calibrated to the test result before it can be used. For example, as the required design life for the F/A-18 was 6,000 flight hours, under "severe" USN usage, the crack initiation module CRACKI within the SAFE software was conservatively calibrated by MDA to produce a damage of 1.0 at 6,000[11] spectrum flight hours using the fatigue test spectrum (ST16). The following should be considered in the calibration process.

5.1 Spectra Reference Conditions

In order to determine the relative fatigue damage between an aircraft's usage and the full scale fatigue test spectrum, a reference flight condition is required to relate both spectra to a stress level at the location on the structure at which the fatigue index is being calculated. For example the reference condition (or PITS) chosen for the F/A-18 wing was a 7.5*g* steady state pull-up (SSPU) manoeuvre at Mn = 1.0 at 15,000 ft. From the MDA load demonstration aircraft (F4) flight trials, this condition produced a WRBM of 6,390,000 inlb.

[11] This assumes that all relevant test failure locations are modified to give full life on operational aircraft.

The fatigue test stress life curves for the F/A-18 were established by inputting the ST16 test spectrum through the crack initiation program (CRACKI) and outputting results for a range of design limit stresses (DLS) multiplied by a stress concentration factor (K_t) i.e. K_tDLS. Before the test spectrum is input to CRACKI, in terms of the test target[12] WRBM, it is normalised by dividing by the reference WRBM[13] defined above. The reference stress was then established by entering the calculated fatigue test stress-life curve for the relevant material at the required ST16 test demonstration life of 12,000 hours (i.e. 6,000*SF_2) and reading off the appropriate stress level, see Ref 3.

5.2 Data Processing

When conducting the above procedure it is important that the damage model processes the test data in the same manner as it is intended to process fleet data. In Figure 5, the ST16 test WRBM spectrum[14] has been processed through CRACKI for the WR strain gauge location (titanium WR lug) to illustrate the sensitivity of the crack initiation program to different ways of compiling the WRBM sequence. These include:

- entire spectrum processed on a flight by flight (F by F) or load line by load line (L by L) basis;
- RFC;
- WRBM discretised and blocked;
- processed by blocking the resulting discretised data from highest to lowest amplitude blocks (Hi to Lo);
- the spectrum divided into 10 by 30 hour segments; and
- with the spectrum Ground-Air-Ground (GAG) coupled. A GAG cycle is the coupling of the highest peak stress with the lowest minimum stress within each single flight, with all other PV couplings unchanged.

As can been seen in Figure 5 significant differences in the resulting reference stress can occur. The effect of RFC (or GAG) is also seen to be significant. It has been shown, Ref 1 and 9, by comparing experimental data to fatigue predictions, that the closest agreement is obtained when the spectra are RFC before the prediction is made[15].

[12] Theoretical or desired spectrum to be applied to the test article

[13] Note: this itself induces an error as the WRBM is PITS dependent. However it is considered impractical to normalise to each PITS experienced by the aircraft.

[14] The spectrum consists of 250 individual flights, for a total of 300 hours.

[15] This is also the case for crack growth predictions for short cracks (Ref 9).

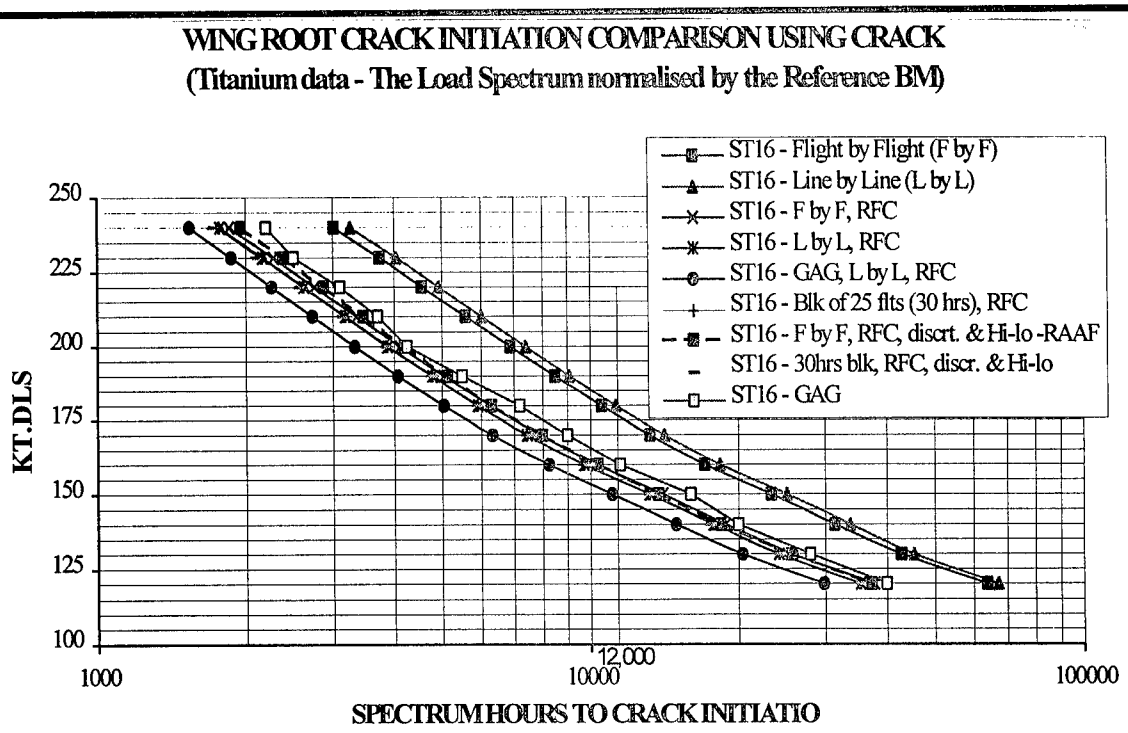

Figure 5: Various Data Processes for ST-16 Spectrum

5.3 Material Data

The choice of material fatigue data is also an important consideration in the calibration process. For modern aircraft which have highly optimised structures, it is possible that many locations will determine the LOT. Therefore it may be attractive or economical to assume that a sensor placed at one location can be used to monitor significant portions of the airframe, assuming that each has been tested to the same severity, by calculating fatigue damage based on material data relevant to that sensor location. For example, fatigue analysis using material relevant to the F/A-18 WR sensor location, the titanium wing lug, was used initially to monitor both the inner wing and centre fuselage bulkheads and frames. However, this assumption is invalidated with the use of fatigue models that attempt to account for material hysteresis[16], in particular the effect of plasticity on suppressing fatigue damage[17] or crack growth, since hysteresis is material dependant. For instance, if titanium fatigue data was used, and the aircraft loading caused the model to predict that the local notch stress had exceeded the plastic limit, it would then effectively process subsequent cycles about a mean compressive residual stress. This would produce a reduction in subsequent tensile cyclic amplitude and lead to a calculated suppression of damage. This may lead to significantly unconservative predictions of damage at locations fabricated of other material, eg. aluminium[18]. The location which experienced the most significant damage during fatigue testing should determine the choice of material fatigue data used.

[16] Material hysteresis models can also be used for RFC systems, as long as the data is collected on a flight by flight basis, as sequence effects within a flight are not considered significant.
[17] Literature reviewed in Ref 1 produced conflicting evidence as to whether this is a permanent effect or not.
[18] Ref 1 demonstrates that hysteresis effects are more marked for titanium than aluminium.

The choice of material may also produce conflicting predictions of the severity between spectra. Two relatively severe F/A-18 usage spectra, SPEC1 and SPEC2, have been compared to the ST-16 design spectrum, for titanium and aluminium fatigue data respectively in Figure 6 and Figure 7. From these two figures it can be seen that the relative severity of the two usage spectra in relation to the design spectrum are significantly changed between the two materials.

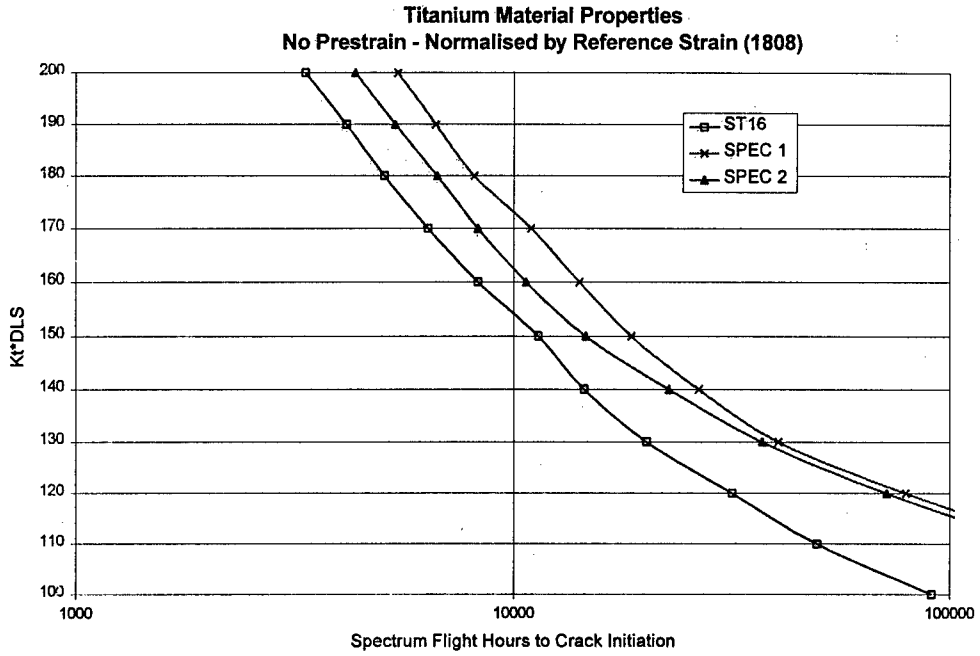

Figure 6: Comparison of Spectra - Titanium Fatigue Data

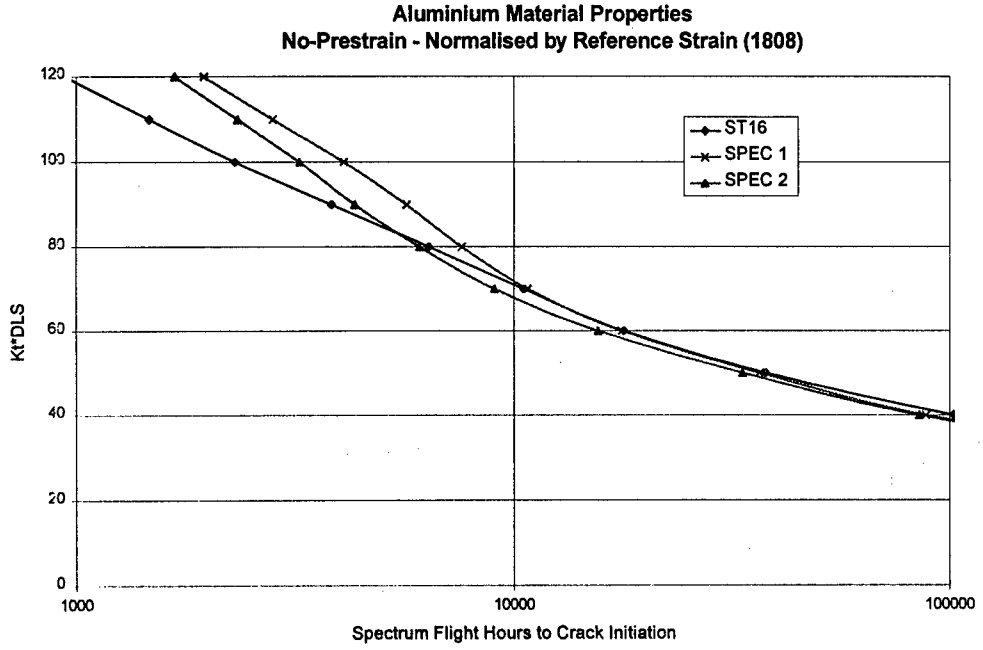

Figure 7: Comparison of WR Strain Spectra - Aluminium Fatigue Data

5.4 Fatigue Test Interpretation

Once the crack initiation model has been calibrated to match the fatigue test result it is important that all fleet spectrums are processed in an identical manner. As stated earlier the damage model for the F/A-18 was calibrated using the target test WRBM. However, WRBM is not measured on fleet aircraft, and thus the WR strain data are used to monitor the fleet. In order to be consistent, it is considered that both the fleet and test article should be assessed in the same manner, thus WR strain data should be used for both. Corrections should be made for the sensor characteristics described in Sections 4.2 to 4.4 and the strain sequences should be normalised using appropriate reference strain levels. The following example from the F/A-18 illustrates the care needed in processing the spectra.

For the flight loads demonstration aircraft, zero strain corresponds to zero *g* in-flight and the strain reading at the reference flight condition with a WRBM of 6,390,000 inlb is 1,808 με. For the ST16 test article zero strain corresponds to zero WRBM, and the strain reading at the reference flight condition is 1717 με. The strain recorded at the reference condition is referred to as the reference strain. In each case the zero strain offset should be taken into account and the strain signals normalised to provide a value of unity at the reference flight condition. Figure 8 illustrates the substantial errors which can arise in the crack initiation curves when the strain sequence is normalised with the incorrect reference strain.

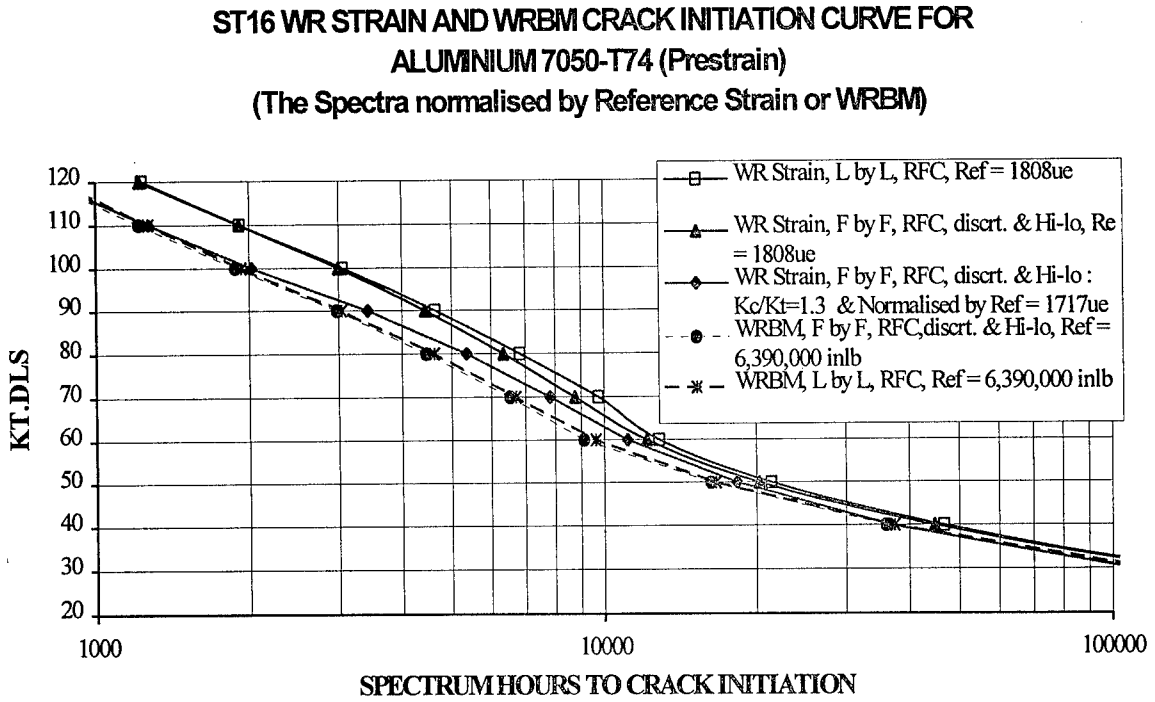

Figure 8: ST-16 WRBM and WR Strain Data Comparison

In Figure 8 the life curves generated for the ST-16 WRBM and WR strain spectra are shown normalised by 6,390,000 inlb and 1808 με, along with the case that the WR spectrum has

been normalised with a reference strain of 1717 με and account has been taken of the bi-linear response of the gauge[19].

5.5 Model Validation

Before the damage model is used to assess fleet aircraft, it must be validated against available fatigue test data, in order to ensure that the model can accurately scale between spectra of varying severity and that it is capable of reasonably reproducing the test results in terms of either total life or crack growth. In the case of the CRACKI model this validation was done using limited coupon test results, for spectra of incremental varying severity, see Ref 1. The model should also be validated using test results for spectra of significantly varying severity.

Finally, the predicted reference stress should also correlate well with the maximum stress experienced at the fatigue test failure locations. It can be shown (in Ref 1), that the reference stress obtained from Figure 8, using the strain spectrum normalised by 1717 με and corrected for bi-linearity, agrees well with that measured at the critical location on the ST16 test article.

6. Conclusions

This paper discussed some of the significant issues arising from a review of the RAAF's F/A-18 fatigue monitoring system. Although it cannot be claimed that these are original or unique findings, and are not only restricted to the RAAF's system, they have been presented here in an attempt to aid a fatigue manager in defining a reliable and accurate tracking system. Not only is the design of the data recording system important, but similar consideration needs to be given to the complexity and effort required before the data can be used (post-processing) to assess the fatigue usage of an aircraft.

In summary, the issues and observations presented in this paper were:

1. Choice of strain sensor location is critical. The location should respond predominantly to the principal damaging load, be in a low stress gradient area, should be capable of accounting for asymmetric flight conditions, should not be subjected to sensor drift and should be readily replaceable.
2. Fleet strain sensor responses are required to be normalised against the response of the sensors on the fatigue test article being used for damage comparison,
3. Sensor calibration and correcting for drift can be achieved if sufficient in-flight recorded flight parameters are available,
4. Maximum Nz does not always relate to maximum bending moment,
5. If the fatigue strain sensors experience a bi-linear response at a critical location, this needs to be accounted for in the damage calculation,
6. The fatigue damage model needs to be carefully calibrated against the fatigue test result, using the same process intended for processing fleet data, and using fatigue material data

[19] This is conveniently accomplished in CRACKI by setting the flag kc/kt equal to the ratio of the positive and negative slopes. For the case of the critical FS488 bulkhead this was set equal to 1.3.

relevant to the most critical location. The model must also be validated against fatigue test results for spectra of varying severity. Care must be exercised when determining reference conditions to be used to normalise spectra. Changes in gauge initialisation conditions can lead to different reference strain values between test articles and flight aircraft,

7. Several data checking processes are require to validate the recorded data. Spurious data, such as strain data spikes, can lead to a significant and unconservative suppression of damage, when using sequence accountable damage models, and
8. As strain gauges become unserviceable in a service environment, therefore a fatigue monitoring system requires several flight parameters recorded synchronously with the strain data, to validate the data, to perform sensor scaling and for filling in of missing or corrupted data.

Even though the simplified systems have only been briefly mentioned in this paper, an important lesson from the review is that to investigate the performance of a complex or sophisticated fatigue tracking system, a simplified system should also be maintained in order to monitor the main monitoring system.

6. Acknowledgments

The author wishes to acknowledge the individual contributions of the members whom contributed to the review which partially lead to this paper, namely: the RAAF Aircraft Structural Integrity Section, DSTO's F/A-18 Life Assessment Task and IFOSTP, and Hawker de Havilland Ltd Victoria. In particular the contributions of Messrs D. Graham and R. Ogden are acknowledged.

7. References

1. Molent, L. and Ogden, R. (editors), " Review of RAAF F/A-18 Structural Appraisal of Fatigue Effects (SAFE) Version 112, Vol. 1, DSTO-TR-0381 (in press).
2. Aktepe, B., "Review of RAAF F/A-18 Structural Appraisal of Fatigue Effects (SAFE) Version 112, Vol. 2: Review of F/A-18 Mission Severity Monitoring Program", DSTO-TR-0381, Aug 1996.
3. Adams, P.S., Keys, G.S II, Schutte, R.E. and Smith, D.J., "F/A-18 Hornet Structural Appraisal of Fatigue Effects (SAFE) Software Manual - Final Report", MDC B2027, MDA, Oct 1990.
4. Molent, L., Aktepe, B. and Polanco, F., "F/A-18 Airframe Fatigue Data Analysis System Validation", ARL-TR-54, DSTO, Melbourne, Jan 1994.
5. Molent, L., Ogden, R. W. and Ooi, Y. Guan, "Development of Analytical Techniques for Calibration of F/A-18 Horizontal Stabilator and Wing Fold Strain Sensors", DSTO-TR-0205, Jul 95.
6. Walker, K. and Molent, L., "Development of an Automated Procedure for Correlation of Two Sets of Range Mean Pair Fatigue Sensor Data", **Proc. of USAF Structural Integrity Program Conference, San Antonio, TX, 6 - 8th. Dec. 1994**

7. FLTLT T. Bueker, "Wing Root Strain Gauge Calibration Program - Evaluation and Recommendations for Modification", RAAF, ASI1A-HQLC, March 1993.
8. Molent, L., Ogden, R.W., Polanco, F. and Ooi, Y. Guan., "Development of Parametric Strain Equations for Fatigue Sensors on the F/A-18", DSTO-TR-0140, Melb, Aust, Jan 1995.
9. Finney, J.M. and Denton, A.D., "Cycle Counting and Reconstitution, with Application to Aircraft Fatigue Data Analysis", Int Conf on Fatigue of Engineering Materials and Structures, Univ of Sheffield, **Proc of Inst Mech Eng, Vol 1**, Sept 1986, pp 231-240.

1996 USAF Aircraft Structural Integrity Program Conference

FINAL ATTENDANCE LIST

MR JAMES ABEL
RAYTHEON E-SYSTEMS
PO BOX 6056 CBN 192
MS 192
GREEENVILLE TX 75403-6056
PH:(903)-457-7708 Fax:(903)-457-4888

MS LEIGH ALTMAN
BELL HELICOPTER TEXTRON INC
FATIGUE ANALYSIS
PO BOX 482
FT WORTH TX 76101-0001
PH:(817)-280-5662 Fax:(817)-280-8772

MR NOBORU ARATA
JAPAN DEFENSE AGY
DEPT OF 3RD RSCH CTR
1-2-10 SAKAE-CHO
TATHIKAWA TOKYO JAPAN 190-0001

DR JOHN BAKUCKAS
FAA DEPT OF TRANS
MC AAR 430 BLDG 210
WILL J HUGHES TECH CTR
ATLANTIC CITY NJ 08405-0001
PH:(609)-485-4784 Fax:(609)-485-4569

DR THEODOR BEIER
MCDONNELL DOUGLAS AERO
DEPT 341N M/S S102-2147
PO BOX 516
ST LOUIS MO 63166-0516
PH:(314)-232-0634 Fax:(314)-234-8915

MR RONALD BIRDSEYE
LOCKHEED MARTIN AERO SYS
C-130 STRUCTURAL INTEGRITY
86 SOUTH COBB DR
MARIETTA GA 30063-0001
PH:(770)-494-3100 Fax:(770)-494-9610

MR JOHN ALCOTT
ARINC
2551 RIVA RD
ANNAPOLIS MD 21401-0001
PH:(410)-266-4472

MR ROBERT ANDREWS
UDRI
M/S CSC-201
300 COLLEGE PARK
DAYTON OH 45469-0120
PH:(513)-229-4417 Fax:(513)-229-3712

MR ROBERT BADER
CONSULTANT
1613 KINGSWAY DR
XENIA OH 45385-9589
PH:(513)-255-0193 Fax:(513)-255-3740

MR DALE BALL
LOCKHEED FT WORTH CO
M/Z 2846
PO BOX 748
FT WORTH TX 76101-0001
PH:(817)-777-3760 Fax:(817)-777-2115

MR ROBERT BELL
LOCKHEED MARTIN AERO SYS
DEPT 73-25 ZONE 0160
86 S COBB DR
MARIETTA GA 30063-0160
PH:(770)-494-5600 Fax:(770)-494-9610

MR EDWARD BITTEL
ROYAL AIR FORCE
RAF WYTON
HUNTINGDON CAMBS PE17 2DL-0001
PH:(071)-305-6688 Fax:(071)-305-6653

MR RUSSELL ALFORD
US AIR FORCE
WR-ALC/LJLE
270 OCMULGEE CT
ROBINS AFB GA 31098-1646
PH:(912)-926-9146 Fax:(912)-926-9142

MR CHARLES ANNIS
PRATT & WHITNEY
M/S 707-22
PO BOX 109600
W PALM BEACH FL 33410-9600
PH:(407)-796-6565 Fax:(407)-796-7454

MR ASAD BAIG
CAE AVIATION LTD
EDMONTON INTL AIRPORT
EDMONTON CANADA T5J-2T2
PH:(403)-890-6300

DR ASIT BASU
UNIV OF MISSOURI-COLUMBIA
DEPT OF STATS
222 MATH SCIENCES BLDG
COLUMBIA MO 65211-0001
PH:(573)-882-8283 Fax:(573)-885-5524

MR STANLEY BERKLEY
FATIGUE MGMT ASSO
1000 N US HWY
MS #615
JUPITER FL 33477-4481
PH:(407)-743-0600 Fax:(407)-743-6777

MR M THOMAS BIVINS JR
MCDONNELL DOUGLAS CORP
M/S C052-0225
2401 E WARDLOW RD
LONG BEACH CA 90807-4418
PH:(310)-593-2902 Fax:(310)-982-5164

MR ROBERT ALLEN
LOCKHEED MARTIN AERO SYS
DEPT 73-51 M/S 0484
86 S COBB DR
MARIETTA GA 30063-0001
PH:(770)-494-5991 Fax:(770)-494-2028

MR HANS ANSELL
SAAB MILITARY AIRCRAFT
SAAB SCANIA AB
MS TUDLB
LINKOPING SWEDEN S 58188-0001

MS DEBORAH BAILEY
US AIR FORCE ASC/SMA
BLDG 16
2145 MONAHAN WAY
WRIGHT-PATTERSON AFB OH 45433-7017
PH:(513)-255-6053 Fax:(513)-255-5105

MR DONALD BEAULIEU
PRATT & WHITNEY
M/S 715-09
PO BOX 109600
W PALM BEACH FL 33410-9600
PH:(561)-796-5979 Fax:(561)-796-5825

DR CATHERINE BIGELOW
FEDERAL AVIATION ADMIN
WILLIAM J HUGHES TECH CNTR
AAR-430 BLDG 210
ATLANTIC CITY INTL NJ 08405-0001
PH:(609)-485-6662 Fax:(609)-485-4569

MR NEIL BLAYLOCK
SOUTHWEST RES INST
BLDG 53
6220 CULEBRA RD
SAN ANTONIO TX 78238-0001
PH:(210)-522-3238 Fax:(210)-522-5606

MR SCOTT BLEDSOE
US NAVY
AV 88 IN SERVICE SUP TEAM
PSC 8021
MCAS CHERRY POINT NC 28533-0021
PH:(919)-466-8517 Fax:(919)-466-8502

DR DAVID BOWLES
NASA LANGLEY RESC CTR
CTO.ASP RESEARCH CTR
6 E TAYLOR ST MS 254
HAMPTON VA 23681-0001
PH:(757)-864-3095 Fax:(757)-864-8291

MR KEVIN BOYD
US AIR FORCE
WL/FIBEC FRACTURE TEST FAC
2130 EIGHTH ST/STE 1
WRIGHT-PATTERSON AFB OH 45433-7542
PH:(513)-255-0434 Fax:(513)-476-7379

MR ELI BRADLEY
FATIGUE MGMT ASSO
71 CRESTWOOD RD
W HARTFORD CT 06107-0001
PH:(860)-521-2075 Fax:(860)-521-2075

MR BRADLEY BRAUN
SYS & ELECTRONICS INC
190 GORDON ST
ELK GROVE VILLAGE IL 60007-0001
PH:(847)-228-0985 Fax:(847)-228-1164

MR CRAIG BROOKS
APES INC
3544 OXFORD AVE
ST LOUIS MO 63143-0001
PH:(314)-644-6040 Fax:(314)-644-0229

MR ABRAHAM BROT
ISRAEL AIRCRAFT INDUSTRIES
DEPT 4441
BEN-GURION INTL AIRPORT
ISRAEL --

MR ALBERT BRUETSCH
USAF SM-ALC
LAFME
5020 DUDLEY BLVD
MCCLELLAN AFB CA 95652-1391
PH:(916)-643-5300 Fax:(916)-643-1405

DR FREDERICK BRUST
BATTELLE
505 KING AVE
COLUMBUS OH 43201-2693
PH:(614)-424-5034 Fax:(614)-424-3457

DR ROBERT BUCCI
ALCOA TECH CTR
100 TECHNICAL DR
ALCOA CTR PA 15069-0001
PH:(412)-337-2671 Fax:(412)-337-5436

MR WILLIAM BUCKEY
US AIR FORCE
2100 MONAHAN WAY
FLIGHT TRAINING SPO
WRIGHT-PATTERSON AFB OH 45433-0001
PH:(937)-255-7076 Fax:(937)-255-8516

MR KIM BUHLER
ROYAL AUSTRALIAN AF
AIRCRAFT STRUCTURAL INT-LOG SYS AGY
RAAF WILLIAMS
LAVERTON VICTORIA AUSTRALIA-3027

MR STEVEN BULLOCK
LOCKHEED MARTIN SKUNK WORKS
BLDG 611-2 DEPT 72-16
1011 LOCKHEED WAY
PALMDALE CA 93599-7216
PH:(805)-572-7808 Fax:(805)-572-7515

MR JAMES BURD
GULFSTREAM AERO CORP
PO BOX 2206
M/S D04
SAVANNAH GA 31402-0001
PH:(912)-965-3591 Fax:(912)-965-4812

MR GARY BURKHARDT
SOUTHWEST RES INC
PO BOX 28510
6220 CULEBRA RD
SAN ANTONIO TX 78228-5166
PH:(210)-522-2705 Fax:(210)-684-4822

DR O HAL BURNSIDE
SOUTHWEST RES INST
6220 CULEBRA RD
SAN ANTONIO TX 78238-5166
PH:(210)-522-2332 Fax:(210)-522-3042

CAPT LAWRENCE BUTKUS
GEORGIA TECH
3819 DONALDSON DR
CHAMBLEE GA 30341-0001
PH:(404)-894-2853 Fax:(404)-853-9140

MR DAVID CAMPBELL
LOCKHEED MARTIN AERO CO
MS 0160
86 S COBB DR
MARIETTA GA 30063-0001
PH:(770)-494-6990 Fax:(770)-494-9610

MR VICENTE CANDELA
SPANISH AIR FORCE
ROMERO ROBLEDO 8
MADRID SPAIN 28008-0001

MR JOE CARDINAL
SOUTHWEST RES INST
6220 CULEBRA RD
SAN ANTONIO TX 78238-5166
PH:(210)-522-3323 Fax:(210)-522-3042

MR DOUGLAS CARMODY
NORTHROP GRUMMAN
PO BOX 9650
M/S H11-223
MELBOURNE FL 32902-9650
PH:(407)-726-7821 Fax:(407)-951-6115

MR YUAN CARON
DIR OF TECH AIRWORTHINESS
101 COL BY
OTTAWA ONTARIO CANADA K1A-0K2
PH:(613)-991-9543 Fax:(613)-998-6922

MR STEVE CHAMBERLAIN
RAF ST ATHAN
NDTS
BARRY
VALE OF GLAMORGAN UK CF624WA-0001

DR CHRISTOS CHAMIS
NASA LEWIS RES CTR
MS 5-11
21000 BROOKPARK RD
CLEVELAND OH 44135-0001
PH:(216)-433-3252 Fax:(216)-433-5802

MR GEORGE CHELL
SOUTHWEST RESEARCH INST
6220 CULEBRA RD
PO DRAWER 28510
SAN ANTONIO TX 78228-5166

MR BRIAN CLINCH
APES INC
3544 OXFORD AVE
ST LOUIS MO 63143-0001
PH:(314)-644-6040

MR THOMAS COOPER
UNIVERSAL TECHNOLOGY CORP
4031 COLONEL GLENN HWY
DAYTON OH 45431-0001
PH:(937)-426-8530 Fax:(937)-426-8755

MR WILLIAM COWIE
GE AIRCRAFT ENGINES
M/D Q105
ONE NEUMANN WAY
CINCINNATI OH 45215-6301
PH:(513)-552-4908 Fax:(513)-552-4921

MR RICHARD DALRYMPLE
NAVAL AIR WARFARE CTR
22541 MILLSTONE RD
CODE 4.1.2.1 M/S 03
PATUXENT RIVER MD 20670-5304
PH:(301)-342-0209 Fax:(301)-342-0227

MR ANTHONY DENYER
ROCKWELL INTL
2600 WESTMINSTER BLVD
PO BOX 3644/MS SL-15
SEAL BEACH CA 90740-7644
PH:(310)-797-2825 Fax:(310)-797-3756

DR HARN CHEN
NORTHROP GRUMMAN CORP
ONE HORNET WAY
M/S 9874/63
EL SEGUNDO CA 90245-0001
PH:(310)-332-9628 Fax:(310)-332-0583

MR JOSEPH COCHRAN
LOCKHEED AERO SYS CO
DEPT 73-25 ZONE 0160
86 S COBB DR
MARIETTA GA 30063-0160
PH:(770)-494-2166 Fax:(770)-494-9610

MR ALAN COPELAND
NORTHROP GRUMMAN
DEPT 9B74 MS 63
ONE HORNET WAYAY
EL SEGUNDO CA 90245-2804
PH:(310)-332-9401 Fax:(310)-332-0583

MR DAVID CRAIG
PRATT & WHITNEY CANADA
M/S 01 MA3
1000 MARIE VICTORIA
LONGUEIL MONTREAL CANADA J4G-1A1
PH:(514)-647-3736 Fax:(514)-647-2319

MR JAMES DALY
METAL IMPROVEMENT CO
10 FOREST AVE
PARAMUS NJ 07652-0001
PH:(201)-843-7800 Fax:(201)-843-3460

DR PAUL DOMAS
GE AIRCRAFT ENGINES
PO BOX 156301
ONE NEUMANN WAY MZ Q105
CINCINNATI OH 45215-6301
PH:(513)-552-4923 Fax:(513)-552-4921

MR JOSEPH CHOY
LOCKHEED MARTIN SKUNK WORKS
DEPT 25-42 BLDG 611-2
1011 LOCKHEED WAY
PALMDALE CA 93599-2542
PH:(805)-572-7809 Fax:(805)-572-7515

MR HAIM COHEN
ISRAELI AIR FORCE
7 BARAK ST
HERZELIA ISRAEL

MR DOUGLAS CORNOG
US AIR FORCE ASC/ENFS
2530 LOOP RD WEST
WRIGHT-PATTERSON AFB OH 45433-7101
PH:(937)-255-8375 Fax:(937)-476-4546

MR NORMAN CRAWLEY
DEPT NATL DEFENCE CANADA
DTA 3
NDHQ, MGGV GEORGE R PEARKES BLDG
OTTAWA ONTARIO CANADA K1A-OK2
PH:(613)-993-9155 Fax:(613)-998-6922

MR MARK DEAN
USAF SA-ALC/LFES
F-5 TCG
303 WILSON BLVD
KELLY AFB TX 78241-5443
PH:(210)-925-4284 Fax:(210)-925-0097

MR DAVID DOUGLAS
ARINC
USN (USMC)
2551 RIVA RD
ANNAPOLIS MD 21403-0001
PH:(410)-266-4432

MR DON CLARK
LOCKHEED MARTIN AERO SYS
DEPT 73-05 CC 22 Z/0199
86 SOUTH COBB DRIVE
MARIETTA GA 30063-0001
PH:(770)-494-1803 Fax:(770)-494-5414

LT DAVID CONLEY
USAF WL/FIBEC
2130 EIGHTH ST STE 1
BLDG 45
WRIGHT-PATTERSON AFB OH 45433-0001
PH:(513)-255-3144 Fax:(513)-656-4999

MR THOMAS COURBE
FRENCH MINISTRY OF DEFENCE
DEPT STPA
26 BLVD VICTOR
PARIS FRANCE 00460 ARMEES-0001

DR MATTHEW CREAGER
STRUCTURAL INTEGRITY ENGRG
STE 200
9560 TOPANGA CANYON BLVD
CHATSWORTH CA 91311-0001
PH:(817)-718-2195 Fax:(818)-718-2212

DR EDVINS DEMUTS
US AIR FORCE WL/FIBEC
2130 8TH ST STE 111
WRIGHT-PATTERSON AFB OH 45433-7542
PH:(937)-255-6104 Fax:(937)-656-4999

MR MIKE DUBBERLY
FATIGUE TECH INC
6250 TERRAPIN DR
MANASSAS VA 22111-3807
PH:(703)-791-3634 Fax:(703)-791-5467

DR VERONIQUE DUBOIS
SWISS AIRCRAFT & SYS CO
SYS MGMT & FATIGUE ENGRG
PO BOX 301
EMMEN SWITZERLAND 6032-0001

LTCOL RICHARD DUGAN
HQ USAF/LGMY AS&S
1030 AIR FORCE PENTAGON
WASHINGTON DC 20330-1030
PH:(202)-208-1630 Fax:(202)-501-3488

MR RANDAL EDWARDS
ROCKWELL INTL-NAAD
PO BOX 3644/MS SL 15
2600 WESTMINSTER BLVD
SEAL BEACH CA 90740-7644
PH:(310)-797-2842 Fax:(310)-797-3756

MR JOSEF EIBLMEIER
MARTEC LTD
221 CHEMIN FREEMAN
STE 150
HULL QUEBEC J8Z 2A8-0001
PH:(819)-595-4816 Fax:(819)-595-1739

MR JOHN ELSNER
ANALYTICAL SERVICES & MATLS INC
FATIGUE & FRAC TEST FAC
BLDG 65 AREA B
WRIGHT-PATTERSON AFB OH 45433-0001
PH:(513)-255-0434 Fax:(513)-476-7379

MR PAUL ELWELL
MOOG ESPRIT
SENECA & JAMISON RDS
PLANT 4
E AURORA NY 14052-0018
PH:(716)-687-4478 Fax:(716)-652-0633

MS ANN EMBREY
FEDERAL AVIATION ADMIN
M/S AVN-347
6500 S MCARTHUR
OKLAHOMA CITY OK 73125-4932
PH:(405)-954-8713 Fax:(405)-954-9532

MR JOSEPH EVANCHO
STRUCTURAL LAMINATES CO
510 CONSTITUTION BLVD
NEW KENSINGTON PA 15068-0001
PH:(412)-339-6888 Fax:(412)-339-6978

MR ROBERT EVANS
US AIR FORCE OC-ALC/LABEF
STE 2AB85A
3001 STAFF DR
TINKER AFB OK 73145-0001
PH:(405)-736-5194 Fax:(405)-733-8555

MR RICHARD EVERETT
US ARMY VEHICLE STRUCTURES DIR
M/S 188E
2 W REID ST
HAMPTON VA 23681-0001
PH:(804)-864-3459 Fax:(804)-864-8911

MR ALBERT EWELL
US AIR FORCE
WR-ALC/LFIT
296 COCHRAN ST
ROBINS AFB GA 31098-0001
PH:(912)-926-1267 Fax:(912)-929-0171

MR JOAO FALCAO
NORTHROP GRUMMAN CORP
M/S H11-223
PO BOX 9650
MELBOURNE FL 32904-9650
PH:(407)-951-6467 Fax:(407)-951-6115

MR TIMOTHY FALLON
NAWCAD
ASLS M/S 3
PAXTUXENT RIVER MD 00000-0001
PH:(301)-342-9325 Fax:(301)-342-9402

MR MICHAEL FALUGI
USAF WL/FIBAA
2130 EIGHTH ST STE 1
WRIGHT-PATTERSON AFB OH 45433-7542
PH:(513)-255-6639 Fax:(513)-255-7723

MR PHILLIP FARLEY
US AIR FORCE
SA-ALC/F-5TCG
KELLY AFB TX 78241-5443
PH:(210)-925-4284 Fax:(210)-925-0097

DR JIRI FIDRANSKY
AERO VODOCHODY
ODOLENA VODA
PRAGUE
CZECH REPUBLIC 250 70-0001

MR JOHN FLOOD
MCDONNELL DOUGLAS AERO
PO BOX 516
M/SS111-1221
ST LOUIS MO 63166-0001
PH:(314)-232-7623 Fax:(314)-232-1394

MR LUPE FLORES
US AIR FORCE
SA-ALC/LADD
514 SHOP LN/STE 2
KELLY AFB TX 78241-6434
PH:(210)-925-4525 Fax:(210)-925-1416

DR THOMAS FLOURNOY
FEDERAL AVIATION ADMIN
WILLIAM J HUGHES TECH CNTR
AGING AIRCRAFT AAR 433
ATLANTIC CITY NJ 08405-0001
PH:(609)-485-5327 Fax:(609)-485-4569

MR DENNIS FLYNN
US NAVY
CBN 027 PO BOX 6056
HWY 1570 @ MAJORS FLD
GREENVILLE TX 75403-6056
PH:(903)-457-6427 Fax:(903)-457-6530

MR SYLVAIN FORGUES
BOMBARDIER INC
10000 CARGO A-4 ST
MONTREAL INTL AIRPORT
MIRABEL QUEBEC CANADA J7N-1H3
PH:(514)-476-4201 Fax:(514)-476-4207

MR ROYCE FORMAN
NASA JOHNSON SPACE CTR
MATERIALS BRANCH (EM2)
HOUSTON TX 77058-0001
PH:(713)-483-8926 Fax:(713)-244-2319

MR MICHAEL FOSTER
GEORGIA TECH RES INST
7220 RICHARDSON RD
SMYRNA GA 30080-0001
PH:(770)-528-7886 Fax:(770)-528-3271

MR JOBST FRANK
GERMAN MOD
AMC PO BOX 33668
WRIGHT-PATTERSON AFB OH 45433-0668
PH:(513)-255-6660 Fax:(513)-476-7744

MAJ ROBERT FREDELL
HQ USAFA/DFEM
STE 6H2
2354 FAIRCHILD DR
US AIR FORCE ACADEMY CO 80840-6240
PH:(719)-333-2531 Fax:(719)-333-2944

MR CARL FRENCH
BOEING DEF & SPC GRP
2601 LIBERTY PKWY
MIDWEST CITY OK 73110-0001
PH:(405)-739-1410 Fax:(405)-739-1416

DR JOSEPH GALLAGHER
US AIR FORCE WL/CCI
BLDG 45
WRIGHT-PATTERSON AFB OH 45433-0001
PH:(937)-255-4269 Fax:(937)-656-4646

MR FERNANDO GARCIA
CORPUS CHRISTI ARMY DEPOT
DIR LOG SUPPORT
M/S 51
CORPUS CHRISTI TX 78418-0001
PH:(512)-939-3282 Fax:(512)-939-4206

MR MARIO GARZA
MOOG ESPRIT
SENECA AND JAMISON RDS
PLANT 4
E AURORA NY 14052-0001
PH:(716)-687-4434 Fax:(716)-652-0633

MR HAROLD GAY
NAVAL AVIATION DEPOT
PSC 8021
MCAS CHERRY POINT
CHERRY POINT NC 28533-0021
PH:(919)-466-8517 Fax:(919)-466-8517

MR WILLIAM GEESE
USAF ASC/YPR6
1981 MONOHAN WAY
WRIGHT-PATTERSON AFB OH 45433-7205
PH:(513)-255-6605 Fax:(513)-656-4896

MR ROBERT GERAMI
US AIR FORCE ASC/ENGS
2530 LOOP RD WEST
WRIGHT-PATTERSON AFB OH 45433-7101
PH:(937)-255-3330 Fax:(937)-656-4546

MR ALI GHANNADAN
MOOG ESPRIT
140 MAYHEW WAYON RD
BLDG E STE 1003
PLEASANT HILL CA 94523-0001
PH:(510)-947-0400 Fax:(510)-947-0900

SQNLDR ALEX GIBBS
ROYAL AUSTRALIAN AF
WR-ALC/EM-AT
480 SECOND ST STE 200
ROBINS AFB GA 31098-1640
PH:(912)-926-2580 Fax:(912)-328-3502

MR BRUCE GIBSON
FATIGUE TECH INC
100 ANDOVER PARK W
SEATTLE WA 98188-0001
PH:(206)-246-2010 Fax:(206)-246-9886

MR JOHN GOODMAN
TENSIODYNE
11735 W OLYMPIC BLVD
STE 705 EAST TOWER
LOS ANGELES CA 90064-0001
PH:(310)-813-9211 Fax:(310)-318-2535

MR MARKUS GOTTIER
MCDONNELL DOUGLAS CORP
M/S S2704396
5775 CAMPUS PKWY
ST LOUIS MO 63042-0516
PH:(314)-232-4932 Fax:(314)-232-1672

DR ALTEN GRANDT
PURDUE UNIV
AERO & ASTRO
1282 GRISSOM HALL
W LAFAYETTE IN 47907-1282
PH:(317)-494-5141 Fax:(317)-494-0307

SQN LDR ANDREW GREEN
USAF WL/POTC
BLDG 18
1950 FIFTH ST
WRIGHT-PATTERSON AFB OH 45433-7251
PH:(937)-255-2734 Fax:(937)-255-2660

DR DANIEL GREVING
ALLIED SIGNAL ENGINES
111 S 34TH ST
M/S 93-77/301-227
PHOENIX AZ 85072-2181
PH:(602)-231-2227 Fax:(602)-231-1428

DR KENNETH GRIFFIN
SOUTHWEST RESEARCH
6220 CULEBRA RD
SAN ANTONIO TX 78238-5166
PH:(210)-522-6873 Fax:(210)-522-3042

MR FRANK GRIMSLEY
US AIR FORCE
ASC/YC
WRIGHT-PATTERSON AFB OH 45440-0001
PH:(513)-255-1049

CAPT DAN GRONER
USAF WL/FIBA
2130 EIGHTH ST STE 1
WRIGHT-PATTERSON AFB OH 45433-7542
PH:(937)-255-5664 Fax:(937)-656-7723

MR MICHAEL GRUBER
BOEING
PO BOX 3707
MS 67-FF
SEATTLE WA 98124-2207
PH:(206)-237-6759 Fax:(206)-234-1499

MR CORNELIS GUIJT
HQ USAFA/DFEN
STE 6H2
2354 FAIRCHILD DR
US AIR FORCE ACADEMY CO 80840-6240
PH:(719)-333-3043 Fax:(719)-333-2944

MR SCOTT GULICK
FATIGUE TECHNOLOGY INC
100 ANDOVER PARK W
SEATTLE WA 98188-0001
PH:(206)-246-2010 Fax:(206)-244-9886

MR GEORG GUNTHER
DASA
LMT22
PO 801160
MUNICH GERMANY 81663-0001

MRS MOHINI GUPTA
PRATT & WHITNEY CANADA
1000 MARIE-VICTORIN
MS OILE4
LONGUEUIL QUEBEC CANADA J4G-1A1
PH:(514)-677-9411 Fax:(514)-647-7461

MR RICHARD HADCOCK
RNH ASSOCIATES INC
6 SUE CIRCLE
HUNTINGTON NY 11743-1979
PH:(516)-271-7037 Fax:(516)-271-7137

MR DENNIS HAGER
USAF WL/MLSS
2179 TWELFTH ST
WRIGHT-PATTERSON AFB OH 45433-7718
PH:(513)-255-3370 Fax:(513)-476-7844

MR STEPHEN HALL
CELERIS AERO CANADA INC
255 CENTRUM BLVD
STE 300
ORLEANS ONTARIO CANADA K1E-3V8
PH:(613)-837-1161 Fax:(613)-834-6420

MR DAVID HARPER
US AIR FORCE HQ AFSC/SEF
9700 AVE G SE
KIRTLAND AFB NM 87185-5670
PH:(505)-846-0996 Fax:(505)-846-6826

MR JAMES HARPER
USAF WR-ALC/LBRA
265 OCMULGEE CT
ROBINS AFB GA 31098-1647
PH:(912)-926-7980 Fax:(912)-926-2211

DR CHARLES HARRIS
NASA LANGLEY RES CTR
M/S 188E
HAMPTON VA 23681-0001
PH:(757)-864-3447 Fax:(757)-864-7729

MR JIM HARRISON
METAL IMPROVEMENT CO INC
1618 S IDA
WICHITA KS 67211-0001
PH:(316)-267-8201 Fax:(316)-267-5735

MR KARL HART
US AIR FORCE HQ AMC/LGXR
402 SCOTT DR UNIT 2A2
SCOTT AFB IL 62225-5308
PH:(618)-256-6698 Fax:(618)-256-2009

MR JAMES HARTER
USAF/ANALYTICAL SERV & MATLS
BLDG 45
2130 EIGHTH STREET STE 1
WRIGHT-PATTERSON AFB OH 45433-7542
PH:(513)-255-6104 Fax:(513)-476-4999

MAJ JURGEN HEILIG
HQ NAEWFC
NATO AEW
B-7010 SHAPE BELGIUM
APO AE 09705 BFPO 26 CFPO 5048-0001

MR MICHAEL HEINER
US AIR FORCE OO-ALC/LFIT
6089 WARDLEIGH RD
HILL AFB UT 84056-5838
PH:(801)-777-9318 Fax:(801)-773-9782

MR MARKUS HEINIMANN
PURDUE UNIVERSITY
1282 GRISSOM HALL
W LAFAYETTE IN 47907-1282
PH:(217)-494-1378 Fax:(317)-494-0307

MR LAWRENCE HEITZMANN
DAYTON T BROWN
555 CHURCH ST
BOHEMIA NY 11716-0001
PH:(516)-244-6230 Fax:(516)-467-9045

MR JAMES HELBLING
NORTHROP GRUMMAN
M/S 9870/89
ONE NORTHROP AVE
EL SEGUNDO CA 90245-2804
PH:(310)-332-6004 Fax:(310)-331-6648

MR GRANT HERRING
OGDEN ALC/LACM
F4 STRUCTURES
7278 4TH ST
HILL AFB UT 84056-5205
PH:(801)-777-0535 Fax:(801)-777-9482

MS PAMELA HERZOG
US AIR FORCE OC-ALC/LAKRA
STE 2AH110
3001 STAFF DR
TINKER AFB OK 73145-3022
PH:(405)-736-2559 Fax:(405)-736-5412

DR PAUL HEULER
IABG
TA 31 EINSTEINSTRASSE 20
OTTOBRUNN GERMANY D 85521-0001

MR RICHARD HEUSSER
WEST COAST INDUSTRIES
14900 WHITMAN AVE N
SEATTLE WA 98133-0001
PH:(206)-365-7513 Fax:(206)-365-7483

MR JAMES HILL
USAF OC-ALC/TILO
7851 SECOND ST
RM127/BLDG 3
TINKER AFB OK 73145-9145
PH:(405)-736-2663 Fax:(405)-736-3086

MR KURT HILL
ROYAL AIR FORCE
HQ LOGISTICS CMD
WYTON HUNTINGDON
PETERBOROUGH ENGLAND PE172PY565-0001

MR GREGORY HOFFMAN
ROYAL AUSTRALIAN AF
5111 ROBERTS AVE
STE 4
MCCLELLAN AFB CA 95652-0001
PH:(916)-643-6445 Fax:(916)-649-0568

MR RICHARD HOLZWARTH
USAF WL/FIBA
BLDG 45
2130 8TH ST STE 1
WRIGHT-PATTERSON AFB OH 45433-7542
PH:(513)-255-6639 Fax:(513)-255-7723

DR MASAMICHI HONGOH
PRATT & WHITNEY CANADA
1000 MARIE-VICTORIN
MAIL CODE 01SA4
LONGUEUIL QUEBEC CANADA J4G-1A1
PH:(514)-677-9411 Fax:(514)-647-2553

MR WALLY HOPPE
SYSTEMS RES LABS
2800 INDIAN RIPPLE RD
DAYTON OH 45440-3696
PH:(513)-427-7761 Fax:(513)-427-7745

MR YOSHIYUKI HOTEI
MITSUBISHI HEAVY IND LTD
1 TOYOBA TOYOYOMA-CHO
NISHIKASUGAI-GUN
AICHI-KEN 480-02 JAPAN-0001

DR PETER HOVEY
UNIV DAYTON RES INST
300 COLLEGE PARK
M/S 0120
DAYTON OH 45469-0120
PH:(937)-229-4027 Fax:(937)-229-3712

MR ROGER HOWELL
OGDEN AIR LOG CTR
7278 4TH ST
HILL AFB UT 84056-5205
PH:(801)-777-0535 Fax:(801)-777-9482

MR ANTHONY HUG
BOEING COMMERCIAL AIRPLANE CO
3801 S OLIBER
MS K 78-16
WICHITA KS 67210-0001
PH:(316)-526-4611 Fax:(316)-526-8535

MR HENRY HUGGINS
LOCKHEED MARTIN AERO SYS
86 S COBB DR
DEPT 73-25
MARIETTA GA 30063-0160
PH:(770)-494-7693 Fax:(770)-494-9610

MR TROY HULLANDER
NAVAL AVIATION DEPOT
500A HWY 70 W
PO BOX 8021
CHERRY POINT NC 28533-0021
PH:(919)-466-8519 Fax:(919)-466-8502

MR LEX HUTCHESON
SVERDRUP TECH INC
4538 CENTERVIEW DR
SUITE 130
SAN ANTONIO TX 78228-0001
PH:(210)-733-3383 Fax:(210)-733-3389

MR NEIL HYGATE
ROYAL NEW ZEALAND AF
HQ NEW ZEALAND DEFENCE FORCE
PRIVATE BAG
WELLINGTON NEWZEALAND-0001

MR J EDWARD INGRAM
LOCKHEED MARTIN AERO SYS
ADV STRUC & MATLS 73-C2
86 S COBB DR M/S 0648
MARIETTA GA 30063-0648
PH:(770)-494-8172 Fax:(770)-494-8345

MR WILLIAM IRBY
LOCKHEED MARTIN AERO SYS
M/S 0303 DEPT 73-71
86 S COBB DR
MARIETTA GA 30063-0303
PH:(770)-494-2873 Fax:(770)-494-7738

MAJ YASUHIRO ISAKARI
JAPAN DEFENSE AGY
1-2-24 IKEJIRI
SETAGAYA-KU
TOKYO JAPAN 154-0001

MR WAFAA ISHAK
BELL HELI TEXTRON CANADA
12800 RUE DE L'AVENIR
MIRABEL QUEBEC CANADA J7J-IRA
PH:(514)-437-2795 Fax:(514)-437-6382

MR ANTHONY JACKSON
LOCKHEED MARTIN AERO SYS
DEPT 73-C1 ZONE 0648
86 S COBB DRIVE
MARIETTA GA 30063-0648
PH:(770)-494-8164 Fax:(770)-494-0799

MR ROBERT JANNARONE
RAPID CLIP NAVAL SYSTEMS
430 10TH ST
ATLANTA GA 30318-0001
PH:(404)-607-1166 Fax:(404)-607-0038

MR RANDY JANSEN
US AIR FORCE
WR-ALC/TIEDD
420 2ND ST/STE 100
ROBINS AFB GA 31098-1640
PH:(912)-926-4228 Fax:(912)-926-1743

MR MARK JARVIS
LOCKHEED MARTIN AERO SYS
S-38/ES-3A ENGRG PROG OFF
86 S COBB DR M/S 0580
MARIETTA GA 30063-0001
PH:(770)-494-3643 Fax:(770)-494-8478

DR DAVID JEONG
US DEPT OF TRANS
M/S DTS-76
KENDALL SQ
CAMBRIDGE MA 02142-1093
PH:(617)-494-3654 Fax:(617)-494-3066

MR JAMES JOBSON
LOCKHEED MARTIN AERO SYS
DEPT 73-25/MS 0160
86 S COBB DR
MARIETTA GA 30063-0001
PH:(770)-494-2981 Fax:(770)-494-9610

MR HERMAN JOHNSON
PRATT & WHITNEY (GESP)
M/S 714-03
PO BOX 109600
W PALM BEACH FL 33410-9600
PH:(407)-796-5151 Fax:(407)-796-8993

DR CRAIG JONES
SANDIA NATL LABS
M/S 0615
PO BOX 5800
ALBUQUERQUE NM 87185-0615
PH:(505)-843-8722 Fax:(505)-843-8760

MR KEVIN JONES
LOCKHEED MARTIN AERO
86 S COBB DR
DEPT 73-25 M/S 0160
MARIETTA GA 30003-0160
PH:(770)-494-3537 Fax:(770)-494-9610

LTCOL JOHN JOOSTEN
ROYAL NETHERLANDS AF
BINCKHORSTLAAN 135
PO BOX 20703
THE HAGUE HOLLAND 2500ES-0001

MR VICTOR JUAREZ
LOCKHEED MARTIN
PO BOX 101654
FT WORTH TX 76185-0001
PH:(817)-762-2710 Fax:(817)-762-2634

MR KIM JUHALA
FINNISH AF DEPOT
PO BOX 210
TAMPERE FINLAND 33101-0001

MR DAVID KANE
NORTHROP GRUMMAN CORP
ONE HORNET WAY
M/S 9B74/N8
EL SEGUNDO CA 90245-0001
PH:(310)-332-9623 Fax:(310)-332-9160

DR ROBERT KIANG
NAVAL AIR WARFARE CTR
M/S 3 CODE 4.4.7.2 BLDG 106
22467 MILLSTONE RD
PATUXENT RIVER MD 20670-0001
PH:(301)-342-7850 Fax:(301)-342-1867

MR PHILLIP KLOOS
MTS SYSTEMS CORP
M/S 231
14000 TECHNOLOGY DR
EDEN PRARIE MN 55344-2290
PH:(612)-937-4854 Fax:(612)-937-4515

DR H KONISH
ALCOA TECH CTR
100 TECHNICAL DR
BLDG D-18-ED
ALCOA CTR PA 15069-0001
PH:(412)-337-2736 Fax:(412)-337-5436

MR ROBERT KURTH
BATTELLE
ENGRG MECH GRP
505 KING AVE
COLUMBUS OH 43201-2693
PH:(614)-424-7151 Fax:(614)-424-3457

MAJ MARCEL LAMBRICHS
ROYAL NETHERLANDS AF
BINCHORSTLAAN 135
PO BOX 20703
THE HAGUE NETHERLAND 2500ESA-0001

LTC ROLF KEIMER
GERMAN AIR FORCE MATERIEL OFF
WASBE F4 PHANTOM
D-51140
COLOGNE GERMANY

MR JON KIMMEL
USAF OC-ALC/LAKRA
STE 2AH110
3001 STAFF DR
TINKER AFB OK 73145-0001
PH:(405)-736-2559 Fax:(405)-736-5412

MR JAMES KOKORIS
NORTHROP GRUMMAN CORP
M/S B13-025
S OYSTER BAY RD
BETHPAGE NY 11714-0001
PH:(516)-346-8814 Fax:(516)-346-3290

MR HENRY KONOPKA
SIKORSKY AIRCRAFT
6900 MAIN ST
M/S S313AZ
STRATFORD CT 06497-0001
PH:(203)-386-4725 Fax:(203)-386-3717

MR JOSEPH KUZNIAR
US AIR FORCE WL/CCI
BLDG 45
2130 EIGHTH ST/STE 1
WRIGHT-PATTERSON AFB OH 45433-7562
PH:(937)-255-4843 Fax:(937)-255-1522

MR RICHARD LAURIDIA
NORTHROP GRUMMAN
M/S 49L-35
9314 W JEFFERSON BLVD
DALLAS TX 75265-5907
PH:(214)-266-4267 Fax:(214)-266-2407

MR ALAN KERR
ARTI/DYNCORP
1 RIDGMAR CENTRE
6500 W FREEWAY
FT WORTH TX 76116-2187
PH:(817)-737-1656 Fax:(817)-737-1605

MR RICHARD KINZIE
USAF
STE 100
420 2ND ST
ROBINS AFB GA 31098-1640
PH:(912)-926-3284 Fax:(912)-926-6619

MR JERZY KOMOROWSKI
NATL RES COUNCIL
MONTREAL RD M-14
OTTAWA ONTARIO -- CANADA K1A-0R6
PH:(613)-993-3999 Fax:(613)-952-7136

MR STEVEN KRAMER
RAYTHEON E SYSTEMS
CBN 170
PO BOX 6056
GREENVILLE TX 75403-6056
PH:(903)-457-7096 Fax:(903)-408-8793

COL HANK LAAKMAN
BOEING DEFENSE & SPACE GRP
2601 LIBERTY PKWY
MS RM-00
MIDWEST CITY OK 73130-0001
PH:(405)-739-1407 Fax:(405)-739-1416

PROF LUIGI LAZZERI
UNIV OF PISA
DEPT OF AERO ENGR
VIA DIOTISALVI 2
PISA ITALY I-56426-0001

MR GUY KERRICK
LOCKHEED MARTIN/FT WORTH
PO BOX 748
M/S 4272
FT WORTH TX 76101-0001
PH:(817)-763-2876 Fax:(817)-777-2215

MR TED KIRCHNER
FOSTER-MILLER INC
195 BEAR HILL RD
WALTHAM MA 02154-1198
PH:(617)-684-4169 Fax:(617)-290-0693

DR SHUNICHI KONDO
ISHIKAWAJIMA-HARIMA HVY IND CO
3-5-1 MUKODAI-CHO
TANASHI-SHI
TOKYO JAPAN-188

MR SRINIYAS KRISHNAN
AS&M
FATIGUE & FRAC TEST FAC
BLDG 65 AREA B
WRIGHT-PATTERSON AFB OH 45433-0001
PH:(513)-255-0434 Fax:(513)-476-7379

DR CAMPBELL LAIRD
UNIV OF PENNSYLVANIA
3231 WALNUT ST
PHILADELPHIA PA 19104-6272
PH:(215)-898-6664 Fax:(215)-573-2128

MR TOMAS LEIJOU
FMV
S-11588
STOCKHOLM SWEEDEN

MR KALMEN LEIKACH
US NAVY
M/S 4 3 3
1421 JEFFERSON DAVIS HWY
ARLINGTON VA 22243-0001
PH:(703)-604-3400 Fax:(703)-604-4396

MR KO-WEI LIU
MCDONNELL DOUGLAS CORP
M/S C052-0225
2401 E WARDLOW ROAD
LONG BEACH CA 90807-5309
PH:(310)-982-5422 Fax:(310)-982-5164

MR AUDGEIR LUNDE
ROYAL NORWEGIAN AF MATL CMD
M/S DFIS
PO BOX 10
N2007 KJELLER NORWAY

CAPT THOMAS MANNING
US AIR FORCE ELEC SYS CTR
75 VANDEN BERG DR
HANSCOM AFB MA 01731-2119
PH:(617)-377-6805 Fax:(617)-377-4292

MR DANIEL MCCRAY
AS&M
FATIGUE & FRACTURE TEST FACILITY
BLDG 65 AREA B
WRIGHT-PATTERSON AFB OH 45433-0001
PH:(513)-255-0434 Fax:(513)-656-7379

MR THOMAS MEYER
UNITED TECH RESCH CTR
411 SILVER LN
M/S 129-73
E HARTFORD CT 06108-0001
PH:(860)-610-7340 Fax:(860)-610-7526

MAJ PATRICK LEMMERS
US AIR FORCE HQ AMC
UNIT 2A2
402 SCOTT DR
SCOTT AFB IL 62225-5308
PH:(618)-256-2059 Fax:(618)-256-5544

MR ANTHONY LIZZA
US AIR FORCE WL/FIBEC
2275 D ST STE 16
WRIGHT-PATTERSON AFB OH 45433-7233
PH:(937)-255-0935 Fax:(937)-656-4102

MR JOSEPH LUZAR
BOEING PROD SUPPORT DIV
M/S K86-81
PO BOX 7730
WICHITA KS 67277-7730
PH:(316)-523-5408 Fax:(316)-523-5705

MR ROBERT MARKER
SYSTEMS RESEARCH LABS
9601 MCALLISTER FREEWAY STE 1165
SAN ANTONIO TX 78216-4605
PH:(210)-922-4971 Fax:(210)-922-4972

DR PETER MCKEIGHAN
SOUTHWEST RESEARCH INST
6220 CULEBRA RD
PO DRAWER 28510
SAN ANTONIO TX 78228-0510
PH:(210)-522-3617 Fax:(210)-522-5122

MR RICHARD MICKLOS
FAA TECHNICAL CTR
CODE AAR432
ATLANTIC CITY INTL NJ 08405-0001
PH:(609)-485-6531 Fax:(609)-485-4569

DR JOHN LINCOLN
USAF ASC/EN
BLDG 560
2530 LOOP RD W
WRIGHT-PATTERSON AFB OH 45433-7101
PH:(937)-255-5312 Fax:(937)-656-4546

FLT LT PAUL LOCKHART
ROYAL AIR FORCE
HQ LOG CMD
RAF WYTON HUNTINGDON
PETERBOROUGH ENGLAND PE17 2DL-0001

DR PAUL LYNN
NATL TECH SYS-RYE CANYON
BLDG 202
25100 RYE CANYON RD
VALENCIA CA 91355-0001
PH:(805)-259-8184 Fax:(805)-257-3539

CAPT VERNON MAY
USAF WL/DOL-F
2130 EIGHTH ST
WRIGHT-PATTERSON AFB OH 45433-0001
PH:(937)-255-5664 Fax:(937)-656-7723

MR ROBERT McKINLEY
US AIR FORCE
ASC/YTJVA/BLDG 56
2100 MONAHAN WAY
WRIGHT-PATTERSON AFB OH 45433-7014
PH:(937)-255-9306 Fax:(937)-255-8516

MS PEGGY MIEDLAR
UNIV DAYTON RES INST
300 COLLEGE PK
M/S 0120
DAYTON OH 45469-0120
PH:(937)-229-4417 Fax:(937)-229-3712

MR ALEXANDER LITVINOV
ASSM
FATIGUE AND FRACTURE
BLDG 65
WRIGHT-PATTERSON AFB OH 45433-0001
PH:(513)-255-0436

MR RONALD LOVELAND
DAYTON T BROWN INC
STRUC FATIGUE TEST
CHURCH ST
BOHEMIA NY 11716-0001
PH:(516)-244-6224 Fax:(516)-567-9045

MR JAMES MALINAK
BOEING DEF & SPC GRP
STE 400
2600 PARAMOUNT PL
FAIRBORN OH 45324-6765
PH:(513)-427-1767 Fax:(513)-427-5255

DR ROBERT MCCLUNG
SOUTHWEST RES INST
6220 CULEBRA
PO DRAWER 28510
SAN ANTONIO TX 78228-0510
PH:(210)-522-2422 Fax:(210)-522-5122

MR ROBERT MELLYN
ELECTRODYNAMICS INC
1200 HICKS RD
ROLLING MEADOWS IL 60008-0001
PH:(847)-259-0740 Fax:(847)-255-3827

MAJ JAMES MILLER
DEPT OF NATL DEFENCE
DIR OF TECH AIRWORTHINESS
101 COLONEL BY DR
OTTAWA ONTARIO K1A 0K2-0001
PH:(613)-993-2320 Fax:(613)-998-6922

MR GERALD MINTZ
ROCKWELL INTL
M/S AD46 DEPT 270
12214 LAKEWOOD BLVD
DOWNEY CA 90241-0001
PH:(310)-922-3358 Fax:(310)-922-2523

MR KOUICHI MURAYAMA
MITSUBISHI HEAVY IND LTD
NAGOYA AERO SYS
10 OYE-CHO MINATO-KU
NAGOYA JAPAN 455-0001

MR TOM NGUYEN
LEARJET INC
PO BOX 7707
MS 29
WICHITA KS 67277-7707
PH:(316)-946-6367 Fax:(316)-946-2990

MR GORDON NISBET
ROYAL AIR FORCE
HQ LOG CMD
RAF WYTON HUNTINGDON
PETERBOROUGH ENGLAND PE17-2DL-0001

MR MITSUGI OHKI
MITSUBISHI HEAVY IND LTD
NISHIKASUGAI-GUN
AICHI-KEN 480-02
JAPAN

MR STEVE OWENS
LOCKHEED MARTIN TAS
M/Z 2803
PO BOX 748
FT WORTH TX 76126-0001
PH:(817)-777-2142 Fax:(817)-777-4254

MR W CRAIG MITCHELL
US AIR FORCE
OO-ALC/LAIA F-4 TCG
6089 WARDLEIGH RD
HILL AFB UT 84056-5838
PH:(801)-777-5891 Fax:(801)-773-7620

MR ARNOLD NATHAN
ISRAEL AIRCRAFT IND
FATIGE & DAMAGE TOLERANCE 4441
BEN GURION INTL AIRPORT
ISRAEL

MR TRUNG NGUYEN
NAVAL AIR WARFARE CTR
AIR VEHICLE STRUCTURES
BLDG 2187 CODE 4332 M/S 3
PATUXENT RIVER MD 20670-0001
PH:(301)-342-9329 Fax:(301)-342-9302

MR MILES NOMURA
MCDONNELL DOUGLAS
3855 LAKEWOOD BLVD
MS 0035-0035
LONG BEACH CA 90846-0001
PH:(310)-982-2698 Fax:(310)-593-7710

MR CRAIG OLKIEWICZ
SYSTEMS & ELECTRONICS INC
190 GORDON ST
ELK GROVE VILLAGE IL 60007-0001
PH:(847)-228-0985 Fax:(847)-228-1164

MR TIM PADFIELD
CAE AVIATION LTD
PO BOX 9864
EDMONTON INTL AIRPORT
EDMONTON ALBERTA CANADA T5J-2T2
PH:(403)-890-6498 Fax:(403)-890-6543

MR JOSEPH MOSHER
US AIR FORCE ASC/SMA
2145 MONAHAN WAY
WRIGHT-PATTERSON AFB OH 45433-7017
PH:(513)-255-6053 Fax:(513)-255-5105

MR GEORGE NEAT
US DOT/VOLPE CTR
KENDALL SQUARE
M/S DTS-74
CAMBRIDGE MA 02142-1093
PH:(617)-494-2679 Fax:(617)-494-3096

MR KURT NIEDRAUER
USAF WR-ALC/LKSA
460 2ND ST STE 221
ROBINS AFB GA 31098-1640
PH:(912)-926-0756 Fax:(912)-926-1646

MR THOMAS O'CONNOR
ARTI/DYNCORP
ONE RIDGMAR CENTRE
6500 W FREEWAY
FT WORTH TX 76116-2187
PH:(817)-737-1680 Fax:(817)-737-1605

MR MATS-OLOF OLSSON
FMV
S-115 88
STOCKHOLM SWEDEN

MR RALPH PAGLIA
USAF WL/MLS-OL
485 QUENTIN ROOSEVELT RD
STE 7
KELLY AFB TX 78241-6426
PH:(210)-925-6408 Fax:(210)-925-2726

LT COL ERICH MULLER
GERMAN AIR FORCE
CIS AIR ARMAMENT
HEIDESTRASS 245 M/S 51140
KOLN GERMANY

MR ROGER NESJE
ROYAL NORWEGIAN AF
MATERIAL COMMAND
PO BOX 10
KJELLER NORWAY N2007-0001

MR DONALD NIESER
USAF OC-ALC/LACRA
STE 2AC489D
3001 STAFF DR
TINKER AFB OK 73145-3019
PH:(405)-736-3832 Fax:(405)-736-5604

MR STEFAN OESCH
SWISS AIRCARFT & SYS CO
SYS MGRM & FATIGUE ENGRG
PO BOX 301
EMMEN SWITZERLAND 6032-0001

DR IREWOLE ORISAMOLU
MARTEC LIMITED
STE 400
1888 BRUNSWICK ST
HALIFAX NOVA SCOTIA B3J-3J8
PH:(902)-425-5101 Fax:(902)-421-1923

MR ARMAND PAQUIN
BOMBARDIER INC
INTL AIRPORT
10,000 CARGO A-4 ST
MIRABEL QUEBEC CANADA J7N-1H3
PH:(514)-476-4201 Fax:(514)-476-4207

MR SUBHASH PATEL
PRATT & WHITNEY
400 MAIN ST
E HARTFORD CT 06108-0001

MR MICHAELA PATER
CCAD
308 CRECY
M/S 6
CORPUS CHRISTI TX 78410-0001
PH:(512)-939-4683 Fax:(512)-939-4206

MR CHARLES PELLERIN
US AIR FORCE WL/MLSE
2179 TWELFTH ST/STE 1
WRIGHT-PATTERSON AFB OH 45433-7718
PH:(513)-255-3953 Fax:(513)-476-4378

DR RIGO PEREZ
MCDONNELL DOUGLAS AERO
DEPT 350N M/S S1022147
JS MCDONNELL BLVD
BERKELEY MO 63134-0001
PH:(314)-234-0656 Fax:(314)-234-8915

MR JOHN PERKINS
BRITISH AERO
STRUC DEPT
WARTON INTERNALPOSTCODE W310C
PRESTON LANCASHIRE ENGLAND PR-4ONB

MR DONALD PETTIT
LOCKHEED MARTIN AERO SYS
73-51 TEST LAB M/S 0484
86 S COBB DR
MARIETTA GA 30063-0484
PH:(770)-494-5313 Fax:(770)-494-2028

MR REINALD PFAU
DASA
LMT 224
PO 801160
MUNICH GERMANY 81603-0001

MR NEAL PHELPS
US AIR FORCE
OO-ALC/LFSS BLDG 1212
1594 E 2475 N
LAYTON UT 84040-0001
PH:(801)-775-4892 Fax:(801)-777-3928

MR SWEE-PHENG PHUA
SINGAPORE TECH AERO LTD
AIR STRUC DEPT
540 AIRPORT RD
SINGAPORE 539938-0001

DR ROBERT PIASCIK
NASA LANGLEY RES CTR
M/S 188E
TWO W REID ST
HAMPTON VA 26381-0001
PH:(757)-864-3483 Fax:(757)-864-8911

MR PAUL PIPER
USAF SA-ALC/LFES
303 WILSON BLVD
BLDG 1562
KELLY AFB TX 78241-5443
PH:(210)-925-4284

MR CHRISTOPHER POMFRET
ABDA
STE 201
3040 PRESIDENTIAL DR
FAIRBORN OH 45324-6272
PH:(937)-427-2229 Fax:(937)-427-1937

CDR SOMCHAT PRASERTSUK
ROYAL THAI NAVY AIR DIV
99/43 M.2 DARATORN 4
SOI SALADANG
PLUTALUANG CHOLGURI THAILAND 2-0180

MR BRAD PREVALLET
LOCKHEED MARTIN/FT WORTH
PO BOX 738
M/S 2846
FT WORTH TX 76101-0001
PH:(817)-763-2517 Fax:(817)-777-2115

MR ADARSH PUN
NORTHROP GRUMMAN
M/S 9B70/W8
ONE NORNET WAY
HAWTHORNE CA 90505-0001
PH:(310)-332-4200 Fax:(310)-332-4160

DR MOHAN RATWANI
R-TEC
4 LATIGO LANE
ROLLING HILLS ESTATE CA 90274-0001
PH:(310)-378-9236 Fax:(310)-378-7697

MR LEONARD REID
FATIGUE TECH INC
100 ANDOVER PARK W
SEATTLE WA 98188-2868
PH:(206)-246-2010 Fax:(206)-244-9886

MR WALTER REIMANN
8220 WELLINGTON NECK
FRANKTOWN VA 23354-0001
PH:(757)-442-6377 Fax:(757)-442-6377

MR THEODORE REINHART
USAF WL/MLSE
BLDG 652
2179 TWELFTH ST STE 1
WRIGHT-PATTERSON AFB OH 45433-7718
PH:(513)-255-3691 Fax:(513)-476-4419

MR KARI RENKO
FINNISH AIR FORCE
AIRCRAFT & WEAPON SYS DIV
PO BOX 30
TIKKAKOSKI FINLAND FIN 41161-0001

MR ROBERT RENNELL
ARINC INC
6205 S SOONER RD
OKLAHOMA CITY OK 73135-0001
PH:(405)-739-0939 Fax:(405)-739-0003

MR BRIAN RICE
US AIR FORCE ASC/ENFS
2530 LOOP RD WEST
WRIGHT-PATTERSON AFB 44 45433-7101
PH:(937)-255-6966 Fax:(937)-255-5677

MR YVES RICHARD
BOMBARDIER INC
INTL AIRPORT
10000 CARGO A-4 ST
MIRABEL QUEBEC CANADA J7N-1H3
PH:(514)-476-4357 Fax:(514)-476-4416

MR MICHAEL ROEMER
STRESS TECH INC
1800 BRIHEN TOWNLINE RD
ROCHESTEER NY 14623-0001
PH:(716)-424-2010 Fax:(716)-272-7201

DR LYNN ROGERS
CSA ENGRG INC
2850 W BAYSHORE RD
PALO ALTO CA 94303-3843
PH:(415)-494-7351 Fax:(415)-494-8749

MR DENNIS ROMANO
NADEP NORTH ISLAND
302 DIABLO CREEK CT
M/S 4.3.3
CLAYTON CA 94517-0001
PH:(619)-545-0626 Fax:(619)-545-0763

MR KAJ ROSANDER
SAAB MILITARY AIRCRAFT
STRUCTURAL TECH
LINKOPING SWEDEN 58188-0001

MR JAMES RUDD
USAF WL/FIB
2130 EIGHTH ST/STE 1
BLDG 45 RM 203A
WRIGHT-PATTERSON AFB OH 45433-6553
PH:(513)-255-3031 Fax:(513)-255-3740

MR JOSEPH RUDD
ARTI/DYNCORP
ONE RIDGMAR CENTRE
6500 W FREEWAY
FT WORTH TX 76116-2187
PH:(817)-737-1680 Fax:(817)-737-1605

MR JAMES RUSS
LOCKHEED MARTIN AERO SYS
DEPT 73-22 MS Z0199
86 S COBB DR
MARIETTA GA 30063-0001
PH:(770)-494-2573 Fax:(770)-494-9617

MR JOHN SAENZ
US AIR FORCE
OC-ALC/LIINT
TINKER AFB OK 73145-0001
PH:(405)-736-2509 Fax:(405)-736-7262

MR CHARLES SAFF
MCDONNELL AIRCRAFT CORP
DEPT 350N M/S S102-1322
JS MCDONNELL BLVD
BERKELEY MO 63134-0001
PH:(314)-233-8623 Fax:(314)-777-1171

MAJ MICHAEL SAGASER
US NAVY
CODE 01505
PSC BOX 8026
CHERRY POINT NC 28532-0026
PH:(919)-466-7896 Fax:(919)-466-8477

MR PEDRO SALVADA
PORTUGUESE AIR FORCE
DIRECCAO DE MECANICA E AERO
AV FORCA AEREA PORTUGUESA
2720 ALFRAGIDE PORTUGAL-0001

PROF A SALVETTI
UNIVERSITA PISA
VIA DIOTISALVI 2
PISA ITALY I-56426-0001

MR RONALD SAMSON
MOOG ESPRIT
SENECA AND JAMISON RDS
E AURORA NY 14052-0001
PH:(716)-687-4279 Fax:(716)-652-0633

MR FORREST SANDOW
USAF WL/FIBAA
2130 EIGHTH ST STE 1
BLDG 45
WRIGHT-PATTERSON AFB OH 45433-7542
PH:(937)-255-5664 Fax:(937)-476-7723

MR GILLES SARRAZIN
BOMBARDIER INC
10000 CARGO A-4 ST
MONTEAL INTL AIRPORT
MIRABEL QUEBEC CANADA J7N-1H3
PH:(514)-476-4655 Fax:(514)-476-4451

MS MARY SCHLEIDER
MERCER ENGR RES CTR
ENGR ANALYSIS & DESIGN
1861 WATSON BLVD
WARNER ROBINS GA 31093-0001
PH:(912)-929-6400 Fax:(912)-929-6479

MR KURT SCHRADER
SOUTHWEST RES INST
6220 CULEBRA RD
SAN ANTONIO TX 78228-0510
PH:(210)-522-3322 Fax:(210)-522-4826

MR PAUL SCREEN
ROYAL AIR FORCE
RAF WADDINGTON
ENGLAND LN5 9NB--

MR IAN SEARLE
BOEING DEF & SPACE GRP
M/S 82-97
20403 68TH S 18-28 BLDG
KENT WA 98032-0001
PH:(206)-773-3894 Fax:(206)-773-4946

DR MICHAEL SHIAO
GALAXY SCIENTIFIC CORP
BLDG 11
2500 ENGLISH CREEK AVE
EGG HARBOR TOWNSHIP NJ 08234-0001
PH:(609)-645-0900

MR DAVID SIMPSON
NATL RES COUNCIL OF CANADA
INST FOR AERO RES
MONTREAL RD
OTTAWA ONTARIO CANADA K1A-0R6
PH:(613)-993-0899 Fax:(613)-952-7136

MR TIMOTHY SITAR
USAF/AFMC
74 WASHINGTON AVE N
STE 8
BATTLE CREEK MI 49017-3094
PH:(616)-961-5444 Fax:(616)-961-5660

MR JOHN SLYE
US AIR FORCE
ASC/YTJVA
BLDG 56 2100 MONAHAN WAY
WRIGHT-PATTERSON AFB OH 45433-7014
PH:(937)-255-9306 Fax:(937)-255-8516

MR JOHNNY SMITH
RAYTHEON AIRCRAFT CO
9709 E CENTRAL
PO BOX 85/DEPT 918
WICHITA KS 67201-0085
PH:(316)-676-7719 Fax:(316)-676-8556

MS MARTY SMITH
ARTI/DYNCORP
ONE RIDGMAR CENTRE
6500 W FREEWAY
FT WORTH TX 76116-0001
PH:(817)-737-1655 Fax:(817)-737-1605

MR JAMES SONG
US AIR FORCE
WL/MLS-OL
5225 BAILEY LP/BLDG 243E
MCCLELLAN AFB CA 95652-2510
PH:(916)-643-3810 Fax:(916)-643-0487

MR TIMOTHY SORENSEN
US AIR FORCE
OO-ALC/LFSS
6080 GUM LANE
HILL AFB UT 84056-5825
PH:(801)-777-9601 Fax:(801)-777-3928

MR WILLIAM SPARKS
31220 POST OAK TRAIL
FAIR OAKS RANCH TX 78015-0510
PH:(210)-981-8725

MR DIRK-JAN SPIEKHOUT
NATL AEROSPACE LAB
VOORSTERWEG
M/S 31
MARKNESSE NETHERLAND 8316PR-0001

MR HUGO STEIN
USAF SA-ALC/LFE
303 WILSON BLVD
STE 1
KELLY AFB TX 78241-5443
PH:(210)-925-6311 Fax:(210)-925-0097

MR BARRY STOCKS
ROYAL AIR FORCE
HQ LOG CMD
RAF WYTON HUNTINGDON
PETERBOROUGH ENGLAND PE17 2DL-0001

MR BARRY STURGIS
NAVAIRSYSCOM
M/S AIR 4 3 3
1421 JEFFERSON DAVIS HWY
ARLINGTON VA 22243-0001
PH:(703)-604-3400 Fax:(703)-604-4396

DR THOMAS SWIFT
FED AVIATION ADMIN
NRS/FRACTURE ANM 105N
3960 PARAMOUNT BLVD
LAKEWOOD CA 90712-0001

DR REDA TADROS
BMW ROLLS RR
ESCHWENWEG 11
M/S ED-3
DAHLEWITZ GERMANY D-15827-0001

MAJ HISATAKA TAGUCHI
JAPAN DEFENSE AGY
DEV DEPT/AIR STAFF OFF
9-7-45 AKASAKA
MINATO-KU TOKYO 107 JAPAN-0001

DR PAUL TAN
FAA
AAR-433
ATLANTIC CITY INTL AIR
ATLANTIC CITY NJ 08405-0001
PH:(609)-485-6665 Fax:(609)-485-4569

MR LARRY TARRANT
US AIR FORCE
OC-ALC/TILOF
7851 2ND ST/RM 107
TINKER AFB OK 73145-9145
PH:(405)-736-5424 Fax:(405)-736-3086

MR MALCOLM THOMAS
ALLISON ENGINE CO
M/S W08
PO BOX 420
INDIANAPOLIS IN 42606-0420
PH:(317)-230-4545 Fax:(317)-230-4470

MR MARK THOMAS
NAVAL AIR WARFARE CTR
MS03 CODE 4333
BLDG 2187
WARMINSTER PA 18974-0591
PH:(215)-441-3971 Fax:(215)-441-2797

MR BRIAN THOMPSON
ROYAL AIR FORCE
HQ LOG CMD
RAF WYTON HUNTINGDON
PETERBOROUGH ENGLAND PE17 2DL-0001

MR STEVEN THOMPSON
USAF WL/MLSE
2179 TWELFTH ST STE 1
WRIGHT-PATTERSON AFB OH 45433-7718
PH:(513)-255-5063 Fax:(513)-476-4419

MR PETER TO
deHAVILLAND
123 GARRETT ST
M/S N18-10
DOWNSVIEW ONTARIO CANADA M3K-1Y5
PH:(416)-373-7349 Fax:(416)-373-7766

MR PAUL TOIVONEN
MCDONNELL DOUGLAS AERO
86 PARK DR
GLEN CARBON IL 62034-1021
PH:(314)-234-4912 Fax:(314)-232-1394

MR PETER TOIVONEN
MCDONNELL DOUGLAS AERO
M/C S270-4320
PO BOX 516
ST LOUIS MO 63166-0516
PH:(314)-232-6439 Fax:(314)-232-3418

MR JEFF TOM
MCDONNELL DOUGLAS
3855 LAKEWOOD BLVD
M/S 801-45
LONG BEACH CA 90846-0001
PH:(310)-496-6921 Fax:(310)-982-7755

MR DAVID TONKS
ROYAL AIR FORCE
RAF BRIZE NORTON
M/S CAREGON
OXON UK OE18 35D-0001

MR DOUGLAS TRITSCH
UNIV DAYTON RES INST
STRUCTURAL INTEGRITY
300 COLLEGE PK
DAYTON OH 45469-0120
PH:(937)-229-4417 Fax:(937)-229-3712

MR BILLY TRUSSELL
US AIR FORCE
WR-ALC/LFEFS
296 COCHRAN ST
ROBINS AFB GA 31098-1622
PH:(912)-926-5482 Fax:(912)-926-5463

MR JIMMY TURNER
US AIR FORCE
SA-ALC/LADD
514 SHOP LN/STE 2
KELLY AFB TX 78241-6434
PH:(210)-925-4525

MS LINDA TWEEDY
SOUTHWEST RES INST
6220 CULEBRA RD
SAN ANTONIO TX 78228-0510
PH:(210)-522-2308 Fax:(210)-522-4826

MR ROB VAN OOST
STRUCTURAL LAMINATES CO
KLUYVERWEG #4
2629 HT
DELFT NETHERLANDS 262985-0001

LT COL MARINUS VOS
ROYAL NETHERLANDS AIR FORCE
OO-ALC/LFA-NE
6061 GUM LN
HILL AFB UT 84056-0001
PH:(801)-777-7741 Fax:(801)-773-7250

MR RAY WALDBUSSER
US AIR FORCE
WR-ALC/LBLRS
265 OCMULGEE CT
ROBINS AFB GA 31098-1647
PH:(912)-926-9602 Fax:(912)-926-2211

MR DOUG WALLING
NADEP
AV-8B IN SERVICE SUPPORT TEAM
PSC 8021
MCAS CHERRY POINT NC 28533-0021
PH:(919)-466-8517 Fax:(919)-466-8502

MR MICHAEL WHISNANT
MOOG ESPRIT
140 MAYHEW WAY
BLDG E STE 1003
PHEASANT HILL CA 94523-0001
PH:(510)-947-0400 Fax:(510)-947-0900

MR MICHAEL TYSON
LOCKHEED-MARTIN AERO
D/73-76 ZONE 0160
86 S COBB DR
MARIETTA GA 30068-0160
PH:(770)-494-1869 Fax:(770)-494-9610

MR BRADLEY VAN PEURSEM
WEST COAST INDUSTRIES
14900 WHITMAN AVE N
SEATTLE WA 98133-0001
PH:(206)-365-7513 Fax:(206)-365-7483

MR MICHAEL WADDELL
USAF WL/MTPN
BLDG 653 STE 6
2977 P ST
WRIGHT-PATTERSON AFB OH 45433-7739
PH:(513)-255-7277 Fax:(513)-476-4420

MR KEVIN WALKER
AERO & MARITIME RES LAB
506 LORIMER ST
FISHBCMENS BEND
VICTORIA AUSTRALIA

MR TONY WAYNE
NAVAL AIR SYS CMD
1421 JEFF DAVIS HGWY
PMA 200
ARLINGTON VA 22243-5120
PH:(703)-604-2060

MR DAVID WHITE
CONSULTANT
2 SILVER BROOK LANE
NORTH GRANBY CT 06060-0001
PH:(860)-653-5481 Fax:(860)-653-9295

CAPT ARNOLD VAN DEN HOEVEN
CANADIAN AIR FORCE
6287 FORTUNE DR
ORLEANS ONTARIO K1C 2A9-0001
PH:(613)-998-7951

MR HANAN VAX
RADA ELEC IND LTD
12 MEDIMAT HAYEHUDIM ST
PO BOX 2059
HERZLIYA B ISRAEL 46120-0001

MR TOM WADE
US COAST GUARD HQ
2100 2ND ST SW
WASHINGTON DC 20593-0001
PH:(202)-267-2816 Fax:(202)-267-4135

MR SIMON WALKER
BRITISH AEROSPACE
SALTGROUNDS RD
BROUGH
EAST YORKS ENGLAND HU15 1EQ-0001

MR GREG WEITZ
LOCKHEED MARTIN
M/S D/73-25 Z0160
86 S COBB DR
MARIETTA GA 30063-0001
PH:(770)-494-4550 Fax:(770)-494-9610

MR DAVID WIELAND
SOUTHWEST RES INST
6220 CULEBRA RD
SAN ANTONIO TX 78228-5166
PH:(210)-522-3864 Fax:(210)-522-3042

MR MICHAEL VAN DERNOOT
MCDONNELL DOUGLAS AERO
DEPT 257J M/S S102-2147
JS MCDONNELL BLVD
BERKELEY MO 63134-0001
PH:(314)-234-9030 Fax:(314)-234-8915

MR JAN VERHOEVEN
RADA EUROPEAN REPR
STRATUMSEDYK 20
PO BOX 6422 5600 HK
EINDHOVEN HOLLAND 56-00HK

MR GARY WAGGONER
USAF WL/MLS
BLDG 652
2179 TWELFTH ST STE 1
WRIGHT-PATTERSON AFB OH 45433-7718
PH:(513)-255-4651 Fax:(513)-476-4419

MS SHEILA WALL
USAF ASC/YTJVA
BLDG 56
2100 MONAHAN WAY
WRIGHT-PATTERSON AFB OH 45433-7014
PH:(937)-255-9306 Fax:(937)-255-8516

MR EDWIN WELLS
USAF ASC/YS
2275 D ST STE 4
WRIGHT-PATTERSON AFB OH 45433-0001
PH:(937)-255-9519 Fax:(937)-656-4276

LTCOL PETER WILCKE
GERMAN AF LIAISON OFF
5490 PEARSON RD
WRIGHT-PATTERSON AFB OH 45433-5332
PH:(937)-257-7222 Fax:(937)-656-1236

MR ROBERT WILKINS
ROCKWELL INTL SPACE SYS
MC AC04 DEPT 287
12214 LAKEWOOD BLVD
DOWNEY CA 90241-7009
PH:(310)-922-3609 Fax:(310)-922-3728

SQN LDR JOHN WILTSHIRE
USAF OC-ALC/LAKI-UK
UK AEW LAISON OFF
3001 STAFF DR/STE 2AH110
TINKER AFB OK 73120-0001
PH:(405)-736-5170 Fax:(405)-736-7659

MR RICHARD WURM
US AIR FORCE
OO-ALC/LACI F-4 TCG
6089 WARDLEIGH RD
HILL AFB UT 84056-5838
PH:(801)-777-6886 Fax:(801)-773-7620

MR JAMES YOST
DCMC-BELL HELICOPTER
DLA
4105 PLANTATION DR
FT WORTH TX 76116-1605
PH:(817)-280-7609 Fax:(817)-280-7061

MR MICHAEL ZEIGLER
USAF WL/FIBEC
BLDG 45
2130 EIGHTH ST/STE 1
WRIGHT-PATTERSON AFB OH 45433-7542
PH:(513)-255-5664 Fax:(513)-476-7723

MR BILL WILKINSON
PRATT & WHITNEY CANADA
1000 MARIE VICTORIA
M/S 01LE4
LONGUEUIL QUEBEC CANADA J4G-1A1
PH:(514)-647-2241 Fax:(514)-647-7461

MR RICHARD WOLF
BOEING PROD SUPPORT DIV
M/S K86-92
PO BOX 7730
WICHITA KS 67277-7730
PH:(316)-526-8220 Fax:(316)-523-2972

DR HSING YEH
US AIR FORCE ASC/ENGS
BLDG 125
2530 LOOP RD W
WRIGHT-PATTERSON AFB OH 45433-7101
PH:(937)-255-6583 Fax:(937)-656-4546

MR GREGORY YOUNG
ROYAL AUSTRALIAN AIR FORCE
NATL RES COUNCIL
BLDG M-14 MONTREAL RD
OTTAWA ONTARIO CANADA K1A-0R6
PH:(613)-990-5019 Fax:(613)-952-7136

MR MICHAEL WILLIAMS
US AIR FORCE SM/ALC
5020 DUDLEY BLVD
SM/ALC/LAFME
MCCLELLAN AFB CA 95652-1391
PH:(916)-643-0253 Fax:(916)-643-1405

MR JAMES WONG
ALLISON ADVANCED DEV CO INC
PO BOX 7162
M/S S50
INDIANAPOLIS IN 46206-7162
PH:(317)-230-2300 Fax:(317)-230-3307

MR AKIRA YOKOYAMA
JAPAN DEFENSE AGY
THIRD RESEARCH CTR
1-2-10 SAKAE
TACHIKAWA TOKYO JAPAN 190-0001

MR JESS YOUNG
OGDEN ALC/LACM
7278 4TH ST
HILL AFB UT 84056-5205
PH:(801)-777-5262 Fax:(801)-777-9482

MR DAVID WILLIE
DIFFRACTO
2835 KEW DRIVE
WINDSOR ONT CANADA N8T3B7-0001
PH:(519)-945-6373 Fax:(519)-945-1467

DR SPENCER WU
AFOSR/NA
STE B-115
110 DUNCAN AVE
WASHINGTON DC 20332-0001
PH:(202)-767-6962 Fax:(202)-767-4988

MAJ SHINJI YOSHIKAWA
JAPAN DEFENSE AGY
SYS MGMT OFF
5-1 LCHIGAYA
SHINJUKUKU TOKYO JAPAN 162-0001

DR JIN YU
MCDONNELL DOUGLAS AERO
2401 E WARDLOW RD
M/S 71-34
LONG BEACH CA 90807-5309
PH:(310)-593-1800 Fax:(310)-982-7787